Using the Eye to Predict Risk for Cardiovascular Disease- The Living Lab

Presented by

Miss Julie Sharon Moore

BSc First Class Hons, MSc (B00686953)

In fulfilment of the requirements for the degree of

Doctor of Philosophy (PhD)

Submitted 1st October 2022

School of Biomedical Sciences

Faculty of Life and Health Sciences

Ulster University

TABLE OF CONTENTS

Declaration

I hereby declare that with effect from the date on which the thesis is deposited in Research Student Administration of Ulster University, I permit

1. the Librarian of the University to allow the thesis to be copied in whole or in part without reference to me on the understanding that such authority applies to the provision of single copies made for study purposes or for inclusion within the stock of another library.
2. the thesis to be made available through the Ulster Institutional Repository and/or EThOS under the terms of the Ulster eTheses Deposit Agreement which I have signed.*

IT IS A CONDITION OF USE OF THIS THESIS THAT ANYONE WHO CONSULTS IT MUST RECOGNISE THAT THE COPYRIGHT RESTS WITH THE AUTHOR AND THAT NO QUOTATION FROM THE THESIS AND NO INFORMATION DERIVED FROM IT MAY BE PUBLISHED UNLESS THE SOURCE IS PROPERLY ACKNOWLEDGED.

This thesis is the sole work of the author and has not been submitted for any previous application for a higher degree.

I Confirm that this thesis is less than 100,000 words.

Julie Moore

Preface

Investigation of the microcirculatory system imparts both opportunities and challenges in clinical practice. Ideally, a highly specific, sensitive and non-invasive method of examining the microcirculation that requires no ionising radiation would be instrumental in the investigation of vascular disease. The conjunctival microvasculature imaging tool developed by our multi-disciplinary team attempts to fulfil these requirements.

Building upon early versions of the hardware and software in this arm of the research project, the imaging system and application were further developed, automated, tested and verified. Subsequently, 94 severe aortic stenosis patients undergoing transcatheter aortic valve implantation (TAVI), as well as 49 older control subjects and 119 patients referred for pressure wire were recruited. More than 1400 conjunctival videos have been processed and over 7200 vessel segments analysed since October 2020.

This thesis examines the adeptness of the conjunctival microvasculature imaging tool with consideration to specific patient cohorts and pathological phenotypes, such as coronary microvascular disease and valvular heart disease (severe aortic stenosis patients referred for TAVI). Parameters of the conjunctiva microcirculation were measured in concurrence with other clinical measurements, such as blood

biomarkers to support characterisation of cardiovascular risk. The work detailed in this thesis also explores data collected within the earlier studies further to assess cardiac remodeling and heart rhythm. This work investigates potential additional biomarkers reported from studies of the retinal vasculature. The final chapter within this thesis is dedicated to the COVID-19 research conducted during the pandemic, while patient recruitment to the cardiovascular risk prediction project was suspended.

Acknowledgements:

Sincerest thanks to my project supervisors Professor Tara Moore, Dr Andrew Nesbit, Professor Jim McLaughlin, and Dr Mark Spence, with special mention to Professor Tara Moore and Dr Andrew Nesbit for the continual support and encouragement shown over the past three years. You are both truly fantastic mentors! I am also grateful to Dr Louise Robertson for her guidance and friendship (long distance cheers!). I would like to thank Dr Jonathan Mailey for his efforts throughout this project, particularly, with recruitment and vessel labelling. I would also like to extend my thanks to Dr Min Jing and William Burns for all their work on the app development. Thanks also to Dr Paul Brennan and Dr Agnes Awuah for their training and valuable input that enabled the continuation of the project. Special thanks to the brilliant Dr Ruth Price for her support. Thank you to Northern Ireland Chest Heart and Stroke and the Heart Trust Fund for funding the project. Importantly, thank you to the participants who took the time to help with this research. Finally, a big heartfelt thank you to my family and friends.

It has been a real privilege to work on this PhD project and as part of a brilliant team within both Professor Tara Moore's Living Lab Research Group and the Pandemic Study team.

Publications- arising from this body of research submitted for the award of PhD

1. Awuah, A., **Moore, J.S.**, Nesbit, M.A., Ruddock, M.W., Brennan, P.F., Mailey, J.A., McNeil, A.J., Jing, M., Finlay, D.D., Trucco, E. and Kurth, M.J., 2022. A novel algorithm for cardiovascular screening using conjunctival microcirculatory parameters and blood biomarkers. *Scientific reports*, *12*(1), pp.1-9. I performed patient recruitment, consenting and data collection, research database preparation and auditing, research data analysis, manuscript preparation and editing.
2. Brennan, P.F., McNeil, A.J., Jing, M., Awuah, A., **Moore, J.S.**, Mailey, J., Finlay, D.D., Blighe, K., McLaughlin, J.A., Nesbit, M.A. and Trucco, E., 2021. Assessment of the conjunctival microcirculation for patients presenting with acute myocardial infarction compared to healthy controls. *Scientific reports*, *11*(1), pp.1-9. I performed patient recruitment, consenting and data collection.
3. Mailey, J.A., **Moore, J.S.**, Brennan, P.F., Jing, M., Awuah, A., McLaughlin, J.A., Nesbit, M.A., Moore, T. and Spence, M.S., 2021. A Novel Method of Conjunctival Vascular Screening to Detect Hemodynamic Alterations in Patients with Coronary Microvascular Disease. *Circulation*, *144*(Suppl_1), pp. A11054-A11054. I obtained ethical approval for the study, patient recruitment, consenting and data collection and analysis, research database preparation and auditing, research data analysis, manuscript preparation and editing.

4. Faustini, S., Shields, A., Banham, G., Wall, N., Al-Taei, S., Tanner, C., Ahmed, Z., Efstathiou, E., Townsend, N., Goodall, M., Plant, T., Perez-Toledo, M., Jasiulewicz, A., Price, R., McLaughlin, J., Farnan, J., **Moore, J.**, Robertson, L., Nesbit, A., Curry, G., Black, A., Cunningham, A., Harper, L., Moore, T., Drayson, M. and Richter, A. 2022. Cross reactivity of spike glycoprotein induced antibody against Delta and Omicron variants before and after third SARS-CoV-2 vaccine dose in healthy and immunocompromised individuals. *Journal of Infection*. I obtained ethical approval for the study, coordinated study participant attendance, performed sample collection and processing and laboratory analyses.
5. Jing, M., Bond, R., Robertson, L.J., **Moore, J.**, Kowalczyk, A., Price, R., Burns, W., Nesbit, M.A., McLaughlin, J. and Moore, T., 2022. User experience of home-based AbC-19 SARS-CoV-2 antibody rapid lateral flow immunoassay test. *Scientific Reports*, *12*(1), pp.1-18. I obtained ethical approval for the study, coordinated study participant attendance, data collection and ensured adherence to all research governance issues, reviewed the manuscript and approved its final version.
6. Jing, M., Bond, R., Robertson, L.J., **Moore, J.**, Kowalczyk, A., Price, R., Burns, W., Nesbit, M.A., McLaughlin, J. and Moore, T., 2021. User experience analysis of AbC-19 Rapid Test via lateral flow immunoassays for self-administrated SARS-CoV-2 antibody testing. *Scientific Reports*, *11*(1), pp.1-13. I obtained ethical approval, coordinated car park data collection and ensured adherence to all research governance issues.
7. **Moore, J.S.**, Robertson, L.J., Price, R., Curry, G., Farnan, J., Black, A., Nesbit, M.A., McLaughlin, J.A. and Moore, T., 2022. Evaluation of the

Performance of a Lateral Flow Device for Quantitative Detection of Anti-SARS-CoV-2 IgG. *Clinical Immunology Communications*. I performed sample collection and processing, laboratory analyses, data and statistical analyses/interpretations and wrote the manuscript and produced figures.

8. Robertson, L.J., Price, R., **Moore, J.S.**, Curry, G., Farnan, J., Black, A., Blighe, K., Nesbit, M.A., McLaughlin, J.A. and Moore, T., 2022. IgG antibody production and persistence to 6 months following SARS-CoV-2 vaccination: A Northern Ireland observational study. *Vaccine*, *40*(18), pp.2535-2539. I co-ordinated participant attendance, performed sample collection and processing, laboratory analyses, data and statistical analyses/interpretations and wrote the manuscript and produced figures.
9. Robertson, L.J., **Moore, J.S.**, Blighe, K., Ng, K.Y., Quinn, N., Jennings, F., Warnock, G., Sharpe, P., Clarke, M., Maguire, K. and Rainey, S., 2021. Evaluation of the IgG antibody response to SARS CoV-2 infection and performance of a lateral flow immunoassay: cross-sectional and longitudinal analysis over 11 months. *BMJ open*, *11*(6), p.e048142. I co-ordinated participant attendance, performed sample collection and processing, laboratory analyses, data and statistical analyses/interpretations and wrote the manuscript and produced figures.

Abstracts:

1. A Semi-automated Method to Evaluate Microvascular Physiology in the Conjunctival Microcirculation (British Society of Cardiovascular Research (BSCR) 2022 Poster Presentation).

2. Non-invasive evaluation of conjunctival microvascular physiology in patients with invasive evidence of coronary microvascular dysfunction (British Society of Cardiovascular Research (BSCR) 2022 Poster Presentation).

Pre-publication Manuscripts:

1. Performance of an Enzyme-Linked Immunosorbent Assay for the Serological Detection of Anti-SARS-CoV-2 IgG Across >1100 Samples. (Written for ProAxsis July 2022). Under review by AstraZeneca.

2. Cardiovascular disease risk prediction review. Literature review submitted to Current Cardiology Reviews, September 2022.

Thesis Abstract

Introduction

Cardiovascular disease is associated with both structural and functional alterations and remodeling of the microcirculation. Chapter 1 (along with papers 1, 2 and 3) outline the investigation of conjunctival microvascular function as a strategy that may support cardiovascular risk prediction, as the microvasculature of the conjunctiva is ideal for non-invasive imaging. The main aim of this thesis is to examine measurements of the conjunctival microcirculation for application in cardiovascular disease risk prediction.

Methods

The first study of this thesis is described in Chapter 2. It investigates prior knowledge obtained from retinal research to determine the methods used, and to investigate their potential application within the conjunctival microvascular imaging application to measure various additional ocular parameters. Chapter 3 detail methods of recruitment to include the controls and high-risk cardiovascular disease cohorts recruited such as coronary microvascular disease patients and severe aortic stenosis patients referred for transcatheter aortic valve implantation (TAVI). The slit-lamp at a magnification of x40 and iPhone 11 Pro at x2 zoom was used in this optimised 4K imaging system following calibration. Image acquisition involved 10 second videos of the left temporal, left nasal, right temporal and right nasal conjunctival vessel view being obtained and a minimum of 60 stable and high quality frames were required for image processing. Chapter 4 comprises of the processes

such as Manhattan Scoring and Convolutional Neural Networks involved in the development of a fully automated application (app) for processing the conjunctival vessel videos.

Results

As discussed within chapter 5, alterations of conjunctival arteriolar axial and cross-sectional velocities (0.57±0.12 mm/s to 0.62±0.12 mm/s, p=0.006 and 0.40±0.08 mm/s to 0.44±0.08 mm/s, p=0.001) wall shear rate (161±71 s^{-1} to 194±94 s^{-1}, p=0.019), as well as venular wall shear stress (7.98±2.50 dynes/cm² to 6.57±1.63 dynes/cm², p<0.001) were detected by the conjunctival vessel imaging application within the TAVI cohort between pre and post TAVI, respectively. Chapter 6 reports reductions in conjunctival axial and cross-sectional velocities (0.55±0.06 mm/s vs 0.53±0.04 mm/s, p=0.036 and 0.38±0.04 mm/s vs 0.37±0.03 mm/s, p=0.038) within the coronary microvascular disease (CMD) cohort when compared to controls, using the conjunctival vessel imaging application. Chapter 7 evaluates haemodynamics and risk scoring, and an area under the curve of 0.899 was reported for the multi-biomarker approach combining conjunctival vessel axial velocity, heart rate, N-terminal pro B-type natriuretic peptide, fibrinogen for all subjects classed into low risk (controls) or high risk (cardiovascular disease) groups. Chapter 8 discusses research outcomes in relation to the past and present knowledge, and how future studies could enhance implementation of healthcare through the use of the conjunctiva microvascular imaging application. Lastly, Chapter 9 (along with papers 4, 5, 6, 7, 8 and 9) detail the results of the COVID-19 research such as the finding of SARS-CoV-2 IgG antibodies being detected over 10 months. This research was conducted during a pause in recruitment to the Cardiovascular Risk Prediction project due to the pandemic.

Conclusion

The findings presented in this thesis and related publications suggest that this objective ocular imaging tool may be able to detect changes in haemodynamics due to valvular disease, macro and micro-vascular disease, as impacted by cardiac structure and rhythm, providing an indication of cardiovascular health. Further longitudinal and serial imaging is required to better assess and stratify risk within the general population. The COVID-19 research had an international impact, but future research could also consider the impact of COVID-19 on the cardiovascular system.

Graphical Abstract:

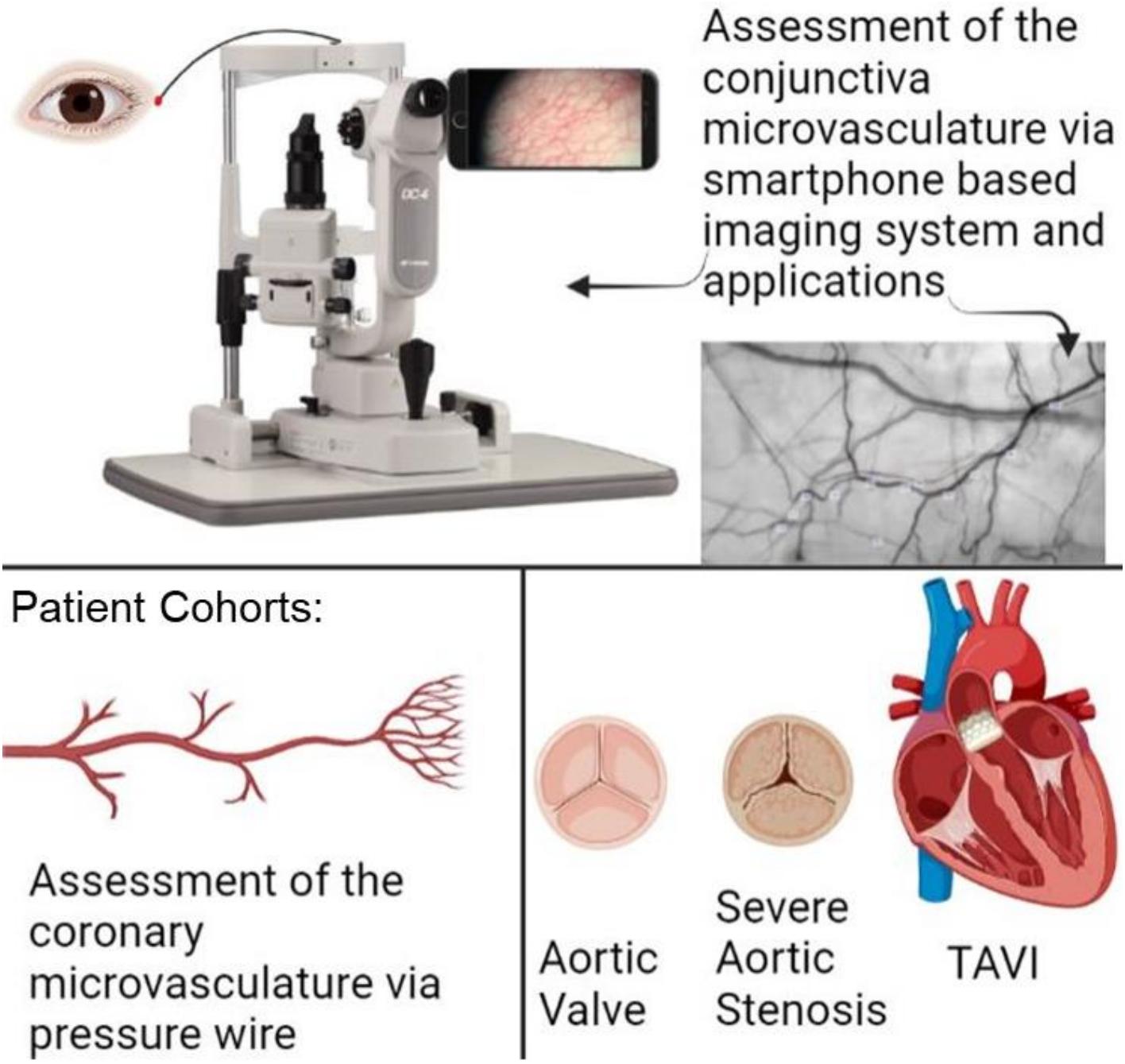

Abbreviations

ACE	Angiotensin-Converting Enzyme
AF	Atrial Fibrillation
ARB	Angiotensin II Receptor Blocker
ARNI	Angiotensin Receptor-Neprilysin Inhibitor
AUC	Area Under the Curve
BPH	Benign Prostatic Hyperplasia
CCHD	Cyanotic Congenital Heart Disease
CFR	Coronary Flow Reserve
CMD/MVD	Coronary Microvascular Disease
COPD	Chronic Obstructive Pulmonary Disorder
CRP	C-Reactive Protein
CSV	Cross-Sectional Velocity
DBP	Diastolic Blood Pressure
DM	Diabetes Mellitus
FFR	Fractional Flow Reserve
HbA1C	Haemoglobin A1C
HCT	Haematocrit
HDL	High Density Lipoprotein
HF	Heart Failure
IgA/IgG/IgM	Immunoglobulin A/ Immunoglobulin G/Immunoglobulin M
IHD	Ischemic Heart Disease
IMR	Index of Microvascular Resistance
LDL	Low Density Lipoprotein
MI	Myocardial Infarction
MRA	Mineralocorticoid Receptor Antagonist
NTproBNP	N-terminal pro B-type natriuretic peptide
PAF	Paroxysmal Atrial Fibrillation
PCI	Percutaneous Coronary Intervention
PCR	Polymerase Chain Reaction
PMR	Polymyalgia Rheumatica
PPM	Permanent Pacemaker
PVD	Peripheral Vascular Disease
Q	Blood Flow Rate
SBP	Systolic Blood Pressure
STI	Spatial Temporal Imaging
TAVI	Transcatheter Aortic Valve Implantation
TIA	Transient Ischemic Attack
Va	Axial Velocity
VTE	Venous Thromboembolism
WSR	Wall Shear Rate
WSS	Wall Shear Stress

Chapter 1

Introduction

Chapter 1: Introduction

1.1 *Background*

The microvasculature of the conjunctiva was first evaluated as a potential screening tool for cardiovascular disease in a feasibility study by Professor Moore and Dr Spence (Brennan *et al*. in 2019). The highly vascularised conjunctiva is clearly visible in contrast with the sclera and is ideal for non-invasive imaging and serial imaging of blood vessels requiring no ionising radiation. Monitoring of the conjunctival microvasculature also has the advantage of elimination of pressure artefact that may be seen when monitoring the sublingual microcirculation. It is proposed that this screening tool may support the detection of endothelial dysfunction and therein, subclinical identification of cardiovascular disease, as well as to potentially model optimal treatment options tailored to the patient. The conjunctival microvasculature and haemodynamics have previously remained largely unexplored, particularly when compared to the literature assessing the retinal vessels. Retinal vessels are already assessed clinically in relation to diabetes, and thus the possibility of assessing the conjunctival vessels clinically remains. Therefore, the study detailed in this thesis attempts to further investigate and improve the application and understanding of the microcirculation of the conjunctiva in relation to cardiovascular health.

Previously, several studies explored the subject of the conjunctival microcirculation. For example, Wanek *et al*. (2013) evaluate the therapeutic potential of the assessment of the conjunctival vasculature in sickle cell disease (SCD), grouping cohorts into SCD haemoglobin Sickle Cell Anaemia (SS) or Sickle Haemoglobin-C Disease (SC). This study evaluates the relationships between haemoglobin, blood viscosity and variation of the haemodynamics and vessel diameter groupings (group 1 <15µm and group 2 >15µm). Individuals with the SC variant typically present with higher blood viscosity levels when compared to their SS counterparts. The study found that in individuals with SS disease, as well as in healthy individuals, the diameters and velocity are positively correlated. However, the increased blood viscosity may disrupt the relationship between diameter and velocity for the SC group as no significant correlation was found, and blood velocities were lower overall for the SC cohort in both vessel groups 1 and 2 (0.42 ± 0.16 mm/s and 0.50 ± 0.20 mm/s) when compared with the healthy individual and SS disease groups (0.48 ± 0.12 mm/s and 0.66 ± 0.22 mm/s vs 0.32 ± 0.08 mm/s and 0.60 ± 0.18 mm/s, respectively). As a result, plasma viscosity was a biomarker assessed within this research project, as detailed within the biomarker analysis section in chapter 3 of this thesis.

Karanam *et al*. (2019) also described differences found in the conjunctival haemodynamics between different ethnicities. Prasanna *et al*. (2021) further emphasise the importance of reducing health inequalities and representation of ethnic minority groups in cardiovascular research. Conversely, our study is

representative of the general population in Northern Ireland comprising of 98% of the population of Northern Ireland being white according to the 2011 census.

The conjunctival microvascular imaging research studies conducted by Koutsiaris *et al*. (2013) and Kansari *et al*. (2016) also underpin our initial feasibility study. Interestingly, Kansari *et al*. describe a different method for analysing flow called variance filtering. They also still describe a manual method for vessel classification, despite the potential of automated vessel classification with the above stated method. Wang *et al*. (2016) propose a sampling size of 15 vessels per patient to be feasible. This target of 15 vessels per patient was exceeded within the feasibility study. Van Zijderveld *et al*. (2014) also present differing methods via imaging, analysing and comparing inferior and superior views rather than the nasal and temporal views. It could be argued that imaging of the nasal and temporal views is more advantageous, as it offers a more complete vascular view, although there may also be bias in imaging the denser vascular regions.

Currently, the need for a tool that can effectively and sub-clinically identify cardiovascular disease is reflected in the rates of mortality due to cardiovascular disease remaining the highest globally. To compare, COVID-19 infection was responsible for at least 3 million deaths in 2020, whilst in the same period approximately 17.9 million people died of cardiovascular disease (World Health Organisation, 2020; World Health Organisation, 2021). These rates may also be further exacerbated by the recent COVID-19 pandemic, with lockdown and virus-induced cardiac injury likely to have increased risk factors (Sebastian *et al*., 2020).

These high mortality rates remain even within the younger population, despite the impact of many campaigns raising awareness about cardiovascular health and the better understanding of not smoking, not drinking to excess, exercising, and getting a balanced diet. Current investigations of non-traditional risk factors are imperative (Libby, 2021).

1.2 *Literature Review; Measurements from Conjunctival Microcirculation Imaging*

An Overview of Conjunctival Microcirculation and Cardiovascular Disease:

There is a deficiency of research surrounding measurements of the conjunctival microcirculation and cardiovascular disease, as evident from the following literature review. Only a couple of studies out of the 25 studies assessed within this review examined the relationship between cardiovascular disease and conjunctival haemodynamic measurements, with 2 studies assessing diabetic subjects, 5 studies examining contact lens wearers and 13 studies looking at healthy subjects. This would suggest that investigation of the conjunctival vessels of cardiovascular disease subjects is a niche area of research. One of these studies was the study conducted by Karanam *et al.* (2014) that looked at Framingham risk scores in association with measurements of vessel diameter, blood flow axial velocity, cross-sectional velocity and blood flow rate. The findings of this study suggest a reduction of axial velocity (low risk=0.54 ± 0.13 mm/s vs high risk= 0.42 ± 0.15 mm/s) and cross-sectional velocity (low risk=0.37 ± 0.09 mm/s vs high risk= 0.29 ± 0.10 mm/s), but increased blood flow rate with increased cardiovascular risk (low risk=133.4 ±

59.6 pl/s vs high risk= 121.9 ± 52.6 pl/s). Similarly, Valeshabad *et al.* (2015) investigated the conjunctival haemodynamic parameters of unilateral ischemic stroke patients, and also found a reduction in the conjunctival blood flow axial velocity in the ipsilateral eyes (0.39 ± 0.13 mm/s) compared to the contralateral eyes (0.49 ± 0.16 mm/s) of the stroke patients. The further work detailed within this thesis adds to the body of evidence with a coronary microvascular disease cohort and a valvular disease cohort undergoing transcatheter aortic valve implantation, as the conjunctival microcirculation of these cohorts had not been previously investigated.

Abstract:

Introduction

Imaging developments have advanced screening of the conjunctiva microcirculation. Consequently, the haemodynamics of the conjunctiva may now be quantitatively and non-invasively assessed, as investigated within this thesis. This literature review attempts to gather the data to compare the measurements of diameter, axial velocity, cross-sectional velocity, blood flow rate, wall shear rate and wall shear stress throughout the literature.

Methods

The databases searched include Ovid, Pubmed, Web of Science and Cumulative Index to Nursing and Allied Health Literature (CINAHL) from 2009-2022. The databases were last searched on the 1st of July 2022. The selection criteria included

all studies focused on quantitative measurement of the conjunctival microcirculation. Data was extracted using a data extraction form and assessed using a critical appraisal checklist.

Results

The search resulted in 25 studies being included for review. The ranges of the diameter, axial velocity, cross-sectional velocity, blood flow rate, wall shear rate and wall shear stress measurements were 6.00-71.25 µm, 0.25-3.26 mm/s, 0.2-1.2 mm/s, 13.0-296.9 pl/s, 190-3515 s^{-1} and 5.4-211.0 N/m^2, respectively.

Conclusion

The literature indicates the possibility of an objective and quantitative approach to assessment of the conjunctival microvasculature for monitoring alterations within the microcirculation. Future research should focus on longitudinal studies and standardisation of the technique.

Introduction

The global mortality rate due to cardiovascular disease remains elevated. However, advancements in medical imaging, technology and machine learning applications should be reflected in cardiovascular healthcare and prevention strategies. Furthermore, it should be acknowledged that non-invasive, real-time assessment of the microcirculation is accessible from imaging of the conjunctiva vasculature. Typically, and in the case of the methodology of this research project, the

microcirculation of the conjunctiva is imaged using a slit lamp and camera system. The acquired images may then be analysed to assess the vessel parameters, and to track the movement of the erythrocytes over time. The aim of this review is to report and evaluate the literature surrounding the imaging and analysis of the conjunctival microvasculature.

Methods

Multiple databases were searched to include OVID, Cumulative Index to Nursing and Allied Health Literature (CINAHL), Pubmed and Web of Science. Hand-searching was also carried out to obtain as many relevant manuscripts as possible. The search was restricted to open access manuscripts, written in English and published between 2009 and 2022. Data was extracted using a pre-designed form and assessed using a critical appraisal tool.

Results

Twenty-five studies were included for review. The results of the data extraction are presented in Table 1 below. The conjunctival vessel diameter was reported in 21 of the included studies, and the results ranged from 6 μm to 71.25 μm. The axial velocity ranged from 0.25-3.26 mm/s, as reported in 22 of the included studies. Cross-sectional velocity was reported in 5 of the included studies. The cross-sectional velocity ranged from 0.2-1.2 mm/s. The blood flow rate ranged from 13.0-

296.9 pl/s. Wall shear rate results were reported in two of the studies included for review. The results from 11 studies ranged from 190-3515 s^{-1}. Lastly, wall shear stress results were also reported in two studies included for review. The results ranged from 5.4-211 N/m^2.

Several studies compared the differences within the conjunctival haemodynamics of contact lens wearers to non-contact lens wearers (Chen *et al*., 2020; Cheung *et al*., 2012; Hu *et al*., 2018; Shi *et al*., 2018; Wang *et al*., 2019). The results of these studies showed overall the conjunctival vessel velocity and blood flow rate was increased for contact lens wearers compared to non-contact lens wearers. A selection of studies also evaluated cohorts at increased cardiovascular risk including those from the studies by Hwang *et al*. (2021), Karanam *et al*. (2014), Khansari *et al*. (2017), Valeshabad *et al*. (2014), Valeshabad *et al*. (2015) and Wanek *et al*. (2013). For most studies assessing alterations in haemodynamics in association with disease vs control groups, the ranges were markedly reduced for axial velocity, cross-sectional velocity and wall shear rate. However, velocity was increased for the diabetes without complications cohort as reported by Hwang *et al*., as well as in the study by Wanek *et al*. that evaluates the differences in the conjunctival parameters of patients with sickle cell disease. Diameter typically remained the same throughout the reviewed studies, whilst the results of blood flow rate were varied. Blood flow rate was reduced in the study by Karanam *et al*. as well as within the study by Khansari *et al*.

Table 1. Data extraction

Study	**Participants**	**Imaging Method**	**Diameter µm**	**Velocity mm/s**	**Blood Flow Rate pl/s**	**WSR s^{-1} WSS dyne/ cm^2**
Akagi et al., 2018	10 healthy subjects	Anterior Segment-OCT	Average: 17.2 ± 0.6 Nasal: 18.0 ± 0.8 Temporal: 17.0 ± 0.4 Inferior: 17.6 ± 1.2 Superior: 16.3 ± 1.1	n/a	n/a	n/a
Chen et al., 2020	13 HCL and 14 NCL	FSLB	HCL (baseline): 17.4 ± 3.9 NCL (baseline): 16.9 ± 2.8	HCL (baseline): Va= 0.52 ± 0.17, CSV= 0.37 ± 0.12 NCL (baseline): Va= 0.47 ± 0.15, CSV= 0.34 ± 0.11	HCL (baseline) : 136.0 ± 115.1 NCL (baseline) : 109.3 ± 51.7	n/a

Chen et al., 2017a	22 Healthy subjects	FSLB	Baseline= 17.8 ± 1.8	Baseline= 0.51 ± 0.20	n/a	n/a
Chen et al., 2017b	56 Dry eye patients	FSLB	Baseline= 22.13 ± 1.84	Baseline= 0.50 ± 0.15	n/a	n/a
Cheung et al., 2012	102 Contact lens users and 29 controls	Computer-assisted intravital microscopy	User= 71.25 ± 12.09 Control= 52.20 ± 5.10	n/a	n/a	n/a
Hu et al., 2018	91 NCL wearers and 75 HCL wearers	FSLB	n/a	NCL= 0.50 ± 0.14 HCL= 0.61 ± 0.15	n/a	n/a
Hwang et al., 2021	98 Controls (C), 13 diabetics without complication (D-C) and 21 diabetics with complication (D+C)	FSLB	n/a	Va; C= 0.51 ± 0.17 D-C= 0.62 ± 0.17 D+C= 0.45 ± 0.17 CSV; C= 0.35 ± 0.12 D-C= 0.43 ± 0.13 D+C= 0.32 ± 0.13	n/a	n/a

Jiang et al., 2013	5 Healthy subjects	RFI, Optical Imaging Ltd, Rehovot, Israel	n/a	Without CL: 0.86 ± 0.08 With CL: 0.99 ± 0.11	n/a	n/a
Jiang et al., 2014	6 Subjects	FSLB	Baseline= 18.8 ± 2.7	Baseline= 0.60 ± 0.12	Baseline= 129.8 ± 59.9	n/a
Jo et al., 2021	5 Healthy males	Custom-built optical imaging system	Average= 11.6	Average= 0.15	n/a	n/a
Karanam et al., 2014	84 subjects (11 low Framingham risk score, 14 intermediate Framingham risk score and 59 high Framingham score)	FSLB	Low= 19.5 ± 3.2 Intermediate = 21.5 ± 2.0 High= 21.3 ± 2.8	Va; Low= 0.54 ± 0.13 Intermediate = 0.44 ± 0.13 High= 0.42 ± 0.15 CSV; Low= 0.37 ± 0.09 Intermediate = 0.30 ± 0.09 High= 0.29 ± 0.10	Low= 133.4 ± 59.6 Intermediate= 123.6 ± 39.3 High= 121.9 ± 52.6	n/a

Khansari et al., 2015	15 Healthy subjects	FSLB	Arterioles= 15 ± 3 Venules= 18 ± 2	Arterioles= 0.63 ± 0.17 Venules= 0.54 ± 0.13	Arterioles = 86 ± 33 Venules= 140 ± 55	Arterioles = 320 ± 132 Venules= 190 ± 46
Khansari et al., 2017	Non-diabetic control (C, n = 34), no clinically visible DR (NDR, n = 47), non-proliferative DR (NPDR, n = 45), and proliferative DR (PDR, n = 35)	FSLB	C= 18 ± 5 NDR= 19 ± 4 NPDR= 18 ± 4 PDR= 18 ± 5	C= 0.70 ± 0.23 NDR= 0.54 ± 0.22 NPDR= 0.62 ± 0.24 PDR= 0.64 ± 0.27	C= 144 ± 118 NDR= 124 ± 98 NPDR= 135 ± 90 PDR= 146 ± 115	WSS; C= 8.6 ± 5.0 NDR= 5.4 ± 3.2 NPDR= 6.2 ± 3.3 PDR= 6.6 ± 3.7
Koutsiaris et al., 2013	15 Normal volunteers	FSLB	6-12	0.52-3.26	13-202	WSR= 587-3515 WSS= 17-211
Koutsiaris et al., 2010	15 Normal volunteers	FSLB	6-12	0.52-3.26	n/a	n/a
Shahidi et al., 2010	1 Healthy subject	FSLB	8.7-24.3 (mean= 15.5)	Va= 0.3-1.6 (mean= 0.9) CSV= 0.2-1.2 (mean= 0.7)	27.3-296.9 (mean= 111.8)	n/a
Shi et al., 2019	58 Normal subjects	FSLB	n/a	0.49	90	n/a

Shi et al., 2018	20 HCL and 40 NCL	FSLB	HCL= 16.9 ± 1.3 NCL= 17.3 ± 1.6	HCL= 0.59 ± 0.19 NCL= 0.48 ± 0.17	HCL= 119 ± 38 NCL= 92 ± 39	n/a
Valeshabad et al., 2015	15 Healthy controls and 12 subjects with a diagnosis of unilateral ischemic stroke	FSLB	Controls right eye= 20.5 ± 4.2 Controls left eye= 20.3 ± 4.5 Stroke contralateral eye= 21.2 ± 3.9 Stroke ipsilateral eye= 20.6 ± 4.4	Controls right eye= 0.42 ± 0.13 Controls left eye= 0.43 ± 0.14 Stroke contralateral eye= 0.49 ± 0.16 Stroke ipsilateral eye= 0.35 ± 0.13	n/a	n/a
Valeshabad et al., 2014	22 Sickle Cell Retinopathy (SCR) subjects	FSLB	12-26	0.25-1.08	n/a	n/a
van Zijdervelt et al., 2014	21 Volunteers	OPSI	Inferior large segments= 21.14 ± 5.22 Inferior small segments= 8.67 ± 0.74 Nasal large segments= 23.58 ± 5.95	n/a	n/a	n/a

			Nasal small segments= 8.72 ± 0.80			
Wanek et al., 2013	9 Healthy controls (AA), 24 SC disease subjects and 18 SS disease subjects	EyeFlow™	AA Vessel size 1= 11.2 ± 0.9 Vessel size 2= 19.5 ± 3.0 SS Vessel size 1= 11.7 ± 0.9 Vessel size 2= 20.5 ± 4.0 SC Vessel size 1= 11.1 ± 1.3 Vessel size 2= 19.8 ± 2.5	AA Vessel size 1= 0.32 ± 0.08 Vessel size 2= 0.60 ± 0.18 SS Vessel size 1= 0.48 ± 0.12 Vessel size 2= 0.66 ± 0.22 SC Vessel size 1= 0.42 ± 0.16 Vessel size 2= 0.50 ± 0.20	n/a	n/a
Wang et al., 2019	13 HCL and 15 NCL	FSLB	HCL Visit 1= 18.1 ± 4.0 Visit 2= 16.8 ± 2.3 NCL Visit 1= 17.2 ± 2.4 Visit 2= 16.8 ± 2.6	HCL Visit 1= 0.52 ± 0.15 Visit 2= 0.51 ± 0.17 NCL Visit 1= 0.49 ± 0.13 Visit 2= 0.51 ± 0.16	HCL Visit 1= 150 ± 119 Visit 2= 118 ± 62 NCL Visit 1= 116 ± 43	n/a

					Visit 2= 117 ± 53	
Wang et al., 2016	5 Healthy subjects	FSLB	30.4 ± 8.4	0.59 ± 0.035	n/a	n/a
Xu et al., 2015	20 Healthy subjects	FSLB	M1= 21.56 ± 2.44 M2= 21.65 ± 2.58	Va; M1= 0.62 ± 0.31 M2= 0.62 ± 0.32 CSV; M1= 0.44 ± 0.22 M2= 0.44 ± 0.22	M1= 165.61 ± 86.62 M2= 166.83 ± 91.00	n/a

Abbreviations:

CL= Contact Lens, CSV= Cross-Sectional Velocity, DR= Diabetic Retinopathy, FSLB= Functional Slit Lamp Biomicroscopy, HCL= Habitual Contact Lens wearer, M1= Measurement 1, M2= Measurement 2, NCL= Non-Habitual Contact Lens wearer, OCT= Optical Coherence Tomography, OPSI= Orthogonal Polarisation Spectral imaging, RFI= Retinal Functional Imager, SC= Sickle Haemoglobin-C Disease, SS= Sickle Cell Anaemia, Va= Axial Velocity, WSR= Wall Shear Rate, WSS= Wall shear Stress

Discussion

This review ascertained the ranges of the various parameters of the conjunctival microcirculation, to include diameter, axial velocity, cross-sectional velocity, blood flow rate, wall shear rate and wall shear stress. The results of our previously published feasibility study fell within the ranges gathered from the literature reviewed (Brennan *et al*., 2021a). The diameter in this previous study was 21.43 ± 7.57 μm for the 56 control subjects and 22.32 ± 7.66 μm for the 59 myocardial infarction (MI) patients, axial velocity was 0.53 ± 0.15 mm/s for controls vs 0.49 ± 0.17 mm/s for the MI group, blood flow rate was 153 ± 124 pl/s vs 154 ± 125 pl/s, and lastly, wall shear rate was calculated to be 162 ± 93 s^{-1} for controls vs 145 ± 88 s^{-1} for MI (Brennan *et al*., 2021a). Similar reductions were reported for velocity (0.53 ± 0.05 mm/s vs 0.47 ± 0.06 mm/s) and wall shear rate (174 ± 22 s^{-1} vs 153 ± 27 s^{-1}) within the cyanotic congenital heart disease group (CCHD) when compared to controls (Brennan *et al*., 2021b).

Wanek *et al*. (2013) suggested stratification of conjunctival haemodynamic results by vessel size. The results show linear relationships between the velocities of the different vessel size groups. Alternatively, Akagi *et al*. (2018) also demonstrated differences in conjunctival vessel measurements between the different fields of view, whilst Khansari *et al*. (2015) observed the differences between the vessel groups of arterioles and venules, and these factors should be considered when assessing alterations in disease groups to obtain reference ranges. Additionally, as demonstrated within the literature, the use of contact lenses is also associated with

vascular abnormalities, alterations of the conjunctival haemodynamics, as well as increased ocular discomfort that also positively correlates with conjunctival vessel velocity (Fang *et al*., 2021). Consequently, contact lens wear was included within the exclusion criteria of this project.

Limitations:

This review was limited due to lack of standardisation of the conjunctival imaging technique. Diameter and axial velocity are consistently measured throughout all studies, whilst the other parameters are calculated by formulae using these measured values.

Conclusion

This review of the literature reports the findings from previous studies, quantitatively assessing the conjunctival microcirculation and informs future studies by assessing the range of parameters. A limited field of research within the past decade reports alterations of the conjunctival microcirculation in association with disease such as in vascular disease or diabetes, as well as in cases of contact lens use. The work presented within this review warrants further research.

1.3. *Vascular Physiology and Pathophysiology*

The Cardiovascular and Microcirculatory System: Physiology

The cardiovascular system is centered on the heart and blood vessels (arteries, arterioles, veins, venules and capillaries) controlling the haemodynamics. The arteries, arterioles, veins, venules and capillaries all differ in structure and function, with the primary role of the arteries being to deliver oxygenated blood from the heart to the rest of the body, and the key role of veins is to deliver the deoxygenated blood back to the heart. Compared to arteries which need to transport blood under higher pressures, veins have thinner walls with less smooth muscle and connective tissue, as well as valves to prevent the back flow of blood. The thickness of the vessel wall varies with vessel diameter, although basement membrane and endothelial layers remain the same.

The tangential component of the force of the blood flow against the vessel wall is known as the wall shear stress (Gijesen *et al*., 2019). Endothelial cells respond to the fluctuations of wall shear stress and wall shear stress alters cell physiology and is a determinant of endothelial function (Cecchi *et al*., 2011; Santamaria *et al*., 2020). Wall shear stress should gradually decrease from arterioles to venules. The arterioles have a key role in metabolic control and flow distribution whilst only endothelium (that lines all vessels) is present in the capillaries (Taqueti and Di Carli, 2018). Endothelial cells play an important role in cardiovascular homeostasis. The capillaries may be a crucial site to investigate endothelial dysfunction. Additionally, metabolically active tissues will have a more extensive capillary network, and

different endothelial cell phenotypes occur with different organs (Colbert and Schmidt, 2016).

Ohm's law states blood flow is equal to the pressure gradient divided by resistance and Murray's law, based on the assumption of constant blood flow, relates the radius of the parent vessel to that of the downstream daughter vessels. Reynold's number is used to determine if flow is laminar or turbulent, with turbulent blood flow related to increased energy loss and decreased blood flow at a given perfusion pressure (Andersson *et al*., 2019). Additionally, whilst energy is interchanged into various forms within the cardiovascular system to include hydrostatic, oncotic and vascular resistance, Poiseuille's law defines the energy requirement for pumping blood through a vessel. Although such laws exist which help explain various aspects of microhaemorheology and micro-haemodynamics, a standardised and comprehensive model is still needed. This would help to better understand normal micro-vessel physiology, and hence help to identify, categorise and explain abnormalities.

Inside the vessels of the microvascular system, the various components of the blood (e.g., leukocytes, red blood cells and platelets) circulate along with plasma. Although these vessels are small, they play a major role in normal cardiovascular function. The importance of monitoring the microcirculation, particularly for the aspects of convection and diffusion, to ensure tissue perfusion and oxygenation is occurring via a bedside point-of-care device has been previously highlighted (Guven *et al*., 2020). The pathogenesis of microvascular and macrovascular dysfunction is not fully

understood, and it remains unknown if there is a correlation between microvascular and macrovascular dysfunction due to shared risk factors.

Previous assessment of the sublingual microcirculation in critically ill patients established the categorization of microvascular abnormalities into types 1-4:

- Type 1 describes the stagnation of blood which may be seen with sepsis.
- Type 2 describes the conditions of haemodilution (altered viscosity and reduction in shear stress may also occur).
- Type 3 describes flow reduction, increased vascular resistance and/or venous pressure (seen with vasoconstriction/tamponade).
- Lastly, type 4 describes hyperdynamic capillary flow (seen with edema) (Dubin *et al*, 2020).

Further alternative methods of scoring the microvasculature system have also been discussed such as De Backer's score and microvascular flow index (Flick *et al*., 2019).

Pathophysiology:

As discussed above, the cardiovascular system has a key regulatory role in many functions of the body such as delivering oxygen and nutrients whilst removing metabolic wastes, protecting from pathogens and maintaining homeostasis. Therefore, disruption of these mechanisms can have serious implications. Cardiovascular disease is the umbrella term for disease of the heart and blood vessels and includes coronary heart disease, cerebrovascular disease, peripheral

artery disease, rheumatic heart disease and congenital heart disease. Approximately, 31% of all deaths worldwide are due to cardiovascular disease (World Health Organisation, 2021).

Despite the extensive impact of cardiovascular disease, the pathophysiological mechanisms have, as of yet, not been fully explained. Atherosclerosis is frequently reported as the main underlying etiology of cardiovascular disease and may be recognised by the formation of fatty streaks (involving endothelial injury and dysfunction, as well as macrophage activation and the formation of foam cells, which are macrophages engorged with lipid), atheroma and plaque formation within a vessel (Rafieian-Kopaei *et al*., 2014). Various mechanisms of fibrosis, remodeling, inflammation and lipid metabolism have been suggested. Fibrosis has been reported in association with the majority of cardiac pathologies and is not always the primary cause of cardiac dysfunction, but instead a pathological response of the cardiomyocyte to the microenvironment (Frangogiannis, 2021). Fibrosis often contributes to impaired cardiac function and is responsible for various electrophysiological changes, resulting in arrythmias that can be fatal in the case of ventricular tachycardia and ventricular fibrillation. The mechanisms discussed above may also occur simultaneously, as in the example of immune cells triggering an inflammatory cascade and causing myocardial damage, provoking a fibrotic response. Similarly, mechanisms of oxidative stress are found to be associated with cardiac stress and activated fibroblasts. The results from the initial study would further suggest this with the example of the biomarker adiponectin being reduced within the high cardiovascular risk group, and adiponectin is reported to be

cardioprotective reducing inflammation, oxidative stress and involved in lipid metabolism (Awuah *et al*., 2022; Yanai and Yoshida, 2019).

Endothelial Dysfunction:

Vascular disease may ensue from the disruption of endothelial homeostasis. Additionally, endothelial dysfunction may be prompted by various stimuli or conditions (Hamilos *et al*., 2018). Interestingly, Godo *et al*. (2020) suggest that the conventional cardiovascular risk factors do not fully account for the vulnerable plaque formations associated with coronary microvascular endothelial dysfunction in patients with non-obstructive coronaries.

1.4. *A Screening Tool: The Conjunctiva Vasculature, Cardiovascular and Microvascular Disease*

In the last century, a link had been established between retinal microvasculature injury and survival, yet the conjunctival microvasculature is consistently overlooked throughout the research (Litwin, 2020). The conjunctival vasculature is arguably more accessible, found within the anterior segment of the eye. The conjunctival vessels stem from the internal carotid artery that branches off to the ophthalmic artery, and the internal jugular vein that branches off to the ophthalmic vein. In-depth methodology of the tool is explained within the methods section of this thesis. These methods are based on several haematological principles. The fundamental principle is that the size of the erythrocyte is proportional to the measurements found within

the flow analysis applications (approximately 8µm in diameter and 2µm in thickness). The range of vessel diameter measurement is around 5-70µm, as demonstrated within the results. Assumptions of deformability of erythrocytes may also be made, and it is also known that deformation is increased by increased wall shear rate.

This study assessed the conjunctival microcirculation in a cohort of pressure wire patients, and hence reports a selection of pressure wire measurements to include:

- The index of microcirculatory resistance (IMR)- a coronary guidewire-based measurement centered on the principle that resistance is equal to the difference in pressure overflow. Evidence suggests that this may be the most reliable and specific indicator of microvascular disease (Fearon and Kobayashi, 2017).
- Coronary flow reserve (CFR)- measured by indicator thermodilution. The ratio between the resting blood flow through the coronaries to the maximum blood flow through the coronary arteries.
- Fractional flow reserve (FFR)- the ratio of the maximum blood flow through a stenosis to the maximum blood flow with no stenosis (currently, the gold standard for assessing epicardial disease).
- Relative flow reserve (RFR)- similar to FFR but does not require vasodilator medications, as it is a non-hyperemic index.

Often patients presenting with angina or symptoms of ischemia are found to have no obstructions within their coronary arteries. Upon further investigation the smaller vessels are found to have microvascular disease. Likewise, various studies suggest microvasculature disease is likely to be under-diagnosed and may be more prevalent

than macrovascular disease (Sidik *et al.,* 2020). It has been suggested that microvascular lesions are a precursor of epicardial lesions and thus this study cohort should support gaging of risk as proposed in Figure 1.1 below (Knuuti *et al.*, 2020).

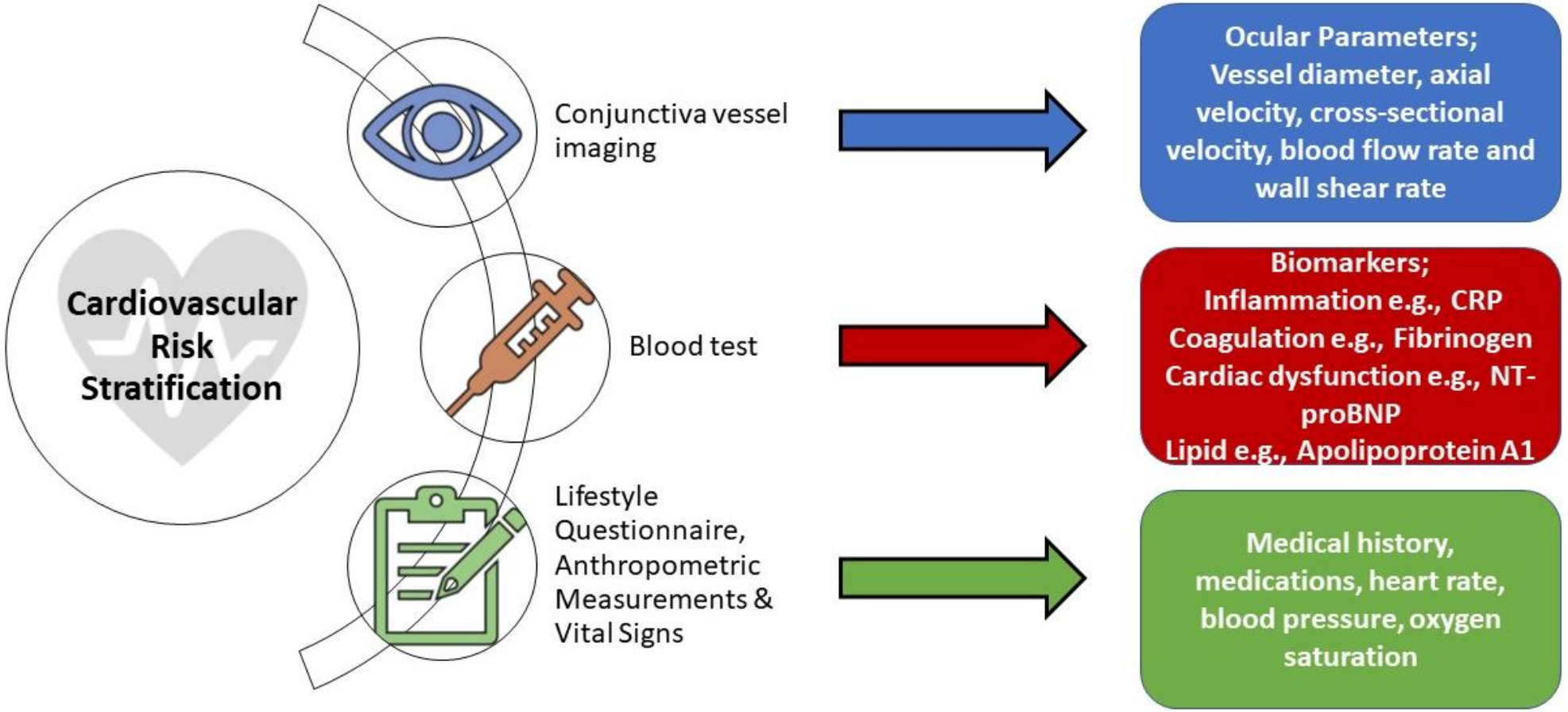

Figure 1.1. Proposed cardiovascular risk stratification

CRP= C-Reactive Protein and NT-proBNP= N-terminal pro B-type natriuretic peptide.

The research project presented herein, hypothesised that the measurements of the pressure wire investigation would correlate with the conjunctival microvascular haemodynamic measurements. The previous studies conducted by the Moore research group also investigated MI patients, as well as MI patients with non-obstructive coronary arteries. It would be of particular interest to compare the results of each group to the results of the pressure wire cohort. Patients with coronary microvascular disease are still at an increased risk of adverse events (Taqueti and Di Carli, 2018).

Coronary microvascular dysfunction may be considered a sub-clinical marker of cardiac remodeling. Additionally, diabetes may predispose metabolic remodeling of the heart, and cardiac remodeling can also be considered a pre-cursor of heart failure. A non-invasive and easily accessible screening tool as proposed in this study would be beneficial to identify those at risk, to intervene at an early stage, and ultimately to prevent adverse events occurring. Although the gold standard software for monitoring the microcirculation is the automated vascular analysis (AVA) software, it has only been assessed with the sublingual microcirculation (Hilty *et al*., 2019). It is expected that the tailored conjunctival software calibrated for the camera system is required for the microvasculature imaging tool.

Assessing Treatment: Severe Aortic Stenosis and Transcatheter Aortic Valve Implantation (TAVI):

A recent study estimated 291,488 people in the UK have severe aortic stenosis, and that almost 60% of these people will die within the next five years if left untreated (Strange *et al*., 2022). Stenosis of the aortic valve is already the most prevalent of the valvular heart diseases (Michail *et al*., 2018). The increasingly older population places further precedence on optimising management and treatment of aortic stenosis.

Severe aortic stenosis is associated with tissue perfusion abnormalities and hence microvascular dysfunction. Patients with severe aortic stenosis may present with heart murmur upon auscultation, and experience symptoms relating to fatigue, dyspnea and angina upon exertion. However, patients with severe aortic stenosis may also be asymptomatic.

Severe aortic stenosis presents with an aortic valve area of less than $1cm^2$ due to leaflet fibrosis and calcification, and an increased blood pressure gradient may be found across the valve (Saikrishnan *et al*., 2014; NICE, 2021). The ejection fraction is often reduced within this cohort of patients, as the left ventricle is required to overcome the stenotic valve. Subsequently, the left ventricle becomes hypertrophied, left ventricular contractile function may deteriorate and thus ejection fraction is lowered (Ito *et al*., 2018). It is this increased cardiac workload that also makes these patients susceptible to potentially fatal arrhythmias and heart failure. Interestingly, secondary microvascular disease may also result within this cohort (Knuuti *et al.*,

2020). Unsurprisingly, the one-year survival rate for aortic stenosis patients who undergo TAVI is 94% compared to 69% for unoperated aortic stenosis patients (Bach, 2011). The TAVI procedure typically involves a new valve being positioned inside the faulty valve via catheter insertion typically through the femoral artery to the aorta (NICE, 2017).

Crucially, Carabello (2013) suggests that upon the onset of aortic stenosis symptoms life expectancy is approximately three years if not treated. However, TAVI was pioneered as a minimally invasive treatment for severe aortic stenosis around two decades ago (Spitzer *et al*., 2020). Improvements in the coronary microcirculation have been reported post-TAVI (Al-Rashid *et al*., 2014).

It is also important to account for several variables associated with TAVI such as pacing, as like most intervention treatments TAVI is also not without risk of complications. This is illustrated in the study by Selle *et al*. (2014) concluding that rapid ventricular pacing in TAVI is associated with impeding recovery of microflow and microcirculatory arrest. Contrastingly, the recent SWEDEHEART observational study conducted by Rück *et al*. (2021) indicates only marginally lower survival rate values for the TAVI cohort who received a permanent pacemaker following surgery (90.0% at 1 year, 52.7% at 5 years and 10.9% at 10 years) compared to those who did not have a permanent pacemaker implanted (92.7% at 1 year, 53.8% at 5 years and 15.3% at 10 years, p=0.692). Pibarot and Dumesnil (2012) suggest more work needs to be done to assess the disease severity both comprehensively and

quantitatively, this may also help to identify the most suitable candidates for TAVI or alternatively, for surgery.

1.5. Ocular, Blood and Clinical Biomarkers

Parameters: Velocity, Blood Flow Rate Wall Shear Rate and Stress:

The methods to obtain the ocular parameters have previously been described within the feasibility study by Brennan *et al*. (2019). To summarise, diameter is measured using the principles of Euclidean distance transform (EDT) in the binary vessel image, whilst axial velocity (the average velocity in a particular direction) is measured using the principles of Fourier transform for spatial temporal imaging (STI) and one dimension+time continuous wavelet transform (1DTCWT). Diameter and axial velocity are the two measured ocular parameters, whilst cross sectional velocity, blood flow rate (formula 1) and wall shear rate (formula 2) are then recorded from calculations. Cross-sectional velocity is dependent on a conversion factor, as it is the volumetrically averaged flow velocity. Vasomotion (oscillation in vascular tone) and the resultant fluctuations in diameter will also correspond to fluctuations in cross-sectional velocity (Fredriksson *et al*., 2021).

$$Q = CSV(\frac{\pi D^2}{4})$$

Formula 1. Blood flow rate (Q) calculation

CSV= Cross sectional velocity, D= Diameter

$$WSR = \frac{8CSV}{D}$$

Formula 2. Wall shear rate (WSR) calculation

CSV= Cross sectional velocity, D= Diameter

A selection of variables are likely to affect the axial velocity such as centrifugal and torsional forces. It may be of interest to compare geometrical variables such as tortuosity with variables such as axial velocity and wall shear stress. For example, it would be expected that increased tortuosity or increased number of branches would correlate with a low wall shear rate, as well as a higher viscosity to promote endothelial dysfunction and atherosclerosis (Souihol *et al*., 2020). Patel *et al.* (2022) carried out a meta-analysis study that investigated conjunctival vessel axial velocity, and the findings were ultimately heterogenous for healthy study participants and an overall difference could also be seen overall between healthy and disease groups. Such comparisons may help to develop a better understanding of the mechanics of blood flow within the vasculature of the conjunctiva (Alastruey *et al*., 2012).

Importantly, understanding the blood composition and particularly the interactions and properties of the erythrocytes, may also be fundamental in characterising the haemodynamic measurements recorded. An incompressible, highly concentrated haemoglobin solution can be found within the erythrocytes (Sousa *et al*., 2016). The erythrocytes morphology can also be reversibly altered (unless lysis occurs), and this is what permits the substantial deformation of erythrocytes within the capillaries and the normal function of the microcirculation (Shou *et al*., 2020). Certain erythrocyte

characterisations may also be phenotypical of diseased states, and this should be carefully considered, as in the example of rheumatoid arthritis (also a risk factor of cardiovascular disease as included in the QRISK3 score) where reduced erythrocyte elasticity has previously been reported (Oore-ofe *et al*., 2021). Huang *et al*. (2020) also concur that the morphology of the vessels, disturbed flow patterns (e.g., low wall shear stress) and the rheological properties of blood are crucial factors in the development of atherosclerosis. Wall shear stress may be of particular importance in the monitoring of the microcirculation, as the monitoring of a changing wall shear stress may help to confirm vascular dysfunction. Critically, investigation of viscosity and wall shear stress may help to improve understanding of results in relation to endothelial function, as Gnasso *et al*. (2019) also suggest it influences the regulation of vascular tone.

Blood Biomarkers:

In 2012, Ioannidis and Tzoulaki found a selection of blood biomarkers assessed in relation to cardiovascular disease had been reported around 6000 times each. Despite this, Oury *et al*. (2018) suggest that the application of blood biomarkers, particularly those involved in endothelial dysfunction with endothelial cells and glycocalyx lining vessels within the microcirculation (e.g. Growth Differentiation Factor-15 (GDF-15) also involved in Endothelial Growth Factor Receptor (EGFR) signaling), the regulation of myocardial injury (e.g. Heart-type Fatty Acid Binding Protein (HFABP)), cardiac stretch (e.g. B-type Natriuretic Peptide (BNP)), inflammation (e.g. C-Reactive Protein (CRP)), and coagulation (e.g. Plasma Viscosity) may be beneficial for the risk stratification of TAVI patients. However, the

timings of the blood biomarker testing both pre and post procedure are likely to be critical, as discussed in a study by Sedhagat *et al*. (2016). Ultimately, further investigation and application of cardiac biomarkers could inform and support best clinical practice for these patient cohorts.

During the pandemic it was demonstrated that COVID-19 fingerpick blood lateral flow testing (Robertson *et al*., 2021), for blood biomarkers such as antibodies for SARS-CoV-2 have the potential to be an inexpensive and effective rapid point of care tool- this may be applied to other diseases, and in the context of this project, cardiovascular disease. Correspondingly, there are already well-established cardiac biomarkers used routinely within clinical practice today (including troponin, BNP and CRP). Additionally, certain blood biomarkers have already been accepted for application in cardiovascular risk score algorithms. This is demonstrated in the example of total cholesterol and high density lipoprotein (HDL) (in the form of the cholesterol:HDL ratio) which is requested within the QRISK3 score calculation. A review by Ouyang *et al*. (2021) explores the concept of cardiovascular disease biomarkers and biosensors in great depth, considering both the inequalities and complexities of the disease, as well as the practicalities and numerous possibilities of biomarkers. The work within this thesis also attempts to further address whether blood biomarkers add value to cardiovascular risk prediction through the use of an algorithm-based score system.

Data Collection, Risk Factors and Risk Scores:

Various studies such as the Framingham study have longitudinally observed lifestyles of a general population to identify risk factors, and as a result, there are now several known risk factors of cardiovascular disease including, but not limited to smoking status, level of physical activity, blood pressure, adiposity and family history. A selection of scoring systems also exist, such as QRISK (as previously mentioned), Euro SCORE or Society of Thoracic Surgeons Predicted Risk of Mortality (STS-PROM) score that are continually being updated in accordance with the evidence. However, these scoring systems often consist of complex calculations involving numerous clinical risk factors. Conversely, Zdrenghea *et al*. (2019) propose that risk scores should not only assess risk factors, but also account for protective factors, suggesting that this may encourage individuals to continue with the preventative measures reducing their cardiovascular risk. Comparison of risk versus benefit guided strategy is also listed within the gaps in evidence section of the European Society of Cardiology (ESC) guidelines (Visseren *et al*., 2021). The accuracy of risk stratification is of the highest importance to ensure patients are not being under or over-treated.

The aforementioned ESC guidelines highlight several further shortcomings in current risk prediction methods, and these should be addressed in future studies of risk scores. The National Institute for Health and Care Excellence (NICE) guidelines (2016) also provide an overview on cardiovascular disease prevention, and whilst they look at regular risk assessments for those aged over 40 years old, there is less evidence and advice available for younger age groups. The use of risk assessment tools is also advised against for a large proportion of the population such as those with type 1 diabetes or chronic kidney disease for example. There have been many

studies that look to assess “lifetime risk”. A better implementation of risk scoring may be to assess patients regularly, even if on a remote basis.

1.6. Rationale and Objectives

Research Question:

Is the conjunctival microcirculation a target for risk stratification of cardiovascular disease, and if so, can it be used to tailor treatment options and optimise care pathways?

One-tailed null hypothesis: The conjunctival microcirculation is a target for risk stratification.

One-tailed alternative hypothesis: The conjunctival microcirculation is not a target for risk stratification.

Chapter 1 Objectives:

- Evaluation of the available evidence surrounding the measurement and application of the conjunctival vessel parameters.
- To establish the ranges of the conjunctival vessel parameters (diameter, axial velocity, cross-sectional velocity, blood flow rate, wall shear rate and wall shear stress).

Chapter 2 Objectives:

- Critical review of the more extensively assessed retinal research to gather findings for utilisation in a conjunctival vessel pilot study.
- Assessment of new metrics such as vessel centreline pixel intensity in disease and vessel classification.

Chapter 3 Objectives:

- To outline the specific research design choices and appraise the methods used throughout the project.

Chapter 4 Objectives:

- Full automation of the conjunctiva video processing application for use on 4K video.
- Upload and processing of the video to be done on a single application at the point of capture using the smartphone device.

Chapter 5 Objectives:

- Assessment of the conjunctival microvasculature using the conjunctival microcirculation imaging tool and application before and after TAVI, as well as in a control group for comparison.

Chapter 6 Objectives:

- Non-invasive assessment of systemic microvascular dysfunction using the conjunctival microcirculation imaging application on coronary microvascular disease patients compared to controls.

Chapter 7 Objectives:

- Investigate comorbidities associated with cardiac remodeling and rhythms that may alter conjunctival haemodynamics.
- Identify factors such as inter-eye differences that may augment cardiovascular risk prediction.

Chapter 8 Objectives:

- Discuss and compare the findings, to include the strengths and limitations of the research from Chapters 1-7 in greater depth.
- Summarise the contributions to knowledge.
- Highlight areas for future research.

Chapter 9 Objectives:

This chapter was included in consideration of the substantial COVID-19 research and mass testing studies accomplished during the brief pause in recruitment to cardiovascular disease risk prediction project due to the COVID-19 pandemic.

- To consider the substantial COVID-19 research and mass testing studies accomplished during the brief pause in recruitment to cardiovascular disease risk prediction project due to the COVID-19 pandemic.

The previous feasibility study conducted within Professor Moore's living lab of healthy study participants, cyanotic congenital heart disease patients (CCHD) and myocardial infarction (MI) patients demonstrated significant differences between the healthy and diseased conjunctival vessels (Brennan *et al*., 2021a; Brennan *et al*., 2021b). The purpose of this study was to assess two new cohorts the TAVI and pressure wire cohorts to add more data to this body of work. These cohorts were

selected specifically to test the conjunctival imaging application following discussions with cardiologists. The pressure wire cohort was ideal to permit comparison of the coronary microcirculation with that of the conjunctiva, whilst the TAVI cohort was ideal to permit assessment of the application to detect haemodynamic changes of patients before and after intervention- therefore, addressing limitations of the prior studies by Brennan *et al*. Conclusively, the primary objective of this phase of the study is to assess the ability of the proposed tool in its identification of microcirculatory disease, as well as disease of the larger vessels and valves (the aortic valve).

Research Project Timeline:

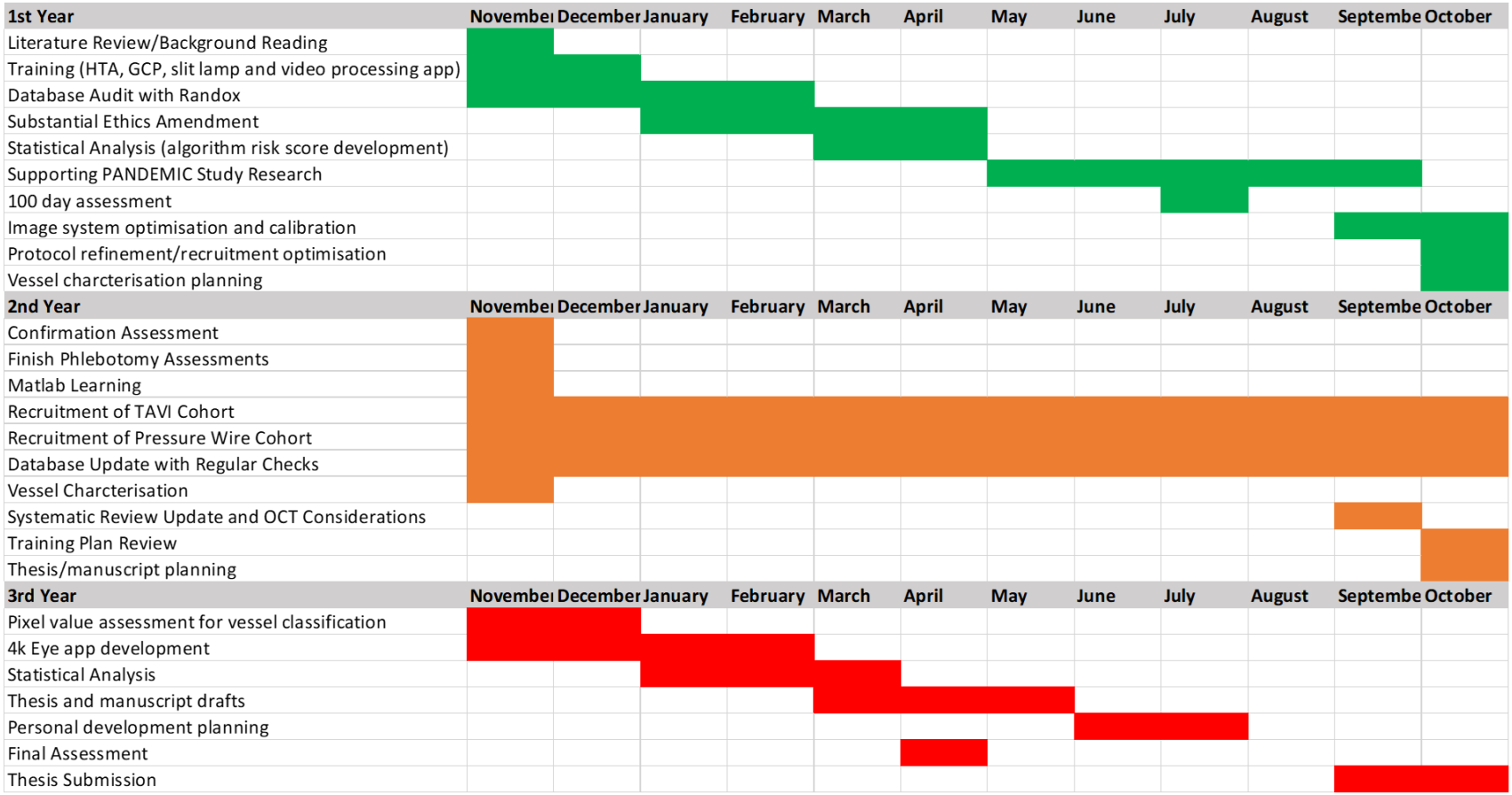

Figure 1.2. GANTT chart

GCP= Good Clinical Practice, HTA= Human Tissue Act, OCT= Optical Coherence Tomography.

Chapter 2

Cardiovascular Disease and Other Ocular Biomarkers

Chapter 2: Cardiovascular Disease and Other Ocular Biomarkers

One-tailed null hypothesis: Ocular parameters assessed throughout the retinal literature can be assessed within the conjunctival microcirculation.

One-tailed alternative hypothesis: Ocular parameters assessed throughout the retinal literature cannot be assessed within the conjunctival microcirculation.

2.1. *Literature Review*

Summary:

Introduction

Imaging of the retina to reflect disease status for conditions such as diabetes is commonplace in day-day ophthalmology clinical practice. Advances in digital health and imaging processing techniques supports current medical imaging practice, reducing workload. Imaging advances allowing ocular vessel classification and pathology recognition may well advance risk prediction with conditions such as cardiovascular disease. This review systematically explores the techniques employed in retinal imaging, along with the accuracy and validity of each technique.

Methods

A pre-defined search strategy was applied. The databases searched included OVID, Web of Science and Pubmed. Manuscripts were excluded if they were published more than 10 years ago, or in a language other than English. Data was analysed in themes of image processing technique. Critical appraisal was carried out on the included observational studies using the Critical Appraisal Skills Programme (CASP, 2018) checklist.

Results

Twenty-three studies were included for review. The retinal image processing techniques included assessment of pixel intensity, central reflex, optical density ratio, tortuosity, fractal dimension and bifurcation angle. The use of deep learning and convolutional neural network was also included for review and reached accuracies of around 97% for vessel classification. The accuracy of disease classification was greatest at around 86% when applying bifurcation angle analysis.

Conclusion

Automated image processing techniques that have been rigorously tested within numerous databases or studies, with high accuracy, as demonstrated within this review for vessel classification are a promising addition for clinical practice; particularly as vessel classification in turn may support disease classification and risk stratification. The research gathered within this review may help to inform other areas of microvascular imaging.

Introduction

Despite the advances in research and the understanding of risk factors, the burden of cardiovascular disease remains. Microvascular dysfunction has been reported to occur both alongside and independent from atherosclerosis (Weber *et al*., 2021). Additionally, an interaction between macrovasculature and microvasculature has been upheld (Cífková *et al*., 2020). The retinal microvasculature has been considerably addressed, the literature surrounding the microcirculation is limited when compared to that of the macrocirculation. This may be reflective of the challenges surrounding imaging of the microcirculation. Particularly, challenges such as the ability to classify the small vessels into arterioles and venules, as well as to classify for disease and to stratify for risk, warrants further investigation. This review seeks to analyse and critically appraise the current retinal vessel imaging techniques.

Methods

Search Strategy:

The search strategy, including the relevant databases and number of records obtained from the search, are documented in Table 2.1. Reviews, abstracts and letters were excluded, and manuscripts that were not open-access or written in a language other than English were also excluded.

Table 2.1. Search strategy

Database	Search	Results	Date Last Searched
OVID	"Cardiovascular" AND "Retinal Vessels"	318	28/05/2021
	"Arterioles" AND "Venules"	246	23/05/2021
	"Cardiovascular" AND Conjunctiva	9	23/05/2021
Web of Science	"Cardiovascular" AND "Retinal Vessels"	671	28/05/2021
	"Arterioles" AND "Venules"	194	23/05/2021
	"Cardiovascular" AND Conjunctiva	158	23/05/2021
Pubmed	"Cardiovascular" AND "Retinal Vessels"	84	28/05/2021
	"Arterioles" AND "Venules"	16	23/05/2021
	"Cardiovascular" AND Conjunctiva	3	23/05/2021
Handsearch	N/a	3	28/5/2021

Data Extraction and Quality Assessment:

Data extraction was themed by the image processing measurement category. Further categories for data extraction within the pre-defined data extraction form included the author and the year of study for study identification, details of the retinal/ocular measurement, data analysis and results of each study included within the review for comparison. The main outcomes of concern are those evaluating the accuracy and validity of the image processing technique. The included observational studies were quality assessed using the Critical Appraisal Skills Programme checklist (CASP, 2018). Risk of bias was assessed using the ROBINS-1 tool (Sterne *et al*., 2016). Lastly, the PRISMA-P protocol was also used to support the structure of the review, as presented in supplementary materials Table S1 (Shamseer *et al.,* 2015).

Results

Manuscript Search and Study Characteristics:

The search returned a total of 1699 manuscripts published within the past 10 years across the three databases searched (OVID, Web of Science and Pubmed). A total of 23 relevant manuscripts were included within this analysis. The results of the data extraction and thematic analysis from all the included papers are documented in the supplementary tables, and only studies with a moderate-high score when critically appraised via GRADE score were included for analysis (Guyatt *et al*., 2013).

Quality Assessment:

The results of the amended CASP (2018) quality assessment and ROBINS-1 risk of bias tool (amended from Sterne *et al*., 2016) are presented in supplementary tables S2 and S3. The CASP tool highlighted some uncertainties with cofounding factors (Mirsharif *et al.,* 2013; Ishikawa *et al.,* 2019; Yin *et al.,* 2019; Huang *et al.,* 2020; Alam *et al.,* 2018) and precision of results for several studies (Mirsharif *et al,* 2013; Morales *et al.,* 2014; Relan *et al.,* 2014; Ding *et al.,* 2015; Vijayakumar *et al.,* 2016; Walikala *et al.,* 2017; Yin *et al.,* 2019; Relan and Relan 2021). A requirement for follow-up was also indicated for three of the included studies (Owen *et al.,* 2019; Huang *et al.,* 2020; Rim *et al.,* 2021). Lastly, due to the nature of the individual observational/experimental studies included, there were generally limited implications for practice.

The results of the ROBINS-1 tool shows uncertainties of bias due to confounding factors agrees with the results from the CASP checklist. Additionally, uncertainties of bias in sample selection (Rim *et al.*, 2021) and outcome measurement were flagged for two studies (Cordina *et al.,* 2015; Rim *et al.,* 2021), and classification bias was considered within one study (Fraz *et al.,* 2014). However, both the overall and individual risk of bias, as shown in supplementary Figure S1, were deemed to be low risk for all included studies.

Pixel Intensity, RGB, HSV and LAB Values:

Eight records included in the review were found to evaluate pixel intensity or Red, Green or Blue (RGB) values. The papers assessed also incorporated methods of deep learning for automation. Six papers within the review specifically assessed the deep learning and convolutional neural network applications. The results

demonstrate the potential application of these methods to be applied for either vessel characterisation or disease classification (with measurements such as central reflex).

The performance metrics show an accuracy ranging from around 77% (Fraz *et al*., 2014) to 97% (Zhang *et al*., 2019), and the results also vary depending on the dataset of retinal images used.

Manuscripts were also collected that assessed pixel values through Optical Density Ratio (ODR) and dual wavelength methods. Two studies included within this review assessing ODR and dual wavelength indicate that this is also a potential method to differentiate between arterioles and venules. The results show 97.06% accuracy for vessel classification in the study conducted by Alam *et al*. (2018), and the mean ODR values of arterioles and venules for the study by Ishikawa *et al*. (2019) were 0.77 ± 0.060 and 1.02 ± 0.067, respectively.

Vessel Tortuosity:

The results from the study by Cordina *et al*. (2015) unexpectedly show that only 62% of cyanotic congenital heart disease patients presented with increased tortuosity. However, these results may be limited by subjective assessment instead of using a quantitative method. Two studies assessed the correlation of tortuosity (quantitatively assessed) with cardiovascular disease risk factors such as blood pressure or body mass index (Owen *et al*., 2019; Tapp *et al*., 2019). Interestingly, no association was found with prevalent myocardial infarction but was found with stroke in the study by Owen *et al*. (2019). Additionally, arteriolar tortuosity was more strongly associated when compared with venular tortuosity in the study by Tapp *et*

al. (2019). Nevertheless, Owen *et al*. propose an association of metabolic dysfunction with increased venular tortuosity.

Fractal Dimension and Bifurcation Angle:

Retinal fractal dimension evaluates branching pattern complexity (Huang *et al*., 2016). Ding *et al*. (2015) and Morales *et al*. (2014) both propose that fractal dimension may be useful to accurately distinguish between healthy and diseased vessel phenotypes. While Huang *et al.* (2020) proposes an increased retinal arteriolar branching angle is associated with increased left ventricular mass index and left atrial size, and hence may be a useful tool to indicate early-stage cardiac remodeling.

Discussion

Vessel Classification Measurements:

The literature often indicates that particular biomarkers are associated with the type of vessel, arterioles or venules. Similarly, it is likely due to disease being expressed differently in arterioles compared to venules, as they differ both structurally and functionally. Indications of disease differing between the vessel types are already recognised in retinal imaging such as arteriolar narrowing in hypertensive retinopathy (Tsukikawa and Stacey, 2020). However, comparative applications between the vessel types are also now recognised such as the arteriole to venule ratio (AlBadawi and Fraz, 2018).

Disease Classification Measurements:

The evidence largely agrees with an association of tortuosity with cardiovascular disease in the large vessels of the coronary arteries. Despite that the larger vessels bifurcate numerous times into smaller vessels, the tortuosity of the microvasculature remains largely unexplored in comparison. It has been suggested that increased tortuosity within the microvasculature may be atheroprotective through increasing the wall shear stress (Allon *et al*., 2021). Comparatively, tortuous collateral arteries also occur through arteriogenesis in a protective effort to maintain perfusion (Della-Morte and Rundek, 2015). Tortuosity of peripheral veins known as varicose veins may also be procoagulant through reduced blood flow. Additionally, elastin degradation due to aging or hypertension may cause wall remodeling and hence tortuosity (Kahe *et al*., 2020). Therefore, this poses debate as to whether vessel tortuosity is an indication or cause of disease. The fractal properties of the vasculature are equally complex, but it has been suggested fractal dimensions change with disease and measures indicating either too high or too low fractality is sub-optimal (Korolj *et al*., 2019).

Conclusion

This review offers a new perspective on the imaging techniques available for microvascular imaging. The medical imaging research and guidelines should acknowledge and adapt to the evolving technologies and processing techniques available. Future directions should focus on application of the novel image processing techniques to further areas of microvascular research.

2.2. *Pilot Study: Cardiovascular Disease and Other Ocular Biomarkers*

Summary

Background

Unlike the conjunctival microvasculature, the retinal microvasculature has been extensively examined. Various ocular parameters have been established within the retinal microvascular research to either distinguish between arterioles and venules or distinguish between healthy and diseased vessels. Therefore, the objective of this pilot study is to apply the ocular parameters measured in the retinal vasculature to the conjunctival microvascular imaging system.

Methods

Conjunctival vasculature images were collected from a cohort of participants elected for pressure wire and grouped by positive (≥25) and negative (<25) index of microcirculatory resistance (IMR), as well as by positive (<2.0) and negative coronary flow reserve (CFR) (≥2.0) result. Images were imported into Image J, and mapped vessel segments were manually assessed for pixel intensity, as well as for vessel tortuosity via the vessel tortuosity index (VTI). Average RGB images were assessed for Red (R), Green (G) and Blue (B) values. The RGB images were converted to HSV images to obtain hue and saturation values, as well as LAB images to obtain luminance values.

Results

A total of 87 arterioles and 536 venules were assessed from 39 patients (21 pressure wire negative and 18 pressure wire positive). The pixel intensity

(arterioles=125 ± 36 vs venules=115 ± 42, p=0.01), G (arterioles=178 ± 23 vs venules=168 ± 23, p<0.001) and B (arterioles=158 ± 25 vs venules=152 ± 23, p=0.015) were significantly increased in the arterioles compared to the venules. G was also significantly increased in the arterioles of the pressure wire positive patients compared to the pressure wire negative (pressure wire negative arterioles= 172 ± 18 vs pressure wire positive arterioles= 185 ± 23, p=0.026). No significant differences were reported in the venules or undifferentiated vessels between pressure wire positive and pressure wire negative groups.

Conclusion

The additional parameters measured in Image J did detect differences in arterioles between both IMR positive and negative groups, as well as differences between arterioles and venules. It is likely that the parameters related to disease are more commonly expressed within the arterioles.

Introduction

Disease of the smaller vessels may have a sizable impact on the mortality rates. Approximately 30% of patients experiencing angina have been found to have coronary microvascular disease, accounting for over half a million people in the United Kingdom alone (Sinha *et al*., 2021). The current invasive gold standard test for assessing microvascular dysfunction within the coronary microcirculation is via pressure wire study measuring the index of microcirculatory resistance (IMR) and coronary flow reserve (CFR) (Dai *et al*., 2021; Groepenhoff *et al*., 2021). An IMR of ≥25, or a CFR <2 are the positive microvascular disease test result cut-off points

(Knuuti *et al*., 2020). A study by Ahn *et al*. (2019) suggests the combination of a positive IMR and CFR performs better for detecting coronary microvascular disease with results of an AUC value of 0.941, compared to 0.87 for IMR and 0.71 for CFR alone.

The current non-invasive gold standard is done via positron emission tomography (PET) scan measuring coronary flow reserve (CFR) or via cardiac magnetic resonance (CMR) imaging measuring myocardial perfusion reserve (MPR) (Marinescu *et al*., 2015). These non-invasive tests both have disadvantages such as the use of ionizing radiation with the PET scan and CMR imaging for some, may feel claustrophobic. CMR imaging is also unsuitable for anyone with metallic implants such as non-CMR compatible pacemakers.

Consequently, an inexpensive, non-invasive imaging method that involves no radiation would be beneficial to assess the microcirculation. Additionally, the evidence reported within retinal microvasculature research proposes that differences can be detected in a range of retinal microvasculature parameters between healthy patients and patients at risk of cardiovascular disease (Cheung *et al*., 2021). The retinal vessels are also routinely assessed in diabetic patients in ophthalmology clinical practice today. The concept that the eye, and thus more specifically, the easily accessible conjunctival microvasculature may be used as a window for cardiovascular health is not unfamiliar. Yet the conjunctival microvasculature has been overlooked in relation to cardiovascular health.

In the previous conjunctival microcirculation studies, vessel segment diameter (D), axial velocity (Va), cross sectional velocity (CSV), blood flow rate (Q) and wall shear

rate (WSR) were assessed (Brennan *et al*., 2019). The primary aim of this pilot study is to evaluate several further parameters from the conjunctival microvasculature images that have been reported within the retinal vessel literature to include vessel tortuosity, pixel intensity, RGB values, hue, saturation and luminance for the differentiated vessel segments. This study will also seek to compare the results with the ocular parameters we previously assessed (D, Va, CSV, Q and WSR) between pressure wire negative and positive individuals.

Methods

Image J Measurements:

Vessel tortuosity index (VTI) and central reflex were measured using the line tool in the ImageJ software (Maryland, USA, https://imagej.nih.gov/ij/). Both measurements were taken from the mean grayscale image with the overlayed vessel ID labels and branch points. The greyscale image was used primarily for the pixel intensity and central reflex width measurement, as during the method development stages it was noted that the central reflex should show an increase in the pixel intensity on the line plot graph. For the purposes of the pilot study the linear distance between vessel segment end points was measured using the line profile tool, and the actual vessel segment length was already measured via the MATLAB version R2021a application. Automation of VTI measurement is possible via MATLAB (Khansari *et al*. 2016; Khansari *et al*. 2021). To calculate VTI the actual length was divided by the linear length, increased VTI values should positively correlate with greater tortuosity.

Pixel intensity and Red, Green and Blue values (RGB) were measured using the intensity profile and RGB profiler in image J. It has been suggested that HSV images are more akin to how we perceive colour, and are invariant to illumination (Palanisamy *et al*., 2018). Hue and Saturation values were obtained through conversion of the RGB image to a HSV image, and similarly, the RGB image was also converted to a LAB image for Luminance to be assessed. Using these primary measures, it is then possible to calculate for weighted intensity (0.299R+0.587G+0.114B), Optical Density Ratio (ODR) (R-G/G) and brightness (RGB/3).

Vessel Differentiation and Classification:

The “ground truth” of the vessel segment type was assessed and labelled on a mapped vessel image as either arteriole, venule or unclassified by a cardiologist on the project. Ground truth was based on the direction of blood flow towards (arteriole) or away (venule) from a bifurcation point.

Statistical Analysis:

For statistical analysis Statistical Package for the Social Sciences (SPSS) for Windows version 27 (property of IBM) was used. Continuous variables were described using the mean, standard deviation of the mean and 95% confidence intervals (CI). Kolmogorov–Smirnov testing was used to assess normality of the continuous variables. Differences between groups of parametric continuous variables were tested using the Student’s t test. Differences between groups of non-parametric continuous variables were tested using the Mann Whitney U test. Binary logistic regression analysis was carried out and receiver operator characteristic

curve generated to assess the area under the curve (AUC). Categorical variables such as comorbidities were expressed as number and percentage, and differences between groups tested using the chi-squared test.

Results

Baseline Characteristics of the Study Participants:

Except for an increased history of chronic obstructive pulmonary disease (COPD) in the pressure wire positive group (negative= 4.8% vs positive= 27.8%, p=0.047) there were no significant differences in baseline characteristics between the groups. The results of the baseline characteristics of the study patients are presented in Table 2.2 below.

Table 2.2. Baseline characteristics

Characteristic	**Pressure Wire Negative (n=21 patients)**	**95% CI**	**Pressure Wire Positive (n=18 patients)**	**95% CI**	***p value**
Age (years) ±*SD*	66.4 ± 7.7	62.9-69.9	67.9 ± 8.2	63.9-72.0	0.530
Gender (% male)	10 (47.6)	n/a	9 (50)	n/a	0.882
Height (cm) ±*SD*	169.0 ± 10.5	164.2-173.8	167.3 ± 9.3	162.7-172.0	0.530

Weight (kg) ±*SD*	86.4 ± 17.9	78.3-94.6	76.4 ± 12.9	70.0-82.8	0.094
Body Mass Index (BMI) (kg/m²) ±*SD*	30.3 ± 5.5	27.7-32.8	27.2 ± 3.4	25.5-28.9	0.069
Mean Systolic Pressure (mmHg) ±*SD*	128.4 ± 15.5	121.4-135.5	123.3 ± 14.8	116.0-130.7	0.234
Mean Diastolic Pressure (mmHg) ±*SD*	74.1 ± 13.5	68.0-80.3	71.7 ± 11.7	65.9-77.6	0.878
Heart Rate (beats per minute) ±*SD*	65.5 ± 8.0	61.9-69.2	73.2 ± 16.1	65.2-81.3	0.223
Resting Oxygen Saturation (%) ±*SD*	96.8 ± 1.6	96.0-97.5	96.9 ± 1.6	96.1-97.8	0.749
Smoking (%)	11 (52.4)	n/a	8 (44.4)	n/a	0.621 $
Hypertension (HTN) (%)	15 (71.4)	n/a	10 (55.6)	n/a	0.303 $
Previous Myocardial Infarction (MI) (%)	4 (19.1)	n/a	4 (22.2)	n/a	0.807 $

Stroke (%)	2 (9.5)	n/a	1 (5.6)	n/a	0.643 $
Previous Transient Ischemic Attack (TIA) (%)	2 (9.5)	n/a	2 (11.1)	n/a	0.871 $
Heart Failure (HF) (%)	2 (9.5)	n/a	1 (5.6)	n/a	0.643 $
Peripheral Vascular Disease (PVD) (%)	0	n/a	3 (16.7)	n/a	0.052 $
Atrial Fibrillation (AF) (%)	3 (14.3)	n/a	5 (27.8)	n/a	0.298 $
Chronic Obstructive Pulmonary Disease (COPD) (%)	1 (4.8)	n/a	5 (27.8)	n/a	**0.047 $**
Family History of Heart Disease (%)	8 (38.1)	n/a	5 (27.8)	n/a	0.575 $
*Mann-Whitney U test, $ Chi-squared test.					

Ocular parameters:

The ocular parameter results are provided in Table 2.3. Only venular axial and cross-sectional velocity were significantly reduced (p=0.041 and p=0.030, respectively) in the pressure wire positive group (axial velocity= 0.55 ± 0.05 mm/s, cross-sectional velocity= 0.38 ± 0.04 mm/s) compared to the negative group (axial velocity= 0.58 ± 0.07 mm/s, cross sectional velocity= 0.40 ± 0.05 mm/s).

Table 2.3. Ocular parameters

	Pressure wire negative n= 21 patients	**95% CI**	**Pressure wire positive n= 18 patients**	**95% CI**	***p value**
Feature					
Diameter (µm) ±*SD*	24.39 ± 3.31	22.88-25.89	25.13 ± 2.61	23.83-25.42	0.666
Axial Velocity (mm/s) ±*SD*	0.57 ± 0.07	0.53-0.60	0.54 ± 0.04	0.52-0.56	0.213
Cross-Sectional Velocity (mm/s) ±*SD*	0.39 ± 0.05	0.37-0.42	0.37 ± 0.03	0.36-0.39	0.140
Blood Flow Rate (pl/s) ±*SD*	201 ± 49	179-223	199 ± 33	183-216	0.587
Wall Shear Rate (s^{-1}) ±*SD*	146 ± 30	132-160	131 ± 19	122-141	0.156

Wall Shear Stress (dynes/cm^2) ±*SD*	20.4 ± 10.2	8.10-11.01	21.8 ± 13.8	7.60-9.44	0.379
		95% CI		**95% CI**	***p value**
Feature (Arterioles) n=14 negative, n=15 positive					
Diameter (µm) ±*SD*	22.08 ± 6.36	18.41-25.75	19.77 ± 3.72	17.71-21.83	0.112
Axial Velocity (mm/s) ±*SD*	0.59 ± 0.12	0.52-0.66	0.54 ± 0.12	0.48-0.61	0.425
Cross-Sectional Velocity (mm/s) ±*SD*	0.42 ± 0.08	0.37-0.46	0.39 ± 0.09	0.34-0.43	0.477
Blood Flow Rate (pl/s) ±*SD*	169 ± 81	122-216	128 ± 76	86-170	0.123
Wall Shear Rate (s^{-1}) ±*SD*	174 ± 83	127-222	177 ± 65	141-212	0.591
Wall Shear Stress (dynes/cm^2) ±*SD*	11.52 ± 7.67	7.09-15.95	10.60 ± 3.51	8.66-12.54	0.813
Feature (Venules) n=20 negative, n=18 positive					

Diameter (µm) ±*SD*	25.52 ± 3.44	23.91-27.13	26.40 ± 2.93	24.94-27.86	0.613
Axial Velocity (mm/s) ±*SD*	0.58 ± 0.07	0.55-0.62	0.55 ± 0.05	0.52-0.57	**0.041**
Cross-Sectional Velocity (mm/s) ±*SD*	0.40 ± 0.05	0.38-0.43	0.38 ± 0.04	0.36-0.40	**0.030**
Blood Flow Rate (pl/s) ±*SD*	223 ± 50	200-246	218 ± 43	196-239	0.534
Wall Shear Rate (s^{-1}) ±*SD*	140 ± 34	124-156	125 ± 21	115-136	0.186
Wall Shear Stress (dynes/cm^2) ±*SD*	9.15 ± 2.94	7.77-10.53	8.14 ± 1.89	7.19-9.08	0.264
Feature (Undifferentiated) n=20 negative, n=18 positive					
Diameter (µm) ±*SD*	23.24 ± 5.41	20.71-25.77	22.35 ± 3.33	20.70-24.01	0.443
Axial Velocity (mm/s) ±*SD*	0.56 ± 0.07	0.53-0.59	0.54 ± 0.09	0.50-0.58	0.633
Cross-Sectional Velocity (mm/s) ±*SD*	0.39 ± 0.04	0.37-0.41	0.38 ± 0.06	0.35-0.41	0.478

Blood Flow Rate (pl/s) ±*SD*	186 ± 77	150-222	164 ± 63	133-195	0.317
Wall Shear Rate (s^{-1}) ±*SD*	155 ± 45	134-176	145 ± 33	128-161	0.496
Wall Shear Stress (dynes/cm^2) ±*SD*	10.02 ± 3.44	8.41-11.63	9.29 ± 2.70	7.95-10.63	0.534
*Mann-Whitney U test					

Vessel differentiation:

The results of the vessel differentiation analysis are presented in Table 2.4 below. At a cut-off point of 0.85, vessel differentiation via the G value resulted in a sensitivity of 60.6% and specificity of 52.4%, and a resultant AUC of 0.506. The results of the mean feature parameters calculated for each patient are shown in Figures 2.1-2.3.

Table 2.4. Vessel differentiation analysis

	Arterioles n= 87	**95% CI**	**Venules n= 536**	**95% CI**	***p value**
Feature					
VTI ±*SD*	1.41 ± 0.21	1.36-1.45	1.44 ± 0.29	1.42-1.47	0.348
Pixel Intensity ±*SD*	125 ± 36	117-133	115 ± 42	111-118	**0.01**
R ±*SD*	221 ± 18	217-225	218 ± 20	217-220	0.203
G ±*SD*	178 ± 23	173-183	168 ± 23	166-170	**<0.001**
B ±*SD*	158 ± 25	153-163	152 ± 23	150-154	**0.015**
Hue ±*SD*	20.4 ± 10.2	18.0-22.5	21.8 ± 13.8	20.6-23.0	0.698
Saturation ±*SD*	59.8 ± 22.4	55.0-64.6	64.1 ± 23.9	62.1-66.2	0.189

Luminance ±*SD*	74.3 ± 7.1	72.8-75.9	73.2 ± 7.4	72.6-73.9	0.303
	Pressure wire negative n= 21 patients	**95% CI**	**Pressure wire positive n= 18 patients**	**95% CI**	***p value**
Feature (Arterioles) n=14 negative, n=15 positive					
VTI ±*SD*	1.39 ± 0.11	1.33-1.45	1.43 ± 0.13	1.36-1.51	0.31
Pixel Intensity ±*SD*	121 ± 28	105-137	132 ± 24	119-146	0.331
R ±*SD*	222 ± 10	216-228	217 ± 22	205-229	0.983
G ±*SD*	172 ± 18	162-182	185 ± 23	172-197	**0.026**
B ±*SD*	152 ± 21	140-164	164 ± 26	150-178	0.102
Hue ±*SD*	21.1 ± 9.7	15.6-26.7	19.8 ± 6.1	16.5-23.2	1.00
Saturation ±*SD*	59.0 ± 23.3	45.5-72.4	59.4 ± 18.9	48.9-69.8	0.683
Luminance ±*SD*	76.3 ± 4.6	73.6-78.9	72.9 ± 8.1	68.4-77.4	0.29
Feature (Venules) n=20 negative, n=18 positive					
VTI ±*SD*	1.48 ± 0.14	1.42-1.55	1.44 ± 0.08	1.40-1.47	0.149
Pixel Intensity ±*SD*	113 ± 18	105-122	115 ± 23	103-126	0.762
R ±*SD*	219 ± 16	211-226	219 ± 14	212-226	0.874

G ±*SD*	174 ± 13	167-180	169 ± 17	161-178	0.443
B ±*SD*	155 ± 17	147-163	152 ± 20	142-162	0.633
Hue ±*SD*	24.7 ± 15.8	17.3-32.2	21.6 ± 6.3	18.5-24.7	0.874
Saturation ±*SD*	61.9 ± 19.2	52.9-70.9	65.5 ± 20.1	55.5-75.5	0.74
Luminance ±*SD*	73.9 ± 5.4	71.4-76.4	73.4 ± 5.8	70.5-76.3	0.633
Feature (Undifferentiated) n=20 negative, n=18 positive					
VTI ±*SD*	1.43 ± 0.10	1.38-1.47	1.49 ± 0.14	1.42-1.56	0.176
Pixel Intensity ±*SD*	120 ± 23	109-131	119 ± 23	108-131	0.573
R ±*SD*	212 ± 21	202-222	218 ± 18	209-226	0.186
G ±*SD*	170 ± 17	162-178	172 ± 20	162-182	0.762
B ±*SD*	153 ± 19	144-162	154 ± 26	141-167	0.573
Hue ±*SD*	21.7 ± 8.2	17.8-25.5	20.2 ± 6.8	16.8-23.6	0.897
Saturation ±*SD*	62.1 ± 18.7	53.4-70.8	65.9 ± 20.0	56.0-75.8	0.573
Luminance ±*SD*	73.6 ± 6.8	70.5-76.8	73.8 ± 8.5	69.6-78.0	0.696

Abbreviations:

VTI= Vessel Tortuosity Index, R= Red, G= Green, B= Blue.

**Mann-Whitney U test*

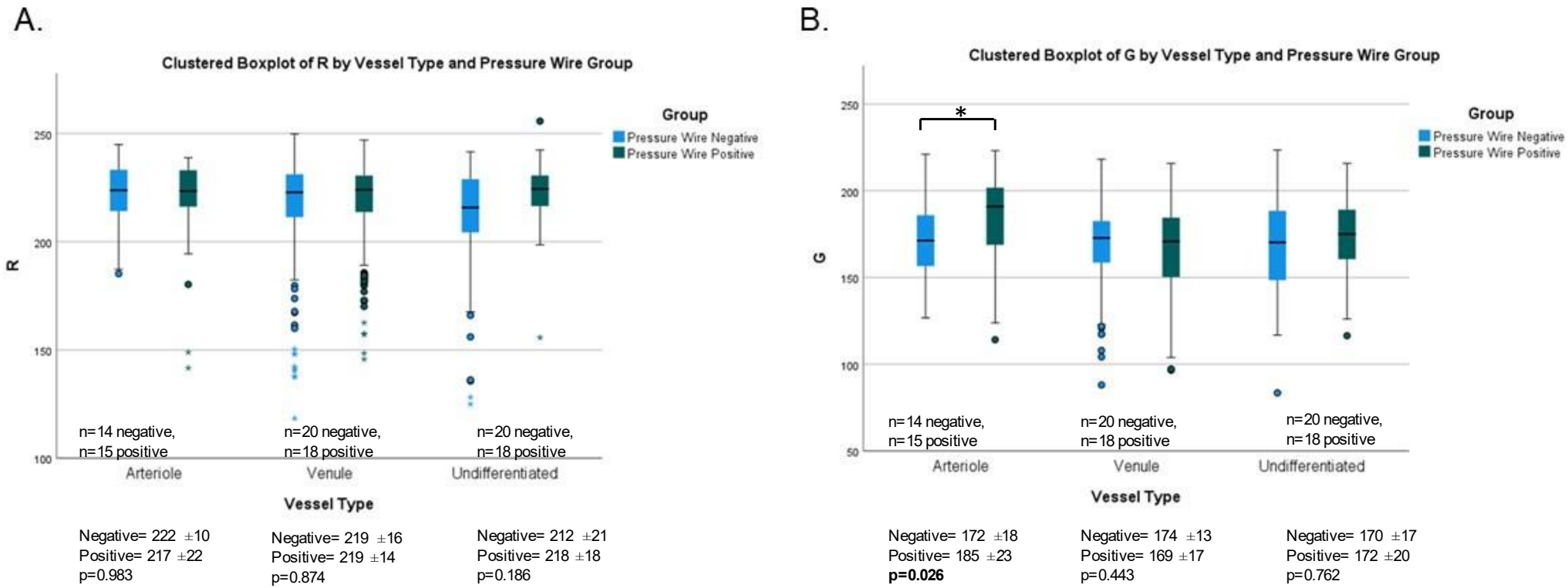

Figure 2.1. Overall patient means for A.) R and B.) G features

*Arterioles n= 14 pressure wire negative (R=222±10, G=172±18) and 15 pressure wire positive subjects (R=217±22, G=185±23). Venules n= 20 pressure wire negative (R=219±16, G=174±13) and 18 pressure wire positive subjects (R=219±14, G=169±17). Undifferentiated n= 20 pressure wire negative (R=212±21, G=170±17) and 18 pressure wire positive subjects (R=218±18, G=172±20). *G of the arterioles significantly different between the pressure wire groups p=0.026. *Mann-Whitney U test.*

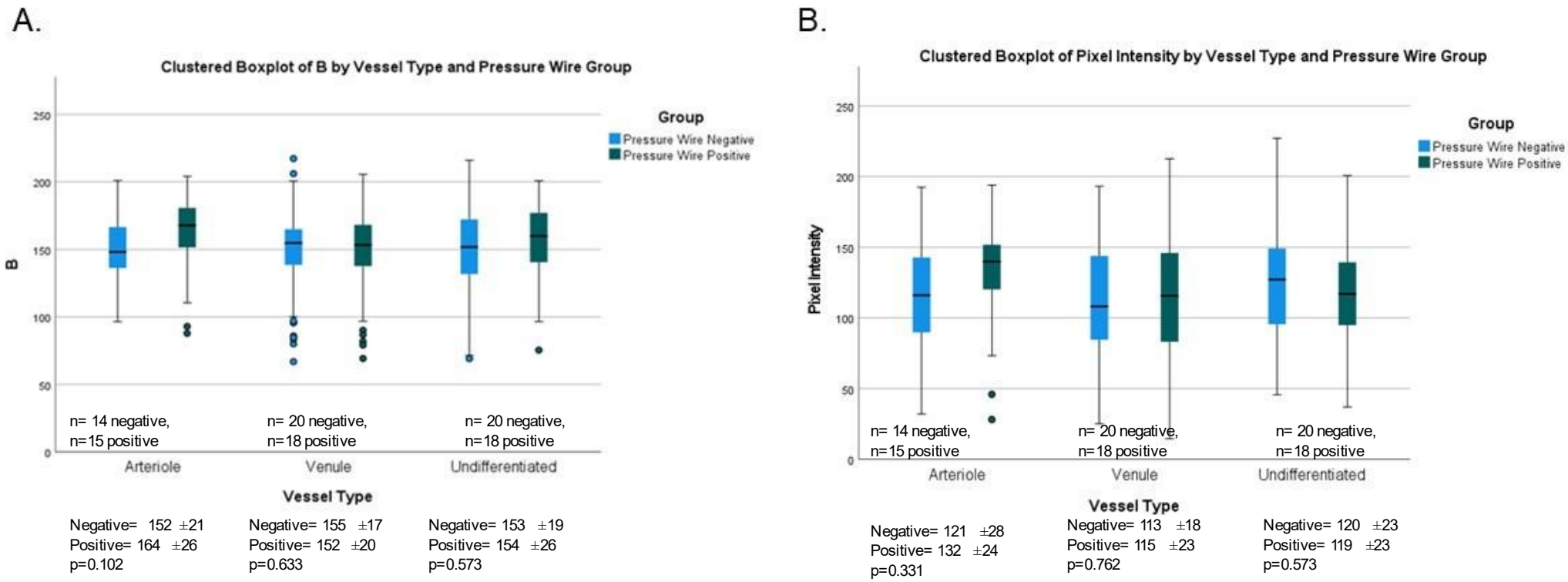

Figure 2.2. Overall patient means for A.) B and B.) pixel intensity (PI) features

*Arterioles n= 14 pressure wire negative (B=152±21, PI=121±28) and 15 pressure wire positive subjects (B=164±26, PI=132±24). Venules n= 20 pressure wire negative (B=155±17, PI=113±18) and 18 pressure wire positive subjects (B=152±20, PI=115±23). Undifferentiated n= 20 pressure wire negative (B=153±19, PI=120±23) and 18 pressure wire positive subjects (B=154±26, PI=119±23). *Mann-Whitney U test.*

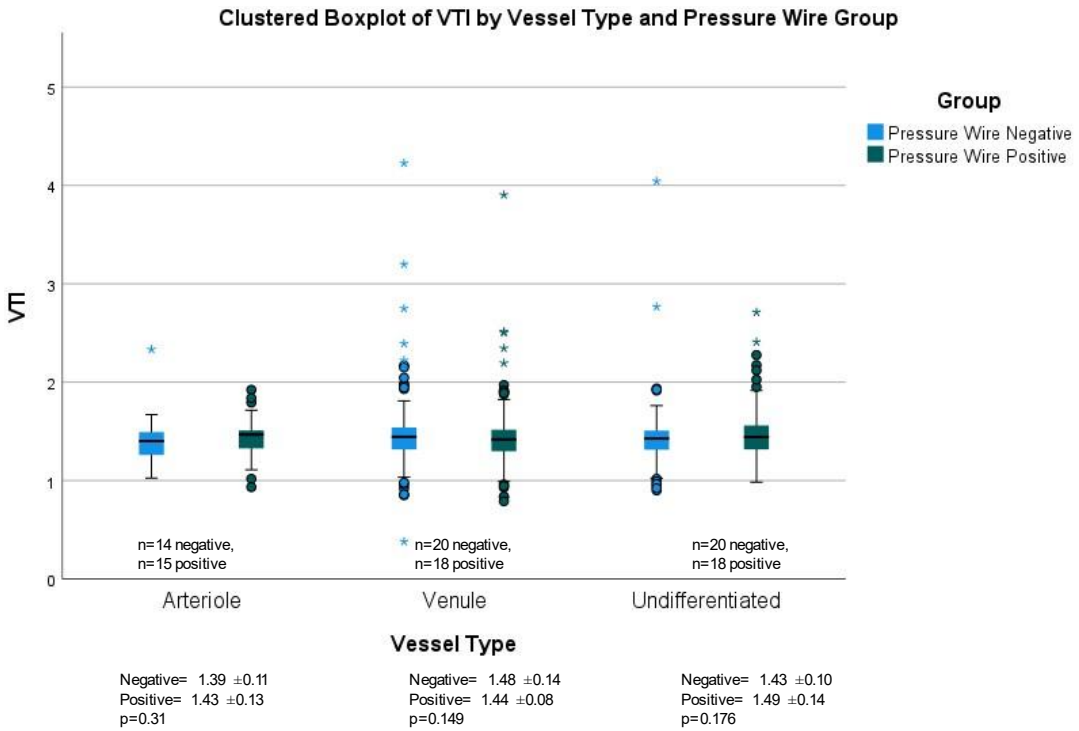

Figure 2.3. Overall patient means for VTI

Arterioles n= 14 pressure wire negative (VTI=1.39±0.11) and 15 pressure wire positive subjects (VTI=1.43±0.13).

Venules n= 20 pressure wire negative (VTI=1.48±0.14) and 18 pressure wire positive subjects (VTI=1.44±0.08).

*Undifferentiated n= 20 pressure wire negative (VTI=1.43±0.10) and 18 pressure wire positive subjects (VTI=1.49±0.14). *Mann-Whitney U test.*

Discussion

The findings of this pilot study suggest that while significant differences may be detected from venular measurements of axial and cross-sectional velocity, the measurement of G within the arterioles also detected significant differences between the negative and positive pressure wire groups. The addition of pixel measurements may be a valuable addition to the conjunctiva video processing applications for detection of microvascular disease. There may be a potential role for pixel measurements for vessel differentiation with G, B and pixel intensity also being significantly different between arterioles and venules, as discussed within the corresponding sections below. Albeit the performance metrics for vessel differentiation of the most significantly different pixel measurement G was disappointing in this pilot study.

VTI:

The VTI results showed a slight increase in arteriole VTI for pressure wire positive patients, but also a slight decrease in venule VTI for the same pressure wire positive patients. The results of the differentiated vessel segments also suggest that the arterioles were less tortuous than venules. This agrees with the findings presented by Khansari *et al*. (2017) reporting that abnormalities of the microvascular circulation are more commonly found in venules, but this may be due to the conjunctival microvasculature comprising of more venules vs arterioles.

Pixel Intensity:

The pixel intensity results were as expected for the vessel classification groups with the arterioles demonstrating a higher pixel intensity when compared to the venules. This conforms with the hypothesis proposing that venules should have a darker appearance (lower pixel intensity) due to lower blood oxygen levels when compared with the arterioles.

RGB, HSV and LAB:

Oxyhaemoglobin absorbs blue-green light. However, the G and B values were significantly higher for the arterioles compared to the venules. Abdulsahib *et al*. (2021) suggest that an increased G value, like pixel intensity, is related to the central reflex characteristic of arterioles. Given the significant difference found within this pilot study this may be a promising variable for both vessel and disease classification, as it is proposed that an increased central reflex occurs as a consequence of wall thickening or atherosclerotic plaque (Bhuiyan *et al*., 2014). Contrastingly, Abdulsahib *et al*. also propose that colour homogeneity is characteristic of venules, but as the standard deviation values report, a similar variation of colour was found within the venules group of this pilot study. No significant differences were reported for hue, saturation or luminance. However, it has been suggested that RGB images are closer to the raw data captured from the camera (Fu *et al.*, 2019).

Limitations:

A limitation within this pilot study was the inability to measure central reflex width. There were too few measurements taken to accurately report for this parameter within the pressure wire cohort. In the majority of cases, the central reflex of vessel

segments was either not apparent or difficult to accurately quantify. As central reflex is dependent on light reflection and the resultant pixel intensity it may be that this is due to varying illumination or potentially refractive error. Similar findings were found when attempting to address the wall to lumen ratio, from the literature this appears to be easier to determine with retinal imaging (Cífková *et al*., 2021; Ott *et al*., 2013; Streese *et al*., 2020). Additionally, there were too few abnormalities identified such as arteriovenous nicking, micro-haemorrhages and aneurysms commented on to compare between groups within the pilot study.

Conclusion

The findings reported within this pilot study suggest that based on the potential to distinguish between controls and coronary microvascular disease, the G value of arterioles may be a valuable addition to the existing conjunctival imaging application. For the added ability to distinguish between vessel types, the pixel intensity, G and blue values may also be useful.

Chapter 3

Methods

Chapter 3: Methods

3.1. *Research Design and Participants*

Research Design:

The research study discussed in this thesis was designed as a prospective, observational, single-centre, multi-cohort study. The participants were allocated an anonymised major adverse cardiac event (MACE) ID number. All videos were saved with the respective ID number for each subject, and the researcher processing the videos was then blinded to the participant groups.

Participants:

Previous Study Participants; Myocardial Infarction and Cyanotic Congenital Heart Disease vs Controls

Myocardial infarction and cyanotic congenital heart disease patients were recruited alongside matched controls in the earlier studies (Brennan *et al*., 2021a; Brennan *et al*., 2021b). The data for each of the anonymised patients was recorded in an encrypted database. The cohorts recruited in this arm of the study (as detailed below) were then recorded on the same database. The database records all results obtained from the data collection questionnaire, as well as the ocular and blood

biomarker results. The ocular parameters of different comorbidities could also be investigated from this larger pooled cohort of 407 subjects.

Inclusion and Exclusion Criteria:

Patients were excluded if they were under 18 years of age, pregnant, had a bleeding disorder for which blood sampling would not be advisable or if they were unable to consent. The Transcatheter Aortic Valve Implantation (TAVI) cohort inclusion criteria involved recruiting only patients referred for TAVI with severe aortic stenosis as assessed via echocardiographic assessment. Further older low-risk control participants (with no evidence of aortic stenosis) were also recruited for comparison with the TAVI cohort.

The pressure wire cohort eligibility criteria included patients referred for pressure wire with suspected coronary microvascular disease, and physiologically non-obstructive coronaries. This meant only patients with a fractional flow reserve (FFR) ≥ 80 were recruited to ensure the focus was not on epicardial disease, but instead only on the presence or absence of microvascular disease within the coronaries. Participants were categorised as pressure wire negative (the controls cohort) if the pressure wire study results show an index of microcirculatory (IMR) <25 and a coronary flow reserve (CFR) of ≥2. All other participants (IMR ≥25 and CFR <2) were classified as pressure wire positive for coronary microvascular disease.

Recruitment:

Patients were recruited through the Royal Victoria Hospital Belfast, Northern Ireland. Patients were informed of the study, and any patients meeting the recruitment criteria and expressing an interest in taking part received the ethically approved patient information leaflet. Informed consent was obtained using the ethically approved consent form. Prior to recruitment of the new cohorts, a substantial ethics amendment had to be approved via the Integrated Research Application System (IRAS) for recruitment of the TAVI and pressure wire cohorts. Recruitment then recommenced in October 2020 and was set to continue until the sample sizes calculated using the power calculation (as described in the succeeding sections) were obtained.

Recruitment of Controls:

Older control subjects were recruited to compare with the TAVI cohort, these were individuals without severe aortic stenosis recruited through the Royal Victoria Hospital. Previously, control subjects were age and sex matched to the myocardial infarction and cyanotic congenital heart disease cohorts.

All patients were imaged within the same clinical environment at the Royal Victoria Hospital in Belfast, and to date, no adverse events were encountered during the study. Imaging for the TAVI cohort was typically carried out at pre-assessment clinic, or on the morning of the procedure. Post-TAVI ocular imaging and blood testing was typically carried out 24 hours after TAVI (to eliminate mitigating factors such as vasodilatory medications administered for TAVI). The pressure wire patients were also typically examined around 4 hours following their procedure so medications would not affect the results of the ocular and blood tests.

Pulse oximeter, blood pressure (average of three readings), temperature and height and weight measurements were taken and recorded for all patients and the ethically approved questionnaire (assessing various risk factors) was also taken (wherein, medications, as well as timings of measurements were also recorded). The questionnaire collected data to include postcode, age, gender, ethnicity, height, weight, blood pressure, smoking status, comorbidities, medications and family history, as these are risk factors required to calculate the QRISK3 score. Other factors recorded included heart rate, oxygen saturation, alcohol intake, occupation details and activity levels as recognised by the European Society of Cardiology Cardiovascular Disease Prevention in Clinical Practice guidelines (Piepoli *et al*., 2016). Handedness was also assessed within the questionnaire and may be of particular interest as this has been suggested as an indicator of cerebral hemisphere dominance (Marcori *et al*., 2020).

Risk Stratification and Scoring:

The National Institute for Clinical Excellence (NICE, 2020) guidelines recommend the employment of QRISK for risk calculations. All eligible participants (all cohorts except for the TAVI and matched TAVI controls due to the exceeding age limits) were consistently assessed using the data collected via questionnaire and electronic health records. The scores were calculated for each patient using the online QRISK3 calculator (https://qrisk.org/three/), as recommended by the National Institute for Health and Care Excellence (NICE, 2020) guidelines, to calculate a person's risk of developing a major adverse cardiac event such as a myocardial infarction or stroke over a 10 year period.

3.2. *Blood Processing and Biomarker Analysis*

The study has ethical approval for the collection of a maximum of 50ml for blood sampling at a possible 3 time points (pre and post procedure, as well as at follow up approximately 3 months after the procedure). The timings of collection, processing and freezing (as well as the timings of eye imaging) are important, and hence are recorded within the data collection questionnaire to allow fair comparisons to be made (timings of medications are also recorded for this purpose). Recruitment of each cohort was standardised. In the TAVI cohort and throughout pre-TAVI recruitment, this occurred either at pre-assessment or on the day of their procedure (the date and time was recorded within the data collection questionnaire). Post-TAVI recruitment did not occur any earlier than 4 hours post procedure, and no later than 24 hours post procedure. This was included in the protocol to correct for any effects from medication, particularly vasodilators, administered for TAVI.

As per protocol, we collect one 4ml blue citrate plasma tube (for routine coagulation and platelet function testing), three of the 4ml yellow top serum tubes (one for routine lipid profile, C-Reactive Protein (CRP), N-terminal pro B-type natriuretic peptide (NtproBNP), electrolyte and urate testing and two for apolipoprotein A1 and B analysis), three of the 4ml EDTA plasma tubes (one for routine full blood count, one for routine glycated haemoglobin A1C (HbA1C) and one for plasma viscosity testing for the purpose of establishing wall shear stress), as well as both an 8ml EDTA plasma and 8ml coagulation activator tube for processing serum for all other additional inflammatory and endothelial markers as associated with cardiovascular disease (primarily analysed via RANDOX biochip) (Awuah *et al.,* 2022). The vacutainer tubes must be collected in the correct order of draw, inverted and processed in accordance with manufacturer instructions, and hence serum tubes are left for thirty minutes to allow for clotting prior to processing. All tubes except the 8ml

plasma and serum vacutainers can be processed by the clinical biochemistry staff within the Kelvin Laboratory, Royal Victoria Hospital, Belfast, UK. However, the blood samples collected for apolipoprotein A1 and B were sent to the Biochemistry Department at Cardiff and Vale University Hospital, UK for testing, and the blood sample collected for plasma viscosity testing was sent to the Ulster Hospital, Dundonald, UK.

The two 8ml research blood tubes for plasma and serum were processed in accordance with the Kelvin Laboratory protocols, and thus centrifuged at 3500rpm for 5 minutes. The plasma and serum were then aliquoted into 0.5ml microcentrifuge tubes pre-labelled with the unique MACE identifier and sample type for the corresponding patient. Approximately, 300µl of whole blood was aliquoted into a labelled microcentrifuge tube from the 8ml EDTA plasma vacutainer prior to processing. Following processing and plasma aliquoting, approximately 300µl of buffy coat was also aliquoted into a further labelled microcentrifuge tube. In total, ten 0.5ml aliquots are typically obtained of both plasma and serum, and two aliquots can then be kept for further testing at Ulster University. All samples are numerically ordered into the Sarstedt freezer boxes and labelled with the study and ethics details. The location details of each sample are recorded on the freezer map.

The remaining samples are sent to Randox for analysis to test both plasma and serum samples for a selection of inflammatory and endothelial dysfunction biomarkers. Each biomarker assessed requires 100µl of patient plasma or serum sample. Subsequently, 2ml of both plasma and serum is required, as 20 biomarkers

are investigated to include interleukins IL-1α, IL-1β, IL-2, IL-4, IL-6, IL-8, IL-10, vascular endothelial growth factor (VEGF), epidermal growth factor (EGF), tumour necrosis factor-α (TNF-α), interferon-ɣ (IFN-ɣ), monocyte chemoattractant protein-1 (MCP-1) (as assessed on the Randox Laboratories Ltd cytokine array, using the Randox Evidence Investigator analyser), heart fatty acid binding protein (H-FABP), adiponectin, homocysteine, high density lipoprotein-3 (HDL-3) (as tested on the Randox RX Imola analyser), folate, vitamin B_{12} (as measured using the Roche Cobas 8000), plasma asymmetric dimethylarginine (ADMA) and plasma leucine-rich alpha-2-glycoprotein-1 (LRG-1) (as assessed using the ELISAgenie ELISA).

Plasma Viscosity and Wall Shear Stress Estimations:

The wall shear stress was estimated within this research project, and this was due to not having access to whole blood viscosity testing, and hence plasma viscosity was measured instead. Characterisation of the rheological properties of plasma are not extensively documented. Nevertheless, plasma is a mixture of proteins and water and behaves as a Newtonian fluid whilst whole blood does not. It is also largely independent of wall shear rate. The Quemada model equation was applied (formula 3), and the estimation of whole blood viscosity was then multiplied by each vessel segment's wall shear rate to obtain the estimated wall shear stress (Mimouni, 2016). It should also be noted that whole blood viscosity may vary within and throughout the length of each vessel segment (as viscosity also varies with other factors such as temperature, and likewise wall shear stress varies with tortuosity, for example), but it was not possible to measure this for each individual segment and thus this average whole blood velocity estimation was applied instead (Balogh and Bagchi, 2019).

$$\eta = \eta_\rho \left(1 - \frac{1}{2} \frac{\kappa_0 + \kappa_\infty \sqrt{\frac{\dot{\gamma}}{\gamma_c}}}{1 + \sqrt{\frac{\dot{\gamma}}{\gamma_c}}} H_t \right)^{-2}$$

Formula 3. Quemada model for estimation of whole blood viscosity

η= whole blood viscosity; η_p = plasma viscosity; K_0= 4.33; K_∞= 2.07; $\dot{\gamma}$= wall shear rate; γ_c= 1.88; H_t= Haematocrit (the volume concentration of red blood cells)

3.3. *Imaging and Video Processing*

Any abnormalities such as inflammation or tears, as well as the quality of the videos taken, were noted within the patient's data collection questionnaire when imaging the conjunctival vessels. Four video recordings of approximately 10 seconds were obtained from each patient, looking at the left temporal, left nasal, right nasal and right temporal views. The operator should aim to select areas with greatest vessel density where possible to maximise the number of vessel segments that may be analysed. Vessel density is quantified within the Dundee conjunctiva video application. There is a high degree of selection bias within this result due to areas of high vessel density being selected for imaging within the conjunctival vasculature of each subject.

The recordings are saved with the unique MACE identifier and field of view and may be accessed from a private Google Drive link. To ensure only the best video frames are selected for analysis, the segmentation selection process was manually carried

out. The selected frames should be focused (including no more than 10% unfocused frames) with minimal movement (drift must be less than 25% of the frame width) and no blinking. The frames can be viewed using a proxy scale of 1/4 (to speed up viewing and to accurately assess image quality) and considered individually using the DJV version 1.3.0 software (available at: https://darbyjohnston.github.io/DJV/). The start and end frames of the 60 consecutive best frames are recorded within a text document and named after the patient's anonymised number, a "_" and either "LN" for left nasal, "LT" for left temporal, "RN" for right nasal and "RT" for right temporal views correspondingly. The videos must also be named as described above and saved to a file named after the anonymised patient ID number within a "conjunctival_videos" file on the C:drive.

The Dundee conjunctival video application then automatically processes the selected video segmentation by the anonymous patient ID number accordingly, via command prompt "the black box system". The black box system utilises the stand-alone MATLAB application by using command prompt, copying and pasting the conjunctival video application location along with the corresponding patient and video number (1=LN, 2=LT, 3=RN and 4=RT). This stand-alone application also offers the below results shown in Figure 3.1 to be output. There is also the option to change the frame limit, as well as the data path. These remained the same throughout this research project. Once the application has finished running and processing a video, the output file can be viewed within the patient's data file.

Figure 3.1. Dundee conjunctival video application results

A.) Histogram of vessel segment widths. B.) Average image. C.) Skeletonised image of vessel segment

For pre and post procedure imaging (in the case of this research project, pre and post TAVI) of the same patient the pre procedure videos must be processed first. The output files should then be transferred to a different pre procedure folder before the post procedure videos can be processed, and then transferred to a post procedure folder. The registered sequence MATLAB file is the most important within the output file, as this file is then input into the eye project application (version 2 with the updated conversion rate for this study) created in collaboration with researchers from Nanotechnology and Integrated Biomedical Engineering Centre (NIBEC), Ulster University. Again, the pre procedure registered sequence must be processed through the NIBEC eye project application before the post procedure registered sequence, and then it is recommended that the output files from this application are transferred to a respective NIBEC eye app pre procedure folder and post procedure folder. Selection of the exact same vessel segments pre and post is limited, as even if the same area is imaged each time, it can be difficult to maintain the same focus and even illumination as carried out previously.

A MATLAB code called “play frames”, developed by Jing (2020), can be used to check the quality of the processed registered sequence video prior to using the NIBEC eye project application. Once the registered sequence has been uploaded to the NIBEC eye project application, the whole focused video is selected for the region of interest (ROI). The video is then edited and played to ensure the video is stable. The frames may be reselected if unstable frames are found upon play back. The sigma value is then set to 7, and the centerlines and binary map are checked. If it appears that the sigma value would need increased from the centrelines and binary map (e.g., typically seen as holes in the larger vessel within the binary map or as

one vessel with more than one centreline), then the ROI must be reselected to exclude the larger vessel(s). The minimum vessel length set at 30 to ensure the maximum number of vessel segments can be analysed. The final step of the application involves selecting only the Space Time Imaging (STI) graphs with analysable yellow motion flow lines and no horizontal or vertical lines. If vertical lines of artefact are seen, the video clip is again rechecked for unstable frames and the frames are reselected.

The Principles and Processes Applied within the Applications:

At the time of recruitment, selecting the best sequence of images from the video taken was a manual process, as previously discussed. Then the Dundee video processing application primarily stabilises the selected segment of the videos and carries out the image registration automatically. The MATLAB application developed by researchers from NIBEC uses the output image registration MATLAB file from the Dundee application to allow the user to manually select the ROI, and although supervised by the user at each stage, the application then automatically carries out the following processes: vessel segmentation, centreline extraction/branch point detection and the EDT as well as the flow (STI graph extraction) analysis and results are then output. EDT was exercised within the application as it determines the distance between to perpendicular points, which was suitable due to the cylindrical profile of the blood vessels (Kipli *et al*., 2020). Additionally, the STI method was the processing method suggested and discussed in the review presented by Shu *et al*. (2019).

Arteriole and Venule Classification:

Initially, the vessel ID maps were developed through MATLAB and used to match the corresponding vessel with the ID on the vessel map to the output csv file results. This permitted manual interrogation, vessel classification and labelling. The principles discussed within a paper by Meyer *et al*. (2018) were considered, and the conjunctival vasculature Audio Visual Interleave (AVI) file output from the NIBEC application was used. Vessel segments with blood flowing towards a bifurcation point were labelled as arterioles, whilst vessel segments with blood flowing away from a bifurcation point were considered to be venules. Although high agreement was found in a preliminary study between four different investigators for vessel classification, a large proportion of vessels remained undifferentiated and the possibility of operator error and misclassification is possible.

Li *et al*. (2020) suggest the initial observations via comprehensive examination and annotations are fundamental in the machine learning processes. Several further avenues, particularly, concerning potential automated methodology were evaluated within the previously discussed literature review and pilot study. These avenues are also considered within the application development section. It was initially proposed that binary logistic regression could be carried out to develop an algorithm that could automatically distinguish between, and thus classify and label selected vessel segments as arterioles and venules from feature extraction.

3.4. *Statistical Analysis*

Prior to data analysis the data collected within the data collection questionnaire was anonymised and recorded within a secure, password-locked database. The database was audited and checked to minimise the risk of incorrect data entry and human error. All statistical analysis was carried out and graphs produced using IBM SPSS Statistics version 27 for Windows (Armonk, N.Y., USA: IBM Corp.). Normality was assessed using the Kolmogorov-Smirnov test.

Parametric continuous results were presented as mean ± standard deviation, and the difference between groups was tested using the Student's t test. The 95% confidence intervals (CI) were also calculated and presented within the results tables. Non-parametric continuous results were presented as median ± interquartile range, and the difference between groups were tested using the Mann-Whitney U test.

Categorical variables were presented as frequency and percentages, and differences between groups tested using the Chi-Square test. For analysis of more than two groups a one-way analysis of variance (ANOVA) test was applied, and Bonferroni post-hoc test was used where equal variance could be assumed, or Games-Howell post-hoc test was used when equal variance could not be assumed. The level of significance was set at $p<0.05$. Correlation analysis was carried out using Spearman's Rho, and correlations were determined to be significant if they were ≥0.7. Intra-observer repeatability was assessed using intra-class correlation coefficients (ICC). Binary logistic regression analysis was also conducted, and receiver operator characteristic curves and straight-line graphs were generated to

create algorithms and patient risk scores. Logistic transformation was applied to variables that were found to be non-normally distributed.

Power Calculations:

Power calculations were conducted using ClinCalc (https://clincalc.com/stats/samplesize.aspx), with an alpha value of 0.05, and based on the early data of the means and standard deviations between the two groups within each cohort (TAVI and pressure wire). The results of the 90% power calculation are based on the initial feasibility study reported by Brennan *et al*. (2021a), that showed a mean axial velocity of 0.53 ± 0.15 mm/s for the control group compared to a reduced axial velocity of 0.49 mm/s for the myocardial infarction (MI) group. Therefore, we estimated the effect size would be approximately halved for the pressure wire cohort, arguably, at reduced cardiovascular risk compared to the MI group. The results of a 3% reduction in mean for the positive pressure wire cohort compared to the negative pressure wire cohort, at an enrolment ratio of 1.5, suggested a total of 3847 vessel segments would be required. Although the number of vessel segments varies per person, the average number was previously reported to be 36 (Brennan *et al*., 2021a), and hence 107 participants would be required. Group 1 (the pressure wire negative group) results show 1539 vessel segments, or 43 participants would be required, and Group 2 (the pressure wire positive group) results show 2308 vessel segments, or 65 participants would be required. The 80% power calculation for this cohort suggests 1150 vessel segments (approximately 32 participants) would be required in Group 1, and 1725 vessel segments (approximately 48 participants) would be required in Group 2. Similarly, for the TAVI

cohort we estimated that 77 participants (2760 vessel segments/ average of 36 vessel segments per person) would be required for 80% power calculation. Whilst 103 participants (3694 vessel segments/ average of 36 vessel segments per person) would be required for 90% power calculation.

3.5. *Ethics and Risk Assessment*

Ethical approval was granted through IRAS and the South Birmingham Research Ethics Committee (IRAS number 166742), as well as by the Belfast Health and Social Care Trust and Ulster University. The study complied with The Declaration of Helsinki, Good Clinical Practice Guidelines and the Human Tissue Act, and was designed in accordance with the Standards for Reporting Diagnostic accuracy studies (STARD) 2015 recommendations (Cohen *et al*., 2016). Data obtained from the study was managed in accordance with the Data Protection Act 2018. Laboratory regulations and the Ulster University local rules for phlebotomy were adhered too throughout. Infection control regulations (particularly considering the COVID-19 pandemic) were also adhered too. Further key risks were considered in association with the COVID-19 pandemic as detailed in Figure 3.2. Additionally, the appropriate Control of Substances Hazardous to Health, risk assessments and personal protective equipment were used.

Figure 3.2. Key risks identified from risk assessments for recommencing recruitment

CVD= Cardiovascular Disease and PPE= Personal Protective Equipment.

Chapter 4

Imaging System Optimisation and Application (App) Development

Chapter 4: Imaging System Optimisation and Application (App) Development

One-tailed null hypothesis: The conjunctival imaging application can be enhanced to permit fully automated processing of 4K videos in a single application.

One-tailed alternative hypothesis: The conjunctival imaging application cannot be enhanced to permit fully automated processing of 4K videos in a single application.

4.1 *Abstract*

In line with the optimisation and recalibration of the imaging system, the video processing application also had to be updated. The main objective was to develop the smartphone-based application to enable fully automated 4K Ultra High Definition (UHD) video processing, from the point of image acquisition and video segment selection, right through to the flow analysis and output of the conjunctival vessel parameters (vessel diameter, axial/cross-sectional velocity, blood flow rate and wall shear rate). The updates involved collaborating with software development experts to create a python executable in Linux, that would then be deployed to a cloud-based web server. The identification of vessel segment centrelines, detection of branch points and measurement of the vessel segment diameter has already been

automated for the older 1080p semi-automated processing application using a segmentation algorithm and the principle of Euclidean distance transform (EDT). This process could be easily transferred for the new 4K application through update of the conversion factor using MATLAB. New techniques that were utilised included Manhattan scoring for automated image registration and convolutional neural network applied to support automated selection of high quality space time image spectrograms for the assessment of blood flow axial velocity. The end result of the fully automated application is beneficial, as after the beginning stage of video upload, the stages of video processing through to the generation and output of results are carried out objectively without manual input through this in-house developed application.

4.2 *Introduction*

The optimisation of the imaging system paved the way for optimisation of the corresponding processing applications. Additional challenges paired with the processing of higher resolution images, such as the increased file sizes. It is also important that both the application and device are fit for purpose, usable and easily adaptable with evolving technology. In order to optimise the camera system and to ensure the application is adaptable with developments in technology, the application was developed in collaboration with researchers from Nanotechnology and Integrated Biomedical Engineering Centre (NIBEC), to allow processing of 4K videos from the image registration stage right through the vessel segmentation, centreline

extraction/branch point detection, euclidean distance transform (EDT) and flow analysis stages as demonstrated in Figure 4.1 below. The application will require less human input with the sigma value and minimum vessel length being pre-defined in the protocol. The space time image (STI) graph selection stage was manual up until this point of development, to ensure only spectrograms that were of high quality i.e., with no image artefact were selected.

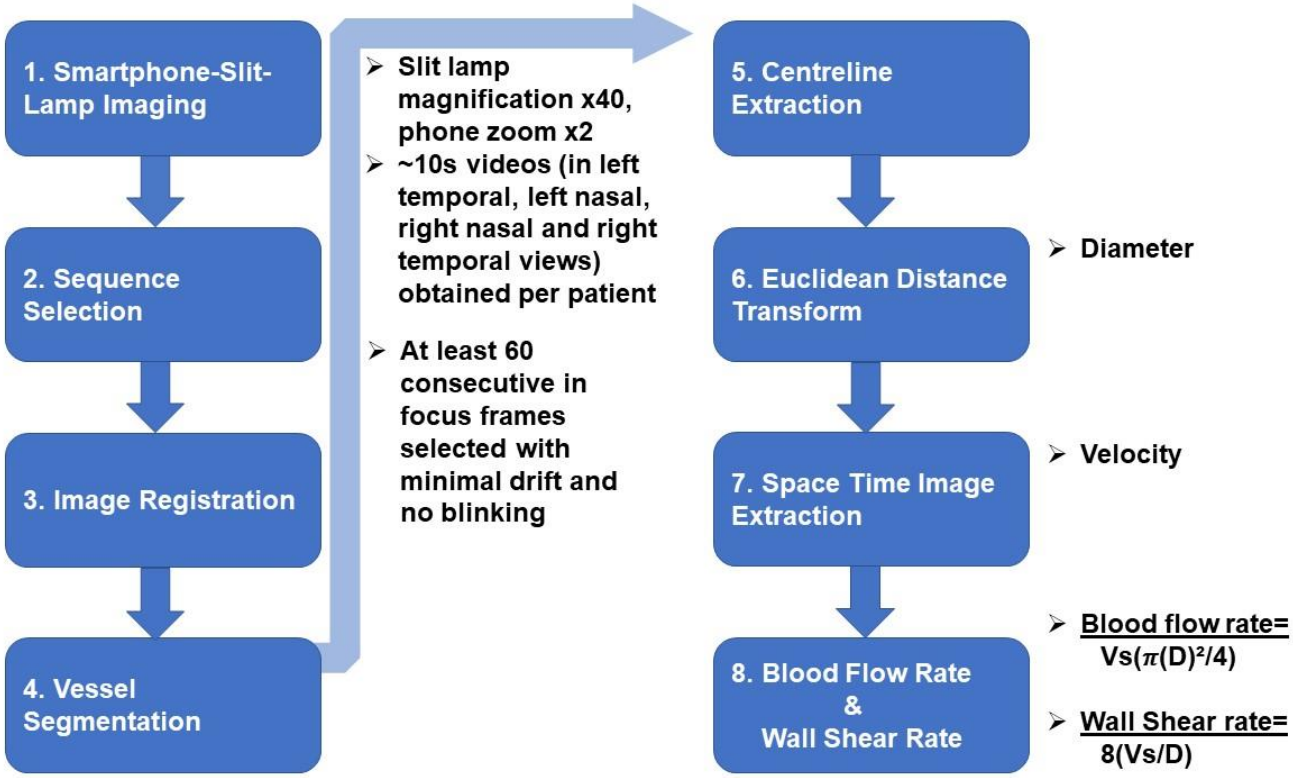

Figure 4.1. Conjunctiva vessel video processing and parameter measurement summary

D= Diameter and Vs= Cross-Sectional Velocity

Consequently, amendments to processing workflow were required, and the following list of objectives was created:

- Combining the image registration application (the “Conjunctiva_Video_App”) that is a stand-alone “black box” application created by researchers at Dundee, with the flow analysis MATLAB application (“eyeprojectAPP”) created by researchers at NIBEC to create a single and independently owned application.
- Increased automation by amending semi-automated or manual stages such as the segmentation selection, region of interest selection and spatial temporal image extraction.
- Faster processing speeds with the opportunity to process more than one video at a time.
- Based on pilot study findings, the extraction of centreline line mean pixel intensity values for each vessel segment.
- Transferring the application to a web based server for easier access from the smartphone device, and thus video upload and processing could be done immediately from the smartphone at the point of capture.

4.3 *Methods*

Imaging system:

The function of the slit lamp biomicroscope is to produce an intense slit beam of light from the lamp which is then focused onto the patient’s eye. The eye is then observed

via magnification with the microscope. A fixation point was also attached to the slit lamp to help the patient focus in the direction of the fixation point, reducing movement to obtain a more stable video. If the patient is more comfortable this may also reduce movement. The height of the slit lamp, as well as the chin rest can also be adjusted to suit the patient. The patient rests their chin on the chin rest (assessed using the alignment mark) and forehead on the forehead band for ocular examination and imaging. Alternatively, the patient's bed or chair may also need to be adjusted, to ensure a clear, focused and stable video can be produced for analysis. The joystick is used to span across each of the views; left temporal, left nasal, right nasal and right temporal, respectively. In terms of infection control, focus should be placed on the chin rest and forehead band when cleaning the slit lamp with an alcohol wipe before and after each use.

The initial imaging system comprised of a Topcon SL-D4 slit lamp (set at a magnification of 40x) (Topcon Medical Images Inc., USA) and ZARF adaptor (ZARF Enterprises, USA) for the iPhone 6S (Apple Inc., USA) to attach to the slit lamp. The 2x magnification setting on the iPhone along with the 40x on the slit lamp results in an overall magnification of 80x. This phase of the study seen an iPhone 11 Pro (Apple Inc., USA) used instead due to the option of 4K (higher resolution) imaging, video stabilisation and a better depth of field. Although various other third-party smart phone applications were explored to control the iPhone imaging settings, for consistency the decision was made to use the same ProMovie Recorder application (www.promovieapp.com) as before. The same settings within the application were also used (including the ISO (light intensity) settings at the minimum setting of 25 to reduce noise artefact), with the only difference being that 4K resolution was used

instead of the previous 1080p setting. Despite the use of the 4K video recording settings, the videos within this phase were both saved as 4K, and a converted 1080p recording.

Calibration:

The 1080p video was derived through converting the original 4K video using the free MOV converter application (https://www.freeconvert.com/mov-converter/) at the same frame rate (60fps) and MOV setting. This resolution conversion was required due to the large amounts of output data that was considered to be difficult to handle at this stage, through the current conjunctiva video processing applications developed in collaboration with Dundee and NIBEC. Due to the change of iPhone camera, the imaging system also had to be recalibrated to obtain an accurate pixel/mm conversion factor. There is the potential for further application development and 4K video processing in future studies (as discussed later). Advancing the applications to permit 4K processing would be highly advantageous, as it is hypothesised that this would permit better visualisation of blood flow and increase both the precision and accuracy of the measurements obtained. Chapter 2 discussed the various studies that have previously relied on pixel measurements in the classification of vessels, and inclusion of this development may also support the automation of vessel classification.

The new camera system was calibrated by imaging a calibration slide (a reticle), using the same set-up and settings as a patient's conjunctival vessels would be imaged. Therefore, the focus remained at 0.5 and the lens-target distance at 100 ±

2mm throughout the calibration process. Five videos were taken for each different iPhone set-up, for the purposes of comparison the iPhone 11 Pro was imaged in both 4K and 1080p settings and the iPhone 6S was also recalibrated. The iPhone 11 Pro camera is made up of three lenses. The ultra-wide lens was found to not be compatible with the application. Calibration was also carried out for the iPhone 11 Pro telephoto lens at 4K resolution settings, and this lens was found to have a higher pixel/mm conversion factor. The estimated depth of field for this lens was poorer than that of the standard wide lens.

Once the videos were obtained, they were first loaded into the VirtualDub software (32 bit windows version 1.10.4 recommended within Image J user guide, available at: http://www.virtualdub.org). Segmentation selection was then carried out to select the most stable and focused 60 frames, as this same process is carried out when processing a patient's conjunctival video. A non-compressed PNG image sequence file for each video was then imported as an image sequence to Image J (Maryland, USA: https://imagej.nih.gov/ij/), and an average image of each image sequence was obtained using the projection Z plugin. Upon obtaining the average image, the line tool was used to measure the distance in pixels between the twenty 0.05mm markings on both the top and bottom of the calibration slide as shown in Figure 4.2. A plot could then be produced in image J; the results were exported to Excel and a mean and standard deviation pixel/mm conversion factor was obtained for each video. The results of the calibration were also independently checked by experts at NIBEC.

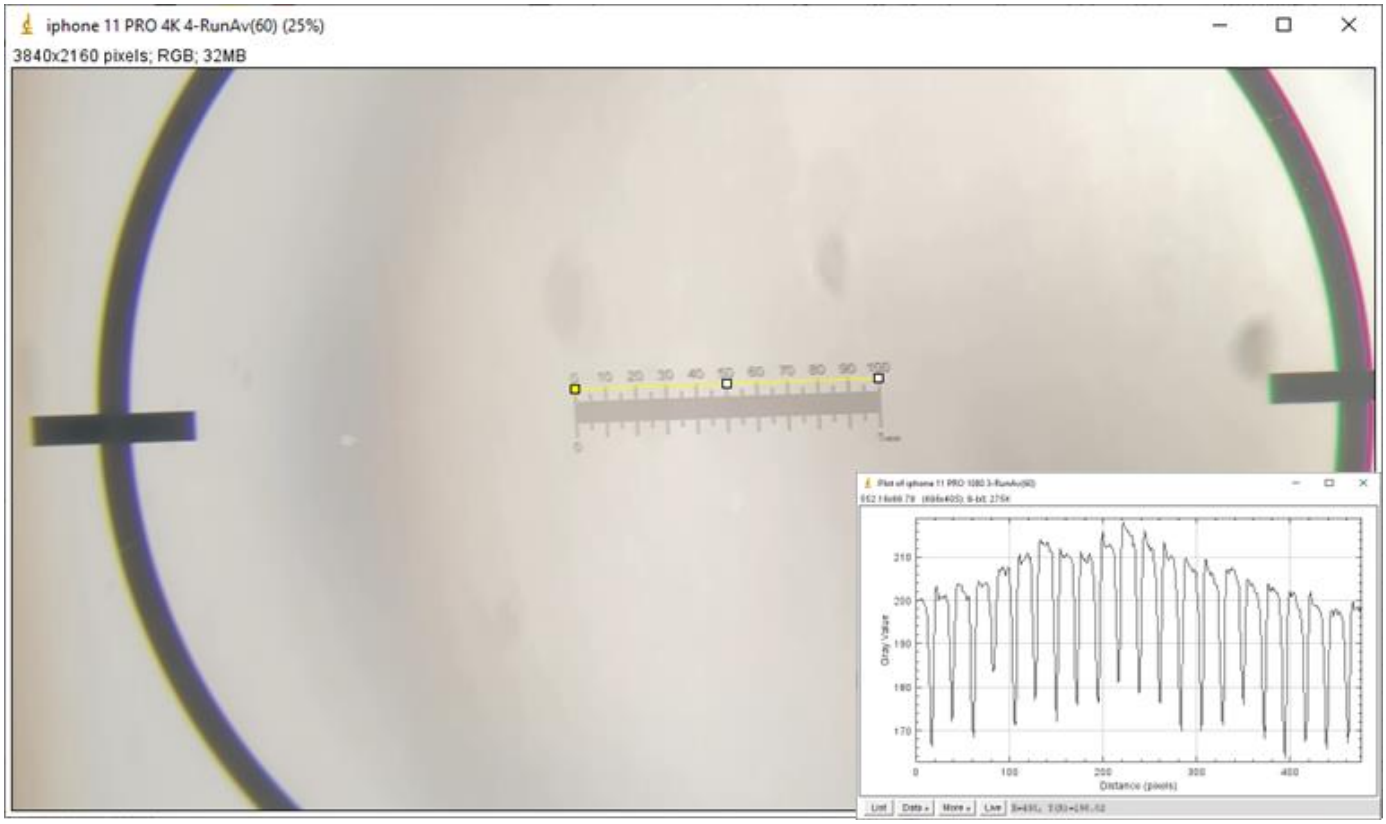

Figure 4.2. Calibration slide measurements

Repeatability:

The intra-observer repeatability analysis was carried out previously by researchers at NIBEC for the iPhone 6S, and then again within this thesis for the iPhone 11. The analysis was carried out re-analysing a total of 16 videos for 4 subjects and comparing the results of the re-analysis to that of the original analysis. The diameter, axial velocity, cross-sectional velocity, blood flow rate and wall shear rate were calculated and compared for 221 matched vessel segments.

For the inter-visit repeatability analysis, a total of 48 videos were processed, 24 for each for subject (4 fields of view; left temporal, left nasal, right nasal and right

temporal imaged across 6 timepoints). The vessel segments for each of the two subjects, with no known evidence of cardiovascular disease, were matched across the same 6 timepoints scheduled throughout a working day, as shown in Table 4.1 below. The mean and standard deviation (SD) were calculated for the separate parameters (diameter, axial velocity, cross-sectional velocity, blood flow rate and wall shear rate) at each timepoint for both individuals. The maximum mean difference for the parameters of each subject were also assessed individually, and the coefficients of repeatability and 95% confidence intervals (CI) were calculated.

Table 4.1. Timepoint descriptions

Timepoint (TP)	**Description**
1	10am
2	11am
3	12pm
4	1pm
5	2pm
6	3pm

Data management:

Originally, the conjunctiva videos were saved to a secure cloud and then processed separately through the two different applications for image registration and flow analysis. A more efficient method of uploading and processing videos directly via a single web server application will be executed at this application development stage. The output results of the application would be emailed to the user.

Sequence Selection:

Previously sequence selection was conducted manually. However, through using a Manhattan Scoring technique for each consecutive frame, the process became fully automated with the option for manual selection still possible. The application can now process multiple potential video segment combinations at a single time. The smartphone access to the web server application at the time of capture means that if the video does not return frames of satisfactory quality (i.e., there is eye movement) the video can be recaptured and reassessed.

Image Registration:

In order to optimise the camera system and to ensure the application is adaptable with developments in technology, the application was developed to allow processing of 4K videos. The output registered sequence file is then automatically input into the eyeprojectAPP version 4 application (version 3 was updated for 4K processing, and version 4 includes the automated STI update), that was developed in MATLAB for processing. The eyeprojectAPP was packaged into a stand-alone executable file for Linux operating systems in order to transfer this on to the server. No manual input will be required from the user throughout this stage using the web server application. Although the registered sequence file is saved and automatically emailed to the user within a zip file, the previous semi-automated method of processing is still accessible.

Vessel Segmentation, Centreline Extraction, Branch Point Detection and EDT:

Vessel segmentation, centreline extraction, branch point detection and EDT were already automated, and thus except for the transferal to a web-based server these stages remain relatively unchanged. The minimum vessel segment length is now automatically set to 40 pixels, and the sigma value to 13. Accordingly, less input is required when compared to the previous applications, as the user does not need to navigate through each stage.

Space Time Image (STI) Graphs and Axial Velocity:

Automation was made possible via application of convolution neural networks (CNN). The highest accuracy was reported for the vgg19 CNN at 86% (training time= 150 minutes), with googlenet having the shortest training time at 26 minutes as well as demonstrating similar accuracy at 84%. Similarly, 84% accuracy was also demonstrated for resnet (training time= 68 minutes) (Jing *et al*., 2022a). Therefore, CNN was applied for automatic processing. The NIBEC app was updated with the option to review all selected STI graphs, including all possible vessel segments with their respective measurements. Figure 4.3. provides the amended workflow diagram that incorporates all of the aforementioned updates.

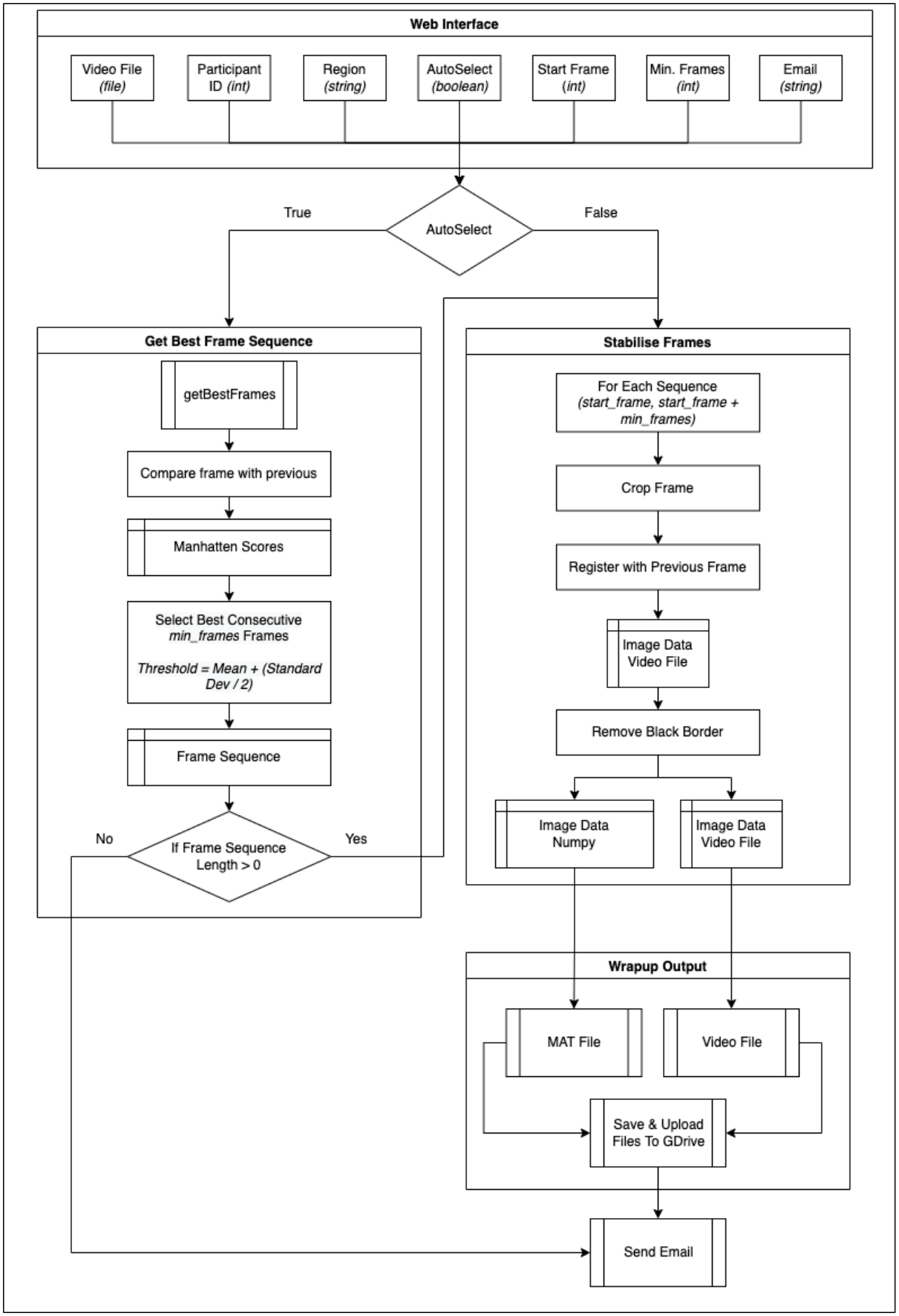

Figure 4.3. Amended workflow diagram reflecting application development updates

Statistical Analysis:

Continuous variables were described using the mean and standard deviation of the mean. Kolmogorov–Smirnov testing was used to assess normality of the continuous variables. For calibration a mean and standard deviation of the pixel/mm conversion factor was obtained from the 40 measurements of each of the 5 videos per iPhone set-up and calculated using excel. For intra-observer repeatability, intraclass correlation coefficients (ICC) were applied with 95% CI. Lastly, coefficients of repeatability with 95% CI were calculated to assess inter-visit repeatability.

4.4 *Results*

Calibration:

The resultant conversion factors from the calibration were as follows; iPhone 6s= 540.9 ± 36.7 pixels/mm, iPhone11 Pro 1080p= 454.8 ± 22.4 pixels/mm and iPhone11 Pro 4K= 894.7 ± 53.6 pixels/mm. The previous calibration factor for the iPhone 6s was 1.81 µm/pixel but following the change of camera sensor this changed by approximately 20% to 2.22 µm/pixel. The graph showing the calibration factor in pixels/mm for each iPhone set-up is presented in Figure 4.4.

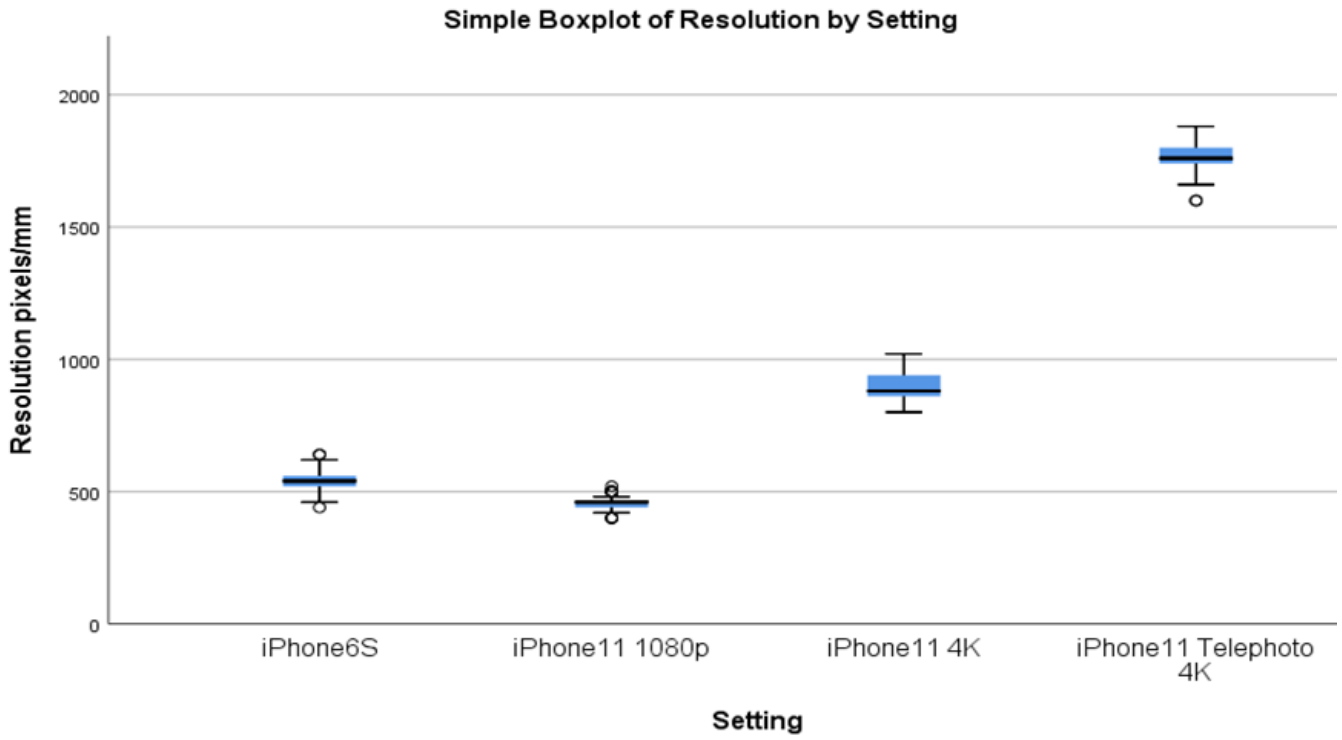

Figure 4.4. Boxplot showing the mean calibration factor(pixels/mm) for each iPhone set-up

40 resolution measurements taken per video; 5 videos taken per setting= 200 measurements recorded in total for each setting.

Repeatability:

Prior to the web server application and the higher resolution video processing, the "black box system" created by Dundee was utilised for image registration. The process of manual segmentation selection was independently assessed by two different researchers. The results shown in Figure 4.5 suggest overlap of start and end frames for both researchers for ten (66.7%) videos; 1, 4, 5, 7, 8, 9, 10, 12, 13 and 15. Selections for videos 7 and 9 were almost identical, and only differed by a

maximum of 6 frames. However, the updated automatic analysis assures 100% repeatability using Manhattan scoring.

	Andrew		Julie	
Video Name	Start	End	Start	End
1	375	738	205	746
2	1	78	372	436
3	1	44	95	274
4	162	448	59	477
5	64	95	30	103
6	1	42	450	540
7	1188	1249	1187	1253
8	633	1020	500	838
9	3	332	8	326
10	82	418	197	355
11	3	248	240	300
12	2	404	22	140
13	11	56	10	92
14	24	66	228	325
15	43	541	210	350

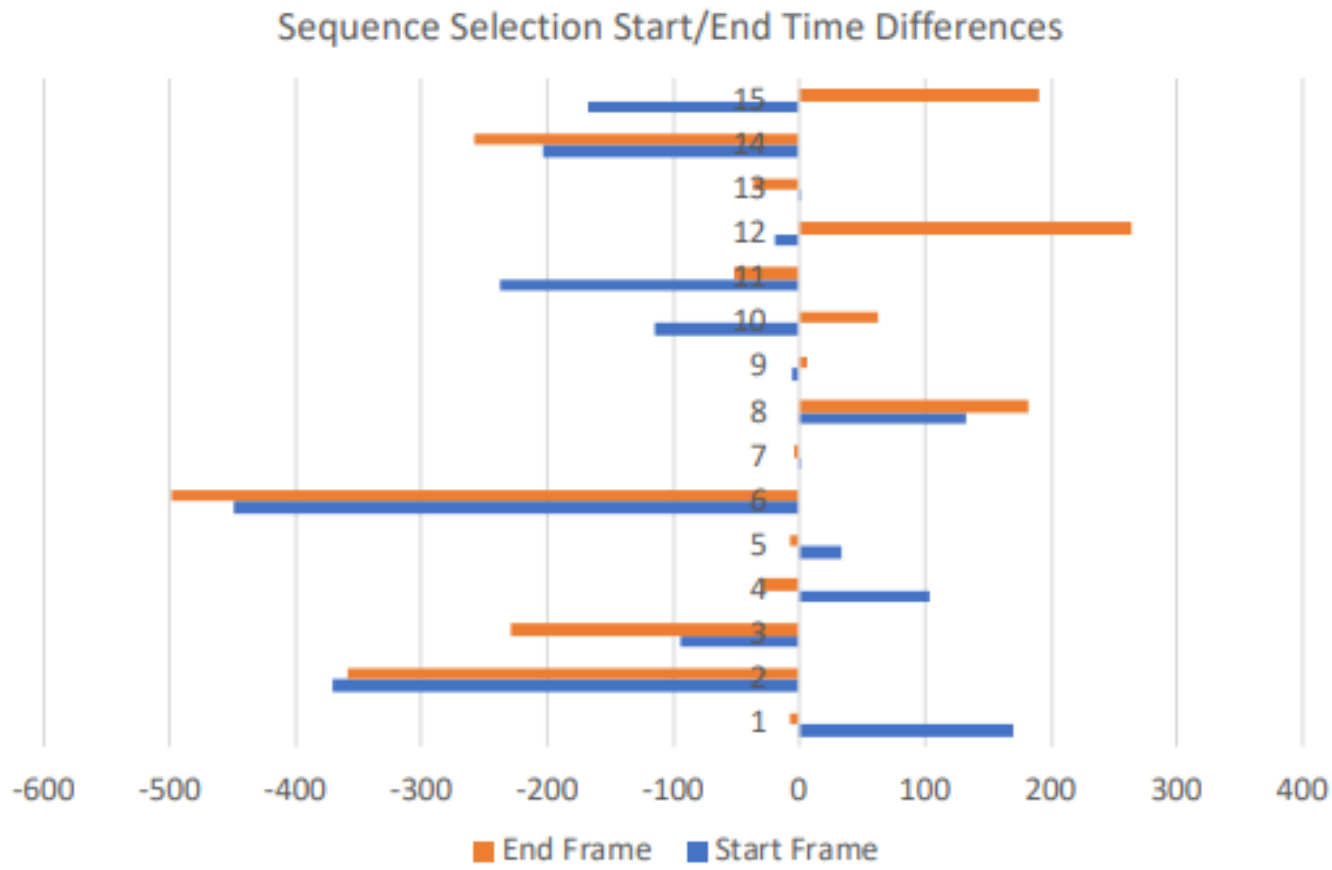

Figure 4.5. Inter-observer repeatability of the manual video segmentation selection

The intra-observer repeatability analysis of the slit lamp and iPhone 11 pro combination used within this study found this method to be repeatable. The results of the mean difference (ICC, 95% CI) for each of the ocular parameters were: diameter= 0.02 ± 0.31 µm (0.999, 95% CI 0.999 – 0.999), axial velocity= 0.002 ± 0.02 mm/s (0.986, 95% CI 0.981 – 0.989), cross-sectional velocity= 0.001 ± 0.02 mm/s (0.985, 95% CI 0.980 – 0.988), blood flow rate= 0.08 ± 11.31 pl/s (0.997, 95% CI 0.996 – 0.998) and wall shear rate= 0.98 ± 8.39 s^{-1} (0.988, 95% CI 0.985 – 0.991).

Xu *et al*. (2015) reported acceptable inter-observer and inter-visit repeatability. For the inter-visit repeatability assessment within this study there was a total maximum mean difference for; diameter= 4.08 µm (coefficient of repeatability (CR)=1.47 (95% confidence intervals= -2.61-5.55), axial velocity= 0.07 mm/s (CR=0.04 (-0.03-0.11), cross-sectional velocity= 0.06 mm/s (CR=0.03 (-0.03-0.09)), blood flow rate= 43.06 pl/s (CR=13.37 (-26.69-56.43)) and wall shear rate= 71.10 s^{-1} (CR=25.01 (-46.09-96.11)). The findings of this study also suggest acceptable variation between the conjunctival haemodynamic measurements across the 6 timepoints for both subjects. The results for two subjects at each of the 6 timepoints are presented in Table 4.2, whilst Table 4.3 summarizes the maximum and minimum results (and at what time point those results occur) for each ocular parameter. The results of the maximum difference alongside the coefficients of repeatability in Table 4.4 support acceptable repeatability. The graphs for each of the parameters measured for both subjects over the 6 timepoints is shown in Figures 4.6-4.8.

Table 4.2. Mean ocular parameters for subjects 1 and 2 at 6 timepoints (TP1-6).

TP	Subject	Diameter µm	Axial Velocity mm/s	Cross-Sectional Velocity mm/s	Blood Flow Rate pl/s	Wall Shear Rate s^{-1}
1	1	20.27	0.44	0.31	114.00	148.57
2	1	20.73	0.45	0.32	121.01	133.54
3	1	21.31	0.44	0.32	131.42	150.63
4	1	17.54	0.46	0.33	94.80	163.96
5	1	22.06	0.48	0.35	132.01	208.11
6	1	18.11	0.51	0.37	87.24	197.67
Total mean ± SD	1	20.00 ± 1.80	0.46 ± 0.03	0.33 ± 0.02	113.41 ± 7.66	167.08 ± 29.55
1	2	19.29	0.52	0.38	117.68	175.70
2	2	17.39	0.54	0.39	100.16	210.88
3	2	17.73	0.49	0.36	95.03	183.10
4	2	15.87	0.56	0.41	91.95	243.32
5	2	18.10	0.54	0.39	108.32	202.42
6	2	19.52	0.55	0.39	133.31	178.26
Total mean ± SD	2	17.98 ± 1.34	0.53 ± 0.02	0.39 ± 0.02	107.74 ± 15.63	198.95 ± 25.86

Table 4.3. Minimum and maximum values for the ocular parameters of subjects 1 and 2.

RANGE	Diameter µm	Axial Velocity mm/s	Cross-Sectional Velocity mm/s	Blood Flow Rate pl/s	Wall Shear Rate s^{-1}
Subject 1 *Minimum*	17.54 (TP4)	0.44 (TP1, TP3)	0.31 (TP1)	87.24 (TP6)	133.54 (TP2)
Maximum	22.06 (TP5)	0.51 (TP6)	0.37 (TP6)	132.01 (TP5)	208.11 (TP5)
Subject 2 *Minimum*	15.87 (TP4)	0.49 (TP3)	0.36 (TP3)	91.95 (TP4)	175.70 (TP1)
Maximum	19.52 (TP6)	0.56 (TP4)	0.41 (TP4)	133.31 (TP6)	243.32 (TP4)

Table 4.4. The greatest difference in ocular parameters for subjects 1 and 2.

Maximum Difference	Diameter µm	Axial Velocity mm/s	Cross-Sectional Velocity mm/s	Blood Flow Rate pl/s	Wall Shear Rate s^{-1}
Subject 1	4.52	0.07	0.06	44.77	74.57
Subject 2	3.64	0.07	0.06	41.35	67.62
Total Mean	4.08	0.07	0.06	43.06	71.10
Total CR (95% CI)	1.47 (-2.61-5.55)	0.04 (-0.03-0.11)	0.03 (-0.03-0.09)	13.37 (-26.69-56.43)	25.01 (-46.09-96.11)

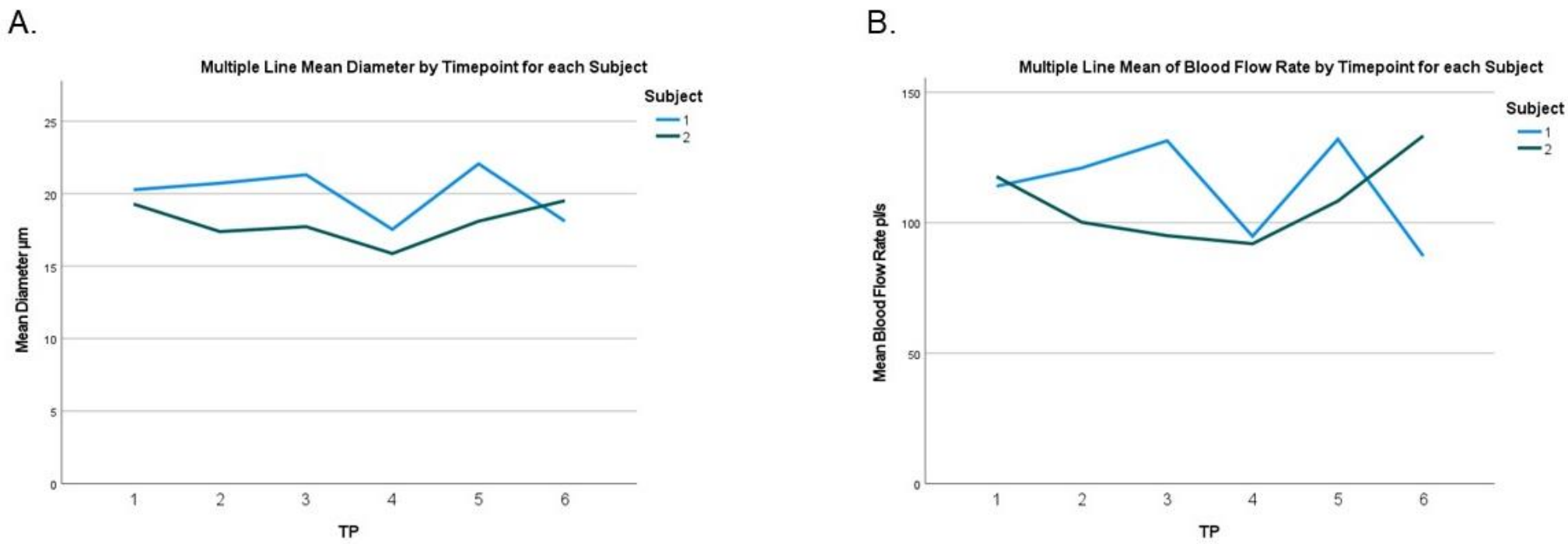

Figure 4.6. Inter-visit repeatability assessment for A.) diameter (µm) and B.) blood flow rate (pl/s)

TP= Timepoint

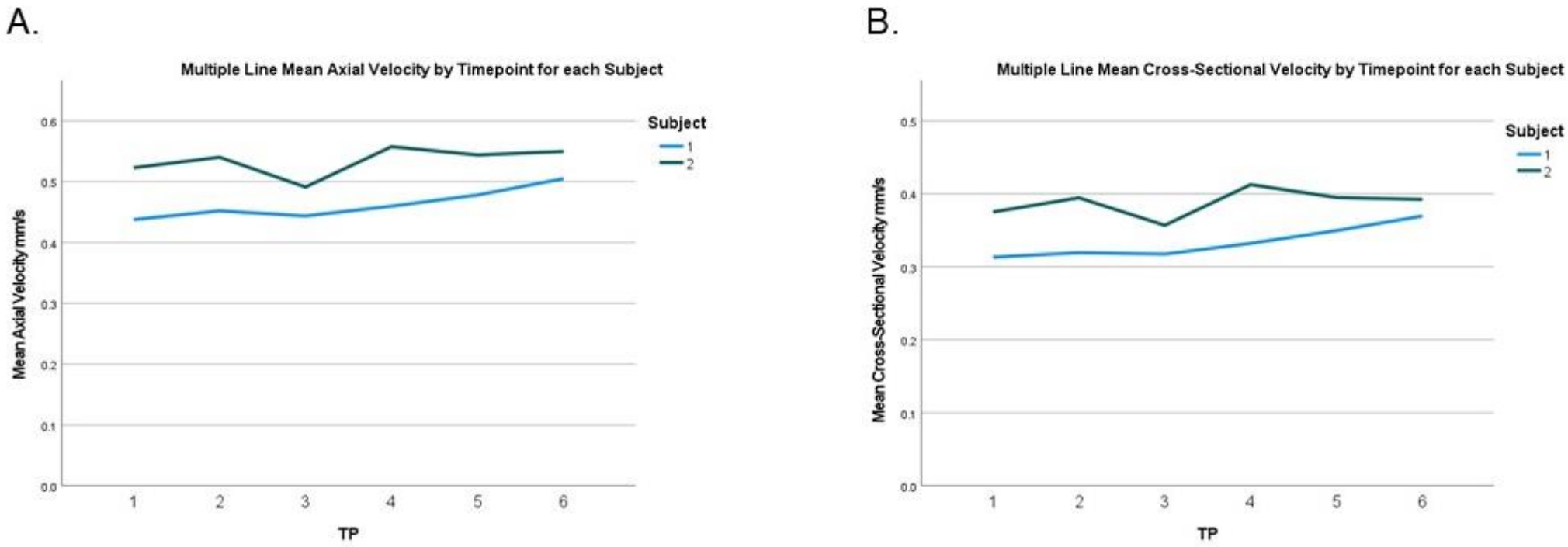

Figure 4.7. Inter-visit repeatability assessment for A.) axial velocity (mm/s) and B.) cross-sectional velocity (mm/s)

TP= Timepoint

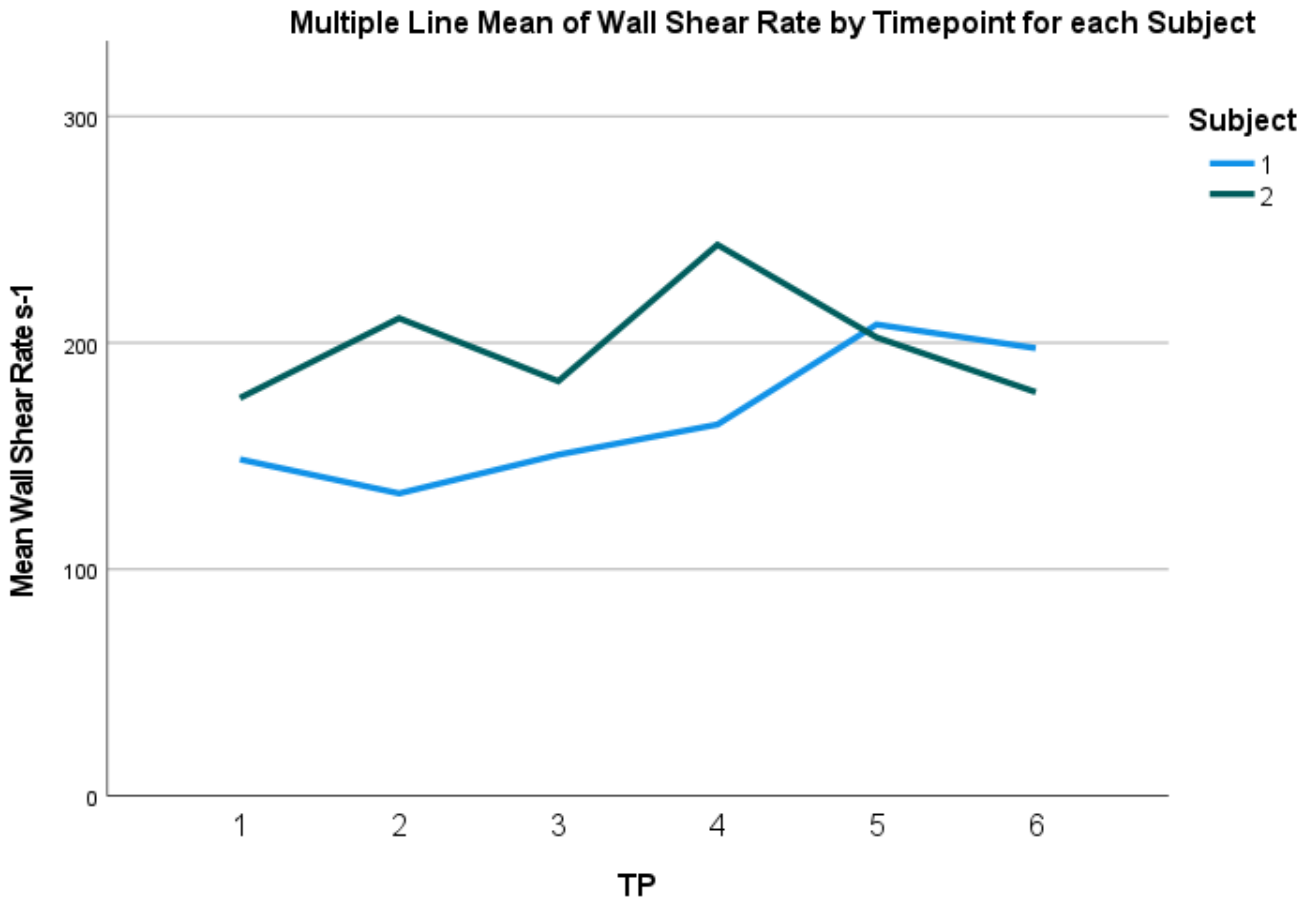

Figure 4.8. Inter-visit repeatability assessment for wall shear rate (s^{-1})

TP= Timepoint

App Testing (Manual vs Automated):

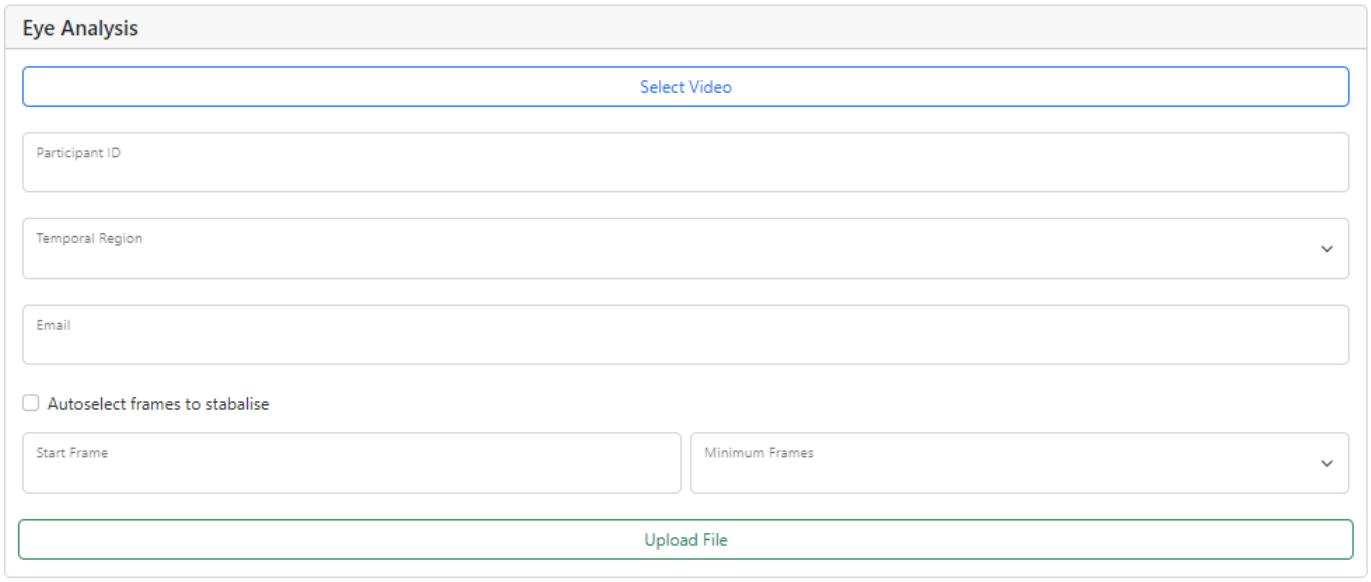

Figure 4.9. Graphical user interface of the updated web server application

The initial testing of 12 matched vessel segments for one subject assessing all fields of view found the mean difference (ICC scores, 95% CI) of; diameter= 0.29 μm (0.995, 0.981-0.998), axial velocity= 0.009 mm/s (0.881, 0.640-0.964), cross-sectional velocity= 0.007 mm/s (0.865, 0.598-0.959), blood flow rate= 7.26 pl/s (0.982, 0.939-0.995) and wall shear rate= 3.22 s^{-1} (0.900, 0.690-0.970). The results of the ICC analysis show good to excellent reliability between the manual and automated methods for all ocular parameters. The new application interface is presented in Figure 4.9.

4.5 *Discussion*

The Medicines and Healthcare Regulatory Authority (MHRA, 2022) state that software required for medical devices and associated applications need to be CE-marked, and under this definition the conjunctival imaging application may belong in class IIa to inform clinical management. Additionally, the Medical Devices Coordination Group (MDCG, 2020) advise that scientific validity should be determined through review of the literature, and technical and clinical performance should be appraised, analysed and documented. Thus far these guidelines do not give specific test values for accuracy or repeatability. Despite a lack of definitive application performance guidelines, the findings within our previous algorithm-based risk score study (that utilises the conjunctival eye application measurements) report good performance metrics to include a sensitivity of 93.0%, specificity of 91.5% and an area under the curve of 0.967 (Awuah *et al*., 2022). The repeatability analysis showed acceptable repeatability also, as the coefficient of repeatability fell within the 95% confidence intervals across the 6 time points of the 2 subjects.

The 4K videos produced from this optimised conjunctival imaging system are of cinematic quality, and inter-phone repeatability was also confirmed. It has been suggested that the resulting quality improvement from 1080p to 4K resolution offers significantly improved visual effects that is of great benefit to both education and medical imaging (Ichihashi *et al*., 2017). It is expected with 4K resolution that processing time would significantly increase, but the videos can now be fully processed within approximately 20 minutes. This is an improvement of at least 10

minutes faster per video from the manual application processing. The new application now lends itself to the possibility of selecting more than 60 frames, granting, 60 frames or less is often more accurate with less chance of artefact/noise. Similarly, less vessel segments were identified via the automated flow analysis STI selection steps (n=30) when compared to the manual selection (n=64). The automated method remains most beneficial as the opportunity to look through all the STI graphs is optional. The fully automated method also removes any subjectivity, markedly improving repeatability, as the same uploaded video will output the exact same result each time.

Conclusion

These findings suggest the conjunctival imaging application is robust and adaptable to the advancements of camera and smartphone technology. The development of this 4K conjunctival video processing application enabled improved image quality, automation and processing speed.

Key Points:

- 4K (UHD) video imaging has been made possible through the calibration and optimisation of the imaging system, and this demonstrates that the imaging system is adaptable to new smartphone cameras.
- Acceptable repeatability was demonstrated for this imaging method.

- 4K video processing has been made possible for image registration and flow analysis.
- Manual input is no longer needed at each stage of application (the segment and STI selection stages are now fully automated using Manhattan Scoring and convolutional neural networks, respectively).

Chapter 5

Use of an In-House Developed Application in the Transcatheter Aortic Valve Implantation (TAVI) Cohort

Chapter 5: Use of an In-House Developed Application in the Transcatheter Aortic Valve Implantation (TAVI) Cohort

One-tailed null hypothesis: Haemodynamic alterations can be detected from pre to post-TAVI using the in-house developed application on the TAVI cohort.

One-tailed alternative hypothesis: Haemodynamic alterations cannot be detected from pre to post-TAVI using the in-house developed application on the TAVI cohort.

5.1 *Abstract*

Introduction:

It is well known that disease of the aortic valve disrupts coronary blood flow and is associated with endothelial dysfunction. Stenosis of the aortic valve has also been reported to provoke alterations of the microcirculation. Patients with severe aortic stenosis often present with chest pain in the absence of epicardial disease. These patients are often referred for TAVI, and TAVI is linked with improvements of haemodynamics. The aim of this study is to assess for systemic microvascular dysfunction by using the conjunctival microcirculation imaging tool and application before and after TAVI, as well as in a control group for comparison.

Methods:

Patients with severe aortic stenosis, referred for TAVI, were recruited to the study after fully informed consent was obtained. An ethically approved data collection questionnaire was used to record the lifestyle and patient information. The conjunctival imaging of the microcirculation was performed using the previously evaluated iPhone and slit lamp imaging system, and the corresponding video processing application.

Results:

Ninety-four severe aortic stenosis patients referred for TAVI were included in the study. The results demonstrate a significant increase in arteriolar axial/cross-sectional velocity (0.57 ± 0.12 mm/s to 0.62 ± 0.12 mm/s, p=0.006 and 0.40 ± 0.08 mm/s to 0.44 ± 0.08 mm/s, p=0.001, respectively) and wall shear rate (161 ± 71 s^{-1} to 194 ± 94 s^{-1}, p=0.019) post-TAVI. The results also suggest a significant reduction of venular wall shear stress from pre- to post-TAVI (7.98 ± 2.50 dynes/cm^2 to 6.57 ± 1.63 dynes/cm^2, p<0.001).

Conclusion:

The assessment of the TAVI cohort permitted matched and serial assessment of the conjunctival microvascular vessel parameters following treatment. Use of the ocular application for conjunctival microcirculation imaging enabled the viewing and documentation of increased axial/cross-sectional velocity and wall shear rate of arterioles, as well as a significant reduction in wall shear stress of the venules assessed from pre to post-TAVI. Future observational studies should report longer term follow-up results to better assess the potential changes in haemodynamics over time.

5.2 *Introduction*

Disease of the aortic valve is the most common valvular disease, and the only effective treatment for severe aortic stenosis is replacement of the valve (TAVI). An aging population means the already elevated incidence of severe aortic stenosis is only going to increase further. Accordingly, the incidence of coronary microvascular disease (CMD) would also increase, as coronary microvascular function has been reported to be impaired concomitant of aortic stenosis (Zhou *et al*., 2022). Konst *et al*. (2020) refer to this microvascular function impairment as type 2 CMD. Although, coronary microvascular dysfunction is poorly defined in this valvular disease cohort. Consequently, screening, risk prediction and the potential ability to tailor treatment and management of the disease becomes ever more important. We previously and systemically demonstrated alterations in the conjunctival microvasculature of patients with epicardial vascular disease (Brennan *et al*., 2021a). Therefore, this study seeks to systemically assess the microvasculature within this valvular disease cohort of severe aortic stenosis patients referred for TAVI, non-invasively, using the conjunctival microcirculation imaging tool.

5.3 *Methods*

The key inclusion criteria for the TAVI cohort included that the subjects had to have been referred for TAVI as a result of having severe aortic stenosis. Exclusion criteria included an inability to consent. The blood samples were collected, and the conjunctival microcirculation of the participants were imaged at pre-assessment or

just prior to TAVI. Post-TAVI images of the conjunctival microcirculation were again collected at least 4 hours post procedure. This was to allow comparison of the conjunctival haemodynamic parameters between pre and post-TAVI for the severe aortic stenosis patients. A study was also undertaken to assess the same vessel segments, where possible, from pre- to post-TAVI. Control patients who were ≥60 years old without aortic stenosis were also recruited. The conjunctival microcirculation of these subjects was also imaged using the smartphone and slit lamp imaging system and corresponding processing application, to enable comparisons between the severe aortic stenosis patients and a control group.

Statistical Analysis:

Data collected from the data collection questionnaire, the ocular examination and blood sample results were recorded within a secure and encrypted database. All analyses were performed using IBM SPSS version 27. Normality was assessed using the Kolmogorov-Smirnov test. The means, standard deviations and 95% confidence intervals (CI) were calculated for continuous parametric variables. Categorical variables were presented as frequencies and percentages. Differences between pre and post and controls vs TAVI ocular parameters and blood biomarkers were assessed using Mann-Whitney U test. Differences between categorial variables from pre to post TAVI, or between the control and TAVI groups were assessed using the chi squared (χ^2) test.

5.4 *Results*

Cohort Baseline Characteristics:

A total of 94 patients were recruited to the TAVI cohort, 42 male and 52 females. The mean age of this cohort was 78.7 ± 6.2 years. The mean BMI was overweight at 27.7 ± 5.4 kg/m², with the mean height being 1.64 ± 0.10 m and the mean weight at 74.8 ± 17.6 kg. The mean systolic blood pressure was pre-hypertensive at 135.8 ± 20.5 mmHg, and the mean diastolic blood pressure was 68.9 ± 12.2 mmHg. The mean heart rate was within normal limits (60-100 bpm) at 75.0 ± 12.5 bpm, and the resting oxygen saturation was also within normal limits (95-100%) at 97.4 ± 1.6%.

A total of 49 participants were recruited to the control group for comparison. A further 36 older pressure wire negative patients were also considered within the control cohort for comparison, and hence 85 participants were included in the TAVI control group. Although baseline characteristics between the two cohorts were similar, the age of the control group was significantly younger than the TAVI group (78.7 ± 6.2 years vs 82.1 ± 5.9 years, respectively, $p<0.001$). Heart rate was also significantly increased in the TAVI cohort (75.0 ± 12.5 bpm) compared to controls (70.3 ± 12.6 bpm, $p<0.007$). Additionally, alcohol intake was significantly increased for controls (3.5 ± 6.9 units per week) compared to the TAVI cohort (1.1 ± 4.2 units per week, $p=0.001$). The baseline characteristics are presented in Table 5.1.

Table 5.1. TAVI cohort characteristics

Patient Characteristic	**TAVI Controls n= 85**	**95% CI**	**TAVI n= 94**	**95% CI**	***p value**
Age (years)	78.7 ± 6.2	77.3-80.0	82.1 ± 5.9	80.9-83.3	**<0.001**
Gender (no. (%) male)	41 (48.2)	n/a	42 (44.7)	n/a	0.634 $
Handedness (no. (%) right)	80 (94.12)	n/a	91 (96.81)	n/a	0.384 $
Height (cm)	165.8 ± 9.2	163.8-167.8	163.7 ± 10.2	161.6-165.8	0.164
Weight (kg)	78.4 ± 17.2	74.7-82.1	74.8 ± 17.6	71.2-78.5	0.156
Body Mass Index (BMI) (kg/m^2)	28.5 ± 5.5	27.3-29.6	27.7 ± 5.4	26.6-28.8	0.337
Clinical					
Mean Systolic Blood Pressure (mmHg)	134.6 ± 19.5	130.4-138.8	135.8 ± 20.5	131.6-140.0	0.798
Mean Diastolic Blood Pressure (mmHg)	70.4 ± 9.6	68.4-72.5	68.9 ± 12.2	66.4-71.4	0.229
Systolic Blood Pressure SD	6.0 ± 6.3	4.6-7.4	5.8 ± 5.9	4.6-7.0	0.832
Heart Rate (bpm)	70.3 ± 12.6	67.6-73.0	75.0 ± 12.5	72.4-77.5	**0.007**

Resting Oxygen Saturation (%)	97.4 ± 1.7	97.0-98.0	97.4 ± 1.6	97.1-97.7	0.782
Temperature (°C)	36.1 ± 0.5	36.0-36.3	36.2 ± 0.5	36.0-36.3	0.51
Risk Factor					
Smoking Years	11.6 ± 17.8	7.8-15.5	14.2 ± 22.2	9.6-18.8	0.616
Number Cigarettes per Day	5.9 ± 9.3	3.9-7.9	5.9 ± 9.0	4.0-7.7	0.908
Years Since Stopped Smoking	6.1 ± 11.6	3.5-8.6	7.7 ± 14.8	4.6-10.7	0.645
Smoking Pack Years	9.7 ± 16.4	6.1-13.2	11.2 ± 21.4	6.8-15.6	0.818
Alcohol Intake days/week	0.9 ± 1.8	0.6-1.3	0.4 ± 1.4	0.1-0.7	**0.001**
Units Alcohol per Week	3.5 ± 6.9	2.0-5.0	1.1 ± 4.2	0.3-2.0	**0.001**
Days Exercise per Week	1.9 ± 2.8	1.3-2.5	1.7 ± 3.0	1.1-2.3	0.281
Smoking History (yes (%))	30 (35.3)	n/a	35 (37.2)	n/a	0.788 $
Exercise (yes (%))	31 (36.5)	n/a	24 (25.5)	n/a	0.113 $
*Mann-Whitney U test, $ Chi-squared test.					

Comorbidities:

Peripheral vascular disease (control= 3.5% vs TAVI= 13.8%, p=0.016), renal disease (control= 36.5% vs TAVI= 59.6%, p=0.002) and heart failure (control= 3.5% vs

TAVI= 37.2%, p<0.001) were significantly increased in the TAVI cohort compared to the controls. Ischemic heart disease (IHD) (control= 51.8% vs TAVI= 28.7%, p=0.002) and a family history of heart disease were more common in the control cohort (control= 25.9% vs TAVI= 9.6%, p=0.004). There were more controls with a pacemaker implanted when compared to the TAVI cohort (control= 25.9% vs TAVI= 9.6%, p=0.004). These results are recorded in Table 5.2.

Table 5.2. TAVI cohort comorbidities

Comorbidities (Frequency (% yes))	**Controls n= 85**	**TAVI n= 94**	***p value**
Hypertension	57 (67.1)	61 (64.9)	0.76
Diabetes	27 (31.8)	28 (29.8)	0.775
COPD	9 (10.6)	9 (9.6)	0.822
Hypercholesterolaemia	60 (70.6)	60 (63.8)	0.337
IHD	44 (51.8)	27 (28.7)	**0.002**
Previous MI >90days	13 (15.3)	13 (13.8)	0.781
Heart Failure	3 (3.5)	35 (37.2)	**<0.001**
Previous PCI	22 (25.9)	24 (25.5)	0.957
Stroke	9 (10.6)	5 (5.3)	0.19
TIA	8 (9.4)	11 (11.7)	0.619
AF	31 (36.5)	27 (28.7)	0.269
AF TYPE Type 1= PAF Type 2= Permanent	11 (12.9)=type 1, 20 (23.5)=type 2	13 (13.8)=type 1, 14 (14.9) =type 2	

PPM	22 (25.9)	9 (9.6)	**0.004**
PVD	3 (3.5)	13 (13.8)	**0.016**
CKD	31 (36.5)	56 (59.6)	**0.002**
VTE	2 (2.4)	3 (3.2)	0.734
Bronchiectasis	2 (2.4)	3 (3.2)	0.734
PF	0	1 (1.1)	0.34
RA	1 (1.2)	3 (3.2)	0.362
Family History (Frequency (% yes))			
Cancer	7 (8.2)	14 (14.9)	0.353
Diabetes	3 (3.5)	6 (6.4)	0.383
Heart Disease	22 (25.9)	9 (9.6)	**0.004**
Stroke	9 (10.6)	4 (4.3)	0.103
Alzheimer's	0	1 (1.1)	0.34
Parkinson's	1 (1.2)	0	0.292

Abbreviations:

*AF= Atrial Fibrillation, CKD= Chronic Kidney Disease, COPD= Chronic Obstructive Pulmonary Disorder, IHD= Ischemic Heart Disease, MI= Myocardial Infarction, PAF= Paroxysmal Atrial Fibrillation, PCI= Percutaneous Coronary Intervention, PF= Pulmonary Fibrosis, PPM= Permanent Pacemaker, PVD= Peripheral Vascular Disease, RA= Rheumatoid Arthritis, TIA= Transient Ischemic Attack, VTE= Venous Thromboembolism. *Chi-squared.*

Medications:

Medications were also similar between the TAVI and control cohort, as shown in Table 5.3. However, more TAVI patients were on P2YI2 inhibitors (controls= 12.9% vs TAVI= 28.7%, p=0.01), angiotensin converting enzyme (ACE) inhibitors (controls= 36.5% vs TAVI= 17.0%, p=0.003) and loop diuretics (controls= 27.1% vs TAVI= 47.9%, p=0.04) than controls. Additionally, more controls were on ranolazine (controls= 5.9% vs TAVI= 0%, p=0.017), nicorandil (controls= 3.5% vs TAVI= 0%, p=0.066), nitrates (controls= 24.7% vs 0%, p<0.001) and statins (controls= 75.3% vs TAVI= 60.6%, p=0.036) than the TAVI patients.

Table 5.3. TAVI cohort medications

Medications (Frequency (% yes))	**Controls n= 85**	**TAVI n= 94**	***p value**
Aspirin	49 (57.7)	37 (39.4)	0.378
P2YI2 inhibitor	11 (12.9)	27 (28.7)	**0.01**
Warfarin	0	2 (2.1)	0.176
NOAC	33 (38.8)	33 (35.1)	0.607
ACE	31 (36.5)	16 (17.0)	**0.003**
ARB	17 (20.0)	14 (14.9)	0.367
MRA	1 (1.2)	3 (3.2)	0.362
SGLT2 Inhibitor	4 (4.7)	5 (5.3)	0.851
Beta Blocker	48 (56.5)	53 (56.4)	0.991
Ca-Channel Blocker	31 (36.5)	24 (25.5)	0.113

Thiazide-like Diuretic	8 (9.4)	7 (7.5)	0.636
Loop Diuretic	23 (27.1)	45 (47.9)	**0.04**
Alpha Blocker	18 (21.2)	16 (17.0)	0.479
Ranolazine	5 (5.9)	0	**0.017**
Nicorandil	3 (3.5)	0	0.066
Nitrate	21 (24.7)	0	**<0.001**
Statin	64 (75.3)	57 (60.6)	**0.036**
Cholesterol absorption inhibitor	3 (3.5)	3 (3.2)	0.9
Abbreviations: *ACE= Angiotensin-Converting Enzyme, ARB= Angiotensin Receptor Blocker, Ca= Calcium, MRA= Mineralocorticoid Receptor Antagonist, NOAC= Non-vitamin K antagonist oral anticoagulant, SGLT2= Sodium-Glucose Cotransporter-2. *Chi-squared.*			

Blood Biomarkers: TAVI vs Controls

Significant differences between the control and the TAVI cohort respectively, were found for the following mean blood biomarkers; urea (7.19 ± 3.10 mmol/L vs 8.02 ± 2.88 mmol/L, p=0.01), creatinine (94.56 ± 46.53 µmol/L vs 102.46 ± 39.97 µmol/L, p=0.025), creatinine clearance (calculated using the Cockcroft-Gault formula (Péquignot et al., 2009)) which was reduced for both cohorts but significantly reduced for the TAVI cohort compared to controls (68.90 ± 21.59 mL/min vs 56.48 ± 20.14 mL/min, p<0.001), haematocrit (HCT) (0.39 ± 0.04 L/L vs 0.37 ± 0.05 L/L, p=0.045), N-terminal pro B-type natriuretic peptide (NTproBNP) results were elevated for both cohorts but significantly increased in the TAVI cohort (1071.45 ± 2533.35 ng/L vs 2531.16 ± 3510.94 ng/L, p<0.001), total cholesterol (3.55 ± 0.82

mmol/L vs 4.15 ± 1.07 mmol/L, p=0.001), high density lipoprotein (HDL) (1.30 ± 0.36 mmol/L vs 1.42 ± 0.40 mmol/L, p=0.044), low density lipoprotein (LDL) (1.60 ± 0.64 mmol/L vs 2.12 ± 0.92 mmol/L, p=0.001), non-HDL (2.23 ± 0.68 mmol/L vs 2.73 ± 0.96 mmol/L, p=0.001), activated partial thromboplastin time (APTT) was significantly reduced to a low level in the TAVI cohort (30.67 ± 14.11 s vs 26.24 ± 4.98 s, p=0.008), fibrinogen (3.67 ± 0.90 g/L vs 4.00 ± 0.96 g/L, p=0.031) and urate (0.32 ± 0.09 mmol/L vs 0.39 ± 0.12 mmol/L, p=0.006).

However, no significant differences were reported for haemoglobin A1C (HbA1C) and both cohort means were pre-diabetic (43.77 ± 9.89 mmol/mol vs 44.13 ± 12.95 mmol/mol, p=0.327), sodium (139.12 ± 3.27 mmol/L vs 138.86 ± 2.97 mmol/L, p=0.569), potassium (4.35 ± 0.42 mmol/L vs 4.41 ± 0.42 mmol/L, p=0.569), haemoglobin (HGB) (128.59 ± 14.24 g/L vs 124.98 ± 16.72 g/L, p=0.193), white cell count (WCC) (7.16 ± 1.71 vs 7.24 ± 2.25, p=0.791), platelet count (234.52 ± 74.24 vs 233.31 ± 74.99, p=0.913), mean corpuscular volume (MCV) (90.59 ± 5.88 fl vs 89.38 ± 6.72 fl, p=0.17), triglyceride (1.43 ± 0.67 mmol/L vs 1.36 ± 0.74 mmol/L, p=0.313), cholesterol:HDL ratio (2.85 ± 0.72 vs 3.04 ± 0.87, p=0.153), prothrombin time (11.92 ± 1.53 s vs 12.21 ± 1.91 s, p=0.388) and C-reactive protein (CRP) (4.23 ± 5.98 mg/L vs 6.21 ± 9.36 mg/L, p=0.064). These results are reported in Table 5.4.

Table 5.4. TAVI cohort blood biomarkers

Blood Biomarkers	**TAVI Controls n= 85**	**95% CI**	**TAVI n= 94**	**95% CI**	***p value**

HbA1C mmol per mol	43.77 ± 9.89	41.56-45.99	44.13 ± 12.95	41.38-46.87	0.327
Sodium mmol per L	139.12 ± 3.27	138.41-139.82	138.86 ± 2.97	138.25-139.47	0.569
Potassium mmol per L	4.35 ± 0.42	4.26-4.44	4.41 ± 0.42	4.33-4.50	0.474
Urea mmol per L	7.19 ± 3.10	6.52-7.86	8.02 ± 2.88	7.43-8.61	**0.01**
Creatinine µmol per L	94.56 ± 46.53	84.53-104.60	102.46 ± 39.97	94.27-110.64	**0.025**
Creatinine (Formula mg per L)	1.07 ± 0.53	0.96-1.81	1.16 ± 0.45	1.07-1.25	**0.025**
Creatinine Clearance mL per min	68.90 ± 21.58	54.71-62.69	56.48 ± 20.14	44.52-51.52	**<0.001**
HGB g per L	128.59 ± 14.24	125.52-131.66	124.98 ± 16.72	121.55-128.40	0.193
Haematocrit L per L	0.39 ± 0.04	0.38-0.40	0.37 ± 0.05	0.36-0.38	**0.045**
White cell count	7.16 ± 1.71	6.79-7.53	7.24 ± 2.25	6.78-7.70	0.791
Platelet count	234.52 ± 74.24	218.51-250.53	233.31 ± 74.99	217.95-248.67	0.913

MCV fl	90.59 ± 5.88	89.32-91.86	89.38 ± 6.72	88.01-90.76	0.17
NtproBNP ng per L	1071.45 ± 2533.35	438.64-1704.26	2531.16 ± 3510.94	1812.05-3250.27	**<0.001**
Total Cholesterol mmol per L	3.55 ± 0.82	3.35-3.74	4.15 ± 1.07	3.92-4.37	**0.001**
Triglyceride mmol per L	1.43 ± 0.67	1.28-1.59	1.36 ± 0.74	1.20-1.51	0.313
HDL mmol per L	1.30 ± 0.36	1.21-1.38	1.42 ± 0.40	1.34-1.50	**0.044**
LDL mmol per L	1.60 ± 0.64	1.45-1.75	2.12 ± 0.92	1.93-2.31	**0.001**
Non-HDL mmol per L	2.23 ± 0.68	2.07-2.38	2.73 ± 0.96	2.53-2.93	**0.001**
Cholesterol: HDL Ratio	2.85 ± 0.72	2.68-3.02	3.04 ± 0.87	2.87-3.23	0.153
Prothrombin Time secs	11.92 ± 1.53	11.51-12.51	12.21 ± 1.91	11.81-12.61	0.388
APTT secs	30.67 ± 14.11	26.18-35.10	26.24 ± 4.98	25.19-27.28	**0.008**
Fibrinogen g per L	3.67 ± 0.90	3.37-3.96	4.00 ± 0.96	3.80-4.20	**0.031**
Urate mmol per L	0.32 ± 0.09	0.29-0.35	0.39 ± 0.12	0.36-0.41	**0.006**

CRP mg per L	4.23 ± 5.98	2.61-6.41	6.21 ± 9.36	4.26-8.15	0.064

Abbreviations:

*APTT= Activated Partial Thromboplastin Time, CRP= C-Reactive Protein, HbA1C= Haemoglobin A1C, HGB= Haemoglobin, HDL= High Density Lipoprotein, LDL= Low Density Lipoprotein, MCV= Mean Corpuscular Volume, NtproBNP= N-terminal Pro-Brain type Natriuretic Peptide. *Mann-Whitney U test.*

TAVI Pre vs Post:

Significant differences were also reported when comparing blood biomarkers pre- and post-TAVI respectively; sodium (138.86 ± 2.97 mmol/L vs 137.42 ± 3.08 mmol/L, p=0.002), potassium (4.41 ± 0.42 mmol/L vs 4.21 ± 0.43 mmol/L, p=0.001), creatinine clearance (48.02 ± 17.08 mL/min vs 57.20 ± 19.41 mL/min, p<0.001), HGB which was significantly reduced to low levels post-TAVI (124.98 ± 16.72 g/L vs 115.57 ± 15.96 g/L, p<0.001), HCT (0.37 ± 0.05 L/L vs 0.35 ± 0.04 L/L p<0.001), WCC (7.24 ± 2.25 vs 8.97 ± 3.17, p<0.001), platelet count (233.31 ± 74.99 vs 193.90 ± 63.41, p<0.001), CRP significantly increased to high levels post-TAVI (6.20 ± 9.36 mg/L vs 15.57 ± 13.09 mg/L, p<0.001) and prothrombin time (12.21 ± 1.91 s vs 12.80 ± 2.11 s, p=0.023). No significant differences were reported for MCV (89.38 ± 6.72 fl vs 89.41 ± 6.62 fl, p=0.991), APTT (26.23 ± 4.98 s vs 27.98 ± 9.66 s, p=0.186), fibrinogen (4.00 ± 0.96 g/L vs 3.89 ± 0.93 g/L, p=0.429) or plasma viscosity (1.75 ± 0.16 mPa vs 1.72 ± 0.17 mPa, p=0.197). Although, the mean plasma viscosity result was reduced to the upper limits of the normal reference range post-TAVI. The results of the pre vs post-TAVI biomarker analysis are presented in Table 5.6.

Table 5.6. TAVI: pre vs post blood biomarkers

Blood Biomarkers	**TAVI Pre n= 94**	**95% CI**	**TAVI Post n= 94**	**95% CI**	***p value**
Sodium mmol per L	138.86 ± 2.97	136.79-138.06	137.42 ± 3.08	138.25-139.47	**0.002**
Potassium mmol per L	4.41 ± 0.42	4.13-4.30	4.21 ± 0.43	4.33-4.50	**0.001**
Urea mmol per L	8.02 ± 2.88	6.81-7.99	7.40 ± 2.86	7.43-8.61	0.105
Creatinine µmol per L	102.46 ± 39.97	92.75-113.17	102.96 ± 49.31	94.27-110.64	0.735
Formula mg per L	1.16 ± 0.45	1.05-1.28	1.16 ± 0.56	11.07-1.25	0.681
Creatinine Clearance mL per min	48.02 ± 17.08	53.16-61.25	57.20 ± 19.41	44.52-51.52	**<0.001**
HGB g per L	124.98 ± 16.72	121.55-128.40	115.57 ± 15.96	112.26-118.87	**<0.001**
Haematocrit L per L	0.37 ± 0.05	0.36-0.38	0.35 ± 0.04	0.34-0.35	**<0.001**
White cell count	7.24 ± 2.25	6.78-7.70	8.97 ± 3.17	8.32-9.63	**<0.001**
Platelet count	233.31 ± 74.99	217.95-248.67	193.90 ± 63.41	180.77-207.03	**<0.001**

MCV fl	89.38 ± 6.72	88.01-90.76	89.41 ± 6.62	88.04-90.78	0.991
CRP mg per L	6.2 ± 9.36	4.26-8.15	15.57 ± 13.09	11.44-19.70	**<0.001**
Prothrombin Time secs	12.21 ± 1.91	11.81-12.61	12.80 ± 2.11	12.33-13.26	**0.023**
APTT secs	26.23 ± 4.98	25.19-27.28	27.98 ± 9.66	25.84-30.11	0.186
Fibrinogen g per L	4 ± 0.96	3.80-4.20	3.89 ± 0.93	3.69-4.10	0.429
Plasma Viscosity mPa	1.75 ± 0.16	1.71-1.78	1.72 ± 0.17	1.68-1.75	0.197
Abbreviations: *APTT= Activated Partial Thromboplastin Time, CRP= C-Reactive Protein, HGB= Haemoglobin, MCV= Mean Corpuscular Volume. *Mann-Whitney U test.*					

Ocular Parameters; TAVI vs Controls

No significant differences were found between the severe aortic stenosis TAVI cohort and the controls for the following ocular parameters; diameter, axial velocity, cross sectional velocity, blood flow rate or wall shear rate, as demonstrated in Table 5.7. The results of the vessel segment analysis are provided in Table S4.

Table 5.7. TAVI cohort ocular parameters

Overall Comparison	**TAVI Controls n= 85 patients**	**95% CI**	**TAVI n= 94 patients**	**95% CI**	***p value**
Mean Diameter(D) µm	25.32 ± 2.66	24.75-25.90	25.52 ± 3.60	24.77-26.26	0.806
Mean Axial Velocity(Va) mm/s	0.55 ± 0.05	0.54-0.56	0.56 ± 0.06	0.55-0.57	0.312
Mean Cross Sectional Velocity(CSV) mm/s	0.38 ± 0.04	0.38-0.39	0.39 ± 0.04	0.38-0.40	0.388
Mean Blood Flow Rate(Q) pl/s	211 ± 49	201-222	219 ± 65	205-232	0.513
Mean Wall Shear Rate(WSR) s^{-1}	138 ± 27	133-144	139 ± 27	133-144	0.739
Arteriole					
Mean Diameter(D) µm	22.90 ± 5.72	21.58-24.23	23.15 ± 6.04	21.79-24.51	0.621
Mean Axial Velocity(Va) mm/s	0.57 ± 0.11	0.55-0.60	0.57 ± 0.12	0.55-0.60	0.822
Mean Cross Sectional Velocity(CSV) mm/s	0.40 ± 0.08	0.38-0.42	0.40 ± 0.08	0.38-0.42	0.774
Mean Blood Flow Rate(Q) pl/s	182 ± 97	159-204	185 ± 95	163-206	0.688

Mean Wall Shear Rate(WSR) s^{-1}	160 ± 61	146-174	161 ± 71	145-177	0.661
Venule					
Mean Diameter(D) µm	25.98 ± 3.34	25.25-26.71	25.84 ± 3.90	25.03-26.64	0.651
Mean Axial Velocity(Va) mm/s	0.55 ± 0.07	0.54-0.57	0.56 ± 0.07	0.55-0.58	0.461
Mean Cross Sectional Velocity(CSV) mm/s	0.38 ± 0.05	0.37-0.39	0.39 ± 0.05	0.38-0.40	0.435
Mean Blood Flow Rate(Q) pl/s	220 ± 55	208-232	225 ± 75	210-241	0.966
Mean Wall Shear Rate(WSR) s^{-1}	135 ± 33	127-142	136 ± 31	130-143	0.582
Undifferentiated					
Mean Diameter(D) µm	23.72 ± 6.87	22.06-25.39	24.16 ± 6.98	22.43-25.89	0.679
Mean Axial Velocity(Va) mm/s	0.55 ± 0.09	0.53-0.57	0.56 ± 0.10	0.53-0.58	0.311
Mean Cross Sectional Velocity(CSV) mm/s	0.38 ± 0.07	0.37-0.40	0.39 ± 0.07	0.37-0.41	0.397
Mean Blood Flow Rate(Q) pl/s	189 ± 118	160-217	193 ± 110	166-220	0.627
Mean Wall Shear Rate(WSR) s^{-1}	147 ± 55	134-161	146 ± 54	133-160	0.939
*Mann-Whitney U test.					

TAVI Pre vs Post:

Comparisons between pre- and post-TAVI found a significant reduction in venular wall shear stress from pre- to post-TAVI respectively (7.98 ± 2.50 dynes/cm² vs 6.57 ± 1.63 dynes/cm², p<0.001), with only a slight increase in arteriolar wall shear stress (9.24 ± 4.38 dynes/cm² vs 9.61 ± 4.32 dynes/cm², p=0.521). These findings are documented in Table 5.8 and depicted in Figures 5.1 and 5.2. The vessel segment analysis results are provided in Table S5.

Contrastingly, significant increases in arteriolar wall shear rate (161 ± 71 s^{-1} vs 194 ± 94 s^{-1}, p=0.019) as well as arteriolar axial (0.57 ± 0.12 mm/s vs 0.62 ± 0.12 mm/s, p=0.006) and cross-sectional velocities (0.40 ± 0.08 mm/s vs 0.44 ± 0.08 mm/s, p=0.001) were also found post-TAVI, with only slight reductions in venular wall shear rate (136 ± 31 s^{-1} vs 130 ± 26 s^{-1}, p=0.11), axial (0.56 ± 0.07 mm/s vs 0.55 ± 0.06 mm/s, p=0.619) and cross-sectional velocity (0.39 ± 0.05 mm/s vs 0.38 ± 0.04 mm/s, p=0.506) as shown in Figures 5.3 and 5.4.

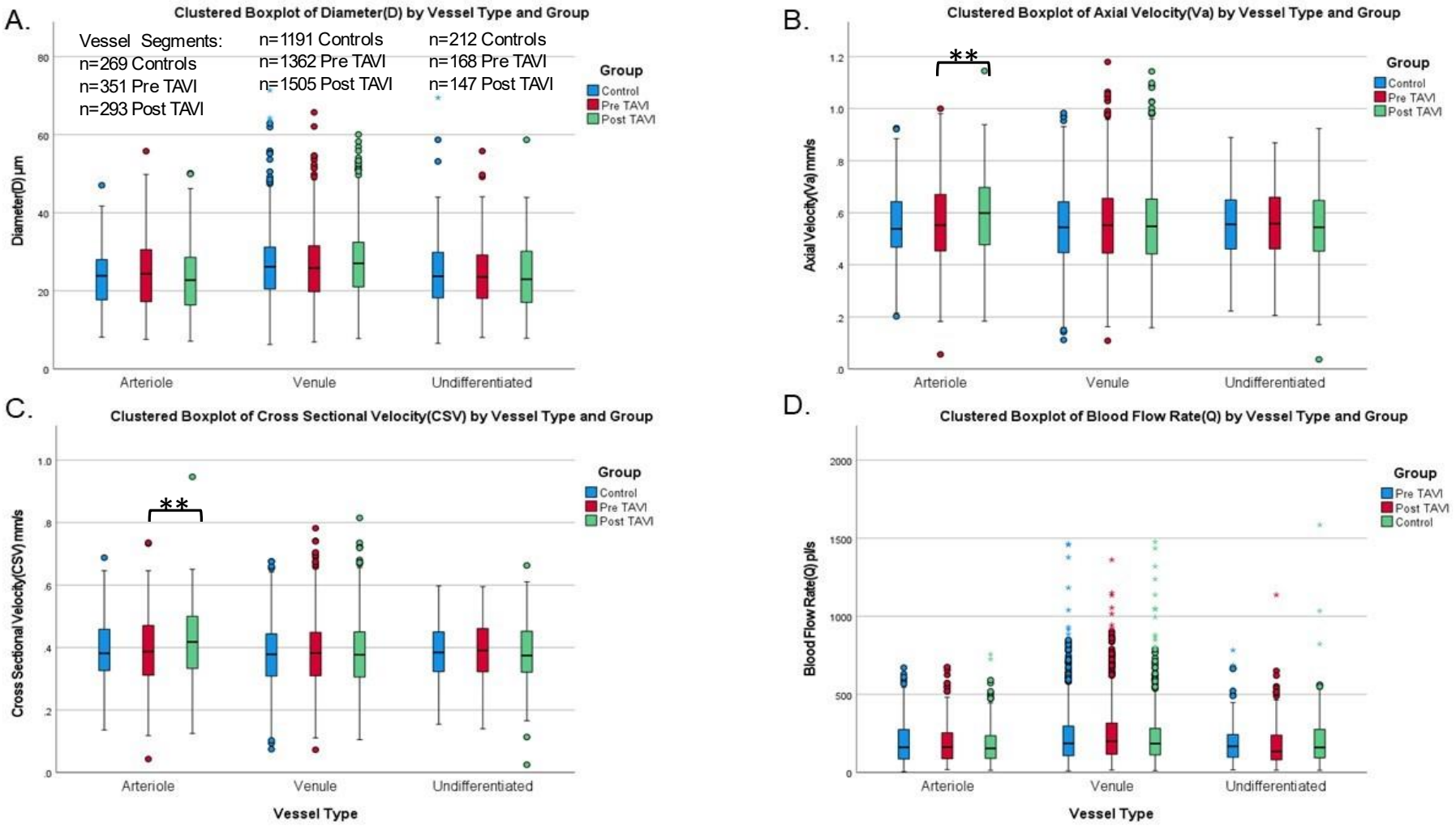

Figure 5.1. Box plot of A.) Diameter (D) µm, B.) Axial Velocity (Va) mm/s, C.) Cross-Sectional Velocity (CSV) mm/s and D.) Blood Flow Rate (Q) pl/s results for pre-TAVI, post-TAVI and control groups.

*A.) Control arterioles= 22.9±5.72 µm, venules=25.98±3.34 µm, undifferentiated=23.72±6.87 µm; Pre TAVI arterioles=23.15±6.04 µm, venules=25.84±3.90 µm, undifferentiated=24.16±6.98 µm; Post TAVI arterioles=22.22±7.28 µm, venules=26.62±3.47 µm, undifferentiated=23.80±6.46 µm. B.) Control arterioles=0.57±0.11mm/s, venules=0.55±0.07 mm/s, undifferentiated=0.55±0.09 mm/s; Pre TAVI arterioles=0.57±0.12 mm/s, venules=0.56±0.07 mm/s, undifferentiated=0.56±0.10 mm/s; Post TAVI arterioles=0.62±0.12 mm/s, venules=0.55±0.06 mm/s, undifferentiated=0.55±0.10 mm/s. C.) Control arterioles=0.40±0.08 mm/s, venules=0.38±0.05 mm/s, undifferentiated=0.38±0.07 mm/s; Pre TAVI arterioles=0.40±0.08 mm/s, venules=0.39±0.05 mm/s, undifferentiated=0.39±0.07 mm/s; Post TAVI arterioles=0.44±0.08 mm/s, venules=0.38±0.04 mm/s, undifferentiated=0.38±0.07 mm/s. D.) Control arterioles=182±97pl/s, venules=220±55pl/s, undifferentiated=189±118pl/s; Pre TAVI arterioles=185±95pl/s, venules=225±75pl/s, undifferentiated=193±110pl/s; Post TAVI arterioles=191±126pl/s, venules=233±64pl/s, undifferentiated=196±110pl/s. Mann-Whitney U test *p<0.05, **p<0.01.*

Pre-TAVI n=94, Post-TAVI n=94 and Control group n=85.

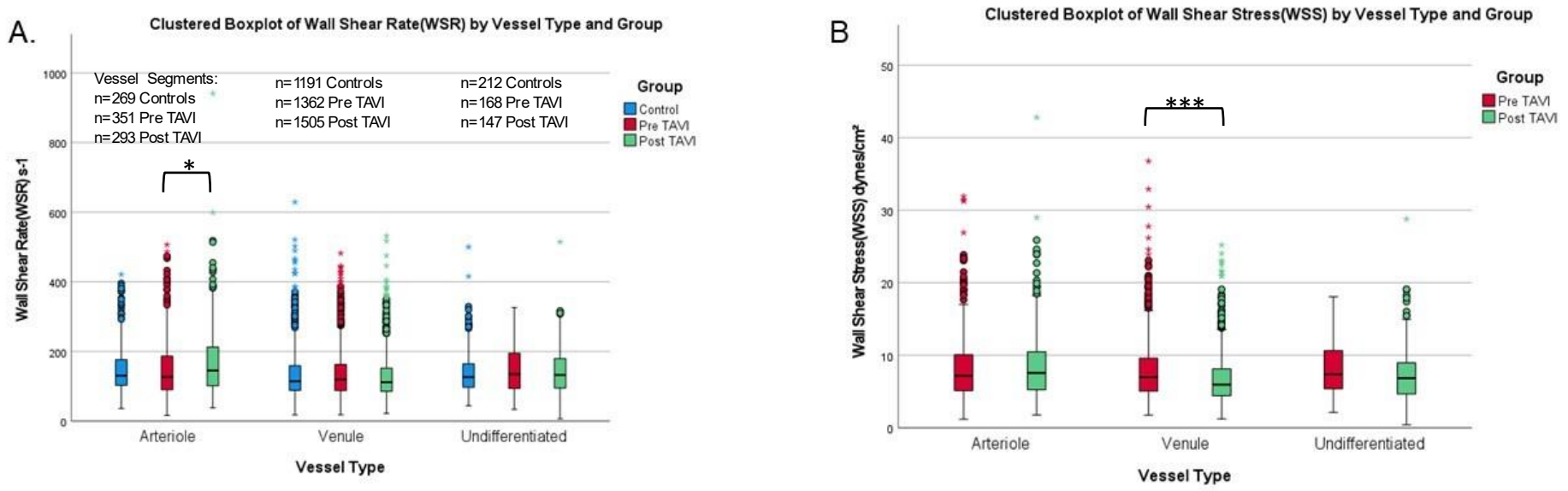

Figure 5.2. Box plot of Wall Shear Rate (WSR) s^{-1} and Wall Shear Stress (WSS) dynes/cm² results

*A.) WSR control arterioles=160±61 s^{-1}, venules=135±33 s^{-1}, undifferentiated=147±55 s^{-1}; Pre TAVI arterioles=161±71 s^{-1}, venules=136±31 s^{-1}, undifferentiated=146±54 s^{-1}; Post TAVI arterioles=194±94 s^{-1}, venules=130±26 s^{-1}, undifferentiated=147±47 s^{-1}. B.) WSS for pre-TAVI arterioles=9.24±4.38 dynes/cm², venules= 7.98±2.50 dynes/cm², undifferentiated= 8.32±3.09 dynes/cm²; Post TAVI arterioles=9.61±4.32 dynes/cm² , venules=6.57±1.63 dynes/cm², undifferentiated=7.46±2.82 dynes/cm². Mann-Whitney U test *p<0.05,***p<0.001.*

Pre-TAVI n=94, Post-TAVI n=94 and Control group n=85

Table 5.8. TAVI: pre vs post ocular parameters

Overall Comparison	**TAVI Pre n= 94 patients**	**95% CI**	**TAVI Post n= 94 patients**	**95% CI**	***p value**
Mean Diameter(D) µm	25.52 ± 3.60	24.77-26.26	25.93 ± 3.37	25.22-26.64	0.489
Mean Axial Velocity(Va) mm/s	0.56 ± 0.06	0.55-0.57	0.56 ± 0.05	0.55-0.57	0.774
Mean Cross Sectional Velocity(CSV) mm/s	0.39 ± 0.04	0.38-0.40	0.39 ± 0.04	0.38-0.40	0.821
Mean Blood Flow Rate(Q) pl/s	219 ± 65	205-232	225 ± 62	212-238	0.661
Mean Wall Shear Rate(WSR) s^{-1}	139 ± 27	133-144	138 ± 27	133-144	0.715
Mean Wall Shear Stress(WSS) dynes/cm^2	8.06 ± 2.40	7.56-8.56	6.96 ± 1.72	6.60-7.32	**0.001**
Arteriole					
Mean Diameter(D) µm	23.15 ± 6.04	21.79-24.51	22.22 ± 7.28	20.58-23.86	0.349
Mean Axial Velocity(Va) mm/s	0.57 ± 0.12	0.55-0.60	0.62 ± 0.12	0.60-0.65	**0.006**

Mean Cross Sectional Velocity(CSV) mm/s	0.40 ± 0.08	0.38-0.42	0.44 ± 0.08	0.42-0.46	**0.001**
Mean Blood Flow Rate(Q) pl/s	185 ± 95	163-206	191 ± 126	162-219	0.728
Mean Wall Shear Rate(WSR) s^{-1}	161 ± 71	145-177	194 ± 94	173-216	**0.019**
Mean Wall Shear Stress(WSS) dynes/cm²	9.24 ± 4.38	8.24-10.24	9.61 ± 4.32	8.64-10.59	0.521
Venule					
Mean Diameter(D) µm	25.84 ± 3.90	25.03-26.64	26.62 ± 3.47	25.90-27.35	0.154
Mean Axial Velocity(Va) mm/s	0.56 ± 0.07	0.55-0.58	0.55 ± 0.06	0.54-0.57	0.619
Mean Cross Sectional Velocity(CSV) mm/s	0.39 ± 0.05	0.38-0.40	0.38 ± 0.04	0.37-0.39	0.506
Mean Blood Flow Rate(Q) pl/s	225 ± 75	210-241	233 ± 64	219-246	0.402
Mean Wall Shear Rate(WSR) s^{-1}	136 ± 31	130-143	130 ± 26	124-135	0.11
Mean Wall Shear Stress(WSS) dynes/cm²	7.98 ± 2.50	7.46-8.50	6.57 ± 1.63	6.23-6.91	**<0.001**
Undifferentiated					

Mean Diameter(D) µm	24.16 ± 6.98	22.43-25.89	23.80 ± 6.46	22.07-25.53	0.876
Mean Axial Velocity(Va) mm/s	0.56 ± 0.10	0.53-0.58	0.55 ± 0.10	0.52-0.57	0.46
Mean Cross Sectional Velocity(CSV) mm/s	0.39 ± 0.07	0.37-0.41	0.38 ± 0.07	0.36-0.40	0.464
Mean Blood Flow Rate(Q) pl/s	193 ± 110	166-183	196 ± 110	166-225	0.888
Mean Wall Shear Rate(WSR) s^{-1}	146 ± 54	133-160	147 ± 47	135-160	0.763
Mean Wall Shear Stress(WSS) dynes/cm^2	8.32 ± 3.09	7.54-9.10	7.46 ± 2.82	6.70-8.21	0.166
*Mann-Whitney U test.					

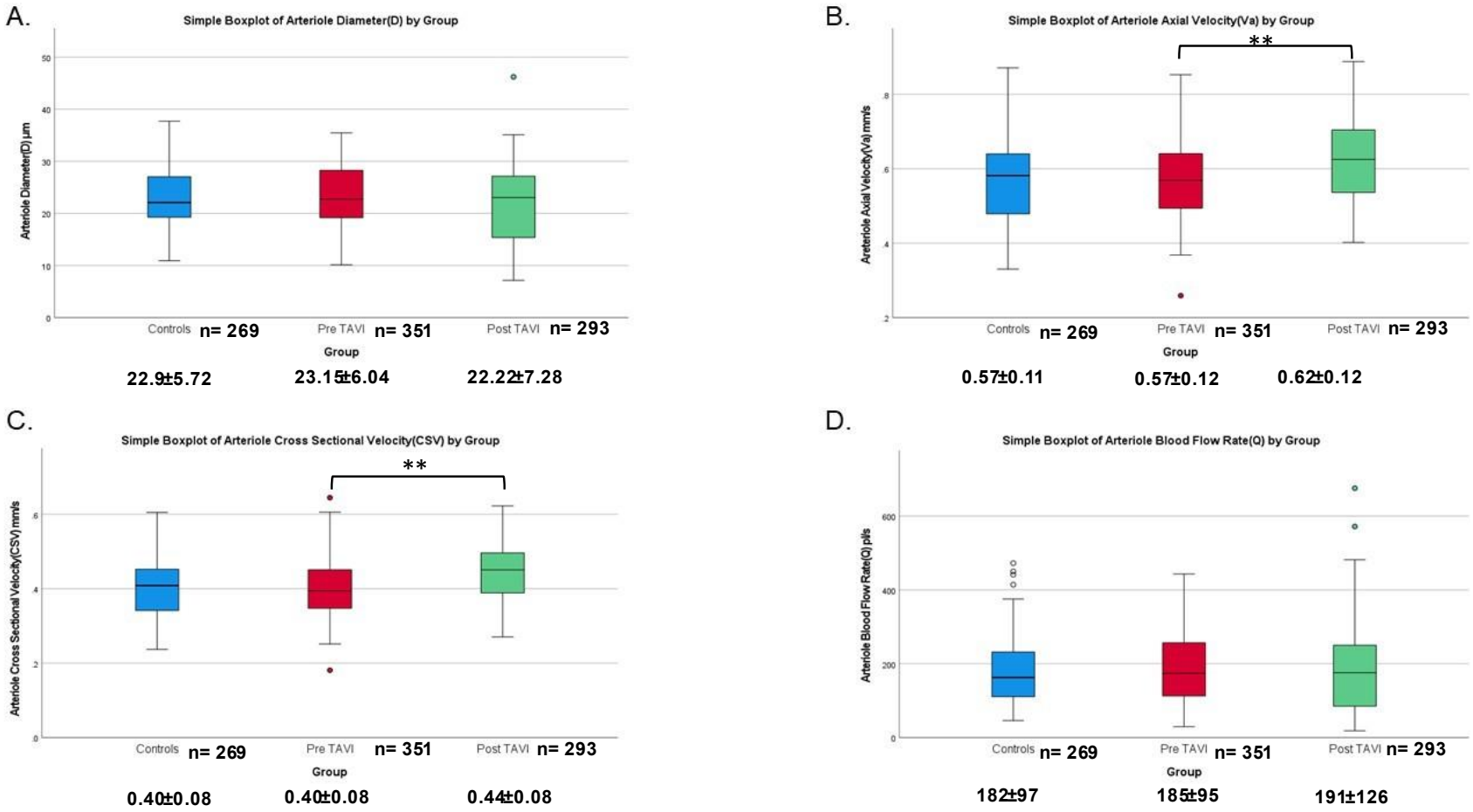

Figure 5.3. Box plot of arteriolar A.) Diameter µm, B.) Axial Velocity mm/s, C.) Cross-Sectional Velocity mm/s and D.) Blood Flow Rate pl/s results for pre-TAVI, post-TAVI and control groups. Mann-Whitney U test **p<0.05,***p<0.001.*

Pre-TAVI n=94, Post-TAVI n=94 and Controls n=85.

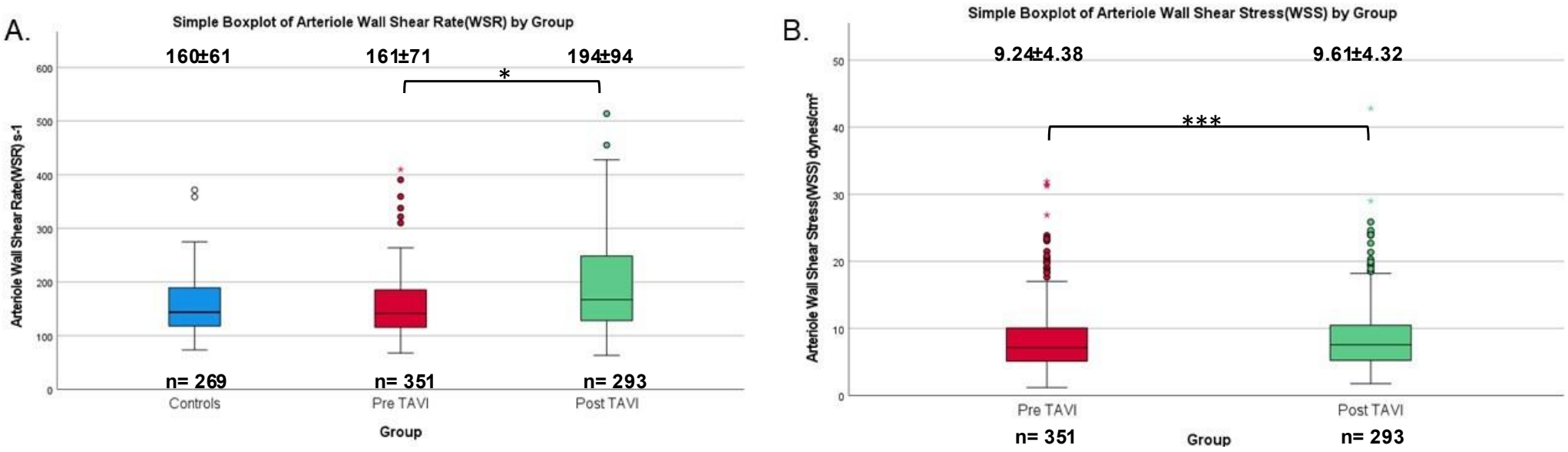

Figure 5.4. Box plot of arteriolar Wall Shear Rate (WSR) s^{-1} and Wall Shear Stress (WSS) dynes/cm²

A.) WSR s^{-1} *results for pre-TAVI, post-TAVI and control groups B.) WSS* dynes/cm² *results for pre-TAVI and post-TAVI group*

*Pre-TAVI n=94, Post-TAVI n=94 and Controls n=85. Mann-Whitney U test *p<0.05,***p<0.001.*

A total of 94 patients with severe aortic stenosis referred for TAVI were recruited to the study, but matching vessels pre- and post-TAVI were only found for 37 patients. There were 71 vessels found to match between the pre and post imaging for assessment. The baseline characteristics of the participants are presented in Table 5.9 below. The results of the ocular parameters from the conjunctival imaging pre- and post-TAVI are presented in Table 5.10. The WSS was significantly reduced from pre- to post-TAVI (7.91 ± 3.91 to 6.47 ± 2.97 dynes/cm², p=0.014) as shown in Figure 5.5. However, no further significant differences in the ocular parameters (to include diameter, axial velocity, cross-sectional velocity and wall shear rate) were reported in the matched vessel segments pre- vs post-TAVI.

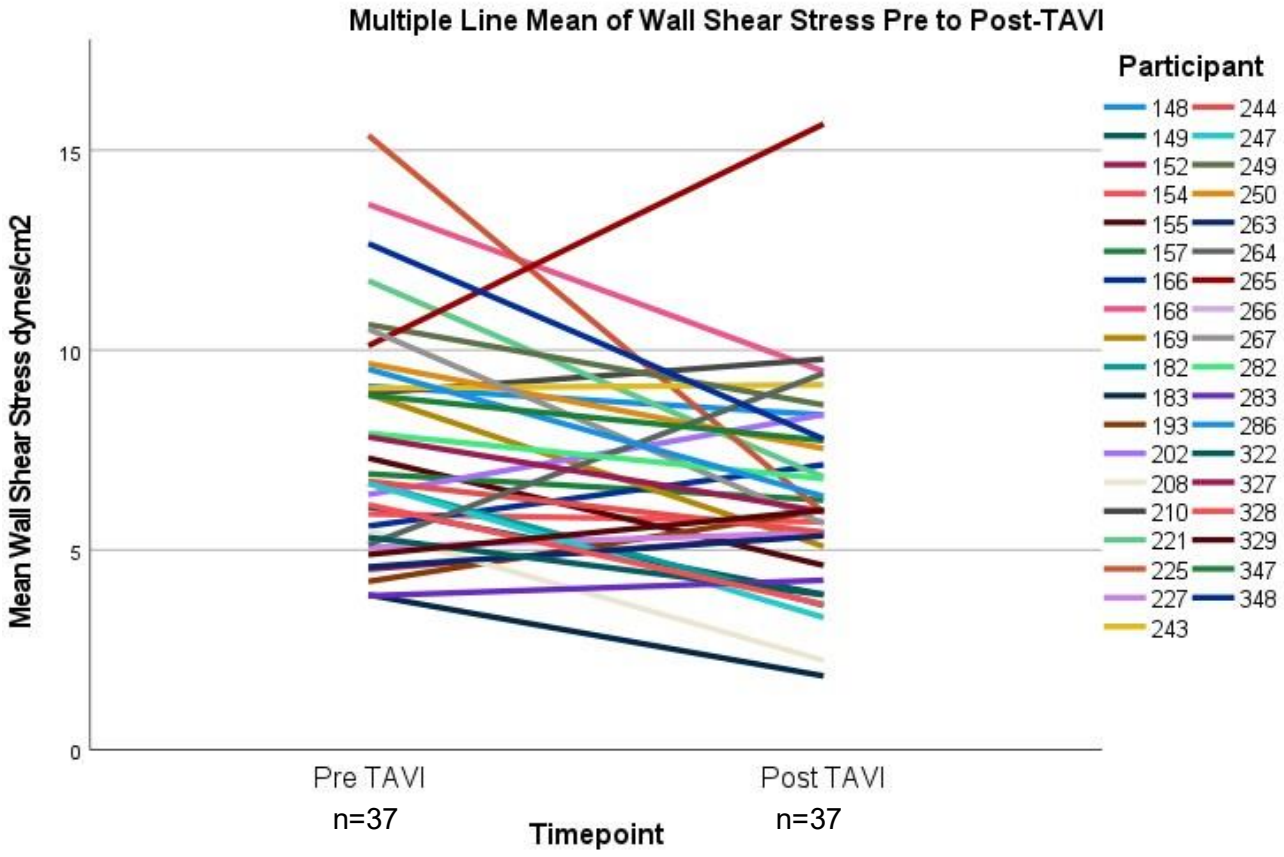

Figure 5.5. Line graph showing reduction of Wall Shear Stress (WSS) dynes/cm² from pre- to post-TAVI. *Pre- to post-TAVI n=37.*

Table 5.9. Baseline characteristics: matched vessel TAVI cohort

Characteristic	**Matched Vessel TAVI Cohort** **n=37**
Age (years)	82.0 ± 6.9
Gender (no. (%) male)	12 (32.4)
Height (m)	1.63 ± 0.10
Weight (kg)	72.3 ± 16.2
Heart Rate (bpm)	76 ± 11
Systolic Blood Pressure (mmHg)	140 ± 20
Diastolic Blood Pressure (mmHg)	70 ± 13
Medical History (no. (%) yes) Hypertension Diabetes Mellitus Hypercholesterolaemia MI Stroke TIA PVD	 23 (62.2) 11 (29.7) 25 (67.6) 2 (5.4) 3 (8.1) 3 (8.1) 6 (16.6)
Medications (no. (%) yes) Antiplatelet Anticoagulant	 27 (73.0) 10 (27.0)

ACE inhibitor ARB Beta blocker Ca-channel blocker Diuretic Statin	7 (18.9) 4 (10.8) 18 (48.6) 10 (27.0) 17 (46.0) 22 (59.5)		
Clinical Measurements	**Pre-TAVI n=37**	**Post-TAVI n=37**	***p Value**
Oxygen Saturation (%)	97.5 ± 1.8	98.1 ± 2.1	0.125
Intra-aortic Systolic Pressure (mmHg)	159.1 ± 25.7	149.5 ± 21.6	0.092
Intra-aortic Diastolic Pressure (mmHg)	63.8 ± 13.0	56.5 ± 11.3	**0.017**
Left Ventricular Ejection Fraction (%)	54.3 ± 10.6	56.8 ± 8.3	0.279
Abbreviations: *ACE= Angiotensin Converting Enzyme, ARB= Angiotensin Receptor Blocker, Ca= Calcium, MI= Myocardial Infarction, PVD= Peripheral Vascular Disease, TIA= Transient Ischemic Attack. *Mann-Whitney U test.*			

Table 5.10. Ocular parameters of the matched vessel TAVI cohort

Ocular parameter	**Pre-TAVI (severe aortic stenosis) n=71**	**Matched Post-TAVI n=71**	***p value**
Diameter (μm)	27.57 ± 8.23	28.20 ± 8.12	0.341
Axial Velocity (mm/s)	0.59 ± 0.17	0.58 ± 0.17	0.885
Cross-Sectional Velocity (mm/s)	0.40 ± 0.12	0.39 ± 0.11	0.853
Blood Flow Rate (pl/s)	259 ± 161	263 ± 155	0.911
Wall Shear Rate (s^{-1})	129 ± 57	124 ± 58	0.619
Wall Shear Stress (dynes/cm^2)	7.91 ± 3.91	6.47 ± 2.97	**0.014**
*Mann-Whitney U test.			

5.5 *Discussion (in-depth discussion continued in Chapter 8)*

Comparison of the controls against the TAVI cohort showed no significant differences between the ocular parameters. However, it was noted that the blood flow rate was markedly increased for both these groups, who were considerably older in comparison to our previous high risk cardiovascular disease (age= 57 ± 12

years, blood flow rate= 154 ± 125 pl/s) and control group (age= 53 ± 10 years, blood flow rate= 153 ± 124 pl/s) (Brennan *et al*., 2021a). This suggests that aging, or senescence, may be an important factor in determining the blood flow rate. Older age is also associated with an increased number of comorbidities and medications as demonstrated within the results. These findings are emulated in the study by Ungvari *et al*. (2010) that also indicate aging to be associated with endothelial dysfunction in the absence of other cardiovascular disease risk factors.

The blood biomarkers suggest significant differences in lipid, coagulation and inflammatory markers that may reflect atherosclerotic processes to include lipid-infiltration, inflammation and fibrosis (Phua *et al*., 2022). NTproBNP was significantly increased and may reflect the increased number of subjects in the TAVI cohort with heart failure. Biomarkers such as increased urea, creatinine and reduced creatinine clearance may also reflect the increased number of subjects in the TAVI cohort with renal disease. Creatinine clearance was found to significantly improve post-TAVI. There was still a reduction in haematocrit and haemoglobin, potentially, due to bleeding complications. Reduction in platelet count was also found, as well as an increase in white cell count, prothrombin time and CRP post-TAVI this may indicate platelet activation and a systemic thromboinflammatory response (Gallet *et al*., 2013; Kalińczuk *et al*., 2019).

The pre- vs post-TAVI study revealed the conjunctival imaging application was able to detect arteriolar improvements of axial velocity, cross-sectional velocity and wall shear rate, and reductions in venular wall shear stress. The increased axial and

cross-sectional velocity agree with findings from Camuglia *et al*. (2014) and Vendrik *et al*. (2020) that suggest immediate and long-term (6-12 months) improvement of coronary microvascular function. A reduction of venular wall shear stress may be due to thrombogenic activity associated with TAVI (Ranasinghe *et al*., 2019; Balogh *et al*., 2019; Laflamme *et al*., 2015). Reductions of wall shear stress were also found for the matched pre- vs post-TAVI vessel segments in this study. Similarly, Ishii *et al.* (2019) also found a reduction in aortic wall shear stress. A reduction of intra-aortic diastolic blood pressure was also reported post-TAVI for this cohort, and this finding reiterates results from the study by Perlman *et al*. (2013), suggesting this may be due to mild aortic regurgitation post-TAVI.

Conclusion

To the best of our knowledge, this study was the first to assess the conjunctival microcirculation of valvular disease, specifically, of severe aortic stenosis patients before and after TAVI. This study highlights the possibilities of the non-invasive conjunctival microvascular imaging tool as a means to assess microvascular function in valvular heart disease. The increased axial and cross-sectional velocity of arterioles post-TAVI demonstrates an improvement in the haemodynamics of the conjunctival microcirculation following TAVI. Future research should longitudinally assess these haemodynamic parameters.

Chapter 6

Use of an In-House Developed Application in Coronary Microvascular Disease (CMD)

Chapter 6: Use of an In-House Developed Application in Coronary Microvascular Disease (CMD)

One-tailed null hypothesis: The in-house developed application can detect alterations of the conjunctival microcirculation within the CMD cohort.

One-tailed alternative hypothesis: The in-house developed application cannot detect alterations of the conjunctival microcirculation within the CMD cohort.

6.1 *Abstract*

Introduction:

The larger epicardial coronary vessels have been extensively assessed through coronary angiography. Pathophysiology of the coronary microcirculation is not fully understood, and this may be in part due to the nature of invasive testing. Coronary microvascular dysfunction is also linked to an increased risk of cardiovascular disease. The aim of this study was to conduct non-invasive assessment of systemic microvascular dysfunction using the conjunctival microcirculation imaging application on CMD patients compared to controls.

Methods:

Patients referred for pressure wire study due to chest pain or shortness of breath, but no significant evidence of epicardial disease, were recruited to the study only after fully informed consent was obtained. Lifestyle demographics, anthropometric and clinical measurements were gathered within the data collection questionnaire. All study participants had an ocular examination, whereby the conjunctival vessels were imaged using the slit lamp and iPhone system. Collected videos were processed using the smartphone-based application. Blood samples were also collected and tested for a selection of markers to include electrolytes, lipids and inflammatory markers.

Results:

48 CMD and 68 controls were included in the study. Significant reductions of axial and cross sectional velocities (0.55 ± 0.06 mm/s to 0.53 ± 0.04 mm/s, p=0.036 and 0.38 ± 0.04 to 0.37 ± 0.03 mm/s, p=0.038, respectively) were observed within the CMD cohort. Comparably, a selection of lipid and inflammatory blood biomarkers to include NTproBNP, triglyceride and fibrinogen were also elevated in the CMD cohort.

Conclusion:

The pressure wire measurements of the coronary microvasculature may also be detected from the measurements of the conjunctival microvasculature using the app. The conjunctival vessel measurements alongside blood biomarkers such as NTproBNP, HDL, triglyceride and fibrinogen may support cardiovascular risk assessment.

6.2 *Introduction*

Coronary microvascular dysfunction is an important contributor to the pathophysiology of cardiovascular disease, but often goes undiagnosed. Presently, the gold standard diagnostic test for coronary microvascular disease (CMD) is invasive coronary function testing that exposes the patient to ionising radiation (Mileva *et al*., 2019). If microvascular dysfunction can be identified beyond the coronaries, using the non-invasive method of imaging the conjunctival microcirculation, this may have the potential to support non-invasive diagnosis of CMD, as well as augment cardiovascular risk prediction. The primary aim of this study was to compare and evaluate the haemodynamic parameters of the conjunctiva in a CMD group compared to controls, using the conjunctival imaging tool and processing application.

6.3 *Methods*

The key inclusion criteria for the pressure wire cohort included patients recruited following invasive coronary angiography investigating symptoms of angina or shortness of breath. The fractional flow reserve of all patients recruited to the study had to be ≥80. All subjects underwent a pressure wire study to investigate index of microcirculatory resistance (IMR) and coronary flow reserve (CFR). The pressure wire positive group included those with a diagnosis of CMD (IMR ≥25 or CFR <2.0). The negative pressure wire group included those without a diagnosis of CMD (IMR <25 or CFR ≥2.0). The exclusion criteria included <18 years of age, pregnant,

inability to consent, history of conjunctival inflammation or contact lens use in the 24 hours prior to recruitment, haemodynamically significant valvular heart disease, left ventricular ejection fraction <40% or previous coronary artery bypass graft (CABG). Using the smartphone and slit lamp imaging system and corresponding processing application, the conjunctival vascular imaging was conducted for both the CMD and control groups, and the clinical demographics and blood biomarkers were also tested.

Statistical Analysis:

Statistical analyses were performed using IBM SPSS v 27. Descriptive statistics (mean ± standard deviation (SD) and 95% confidence intervals (CI)) were used for parametric continuous data. Percentages were used for summarising categorical data. Chi-squared test was used to determine the association between categorical variables. Student's t-test was used to examine the differences between group means for parametric data. Where the assumptions of the Student's t-test were unmet, the Mann Whitney U test was used. Normality of continuous variables was assessed using the Kolmogorov-Smirnov test.

6.4 *Results*

Cohort Baseline Characteristics:

A total of 119 patients were recruited to the pressure wire cohort. However, 8 patients were excluded due to inaccuracies within the pressure wire measurements.

The negative pressure wire cohort consisted of 68 patients and the positive pressure wire cohort consisted of 43 patients. As recorded in Table 6.1, no significant differences in baseline characteristics were reported between the negative and positive pressure wire groups except for heart rate. Heart rate was significantly increased in the positive pressure wire group compared to the negative pressure wire group (65.2 ± 9.2 bpm vs 72.6 ± 14.3 bpm, p=0.009).

Table 6.1. Pressure wire cohort baseline characteristics

Patient Characteristic	**Pressure wire negative (Controls) n= 68 patients**	**95% CI**	**Pressure wire positive (CMD) n= 43 patients**	**95% CI**	***p value**
Age (years)	63.1 ± 9.2	60.9-65.3	66.0 ± 9.8	63.0-69.0	0.077
Gender (no. (%) male)	42 (61.8)	n/a	21 (48.8)	n/a	0.18 $
Handedness (no. (%) right)	59 (86.8)	n/a	38 (88.4)	n/a	0.52 $
Height (cm)	169.5 ± 9.4	167.3-171.8	167.7 ± 8.7	165.0-170.4	0.258
Weight (kg)	89.0 ± 20.4	84.1-94.0	82.8 ± 16.7	77.7-87.9	0.129
BMI (kg/m^2)	31.0 ± 6.8	29.3-32.6	29.4 ± 5.7	27.7-31.2	0.132
Clinical					

Mean Systolic Blood Pressure (mmHg)	125.2 ± 15.8	121.5-129.1	124.6 ± 17.0	119.3-129.8	0.58
Mean Diastolic Blood Pressure (mmHg)	72.4 ± 10.7	69.8-75.0	70.5 ± 9.6	67.6-73.5	0.635
Systolic Blood Pressure SD	8.0 ± 5.0	6.8-9.2	7.5 ± 5.7	5.7-9.2	0.325
Heart Rate (bpm)	65.2 ± 9.2	63.0-67.5	72.6 ± 14.3	68.2-77.0	**0.009**
Resting Oxygen Saturation (%)	97.2 ± 1.5	96.9-97.6	96.9 ± 1.5	96.4-97.3	0.298
Temperature (°C)	36.1 ± 0.5	36.0-36.2	36.0 ± 0.5	35.9-36.2	0.947
QRISK3 Score	18.61 ± 11.91	15.73-21.50	21.90 ± 15.84	17.02-26.77	0.333
Score of healthy person with same age, sex and ethnicity (%)	10.69 ± 6.32	9.16-12.22	12.87 ± 6.51	10.87-14.88	0.051
Relative Risk	2.21 ± 2.09	1.71-2.72	1.87 ± 1.56	1.39-2.35	0.452

Factor					
Smoking Years	14.8 ± 17.8	10.4-19.1	17.19 ± 20.4	10.9-23.5	0.619
Number Cigarettes per Day	10.6 ± 14.4	7.1-14.1	12.9 ± 17.0	7.6-18.2	0.701
Years Since Stopped Smoking	6.7 ± 11.9	3.8-5.4	7.6 ± 11.8	3.8-11.3	0.935
Smoking Pack Years	14.9 ± 23.0	9.3-20.6	21.4 ± 31.4	11.7-31.2	0.454
Alcohol Intake days/week	2.0 ± 1.6	1.5-2.5	2.6 ± 2.8	1.5-3.8	0.865
Units Alcohol per Week	11.1 ± 19.1	5.01-17.08	11.8 ± 18.8	4.2-19.4	0.556
Days Exercise per Week	2.7 ± 3.0	2.0-3.4	2.1 ± 2.8	1.2-3.0	0.271
Smoking History (yes (%))	35 (51.5)	n/a	23 (53.5)	n/a	0.836 $
Exercise (yes (%))	36 (52.9)	n/a	18 (41.9)	n/a	0.255 $
*Mann-Whitney U test, $ Chi-squared test.					

Comorbidity:

Asthma was the only comorbidity that was significantly increased in the positive pressure wire group compared to the negative (0% vs 7%, p=0.027). Family history of comorbidities was similar between the groups also, as shown in Table 6.2.

Table 6.2. Pressure wire cohort comorbidities

Comorbidities (Frequency (% yes))	**Controls n= 68**	**CMD n= 43**	***p value**
Hypertension	36 (52.9)	22 (51.2)	0.855
Diabetes	21 (30.9)	13 (30.2)	0.942
COPD	4 (5.9)	6 (14.0)	0.148
Hypercholesterolaemia	51 (75.0)	37 (86.0)	0.162
IHD	26 (38.2)	13 (30.2)	0.39
Previous MI >90days	16 (23.5)	10 (23.3)	0.974
Heart Failure	4 (5.9)	3 (7.0)	0.817
Previous PCI	25 (36.8)	13 (30.2)	0.48
Cardiac Surgery	1 (1.5)	0	0.424
Stroke	6 (8.8)	4 (9.3)	0.932
TIA	3 (4.4)	5 (11.6)	0.152
AF	6 (8.8)	8 (18.6)	0.131
PPM	0	2 (4.7)	0.073
PVD	1 (1.5)	3 (7.0)	0.129
VTE	0	1 (2.3)	0.207

Bronchiectasis	0	2 (4.7)	0.073
Asthma	0	3 (7.0)	**0.027**
Benign Prostatic Hyperplasia	2 (2.9)	0	0.256
Breast Cancer	1 (1.5)	0	0.424
Cataract	1 (1.5)	4 (9.3)	0.053
Depression	1 (1.5)	3 (7.0)	0.129
Dry Eyes	1 (1.5)	1 (2.3)	0.741
Fibromyalgia	0	1 (2.3)	0.207
Glaucoma	2 (2.9)	0	0.256
Gout	1 (1.5)	1 (2.3)	0.741
Hypothyroidism	3 (4.4)	1 (2.3)	0.566
Lymphoma	0	1 (2.3)	0.207
Migraine	0	1 (2.3)	0.207
Musculoskeletal	0	1 (2.3)	0.207
Osteoarthritis	11 (16.2)	5 (11.6)	0.506
PAF	5 (7.4)	4 (9.3)	0.714
Prostate Cancer	2 (2.9)	1 (2.3)	0.846
Psoriasis	2 (2.9)	0	0.256
Renal	9 (13.2)	7 (16.3)	0.656
Renal Calculus	1 (1.5)	0	0.424
Retinal Detachment	0	1 (2.3)	0.207
Sleep Disorder	2 (2.9)	0	0.256
Family History (Frequency (% yes))			
Cancer	9	9	0.236

Diabetes	10	6	0.912
Heart Disease	37	17	0.155
Ischemic Heart Disease	37	18	0.198
Stroke	8	8	0.318
Alzheimer's	2	1	0.846
Parkinson's	1	0	0.424

Abbreviations:

AF= Atrial Fibrillation, COPD= Chronic Obstructive Pulmonary Disorder, IHD= Ischemic Heart Disease, MI= Myocardial Infarction, PAF= Paroxysmal Atrial Fibrillation, PCI= Percutaneous Coronary Intervention, PF= Pulmonary Fibrosis, PPM= Permanent Pacemaker, PVD= Peripheral Vascular Disease, TIA= Transient Ischemic Attack, VTE= Venous Thromboembolism

**Chi-squared test.*

Medications:

Table 6.3 shows that the medications taken by the participants were similar between the two pressure wire groups, with significant differences only for anticoagulants (controls= 5% vs CMD= 9%, p=0.036) angiotensin receptor blockers (ARB) (controls= 5% vs CMD= 10%, p=0.017) and loop diuretics (controls= 2% vs CMD= 6%, p=0.029).

Table 6.3. Pressure wire cohort medications

Medications (Frequency (% yes))	**Controls n= 68**	**CMD n= 43**	***p value**
Aspirin	41 (60.3)	29 (67.4)	0.447
P2Y12 inhibitor	20 (29.4)	11 (25.6)	0.661
Anticoagulant	5 (7.4)	9 (20.9)	**0.036**
ACE	29 (42.6)	20 (46.5)	0.69
ARB	5 (7.4)	10 (23.3)	**0.017**
MRA	1 (1.5)	1 (2.3)	0.741
SGLT2 inhibitor	4 (5.9)	7 (16.3)	0.074
Beta Blocker	41 (60.3)	31 (72.1)	0.205
Ca-Channel Blocker	15 (22.1)	14 (32.6)	0.22
Thiazide diuretic	5 (7.4)	5 (11.6)	0.443
Loop diuretic	2 (2.9)	6 (14.0)	**0.029**
Other anti-hypertensive	5 (7.4)	3 (7.0)	0.94
Ranolazine	5 (7.4)	8 (18.6)	0.073
Nicorandil	3 (4.4)	4 (9.3)	0.302
Nitrate	25 (36.8)	18 (41.9)	0.591
Statin	55 (80.9)	37 (86.0)	0.482
Cholesterol absorption inhibitor	2 (2.9)	3 (7.0)	0.318

Abbreviations:

*ACE= Angiotensin-Converting Enzyme, ARB= Angiotensin Receptor Blocker, Ca= Calcium, MRA= Mineralocorticoid Receptor Antagonist, SGLT2= Sodium-Glucose Cotransporter-2. *Chi-squared test.*

Blood Biomarkers:

Comparable to the transcatheter aortic valve implantation (TAVI) controls vs the TAVI cohort, N-Terminal pro B-type natriuretic peptide (NTproBNP) was significantly increased for the pressure wire positive (CMD) group (910.00 ± 3000.54 ng/L) compared to the pressure wire negative (Control) group (199.36 ± 290.64 ng/L, p=0.01). High Density Lipoprotein (HDL) (Control= 1.20 ± 0.31 mmol/L vs CMD= 1.32 ± 0.39 mmol/L, p=0.042) and fibrinogen (Control= 3.34 ± 0.63 g/L vs CMD= 3.76 ± 0.85 g/L, p=0.016) were also significantly elevated in the positive group. However, triglyceride (Control= 1.80 ± 0.88 mmol/L vs CMD= 1.65 ± 1.51 mmol/L, p=0.046) and cholesterol:HDL (Control= 3.41 ± 1.24 vs CMD= 2.92 ± 0.70, p=0.044) were significantly reduced in the positive group.

No significant differences were found for the following biomarkers between the pressure wire negative and the pressure wire positive group respectively; glycated haemoglobin A1C (HbA1C) (44.15 ± 12.76 mmol/L vs 43.74 ± 15.80 mmol/L, p=0.381), sodium (139.06 ± 2.17 mmol/L vs 139.56 ± 2.81 mmol/L, p=0.185), potassium (4.31 ± 0.35 mmol/L vs 4.30 ± 0.41 mmol/L, p=0.413), urea (5.48 ± 1.52 mmol/L vs 5.76 ± 2.02 mmol/L, p=0.667), creatinine (84.26 ± 15.49 µmol/L vs 79.93 ± 23.66 µmol/L, p=0.057), creatinine clearance (104.60 ± 39.71 ml/min vs 99.14 ± 30.57 ml/min, p=0.73), Haemoglobin (HGB) (138.93 ± 13.57 g/L vs 137.05 ± 12.58 g/L, p=0.622), Haematocrit (HCT) (0.41 ± 0.04 L/L vs 0.41 ± 0.03 L/L, p=0.57), White Cell Count (WCC) (7.35 ± 1.71 vs 7.87 ± 2.61, p=0.584), platelet count (244.9 ± 59.39 vs 258.86 ± 65.45, p=0.361), Mean Corpuscular Volume (MCV) (88.47 ± 5.54 fl vs 89.77 ± 5.46 fl, p=0.122), total cholesterol (3.86 ± 1.08 mmol/L vs 3.74 ± 0.92 mmol/L, p=0.754), Low Density Lipoprotein (LDL) (1.86 ± 0.96 mmol/L vs 1.71 ± 0.76 mmol/L, p=0.948), non-HDL (2.67 ± 1.09 mmol/L vs 2.43 ± 0.77 mmol/L, p=0.441),

prothrombin time (11.79 ± 1.39 s vs 11.61 ± 1.08 s, p=0.57), Activated Partial Thromboplastin Time (APTT) (31.61 ± 16.70 s vs 31.51 ± 14.30 s, p=0.927), urate (0.33 ± 0.07 mmol/L vs 0.33 ± 0.08 mmol/L, p=0.567), C-Reative Protein (CRP) (2.79 ± 3.31 mg/L vs 3.61 ± 5.02 mg/L, p=0.598), plasma viscosity (1.67 ± 0.11 mPa vs 1.68 ± 0.09 mPa, p=0.443), apolipoprotein A1 (1.39 ± 0.25 g/L vs 1.42 ± 0.24 g/L, p=0.215) and apolipoprotein B (0.79 ± 0.28 g/L vs 0.75 ± 0.16 g/L, p=0.977). Table 6.4 presents the blood biomarker results of the CMD group compared to the controls.

Table 6.4. Pressure wire cohort blood biomarkers

Blood Biomarkers	**Controls n= 68**	**95% CI**	**CMD n= 43**	**95% CI**	***p value**
HbA1C mmol per L	44.15 ± 12.76	41.06-47.24	43.74 ± 15.80	38.82-48.66	0.381
Sodium mmol per L	139.06 ± 2.17	138.53-139.58	139.56 ± 2.81	138.69-140.42	0.185
Potassium mmol per L	4.31 ± 0.35	4.22-4.39	4.30 ± 0.41	4.17-4.42	0.413
Urea mmol per L	5.48 ± 1.52	5.11-5.85	5.76 ± 2.02	5.14-6.38	0.667
Creatinine µmol per L	84.26 ± 15.49	80.52-88.01	79.93 ± 23.66	72.65-87.21	0.057
Formula mg per L	0.95 ± 0.18	0.91-1.0	0.90 ± 0.27	0.82-0.99	0.057

Creatinine Clearance mL per min	104.60 ± 39.71	94.99-114.21	99.14 ± 30.57	89.73-108.55	0.73
HGB g per L	138.93 ± 13.57	135.64-142.21	137.05 ± 12.58	133.17-140.92	0.622
Haematocrit L per L	0.41 ± 0.04	0.40-0.42	0.41 ± 0.03	0.40-0.42	0.57
White cell count	7.35 ± 1.71	6.94-7.77	7.87 ± 2.61	7.07-8.68	0.584
Platelet count	244.9 ± 59.39	230.52-259.27	258.86 ± 65.45	238.72-279.00	0.361
MCV fl	88.47 ± 5.54	87.13-89.81	89.77 ± 5.46	88.09-91.45	0.122
NtproBNP ng per L	199.36 ± 290.64	126.76-271.96	910.00 ± 3000.54	25.03-1845.03	**0.01**
Total Cholesterol mmol per L	3.86 ± 1.08	3.59-4.12	3.74 ± 0.92	3.46-4.02	0.754
Triglyceride mmol per L	1.80 ± 0.88	1.58-2.00	1.65 ± 1.51	1.19-2.12	**0.046**
HDL mmol per L	1.20 ± 0.31	1.12-1.27	1.32 ± 0.39	1.21-1.43	**0.042**
LDL mmol per L	1.86 ± 0.96	1.63-1.80	1.71 ± 0.76	1.48-1.95	0.948

NonHDL mmol per L	2.67 ± 1.09	2.40-2.94	2.43 ± 0.77	2.19-2.66	0.441
Cholesterol:HDL Ratio	3.41 ± 1.24	3.11-3.71	2.92 ± 0.70	2.71-3.14	**0.044**
Prothrombin Time secs	11.79 ± 1.39	11.43-12.14	11.61 ± 1.08	11.25-11.97	0.57
APTT secs	31.61 ± 16.70	27.34-35.89	31.51 ± 14.30	26.74-36.27	0.927
Fibrinogen g per L	3.34 ± 0.63	3.17-3.50	3.76 ± 0.85	3.48-4.05	**0.016**
Urate mmol per L	0.33 ± 0.07	0.31-0.35	0.33 ± 0.08	0.30-0.35	0.567
CRP mg per L	2.79 ± 3.31	1.97-3.61	3.61 ± 5.02	2.05-5.17	0.598
Plasma Viscosity mPa	1.67 ± 0.11	1.65-1.70	1.68 ± 0.09	1.65-1.71	0.443
Apolipoprotein A1 g per L	1.39 ± 0.25	1.32-1.45	1.42 ± 0.24	1.35-1.50	0.215
Apolipoprotein B g per L	0.79 ± 0.28	0.72-0.86	0.75 ± 0.16	0.70-0.80	0.977

Abbreviations:

APTT= Activated Partial Thromboplastin Time, CRP= C-Reactive Protein, HbA1C= Haemoglobin A1C, HGB= Haemoglobin, HDL= High Density Lipoprotein, LDL=

*Low Density Lipoprotein, MCV= Mean Corpuscular Volume, NtproBNP= N-terminal Pro-Brain type Natriuretic Peptide. *Mann-Whitney U test.*

Ocular Parameters of the Pressure Wire Negative Group vs the Pressure Wire Positive Group:

As shown in Table 6.5 and by Figure 6.1, mean axial and cross-sectional velocity were significantly reduced in the pressure wire positive group compared to the pressure wire negative group (mean axial velocity; Control= 0.55 ± 0.06 mm/s vs CMD= 0.53 ± 0.04 mm/s, p=0.036, mean cross-sectional velocity; Control= 0.38 ± 0.04 mm/s vs CMD= 0.37 ± 0.03 mm/s, p=0.038). Figure 6.2 illustrates the results of mean diameter, blood flow rate, wall shear rate and wall shear stress. The results of the vessel differentiation show that this difference may be largely due to the venules (mean axial velocity; Control venules= 0.55 ± 0.07 mm/s vs CMD venules= 0.53 ± 0.05 mm/s, p=0.042, mean cross-sectional velocity; Control venules= 0.38 ± 0.05 mm/s vs CMD venules= 0.37 ± 0.03 mm/s p=0.044) as shown by Figure 6.3. Figure 6.4 shows the vessel differentiation results for diameter, blood flow rate, wall shear rate and wall shear stress. The results of the vessel segment analysis are provided in Table S6.

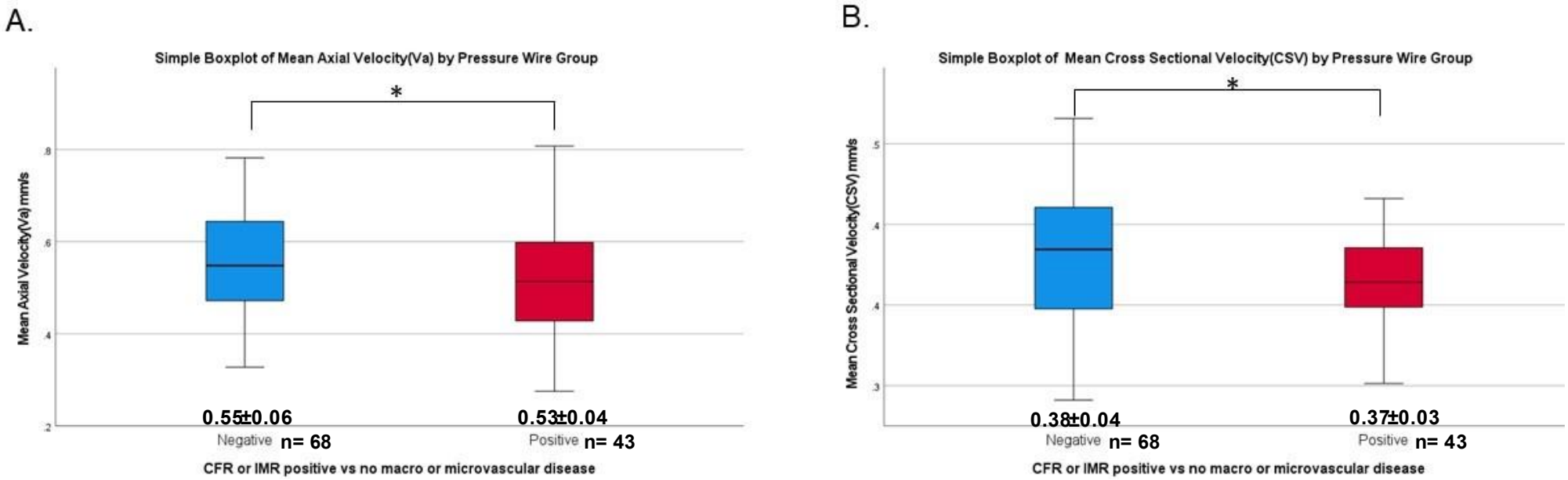

Figure 6.1. Box plot of A.) Axial Velocity mm/s (p=0.036) and B.) Cross-Sectional Velocity mm/s (p=0.038) results for negative (controls) versus positive (CMD) pressure wire groups

*Controls n=68 and CMD n=43. Mann-Whitney U test *p<0.05.*

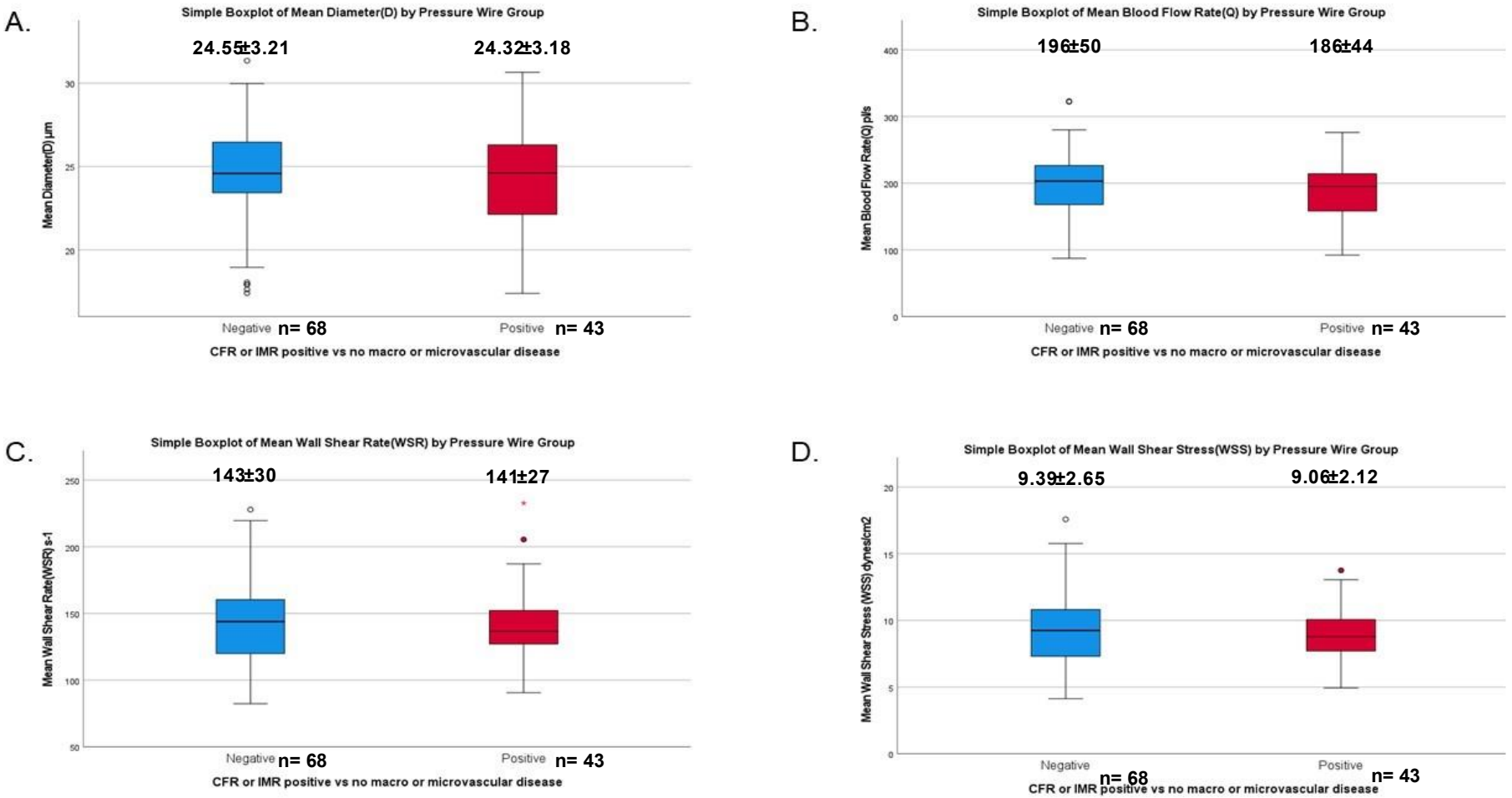

Figure 6.2. Box plot of A.) Diameter µm (p=0.59), B.) Blood Flow Rate pl/s (p=0.287), C.) Wall Shear Rate s^{-1} (p=0.624) and D.) Wall Shear Stress dynes/cm² (p=0.057) results for negative (controls) versus positive (CMD) pressure wire group. *Controls n= 68 and CMD n=43. *Mann-Whitney U test.*

Table 6.5. Pressure wire cohort ocular parameters

Overall Comparison	**Controls n= 68 patients**	**95% CI**	**CMD n= 43 patients**	**95% CI**	***p value**
Mean Diameter(D) µm	24.55 ± 3.21	23.77-25.33	24.32 ± 3.18	23.34-25.30	0.59
Mean Axial Velocity(Va) mm/s	0.55 ± 0.06	0.53-0.56	0.53 ± 0.04	0.51-0.54	**0.036**
Mean Cross Sectional Velocity(CSV) mm/s	0.38 ± 0.04	0.37-0.39	0.37 ± 0.03	0.36-0.38	**0.038**
Mean Blood Flow Rate(Q) pl/s	196 ± 50	184-208	186 ± 44	172-199	0.287
Mean Wall Shear Rate(WSR) s^{-1}	143 ± 30	136-150	141 ± 27	132-149	0.624
Mean Wall Shear Stress(WSS) dynes/cm^2	9.39 ± 2.65	8.75-10.03	9.06 ± 2.12	8.40-9.71	0.557

Arteriole					
Mean Diameter(D) µm	21.56 ± 6.39	19.78-23.34	20.78 ± 5.15	19.09-22.47	0.311
Mean Axial Velocity(Va) mm/s	0.55 ± 0.12	0.52-0.59	0.53 ± 0.12	0.49-0.57	0.285
Mean Cross Sectional Velocity(CSV) mm/s	0.39 ± 0.08	0.37-0.42	0.37 ± 0.09	0.35-0.40	0.327
Mean Blood Flow Rate(Q) pl/s	156 ± 91	131-181	142 ± 82	115-169	0.369
Mean Wall Shear Rate(WSR) s^{-1}	171 ± 84	148-195	164 ± 62	143-184	0.922
Mean Wall Shear Stress(WSS) dynes/cm^2	11.18 ± 5.45	9.67-12.70	10.52 ± 3.74	9.29-11.75	0.941
Venule					

Mean Diameter(D) µm	25.08 ± 3.55	24.20-25.95	25.24 ± 4.00	24.00-26.49	0.777
Mean Axial Velocity(Va) mm/s	0.55 ± 0.07	0.54-0.57	0.53 ± 0.05	0.52-0.55	**0.042**
Mean Cross Sectional Velocity(CSV) mm/s	0.38 ± 0.05	0.37-0.40	0.37 ± 0.03	0.36-0.38	**0.044**
Mean Blood Flow Rate(Q) pl/s	204 ± 56	191-218	200 ± 54	183-217	0.835
Mean Wall Shear Rate(WSR) s^{-1}	139 ± 33	131-147	138 ± 33	127-148	0.715
Mean Wall Shear Stress(WSS) dynes/cm^2	9.10 ± 2.63	8.45-9.75	8.93 ± 2.36	8.20-9.66	0.738
Undifferentiated					
Mean Diameter(D) µm	23.73 ± 6.57	21.88-25.58	21.69 ± 4.20	20.15-23.23	0.137

Mean Axial Velocity(Va) mm/s	0.55 ± 0.08	0.53-0.57	0.51 ± 0.09	0.48-0.55	0.099
Mean Cross Sectional Velocity(CSV) mm/s	0.39 ± 0.06	0.37-0.40	0.36 ± 0.06	0.34-0.38	0.182
Mean Blood Flow Rate(Q) pl/s	192 ± 118	159-225	147 ± 65	123-171	0.055
Mean Wall Shear Rate(WSR) s^{-1}	150 ± 51	136-164	147 ± 43	131-163	0.981
Mean Wall Shear Stress(WSS) dynes/cm^2	9.92 ± 3.62	8.90-10.94	9.35 ± 2.84	8.31-10.39	0.643
*Mann-Whitney U test.					

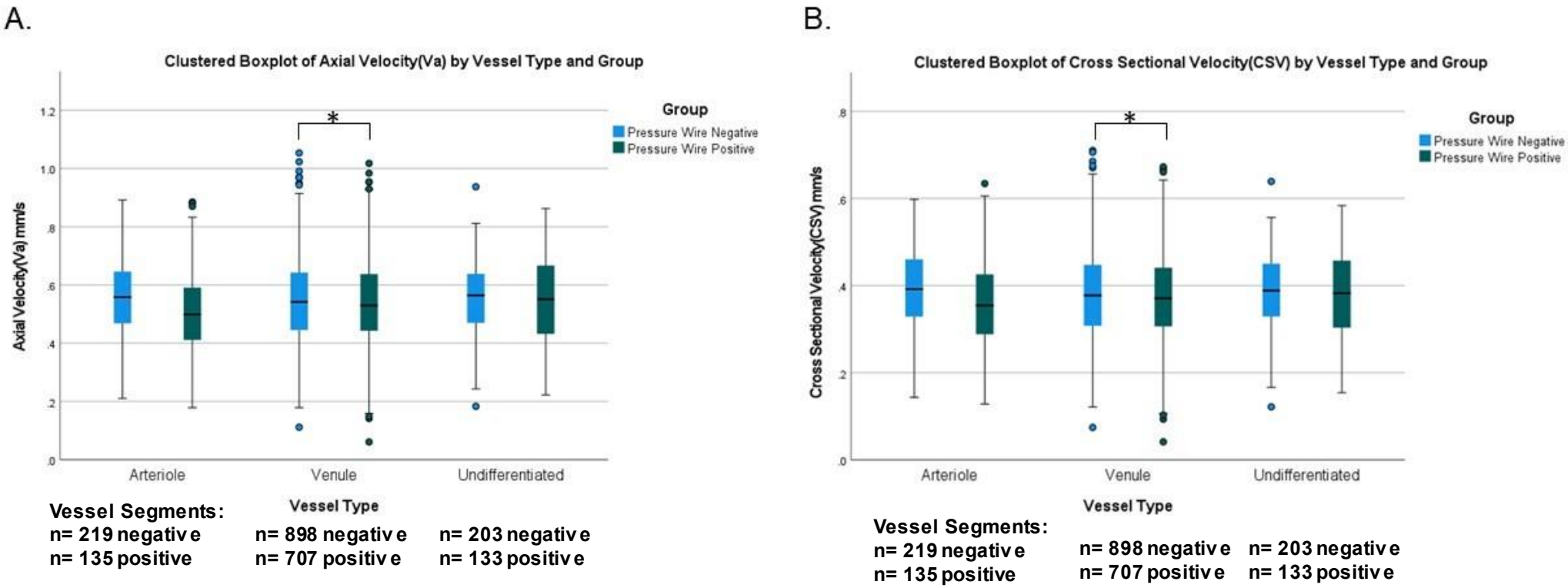

Figure 6.3. Vessel differentiation of A.) Axial Velocity (Va) mm/s and B.) Cross-Sectional Velocity (CSV) mm/s for negative (controls) versus positive (CMD) pressure wire groups. *Mann-Whitney U test.

A.) Arteriole Pressure Wire Negative=0.55±0.12mm/s, Venule Pressure Wire Negative=0.55±0.07mm/s, Undifferentiated Pressure Wire Negative=0.55±0.08mm/s; Arteriole Pressure Wire Positive=0.53±0.12mm/s, Venule Pressure Wire Positive=0.53±0.05mm/s,

*Undifferentiated Pressure Wire Positive=0.51±0.09mm/s. B.) Arteriole Pressure Wire Negative=0.39±0.08mm/s, Venule Pressure Wire Negative=0.38±0.05mm/s, Undifferentiated Pressure Wire Negative=0.39±0.06mm/s; Arteriole Pressure Wire Positive=0.37±0.09mm/s, Venule Pressure Wire Positive=0.37±0.03mm/s, Undifferentiated Pressure Wire Positive=0.36±0.06mm/s. Controls n=68 and CMD n=43. *p<0.05.*

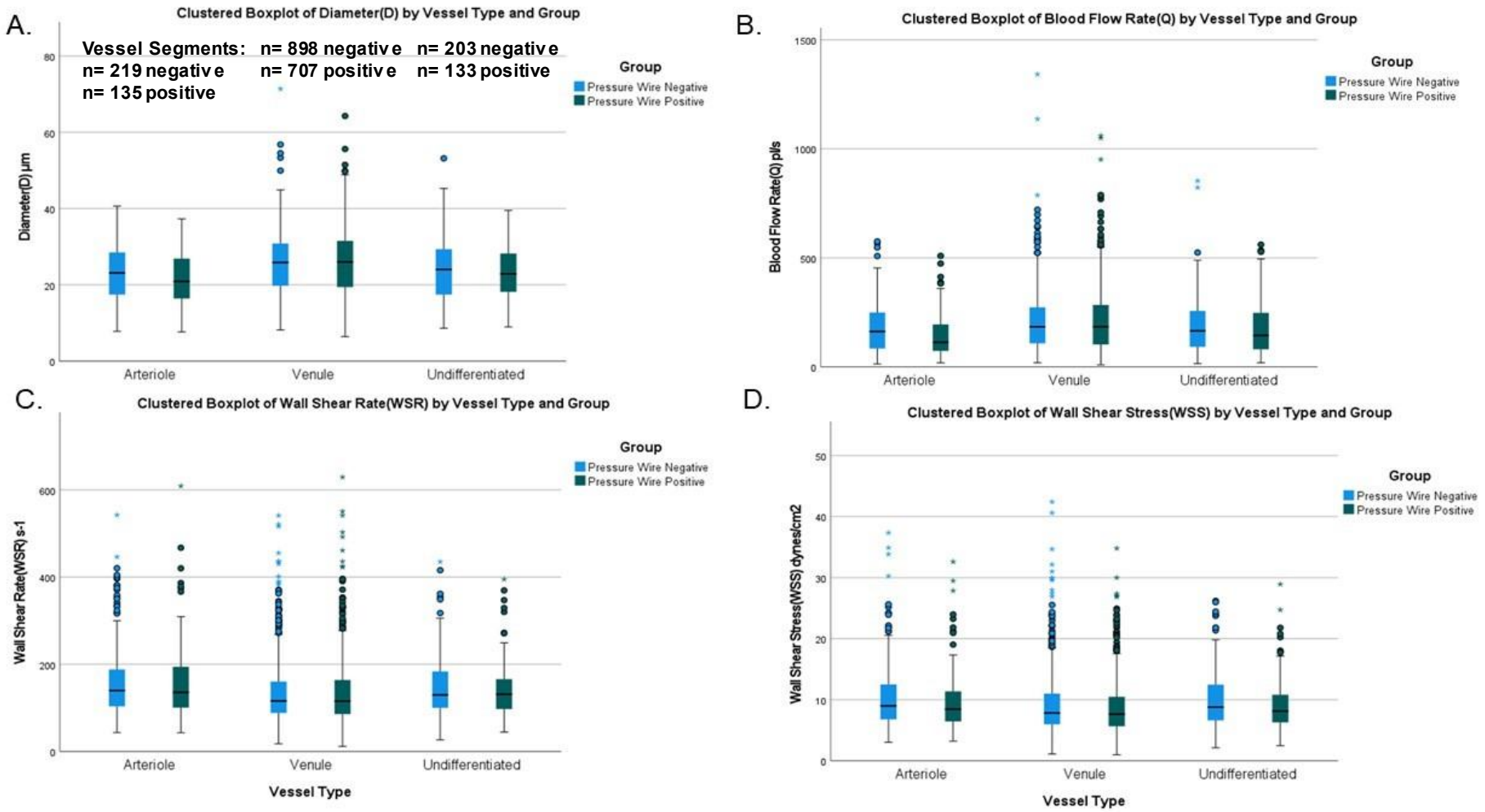

Figure 6.4. Vessel differentiation of A.) Diameter (D) µm, B.) Blood Flow Rate (Q) pl/s, C.) Wall Shear Rate (WSR) s^{-1} and D.) Wall Shear Stress (WSS) dynes/cm² for negative (controls) versus positive (CMD) pressure wire groups. *Controls n=68 and CMD n=43.*

*A.) Arteriole Pressure Wire Negative=21.36±6.31µm, Venule Pressure Wire Negative=25.08±3.55µm, Undifferentiated Pressure Wire Negative=23.73±6.57µm, Arteriole Pressure Wire Positive=20.78±5.15µm, Venule Pressure Wire Positive=25.24±400µm, Undifferentiated Pressure Wire Positive=21.69±4.20µm; B.) Arteriole Pressure Wire Negative=156±91pl/s, Venule Pressure Wire Negative=204±56 pl/s, Undifferentiated Pressure Wire Negative=192±118 pl/s, Arteriole Pressure Wire Positive=142±82 pl/s, Venule Pressure Wire Positive=200±54 pl/s, Undifferentiated Pressure Wire Positive=147±65 pl/s; C.) Arteriole Pressure Wire Negative=171±84s^{-1}, Venule Pressure Wire Negative=139±33s^{-1}, Undifferentiated Pressure Wire Negative=150±51s^{-1}, Arteriole Pressure Wire Positive=164±62s^{-1}, Venule Pressure Wire Positive=138±33s^{-1}, Undifferentiated Pressure Wire Positive=147±43s^{-1}; D.) Arteriole Pressure Wire Negative=11.18±5.45dynes/cm², Venule Pressure Wire Negative=9.1±2.63 dynes/cm², Undifferentiated Pressure Wire Negative=9.92±3.62 dynes/cm², Arteriole Pressure Wire Positive=10.52±3.74 dynes/cm², Venule Pressure Wire Positive=8.93±2.36 dynes/cm², Undifferentiated Pressure Wire Positive=9.35±2.84 dynes/cm². *Mann-Whitney U test.*

6.5 *Discussion (in-depth discussion continued in Chapter 8)*

The finding of increased heart rate in the CMD compared to the control group agrees with the study by Haider *et al*. (2019) that reports a significantly higher baseline heart rate in patients with abnormal coronary flow reserve ($p<0.001$). Similarly, the number of subjects with a history of asthma was increased in the CMD group, and it is possible that this may have been a cofounding factor. Tikhonova *et al*. (2015) found alterations of the blood flow oscillations in subjects with asthma compared to the control group.

In this study, the biomarkers that showed significant differences between the CMD and control groups included NTproBNP, HDL, triglyceride and Fibrinogen. A recent study by Östlund-Papadogeorgos also demonstrated a correlation between NTproBNP levels and CMD. However, the evidence is mixed with Jones *et al*. (2014) suggesting no correlation between NTproBNP levels and CMD in a study of 224 women. Therefore, future larger studies may be required to investigate this relationship. A study by Liu *et al*. (2020) reports similar results to the study presented here, supporting the use of the biomarker triglyceride as a sub-clinical marker of myocardial injury. Lastly, fibrinogen has also previously been reported in the study by Lassé *et al*. (2021) to be a potential predictor of cardiovascular risk.

Expectedly, as based on the results of the earlier studies of this project, this study also found overall reductions of wall shear stress, axial velocity and cross-sectional velocity using the conjunctival imaging tool and processing application. This is also

the first study with results to suggest alterations of conjunctival microvascular function reflect those of coronary microvascular function. The results suggest the finding of a reduction in axial/cross-sectional velocity is more prevalent in venules, but this may be due to the conjunctival vasculature consisting of more venules. A review by Feuer *et al*. (2022) proposes that alterations in microvascular function are reflective of systemic pathophysiology.

Limitations:

Except for angiotensin receptor blockers (ARB) and loop diuretics used to treat high blood pressure, and anticoagulants, used to reduce the risk of blood clots, no significant differences in medications were reported between the groups. In-depth analysis of the effect of these medications showed no significant association with the conjunctival microcirculation parameters of axial/cross-sectional velocity or wall shear stress.

Conclusion

The findings presented in this study support the hypothesis that alterations in the coronary microcirculation may also be identified beyond the coronaries, in the conjunctival microcirculation, due to systemic microvascular dysfunction. This study imparts substantiating evidence and pre-clinical data on the efficacy of this pre-clinical application to predict microvascular disease.

Chapter 7

Haemodynamics and Risk Scoring

Chapter 7: Haemodynamics and Risk Scoring

One-tailed null hypothesis: The conjunctival microcirculation is a target for risk stratification, and haemodynamic alterations can be detected between healthy and cardiovascular disease groups using the in-house developed application.

One-tailed alternative hypothesis: The conjunctival microcirculation is not a target for risk stratification, and haemodynamic alterations cannot be detected between healthy and cardiovascular disease groups using the in-house developed application.

7.1 *Abstract*

Introduction:

Conjunctival haemodynamic parameters may be influenced by structural changes such as with cardiac remodeling, or with electrical changes such as with arrhythmia or pacing. Additionally, increased inter-arm blood pressure differences have been associated with increased cardiovascular disease risk. Inter-eye differences of the conjunctival microcirculation have not been assessed before. This study aims to firstly, investigate comorbidities associated with cardiac remodeling and rhythms that

may alter conjunctival haemodynamics, and secondly, identify factors such as inter-eye differences that may augment cardiovascular risk prediction.

Methods:

To investigate cardiac remodeling the ocular parameters of the coronary microvascular disease (CMD), diabetes mellitus (DM) and heart failure (HF) groups were compared along with a control group. The controls cohort included subjects with no history of DM, HF, hypertension, hypercholesterolemia, myocardial infarction, stroke, transient ischemic attack, peripheral vascular disease, cyanotic congenital heart disease or aortic stenosis. The CMD group comprised of all individuals from the entire dataset with CMD but no history of DM or HF, likewise, the DM group consisted of all the individuals with DM but no CMD or HF and the HF group consisted of all the individuals with HF. To investigate the impact of rhythm on the conjunctival haemodynamics, an atrial fibrillation group and a paced group of subjects were also compared to controls. Similarly, the atrial fibrillation group included all individuals with atrial fibrillation within the entire dataset, and the paced group contained all individuals known to have a paced heart rhythm. The inter-eye study compared the inter-eye ocular parameter differences of the entire CMD (pressure wire positive) group to that of the control (pressure wire negative) group. To identify factors that may augment risk prediction, binary logistic regression analysis was performed to identify the best predictor variables of the full database (consisting of 407 subjects classed into the high risk cardiovascular disease group or the control group). Lastly, this control group was stratified by QRISK3 score and the ocular parameters were compared.

Results:

Wall shear rate was significantly reduced for CMD, DM and HF compared to controls. The area under the curve (AUC) for CMD=0.772, DM=0.686 and HF=0.729. Wall shear rate was also significantly reduced in the paced group compared to controls (147 ± 31 s^{-1} vs 132 ± 22 s^{-1} p=0.027). For the atrial fibrillation group, all ocular parameters assessed, except for wall shear rate, were significantly increased ($p<0.05$). Inter-eye differences were increased in the CMD group compared to controls. Full database analysis found the best predictors of cardiovascular risk classification to be heart rate, axial velocity, N-terminal pro B-type natriuretic peptide (NTproBNP) and fibrinogen with an AUC=0.899. QRISK3 score stratification of the controls also detected significant differences in ocular parameters between the low, moderate and high risk classes.

Conclusion:

The findings suggest that conjunctival haemodynamics are influenced by both alterations of cardiac structure and rhythm. Conjunctival haemodynamic parameters measured using the conjunctival imaging tool and application to include inter-eye differences, as well as other biomarkers such as heart rate, NTproBNP and fibrinogen may have utility in a multi-biomarker approach to support cardiovascular risk prediction.

7.2 *Introduction*

Both structural and electrical changes may impact haemodynamic parameters and cardiovascular risk. Therefore, this study aims to assess ocular parameter differences in groups of patients where cardiac remodeling may occur to include CMD (microvascular remodeling), DM (metabolic-related remodeling) and HF often occurring consequent to cardiac remodeling. The study also aims to assess the differences of groups of patients with electrical changes to include atrial fibrillation and paced groups. Inter-eye differences were also investigated for the CMD group. To better assess cardiovascular risk, the full database of ocular parameters for 407 subjects is considered within the cardiovascular disease and control cohorts they were recruited to. Lastly, the controls are stratified by QRISK3 score and the ocular parameters defined for a low (<10), moderate (10-20) or high QRISK3 score (>20).

7.3 *Methods*

This multi-cohort study quantitatively assesses the conjunctival microcirculation using the conjunctival imaging tool and processing application. The cohorts investigated included controls, patients referred for pressure wire with non-obstructive coronary arteries but a resulting index of microvascular resistance (IMR) ≥25 or coronary flow reserve (CFR) <2.0 (CMD group), patients with known DM, HF, atrial fibrillation and those with a paced heart rhythm. Fully informed consent was obtained from participants prior to enrolment in the study. Participants were recruited at the Royal Victoria Hospital, Belfast, UK between January 2018 and March 2022

(Integrated Research Application System study number 166742). The study conformed to Good Clinical Practice and the Declaration of Helsinki.

Statistical Analysis:

Normality was tested using the Kolmogorov-Smirnov test. Continuous variables were presented as mean ± standard deviation (SD). A one-way analysis of variance (ANOVA) comparison with Games Howell post hoc was used to assess the difference between groups of continuous variables. Categorical variables were presented as number (%). The Chi-Square test with post hoc testing (adjusted standardised residuals and Bonferroni correction) was used to assess the difference between categorical variables. To assess the mean inter-eye difference the mean results for each patient were calculated for each field of view, and the left side was subtracted from the right. Binary logistic regression (using forward wald, backward wald and forced entry) was carried out to assess for cardiovascular disease risk predictor variables, and receiver operator characteristic (ROC) curves were generated.

7.4 *Results*

Cardiac Remodeling:

The controls cohort included 47 individuals with no history of DM, HF, hypertension (HTN), hypercholesterolemia (HCL), myocardial infarction (MI), stroke, transient ischemic attack (TIA), peripheral vascular disease (PVD), cyanotic congenital heart disease (CCHD) or aortic stenosis (AS). The CMD cohort included 29 individuals

with no diagnosis of DM or HF. The DM cohort included 67 individuals with no diagnosis of CMD or HF. The HF group included 55 individuals. Within the HF cohort, 2 individuals had co-existing CMD and 18 individuals had co-existing DM. The baseline characteristics and ocular results for each cohort are presented in Tables 7.1 and 7.2 below.

Table 7.1. Cardiac remodeling cohorts: baseline characteristics

Characteristic	**Control (n=47)**	**CMD (n=29)**	**DM (n=67)**	**HF (n=55)**	***p value**
Age (years)	54.46 ± 14.3	65.59 ± 9.1	70.48 ± 13.3	70.55 ± 18.1	**<0.001**
Gender (no., (%) male)	31 (68.9)	14 (48.3)	44 (65.7)	32 (58.2)	0.353 $
Height (m)	1.68 ± 0.1	1.68 ± 0.1	1.68 ± 0.1	1.68 ± 0.1	0.965
Weight (kg)	76.5 ± 19	77.4 ± 13	87.1 ± 22	78.9 ± 17	**0.013**
Heart Rate (bpm)	70 ± 10	69 ± 12	72 ± 12	75 ± 13	**0.042**
Systolic Blood Pressure (mmHg)	129 ± 18	127 ± 18	130 ± 16	125 ± 18	0.528
Diastolic Blood Pressure (mmHg)	75 ± 10	71 ± 9	70 ± 9	68 ± 11	**0.008**

Medical History (no., (%))	N/a				
HTN		12 (41.4)	45 (67.2)	37 (67.3)	**<0.001 $**
HCL		24 (82.8)	52 (77.6)	36 (65.5)	**<0.001 $**
MI		5 (17.2)	10 (14.9)	14 (25.5)	**0.004 $**
Stroke		2 (6.9)	6 (9.0)	3 (5.5)	0.227 $
TIA		1 (3.5)	5 (7.5)	8 (14.6)	**0.031 $**
PVD		1 (3.5)	3 (4.5)	9 (16.4)	**0.005 $**
CCHD		0	0	7 (12.7)	**<0.001 $**
AS		0	16 (23.9)	35 (63.6)	**<0.001 $**

Abbreviations:

*AS= Aortic Stenosis, CCHD= Cyanotic Congenital Heart Disease, CMD= Coronary Microvascular Disease, DM= Diabetes Mellitus, HCL= Hypercholesterolemia, HF= Heart Failure, HTN= Hypertension, MI= Myocardial Infarction, PVD= Perioheral Vascular Disease, TIA= Transient Ischemic Attack. *Mann-Whitney U test. $ Chi-squared test.*

The mean blood flow rate (Q) was increased in CMD (189 ± 40 pl/s), DM (204 ± 60 pl/s) and HF (207 ± 72 pl/s) compared to the controls (155 ± 55 pl/s). Mean wall shear rate (WSR) was reduced in CMD (134 ± 23 s^{-1}), DM (142 ± 29 s^{-1}) and HF (138 ± 27 s^{-1}) compared to the controls (166 ± 39 s^{-1}). ROC analysis of WSR gave an area under the curve (AUC) of 0.772 for controls vs CMD, 0.686 for controls vs DM and 0.729 for controls vs HF as shown in Figure 7.1. The axial and cross-sectional velocities were also significantly increased in the DM cohort (0.55 ± 0.07,

0.38 ± 0.04 mm/s) compared to the CMD cohort (0.52 ± 0.04, 0.36 ± 0.03 mm/s) ($p<0.05$). However, no significant differences were reported in the mean axial or cross-sectional velocity results between the controls and the other groups, but significant differences were reported for the mean diameter.

Table 7.2. Cardiac remodeling cohorts: ocular parameters

Ocular Parameter	**Control (n=47)**	**CMD (n=29)**	**DM (n=67)**	**HF (n=55)**	***p value**
Diameter (µm)	21.4 ± 3.4	24.8 ± 3.0	24.7 ± 3.4	25.0 ± 4.2	**<0.001**
Axial Velocity (mm/s)	0.53 ± 0.06	0.52 ± 0.04	0.55 ± 0.07	0.54 ± 0.07	**<0.001**
Cross-Sectional Velocity (mm/s)	0.38 ± 0.04	0.36 ± 0.03	0.38 ± 0.04	0.38 ± 0.05	**0.001**
Blood Flow Rate (pl/s)	155 ± 55	189 ± 40	204 ± 60	207 ± 72	**<0.001**
Wall Shear Rate (s^{-1})	166 ± 39	134 ± 23	142 ± 29	138 ± 27	**<0.001**

Abbreviations:

CMD= Coronary Microvascular Disease, DM= Diabetes Mellitus, HF= Heart Failure.

**Mann-Whitney U test.*

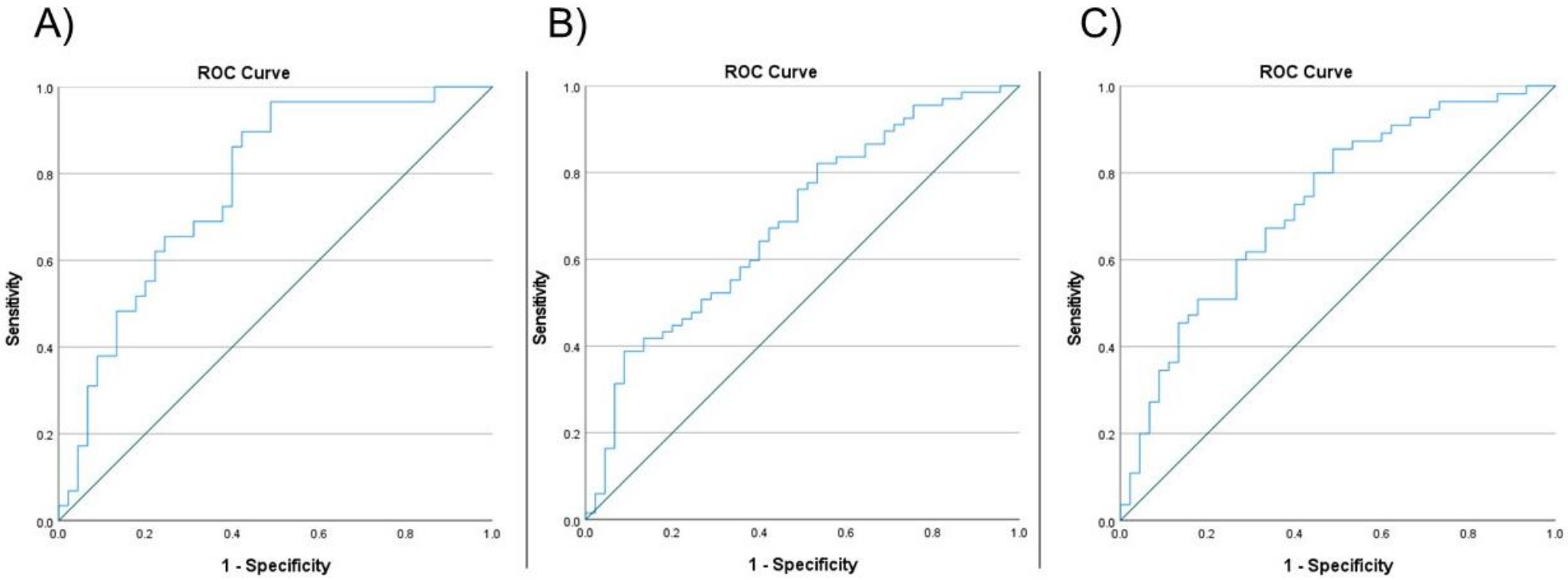

Figure 7.1. WSR ROC graphs

A) Controls (n=47) vs CMD (n=29) (cut off point=0.4, sensitivity=72.4%, specificity=62.2%), B) Controls (n=47) vs DM (n=67) (cut-off point=0.60, sensitivity=62.7%, specificity=60.0%), C) Controls (n=47) vs HF (n=55) (cut-off point=0.55, sensitivity=70.9%, specificity=60.0%)

Heart Rhythm:

Total analysis of the heart rhythm for all cohorts recruited in the study showed that 57 participants recruited to the study had atrial fibrillation (AF), and a separate 21 participants had a paced heart rhythm. There were 20 subjects excluded from the analysis due to undisclosed heart rhythm, or from having another electrocardiographic abnormality such as left bundle branch block. The control group (n=308) consisted of 187 (60.7%) males with a total mean age of 63.7 ± 14.9 years. The controls also had a mean height of 1.68 ± 0.11 m, and a mean weight of 81.51 ± 19.86 kg. The mean heart rate of the controls was 71 ± 12 bpm, and they had a mean systolic blood pressure of 128 ± 19 mmHg and a diastolic blood pressure of 72 ± 11 mmHg. 142 (46.1%) controls had a history of HTN, 69 (22.4%) had DM, 185 (60.0%) had HCL, 44 (14.3%) had a previous MI, 12 (3.9%) had a previous stroke, 17 (5.5%) had a previous TIA, 13 (4.2%) had PVD, 60 (19.5%) had AS, 34 (11.0%) had known CMD and 34 (11.0%) had HF.

The AF group consisted of 36 (63.2%) males (p=0.609) with a total mean age of 76.9 ± 11.7 years, which was significantly increased in comparison to controls (p<0.001). The AF group had a mean height of 1.70 ± 0.10 m and a mean weight of 80.83 ± 17.55 kg (p=0.155 and 0.807, respectively). The mean heart rate of the controls was 74 ± 13 bpm (p=0.203), and they had a mean systolic blood pressure of 127 ± 15 mmHg and a diastolic blood pressure of 71 ± 11 mmHg (p=0.857 and 0.817, respectively). 34 (59.7%) within this group had a history of HTN, and this was significantly increased compared to that of the controls (p=0.045). 16 (28.1%) had a history of DM, and this slight increase in percentage compared to controls was not statistically significant (p=0.426). Analogous with controls, 8 (14.0%) had a previous MI (p=0.996), while the number of participants with HCL was slightly increased for

the AF group at 37 (64.9%) (p=0.426). Expectantly, a history of stroke was significantly increased in the AF group n=7 (13.7%) (p=0.008). 4 (7.0%) had a history of TIA (p=0.630). 6 (11.8%) had PVD, and this was significantly increased in comparison to controls (p=0.044). The percentage of participants with AS n=26 (45.6%) and HF n=17 (29.8%) was also significantly increased in the AF group compared to controls (p<0.001). However, 7 (12.3%) within the AF group had a history of known CMD, thus, whilst this was increased in comparison to controls, there was no statistically significant difference in the number of participants with known CMD between the two groups (p=0.198).

The second and last heart rhythm in this analysis was paced. The paced group was made up of 8 (38.1%) male participants (p=0.832), with a mean age of 76.7 ± 14.5 years that was significantly older than the controls (p<0.001). This group had a mean height of 1.66 ± 0.10 m and weight of 80.00 ± 22.78 kg (p=0.535 and 0.565, respectively). The mean heart rate was 69 ± 13 bpm (p=0.266). The mean systolic blood pressure was significantly increased compared to control at 139 ± 22 mmHg (p=0.017). The mean diastolic blood pressure was similar to that of controls at 72 ± 10 mmHg (p=0.738). 12 (57.1%) paced group participants had a history of HTN (p=0.289), 4 (19.0%) had DM (p=0.753), 9 (42.9%) had HCL (p=0.139), 3 (14.3%) had a previous MI (p=0.972), 2 (9.5%) had a previous stroke (p=0.206), 3 (14.3%) had a previous TIA (p=0.097), 2 (9.5%) had PVD (p=0.248), 7 (33.3%) had AS (p=0.115), 1 (4.8%) had known CMD (p=0.181) and 3 (14.3%) had HF (p=0.629).

All ocular parameters except for wall shear rate were significantly increased in AF compared to controls as shown in Figures 7.2-7.4 (Diameter; controls= 23.56 ± 3.50 µm vs AF= 25.40 ± 3.53 µm, $p<0.001$; Axial Velocity; controls= 0.53 ± 0.06 mm/s vs AF= 0.57 ± 0.05 mm/s, $p<0.001$; Cross-Sectional Velocity; controls= 0.37 ± 0.04 mm/s vs AF= 0.40 ± 0.03 mm/s, $p<0.001$; Blood Flow Rate; controls= 181 ± 57 pl/s vs AF= 221 ± 59 pl/s, $p<0.001$). However, for all participants with paced rhythm compared to controls the mean wall shear rate was significantly reduced (controls mean wall shear rate=147 ± 31 s^{-1} vs paced mean wall shear rate=132 ± 22 s^{-1}, $p=0.027$), whilst the mean diameter was significantly increased (controls mean diameter= 23.56 ± 3.50 µm vs paced mean diameter= 25.45 ± 3.25 µm, $p=0.029$), as shown in Figures 7.5-7.7. All results from this heart rhythm analysis are presented in Table 7.3.

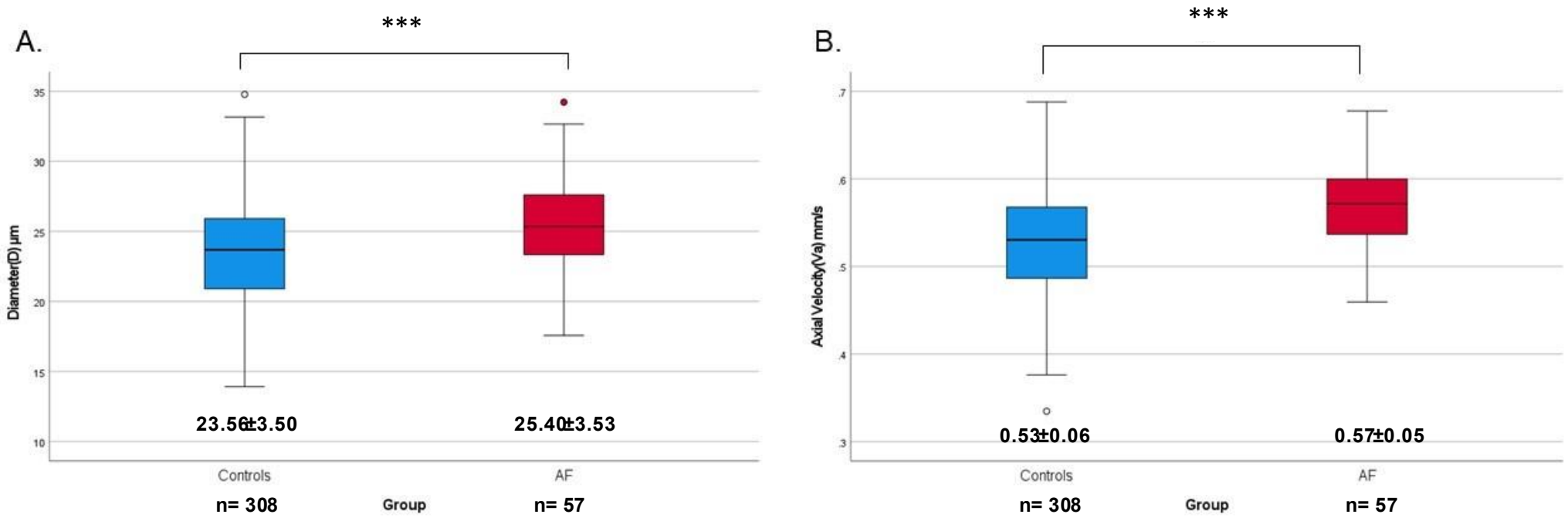

Figure 7.2. Box plot of ocular parameters for AF vs control groups

*A.) Diameter (µm) and B.) Axial Velocity (mm/s). Controls n= 308 and AF n= 57. Mann-Whitney U test ***p<0.001.*

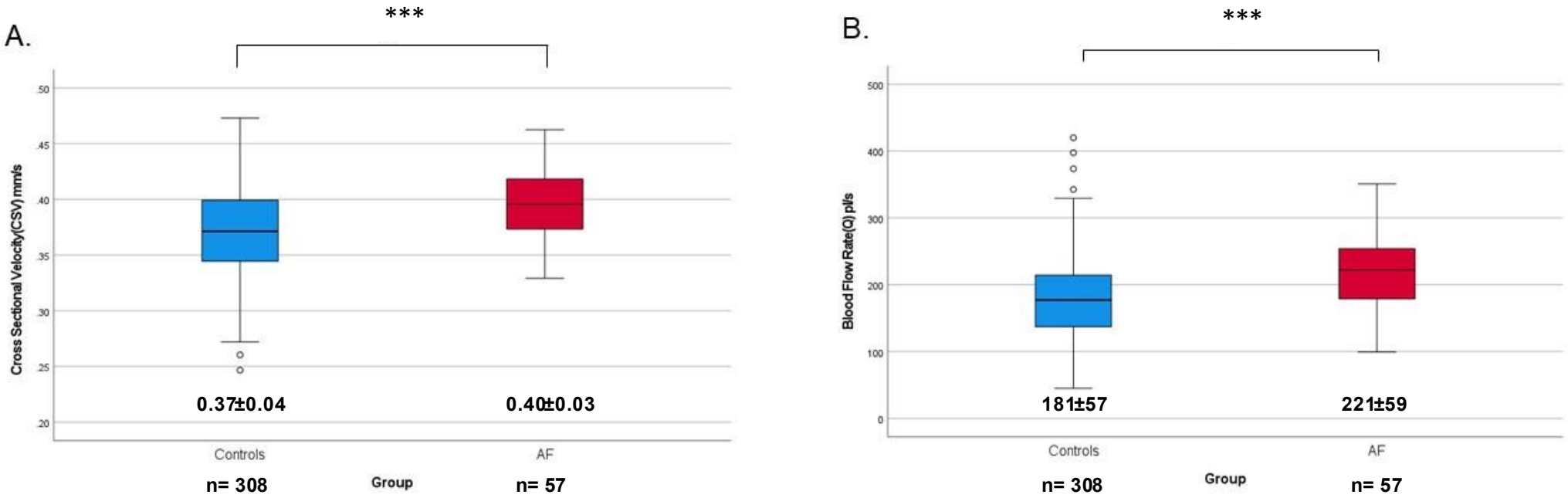

Figure 7.3. Box plot of ocular parameters for AF vs control groups

A.) Cross-Sectional Velocity (mm/s) and B.) Blood Flow Rate (pl/s) Controls n= 308 and AF n= 57. Mann-Whitney U test

****p<0.001.*

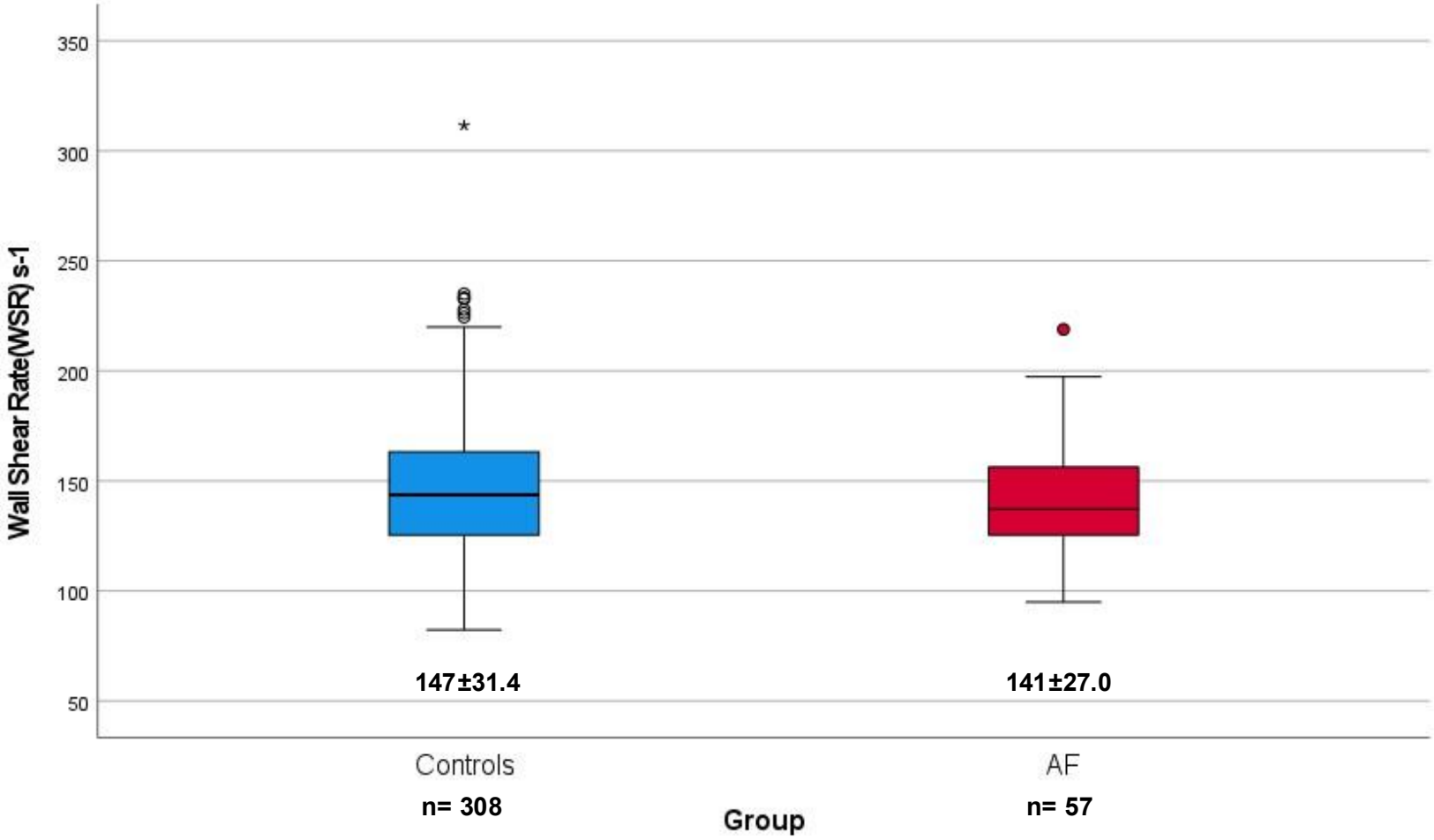

Figure 7.4. Box plot of Wall Shear Rate (s^{-1}) for AF vs control groups

Controls n= 308 and AF n= 57. Mann-Whitney U test p=0.175.

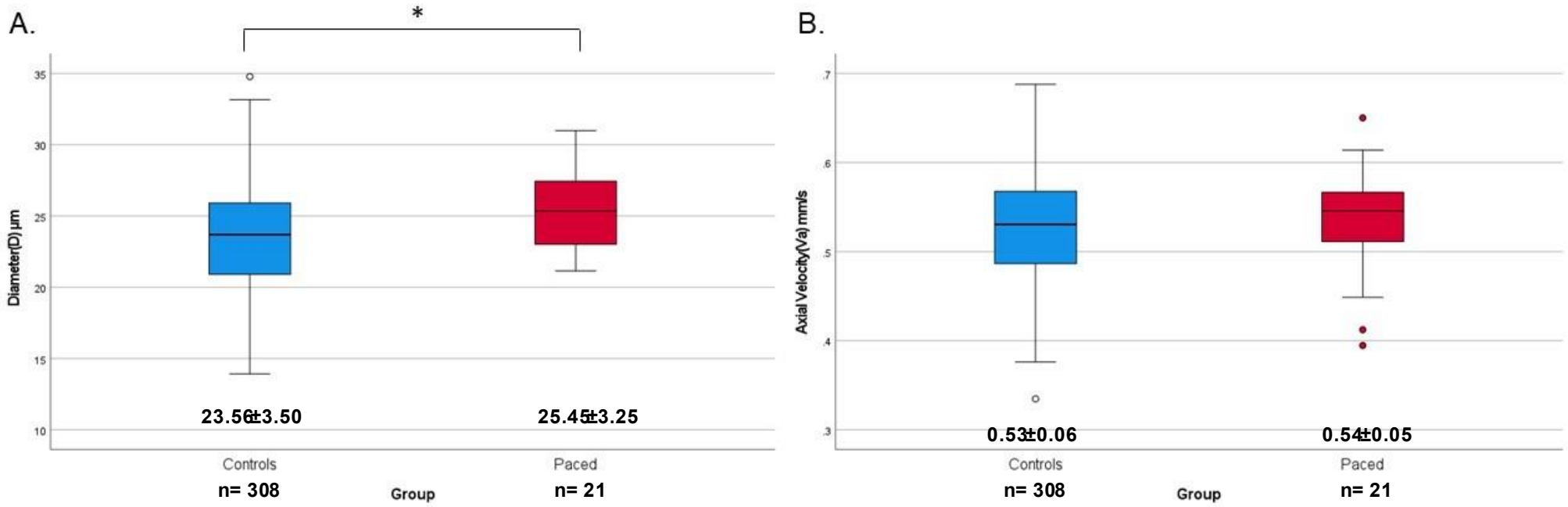

Figure 7.5. Box plot of ocular parameters for paced vs control groups

*A.) Diameter (µm) *p<0.05 and B.) Axial Velocity (mm/s) p=0.555. Controls n= 308 and Paced n= 21. Mann-Whitney U test.*

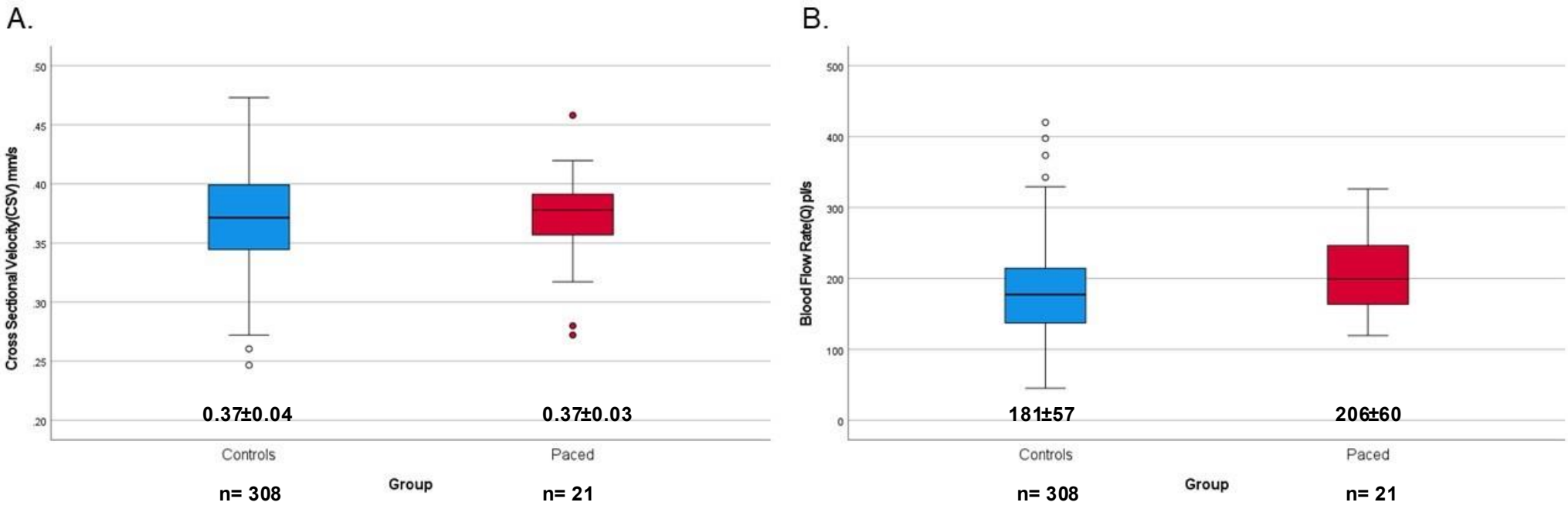

Figure 7.6. Box plot of ocular parameters for paced vs control groups

A.) Cross-Sectional Velocity (mm/s) p=0.859 and B.) Blood Flow Rate (pl/s) p=0.86. Controls n= 308 and Paced n= 21. Mann-Whitney U test.

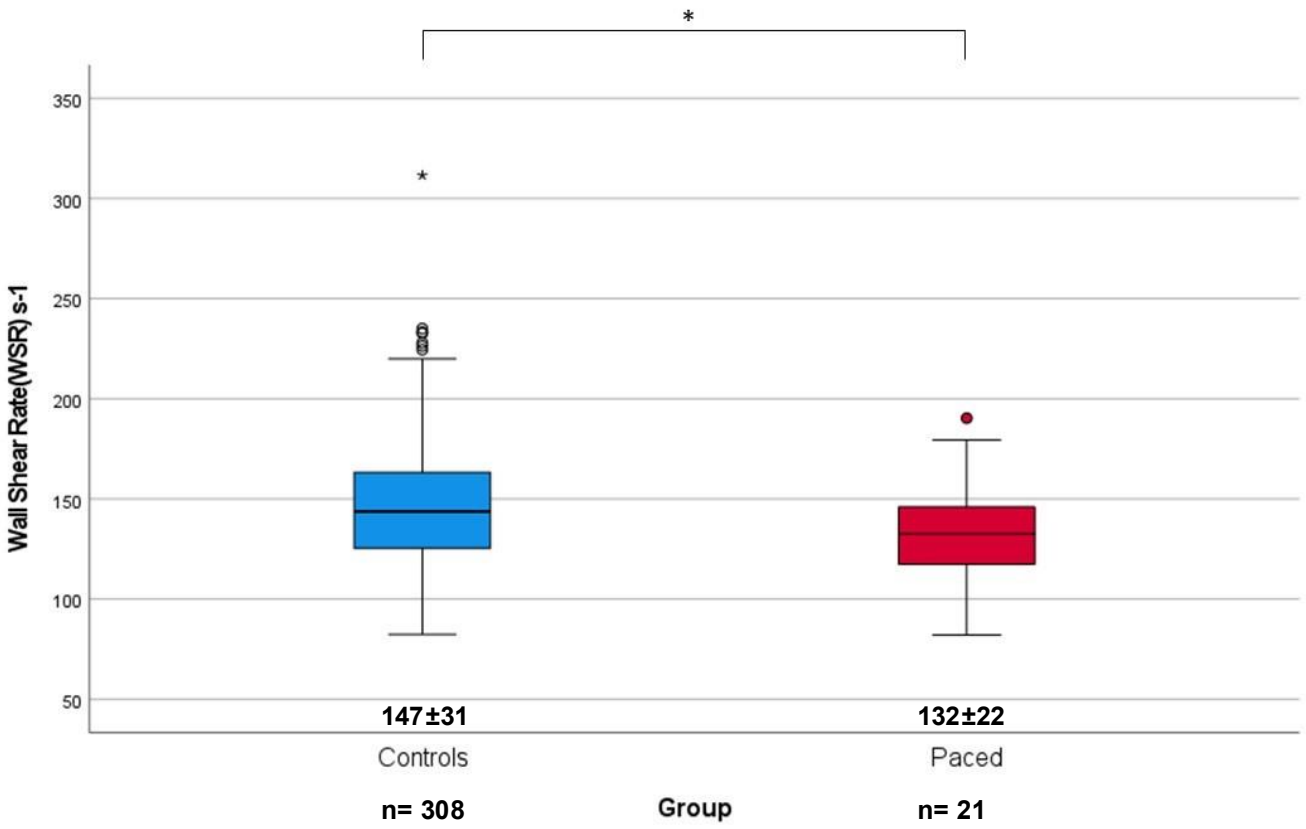

Figure 7.7. Box plot of Wall Shear Rate (s^{-1}) for paced vs control groups

*Controls n= 308 and Paced n= 21. Mann-Whitney U test *p<0.05.*

Table 7.3. Ocular parameters of atrial fibrillation, paced and control groups

Ocular Parameter	**Controls n= 308 patients**	**95% CI**	**Atrial Fibrillation n= 57 patients**	**95% CI**	***p value**
Mean Diameter(D) (µm)	23.56 ± 3.50	23.16-23.95	25.40 ± 3.53	24.49-26.37	**<0.001**
Mean Axial Velocity(Va) (mm/s)	0.53 ± 0.06	0.52-0.54	0.57 ± 0.05	0.56-0.58	**<0.001**
Mean Cross Sectional Velocity(CSV) (mm/s)	0.37 ± 0.04	0.37-0.38	0.40 ± 0.03	0.39-0.40	**<0.001**
Mean Blood Flow Rate(Q) (pl/s)	181 ± 57	175-188	221 ± 59	206-237	**<0.001**
Mean Wall Shear Rate(WSR) (s^{-1})	147 ± 31	144-151	141 ± 27	134-148	0.175
Ocular Parameter	**Controls**	**95% CI**	**Paced**	**95% CI**	***p value**

	n= 308 patients		**n= 21 patients**		
Mean Diameter(D) (µm)	23.56 ± 3.50	23.16-23.95	25.45 ± 3.25	23.97-26.93	**0.029**
Mean Axial Velocity(Va) (mm/s)	0.53 ± 0.06	0.52-0.54	0.54 ± 0.05	0.51-0.56	0.555
Mean Cross Sectional Velocity(CSV) (mm/s)	0.37 ± 0.04	0.37-0.38	0.37 ± 0.03	0.36-0.39	0.859
Mean Blood Flow Rate(Q) (pl/s)	181 ± 57	175-188	206 ± 60	179-234	0.086
Mean Wall Shear Rate(WSR) (s^{-1})	147 ± 31	144-151	132 ± 22	122-142	**0.027**
*Mann-Whitney U test.					

Inter-eye Study:

The results of the difference in the inter-eye conjunctival vascular parameters between the positive pressure wire cohort and controls are recorded in Table 7.4. Significant inter-eye mean differences were reported between diameter (p=0.025), axial velocity (p=0.012), cross-sectional velocity (p=0.008), wall shear rate (p=0.005) and wall shear stress (p=0.005) of the positive pressure wire (indicative of coronary microvascular disease (MVD)) cohort (diameter= 1.61 ± 5.08 µm, axial velocity= -0.041 ± 0.064 mm/s, cross-sectional velocity= -0.032 ± 0.048 mm/s, wall shear rate= -22.45 ± 51.95 s^{-1}, wall shear stress= -1.22 ± 3.05 dynes/cm^2) compared to controls (diameter= -0.70 ± 4.78 µm, axial velocity= -0.003 ± 0.087 mm/s, cross-sectional velocity= -0.001 ± 0.061 mm/s, wall shear rate= 4.42 ± 43.60 s^{-1}, wall shear stress= 0.24 ± 2.44 dynes/cm^2). However, the inter-eye mean difference of blood flow rate was not statistically significant (p=0.087) between the positive pressure wire cohort (11.52 ± 72.33 pl/s) and controls (-11.15 ± 76.97 pl/s). The graphs for the inter-eye mean difference results are presented in Figures 7.8 and 7.9.

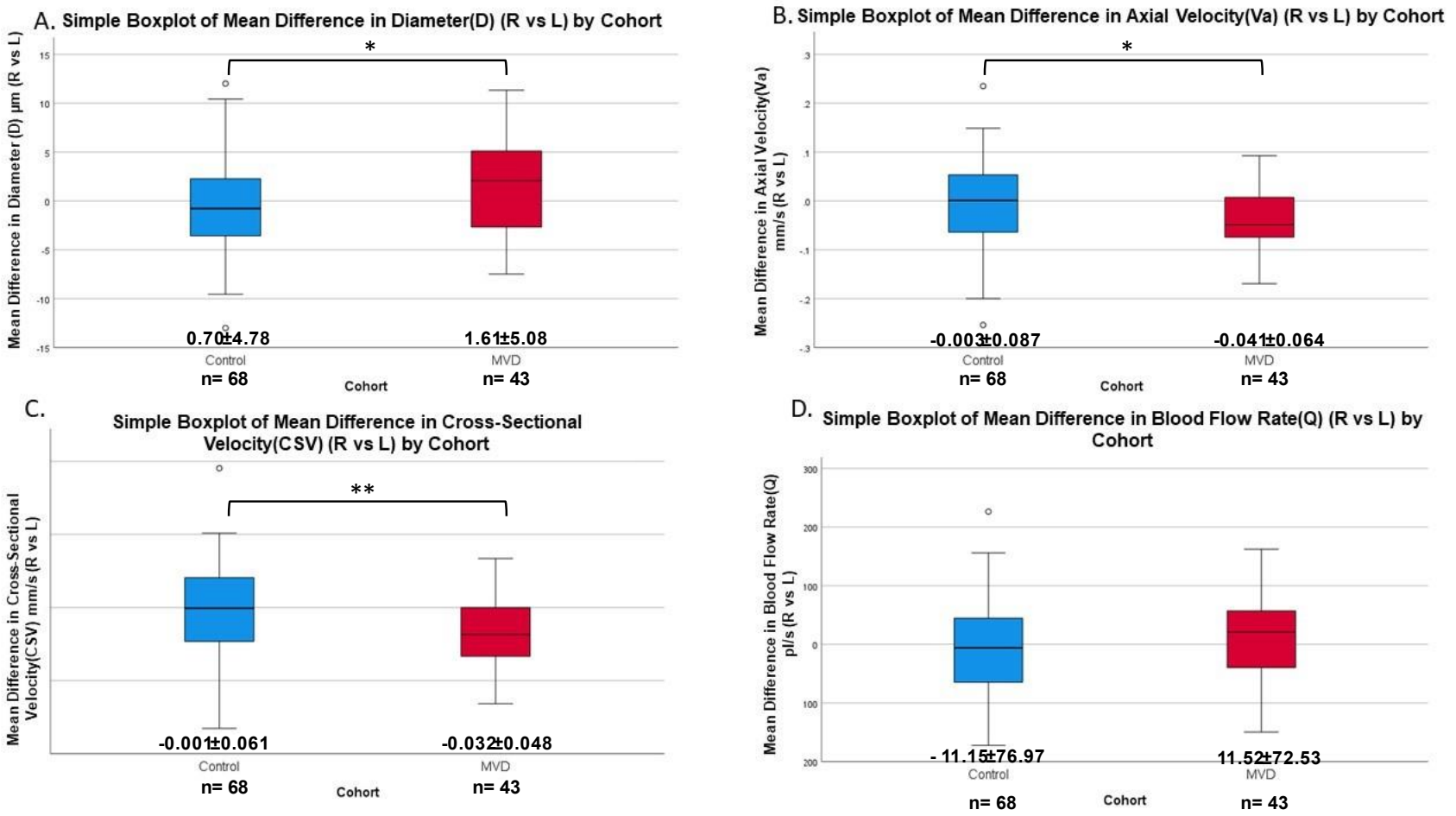

Figure 7.8. Inter-eye mean differences for A.) Diameter(µm), B.) Axial Velocity(mm/s), C.) Cross-Sectional Velocity(mm/s) and D.) Blood Flow Rate(pl/s) between cohorts*. MVD= microvascular disease. Controls n=68 and MVD n=43. Mann-Whitney U test *p<0.05, **p<0.01 and D) p=0.087.*

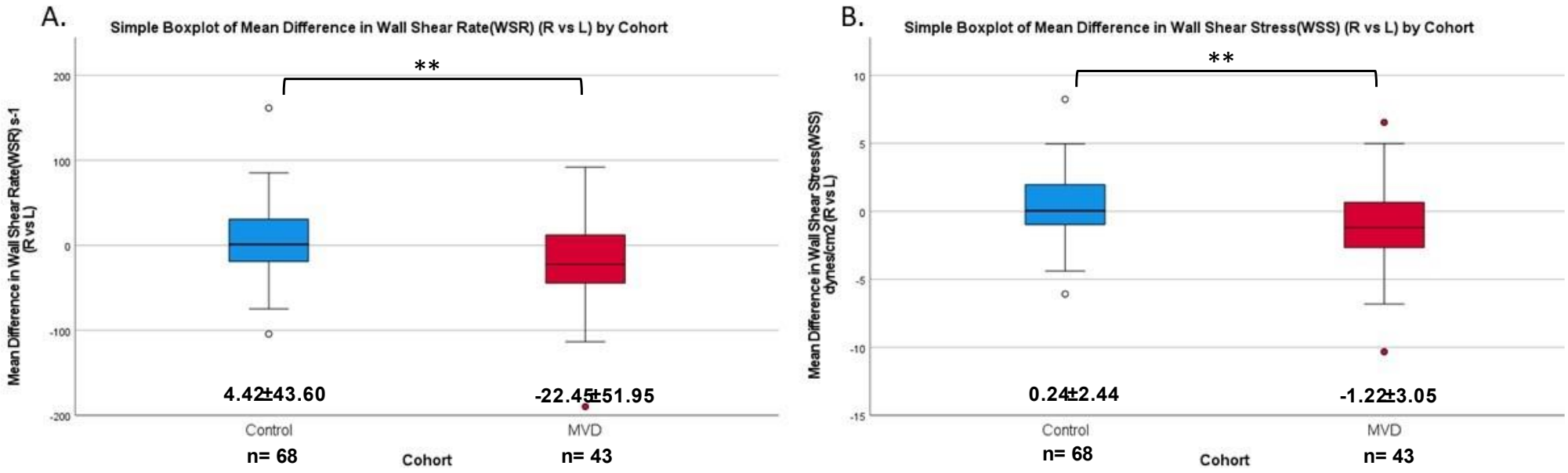

Figure 7.9. Inter-eye mean differences for A.) Wall Shear Rate (s^{-1}) and B.) Wall Shear Stress (dynes/cm^2) between cohorts

*Controls n=68 and MVD n=43. Mann-Whitney U test **p<0.01.*

Table 7.4. Mean inter-eye difference (mean parameters of left eye subtracted from that of the right eye)

Ocular Parameter	**Controls (n=68)**	**MVD (n=43)**	***p value**
Diameter µm	-0.70 ± 4.78	1.61 ± 5.08	**0.025**
Axial Velocity mm/s	-0.003 ± 0.087	-0.041 ± 0.064	**0.012**
Cross-Sectional Velocity mm/s	-0.001 ± 0.061	-0.032 ± 0.048	**0.008**
Blood Flow Rate pl/s	-11.15 ± 76.97	11.52 ± 72.33	0.087
Wall Shear Rate s^{-1}	4.42 ± 43.60	-22.45 ± 51.95	**0.005**
Wall Shear Stress dynes/cm^2	0.24 ± 2.44	-1.22 ± 3.05	**0.005**
*Mann-Whitney U test.			

Table 7.5 reports the right nasal and left nasal field of view mean difference in ocular parameters between the two cohorts. Significant differences were again found for diameter (D) (controls= -0.85 ± 8.65 µm vs MVD= 3.09 ± 7.85 µm, p=0.014), axial velocity (Va) (controls= -0.001 ± 0.108 mm/s vs MVD= -0.065 ± 0.135 mm/s, p=0.023), Cross-Sectional Velocity (CSV) (controls= 0.002 ± 0.079 mm/s vs MVD= -0.052 ± 0.096 mm/s, p=0.005), Wall Shear Rate (WSR) (controls= 10.76 ± 79.75 s^{-1} vs MVD= -42.13 ± 85.62 s^{-1}, p=0.003) and Wall Shear Stress (WSS) (controls= 0.67 ± 4.69 dynes/cm^2 vs MVD= -2.26 ± 4.67 dynes/cm^2, p=0.003). Blood flow rate (Q)

only approached statistical significance (controls= 0.002 ± 0.079 pl/s vs MVD= 28 ± 134 pl/s, p=0.055). The results for the right and left nasal field of view mean differences between cohorts are shown in Figures 7.10 and 7.11. All mean ocular parameters for each field of view are presented in Table S7. Lastly, the results of the temporal field of view analysis are presented in Table S8, and the nasal vs temporal field of view analysis results are presented in Table S9.

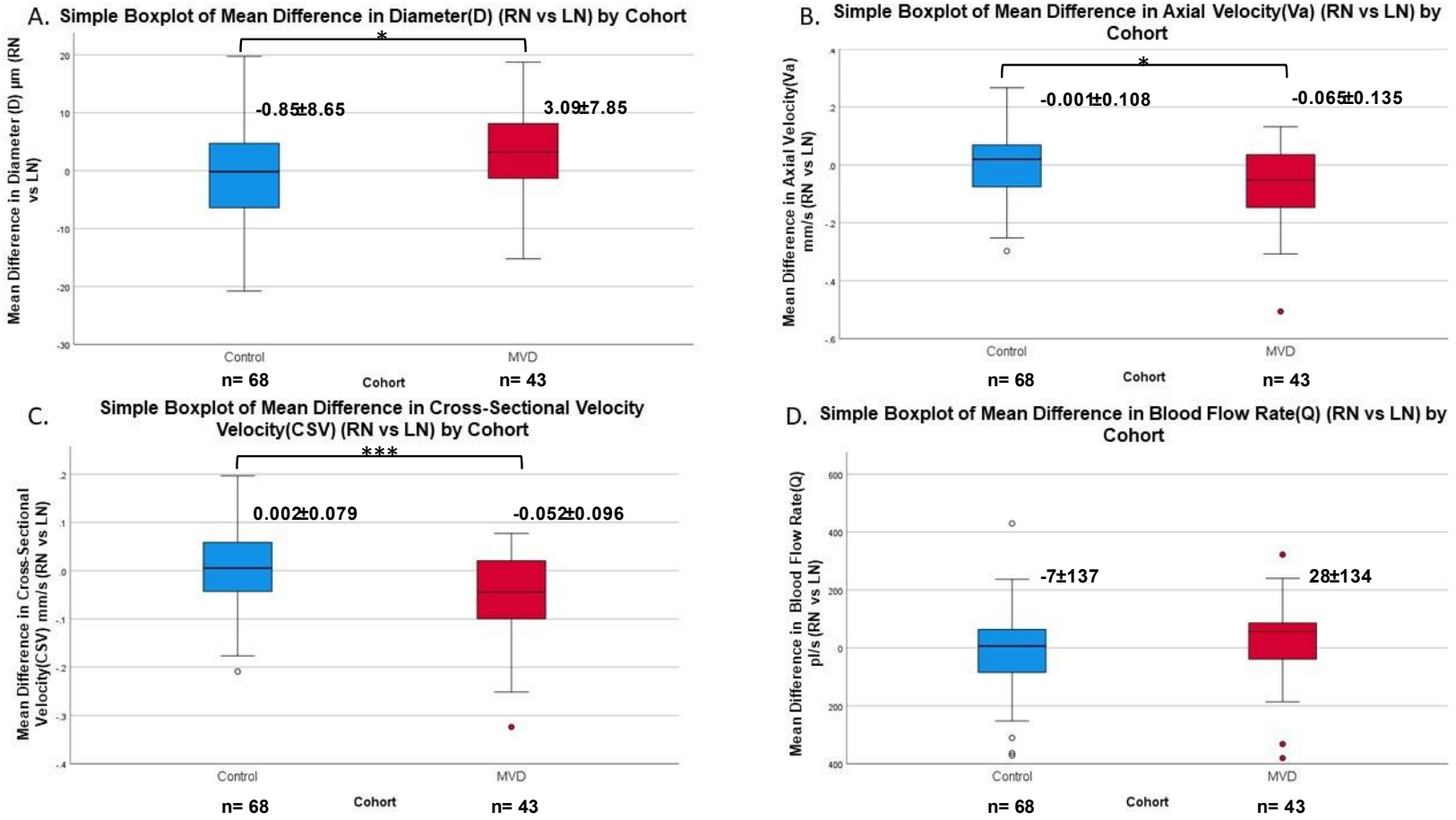

Figure 7.10. Nasal field of view mean differences for A.) Diameter(µm), B.) Axial Velocity(mm/s), C.) Cross-Sectional Velocity(mm/s) and D.) Blood Flow Rate(pl/s) between cohorts

*Controls n=68 and MVD n=43. Mann-Whitney U test *p<0.05, ***p<0.001 and D) p=0.055.*

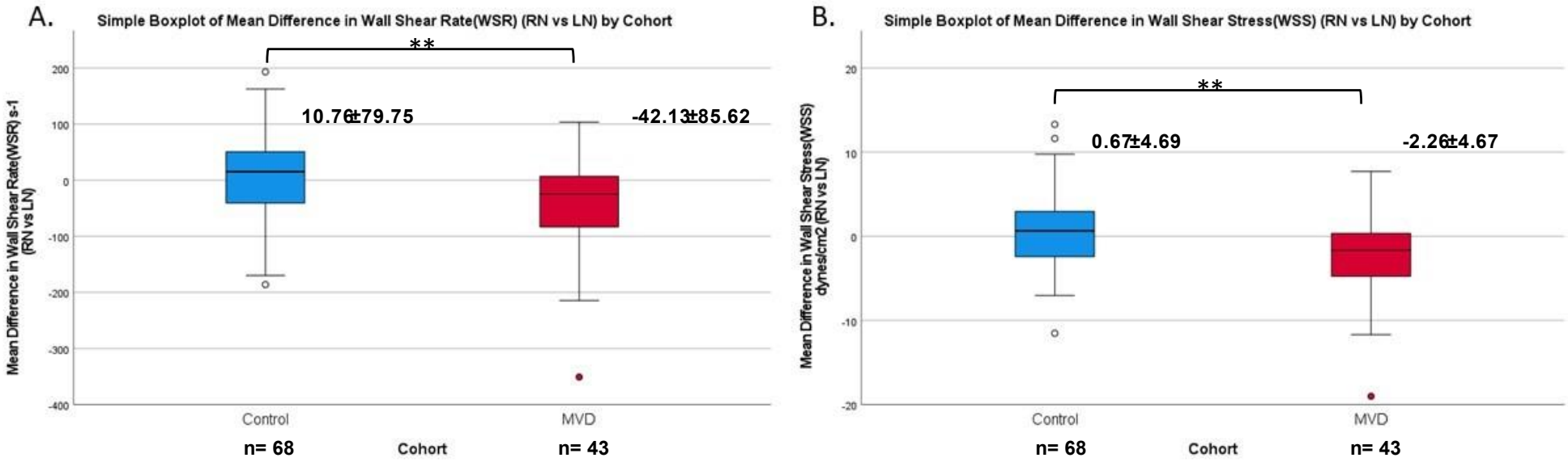

Figure 7.11. Nasal field of view mean differences for A.) Wall Shear Rate(s^{-1}) and B.) Wall Shear Stress (dynes/cm^2) between cohorts

*Controls n=68 and MVD n=43. Mann-Whitney U test **p<0.01.*

Table 7.5. Mean inter-view difference (right nasal vs left nasal)

Ocular Parameter	**Controls (n=68)**	**MVD (n=43)**	***p value**
Diameter µm	-0.85 ± 8.65	3.09 ± 7.85	**0.014**
Axial Velocity mm/s	-0.001 ± 0.108	-0.065 ± 0.135	**0.023**
Cross-Sectional Velocity mm/s	0.002 ± 0.079	-0.052 ± 0.096	**0.005**
Blood Flow Rate pl/s	-7 ± 137	28 ± 134	0.055
Wall Shear Rate s^{-1}	10.76 ± 79.75	-42.13 ± 85.62	**0.003**
Wall Shear Stress dynes/cm^2	0.67 ± 4.69	-2.26 ± 4.67	**0.003**
*Mann-Whitney U test.			

Risk Scoring:

A total assessment of the 407 participants excluding the 8 pressure wire cohort patients (due to inaccuracies within the pressure wire measurements) separated into control (n=183) and cardiovascular disease cohorts as shown in Figure 7.12 (to include transcatheter aortic valve implantation (TAVI), pressure wire positive (CMD), cyanotic congenital heart disease and myocardial infarction within the cardiovascular disease cohort, total n=214), resulted in the generation of a four variable patient risk score with a sensitivity of 88.8% and a specificity of 69.6% for classification of

cardiovascular disease. The baseline characteristics of the two groups are presented in Table 7.6. The variables within the score included axial velocity (controls= 0.55 ± 0.06 mm/s vs cardiovascular disease= 0.53 ± 0.06 mm/s, p=0.022), heart rate (controls= 68.70 ± 10.94 bpm vs cardiovascular disease= 74.18 ± 12.95 bpm, p<0.001), NTproBNP (controls= 316.09 ± 676.394 ng/L vs cardiovascular disease= 1715.58 ± 2965.994 ng/L, p<0.001) and fibrinogen (3.28 ± 0.756 g/L vs 3.90 ± 0.975 g/L, p<0.001) at the cut-off point of 0.47. Table 7.7 presents the contributions of each individual variable. Heart rate, NTproBNP and fibrinogen were not normally distributed, and hence were log transformed. The resultant area under the receiver operator curve was 0.899, as presented in Figure 7.13. Figure 7.14 shows the predicted probability against this multi-biomarker patient score resulted in an R^2 value of 0.894.

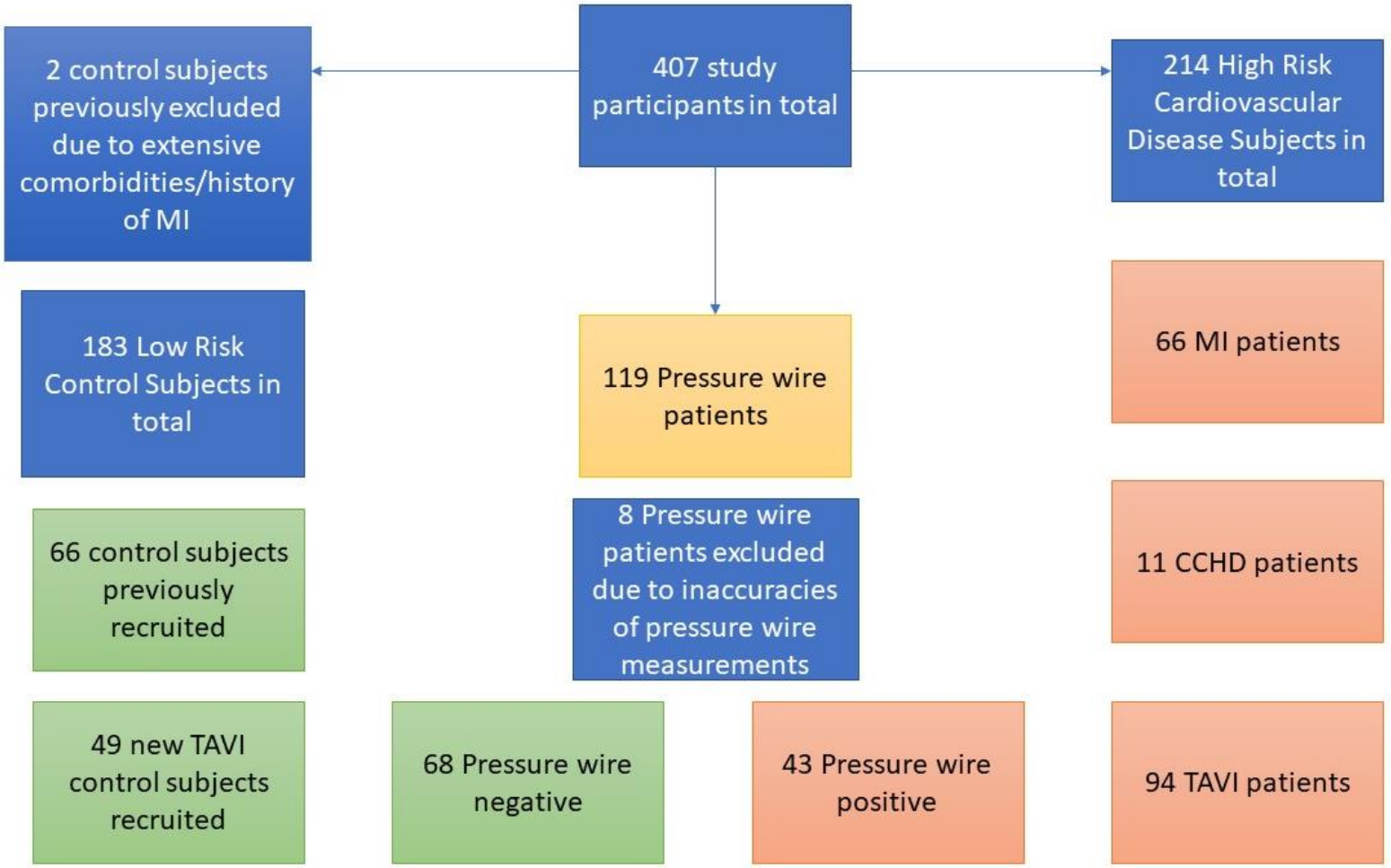

Figure 7.12. Flow chart of all the groups recruited

CCHD= Cyanotic Congenital Heart Disease, MI= Myocardial Infarction, TAVI=Transcatheter Aortic Valve Implantation.

Table 7.6. Baseline characteristics of the total cardiovascular (CVD) and control groups

Baseline Characteristic	**Control n=183**	**CVD n=214**	***p Value**
Age years	64.60 ± 14.36	68.81 ± 16.16	**0.001**
Gender % male	63.4 (116/183)	57.0 (122/214)	0.196 $
Height cm	168.28 ± 9.94	167.08 ± 10.22	0.210
Weight kg	83.35 ± 21.42	78.80 ± 17.29	0.076
Mean Systolic Blood Pressure mmHg	130.02 ± 17.98	128.13 ± 19.54	0.190
Mean Diastolic Blood Pressure mmHg	73.46 ± 10.07	70.42 ± 11.38	**0.015**
Resting Oxygen Saturation %	97.62 ± 1.52	96.50 ± 3.99	**<0.001**
*Mann-Whitney U test, $ Chi-squared test.			

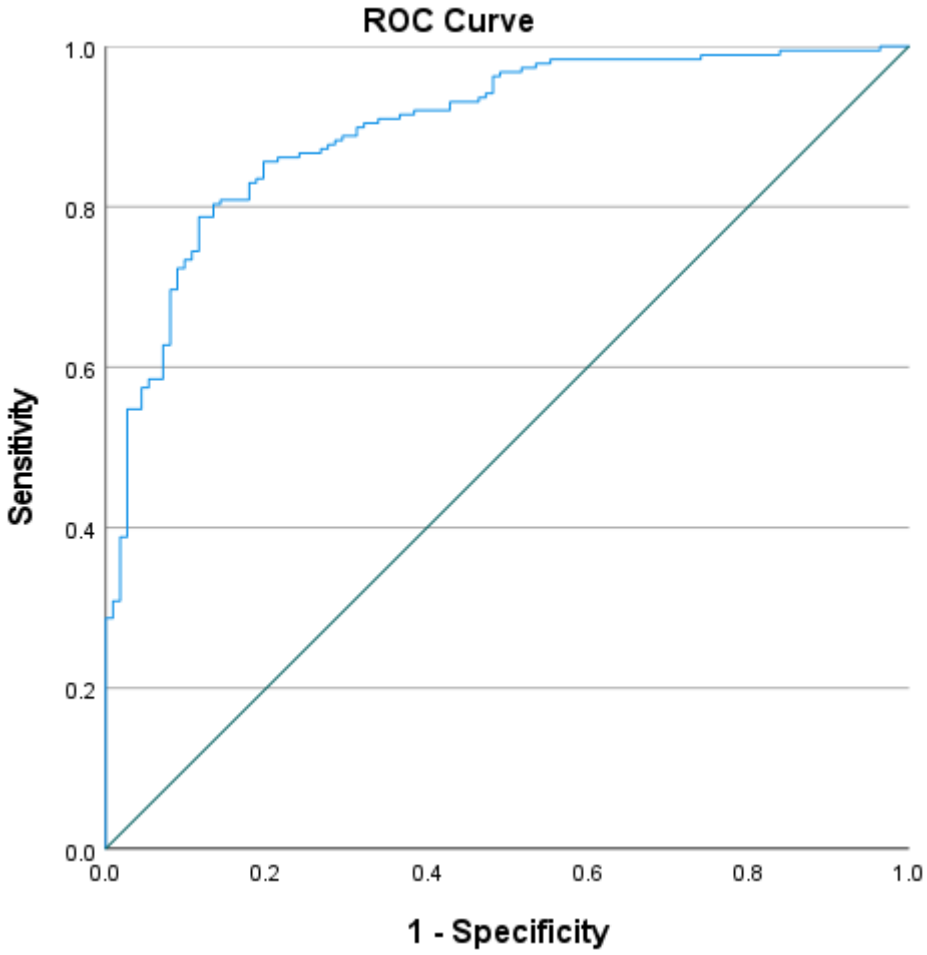

Figure 7.13. ROC of axial velocity, heart rate, N-terminal pro B-type natriuretic peptide and fibrinogen for cardiovascular disease classification of the entire dataset (n=407).

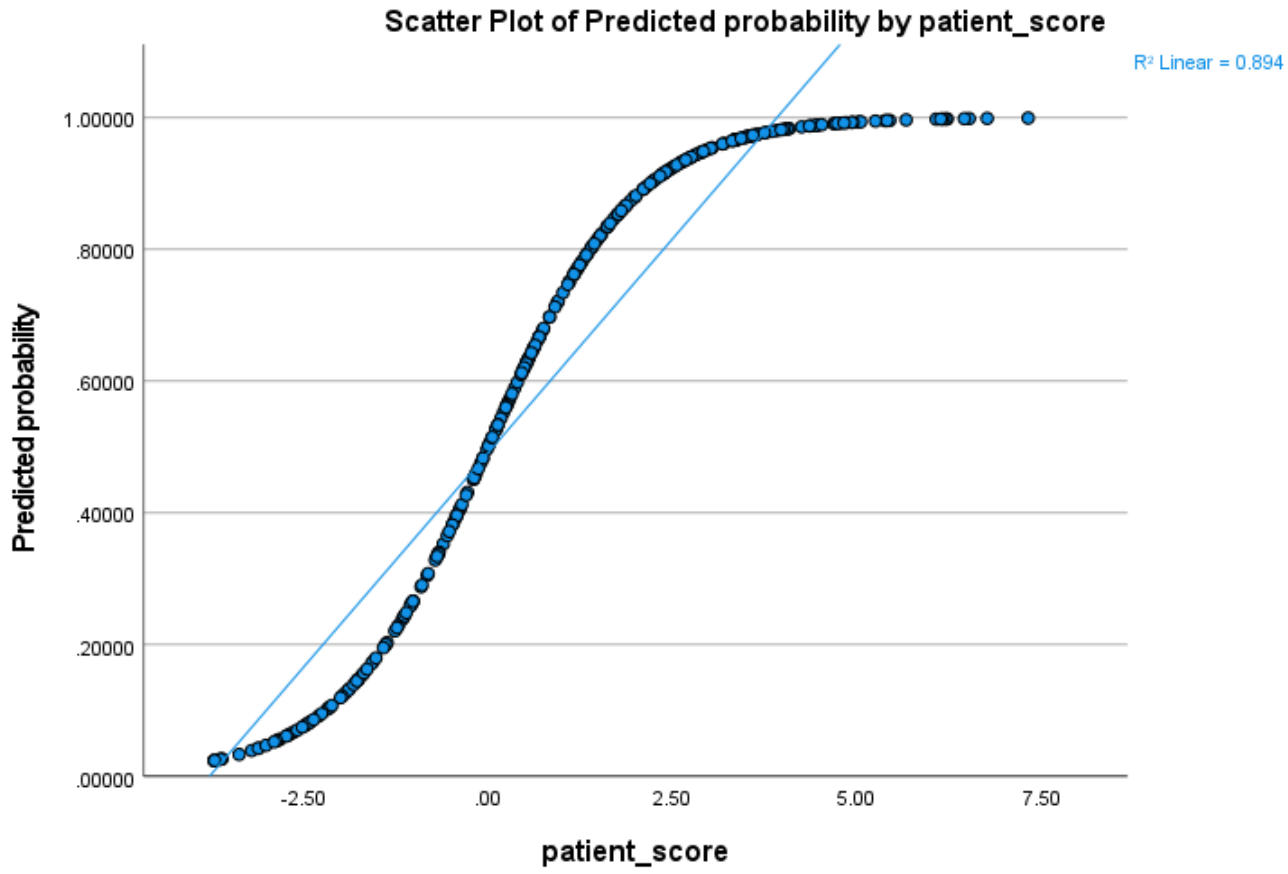

Figure 7.14. Scatterplot of predicted probability by patient score

The formula for the patient score= (Va-9.157) + (Log_{10}(Heart rate)*7.897) + (Log_{10}(BNP)*2.518) + (Log_{10}(Fibrinogen)*4.480) + (-17.264)*

Va=Axial Velocity and BNP= N-terminal pro B-type natriuretic peptide.

Table 7.7. Table of contribution

Biomarker/ocular parameter	AUROC	Sensitivity %	Specificity %
Va	0.567	58.0	47.0
Log10 Heart rate	0.623	60.3	52.8
Log10 BNP	0.814	78.4	75.3

Log10 Fibrinogen	0.700	74.0	56.0
AUROC Area Under Receiver Operator Characteristic Curve, *Va* Axial Velocity, *BNP* N-terminal pro brain natriuretic peptide.			

Risk Classification of Controls:

In order to compare the ocular parameters to current risk scoring methods, the control subjects were classified into low, intermediate and high risk based on their QRISK3 scores: <10= low risk, 10-20= moderate risk and >20= high risk. There were 53 control subjects excluded due to either exceeding the age limit (25-80 years) for QRISK3 calculation, being below the required height (<140cm) and weight (<40kg) limits or due to missing risk factors required for calculation. The baseline characteristics are presented in Table 7.8, and the results of the ocular parameters for each of these classes of risk are presented in Table 7.9 below. The post-hoc analysis results are provided in Table S10 and S11.

Table 7.8. Baseline characteristics of the controls stratified by QRISK3 risk class

Baseline Characteristic	**Low (n=58)**	**Moderate (n=37)**	**High (n=35)**	***p Value**
Age years	50.95 ± 8.39	62.17 ± 6.67	66.52 ± 8.29	**<0.001**

Gender % male	55.2 (32/58)	81.1 (30/37)	65.7 (23/35)	**0.035 $**
Height cm	167.33 ± 10.76	171.73 ± 8.88	168.60 ± 9.44	0.11
Weight kg	82.24 ± 23.84	86.68 ± 19.99	89.98 ± 18.79	0.232
Mean Systolic Blood Pressure mmHg	121.77 ± 16.53	128.89 ± 12.68	132.15 ± 15.87	**0.005**
Mean Diastolic Blood Pressure mmHg	75.21 ± 11.02	74.63 ± 10.01	73.04 ± 9.85	0.621
Heart Rate bpm	67.68 ± 10.45	67.00 ± 10.16	69.15 ± 9.53	0.663
Resting Oxygen Saturation %	97.68 ± 1.34	97.78 ± 1.48	97.03 ± 1.72	0.065
*Mann-Whitney U test, $ Chi-squared test.				

Table 7.9. Ocular parameter results of the controls stratified by QRISK3 risk class

Ocular Parameter	**Low Risk (n=58)**	**Moderate Risk (n=37)**	**High Risk (n=35)**	***p value**
Diameter(D) µm	21.55 ± 3.30	24.27 ± 3.03	23.96 ± 3.13	**<0.001**
Axial Velocity(Va) mm/s	0.53 ± 0.05	0.56 ± 0.06	0.54 ± 0.05	**0.021**

Cross-Sectional Velocity(CSV) mm/s	0.38 ± 0.04	0.39 ± 0.04	0.38 ± 0.04	0.115
Blood Flow Rate(Q) pl/s	155 ± 49	199 ± 47	186 ± 44	**<0.001**
Wall Shear Rate(WSR) s^{-1}	164 ± 38	150 ± 30	146 ± 26	**0.021**
*Mann-Whitney U test.				

7.5 *Discussion (in-depth discussion continued in Chapter 8)*

The results of the binary logistic regression suggest wall shear rate may be a good predictor of cardiac remodeling. Normal laminar wall shear rate and shear stress is a determinant of normal endothelial function. Disturbance of normal wall shear rate and stress stimulates the process of atherosclerosis, and thus myocardial remodeling. This result agrees with the findings of the study by Lee *et al.* (2016) that suggest dysregulation of microvascular haemodynamics may be an important contributor to the pathophysiology of heart failure with preserved ejection fraction.

It was expected that alterations of the microcirculatory haemodynamics would be found for patients with atrial fibrillation, given the results of the study by Corban *et al*. (2020) suggest an absence of vascular endothelial dysfunction is associated with a lower risk of developing atrial fibrillation. Assessment of the atrial fibrillation group compared to controls show all ocular parameters except for wall shear rate were

increased in the atrial fibrillation group. This was not the case for the paced group, where the wall shear rate was significantly reduced.

Inter-arm blood pressure differences are reported to be associated with cardiovascular disease to include both peripheral and cerebral disease (Chang *et al*., 2017). Stergiou *et al*. (2021) recommend that an inter-arm systolic blood pressure difference of 20 mmHg or more should warrant further arterial investigation. Similarly, in this study inter-eye differences were reported to be significantly increased for all parameters except for blood flow rate in the CMD group compared to controls.

Binary logistic regression analysis found resting heart rate, axial velocity, NTproBNP and fibrinogen to be predictors of cardiovascular disease. The resultant AUC of 0.899, whilst not tested on a different cohort was much higher than what has been reported for the other risk prediction models such as the Framingham risk score at an AUC of 0.79 (Bitton and Gaziano, 2010). Stratifying the control group by QRISK3 classification further supported the addition of ocular parameters to cardiovascular risk scores, as significant differences for all ocular parameters except for cross-sectional velocity were reported.

Conclusion

Assessment of indices of the conjunctival microcirculation using the conjunctiva imaging tool and processing application may have the potential to detect haemodynamic differences due to electrical or structural changes. Additionally, inter-arm blood pressure differences should be measured and correlation with inter-eye differences assessed, to further evaluate the application of inter-eye differences. A multi-marker approach including clinical, ocular and blood biomarkers was proposed to successfully classify subjects into high cardiovascular risk and control groups. Significant differences in ocular parameters were found when the control group was stratified by QRISK3 score.

Chapter 8

Discussion

Chapter 8: Discussion

8.1. Discussion

The focal points of this research project included the development of the image processing application to support fully automated analysis, and the ability of the conjunctival microvascular imaging tool to detect differences between controls and macro and microvascular disease states, as well as in valvular disease with severe aortic stenosis patients pre- and post-transcatheter aortic valve implantation (TAVI). The ocular imaging results were also supported by the blood biomarkers, as well as various clinical measurements such as vital signs, anthropometric measurements and comorbidities for example. As previously shown (Awuah *et al*., 2022), the multi-marker risk scoring approach was again optimal for assessing the full 407 participant cohort. Table 8.1. presents a summary of results for discussion. This combination of results indicates alterations in haemodyamics are detectable using the imaging tool and processing application. The trend throughout the results was that axial or cross-sectional velocity and wall shear rate was typically reduced in high risk cardiovascular disease groups compared to a low risk control group. These findings are largely in agreement with the results of the literature review in chapter 1 and the included study by Karanam *et al*. (2014). This work builds on the literature with the findings reported for 2 cohorts that were not previously assessed, as well as evaluating the full 407 subject dataset and the development of the first known fully

automated smartphone based application for processing videos of the conjunctival microcirculation.

Table 8.1. Summary of results

Study	**Key Findings**
TAVI Cohort	• Arteriolar Va increased post-TAVI • Arteriolar CSV increased post-TAVI • Arteriolar WSR increased post-TAVI • Venular WSS reduced post-TAVI
CMD Cohort	• Va was reduced in the CMD group • CSV was reduced in the CMD group
Cardiac Remodeling	• Significant increase in Q of CMD, DM and HF

	groups compared to controls • Significant decrease in WSR of CMD, DM and HF groups compared to controls
Heart Rhythm	• All parameters except WSR significantly increased in AF group compared to controls • WSR significantly reduced in paced group compared to controls
Inter-eye Study	• Increased inter-eye differences of ocular parameters in the CMD group compared to the control group
Risk Scoring	• Predictors of cardiovascular disease= resting heart rate, Va, NTproBNP and fibrinogen • Significant differences for Va, Q and WSR

	between low, moderate and high-risk QRISK3 classes
AF Atrial Fibrillation, *CMD* Coronary Microvascular Disease, *DM* Diabetes Mellitus, *HF* Heart Failure, *TAVI* Transcatheter Aortic Valve Implantation, *Va* Axial Velocity, *CSV* Cross-Sectional Velocity, *Q* Blood Flow Rate, *WSR* Wall Shear Rate, *WSS* Wall Shear Stress, *NTproBNP* N-terminal pro B-type natriuretic peptide.	

Valvular Disease, TAVI and the Conjunctival Microcirculation:

Peripheral vascular and renal disease are commonly found in older individuals. However, significant difference between the controls and the TAVI cohort was demonstrated by Fusini *et al*. (2015) via the higher prevalence of coronary artery disease, as well as carotid and femoral artery disease seen with patients referred for TAVI being associated with significant stenosis, and hence atherosclerotic involvement of peripheral arteries. In severe aortic stenosis the left ventricle pressure overload may not be compensated by hypertrophy, and hence the left ventricular ejection fraction is reduced (Kamperidis *et al*., 2016).

Several studies have previously reported that coronary flow reserve (CFR) is also reduced (<2.0) in severe aortic stenosis, and coronary blood flow is also typically improved following TAVI (Ben-Dor *et al*., 2019). Comella *et al*. (2021) suggests that improvement of CFR and wall shear stress do not occur until much later within the post-operative period, and that this improvement is likely to correlate with the resolving of patient symptoms. This would agree with the results described within our study as wall shear rate would also be expected to improve later than the

approximate 24 hours after TAVI. An increase in wall shear rate is dependent on an increase in axial and cross-sectional velocity as previously described in Formula 2.

Although wall shear rate remained relatively unchanged post-TAVI in this study, it also found conjunctival wall shear stress (particularly venular wall shear stress) to be significantly reduced post-TAVI. This result is likely due to the significant reduction in haematocrit (HCT) post-TAVI. Although, it is possible this could also be due to the effects of pacing, as pacing leads may be implanted via venous access, and as discussed later in this chapter the wall shear rate of paced patients compared to controls was significantly reduced. Nevertheless, only 6 out of the 94 (6.4%) TAVI patients had a paced rhythm post-TAVI who did not have paced rhythm pre-TAVI. Wall shear stress reductions may be statistically significantly reduced for venules and not arterioles, as venules are the more common vessel segment within the conjunctiva microvasculature. A study by Nel *et al*. (2017) found an independent association of coronary microvascular blood flow with calcified aortic valve disease, and assessment between the pre-TAVI cohort with a matched control cohort was deemed necessary. Subsequently, the levels of wall shear stress may be reduced within the TAVI cohort when compared to that of controls. However, plasma viscosity was not measured for the controls within this study, limiting the wall shear stress calculations for that group.

Our previous study compared a cohort of myocardial infarction (MI) patients with patients referred for pressure wire assessment who had non-obstructive coronary artery disease (NOCAD). Similarly, severe aortic stenosis patients may also have

non-obstructive coronary arteries yet experience angina. Therefore, it may be due to microvascular dysfunction, and it has been proposed that normal microcirculatory function should resume post-TAVI (Rolandi *et al*., 2016).

It is acknowledged that cardiac remodeling experienced with severe aortic stenosis may influence microvascular function and haemodynamics. Left ventricular remodeling and hypertrophy would counterbalance the load, reducing wall stress and oxygen requirements, and is also associated with an inadequate capillary density (Zelis *et al*., 2020). It is possible that microvascular haemodynamic changes would not occur instantaneously. Proposedly, improvements may be seen with longer term follow-up of the microcirculation due to reverse remodeling (Minten *et al*., 2021).

Although no studies have assessed the conjunctival microvasculature pre- and post-TAVI, a study by Fusi-Rubiano *et al*. (2017) examined the retinal vessels due to the incidence of cerebrovascular events associated with TAVI. The study found 15% of patients post-TAVI experienced retinal embolic events. Whilst the current conjunctival imaging system does not directly assess embolic events, such events may significantly impact the results. It should be noted that unlike the conjunctival vasculature, the retinal vasculature is autoregulated and affected by an intraocular pressure pulse (Shi *et al*., 2019).

TAVI vs Controls; Blood Biomarkers:

Unsurprisingly, N-terminal pro B-type natriuretic peptide (NTproBNP) was found to be significantly increased in the TAVI cohort compared to the controls. Although,

increased NTproBNP may also be associated with aging, and the control group were significantly younger than the TAVI group but were all ≥60 years old. This finding is largely supported by the literature. Banovic (2017) proposed that NTproBNP values in combination with the non-invasive echocardiographic measurements of the microcirculation (CFR) may be used in risk stratification. The conjunctiva imaging risk stratification tool proposed in this thesis, whilst it is evidently not able to offer structural views of the heart that echocardiograms can, is more easily operated, less time-consuming and requires less contact with patients (of particular benefit during the COVID-19 pandemic).

Urea, creatinine, urate, total cholesterol, high density lipoprotein (HDL), low density lipoprotein (LDL), non-HDL and fibrinogen were significantly increased whilst creatinine clearance, haematocrit and activated partial thromboplastin time (APTT) were all significantly reduced in the TAVI cohort compared to controls. Increased lipids are an associated risk factor of aortic stenosis (Kaltoft *et al*., 2020). Fibrinolytic dysregulation and oxidative stress are also frequent reports in the pathophysiology of aortic stenosis (Siudut *et al*., 2020). Interestingly, increased perceived stress levels, another risk factor of cardiovascular disease, was associated with a shortened APTT in the study by Yin *et al*. (2021).

The renal physiology of older control patients would be expected to be significantly impaired in comparison to younger control patients. This difference is prominent between controls and patients with severe aortic stenosis, as these patients share similar risk factors such as hypertension for example. Urea is likely increased due to a decrease in reabsorption and decline in the number of urea channels, similarly, the increased creatinine levels of TAVI patients compared to controls may be due to

processes such as atrophy increasing the permeability of the proximal tubule (Musso *et al*., 2012). Alternatively, the increased creatinine, urea and urate levels may be a consequence of the significantly increased loop diuretic use of the TAVI cohort (El-Refai *et al*., 2011).

Pre vs Post-TAVI; Blood Biomarkers:

The findings of the increased inflammatory marker C-Reactive Protein (CRP) post-TAVI coincide with the results of previous studies (Ruparelia *et al*., 2016; Navaratnarajah *et al*., 2020). Iglesias-Álvarez *et al*. (2018) suggest that while there is an increase in CRP levels post-TAVI, it is the baseline CRP that is of greatest prognostic value as a marker of mortality post-TAVI. The findings of Iglesias-Álvarez *et al*. are also echoed by Stundl *et al*. (2018).

Similarly, the findings of reduced platelet count post-TAVI are reflective of the results within previous studies. It has also been suggested that the severity of platelet count reduction is associated with an increased frequency of major adverse cardiac events (Gallet *et al*., 2013). However, reports that reduced platelet count also occur with other cardiac procedures may indicate this to be a non-specific finding of TAVI (Mitrosz *et al*., 2017). The haematocrit levels were significantly reduced post-TAVI, and these results may present bias due to haemodilution (Horna *et al*., 2021). The increased prothrombin time may also be explained by the common phenomenon of thrombocytopenia post-TAVI (Mitrosz *et al*., 2017).

White cell count was also significantly increased in the study by Abu *et al*. (2021). It is also reported in this study that an increase in white cell count is associated with increased mortality and adverse events, to include major bleeding and arrhythmia post-TAVI. A further potential indicator of adverse events and mortality is that of the ratio of contrast to creatinine clearance post-TAVI. Venturi *et al*. (2022) suggested this to be useful for risk stratification, with values ≥2.2 associated with acute kidney injury and 90-day mortality. Lastly, incremental drops in haemoglobin are associated with increased mortality in the study by Takagi *et al*. (2021), and hence haemoglobin may also be useful for risk stratification purposes alongside the axial velocity, cross-sectional velocity and wall shear rate of the conjunctival arterioles.

Microvascular Disease, Pressure Wire Measurements and the Conjunctival Microcirculation:

This study found a significant reduction in the conjunctival axial and cross-sectional velocity of patients who were pressure wire positive (diagnosed with coronary microvascular disease (CMD)) compared to those who were pressure wire negative for CMD. The findings of axial and cross-sectional velocity were akin to those presented by Brennan *et al*. (2021a) in the earlier myocardial infarction vs controls study for this project. Consequently, this would suggest that conjunctiva microcirculation imaging may be capable of detecting changes due to pre-clinical myocardial dysfunction, from the earliest stages of the ischemic cascade to myocardial infarction at the later stages (Stillman *et al*., 2018). The axial and cross-sectional velocities may be reduced with these conditions due to the obstruction of blood flow.

Microvascular Disease Blood Biomarkers:

The significantly increased NTproBNP levels in pressure wire positive individuals agree with the literature. A study by Rahman *et al*. (2020) suggests that NTproBNP is increased with functional coronary microvascular disease (patients with increased nitric oxide synthase activity but normal acetylcholine dilation, and hence endothelial function). A more marked elevation was discerned with structural coronary microvascular disease due to endothelial dysfunction with reduced acetylcholine dilation.

Fibrinogen is a biomarker identified for cardiovascular risk due to its role in coagulation and the formation of thrombi. Additionally, elevated levels are associated with myocardial injury. Pieters *et al*. (2021) found from their 14-year long, 4487-person observational study an association of fibrinogen with all-cause and cardiovascular disease mortality. It had also been proposed that fibrinogen and viscoelastic testing may support cardiovascular risk stratification (Levy and Tanaka, 2021). Adverse remodeling and injury may result from dyslipidemia impairing microvascular function. Cholesterol:HDL and triglyceride levels were significantly reduced for the positive pressure wire group compared to the pressure wire negative group, and this may be a protective mechanism and reason as to why these patients have unobstructed epicardial vessels, as there was no significant difference on the number of patients on statins or cholesterol absorption inhibitors between the two groups. However, there were 5.1% more pressure wire negative subjects on statins compared to the pressure wire positive subjects, but 4.1% more pressure wire

positive subjects were on cholesterol absorption inhibitors compared to pressure wire negative subjects.

Ocular Haemodynamic Effects of Heart Rhythm and Cardiac Remodeling:

The findings presented in this thesis support imaging application of the conjunctiva for detecting changes in haemodynamics due to cardiac remodeling (both sub-clinical and clinical) or heart rhythm. The study by Soulat-Dufour *et al*. (2022) demonstrate the impact of arrhythmia on cardiac remodeling, as well as the effect of restoring sinus rhythm on reverse remodeling. This is in concurrence with the results of this study that shows significantly increased axial and cross-sectional velocities and blood flow rate with atrial fibrillation compared to controls. Furthermore, with paced patients the axial and cross-sectional velocities are similar to that of the controls. Unlike the comparison between atrial fibrillation patients and controls, where wall shear rate was only slightly reduced with atrial fibrillation in comparison to controls, wall shear rate was significantly reduced in paced patients compared to controls. As wall shear rate decreases so does wall shear stress, and an *in vivo* rabbit study by Jen *et al*. (2013) also shows a reduction of wall shear stress following rapid pacing. The study concludes that rapid pulse rates modulate endothelial responses. The modulation of the endothelium is key in cardiac contractility and remodeling (Segers *et al*., 2018).

The results assessing CMD, diabetes mellitus (DM) and heart failure (HF) groups in comparison to controls showed a significant increase in blood flow rate that may be due to vasodilation (Duncker *et al*., 2015). The CMD, DM and HF groups also

showed a significant decrease in wall shear rate compared to controls. As previously discussed, this is characteristic of atherosclerosis. The result of the significantly increased blood flow rate in diabetic patients compared to controls was previously reported in the study by Brennan *et al*. (2021a). These results may be due to the significantly older age and increased mean ocular diameter of the CMD, DM and HF groups when compared to the controls. The DM group also had a significantly increased body mass compared to the CMD and control group. The use of the single ocular marker wall shear rate at a cut-off point 0.4, had an area under the curve (AUC) of 0.772 for distinguishing between the CMD and control group. This finding largely agrees with the literature that suggests assessment of wall shear rate, as required for wall shear stress calculations, may support identification of high-risk atherosclerotic plaques (Cecchi *et al*., 2011).

Although the findings of this study show a significantly increased axial and cross-sectional velocity of the DM group compared to the CMD group, Labazi and Trask (2017) suggest there may also be a prognostic value to findings of CMD as an early stage in the development of atherosclerosis in DM. Similarly, whilst CMD may be at the sub-clinical stages of cardiovascular disease and HF at the later clinical stages of cardiovascular disease, it has been addressed by Mohammed *et al*. (2014) that CMD contributes to HF like DM also contributes to HF and vice versa (Braunwald, 2019).

Inter-eye Study:

The key findings of the inter-eye study include a significantly greater mean inter-eye difference for CMD compared to controls for diameter, axial velocity, cross-sectional velocity, wall shear rate and wall shear stress. No significant difference was found for

blood flow rate, yet blood flow rate is estimated using the parameters of diameter and cross-sectional velocity. The differences were also more marked in the left versus right nasal view. In a meta-analysis study conducted by Singh *et al*. (2015), the results indicate inter-limb blood pressure differences in association with cardiovascular risk stratification. The study suggests inter-arm blood pressure differences may be due to subclavian stenosis, and inter-limb differences may also be attributed to peripheral vascular disease. Tanaka *et al*. (2014) also conclude that inter-arm differences of systolic blood pressure may be associated with microvascular complications within a diabetic cohort.

This is the first study to assess inter-eye differences in the conjunctival microcirculation. Strauss *et al*. (2016) report that no significant differences were found within the retinal vasculature for inter-arm systolic blood pressure differences. Although, the study by Strauss *et al*. only considered retinal vessel caliber of younger individuals, and hence further study would be required.

Risk Scoring:

An earlier study within this research project indicated that NTproBNP, adiponectin and ocular velocities may be most valuable for distinguishing between MI and controls (Awuah *et al*., 2022). Comparably, looking at all cardiovascular risk cohorts recruited to this study combined as one high cardiovascular risk cohort, again found NTproBNP and ocular velocity to be accurate variables for distinguishing between the high cardiovascular risk and control groups. In this study, heart rate and fibrinogen were also found to be significant predictor variables via binary logistic

regression. The usefulness of the added biomarker fibrinogen is highlighted in the meta-analysis study by Kunutsor *et al*. (2016) that shows an independent association of fibrinogen with risk of sudden cardiac death. Caetano and Alves (2015) also suggest that heart rate is an independent risk factor for both cardiovascular and all-cause mortality. A risk score was also generated by Gauss *et al*. (2018), but for trauma upon hospital admission that incorporates both fibrinogen and heart rate. The study reported in this thesis did not find a significant correlation between heart rate and fibrinogen, but Whelton *et al*. (2014) found an increased resting heart rate to be significantly and independently associated with markers of inflammation, to include fibrinogen. The significance of fibrinogen as a risk marker of cardiovascular disease was stressed via the Emerging Risk Factors Collaboration (2012), that indicates fibrinogen testing for those determined to be of intermediate cardiovascular risk may support prevention of an adverse cardiovascular event occurring for every 400-500 people.

8.2. Limitations

The post-TAVI assessment typically occurred around 24 hours post procedure. It may be expected that follow-up assessment after a longer period has lapsed from the implanting of the new aortic valve would provide greater differences in results due to reverse cardiac remodelling. The conjunctival vessel analysis can also be limited by the video quality (particularly, for elderly and frail patients that may present with tremor), and the vessels analysed depends on the vessels that were both in view and in focus. Consequently, it can be difficult to assess the exact same vessel

segments in the conjunctival post assessment as were assessed in the conjunctival pre assessment. Furthermore, the average age of the TAVI cohort recruited in this study is 82 years, and thus frailty, and the incidence of ocular disease and other comorbidities, would also be increased within this cohort. A limitation of the pressure wire cohort included that vasospastic angina (that can occur alongside microvascular angina) was not fully investigated via vasoreactivity testing (Ford *et al*., 2018). In the inter-eye study, blood pressure measurements were not measured for each arm. It may have been beneficial to assess potential correlation between differences of inter-arm and inter-eye, comparable to the aforementioned retinal study conducted by Strauss *et al*.

Every effort was made to ensure method consistency, but conjunctival blood flow may be affected by medications (the details of which were recorded), the room lighting and even how the patient presents to the clinic. Additionally, although every effort would be made to ensure the patient was at ease and as comfortable as possible, if the patient presents to clinic stressed or anxious for example in the case of white-coat syndrome, the sympathetic nervous system would be activated (Pioli *et al*., 2018). Consequently, ocular vessel vasoconstriction and reduced ocular blood flow may occur. Ultimately, to better assess cardiovascular risk, consideration for an ambulatory, as well as a population-based multi-generational approach, similar to the Framingham risk study may be required (D'Agostino *et al*., 2013).

8.3. Conclusion

The findings of the matched vessel segment pre- and post-TAVI study suggests that imaging of the conjunctival microcirculation is capable of detecting changes in wall shear stress pre- to post-TAVI. Follow-up ocular imaging would be required to investigate changes in haemodynamics due to reverse cardiac remodeling. The results of the pressure wire study and haemodynamic investigations suggest that alterations of the microvascular haemodynamics within the conjunctiva, may reflect those of the coronary microcirculation. Therefore, the ocular imaging tool investigated within this thesis may support the diagnosis of microvascular dysfunction, as well as risk stratification.

Contributions to Knowledge:

The key message portrayed throughout this thesis is that the ocular microcirculation measurements, extracted from our conjunctival imaging tool and application, may provide an indication of cardiovascular health. The specific cohorts analysed offered a better insight into how these measurements hold potential for application in clinical practice. The results of the TAVI cohort demonstrate the use of the tool for serial measurements, and how treatment could be assessed and tailored for overall optimised patient care. The recruitment of older control subjects for comparison with the TAVI cohort also provided an insight into the effects of age on the microcirculation and latent reference ranges, whereas the pressure wire cohort notably confirms a correlation between the coronary microcirculation and the conjunctival microcirculation. Finally, the work within this thesis should also set the foundation for automation of vessel classification, and a more specific understanding of the structure of the conjunctival microvasculature under different conditions.

8.4. Future Research

Future studies should focus on further performance evaluation of the conjunctival microcirculation imaging and processing tool. Prior to the implementation in clinics, a usability assessment may also need to be conducted. Streamlining the current applications into an IOS or Android application may permit a more user-friendly interface for healthcare professionals or medical practitioners. Similar to other wearable medical devices and related smartphone applications, this imaging tool may also have potential as a remote monitoring device for the general population in future (Ballinger *et al*., 2018), particularly, with the potential of portable slit lamp and phone camera development to offer x80 magnification, in combination with recent advancements such as the application automation. Prospective slit lamp modifications should also seek to permit imaging of patients in the supine position. A device similar to that of a virtual reality headset could be used that has an internal fixation point for the subject to focus on. Additionally, better incorporation of artificial intelligence programming for vessel classification within the application would support a more comprehensive vessel analysis, offering measurements such as the artery to vein ratio. Future work may also assess microvasculature branching patterns and angles in comparison to the echocardiographic results, to investigate vascular and cardiac remodeling.

Further research requires assessment of the ocular imaging tool for long-term investigations. Prospectively, research of this investigative tool may again focus on expansion to examine further cohorts such as for a method of monitoring patients

following cardiac surgery. Monitoring this cohort would also enable comparisons to be made between percutaneous coronary intervention and surgery. It may be beneficial to investigate the ocular parameters in the pathophysiology of other organs such as the brain. Examination of long-COVID patients (particularly as they often experience chest pain or palpitations) may also be of interest, with the microcirculation being a main interface between the parenchymal cells and the blood, as well as an important transport system for inflammatory and immune cells (Guven *et al.,* 2019; Yin *et al.*, 2021). Another interesting area for investigation may be pregnancy, with Moka *et al*. (2020) previously reporting an increase in the axial velocity of pregnant patients. This examination may help to provide further insight into the physiological changes of the microcirculation and conditions such as preeclampsia or gestational diabetes. Ultimately, such investigation of the microcirculation may help uncover novel approaches to treatments and patient care.

Chapter 9

The PANDEMIC (Protective/risk factors, ANtibody response, Dna, gEnoMICs) Study

Chapter 9: The PANDEMIC (Protective/risk factors, ANtibody response, Dna, gEnoMICs) Study

Statement of Inclusion:

This chapter was included in consideration of the substantial COVID-19 research and mass testing studies accomplished during the brief pause in recruitment to cardiovascular disease risk prediction project due to the COVID-19 pandemic.

Summary

From the start of the COVID-19 pandemic (March 2020), there was a pause in recruitment for the cardiovascular risk prediction project outlined in this thesis. The focus shifted to supporting urgent COVID-19 research through study design, risk assessment, ethics application right through to the stages of validating COVID-19 tests. The three main strategies for managing the COVID-19 pandemic appeared to be enforcing preventative measures, testing and vaccination. The aim of the PANDEMIC study centered on investigation of the antibody response to SARS-CoV-2 infection. Between May 2020 and February 2021, over 500 participants were recruited to include members of the general public, Northern Ireland healthcare workers and plasma donors. Following the development and deployment of the SARS-CoV-2 vaccine we also assessed a cohort of vaccinated individuals. World

Health Organization international standards, pre-pandemic samples, microorganism serology samples, as well as serology from emerging SARS-CoV-2 variants of concern were also tested. To date, well over 1000 blood samples have been antibody tested on a selection of different immunoassays. Rapid antigen testing was also carried out to evaluate the performance of several SARS-CoV-2 rapid antigen tests, with postal studies being carried out across Northern Ireland to test SARS-CoV-2 positive samples, as well as clinic days being conducted under the COVID-19 regulations to test SARS-CoV-2 negative samples.

Graphical Abstract:

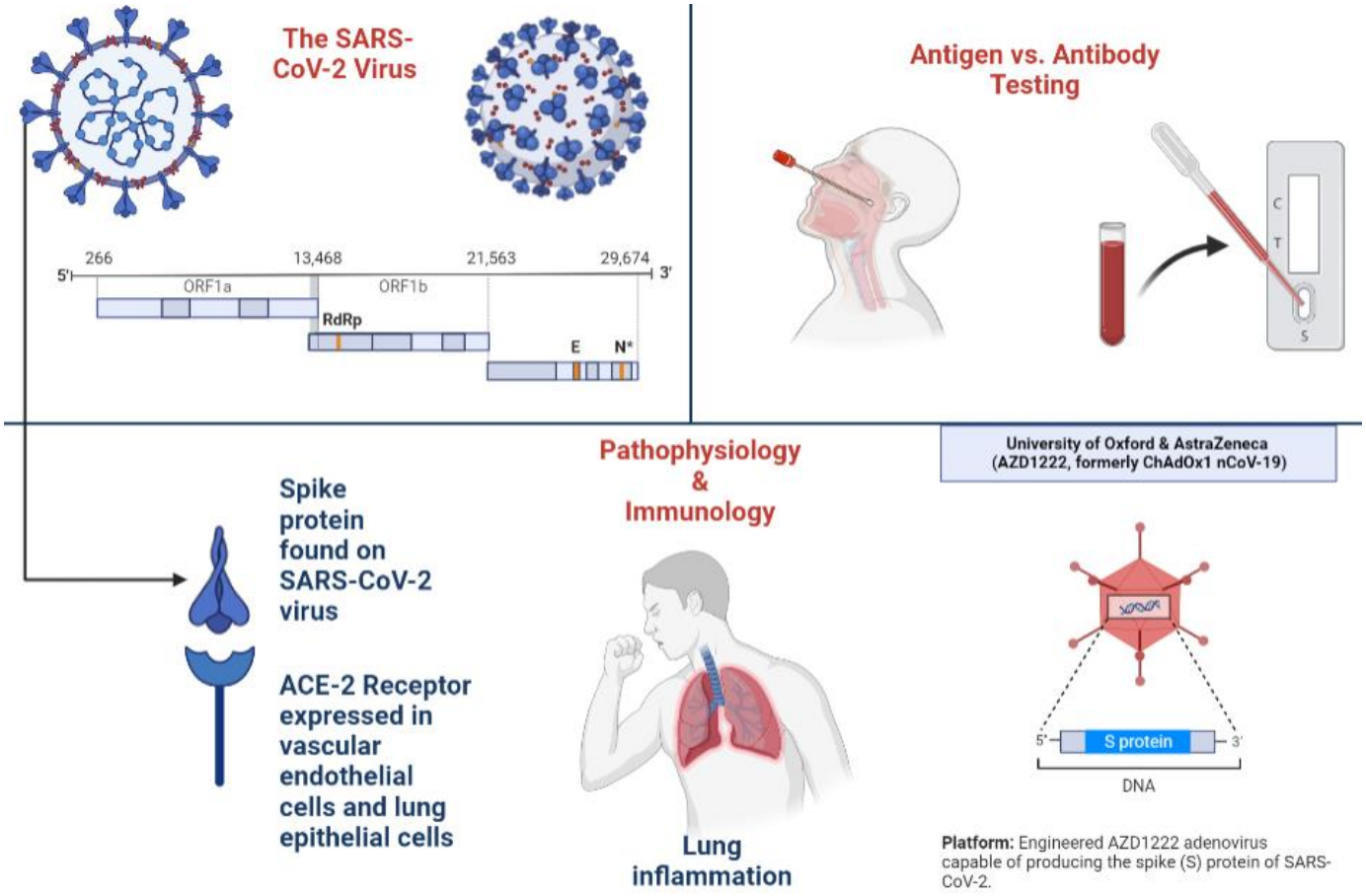

9.2 *Introduction*

The SARS-CoV-2 outbreak began in 2019 and sparked a global pandemic. The symptoms varied extensively; for some, SARS-CoV-2 infection was mild or even asymptomatic, whilst a large majority experienced fever, dry cough and loss of taste/smell. Sadly, for many the virus was life-threatening or even fatal, and hence research to learn how to prevent, manage and treat SARS-CoV-2 infection was urgent.

The impact of SARS-CoV-2 infection on the cardiovascular system has also been vastly reported. The SARS-CoV-2 virus has been found to bind to the angiotensin-converting enzyme 2 (ACE2) receptor, a receptor that has been previously suggested to have a cardioprotective role. Additionally, an inflammatory cascade and cytokine storm has been reported to occur with SARS-CoV-2 infection, and this may also lead to myocardial injury (Cenko *et al*., 2021). The long-term effects of the infection that became known as “long-COVID” still require investigation. This has become more apparent, with a recent large study suggesting that individuals who have had SARS-CoV-2 infection were more likely to develop diabetes or cardiovascular disease over a 12 month period than those who had not been infected (Rezel-Potts *et al*., 2022). The emergence of different variants of concern and the vaccine immune response also requires longitudinal study. Therefore, the main aim of the PANDEMIC study was to test various cohorts of participants and samples, and to evaluate a selection of SARS-CoV-2 antibody and antigen tests.

9.3 *Methods*

Cohorts:

All participants provided fully informed consent prior to enrolment in the study or had provided enduring consent if samples were used from other Ulster University studies. The study was approved by the South Birmingham Research Ethics Service (REC 20/WM/0184, IRAS 286041), and adhered to the Declaration of Helsinki.

SARS-CoV-2 humoral antibody testing was carried out using a selection of different tests as well as samples. Samples were deemed true positives if they tested positive for anti-SARS-CoV-2 IgG on two or more lab-based immunoassays, whilst samples were deemed true negatives if they tested negative on two or more lab-based immunoassays. Pre-pandemic samples were also considered to be true negatives. World Health Organization (WHO) and microorganism serology samples were also assessed.

The vaccine cohort also permitted investigation of the immune response in cohorts of clinically extremely vulnerable (CEV), to include those with cardiovascular disease, compared to non-CEV.

Antibody Testing:

The antibody tests used to investigate the SARS-CoV-2 immune response to infection or vaccination included Roche Elecsys Anti-SARS-CoV-2 IgG/IgA/IgM chemiluminescence immunoassays (CLIA) as tested by the laboratories at Craigavon Hospital, Abbott SARS-CoV-2 IgG CLIA as tested by the laboratories at

Northern Ireland Blood Transfusion Service (NIBTS) and EuroImmun SARS-CoV-2 IgG enzyme-linked immunosorbent assay (ELISA) carried out by PANDEMIC study researchers in accordance with manufacturer instructions. A selection of lateral flow devices (LFDs) to include AbC-19™ were also tested by PANDEMIC study researchers in accordance with the instructions for use/protocol. The ProAxsis Anti-SARS-CoV-2 IgG ELISA was later evaluated and samples tested by PANDEMIC study researchers, again in adherence to the corresponding protocol.

Antigen Testing:

The antigen testing involved evaluating the sensitive SARS-CoV-2 PCR result as the ground truth of infection. Typically, the cycle threshold of ORF1ab and E-gene from the RANDOX home PCR testing kit was compared to the rapid antigen test result of the LFD under investigation. Symptom details as well as time of onset and duration of infection were also often self-reported from participants via questionnaire. For usability investigations, details such as age groups, education levels and ease of use were assessed. Videos were often recorded of the participant (not including their face for anonymity/confidentiality purposes) for assessment of technique, and LFD photos permitted confirmation of test result.

Statistical Analysis:

A 2x2 contingency table was created for the sensitivity and specificity evaluation for each immunoassay under evaluation. Kappa scores were used to assess agreement between tests.

9.4 *Discussion*

Infection:

The first PANDEMIC study report by Robertson *et al*. (2021) found detectable SARS-CoV-2 full trimeric spike protein IgG antibodies 11 months post infection, in a cohort of participants from Northern Ireland. A longitudinal blood plasma donor study was also carried out. Similarly, SARS-CoV-2 antibodies were detected over 10 months for this study. The report described good correlation between the antibody tests evaluated.

Vaccination (including hybrid infection):

Following on from the PANDEMIC study and the report that focused on infection as discussed in the previous section, the vaccine cohort was recruited (Robertson *et al*., 2022). The vaccine cohort again consisted of a sample of patients from a Northern Ireland general practice clinic. Blood samples were collected from patients at time points (TP) 1-7. The TP1 sample was collected pre vaccination, TP2- three weeks post first vaccination, TP3- pre second vaccination, TP4- three weeks post second vaccination, TP5- six months post first vaccination, TP6- nine months post first vaccination and lastly, TP7 was collected post booster vaccination. The study showed that two doses of the Astrazeneca ChAdOx1 nCov-19 vaccine induced a strong anti-spike protein antibody response. The antibody response was detectable in the majority of the cohort to TP5. High-positive SARS-CoV-2 antibody levels were also reported in all individuals assessed at the post-booster timepoint (TP7) (Moore *et al*., 2022).

Faustini *et al*. (2022) assessed three cohorts of individuals post SARS-CoV-2 booster vaccination (Pfizer BioNtech 162b2) for cross-reactivity of the SARS-CoV-2 spike glycoprotein antibodies. The study detected antibodies for all cohorts 4 weeks post vaccination. Antibody levels were increased in the cohort that received the Astrazeneca ChAdOx1 nCov-19 vaccine compared to those who received the Pfizer BioNtech 162b2 for the previous two doses.

Cross-Reactivity; Variants of Concern and Microorganism Serology:

From the Astrazeneca ChAdOx1 nCov-19 cohort in the study by Faustini *et al*. (2022) discussed in the previous section, the results showed antibody levels and reactivity against Delta and Omicron variants significantly declined prior to the booster vaccination. The paper submission entitled “Performance of an Enzyme-Linked Immunosorbent Assay for the Serological Detection of Anti-SARS-CoV-2 IgG Across >1100 Samples” also assesses cross-reactivity, to include variants of concern and microorganism serology, as does the manuscript entitled “Evaluation of the Performance of a Lateral Flow Device for Quantitative Detection of Anti-SARS-CoV-2 IgG” (Moore *et al*., 2022).

Test Usability:

The PANDEMIC study also assessed Northern Ireland cohorts in the usability of the self-administered AbC-19™ rapid point of care antibody LFD test during a large car-park study of 1544 participants (Jing *et al*., 2021), as well as within a later postal study to assess use in the home environment (Jing *et al*., 2022b). These studies were conducted to help with the development and design of rapid point of care tests

for ease of use. The two studies were in agreement that the test was predominantly user-friendly. Difficulties with the collection and application of the capillary blood sample from the participant's finger to the test were noted. Expectedly, the findings also suggest the participant's encountered difficulties in reading faint test results.

Although the focus of the studies was on SARS-CoV-2 IgG antibody testing, the information obtained is transferrable for the development of other rapid point of care serology tests, such as for the cardiovascular blood biomarkers discussed previously. The PANDEMIC study also considered the use of a smartphone application to read the results of the rapid point of care test via the colour intensity of the test band. Moreover, this would be particularly beneficial as smartphone health applications grow more popular. Especially, for the cardiovascular risk application using the ocular and blood biomarkers as proposed in the earlier sections, or as discussed in a different study by Jing *et al*. (2020) that investigates CRP concentrations via T-line intensity changes on LFD. Such technology also gives rise to the potential of remote monitoring that was particularly useful during the pandemic.

The impact of COVID and long-COVID on cardiovascular disease:

Those with cardiovascular disease were considered clinically extremely vulnerable or of high-risk of COVID-19. However, it may be that those infected with COVID-19 are also at high-risk of cardiovascular disease. The angiotensin-converting enzyme-2 (ACE-2) receptor is expressed throughout the cardiopulmonary system and facilitates entry of SARS-CoV-2 into cells (Task Force for the Management of

COVID-19 of the European Society of Cardiology, 2022). ACE-2 has been suggested to be lung-protective, and the binding of the SARS-CoV-2 spike protein the ACE-2 receptors downregulates ACE-2. The vascular endothelial cell damage seen with SARS-CoV-2 infection may occur as a result of this downregulation of ACE-2 (Lei *et al*., 2021; Maccio *et al*., 2021).

A 153,760-person study conducted by Xie *et al*. (2022) indicates that approximately one month post infection increased risks and twelve month burden of cardiovascular diseases ensues. Given long-COVID symptoms may be shared with those of cardiovascular disease such as the symptom of shortness of breath, the importance of cardiovascular investigation is heightened. Particularly from the earliest stages as our ocular imaging tool aims to implement. Sulli *et al*. (2022) also support imaging of the microvasculature following COVID-19 infection, describing alterations in nailfold videocapillaroscopy results to include capillary rarefaction due to COVID-19. Further reports of microvascular injury have also been described owing to microthrombi (with hypercoagulability and thrombosis events systematically increased), elevated inflammatory markers, hypoxia with pulmonary microvascular damage potentially leading to right heart failure (Giacca and Shah, 2022; Raman *et al*., 2022).

Limitations:

While a proportion of patients recruited to the cardiovascular disease risk study that this thesis primarily focuses on, the infection and vaccination status of those patients was not a focus within the data collection form for the study. Furthermore, whilst it was known that a small proportion of the vaccine cohort were clinically extremely

vulnerable due to cardiovascular disease, ocular imaging was not carried out on those individuals. At the commencement of the pandemic, testing was limited and many people who had COVID may not have had a confirmed diagnosis, or were even asymptomatic, and hence unaware they had COVID. The restrictions also made testing difficult, with the older and high-risk populations shielding. The PANDEMIC study attempted to adapt to this, such as with the outdoor carpark study, where extra logistical measures and risk assessment considerations were required.

Moreover, not everyone who was infected with COVID may have elicited a detectable humoral response, and the cellular response was not tested. The timing of antibody testing was also crucial. IgM may be detected shortly following acute infection, but detection of IgG may be as late as 2 weeks after infection. Assessing true positive SARS-CoV-2 IgG samples was also difficult, as no gold-standard SARS-CoV-2 antibody test existed. Lastly, it was expected that a proportion of participants may not be available for follow-up, particularly, given the longitudinal nature of investigating the immune response within the vaccine cohort.

Conclusion

The PANDEMIC study supported both antibody and antigen test evaluation, as well as contributed to the understanding of SARS-CoV-2 transmission and sero-epidemiology in Northern Ireland. The monitoring of the SARS-CoV-2 immune response was of particular importance in reaction to the SARS-CoV-2 vaccination programme, as well as emerging variants of concern. Future research should

investigate long-COVID, specifically, in relation to cardiovascular disease given the inflammatory nature of the infection.

Chapter 10

References

Chapter 10: References

Abdulsahib, A.A., Mahmoud, M.A., Mohammed, M.A., Rasheed, H.H., Mostafa, S.A. and Maashi, M.S., 2021. Comprehensive review of retinal blood vessel segmentation and classification techniques: Intelligent solutions for green computing in medical images, current challenges, open issues, and knowledge gaps in fundus medical images. *Network Modeling Analysis in Health Informatics and Bioinformatics*, *10*(1), pp.1-32.

Abu Khadija, H., Gandelman, G., Ayyad, O., Jaber, M., Poles, L., Jonas, M., Paz, O., Abu Sbaih, F., Sella, G., Shimoni, S. and George, J., 2021. Differential systemic inflammatory responses after TAVI: The role of self versus balloon expandable devices. *PloS one*, *16*(10), p.e0258963.

Ahn, S.G., Hung, O.Y., Lee, J.W., Lee, J.H., Youn, Y.J., Ahn, M.S., Kim, J.Y., Yoo, B.S., Lee, S.H., Yoon, J. and Kwon, W., 2016. Combination of the thermodilution-derived index of microcirculatory resistance and coronary flow reserve is highly predictive of microvascular obstruction on cardiac magnetic resonance imaging after ST-segment elevation myocardial infarction. *JACC: Cardiovascular Interventions*, *9*(8), pp.793-801.

Akagi, T., Uji, A., Huang, A.S., Weinreb, R.N., Yamada, T., Miyata, M., Kameda, T., Ikeda, H.O. and Tsujikawa, A., 2018. Conjunctival and intrascleral vasculatures assessed using anterior segment optical coherence tomography angiography in normal eyes. *American journal of ophthalmology*, *196*, pp.1-9.

Alam, M., Son, T., Toslak, D., Lim, J.I. and Yao, X., 2018. Combining ODR and blood vessel tracking for artery–vein classification and analysis in color fundus images. *Translational vision science & technology*, *7*(2), pp.23-23.

Alastruey, J., Siggers, J.H., Peiffer, V., Doorly, D.J. and Sherwin, S.J., 2012. Reducing the data: Analysis of the role of vascular geometry on blood flow patterns in curved vessels. *Physics of Fluids*, *24*(3), p.031902.

AlBadawi, S. and Fraz, M.M., 2018, June. Arterioles and venules classification in retinal images using fully convolutional deep neural network. In *International Conference Image Analysis and Recognition* (pp. 659-668). Springer, Cham.

Allon, R., Aronov, M., Belkin, M., Maor, E., Shechter, M. and Fabian, I.D., 2021. Retinal microvascular signs as screening and prognostic factors for cardiac disease: A systematic review of current evidence. *The American Journal of Medicine*, *134*(1), pp.36-47.

Al-Rashid, F., Hildebrandt, H., Baars, T., El Chilali, K., Wendt, D., Thielmann, M., Jakob, H., Kottenberg, E., Peters, J., Erbel, R. and Heusch, G., 2014. TCT-717 Coronary Microcirculation during Transfemoral Transcatheter Aortic Valve Implantation. *Journal of the American College of Cardiology*, *64*(11S), pp.B210-B211.

Andersson, M., Ebbers, T. and Karlsson, M., 2019. Characterization and estimation of turbulence-related wall shear stress in patient-specific pulsatile blood flow. *Journal of biomechanics*, *85*, pp.108-117.

Awuah, A., Moore, J.S., Nesbit, M.A., Ruddock, M.W., Brennan, P.F., Mailey, J.A., McNeil, A.J., Jing, M., Finlay, D.D., Trucco, E. and Kurth, M.J., 2022. A novel

algorithm for cardiovascular screening using conjunctival microcirculatory parameters and blood biomarkers. *Scientific reports*, *12*(1), pp.1-9.

Bach, D.S., 2011. Prevalence and characteristics of unoperated patients with severe aortic stenosis. *The Journal of heart valve disease*, *20*(3), pp.284-291.

Ballinger, B., Hsieh, J., Singh, A., Sohoni, N., Wang, J., Tison, G.H., Marcus, G.M., Sanchez, J.M., Maguire, C., Olgin, J.E. and Pletcher, M.J., 2018, April. DeepHeart: semi-supervised sequence learning for cardiovascular risk prediction. In *Thirty-Second AAAI Conference on Artificial Intelligence*.

Balogh, P. and Bagchi, P., 2019. Three-dimensional distribution of wall shear stress and its gradient in red cell-resolved computational modeling of blood flow in in vivo-like microvascular networks. *Physiological reports*, *7*(9), p.e14067.

Banovic, M.D., 2017. NT-proBNP in patients with asymptomatic severe aortic stenosis: relation to coronary microvascular function. *Biomarkers in Medicine*, *11*(6), pp.409-414.

Ben-Dor, I., Malik, R., Goldstein, S.A., Wang, Z., Magalhaes, M.A., Weissman, G., Okubagzi, P.G., Torguson, R., Lindsay, J., Satler, L.F. and Pichard, A.D., 2014.

Coronary blood flow in patients with severe aortic stenosis before and after transcatheter aortic valve implantation. *The American journal of cardiology*, *114*(8), pp.1264-1268.

Bhuiyan, A., Cheung, C.Y., Frost, S., Lamoureux, E., Mitchell, P., Kanagasingam, Y. and Wong, T.Y., 2014. Development and reliability of retinal arteriolar central light reflex quantification system: a new approach for severity grading. *Investigative ophthalmology & visual science*, *55*(12), pp.7975-7981.

Bitton, A. and Gaziano, T., 2010. The Framingham Heart Study's impact on global risk assessment. *Progress in cardiovascular diseases*, *53*(1), pp.68-78.

Braunwald, E., 2019. Diabetes, heart failure, and renal dysfunction: the vicious circles. *Progress in cardiovascular diseases*, *62*(4), pp.298-302.

Brennan, P.F., McNeil, A.J., Jing, M., Awuah, A., Finlay, D.D., Blighe, K., McLaughlin, J.A., Wang, R., Moore, J., Nesbit, M.A. and Trucco, E., 2019. Quantitative assessment of the conjunctival microcirculation using a smartphone and slit-lamp biomicroscope. *Microvascular research*, *126*, p.103907.

Brennan, P.F., McNeil, A.J., Jing, M., Awuah, A., Moore, J.S., Mailey, J., Finlay, D.D., Blighe, K., McLaughlin, J.A., Nesbit, M.A. and Trucco, E., 2021a. Assessment of the conjunctival microcirculation for patients presenting with acute myocardial infarction compared to healthy controls. *Scientific reports*, *11*(1), pp.1-9.

Brennan, P.F., Jing, M., McNeil, A.J., Awuah, A., Mailey, J., Kelly, B., Finlay, D.D., Blighe, K., McLaughlin, J.A., Nesbit, M.A. and Trucco, E., 2021b. Assessment of the conjunctival microcirculation in adult patients with cyanotic congenital heart disease compared to healthy controls. *Microvascular Research*, *136*, p.104167.

Caetano, J. and Alves, J.D., 2015. Heart rate and cardiovascular protection. *European journal of internal medicine*, *26*(4), pp.217-222.

Camuglia, A.C., Syed, J., Garg, P., Kiaii, B., Chu, M.W., Jones, P.M., Bainbridge, D. and Teefy, P.J., 2014. Invasively assessed coronary flow dynamics improve following relief of aortic stenosis with transcatheter aortic valve implantation. *Journal of the American College of Cardiology*, *63*(17), pp.1808-1809.

Carabello, B.A., 2013. Introduction to aortic stenosis. *Circulation research*, *113*(2), pp.179-185.

Cecchi, E., Giglioli, C., Valente, S., Lazzeri, C., Gensini, G.F., Abbate, R. and Mannini, L., 2011. Role of hemodynamic shear stress in cardiovascular disease. *Atherosclerosis*, *214*(2), pp.249-256.

Cenko, E., Badimon, L., Bugiardini, R., Claeys, M.J., De Luca, G., de Wit, C., Derumeaux, G., Dorobantu, M., Duncker, D.J., Eringa, E.C. and Gorog, D.A., 2021. Cardiovascular disease and COVID-19: a consensus paper from the ESC Working Group on Coronary Pathophysiology & Microcirculation, ESC Working Group on Thrombosis and the Association for Acute CardioVascular Care (ACVC), in collaboration with the European Heart Rhythm Association (EHRA). *Cardiovascular research*, *117*(14), pp.2705-2729.

Chang, Y., Choi, G.S., Lim, S.M., Kim, Y.J. and Song, T.J., 2018. Interarm systolic and diastolic blood pressure difference is diversely associated with cerebral atherosclerosis in noncardioembolic stroke patients. *American Journal of Hypertension*, *31*(1), pp.35-42.

Chen, Q., Jiang, H. and Wang, J., 2020. Conjunctival vascular adaptation related to ocular comfort in habitual contact lens wearers. *American journal of ophthalmology*, *216*, pp.99-109.

Chen, W., Xu, Z., Jiang, H., Zhou, J., Wang, L. and Wang, J., 2017a. Altered bulbar conjunctival microcirculation in response to contact lens wear. *Eye & contact lens*, *43*(2), p.95.

Chen, W., Batawi, H.I.M., Alava, J.R., Galor, A., Yuan, J., Sarantopoulos, C.D., McClellan, A.L., Feuer, W.J., Levitt, R.C. and Wang, J., 2017b. Bulbar conjunctival microvascular responses in dry eye. *The ocular surface*, *15*(2), pp.193-201.

Cheung, A.T.W., Hu, B.S., Wong, S.A., Chow, J., Chan, M.S., To, W.J., Li, J., Ramanujam, S. and Chen, P.C.Y., 2012. Microvascular abnormalities in the bulbar conjunctiva of contact lens users. *Clinical hemorheology and microcirculation*, *51*(1), pp.77-86.

Cheung, C.Y., Xu, D., Cheng, C.Y., Sabanayagam, C., Tham, Y.C., Yu, M., Rim, T.H., Chai, C.Y., Gopinath, B., Mitchell, P. and Poulton, R., 2021. A deep-learning system for the assessment of cardiovascular disease risk via the measurement of retinal-vessel calibre. *Nature biomedical engineering*, *5*(6), pp.498-508.

Cífková, R., Harazny, J.M., Bruthans, J., Wohlfahrt, P., Krajčoviechová, A., Lánská, V., Gelžinský, J., Mateřánková, M., Mareš, Š., Filipovský, J. and Mayer Jr, O., 2021. Reference values of retinal microcirculation parameters derived from a population random sample. *Microvascular research*, *134*, p.104117.

Cohen, J.F., Korevaar, D.A., Altman, D.G., Bruns, D.E., Gatsonis, C.A., Hooft, L., Irwig, L., Levine, D., Reitsma, J.B., De Vet, H.C. and Bossuyt, P.M., 2016. STARD 2015 guidelines for reporting diagnostic accuracy studies: explanation and elaboration. *BMJ open*, *6*(11).

Colbert, J.F. and Schmidt, E.P., 2016. Endothelial and microcirculatory function and dysfunction in sepsis. *Clinics in chest medicine*, *37*(2), pp.263-275.

Comella, A., Michail, M., Chan, J., Cameron, J.D., Gooley, R., Mathur, A., Hughes, A.D. and Brown, A.J., 2021. Patients with aortic stenosis exhibit early improved

endothelial function following transcatheter aortic valve replacement: The eFAST study. *International Journal of Cardiology*, *332*, pp.143-147.

Cordina, R., Leaney, J., Golzan, M., Grieve, S., Celermajer, D.S. and Graham, S.L., 2015. Ophthalmological consequences of cyanotic congenital heart disease: vascular parameters and nerve fibre layer. *Clinical & experimental ophthalmology*, *43*(2), pp.115-123.

Critical Appraisal Skills Programme (2018). *CASP cohort study checklist*. [online] Available at: https://casp-uk.b-cdn.net/wp-content/uploads/2018/03/CASP-Cohort-Study-Checklist-2018_fillable_form.pdf

D'Agostino Sr, R.B., Pencina, M.J., Massaro, J.M. and Coady, S., 2013. Cardiovascular disease risk assessment: insights from Framingham. *Global heart*, *8*(1), pp.11-23.

Dai, N., Che, W., Liu, L., Zhang, W., Yin, G., Xu, B., Xu, Y., Duan, S., Yu, H., Li, C. and Yao, K., 2021. Diagnostic Value of Angiography-Derived IMR for Coronary Microcirculation and Its Prognostic Implication After PCI. *Frontiers in cardiovascular medicine*, p.1273.

Dashtbozorg, B., Mendonça, A.M. and Campilho, A., 2013. An automatic graph-based approach for artery/vein classification in retinal images. *IEEE Transactions on Image Processing*, *23*(3), pp.1073-1083.

Della-Morte, D. and Rundek, T., 2015. The role of shear stress and arteriogenesis in maintaining vascular homeostasis and preventing cerebral atherosclerosis. *Brain Circulation*, *1*(1), p.53.

Ding, Y., Ward, W.O., Duan, J., Auer, D.P., Gowland, P. and Bai, L., 2015. Retinal vasculature classification using novel multifractal features. *Physics in Medicine & Biology*, *60*(21), p.8365.

Dubin, A., Edul, V.S.K., Eguillor, J.F.C. and Ferrara, G., 2020. Monitoring Microcirculation: Utility and Barriers–A Point-of-View Review. *Vascular health and risk management*, *16*, p.577.

Duncker, D.J., Koller, A., Merkus, D. and Canty Jr, J.M., 2015. Regulation of coronary blood flow in health and ischemic heart disease. *Progress in cardiovascular diseases*, *57*(5), pp.409-422.

El-Refai, M., Krivospitskaya, O., Peterson, E.L., Wells, K., Williams, L.K. and Lanfear, D.E., 2011. Relationship of loop diuretic dosing and acute changes in renal function during hospitalization for heart failure. *Journal of clinical & experimental cardiology*, *2*(10).

Emerging Risk Factors Collaboration, 2012. C-reactive protein, fibrinogen, and cardiovascular disease prediction. *New England Journal of Medicine*, *367*(14), pp.1310-1320.

Fang, M., Airen, S., Jiang, H. and Wang, J., 2021. Ocular surface microvascular response and its relation to contact lens fitting and ocular comfort: an update of recent research. *Clinical and experimental optometry*, *104*(6), pp.661-671.

Fearon, W.F. and Kobayashi, Y., 2017. Invasive assessment of the coronary microvasculature: the index of microcirculatory resistance. *Circulation: Cardiovascular Interventions*, *10*(12), p.e005361.

Feuer, D.S., Handberg, E.M., Mehrad, B., Wei, J., Merz, C.N.B., Pepine, C.J. and Keeley, E.C., 2022. Microvascular dysfunction as a systemic disease: A review of the evidence. *The American Journal of Medicine*.

Flick, M., Duranteau, J., Scheeren, T.W. and Saugel, B., 2020. Monitoring of the sublingual microcirculation during cardiac surgery: current knowledge and future directions. *Journal of cardiothoracic and vascular anesthesia*, *34*(10), pp.2754-2765.

Ford, T.J., Rocchiccioli, P., Good, R., McEntegart, M., Eteiba, H., Watkins, S., Shaukat, A., Lindsay, M., Robertson, K., Hood, S. and Yii, E., 2018. Systemic microvascular dysfunction in microvascular and vasospastic angina. *European heart journal*, *39*(46), pp.4086-4097.

Frangogiannis, N.G., 2021. Cardiac fibrosis. *Cardiovascular Research*, *117*(6), pp.1450-1488.

Fraz, M.M., Rudnicka, A.R., Owen, C.G., Strachan, D.P. and Barman, S.A., 2014, January. Automated arteriole and venule recognition in retinal images using ensemble classification. In *2014 International Conference on Computer Vision Theory and Applications (VISAPP)* (Vol. 3, pp. 194-202). IEEE.

Fredriksson, I., Larsson, M., Strömberg, T. and Iredahl, F., 2021. Vasomotion analysis of speed resolved perfusion, oxygen saturation, red blood cell tissue fraction, and vessel diameter: Novel microvascular perspectives. *Skin Research and Technology*.

Fu, H., Wang, B., Shen, J., Cui, S., Xu, Y., Liu, J. and Shao, L., 2019, October. Evaluation of retinal image quality assessment networks in different color-spaces. In *International Conference on Medical Image Computing and Computer-Assisted Intervention* (pp. 48-56). Springer, Cham.

Fusi-Rubiano, W.J., Yang, Y.C., Smallwood, A.F., Chavan, R.C., Khogali, S., Narendran, N. and Cotton, J.M., 2017. Retinal embolic events: frequency and impact following transcatheter aortic valve implantation (TAVI) for aortic stenosis. *BMJ open ophthalmology*, *1*(1), p.e000033.

Fusini, L., Mirea, O., Tamborini, G., Muratori, M., Gripari, P., Cefalù, C., Ghulam Ali, S., Maffessanti, F., Andreini, D., Pontone, G. and Bartorelli, A.L., 2015. Incidence and severity of atherosclerotic cardiovascular artery disease in patients undergoing TAVI. *The international journal of cardiovascular imaging*, *31*(5), pp.975-985.

Gallet, R., Seemann, A., Yamamoto, M., Hayat, D., Mouillet, G., Monin, J.L., Gueret, P., Couetil, J.P., Dubois-Randé, J.L., Teiger, E. and Lim, P., 2013. Effect of transcatheter (via femoral artery) aortic valve implantation on the platelet count and its consequences. *The American journal of cardiology*, *111*(11), pp.1619-1624.

Gauss, T., Campion, S., Kerever, S., Eurin, M., Raux, M., Harrois, A., Paugam-Burtz, C. and Hamada, S., 2018. Fibrinogen on Admission in Trauma score. *European journal of anaesthesiology*, *35*(1), pp.25-32.

Giacca, M. and Shah, A.M., 2022. The pathological maelstrom of COVID-19 and cardiovascular disease. *Nature Cardiovascular Research*, *1*(3), pp.200-210.

Gijsen, F., Katagiri, Y., Barlis, P., Bourantas, C., Collet, C., Coskun, U., Daemen, J., Dijkstra, J., Edelman, E., Evans, P. and Van Der Heiden, K., 2019. Expert recommendations on the assessment of wall shear stress in human coronary arteries: existing methodologies, technical considerations, and clinical applications. *European heart journal*, *40*(41), pp.3421-3433.

Godo, S., Corban, M.T., Toya, T., Gulati, R., Lerman, L.O. and Lerman, A., 2020. Association of coronary microvascular endothelial dysfunction with vulnerable plaque

characteristics in early coronary atherosclerosis. *EuroIntervention: journal of EuroPCR in collaboration with the Working Group on Interventional Cardiology of the European Society of Cardiology*, *16*(5), pp.387-394.

Gnasso, A., Cacia, M., Cutruzzolà, A., Minieri, M., Carallo, C., Cortese, C. and Irace, C., 2019. Influence of acute reduction of blood viscosity on endothelial function. *Clinical Hemorheology and Microcirculation*, *72*(3), pp.239-245.

Groepenhoff, F., Klaassen, R.G.M., Valstar, G.B., Bots, S.H., Onland-Moret, N.C., Den Ruijter, H.M., Leiner, T. and Eikendal, A.L., 2021. Evaluation of non-invasive imaging parameters in coronary microvascular disease: a systematic review. *BMC medical imaging*, *21*(1), pp.1-23.

Guven, G. and Ince, C., 2019. Does Monitoring the Microcirculation Make a Difference in Sepsis? Outcome?. *Evidence-Based Practice of Critical Care E-Book*, *19*(3), p.256.

Guven, G., Hilty, M.P. and Ince, C., 2020. Microcirculation: physiology, pathophysiology, and clinical application. *Blood purification*, *49*(1-2), pp.143-150.

Guyatt, G.H., Thorlund, K., Oxman, A.D., Walter, S.D., Patrick, D., Furukawa, T.A., Johnston, B.C., Karanicolas, P., Akl, E.A., Vist, G. and Kunz, R., 2013. GRADE guidelines: 13. Preparing summary of findings tables and evidence profiles—continuous outcomes. *Journal of clinical epidemiology*, *66*(2), pp.173-183.

Hamilos, M., Petousis, S. and Parthenakis, F., 2018. Interaction between platelets and endothelium: from pathophysiology to new therapeutic options. *Cardiovascular diagnosis and therapy*, *8*(5), p.568.

Haider, A., Bengs, S., Maredziak, M., Messerli, M., Fiechter, M., Giannopoulos, A.A., Treyer, V., Schwyzer, M., Kamani, C.H., Patriki, D. and von Felten, E., 2019. Heart

rate reserve during pharmacological stress is a significant negative predictor of impaired coronary flow reserve in women. *European Journal of Nuclear Medicine and Molecular Imaging*, *46*(6), pp.1257-1267.

Hilty, M.P., Guerci, P., Ince, Y., Toraman, F. and Ince, C., 2019. MicroTools enables automated quantification of capillary density and red blood cell velocity in handheld vital microscopy. *Communications biology*, *2*(1), pp.1-15.

Horna, S., Pollari, F., Jessl, J., Vogt, F. and Fischlein, T., 2021. Outcomes for In-Hospital Thrombocytopenia after TAVI. *The Thoracic and Cardiovascular Surgeon*, *69*(S 01), pp.DGTHG-eP100.

Hu, L., Shi, C., Jiang, H., Shi, Y., Sethi, Z. and Wang, J., 2018. Factors affecting microvascular responses in the bulbar conjunctiva in habitual contact lens wearers. *Investigative ophthalmology & visual science*, *59*(10), pp.4108-4114.

Huang, F., Dashtbozorg, B., Zhang, J., Bekkers, E., Abbasi-Sureshjani, S., Berendschot, T.T. and ter Haar Romeny, B.M., 2016. Reliability of using retinal vascular fractal dimension as a biomarker in the diabetic retinopathy detection. *Journal of ophthalmology*, *2016*.

Huang, L., Aris, I.M., Teo, L.L., Wong, T.Y., Chen, W.Q., Koh, A.S. and Li, L.J., 2020. Exploring associations between cardiac structure and retinal vascular geometry. *Journal of the American Heart Association*, *9*(7), p.e014654.

Hwang, J., Karanam, V., Wang, J., Feuer, W.J., Garg, R.K., Tamariz, L. and Galor, A., 2021. Conjunctival Vessels in Diabetes Using Functional Slit Lamp Biomicroscopy. *Cornea*, *40*(8), pp.950-957.

Ichihashi, T., Hirabayashi, Y. and Nagahara, M., 2017. Potential utility of a 4K consumer camera for surgical education in ophthalmology. *Journal of ophthalmology*, *2017*.

Iglesias-Álvarez, D., López-Otero, D., González-Ferreiro, R., Sanmartín-Pena, X., Cid-Álvarez, B., Trillo-Nouche, R. and González-Juanatey, J.R., 2018. Prognostic value of hs-CRP after transcatheter aortic valve implantation. *Circulation: Cardiovascular Interventions*, *11*(12), p.e007213.

Ioannidis, J.P. and Tzoulaki, I., 2012. Minimal and null predictive effects for the most popular blood biomarkers of cardiovascular disease. *Circulation research*, *110*(5), pp.658-662.

Ishii, M., Kaikita, K., Mitsuse, T., Nakanishi, N., Oimatsu, Y., Yamashita, T., Nagamatsu, S., Tabata, N., Fujisue, K., Sueta, D. and Takashio, S., 2019. Reduction in thrombogenic activity and thrombocytopenia after transcatheter aortic valve implantation—The ATTRACTIVE-TTAS study. *IJC Heart & Vasculature*, *23*, p.100346.

Ishikawa, S., Yoshinaga, Y., Kantake, D., Nakamura, D., Yoshida, N., Hisatomi, T., Ikeda, Y., Ishibashi, T. and Enaida, H., 2019. Development of a novel noninvasive system for measurement and imaging of the arterial phase oxygen density ratio in the retinal microcirculation. *Graefe's Archive for Clinical and Experimental Ophthalmology*, *257*(3), pp.557-565.

Ito, S., Miranda, W.R., Nkomo, V.T., Connolly, H.M., Pislaru, S.V., Greason, K.L., Pellikka, P.A., Lewis, B.R. and Oh, J.K., 2018. Reduced left ventricular ejection fraction in patients with aortic stenosis. *Journal of the American College of Cardiology*, *71*(12), pp.1313-1321.

Jiang, H., Ye, Y., DeBuc, D.C., Lam, B.L., Rundek, T., Tao, A., Shao, Y. and Wang, J., 2013. Human conjunctival microvasculature assessed with a retinal function imager (RFI). *Microvascular research*, *85*, pp.134-137.

Jiang, H., Zhong, J., DeBuc, D.C., Tao, A., Xu, Z., Lam, B.L., Liu, C. and Wang, J., 2014. Functional slit lamp biomicroscopy for imaging bulbar conjunctival microvasculature in contact lens wearers. *Microvascular research*, *92*, pp.62-71.

Jing, M. *et al.* Enhance categorisation of multilevel high-sensitivity cardiovascular biomarkers from lateral flow immunoassay images via neural networks and dynamic time warping. In *2020 IEEE International Conference on Image Processing (ICIP)*, 365–369 (IEEE, 2020).

Jing, M., Moore, J.S., Mailey, J.A., Awuah, A., Brennan, P.F., McNeil, A., Robertson, L.J., McLaughlin J.A.D., Nesbit, M.A., Trucco, E., Spence, M.S. and Moore, T. 2022a. Enhancement for Automated Estimation of Blood Flow Axial Velocity from Conjunctival Videos by Deep Learning. Conference: 2022 44th Annual International Conference of the IEEE Engineering in Medicine & Biology Society (EMBC).

Jing, M., Bond, R., Robertson, L.J., Moore, J., Kowalczyk, A., Price, R., Burns, W., Nesbit, M.A., McLaughlin, J. and Moore, T., 2022b. User experience of home-based AbC-19 SARS-CoV-2 antibody rapid lateral flow immunoassay test. *Scientific Reports*, *12*(1), pp.1-18.

Jing, M., Bond, R., Robertson, L.J., Moore, J., Kowalczyk, A., Price, R., Burns, W., Nesbit, M.A., McLaughlin, J. and Moore, T., 2021. User experience analysis of AbC-19 Rapid Test via lateral flow immunoassays for self-administrated SARS-CoV-2 antibody testing. *Scientific Reports*, *11*(1), pp.1-13.

Jo, H.C., Jeong, H., Lee, J., Na, K.S. and Kim, D.Y., 2021. Quantification of blood flow velocity in the human conjunctival microvessels using deep learning-based stabilization algorithm. *Sensors*, *21*(9), p.3224.

Jones, E., Wei, J., Mehta, P., Shufelt, C., Minissian, M., Pepine, C., Handberg, E., Zhang, X., Rogatko, A., Sopko, G. and Merz, C.N.B., 2014. B-type natriuretic peptide does not correlate with invasive or noninvasive measures of coronary microvascular dysfunction in women with preserved ejection fraction: a report from the Women's Ischemia Syndrome Evaluation-Coronary Vascular Dysfunction (WISE-CVD) Study. *Journal of the American College of Cardiology*, *63*(12S), pp.A1411-A1411.

Kahe, F., Sharfaei, S., Pitliya, A., Jafarizade, M., Seifirad, S., Habibi, S. and Chi, G., 2020. Coronary artery tortuosity: a narrative review. *Coronary artery disease*, *31*(2), pp.187-192.

Kalińczuk, Ł., Zieliński, K., Chmielak, Z., Mintz, G.S., Dąbrowski, M., Pręgowski, J., Proczka, M., Michałowska, I., Czerwińska-Jelonkiewicz, K., Łazarczyk, H. and Demkow, M., 2019. Effect on mortality of systemic thromboinflammatory response after transcatheter aortic valve implantation. *The American Journal of Cardiology*, *124*(11), pp.1741-1747.

Kaltoft, M., Langsted, A. and Nordestgaard, B.G., 2020. Triglycerides and remnant cholesterol associated with risk of aortic valve stenosis: Mendelian randomization in the Copenhagen General Population Study. *European Heart Journal*, *41*(24), pp.2288-2299.

Kamperidis, V., Delgado, V., van Mieghem, N.M., Kappetein, A.P., Leon, M.B. and Bax, J.J., 2016. Diagnosis and management of aortic valve stenosis in patients with heart failure. *European Journal of Heart Failure*, *18*(5), pp.469-481.

Karanam, V.C., Tamariz, L., Batawi, H., Wang, J. and Galor, A., 2019. Functional slit lamp biomicroscopy metrics correlate with cardiovascular risk. *The ocular surface*, *17*(1), pp.64-69.

Karanam, V.C., Tamariz, L., Batawi, H., Wang, J. and Galor, A., 2019. Functional slit lamp biomicroscopy metrics correlate with cardiovascular risk. *The ocular surface*, *17*(1), pp.64-69.

Khansari, M.M., Wanek, J., Felder, A.E., Camardo, N. and Shahidi, M., 2015. Automated assessment of hemodynamics in the conjunctival microvasculature network. *IEEE transactions on medical imaging*, *35*(2), pp.605-611.

Khansari, M.M., Wanek, J., Tan, M., Joslin, C.E., Kresovich, J.K., Camardo, N., Blair, N.P. and Shahidi, M., 2017. Assessment of conjunctival microvascular hemodynamics in stages of diabetic microvasculopathy. *Scientific reports*, *7*(1), pp.1-9.

Kipli, K., Enamul Hoque, M., Thai Lim, L., Afendi Zulcaffle, T.M., Kudnie Sahari, S. and Hamdi Mahmood, M., 2020. Retinal image blood vessel extraction and quantification with Euclidean distance transform approach. *IET Image Processing*, *14*(15), pp.3718-3724.

Knuuti, J., Wijns, W., Saraste, A., Capodanno, D., Barbato, E., Funck-Brentano, C., Prescott, E., Storey, R.F., Deaton, C., Cuisset, T. and Agewall, S., 2020. 2019 ESC Guidelines for the diagnosis and management of chronic coronary syndromes: the Task Force for the diagnosis and management of chronic coronary syndromes of the European Society of Cardiology (ESC). *European heart journal*, *41*(3), pp.407-477.

Konst, R.E., Guzik, T.J., Kaski, J.C., Maas, A.H. and Elias-Smale, S.E., 2020. The pathogenic role of coronary microvascular dysfunction in the setting of other cardiac or systemic conditions. *Cardiovascular Research*, *116*(4), pp.817-828.

Korolj, A., Wu, H.T. and Radisic, M., 2019. A healthy dose of chaos: Using fractal frameworks for engineering higher-fidelity biomedical systems. *Biomaterials*, *219*, p.119363.

Koutsiaris, A.G., Tachmitzi, S.V. and Batis, N., 2013. Wall shear stress quantification in the human conjunctival pre-capillary arterioles in vivo. *Microvascular research*, *85*, pp.34-39.

Koutsiaris, A.G., Tachmitzi, S.V., Papavasileiou, P., Batis, N., Kotoula, M.G., Giannoukas, A.D. and Tsironi, E., 2010. Blood velocity pulse quantification in the human conjunctival pre-capillary arterioles. *Microvascular research*, *80*(2), pp.202-208.

Kunutsor, S.K., Kurl, S., Zaccardi, F. and Laukkanen, J.A., 2016. Baseline and long-term fibrinogen levels and risk of sudden cardiac death: A new prospective study and meta-analysis. *Atherosclerosis*, *245*, pp.171-180.

Labazi, H. and Trask, A.J., 2017. Coronary microvascular disease as an early culprit in the pathophysiology of diabetes and metabolic syndrome. *Pharmacological research*, *123*, pp.114-121.

Laflamme, J., Puri, R., Urena, M., Laflamme, L., DeLarochellière, H., Altisent, O.A.J., Del Trigo, M., Campelo-Parada, F., DeLarochellière, R., Paradis, J.M. and Dumont, E., 2015. Incidence and risk factors of hemolysis after transcatheter aortic valve implantation with a balloon-expandable valve. *The American journal of cardiology*, *115*(11), pp.1574-1579.

Lassé, M., Pilbrow, A.P., Kleffmann, T., Andersson Överström, E., von Zychlinski, A., Frampton, C., Poppe, K.K., Troughton, R.W., Lewis, L.K., Prickett, T.C. and Pemberton, C.J., 2021. Fibrinogen and hemoglobin predict near future cardiovascular events in asymptomatic individuals. *Scientific reports*, *11*(1), pp.1-10.

Lee, J.F., Barrett-O'Keefe, Z., Garten, R.S., Nelson, A.D., Ryan, J.J., Nativi, J.N., Richardson, R.S. and Wray, D.W., 2016. Evidence of microvascular dysfunction in heart failure with preserved ejection fraction. *Heart*, *102*(4), pp.278-284.

Lei, Y., Zhang, J., Schiavon, C.R., He, M., Chen, L., Shen, H., Zhang, Y., Yin, Q., Cho, Y., Andrade, L. and Shadel, G.S., 2021. SARS-CoV-2 spike protein impairs endothelial function via downregulation of ACE 2. *Circulation research*, *128*(9), pp.1323-1326.

Levy, J.H. and Tanaka, K.A., 2021. Can We Use Viscoelastic Testing to Evaluate Microvascular Dysfunction in Acute Myocardial Infarction?. *Basic to Translational Science*, *6*(9-10), pp.762-764.

Li, W., Yang, Y., Zhang, K., Long, E., He, L., Zhang, L., Zhu, Y., Chen, C., Liu, Z., Wu, X. and Yun, D., 2020. Dense anatomical annotation of slit-lamp images improves the performance of deep learning for the diagnosis of ophthalmic disorders. *Nature Biomedical Engineering*, *4*(8), pp.767-777.

Libby, P., 2021. The changing landscape of atherosclerosis. *Nature*, *592*(7855), pp.524-533.

Litwin, M., 2020. It Is Time for Microcirculation. *Hypertension,* 76(2), pp.327-329.

Maccio, U., Zinkernagel, A.S., Shambat, S.M., Zeng, X., Cathomas, G., Ruschitzka, F., Schuepbach, R.A., Moch, H. and Varga, Z., 2021. SARS-CoV-2 leads to a small vessel endotheliitis in the heart. *EBioMedicine*, *63*, p.103182.

Liu, Y., Wu, M., Xu, J., Sha, D., Xu, B. and Kang, L., 2020. Association between Triglyceride and glycose (TyG) index and subclinical myocardial injury. *Nutrition, Metabolism and Cardiovascular Diseases*, *30*(11), pp.2072-2076.

Marcori, A.J. and Okazaki, V.H.A., 2020. A historical, systematic review of handedness origins. *Laterality*, *25*(1), pp.87-108.

Marinescu, M.A., Löffler, A.I., Ouellette, M., Smith, L., Kramer, C.M. and Bourque, J.M., 2015. Coronary microvascular dysfunction, microvascular angina, and treatment strategies. *JACC: Cardiovascular imaging*, *8*(2), pp.210-220.

Meyer, P.A.R., 2018. Re-orchestration of blood flow by micro-circulations. *Eye*, *32*(2), pp.222-229.

Medical Devices Coordination Group (MDCG). (2020) Available at: https://health.ec.europa.eu/system/files/2020-09/md_mdcg_2020_1_guidance_clinic_eva_md_software_en_0.pdf [Accessed 29 September 2022].

Medicines and Healthcare Products Regulatory Agency (MHRA). (2022) Available at: https://assets.publishing.service.gov.uk/government/uploads/system/uploads/attachment_data/file/1105233/Medical_device_stand-alone_software_including_apps.pdf [Accessed 29 September 2022].

Michail, M., Davies, J.E., Cameron, J.D., Parker, K.H. and Brown, A.J., 2018. Pathophysiological coronary and microcirculatory flow alterations in aortic stenosis. *Nature Reviews Cardiology*, *15*(7), pp.420-431.

Mileva, N., Nagumo, S., Mizukami, T., Sonck, J., Berry, C., Gallinoro, E., Monizzi, G., Candreva, A., Munhoz, D., Vassilev, D. and Penicka, M., 2022. Prevalence of Coronary Microvascular Disease and Coronary Vasospasm in Patients With Nonobstructive Coronary Artery Disease: Systematic Review and Meta-Analysis. *Journal of the American Heart Association*, *11*(7), p.e023207.

Mimouni, Z., 2016. The rheological behavior of human blood—comparison of two models. *Open Journal of Biophysics*, *6*(02), p.29.

Minten, L., McCutcheon, K., Jentjens, S., Vanhaverbeke, M., Segers, V.F., Bennett, J. and Dubois, C., 2021. The coronary and microcirculatory measurements in patients with aortic valve stenosis study: rationale and design. *American Journal of Physiology-Heart and Circulatory Physiology*, *321*(6), pp.H1106-H1116.

Mirsharif, Q., Tajeripour, F. and Pourreza, H., 2013. Automated characterization of blood vessels as arteries and veins in retinal images. *Computerized Medical Imaging and Graphics*, *37*(7-8), pp.607-617.

Mitrosz, M., Chlabicz, M., Hapaniuk, K., Kaminski, K.A., Sobkowicz, B., Piszcz, J., Dobrzycki, S., Musial, W.J., Hirnle, T. and Tycinska, A.M., 2017. Thrombocytopenia associated with TAVI—The summary of possible causes. *Advances in medical sciences*, *62*(2), pp.378-382.

Mohammed, S.F., Hussain, S., Mirzoyev, S.A., Edwards, W.D., Maleszewski, J.J. and Redfield, M.M., 2015. Coronary microvascular rarefaction and myocardial

fibrosis in heart failure with preserved ejection fraction. *Circulation*, *131*(6), pp.550-559.

Moka, S., Koutsiaris, A.G., Garas, A., Messinis, I., Tachmitzi, S.V., Giannoukas, A. and Tsironi, E.E., 2020. Blood flow velocity comparison in the eye capillaries and postcapillary venules between normal pregnant and non-pregnant women. *Microvascular Research*, *127*, p.103926.

Moore, J.S., Robertson, L.J., Price, R., Curry, G., Farnan, J., Black, A., Nesbit, M.A., McLaughlin, J.A. and Moore, T., 2022. Evaluation of the Performance of a Lateral Flow Device for Quantitative Detection of Anti-SARS-CoV-2 IgG. *Clinical Immunology Communications*.

Morales, S., Naranjo, V., Navea, A. and Alcaniz, M., 2014. Computer-aided diagnosis software for hypertensive risk determination through fundus image processing. *IEEE journal of biomedical and health informatics*, *18*(6), pp.1757-1763.

Musso, C.G., Gregori, J.Á., Jauregui, J.R. and Núñez, J.F.M., 2012. Creatinine, urea, uric acid, water and electrolytes renal handling in the healthy oldest old. *World Journal of Nephrology*, *1*(5), p.123.

Navaratnarajah, A., Bhan, A., Alcock, E., Dew, T., Monaghan, M., Shah, A.M., Wendler, O., MacCarthy, P. and Dworakowski, R., 2020. Systemic inflammation and oxidative stress contribute to acute kidney injury after transcatheter aortic valve implantation. *Cardiology Journal*.

Nel, K., Nam, M.C., Anstey, C., Boos, C.J., Carlton, E., Senior, R., Kaski, J.C., Khattab, A., Shamley, D., Byrne, C.D. and Stanton, T., 2017. Myocardial blood flow reserve is impaired in patients with aortic valve calcification and unobstructed epicardial coronary arteries. *International journal of cardiology*, *248*, pp.427-432.

NICE. *Heart valve disease presenting in adults: investigation and management* (2021) Available at: https://www.nice.org.uk/guidance/GID-NG10122/documents/draft-guideline [Accessed 8 August 2021].

NICE. *CVD risk assessment and management* (2020) Available at: https://cks.nice.org.uk/topics/cvd-risk-assessment-management/management/cvd-risk-assessment/ [Accessed 26 July 2022].

NICE. *Transcatheter aortic valve implantation for severe aortic stenosis* (2017) Available at: https://www.nice.org.uk/guidance/ipg586 [Accessed 8 August 2021].

NICE. *Cardiovascular disease prevention overview* (2016) Available at: https://pathways.nice.org.uk/pathways/cardiovascular-disease-prevention#path=view%3A/pathways/cardiovascular-disease-prevention/cardiovascular-disease-prevention-overview.xml&content=view-index [Accessed 2 November 2021].

Oore-ofe, O., Soma, P., Buys, A.V., Debusho, L.K. and Pretorius, E., 2017. Characterizing pathology in erythrocytes using morphological and biophysical membrane properties: Relation to impaired hemorheology and cardiovascular function in rheumatoid arthritis. *Biochimica et Biophysica Acta (BBA)-Biomembranes*, *1859*(12), pp.2381-2391.

Östlund-Papadogeorgos, N., Ekenbäck, C., Jokhaji, F., Mir-Akbari, H., Witt, N., Jernberg, T., Wallén, H., Linder, R., Törnerud, M., Samad, B.A. and Persson, J., 2020. Blood haemoglobin, renal insufficiency, fractional flow reserve and plasma NT-proBNP is associated with index of microcirculatory resistance in chronic coronary syndrome. *International Journal of Cardiology*, *317*, pp.1-6.

Ott, C., Raff, U., Harazny, J.M., Michelson, G. and Schmieder, R.E., 2013. Central pulse pressure is an independent determinant of vascular remodeling in the retinal circulation. *Hypertension*, *61*(6), pp.1340-1345.

Oury, C., Nchimi, A., Lancellotti, P. and Bergler-Klein, J., 2018. Can blood biomarkers help predicting outcome in transcatheter aortic valve implantation?. *Frontiers in cardiovascular medicine*, *5*, p.31.

Ouyang, M., Tu, D., Tong, L., Sarwar, M., Bhimaraj, A., Li, C., Cote, G.L. and Di Carlo, D., 2021. A review of biosensor technologies for blood biomarkers toward monitoring cardiovascular diseases at the point-of-care. *Biosensors and Bioelectronics*, *171*, p.112621.

Owen, C.G., Rudnicka, A.R., Welikala, R.A., Fraz, M.M., Barman, S.A., Luben, R., Hayat, S.A., Khaw, K.T., Strachan, D.P., Whincup, P.H. and Foster, P.J., 2019. Retinal vasculometry associations with cardiometabolic risk factors in the european prospective investigation of cancer—norfolk study. *Ophthalmology*, *126*(1), pp.96-106.

Palanisamy, G., Ponnusamy, P. and Gopi, V.P., 2018, December. An adaptive enhancement method for low contrast color retinal images based on strucural similarity. In *2018 International Conference on Circuits and Systems in Digital Enterprise Technology (ICCSDET)* (pp. 1-4). IEEE.

Patel, N., Duong, S., Mirbod, P., Xu, J. and Gaynes, B.I., 2022. A meta-analysis of variability in conjunctival microvascular hemorheology metrics. *Microvascular Research*, p.104340.

Péquignot, R., Belmin, J., Chauvelier, S., Gaubert, J.Y., Konrat, C., Duron, E. and Hanon, O., 2009. Renal function in older hospital patients is more accurately

estimated using the Cockcroft-Gault formula than the modification diet in renal disease formula. *Journal of the American Geriatrics Society*, *57*(9), pp.1638-1643.

Perlman, G.Y., Loncar, S., Pollak, A., Gilon, D., Alcalai, R., Planer, D., Lotan, C. and Danenberg, H.D., 2013. Post-procedural hypertension following transcatheter aortic valve implantation: incidence and clinical significance. *JACC: Cardiovascular Interventions*, *6*(5), pp.472-478.

Phua, K., Chew, N.W., Kong, W.K., Tan, R.S., Ye, L. and Poh, K.K., 2022. The mechanistic pathways of oxidative stress in aortic stenosis and clinical implications. *Theranostics*, *12*(11), p.5189.

Pibarot, P. and Dumesnil, J.G., 2012. Improving assessment of aortic stenosis. *Journal of the American College of Cardiology*, *60*(3), pp.169-180.

Piepoli, M.F., 2017. 2016 European Guidelines on cardiovascular disease prevention in clinical practice.

Pieters, M., Ferreira, M., de Maat, M.P. and Ricci, C., 2021. Biomarker association with cardiovascular disease and mortality–The role of fibrinogen. A report from the NHANES study. *Thrombosis Research*, *198*, pp.182-189.

Prasanna, A., Miller, H.N., Wu, Y., Peeler, A., Ogungbe, O., Plante, T.B. and Juraschek, S.P., 2021. Recruitment of Black adults into cardiovascular disease trials. *Journal of the American Heart Association*, *10*(17), p.e021108.

Rafieian-Kopaei, M., Setorki, M., Doudi, M., Baradaran, A. and Nasri, H., 2014. Atherosclerosis: process, indicators, risk factors and new hopes. *International journal of preventive medicine*, *5*(8), p.927.

Rahman, H., Demir, O.M., Khan, F., Ryan, M., Ellis, H., Mills, M.T., Chiribiri, A., Webb, A. and Perera, D., 2020. Physiological stratification of patients with angina due to coronary microvascular dysfunction. *Journal of the American College of Cardiology*, *75*(20), pp.2538-2549.

Raman, B., Bluemke, D.A., Lüscher, T.F. and Neubauer, S., 2022. Long COVID: post-acute sequelae of COVID-19 with a cardiovascular focus. *European heart journal*, *43*(11), pp.1157-1172.

Ranasinghe, M.P., Peter, K. and McFadyen, J.D., 2019. Thromboembolic and bleeding complications in transcatheter aortic valve implantation: insights on mechanisms, prophylaxis and therapy. *Journal of Clinical Medicine*, *8*(2), p.280.

Relan, D., MacGillivray, T., Ballerini, L. and Trucco, E., 2014, August. Automatic retinal vessel classification using a least square-support vector machine in VAMPIRE. In *2014 36th annual international conference of the IEEE Engineering in medicine and biology society* (pp. 142-145). IEEE.

Relan, D. and Relan, R., 2021. Unsupervised sorting of retinal vessels using locally consistent Gaussian mixtures. *Computer Methods and Programs in Biomedicine*, *199*, p.105894.

Rezel-Potts, E., Douiri, A., Sun, X., Chowienczyk, P.J., Shah, A.M. and Gulliford, M.C., 2022. Cardiometabolic outcomes up to 12 months after COVID-19 infection. A matched cohort study in the UK. *PLoS medicine*, *19*(7), p.e1004052.

Rim, T.H., Lee, C.J., Tham, Y.C., Cheung, N., Yu, M., Lee, G., Kim, Y., Ting, D.S., Chong, C.C.Y., Choi, Y.S. and Yoo, T.K., 2021. Deep-learning-based cardiovascular risk stratification using coronary artery calcium scores predicted from retinal photographs. *The Lancet Digital Health*, *3*(5), pp.e306-e316.

Robertson, L.J., Moore, J.S., Blighe, K., Ng, K.Y., Quinn, N., Jennings, F., Warnock, G., Sharpe, P., Clarke, M., Maguire, K. and Rainey, S., 2021. Evaluation of the IgG antibody response to SARS CoV-2 infection and performance of a lateral flow immunoassay: cross-sectional and longitudinal analysis over 11 months. *BMJ open*, *11*(6), p.e048142.

Rolandi, M.C., Wiegerinck, E.M., Casadonte, L., Yong, Z.Y., Koch, K.T., Vis, M., Piek, J.J., Baan Jr, J., Spaan, J.A. and Siebes, M., 2016. Transcatheter replacement of stenotic aortic valve normalizes cardiac–coronary interaction by restoration of systolic coronary flow dynamics as assessed by wave intensity analysis. *Circulation: Cardiovascular Interventions*, *9*(4), p.e002356.

Rück, A., Saleh, N. and Glaser, N., 2021. Outcomes following permanent pacemaker implantation after transcatheter aortic valve replacement: SWEDEHEART observational study. *Cardiovascular Interventions*, *14*(19), pp.2173-2181.

Ruparelia, N., Panoulas, V.F., Frame, A., Ariff, B., Sutaria, N., Fertleman, M., Cousins, J., Anderson, J., Bicknell, C., Chukwuemeka, A. and Sen, S., 2016. Impact of clinical and procedural factors upon C reactive protein dynamics following transcatheter aortic valve implantation. *World journal of cardiology*, *8*(7), p.425.

Saikrishnan, N., Kumar, G., Sawaya, F.J., Lerakis, S. and Yoganathan, A.P., 2014. Accurate assessment of aortic stenosis: a review of diagnostic modalities and hemodynamics. *Circulation*, *129*(2), pp.244-253.

Santamaría, R., González-Álvarez, M., Delgado, R., Esteban, S. and Arroyo, A.G., 2020. Remodeling of the microvasculature: may the blood flow be with you. *Frontiers in Physiology*, *11*, p.586852.

Sebastian, S., Stein, L.K. and Dhamoon, M.S., 2020. Infection as a Cardiovascular Trigger: Associations Between Different Organ System Infections and Cardiovascular Events. *The American Journal of Medicine*, *133*(12), pp.1437-1443.

Sedaghat, A., Falkenberg, N., Sinning, J.M., Kulka, H., Hammerstingl, C., Nickenig, G., Oldenburg, J., Pötzsch, B. and Werner, N., 2016. TAVI induces an elevation of hemostasis-related biomarkers, which is not causative for post-TAVI thrombocytopenia. *International journal of cardiology*, *221*, pp.719-725.

Segers, V.F., Brutsaert, D.L. and De Keulenaer, G.W., 2018. Cardiac remodeling: endothelial cells have more to say than just NO. *Frontiers in physiology*, *9*, p.382.

Selle, A., Figulla, H.R., Ferrari, M., Rademacher, W., Goebel, B., Hamadanchi, A., Franz, M., Schlueter, A., Lehmann, T. and Lauten, A., 2014. Impact of rapid ventricular pacing during TAVI on microvascular tissue perfusion. *Clinical research in cardiology*, *103*(11), pp.902-911.

Shahidi, M., Wanek, J., Gaynes, B. and Wu, T., 2010. Quantitative assessment of conjunctival microvascular circulation of the human eye. *Microvascular research*, *79*(2), pp.109-113.

Shamseer, L., Moher, D., Clarke, M., Ghersi, D., Liberati, A., Petticrew, M., Shekelle, P. and Stewart, L.A., 2015. Preferred reporting items for systematic review and meta-analysis protocols (PRISMA-P) 2015: elaboration and explanation. *Bmj*, *349*.

Shi, C., Jiang, H., Gameiro, G.R. and Wang, J., 2019. Microcirculation in the conjunctiva and retina in healthy subjects. *Eye and Vision*, *6*(1), pp.1-6.

Shi, Y., Hu, L., Chen, W., Qu, D., Jiang, H. and Wang, J., 2018. Evaluated conjunctival blood flow velocity in daily contact lens wearers. *Eye & contact lens*, *44*(Suppl 1), p.S238.

Shou, K., Sarter, M., De Souza, N.R., De Campo, L., Whitten, A.E., Kuchel, P.W., Garvey, C.J. and Stadler, A.M., 2020. Effect of red blood cell shape changes on haemoglobin interactions and dynamics: a neutron scattering study. *Royal Society open science*, *7*(10), p.201507.

Shu, X., Wang, J. and Hu, L., 2019. A review of functional slit lamp biomicroscopy. *Eye and Vision*, *6*(1), pp.1-9.

Sidik, N., Morrow, A. and Berry, C., 2020. Human microcirculation in ischemic heart disease. *Arteriosclerosis, Thrombosis, and Vascular Biology* 40, pp.11-13.

Singh, S., Sethi, A., Singh, M., Khosla, K., Grewal, N. and Khosla, S., 2015. Simultaneously measured inter-arm and inter-leg systolic blood pressure differences and cardiovascular risk stratification: a systemic review and meta-analysis. *Journal of the American Society of Hypertension*, *9*(8), pp.640-650.

Sinha, A., Rahman, H. and Perera, D., 2021. Coronary microvascular disease: current concepts of pathophysiology, diagnosis and management. *Cardiovascular Endocrinology & Metabolism*, *10*(1), p.22.

Siudut, J., Natorska, J., Wypasek, E., Wiewiórka, Ł., Ostrowska-Kaim, E., Wiśniowska-Śmiałek, S., Plens, K., Legutko, J. and Undas, A., 2020. Impaired fibrinolysis in patients with isolated aortic stenosis is associated with enhanced oxidative stress. *Journal of Clinical Medicine*, *9*(6), p.2002.

Souilhol, C., Serbanovic-Canic, J., Fragiadaki, M., Chico, T.J., Ridger, V., Roddie, H. and Evans, P.C., 2020. Endothelial responses to shear stress in atherosclerosis: a novel role for developmental genes. *Nature Reviews Cardiology*, *17*(1), pp.52-63.

Soulat-Dufour, L., Lang, S., Addetia, K., Ederhy, S., Adavane-Scheuble, S., Chauvet-Droit, M., Jean, M.L., Nhan, P., Ben Said, R., Kamami, I. and Issaurat, P., 2022. Restoring sinus rhythm reverses cardiac remodeling and reduces valvular regurgitation in patients with atrial fibrillation. *Journal of the American College of Cardiology*, *79*(10), pp.951-961.

Sousa, P.C., Pinho, F.T., Alves, M.A. and Oliveira, M.S., 2016. A review of hemorheology: Measuring techniques and recent advances. *Korea-Australia Rheology Journal*, *28*(1), pp.1-22.

Spitzer, E., Mylotte, D., Lauten, A. and O'Sullivan, C.J., 2020. TAVI and the Challenges Ahead. *Frontiers in Cardiovascular Medicine*, *7*.

Stergiou, G.S., Palatini, P., Parati, G., O'Brien, E., Januszewicz, A., Lurbe, E., Persu, A., Mancia, G. and Kreutz, R., 2021. 2021 European Society of Hypertension practice guidelines for office and out-of-office blood pressure measurement. *Journal of Hypertension*, *39*(7), pp.1293-1302.

Sterne, J.A., Hernán, M.A., Reeves, B.C., Savović, J., Berkman, N.D., Viswanathan, M., Henry, D., Altman, D.G., Ansari, M.T., Boutron, I., Carpenter, J.R., Chan, A., Churchill, R., Deeks, J.J., Hróbjartsson, A., Kirkham, J., Jüni, P., Loke, Y.K., Pigott, T.D., Ramsay, C.R., Regidor, D., Rothstein, H.R., Sandhu, L., Santaguida, P.L., Schünemann, H.J., Shea, B., Shrier, I., Tugwell, P., Turner, L., Valentine, J.C., Waddington, H., Waters, E., Wells, G.A., Whiting, P.F. and Higgins, J.P. (2016) ROBINS-I: a tool for assessing risk of bias in non-randomised studies of interventions. BMJ, 355, i4919.

Stillman, A.E., Oudkerk, M., Bluemke, D.A., de Boer, M.J., Bremerich, J., Garcia, E.V., Gutberlet, M., van der Harst, P., Hundley, W.G., Jerosch-Herold, M. and

Kuijpers, D., 2018. Imaging the myocardial ischemic cascade. *The international journal of cardiovascular imaging*, *34*(8), pp.1249-1263.

Strange, G.A., Stewart, S., Curzen, N., Ray, S., Kendall, S., Braidley, P., Pearce, K., Pessotto, R., Playford, D. and Gray, H.H., 2022. Uncovering the treatable burden of severe aortic stenosis in the UK. *Open Heart*, *9*(1).

Strauss, M., Smith, W. and Schutte, A.E., 2016. Inter-arm blood pressure difference and its relationship with retinal microvascular calibres in young individuals: the African-PREDICT study. *Heart, Lung and Circulation*, *25*(8), pp.855-861.

Streese, L., Brawand, L.Y., Gugleta, K., Maloca, P.M., Vilser, W. and Hanssen, H., 2020. New frontiers in noninvasive analysis of retinal wall-to-lumen ratio by retinal vessel wall analysis. *Translational Vision Science & Technology*, *9*(6), pp.7-7.

Stundl, A., Busse, L., Leimkühler, P., Weber, M., Zur, B., Mellert, F., Grube, E., Nickenig, G., Werner, N. and Sinning, J.M., 2018. Combination of high-sensitivity C-reactive protein with logistic EuroSCORE improves risk stratification in patients undergoing TAVI. *EuroIntervention: journal of EuroPCR in collaboration with the Working Group on Interventional Cardiology of the European Society of Cardiology*, *14*(6), pp.629-636.

Sulli, A., Gotelli, E., Bica, P.F., Schiavetti, I., Pizzorni, C., Aloè, T., Grosso, M., Barisione, E., Paolino, S., Smith, V. and Cutolo, M., 2022. Detailed videocapillaroscopic microvascular changes detectable in adult COVID-19 survivors. *Microvascular Research*, *142*, p.104361.

Takagi, H., Hari, Y., Kawai, N., Ando, T. and ALICE (All-Literature Investigation of Cardiovascular Evidence) Group, 2019. Meta-analysis of impact of anemia and

hemoglobin level on survival after transcatheter aortic valve implantation. *The American Journal of Cardiology*, *123*(2), pp.306-314.

Tanaka, Y., Fukui, M., Tanaka, M., Fukuda, Y., Mitsuhashi, K., Okada, H., Yamazaki, M., Hasegawa, G., Yoshioka, K. and Nakamura, N., 2014. The inter-arm difference in systolic blood pressure is a novel risk marker for subclinical atherosclerosis in patients with type 2 diabetes. *Hypertension Research*, *37*(6), pp.548-552.

Tapp, R.J., Owen, C.G., Barman, S.A., Welikala, R.A., Foster, P.J., Whincup, P.H., Strachan, D.P., Rudnicka, A.R. and UK Biobank Eye and Vision Consortium, 2019. Associations of retinal microvascular diameters and tortuosity with blood pressure and arterial stiffness: United Kingdom Biobank. *Hypertension*, *74*(6), pp.1383-1390.

Taqueti, V.R. and Di Carli, M.F., 2018. Coronary microvascular disease pathogenic mechanisms and therapeutic options: JACC state-of-the-art review. *Journal of the American College of Cardiology*, *72*(21), pp.2625-2641.

Task Force for the management of COVID-19 of the European Society of Cardiology, Baigent, C., Windecker, S., Andreini, D., Arbelo, E., Barbato, E., Bartorelli, A.L., Baumbach, A., Behr, E.R., Berti, S. and Bueno, H., 2022. European Society of Cardiology guidance for the diagnosis and management of cardiovascular disease during the COVID-19 pandemic: part 1—epidemiology, pathophysiology, and diagnosis. *Cardiovascular Research*, *118*(6), pp.1385-1412.

Tikhonova, I.V., Kosyakova, N.I., Tankanag, A.V. and Chemeris, N.K., 2016. Oscillations of skin microvascular blood flow in patients with asthma. *Microcirculation*, *23*(1), pp.33-43.

Tsukikawa, M. and Stacey, A.W., 2020. A review of hypertensive retinopathy and chorioretinopathy. *Clinical optometry*, *12*, p.67.

Valeshabad, A.K., Wanek, J., Mukarram, F., Zelkha, R., Testai, F.D. and Shahidi, M., 2015. Feasibility of assessment of conjunctival microvascular hemodynamics in unilateral ischemic stroke. *Microvascular research*, *100*, pp.4-8.

Ungvari, Z., Kaley, G., De Cabo, R., Sonntag, W.E. and Csiszar, A., 2010. Mechanisms of vascular aging: new perspectives. *Journals of Gerontology Series A: Biomedical Sciences and Medical Sciences*, *65*(10), pp.1028-1041.

van Zijderveld, R., Ince, C. and Schlingemann, R.O., 2014. Orthogonal polarization spectral imaging of conjunctival microcirculation. *Graefe's Archive for Clinical and Experimental Ophthalmology*, *252*(5), pp.773-779.

Vendrik, J., Ahmad, Y., Eftekhari, A., Howard, J.P., Wijntjens, G.W., Stegehuis, V.E., Cook, C., Terkelsen, C.J., Christiansen, E.H., Koch, K.T. and Piek, J.J., 2020. Long-Term Effects of Transcatheter Aortic Valve Implantation on Coronary Hemodynamics in Patients With Concomitant Coronary Artery Disease and Severe Aortic Stenosis. *Journal of the American Heart Association*, *9*(5), p.e015133.

Venturi, G., Scarsini, R., Pighi, M., Kotronias, R.A., Piccoli, A., Lunardi, M., Del Sole, P., Mainardi, A., Gambaro, A., Tavella, D. and De Maria, G.L., 2022. Volume of contrast to creatinine clearance ratio predicts early mortality and AKI after TAVI. *Catheterization and Cardiovascular Interventions*.

Vijayakumar, V., Koozekanani, D.D., White, R., Kohler, J., Roychowdhury, S. and Parhi, K.K., 2016, August. Artery/vein classification of retinal blood vessels using feature selection. In *2016 38th annual international conference of the IEEE engineering in medicine and biology society (EMBC)* (pp. 1320-1323). IEEE.

Visseren, F.L., Mach, F., Smulders, Y.M., Carballo, D., Koskinas, K.C., Bäck, M., Benetos, A., Biffi, A., Boavida, J.M., Capodanno, D. and Cosyns, B., 2021. 2021

ESC Guidelines on cardiovascular disease prevention in clinical practice: Developed by the Task Force for cardiovascular disease prevention in clinical practice with representatives of the European Society of Cardiology and 12 medical societies With the special contribution of the European Association of Preventive Cardiology (EAPC). *European Heart Journal*, *42*(34), pp.3227-3337.

Wanek, J., Gaynes, B., Lim, J.I., Molokie, R. and Shahidi, M., 2013. Human bulbar conjunctival hemodynamics in hemoglobin SS and SC disease. *American journal of hematology*, *88*(8), pp.661-664.

Wang, J., Hu, L., Shi, C. and Jiang, H., 2019. Inter-visit measurement variability of conjunctival vasculature and circulation in habitual contact lens wearers and non-lens wearers. *Eye and Vision*, *6*(1), pp.1-7.

Wang, L., Yuan, J., Jiang, H., Yan, W., Cintrón-Colón, H.R., Perez, V.L., DeBuc, D.C., Feuer, W.J. and Wang, J., 2016. Vessel sampling and blood flow velocity distribution with vessel diameter for characterizing the human bulbar conjunctival microvasculature. *Eye & contact lens*, *42*(2), p.135.

Weber, B.N., Stevens, E., Barrett, L., Bay, C., Sinnette, C., Brown, J.M., Divakaran, S., Bibbo, C., Hainer, J., Dorbala, S. and Blankstein, R., 2021. Coronary Microvascular Dysfunction in Systemic Lupus Erythematosus. *Journal of the American Heart Association*, p.e018555.

Whelton, S.P., Narla, V., Blaha, M.J., Nasir, K., Blumenthal, R.S., Jenny, N.S., Al-Mallah, M.H. and Michos, E.D., 2014. Association between resting heart rate and inflammatory biomarkers (high-sensitivity C-reactive protein, interleukin-6, and fibrinogen)(from the Multi-Ethnic Study of Atherosclerosis). *The American journal of cardiology*, *113*(4), pp.644-649.

World Health Organisation. *The true death toll of COVID-19 estimating global excess mortality* (2021) Available at: https://www.who.int/data/stories/the-true-death-toll-of-covid-19-estimating-global-excess-mortality [Accessed 21 June 2021].

World Health Organisation. *Cardiovascular diseases (CVDs)* (2021) Available at: https://www.who.int/en/news-room/fact-sheets/detail/cardiovascular-diseases-(cvds) [Accessed 9 June 2021].

Xie, Y., Xu, E., Bowe, B. and Al-Aly, Z., 2022. Long-term cardiovascular outcomes of COVID-19. *Nature medicine*, *28*(3), pp.583-590.

Xu, Z., Jiang, H., Tao, A., Wu, S., Yan, W., Yuan, J., Liu, C., DeBuc, D.C. and Wang, J., 2015. Measurement variability of the bulbar conjunctival microvasculature in healthy subjects using functional slit lamp biomicroscopy (FSLB). *Microvascular research*, *101*, pp.15-19.

Yanai, H. and Yoshida, H., 2019. Beneficial effects of adiponectin on glucose and lipid metabolism and atherosclerotic progression: Mechanisms and perspectives. *International journal of molecular sciences*, *20*(5), p.1190.

Yin, J., Wang, S., Liu, Y., Chen, J., Li, D. and Xu, T., 2021. Coronary microvascular dysfunction pathophysiology in COVID-19. *Microcirculation*, p.e12718.

Yin, H., Cheng, X., Liang, Y., Liu, A., Wang, H., Liu, F., Guo, L., Ma, H. and Geng, Q., 2021. High perceived stress may shorten activated partial thromboplastin time and lead to worse clinical outcomes in patients with coronary heart disease. *Frontiers in Cardiovascular Medicine*, *8*.

Yin, X.X., Irshad, S. and Zhang, Y., 2019. Artery/vein classification of retinal vessels using classifiers fusion. *Health information science and systems*, *7*(1), pp.1-14.

Zdrenghea, D., Guşetu, G., Zdrenghea, M., Cismaru, G., Caloian, B., Vaidean, G. and Pop, D., 2019. CV RISK–A new relative cardiovascular risk score. *Medical hypotheses*, *132*, p.109362.

Zelis, J.M., Tonino, P.A., Pijls, N.H., De Bruyne, B., Kirkeeide, R.L., Gould, K.L. and Johnson, N.P., 2020. Coronary Microcirculation in Aortic Stenosis: Pathophysiology, Invasive Assessment, and Future Directions. *Journal of Interventional Cardiology*, *2020*.

Zhang, S., Zheng, R., Luo, Y., Wang, X., Mao, J., Roberts, C.J. and Sun, M., 2019. Simultaneous arteriole and venule segmentation of dual-modal fundus images using a multi-task cascade network. *IEEE Access*, *7*, pp.57561-57573.

Zhou, W., Sun, Y.P., Divakaran, S., Bajaj, N.S., Gupta, A., Chandra, A., Morgan, V., Barrett, L., Martell, L., Bibbo, C.F. and Hainer, J., 2022. Association of myocardial blood flow reserve with adverse left ventricular remodeling in patients with aortic stenosis: the microvascular disease in aortic stenosis (MIDAS) study. *JAMA cardiology*, *7*(1), pp.93-99.

Bibliography:

Abdu, F.A., Liu, L., Mohammed, A.Q., Yin, G., Xu, B., Zhang, W., Xu, S., Lv, X., Fan, R., Feng, C. and Shi, T., 2021. Prognostic impact of coronary microvascular dysfunction in patients with myocardial infarction with non-obstructive coronary arteries. *European Journal of Internal Medicine*.

Allaqaband, H., Gutterman, D.D. and Kadlec, A.O., 2018. Physiological consequences of coronary arteriolar dysfunction and its influence on cardiovascular disease. *Physiology*, *33*(5), pp.338-347.

American Academy of Family Physicians. *The EveryONE project: advancing health equity in every community* (2021). Available at: https://www.aafp.org/patient-care/social-determinants-of-health/everyone-project.html. [Accessed 8 August 2021].

Comunale, G., Susin, F.M. and Mynard, J.P., 2022. Ventricular wall stress and wall shear stress homeostasis predicts cardiac remodeling during pregnancy: a modeling study. *International Journal for Numerical Methods in Biomedical Engineering*, *38*(1), p.e3536.

Corbacho-Alonso, N., Baldán-Martín, M., López, J.A., Rodríguez-Sánchez, E., Martínez, P.J., Mourino-Alvarez, L., Martin-Rojas, T., Sastre-Oliva, T., Madruga, F., Vázquez, J. and Padial, L.R., 2020. Novel molecular plasma signatures on cardiovascular disease can stratify patients throughout life. *Journal of proteomics*, *222*, p.103816.

Didion, S.P., 2017. Cellular and oxidative mechanisms associated with interleukin-6 signaling in the vasculature. *International journal of molecular sciences*, *18*(12), p.2563.

Erdoes, G., Lippuner, C., Kocsis, I., Schiff, M., Stucki, M., Carrel, T., Windecker, S., Eberle, B., Stueber, F. and Book, M., 2015. Technical approach determines inflammatory response after surgical and transcatheter aortic valve replacement. *PloS one*, *10*(11), p.e0143089.

Girard, F., Kavalec, C. and Cheriet, F., 2019. Joint segmentation and classification of retinal arteries/veins from fundus images. *Artificial intelligence in medicine*, *94*, pp.96-109.

Hemelings, R., Elen, B., Stalmans, I., Van Keer, K., De Boever, P. and Blaschko, M.B., 2019. Artery–vein segmentation in fundus images using a fully convolutional network. *Computerized Medical Imaging and Graphics*, *76*, p.101636.

Huang, Q., Sun, J. and Xu, C., 2021. Effects of waveform shape of pulsatile blood flow on hemodynamics in an artery bifurcation model. *Proceedings of the Institution of Mechanical Engineers, Part C: Journal of Mechanical Engineering Science*, *235*(2), pp.428-440.

Kleinbongard, P. and Heusch, G., 2021. A fresh look at coronary microembolization. *Nature Reviews Cardiology*, pp.1-16.

Liu, C.L., Guo, J., Zhang, X., Sukhova, G.K., Libby, P. and Shi, G.P., 2018. Cysteine protease cathepsins in cardiovascular disease: from basic research to clinical trials. *Nature Reviews Cardiology*, *15*(6), pp.351-370.

Luan, H.H., Wang, A., Hilliard, B.K., Carvalho, F., Rosen, C.E., Ahasic, A.M., Herzog, E.L., Kang, I., Pisani, M.A., Yu, S. and Zhang, C., 2019. GDF15 is an inflammation-induced central mediator of tissue tolerance. *Cell*, *178*(5), pp.1231-1244.

Masi, S., Rizzoni, D., Taddei, S., Widmer, R.J., Montezano, A.C., Lüscher, T.F., Schiffrin, E.L., Touyz, R.M., Paneni, F., Lerman, A. and Lanza, G.A., 2021. Assessment and pathophysiology of microvascular disease: recent progress and clinical implications. *European heart journal*, *42*(26), pp.2590-2604.

Mirna, M., Wernly, B., Paar, V., Jung, C., Jirak, P., Figulla, H.R., Kretzschmar, D., Franz, M., Hoppe, U.C., Lichtenauer, M. and Lauten, A., 2018. Multi-biomarker analysis in patients after transcatheter aortic valve implantation (TAVI). *Biomarkers*, *23*(8), pp.773-780.

Mozos, I., Malainer, C., Horbańczuk, J., Gug, C., Stoian, D., Luca, C.T. and Atanasov, A.G., 2017. Inflammatory markers for arterial stiffness in cardiovascular diseases. *Frontiers in immunology*, *8*, p.1058.

Muller, O., Ntalianis, A., Wijns, W., Delrue, L., Dierickx, K., Auer, R., Rodondi, N., Mangiacapra, F., Trana, C., Hamilos, M. and Valentin, E., 2013. Association of biomarkers of lipid modification with functional and morphological indices of coronary stenosis severity in stable coronary artery disease. *Journal of cardiovascular translational research*, *6*(4), pp.536-544.

Passerini, T., Quaini, A., Villa, U., Veneziani, A. and Canic, S., 2013. Validation of an open source framework for the simulation of blood flow in rigid and deformable vessels. *International journal for numerical methods in biomedical engineering*, *29*(11), pp.1192-1213.

Redfors, B., Furer, A., Lindman, B.R., Burkhoff, D., Marquis-Gravel, G., Francese, D.P., Ben-Yehuda, O., Pibarot, P., Gillam, L.D., Leon, M.B. and Généreux, P., 2017. Biomarkers in aortic stenosis: a systematic review. *Structural Heart*, *1*(1-2), pp.18-30.

Robbins, C.B., Thompson, A.C., Bhullar, P.K., Koo, H.Y., Agrawal, R., Soundararajan, S., Yoon, S.P., Polascik, B.W., Scott, B.L., Grewal, D.S. and Fekrat, S., 2021. Characterization of retinal microvascular and choroidal structural changes in Parkinson disease. *JAMA ophthalmology*, *139*(2), pp.182-188.

Sorop, O., Olver, T.D., van de Wouw, J., Heinonen, I., van Duin, R.W., Duncker, D.J. and Merkus, D., 2017. The microcirculation: a key player in obesity-associated cardiovascular disease. *Cardiovascular research*, *113*(9), pp.1035-1045.

von Knobelsdorff-Brenkenhoff, F., Karunaharamoorthy, A., Trauzeddel, R.F., Barker, A.J., Blaszczyk, E., Markl, M. and Schulz-Menger, J., 2016. Evaluation of aortic blood flow and wall shear stress in aortic stenosis and its association with left ventricular remodeling. *Circulation: Cardiovascular Imaging*, *9*(3), p.e004038.

Welikala, R.A., Foster, P.J., Whincup, P.H., Rudnicka, A.R., Owen, C.G., Strachan, D.P. and Barman, S.A., 2017. Automated arteriole and venule classification using deep learning for retinal images from the UK Biobank cohort. *Computers in biology and medicine*, *90*, pp.23-32.

Chapter 11

Supplementary Materials

Table S1. Amended PRISMA-P (Preferred Reporting Items for Systematic review and Meta-Analysis Protocols) 2015 checklist: recommended items to address in a systematic review protocol*

Section and topic	Item No	Checklist item
INTRODUCTION ✓ pg 60-62		
Rationale	6	Describe the rationale for the review in the context of what is already known
Objectives	7	Provide an explicit statement of the question(s) the review will address with reference to participants, interventions, comparators, and outcomes (PICO)
METHODS ✓ pg 62-64		
Eligibility criteria	8	Specify the study characteristics (such as PICO, study design, setting, time frame) and report characteristics (such as years considered, language, publication status) to be used as criteria for eligibility for the review
Information sources	9	Describe all intended information sources (such as electronic databases, contact with study authors, trial registers or other grey literature sources) with planned dates of coverage
Search strategy	10	Present draft of search strategy to be used for at least one electronic database, including planned limits, such that it could be repeated
Study records: Data management	11a	Describe the mechanism(s) that will be used to manage records and data throughout the review

Selection process	11b	State the process that will be used for selecting studies (such as two independent reviewers) through each phase of the review (that is, screening, eligibility and inclusion in meta-analysis)	
Data collection process	11c	Describe planned method of extracting data from reports (such as piloting forms, done independently, in duplicate), any processes for obtaining and confirming data from investigators	
Data items	12	List and define all variables for which data will be sought (such as PICO items, funding sources), any pre-planned data assumptions and simplifications	
Outcomes and prioritization	13	List and define all outcomes for which data will be sought, including prioritization of main and additional outcomes, with rationale	
Risk of bias in individual studies ✓ **Figure S1**			14
Data synthesis	15a	Describe criteria under which study data will be quantitatively synthesised	
Objectives	15b	If data are appropriate for quantitative synthesis, describe planned summary measures, methods of handling data and methods of combining data from studies, including any planned exploration of consistency (such as I^2, Kendall's τ)	15c
Eligibility criteria	15d	If quantitative synthesis is not appropriate, describe the type of summary planned	
Meta-bias(es)	16	Specify any planned assessment of meta-bias(es) (such as publication bias across studies, selective reporting within studies)	
Confidence in cumulative evidence	17	Describe how the strength of the body of evidence will be assessed (such as GRADE)	

*** It is strongly recommended that this checklist be read in conjunction with the PRISMA-P Explanation and Elaboration (cite when available) for important clarification on the items. Amendments to a review protocol should be tracked and**

dated. The copyright for PRISMA-P (including checklist) is held by the PRISMA-P Group and is distributed under a Creative Commons Attribution Licence 4.0.

From: Shamseer L, Moher D, Clarke M, Ghersi D, Liberati A, Petticrew M, Shekelle P, Stewart L, PRISMA-P Group. Preferred reporting items for systematic review and meta-analysis protocols (PRISMA-P) 2015: elaboration and explanation. BMJ. 2015 Jan 2;349(jan02 1):g7647.

Table S2. Quality assessment (Amended from CASP, 2018)

	Alam *et al*., 2018	Cordina *et al.*, 2015	Dasht-bozorg *et al*., 2013	Ding *et al.*, 2015	Fraz *et al.,* 2014	Girard *et al*., 2019	Hemel-ings *et al*., 2019	Huang *et al.*, 2020	Ishikawa *et al*., 2019	Mirsharif *et al*., 2013	Morales *et al.*, 2014	Owen *et al*., 2019	Relan *et al*., 2014	Relan and Relan, 2021	Rim *et al*., 2021	Tapp *et al*., 2019	Vijayaku-mar *et al*., 2016	Welikala *et al*., 2017	Yin *et al*., 2019	Zhang *et al*., 2019
Did the study address a clearly focused issue?	+	+	+	+	+	+	+	+	+	+	+	+	+	+	+	+	+	+	+	+
Was the cohort recruited in an acceptable way/were the vessels grouped in an acceptable way?	+ (50 non-proliferative diabetic retinopathy fundus images)	+ (13 cyanotic congenital heart disease retinal images)	+ (databases used)	+ (databases used)	+ (3149 vessel segments from 40 fundus images-arterioles and venules classified by an expert)	+ (database used)	+ (databases used)	+ (50 Cardiac Aging Study participants)	+ (61 healthy volunteers and 10 additional volunteers)	+ (database and 13 further images used)	+ (database used)	+ (5947 participants (279802 arterioles and 285791 venules))	+ (70 fundus images and database used)	+ (databases used)	+ (216 152 retinal images used)	+ (The United Kingdom Biobank including 68 550 participants)	+ (database used)	+ (100 retinal images randomly selected from the 135,867 retinal images obtained at the UK Biobank)	+ (databases and 40 further images used)	+ (databases used)
Was the outcome accurately measured to minimize bias?	+ (automated)	? (subjective clinical assessment of	+ (automated)	+ (automated)	+ (automated)	+ (automated)	+ (automated)	+ (semi-automated)	+ (algorithm)	+ (automated)	+ (algorithm)	+ (quantitative)	+ (automated)	+ (automated)	+ (saliency maps)	+ (automated)	+ (automated)	+ (automated)	+ (quantitative)	+ (automated)

		tortuosity)																		
Have the authors identified all important cofounding factors?	?	+	+	+	+	+	+	+	?	+	?	+	+	+	+	+	+	+	?	+
Have the authors accounted for cofounding factors in design/ analysis?	+	+	+	+	+	+	+	-	?	?	+	+	+	+	+	+	+	+	?	+
Was follow-up complete/ long enough?	+	+	+	+	+	+	+	?	+	+	+	?	+	+	?	+	+	+	+	+
What are the results of this study?	97.06% accuracy 97.58, arteriole classification (sensitivity, specificity) =95.89 % vs venule= 97.81, 96.68 %.	62% of patients presented increased vessel tortuosity.	Vessel classification accuracies of 88.3%, 87.4%, and 89.8% reported from the corresponding databases.	Accuracies of 85.5% and 77% for healthy and diseased vasculature classification.	Sensitivity for the classification of arterioles is 90.67% and for the veins is 76.58%.	Vessel classification specificity of 92.9% with a sensitivity of 93.7%.	Accuracies of 94.42% and 94.11% on arteries and veins, respectively.	Each unit increase in a set of cardiac structure indices was associated with larger retinal arteriolar branching angle (β and 95% CI: for left ventricular internal diameter end systole index, 26.93°;	The mean ODR values of arterioles and venules were 0.77 ± 0.060 and 1.02 ± 0.067, respectively. ODR also significantly increased with breath holding ($p<0.05$).	82.65% of arteries within the DRIVE database were correctly classified and 85.74% of venules from the same database were correctly classified.	Overall, 61.19% accuracy for cardiovascular disease classification-56.41% sensitivity and 67.86% specificity reported.	Increased venular tortuosity was associated with higher body mass index (BMI; 2.5%; 95% confidence interval [CI], 1.7%–3.3% per 5 kg/m^2), hemoglobin A1c (HbA1c) level	Mean vessel classification accuracy of 94%.	90.14%, 90.3% and 93.8% classification rates obtained for the respective databases.	AUC of 0·742, 95% CI 0·732–0·753 for predicting the presence of coronary artery calcium.	Greater arteriolar tortuosity was associated with higher systolic BP (relative increase, 1.2%; 95% CI, 0.9; 1.4% per 10 mmHg), higher mean arterial pressure, 1.3%; 0.9, 1.7% per 10 mmHg, and	AUC of 97.2% was obtained on an average of 100 runs of the algorithm.	Arteriole/venule classification accuracy of 86.97% (per pixel basis) over the entire retinal image.	Overall classification accuracies of 87.82%, 90.45% and 93.90% reported in the respective databases.	The arteriovenous classification accuracy evaluated on the automatically detected vessels is 97.27%.

								6.00–47.86; for left ventricular internal diameter end diastole index, 17.86°; 1.61–34.11; for left ventricular mass index, 0.39°; 0.10–0.67; for left atrial volume index, 0.91°; 0.24–1.58).				(2.2%; 95% CI, 1.0%–3.5% per 1%), and prevalent type 2 diabetes (6.5%; 95% CI, 2.8%–10.4%). Arteriolar tortuosity increased with age (5.4%; 95% CI, 3.8%–7.1% per decade), higher systolic blood pressure (1.2%; 95% CI, 0.5%–1.9% per 10 mmHg), in females (3.8%; 95% CI, 1.4%–6.4%), and in those with prevalent stroke (8.3%;				higher pulse pressure (PP, 1.8%; 1.4; 2.2% per 10 mmHg).				

												95% CI, –0.6% to 18%); no association was observed with prevalent myocardial infarction.								
Is the precision of results acceptable?	+	+	+	?	+	+	+	+	+	?	?	+	?	?	+	+	?	?	?	+
Do you believe the results?	+	+	+	+	+	+	+	+	+	+	+	+	+	+	+	+	+	+	+	+
Do the results of this study fit with other available evidence?	+	+	+	+	+	+	+	+	+	+	+	+	+	+	+	+	+	+	+	+
Can the results be applied/ or is there implications for practice?	?	+	?	?	?	?	?	?	?	?	+	?	?	?	+	?	?	?	?	?

Table S3. Risk of Bias assessment (Amended from Sterne *et al*., 2016)

Study	Bias due to cofounding	Bias in participant/vessel selection	Bias in classification	Bias from intended intervention deviation	Bias due to missing data	Bias in outcome measurement	Bias in selection of reported result	Overall Bias
Alam *et al.*, 2021	?	?	+	+	+	+	+	+
Cordina *et al.*, 2015	+	+	+	+	+	?	+	+
Dashtbozorg *et al.*, 2013	+	+	+	+	+	+	+	+
Ding *et al.*, 2015	+	+	+	+	+	+	+	+
Fraz *et al.*, 2014	+	+	?	+	+	+	+	+
Girad *et al.*, 2019	+	+	+	+	+	+	+	+
Hemelings *et al.*, 2019	+	+	+	+	+	+	+	+
Huang *et al.*, 2020	?	+	+	+	+	+	+	+
Ishikawa *et al.*, 2019	?	+	+	+	+	+	+	+
Mirsharif *et al.*, 2013	?	+	+	+	+	+	+	+
Morales *et al.*, 2014	+	+	+	+	+	+	+	+
Owen *et al.*, 2019	+	+	+	+	+	+	+	+

Relan *et al.*, 2014	+	+	+	+	+	+	+	+
Relan and Relan, 2021	+	+	+	+	+	+	+	+
Rim *et al.*, 2021	+	?	+	+	+	?	+	+
Tapp *et al., 2019*	+	+	+	+	+	+	+	+
Vijayakumar *et al.*, 2015	+	+	+	+	+	+	+	+
Welikala *et al.*, 2017	+	+	+	+	+	+	+	+
Yin *et al.*, 2019	?	+	+	+	+	+	+	+
Zhang *et al.*, 2019	+	+	+	+	+	+	+	+
Key: **+: Low risk of bias** **-: High risk of bias** **?: Unclear risk of bias**								

Figure S1. Risk of Bias graph

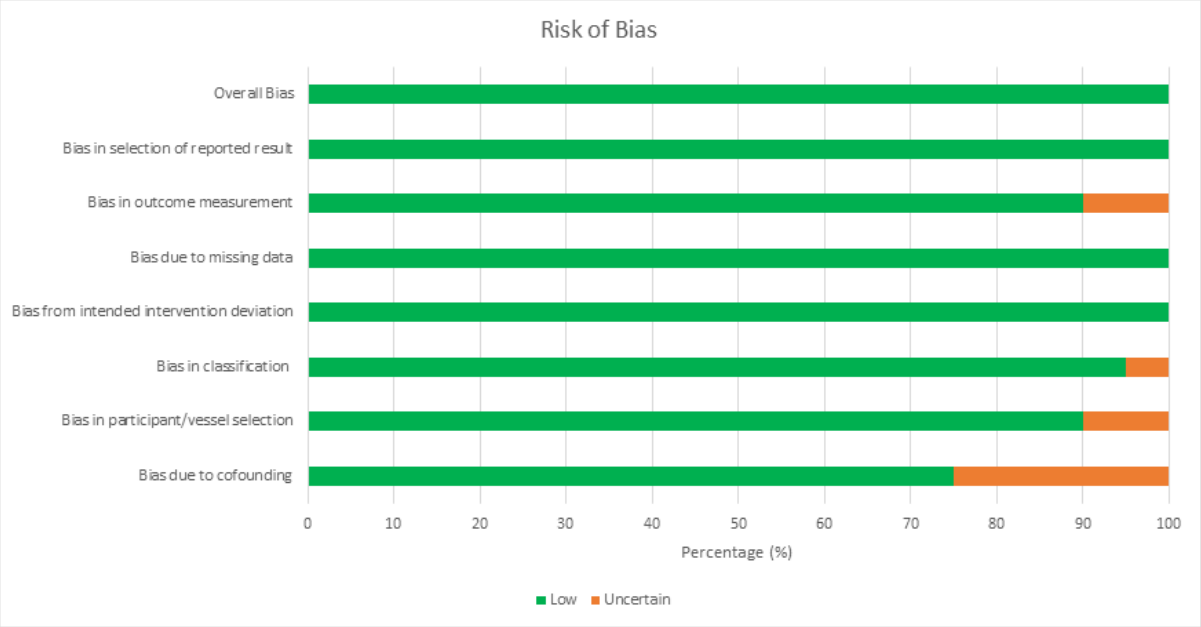

Table S4. TAVI cohort vessel segment analysis

Overall TAVI Comparison	**TAVI Controls n= 1672 vessel segments**	**95% CI**	**TAVI n= 1881 vessel segments**	**95% CI**	**p Value**
Diameter µm	25.37 ± 8.29	24.98-25.77	25.44 ± 8.49	25.06-25.83	0.812
Axial Velocity mm/s	0.55 ± 0.14	0.54-0.56	0.56 ± 0.16	0.55-0.56	0.348
Cross-Sectional Velocity mm/s	0.38 ± 0.10	0.38-0.39	0.39 ± 0.11	0.38-0.39	0.268
Blood Flow Rate pl/s	212 ± 158	204-219	216 ± 159	209-223	0.689

Wall Shear Rate s^{-1}	136 ± 69	133-140	138 ± 71	135-141	0.511
Arteriole TAVI Comparison	**TAVI Controls n= 269**	**95% CI**	**TAVI n= 351**	**95% CI**	**p Value**
Diameter µm	23.09 ± 7.10	22.24-23.94	24.39 ± 8.72	23.48-25.31	0.121
Axial Velocity mm/s	0.55 ± 0.14	0.54-0.57	0.55 ± 0.17	0.54-0.57	0.754
Cross-Sectional Velocity mm/s	0.39 ± 0.10	0.37-0.40	0.39 ± 0.12	0.38-0.40	0.851
Blood Flow Rate pl/s	176 ± 119	162-191	195 ± 135	181-210	0.222
Wall Shear Rate s^{-1}	151 ± 74	142-160	149 ± 86	140-158	0.224
Venule TAVI Comparison	**TAVI Controls n= 1191**	**95% CI**	**TAVI n= 1362**	**95% CI**	**p Value**
Diameter µm	26.05 ± 8.38	25.57-26.52	25.88 ± 8.41	25.44-26.33	0.697
Axial Velocity mm/s	0.55 ± 0.14	0.54-0.56	0.56 ± 0.16	0.55-0.56	0.463
Cross-Sectional Velocity mm/s	0.38 ± 0.10	0.37-0.38	0.38 ± 0.11	0.38-0.39	0.339
Blood Flow Rate pl/s	221 ± 163	212-230	224 ± 166	215-233	0.989
Wall Shear Rate s^{-1}	132 ± 68	128-136	134 ± 66	131-138	0.194

Undifferentiated TAVI Comparison	**TAVI Controls n= 212**	**95% CI**	**TAVI n= 168**	**95% CI**	**p Value**
Diameter µm	24.46 ± 8.55	23.31-25.61	24.08 ± 8.36	22.81-25.35	0.519
Axial Velocity mm/s	0.55 ± 0.14	0.53-0.57	0.56 ± 0.14	0.54-0.58	0.507
Cross-Sectional Velocity mm/s	0.38 ± 0.09	0.37-0.40	0.39 ± 0.10	0.37-0.40	0.434
Blood Flow Rate pl/s	203 ± 170	180-226	191 ± 133	170-211	0.701
Wall Shear Rate s^{-1}	141 ± 66	132-150	148 ± 70	137-158	0.45
L Eye TAVI Comparison	**TAVI Controls n= 684**	**95% CI**	**TAVI n= 911**	**95% CI**	**p Value**
Diameter µm	25.01 ± 8.41	24.38-25.64	25.64 ± 8.64	25.08-26.20	0.181
Axial Velocity mm/s	0.54 ± 0.15	0.53-0.56	0.56 ± 0.16	0.54-0.57	0.166
Cross-Sectional Velocity mm/s	0.38 ± 0.11	0.37-0.39	0.38 ± 0.11	0.38-0.39	0.203
Blood Flow Rate pl/s	204 ± 148	193-215	219 ± 162	208-229	0.122
Wall Shear Rate s^{-1}	139 ± 73	133-144	137 ± 70	132-142	0.806

R Eye TAVI Comparison	**TAVI Controls n= 988**	**95% CI**	**TAVI n= 970**	**95% CI**	**p Value**
Diameter µm	25.62 ± 8.20	25.11-26.13	25.26 ± 8.34	24.73-25.78	0.398
Axial Velocity mm/s	0.55 ± 0.14	0.54-0.56	0.56 ± 0.15	0.55-0.57	0.907
Cross-Sectional Velocity mm/s	0.38 ± 0.10	0.38-0.39	0.39 ± 0.11	0.38-0.39	0.664
Blood Flow Rate pl/s	217 ± 165	206-227	213 ± 155	203-223	0.436
Wall Shear Rate s^{-1}	135 ± 67	131-139	139 ± 71	135-144	0.268
LN TAVI Comparison	**TAVI Controls n= 322**	**95% CI**	**TAVI n= 414**	**95% CI**	**p Value**
Diameter µm	24.65 ± 8.83	23.68-25.62	25.04 ± 8.89	24.18-25.90	0.534
Axial Velocity mm/s	0.55 ± 0..15	0.54-0.57	0.58 ± 0.17	0.56-0.59	0.057
Cross-Sectional Velocity mm/s	0.39 ± 0.10	0.38-0.40	0.40 ± 0.11	0.39-0.41	0.062
Blood Flow Rate pl/s	206 ± 158	188-223	224 ± 176	207-241	0.202
Wall Shear Rate s^{-1}	145 ± 76	136-153	147 ± 75	140-155	0.557

LT TAVI Comparison	**TAVI Controls n= 362**	**95% CI**	**TAVI n= 497**	**95% CI**	**p Value**
Diameter µm	25.33 ± 8.01	24.50-26.16	26.14 ± 8.42	25.40-26.88	0.238
Axial Velocity mm/s	0.53 ± 0.15	0.52-0.55	0.53 ± 0.16	0.52-0.55	0.789
Cross-Sectional Velocity mm/s	0.37 ± 0.10	0.36-0.38	0.37 ± 0.11	0.36-0.38	0.889
Blood Flow Rate pl/s	203 ± 138	189-217	214 ± 150	201-228	0.375
Wall Shear Rate s^{-1}	133 ± 69	126-140	128 ± 65	123-134	0.387
RN TAVI Comparison	**TAVI Controls n= 420**	**95% CI**	**TAVI n= 394**	**95% CI**	**p Value**
Diameter µm	24.82 ± 8.04	24.05-25.59	24.39 ± 7.89	23.61-25.18	0.54
Axial Velocity mm/s	0.56 ± 0.14	0.55-0.57	0.58 ± 0.16	0.56-0.59	0.114
Cross-Sectional Velocity mm/s	0.39 ± 0.10	0.38-0.40	0.40 ± 0.11	0.39-0.41	0.087
Blood Flow Rate pl/s	207 ± 154	192-222	205 ± 137	192-219	0.982
Wall Shear Rate s^{-1}	141 ± 69	135-148	149 ± 73	142-156	0.121

RT TAVI Comparison	**TAVI Controls n= 568**	**95% CI**	**TAVI n= 576**	**95% CI**	**p Value**
Diameter µm	26.21 ± 8.27	25.53-26.90	25.85 ± 8.59	25.15-26.55	0.513
Axial Velocity mm/s	0.55 ± 0.14	0.54-0.56	0.54 ± 0.15	0.53-0.55	0.257
Cross-Sectional Velocity mm/s	0.38 ± 0.09	0.37-0.39	0.37 ± 0.10	0.37-0.38	0.411
Blood Flow Rate pl/s	224 ± 172	210-238	219 ± 167	205-232	0.272
Wall Shear Rate s^{-1}	130 ± 65	124-135	133 ± 69	127-138	0.829
Abbreviations: *L= Left, LN= Left Nasal, LT= Left Temporal, R= Right, RN= Right Nasal, RT= Right Temporal, TAVI= Transcatheter Aortic Valve Implantation*					

Table S5. TAVI pre vs post vessel segment analysis

Overall TAVI Comparison	**Pre-TAVI n= 1881**	**95% CI**	**Post-TAVI n= 1945**	**95% CI**	**p Value**
Mean Diameter(D) µm	25.44 ± 8.49	25.06-25.83	26.22 ± 8.63	25.84-26.61	**0.005**
Diameter SD µm	4.17 ± 2.13	4.08-4.27	4.25 ± 2.04	4.16-4.34	**0.048**

Axial Velocity mm/s	0.56 ± 0.16	0.55-0.56	0.56 ± 0.15	0.55-0.57	0.528
Cross-Sectional Velocity mm/s	0.39 ± 0.11	0.38-0.39	0.39 ± 0.11	0.38-0.39	0.872
Blood Flow Rate pl/s	216 ± 159	209-223	229 ± 165	222-237	**0.01**
Wall Shear Rate s^{-1}	138 ± 71	135-141	135 ± 74	132-138	**0.028**
Wall Shear Stress dynes/cm^2	7.91 ± 4.13	7.72-8.10	7.00 ± 3.70	6.84-7.16	**<0.001**
Arteriole TAVI Comparison	**Pre-TAVI n= 351**	**95% CI**	**Post-TAVI n= 293**	**95% CI**	**p Value**
Mean Diameter(D) µm	24.39 ± 8.72	23.48-25.31	22.97 ± 8.19	22.03-23.91	0.053
Diameter SD µm	3.98 ± 1.84	3.78-4.17	4.16 ± 1.86	3.94-4.37	0.154
Axial Velocity mm/s	0.55 ± 0.17	0.54-0.57	0.60 ± 0.15	0.58-0.61	**0.002**
Cross-Sectional Velocity mm/s	0.39 ± 0.12	0.38-0.40	0.42 ± 0.11	0.41-0.43	**0.001**
Blood Flow Rate pl/s	195 ± 135	181-210	189 ± 132	174-204	0.626

Wall Shear Rate s^{-1}	149 ± 86	140-158	174 ± 105	162-186	**0.001**
Wall Shear Stress dynes/cm^2	8.36 ± 4.93	7.83-8.88	8.72 ± 5.16	8.13-9.32	0.285
Venule TAVI Comparison	**Pre-TAVI n= 1362**	**95% CI**	**Post-TAVI n= 1505**	**95% CI**	**p Value**
Mean Diameter(D) µm	25.88 ± 8.41	25.44-26.33	27.09 ± 8.52	26.66-27.52	**<0.001**
Diameter SD µm	4.12 ± 2.09	4.01-4.23	4.20 ± 2.01	4.10-4.30	0.077
Axial Velocity mm/s	0.56 ± 0.16	0.55-0.56	0.55 ± 0.15	0.54-0.56	0.802
Cross-Sectional Velocity mm/s	0.38 ± 0.11	0.38-0.39	0.38 ± 0.10	0.37-0.38	0.368
Blood Flow Rate pl/s	224 ± 166	215-233	241 ± 170	232-249	**0.003**
Wall Shear Rate s^{-1}	134 ± 66	131-138	126 ± 63	123-129	**<0.001**
Wall Shear Stress dynes/cm^2	7.76 ± 3.95	7.55-7.98	6.61 ± 3.17	6.45-6.77	**<0.001**

Undifferentiated TAVI Comparison	**Pre-TAVI n= 168**	**95% CI**	**Post-TAVI n= 147**	**95% CI**	**p Value**
Mean Diameter(D) µm	24.08 ± 8.36	22.81-25.35	23.83 ± 8.71	22.41-25.25	0.878
Diameter SD µm	5.02 ± 2.75	4.60-5.44	4.96 ± 2.53	4.55-5.38	0.909
Axial Velocity mm/s	0.56 ± 0.14	0.54-0.58	0.54 ± 0.15	0.52-0.57	0.347
Cross-Sectional Velocity mm/s	0.39 ± 0.10	0.37-0.40	0.38 ± 0.10	0.36-0.40	0.402
Blood Flow Rate pl/s	191 ± 133	171-211	192 ± 161	166-218	0.392
Wall Shear Rate s^{-1}	148 ± 70	137-158	148 ± 75	136-160	0.936
Wall Shear Stress dynes/cm^2	8.15 ± 3.60	7.59-8.72	7.54 ± 4.25	6.84-8.23	**0.043**
L Eye TAVI Comparison	**Pre-TAVI n= 911**	**95% CI**	**Post-TAVI n= 876**	**95% CI**	**p Value**
Mean Diameter(D) µm	25.64 ± 8.64	25.08-26.20	26.58 ± 8.79	26.00-27.17	**0.026**
Diameter SD µm	4.25 ± 2.29	4.11-4.40	4.35 ± 1.99	4.22-4.84	**0.013**

Axial Velocity mm/s	0.56 ± 0.16	0.54-0.57	0.56 ± 0.16	0.55-0.57	0.529
Cross-Sectional Velocity mm/s	0.38 ± 0.11	0.38-0.39	0.39 ± 0.11	0.38-0.39	0.8
Blood Flow Rate pl/s	219 ± 162	208-229	235 ± 168	224-246	**0.023**
Wall Shear Rate s^{-1}	137 ± 70	132-142	133 ± 71	128-138	0.078
Wall Shear Stress dynes/cm^2	7.83 ± 4.37	7.54-8.11	6.90 ± 3.55	6.67-7.14	**<0.001**
R Eye TAVI Comparison	**Pre-TAVI n= 970**	**95% CI**	**Post-TAVI n= 1069**	**95% CI**	**p Value**
Mean Diameter(D) µm	25.26 ± 8.34	24.73-25.78	25.93 ± 8.50	25.42-26.44	0.071
Diameter SD µm	4.10 ± 1.97	3.97-4.22	4.16 ± 2.08	4.04-4.29	0.66
Axial Velocity mm/s	0.56 ± 0.15	0.55-0.57	0.56 ± 0.16	0.55-0.57	0.788
Cross-Sectional Velocity mm/s	0.39 ± 0.11	0.38-0.39	0.39 ± 0.11	0.38-0.39	0.989
Blood Flow Rate pl/s	213 ± 155	203-223	224 ± 163	215-234	0.148

Wall Shear Rate s^{-1}	139 ± 71	135-144	137 ± 75	132-141	0.158
Wall Shear Stress dynes/cm^2	7.99 ± 3.89	7.74-8.23	7.08 ± 3.82	6.85-7.31	**<0.001**
LN TAVI Comparison	**Pre-TAVI n= 414**	**95% CI**	**Post-TAVI n= 365**	**95% CI**	**p Value**
Mean Diameter(D) µm	25.04 ± 8.89	24.18-25.90	25.79 ± 8.73	24.89-26.68	0.23
Diameter SD µm	4.43 ± 2.58	4.18-4.68	4.45 ± 1.93	4.25-4.64	**0.043**
Axial Velocity mm/s	0.58 ± 0.17	0.56-0.60	0.57 ± 0.16	0.55-0.58	0.394
Cross-Sectional Velocity mm/s	0.40 ± 0.11	0.39-0.41	0.39 ± 0.11	0.38-0.40	0.277
Blood Flow Rate pl/s	224 ± 176	207-241	228 ± 165	211-245	0.526
Wall Shear Rate s^{-1}	147 ± 75	140-155	139 ± 72	132-147	0.063
Wall Shear Stress dynes/cm^2	8.44 ± 4.85	7.96-8.91	7.25 ± 3.42	6.90-7.60	**0.001**
LT TAVI Comparison	**Pre-TAVI n= 497**	**95% CI**	**Post-TAVI n= 511**	**95% CI**	**p Value**

Mean Diameter(D) µm	26.14 ± 8.42	25.40-26.88	27.15 ± 8.80	26.39-27.92	0.072
Diameter SD µm	4.11 ± 2.01	3.93-4.29	4.29 ± 2.03	4.11-4.46	0.133
Axial Velocity mm/s	0.53 ± 0.16	0.52-0.55	0.55 ± 0.14	0.54-0.56	0.066
Cross-Sectional Velocity mm/s	0.37 ± 0.11	0.36-0.38	0.38 ± 0.10	0.37-0.39	0.116
Blood Flow Rate pl/s	214 ± 150	201-228	240 ± 169	225-255	**0.013**
Wall Shear Rate s^{-1}	128 ± 65	123-134	129 ± 70	123-135	0.701
Wall Shear Stress dynes/cm^2	7.31 ± 3.85	6.97-7.66	6.65 ± 3.63	6.34-6.97	0.002
RN TAVI Comparison	**Pre-TAVI n= 394**	**95% CI**	**Post-TAVI n= 468**	**95% CI**	**p Value**
Mean Diameter(D) µm	24.39 ± 7.89	23.61-25.18	24.82 ± 8.44	24.05-25.58	0.44
Diameter SD µm	4.13 ± 1.88	3.94-4.32	4.15 ± 2.02	3.96-4.33	0.803
Axial Velocity mm/s	0.58 ± 0.16	0.56-0.59	0.57 ± 0.16	0.56-0.59	0.63

Cross-Sectional Velocity mm/s	0.40 ± 0.11	0.39-0.41	0.40 ± 0.11	0.39-0.41	0.671
Blood Flow Rate pl/s	205 ± 137	192-219	212 ± 151	198-226	0.838
Wall Shear Rate s^{-1}	149 ± 73	14-156	151 ± 90	143-159	0.406
Wall Shear Stress dynes/cm^2	8.45 ± 3.94	8.06-8.85	7.79 ± 4.48	7.39-8.20	**<0.001**
RT TAVI Comparison	**Pre-TAVI n= 576**	**95% CI**	**Post-TAVI n= 601**	**95% CI**	**p Value**
Mean Diameter(D) µm	25.85 ± 8.59	25.15-26.55	26.80 ± 8.45	26.12-27.47	0.064
Diameter SD µm	4.08 ± 2.02	3.91-4.24	4.18 ± 2.13	4.01-4.35	0.472
Axial Velocity mm/s	0.54 ± 0.15	0.53-0.55	0.55 ± 0.15	0.53-0.56	0.577
Cross-Sectional Velocity mm/s	0.37 ± 0.10	0.37-0.38	0.38 ± 0.11	0.37-0.38	0.9
Blood Flow Rate pl/s	218 ± 167	205-232	234 ± 172	220-248	0.067
Wall Shear Rate s^{-1}	133 ± 69	127-138	126 ± 59	121-130	0.186

Wall Shear Stress dynes/cm^2	7.67 ± 3.83	7.35-7.99	6.52 ± 3.11	6.27-6.77	**<0.001**
Abbreviations: *L= Left, LN= Left Nasal, LT= Left Temporal, R= Right, RN= Right Nasal, RT= Right Temporal, TAVI= Transcatheter Aortic Valve Implantation*					

Table S6. Pressure wire cohort vessel segment analysis

Overall Controls vs CMD	**Controls n= 1320 vessel segments**	**95% CI**	**CMD n= 975 vessel segments**	**95% CI**	**p value**
Diameter µm	24.80 ± 7.93	24.37-25.22	24.89 ± 8.36	24.37-25.42	0.879
Axial Velocity mm/s	0.55 ± 0.14	0.55-0.56	0.53 ± 0.15	0.52-0.54	**<0.001**
Cross-Sectional Velocity mm/s	0.38 ± 0.10	0.38-0.39	0.37 ± 0.19	0.36-0.37	**<0.001**
Blood Flow Rate pl/s	201 ± 131	193-208	194 ± 133	185-202	0.062
Wall Shear Rate s^{-1}	142 ± 75	138-146	136 ± 76	132-141	**0.026**
Wall Shear Stress dynes/cm^2	9.57 ± 5.05	9.30-9.84	8.80 ± 4.49	8.51-9.08	**<0.001**

Arteriole Controls vs CMD	**Controls n= 219 vessel segments**	**95% CI**	**CMD n= 135 vessel segments**	**95% CI**	**p value**
Diameter µm	23.06 ± 7.91	22.01-24.11	21.35 ± 7.14	20.14-22.57	**0.039**
Axial Velocity mm/s	0.56 ± 0.13	0.54-0.58	0.50 ± 0.14	0.48-0.52	**<0.001**
Cross-Sectional Velocity mm/s	0.40 ± 0.09	0.38-0.41	0.36 ± 0.10	0.34-0.37	**<0.001**
Blood Flow Rate pl/s	180 ± 117	165-196	138 ± 97	121-154	**0.001**
Wall Shear Rate s^{-1}	160 ± 86	149-172	155 ± 90	140-171	0.398
Wall Shear Stress dynes/cm^2	10.48 ± 5.78	9.71-11.25	9.80 ± 5.18	8.91-10.68	0.3
Venule Controls vs CMD	**Controls n= 898 vessel segments**	**95% CI**	**CMD n= 707 vessel segments**	**95% CI**	**p value**
Diameter µm	25.48 ± 7.82	24.97-25.99	25.86 ± 8.59	25.22-26.49	0.535
Axial Velocity mm/s	0.55 ± 0.14	0.54-0.56	0.53 ± 0.15	0.52-0.54	**0.012**

Cross-Sectional Velocity mm/s	0.38 ± 0.10	0.37-0.39	0.37 ± 0.10	0.36-0.37	**0.016**
Blood Flow Rate pl/s	208 ± 134	199-216	207 ± 137	197-217	0.686
Wall Shear Rate s^{-1}	136 ± 72	131-141	132 ± 75	127-138	0.159
Wall Shear Stress dynes/cm^2	9.21 ± 4.88	8.89-9.53	8.60 ± 4.40	8.28-8.93	**0.01**
Undifferentiated Controls vs CMD	**Controls n= 203 vessel segments**	**95% CI**	**CMD n= 133 vessel segments**	**95% CI**	**p value**
Diameter µm	23.66 ± 8.08	22.54-24.78	23.36 ± 7.01	22.16-24.56	0.76
Axial Velocity mm/s	0.56 ± 0.12	0.54-0.58	0.53 ± 0.15	0.51-0.56	0.071
Cross-Sectional Velocity mm/s	0.39 ± 0.08	0.38-0.40	0.37 ± 0.10	0.35-0.39	0.065
Blood Flow Rate pl/s	191 ± 133	173-210	179 ± 128	157-201	0.283
Wall Shear Rate s^{-1}	151 ± 71	141-161	139 ± 62	128-149	0.216
Wall Shear Stress dynes/cm^2	10.17 ± 4.78	9.51-10.83	8.82 ± 4.09	8.12-9.52	**0.01**

L Eye Controls vs CMD	**Controls n= 583 vessel segments**	**95% CI**	**CMD n= 427 vessel segments**	**95% CI**	**p value**
Diameter µm	24.75 ± 7.89	24.10-25.39	23.78 ± 8.05	23.01-24.54	0.058
Axial Velocity mm/s	4.23 ± 1.96	4.07-4.39	3.85 ± 1.96	3.67-4.03	**0.001**
Cross-Sectional Velocity mm/s	0.56 ± 0.15	0.55-0.57	0.54 ± 0.15	0.53-0.56	0.134
Blood Flow Rate pl/s	0.39 ± 0.10	0.38-0.40	0.38 ± 0.10	0.37-0.39	0.287
Wall Shear Rate s^{-1}	201 ± 139	190-212	184 ± 126	172-196	**0.022**
Wall Shear Stress dynes/cm^2	143 ± 73	137-149	150 ± 86	142-158	0.437
Mean Wall Shear Stress	9.60 ± 4.86	9.20-9.99	9.46 ± 4.94	8.99-9.93	0.555
R Eye Controls vs CMD	**Controls n= 737 vessel segments**	**95% CI**	**CMD n= 548 vessel segments**	**95% CI**	**p value**
Diameter µm	24.84 ± 7.98	24.26-25.41	25.76 ± 8.51	25.04-26.47	0.156

Axial Velocity mm/s	4.02 ± 1.94	3.88-4.16	3.99 ± 2.09	3.81-4.16	0.637
Cross-Sectional Velocity mm/s	0.55 ± 0.13	0.54-0.56	0.51 ± 0.14	0.50-0.52	**<0.001**
Blood Flow Rate pl/s	0.38 ± 0.09	0.38-0.39	0.35 ± 0.10	0.35-0.36	**<0.001**
Wall Shear Rate s^{-1}	200 ± 126	191-209	200 ± 138	189-212	0.598
Wall Shear Stress dynes/cm^2	142 ± 76	136-147	126 ± 65	121-132	**<0.001**
Mean Wall Shear Stress	9.55 ± 5.19	9.18-9.93	8.28 ± 4.03	7.94-8.62	**<0.001**
LN Controls vs CMD	**Controls n= 239 vessel segments**	**95% CI**	**CMD n= 191 vessel segments**	**95% CI**	**p value**
Diameter µm	23.88 ± 8.05	22.86-24.91	21.80 ± 7.62	20.71-22.88	**0.01**
Axial Velocity mm/s	4.16 ± 1.91	3.92-4.41	3.83 ± 1.76	3.58-4.08	0.054
Cross-Sectional Velocity mm/s	0.57 ± 0.15	0.55-0.59	0.56 ± 0.16	0.54-0.59	0.625
Blood Flow Rate pl/s	0.40 ± 0.11	0.38-0.41	0.40 ± 0.11	0.38-0.41	0.923

Wall Shear Rate s^{-1}	193 ± 135	176-210	168 ± 130	149-186	**0.008**
Wall Shear Stress dynes/cm^2	152 ± 75	142-161	169 ± 89	156-182	**0.049**
Mean Wall Shear Stress	10.00 ± 4.67	9.41-10.60	10.37 ± 5.18	9.63-11.11	0.662
LT Controls vs CMD	**Controls n= 344 vessel segments**	**95% CI**	**CMD n= 236 vessel segments**	**95% CI**	**p value**
Diameter µm	25.34 ± 7.73	24.52-26.16	25.38 ± 8.04	24.35-26.41	0.975
Axial Velocity mm/s	0.55 ± 0.15	0.54-0.57	0.53 ± 0.14	0.51-0.55	0.101
Cross-Sectional Velocity mm/s	0.38 ± 0.10	0.37-0.39	0.37 ± 0.10	0.35-0.38	0.107
Blood Flow Rate pl/s	207 ± 141	192-222	198 ± 121	182-213	0.577
Wall Shear Rate s^{-1}	137 ± 71	130-145	134 ± 79	124-145	0.364
Wall Shear Stress dynes/cm^2	9.32 ± 4.98	8.79-9.84	8.72 ± 4.62	8.13-9.31	0.156
RN Controls vs CMD	**Controls n= 372**	**95% CI**	**CMD n= 237**	**95% CI**	**p value**

	vessel segments		**vessel segments**		
Diameter µm	24.28 ± 8.31	23.43-25.13	24.52 ± 8.40	23.44-25.60	0.948
Axial Velocity mm/s	0.55 ± 0.13	0.54-0.56	0.52 ± 0.15	0.51-0.54	**0.022**
Cross-Sectional Velocity mm/s	0.39 ± 0.09	0.38-0.39	0.37 ± 0.10	0.35-0.38	**0.016**
Blood Flow Rate pl/s	196 ± 133	182-209	191 ± 148	172-210	0.369
Wall Shear Rate s^{-1}	149 ± 82	141-157	136 ± 69	127-145	0.226
Wall Shear Stress dynes/cm^2	9.83 ± 5.44	9.27-10.38	8.75 ± 4.20	8.22-9.29	0.06
RT Controls vs CMD	**Controls n= 365 vessel segments**	**95% CI**	**CMD n= 311 vessel segments**	**95% CI**	**p value**
Diameter µm	25.41 ± 7.59	24.62-24.19	26.70 ± 8.48	25.76-27.65	0.096
Axial Velocity mm/s	0.55 ± 0.13	0.53-0.56	0.5 ± 0.14	0.49-0.52	**<0.001**
Cross-Sectional Velocity mm/s	0.38 ± 0.09	0.37-0.39	0.35 ± 0.09	0.34-0.36	**<0.001**

Blood Flow Rate pl/s	205 ± 118	192-217	208 ± 130	194-223	0.944
Wall Shear Rate s^{-1}	135 ± 69	128-142	119 ± 61	112-125	**<0.001**
Wall Shear Stress dynes/cm^2	9.27 ± 4.91	8.77-9.78	7.92 ± 3.86	7.49-8.35	**<0.001**
Abbreviations: *CMD= Coronary Microvascular Disease, L= Left, LN= Left Nasal, LT= Left Temporal, R= Right, RN= Right Nasal, RT= Right Temporal.*					

Table S7. Mean inter-eye and field of view ocular parameters of controls vs microvascular disease (MVD) groups

Ocular Parameter (Right Eye)	**Controls (n=68)**	**MVD (n=43)**	**p value**
Diameter µm	24.06 ± 3.73	24.80 ± 3.69	0.326
Axial Velocity mm/s	0.55 ± 0.07	0.51 ± 0.05	**0.002**
Cross-Sectional Velocity mm/s	0.38 ± 0.05	0.35 ± 0.03	**0.002**
Blood Flow Rate pl/s	188 ± 57	187 ± 50	0.998
Wall Shear Rate s^{-1}	146 ± 35	132 ± 30	**0.030**
Wall Shear Stress dynes/cm^2	9.52 ± 2.84	8.53 ± 2.37	0.063
Left Eye			

Diameter µm	24.77 ± 4.18	23.18 ± 4.04	**0.037**
Axial Velocity mm/s	0.55 ± 0.08	0.55 ± 0.06	0.923
Cross-Sectional Velocity mm/s	0.38 ± 0.06	0.39 ± 0.05	0.781
Blood Flow Rate pl/s	199 ± 65	176 ± 61	**0.026**
Wall Shear Rate s^{-1}	142 ± 38	154 ± 40	0.153
Wall Shear Stress dynes/cm^2	9.28 ± 3.02	9.75 ± 2.61	0.321
Nasal Field of View			
Diameter µm	23.9 ± 6.25	22.76 ± 5.56	0.231
Axial Velocity mm/s	0.55 ± 0.09	0.56 ± 0.11	0.912
Cross-Sectional Velocity mm/s	0.39 ± 0.06	0.39 ± 0.08	0.916
Blood Flow Rate pl/s	189 ± 99	176 ± 93	0.292
Wall Shear Rate s^{-1}	150 ± 56	159 ± 61	0.318
Wall Shear Stress dynes/cm^2	9.78 ± 3.98	10.07 ± 3.77	0.562
Temporal Field of View			
Diameter µm	24.86 ± 5.55	25.12 ± 5.08	0.749
Axial Velocity mm/s	0.55 ± 0.10	0.52 ± 0.08	0.142
Cross-Sectional Velocity mm/s	0.38 ± 0.07	0.36 ± 0.06	0.110

Blood Flow Rate pl/s	200 ± 93	193 ± 73	0.831
Wall Shear Rate s^{-1}	139 ± 49	131 ± 42	0.248
Wall Shear Stress dynes/cm^2	9.18 ± 3.52	8.50 ± 2.83	0.218
Left Nasal			
Diameter µm	24.34 ± 6.25	21.21 ± 5.45	**0.012**
Axial Velocity mm/s	0.55 ± 0.10	0.59 ± 0.12	0.156
Cross-Sectional Velocity mm/s	0.39 ± 0.07	0.42 ± 0.09	0.095
Blood Flow Rate pl/s	193 ± 98	162 ± 96	**0.041**
Wall Shear Rate s^{-1}	145 ± 52	180 ± 71	**0.010**
Wall Shear Stress dynes/cm^2	9.45 ± 3.55	11.20 ± 4.12	**0.041**
Left Temporal			
Diameter µm	24.69 ± 5.97	25.03 ± 5.25	0.785
Axial Velocity mm/s	0.55 ± 0.10	0.53 ± 0.08	0.464
Cross-Sectional Velocity mm/s	0.38 ± 0.07	0.37 ± 0.06	0.303
Blood Flow Rate pl/s	200 ± 105	193 ± 78	0.995
Wall Shear Rate s^{-1}	143 ± 55	134 ± 46	0.387

Wall Shear Stress dynes/cm^2	9.37 ± 3.69	8.62 ± 2.85	0.276
Right Nasal			
Diameter µm	23.49 ± 6.27	24.30 ± 5.28	0.421
Axial Velocity mm/s	0.55 ± 0.08	0.52 ± 0.08	0.096
Cross-Sectional Velocity mm/s	0.39 ± 0.06	0.37 ± 0.05	**0.050**
Blood Flow Rate pl/s	186 ± 99	190 ± 88	0.554
Wall Shear Rate s^{-1}	156 ± 60	138 ± 41	0.246
Wall Shear Stress dynes/cm^2	10.10 ± 4.38	8.94 ± 3.04	0.219
Right Temporal			
Diameter µm	25.05 ± 5.12	25.22 ± 4.97	0.785
Axial Velocity mm/s	0.55 ± 0.10	0.52 ± 0.08	0.193
Cross-Sectional Velocity mm/s	0.38 ± 0.07	0.36 ± 0.06	0.225
Blood Flow Rate pl/s	200 ± 79	192 ± 69	0.756
Wall Shear Rate s^{-1}	135 ± 41	129 ± 39	0.449
Wall Shear Stress dynes/cm^2	8.97 ± 3.35	8.38 ± 2.84	0.475

Table S8. Mean inter-view difference (right temporal vs left temporal) of controls vs microvascular disease (MVD) groups

Ocular Parameter	Controls (n=68)	MVD (n=43)	p value
Diameter µm	0.30 ± 7.64	0.19 ± 7.20	0.853
Axial Velocity mm/s	-0.003 ± 0.122	-0.011 ± 0.103	0.667
Cross-Sectional Velocity mm/s	-0.004 ± 0.084	-0.008 ± 0.073	0.780
Blood Flow Rate pl/s	-2.54 ± 128.37	-1.01 ± 102.31	0.967
Wall Shear Rate s^{-1}	-8.25 ± 63.72	-5.00 ± 60.44	0.770
Wall Shear Stress dynes/cm^2	-0.44 ± 3.61	-0.24 ± 3.62	0.672

Table S9. Mean inter-view difference (nasal vs temporal) of controls vs microvascular disease (MVD) groups

Ocular Parameter	Controls (n=68)	MVD (n=43)	p value
Diameter µm	1.08 ± 4.97	2.31 ± 5.02	0.127
Axial Velocity mm/s	-0.008 ± 0.097	-0.027 ± 0.100	0.361
Cross-Sectional Velocity mm/s	-0.009 ± 0.066	-0.024 ± 0.068	0.298
Blood Flow Rate pl/s	10.05 ± 82.74	16.40 ± 79.00	0.397
Wall Shear Rate s^{-1}	-13.72 ± 43.97	-26.04 ± 45.11	0.089

Wall Shear Stress dynes/cm^2	-0.80 ± 2.86	-1.50 ± 2.71	0.09

Table S10. Post-hoc analysis of the baseline characteristics for the QRISK3 classification of controls

Multiple Comparisons							
Games-Howell							
Dependent Variable	(I) Risk Class	(J) Risk Class	Mean Difference (I-J)	Std. Error	Sig.	95% Confidence Interval	
						Lower Bound	Upper Bound
Age (years)	Low	Moderate	-11.219924293684330*	1.554117	0	-14.9246	-7.5152
		High	-15.565508468857537*	1.782494	0	-19.8307	-11.3004
	Moderate	Low	11.219924293684330*	1.554117	0	7.515204	14.92464
		High	-4.345584175173208*	1.779562	0.045	-8.61354	-0.07762
	High	Low	15.565508468857537*	1.782494	0	11.30036	19.83066
		Moderate	4.345584175173208*	1.779562	0.045	0.077624	8.613544
Height (cm)	Low	Moderate	-4.39772	2.03138	0.083	-9.2416	0.4461
		High	-1.27069	2.13173	0.823	-6.3625	3.8211
	Moderate	Low	4.39772	2.03138	0.083	-0.4461	9.2416
		High	3.12703	2.16221	0.323	-2.0521	8.3061
	High	Low	1.27069	2.13173	0.823	-3.8211	6.3625
		Moderate	-3.12703	2.16221	0.323	-8.3061	2.0521
Weight (kg)	Low	Moderate	-4.4397	4.53862	0.593	-15.2638	6.3844
		High	-7.73748	4.45872	0.198	-18.3745	2.8996
	Moderate	Low	4.4397	4.53862	0.593	-6.3844	15.2638

		High	-3.29778	4.56979	0.752	-14.2404	7.6449
	High	Low	7.73748	4.45872	0.198	-2.8996	18.3745
		Moderate	3.29778	4.56979	0.752	-7.6449	14.2404
Mean Systolic Blood Pressure (mmHg)	Low	Moderate	-7.12178	3.008645	0.052	-14.292	0.048468
		High	-10.382266009852260*	3.450164	0.01	-18.634	-2.13057
	Moderate	Low	7.121777	3.008645	0.052	-0.04847	14.29202
		High	-3.26049	3.39687	0.605	-11.4079	4.886924
	High	Low	10.382266009852260*	3.450164	0.01	2.130565	18.63397
		Moderate	3.260489	3.39687	0.605	-4.88692	11.4079
Mean Diastolic Blood Pressure (mmHg)	Low	Moderate	0.576266	2.191758	0.963	-4.65528	5.807807
		High	2.168801	2.205863	0.59	-3.10134	7.438947
	Moderate	Low	-0.57627	2.191758	0.963	-5.80781	4.655275
		High	1.592535	2.341019	0.776	-4.01337	7.198443
	High	Low	-2.1688	2.205863	0.59	-7.43895	3.101344
		Moderate	-1.59254	2.341019	0.776	-7.19844	4.013372
Heart Rate (bpm)	Low	Moderate	0.679	2.195	0.949	-4.57	5.93
		High	-1.468	2.149	0.774	-6.61	3.67
	Moderate	Low	-0.679	2.195	0.949	-5.93	4.57
		High	-2.147	2.353	0.634	-7.79	3.49

	High	Low	1.468	2.149	0.774	-3.67	6.61
		Moderate	2.147	2.353	0.634	-3.49	7.79
Resting Oxygen Satura-tion (%)	Low	Moderate	-0.105	0.301	0.935	-0.83	0.62
		High	0.65	0.342	0.147	-0.17	1.47
	Moderate	Low	0.105	0.301	0.935	-0.62	0.83
		High	0.755	0.379	0.122	-0.15	1.66
	High	Low	-0.65	0.342	0.147	-1.47	0.17
		Moderate	-0.755	0.379	0.122	-1.66	0.15
* The mean difference is significant at the 0.05 level.							

Table S11. Post-hoc analysis of the ocular parameters for the QRISK3 classification of controls

Multiple Comparisons							
Games-Howell							
Dependent Variable	(I) Risk Class	(J) Risk Class	Mean Difference (I-J)	Std. Error	Sig.	95% Confidence Interval	
						Lower Bound	Upper Bound
Diameter (D) µm	Low	Moderate	-2.724737080*	0.664462	0	-4.3109	-1.13857
		High	-2.412423904*	0.688617	0.002	-4.05891	-0.76594
	Moderate	Low	2.724737080*	0.664462	0	1.138574	4.3109
		High	0.312313	0.726104	0.903	-1.4267	2.051322
	High	Low	2.412423904*	0.688617	0.002	0.765941	4.058907
		Moderate	-0.31231	0.726104	0.903	-2.05132	1.426696
Axial Velocity (Va) mm/s	Low	Moderate	-.03369337185*	0.012357	0.022	-0.06329	-0.00410
		High	-0.01387	0.011692	0.465	-0.04186	0.014126

	Moderate	Low	.03369337185*	0.012357	0.022	0.004101	0.063286
		High	0.019828	0.013701	0.323	-0.01298	0.052638
	High	Low	0.013866	0.011692	0.465	-0.01413	0.041857
		Moderate	-0.01983	0.013701	0.323	-0.05264	0.012982
Cross Sectional Velocity (CSV) mm/s	Low	Moderate	-0.0175	0.008818	0.123	-0.03861	0.0036
		High	-0.00406	0.008267	0.876	-0.02383	0.015706
	Moderate	Low	0.017503	0.008818	0.123	-0.0036	0.038605
		High	0.013439	0.009547	0.343	-0.00943	0.036303
	High	Low	0.004064	0.008267	0.876	-0.01571	0.023834
		Moderate	-0.01344	0.009547	0.343	-0.0363	0.009426
Blood Flow Rate(Q) pl/s	Low	Moderate	-44.651934730090430*	10.19227	0	-68.9969	-20.3069
		High	-31.113998689605040*	9.9338	0.007	-54.8473	-7.38066
	Moderate	Low	44.651934730090430*	10.19227	0	20.30692	68.99694
		High	13.53794	10.78236	0.425	-12.2812	39.3571
	High	Low	31.113998689605040*	9.9338	0.007	7.38066	54.84734
		Moderate	-13.5379	10.78236	0.425	-39.3571	12.28123
Wall Shear Rate (WSR) s^{-1}	Low	Moderate	14.28113	7.11439	0.116	-2.67831	31.24057
		High	18.395263846239830*	6.731142	0.021	2.349721	34.44081
	Moderate	Low	-14.2811	7.11439	0.116	-31.2406	2.678313

		High	4.114133	6.574321	0.806	-11.6315	19.85977
	High	Low	-18.395263846239830*	6.731142	0.021	-34.4408	-2.34972
		Moderate	-4.11413	6.574321	0.806	-19.8598	11.6315
* The mean difference is significant at the 0.05 level.							

Chapter 12

Appendix

Appendix I

www.nature.com/scientificreports

scientific reports

Check for updates

OPEN

A novel algorithm for cardiovascular screening using conjunctival microcirculatory parameters and blood biomarkers

Agnes Awuah[1], Julie S. Moore[1], M. Andrew Nesbit[1], Mark W. Ruddock[2], Paul F. Brennan[3], Jonathan A. Mailey[3], Andrew J. McNeil[4], Min Jing[5], Dewar D. Finlay[5], Emanuele Trucco[6], Mary Jo Kurth[2], Joanne Watt[2], John V. Lamont[2], Peter Fitzgerald[2], Mark S. Spence[3], James A. D. McLaughlin[5] & Tara C. B. Moore[1]✉

Microvascular haemodynamic alterations are associated with coronary artery disease (CAD). The conjunctival microcirculation can easily be assessed non-invasively. However, the microcirculation of the conjunctiva has not been previously explored in clinical algorithms aimed at identifying patients with CAD. This case–control study involved 66 patients with post-myocardial infarction and 66 gender-matched healthy controls. Haemodynamic properties of the conjunctival microcirculation were assessed with a validated iPhone and slit lamp-based imaging tool. Haemodynamic properties were extracted with semi-automated software and compared between groups. Biomarkers implicated in the development of CAD were assessed in combination with conjunctival microcirculatory parameters. The conjunctival blood vessel parameters and biomarkers were used to derive an algorithm to aid in the screening of patients for CAD. Conjunctival blood velocity measured in combination with the blood biomarkers (N-terminal pro-brain natriuretic peptide and adiponectin) had an area under receiver operator characteristic curve (AUROC) of 0.967, sensitivity 93.0%, specificity 91.5% for CAD. This study demonstrated that the novel algorithm which included a combination of conjunctival blood vessel haemodynamic properties, and blood-based biomarkers could be used as a potential screening tool for CAD and should be validated for potential utility in asymptomatic individuals.

Cardiovascular disease (CVD) is a major cause of morbidity and mortality in developed countries[1]. It accounts for 17.9 million deaths globally, with up to 80% of these deaths resulting from myocardial infarction (MI) and stroke[1]. Coronary artery disease (CAD) is the most common type of CVD and results from the accumulation of lipid deposits (atherosclerosis) in the coronary arteries[2]. CAD is the leading cause of death in developed countries[3].

CVD not only carries a significant morbidity and mortality burden but has major economic implications. The World Heart Foundation estimated the total cost of CVD was US$863 billion in 2010, with a predicted increase to approximately US$1,044 billion by 2030[4]. The total expenditure on CVD in the EU is €210 billion annually with 53% (€111 billion) due to direct health care expenditures, productivity losses cost 26% (€54 billion), and informal care of patients costs 21% (€45 billion)[5].

Atherosclerosis is the key pathophysiological process that underlies CAD[6]. This process develops over a prolonged period of time and is influenced by a variety of medical and behavioural risk factors[5]. Atherosclerotic plaques in general do not produce symptoms until the affected vessel has significant luminal narrowing and the resulting ischaemic cascade can be silent in its early stages. Prior to atherosclerotic plaque rupture and resultant MI, patients may be asymptomatic. Many predictive approaches, screening and diagnostic methods for atherosclerotic diseases have evolved. These include utilization of independent traditional and biochemical risk factors, general CVD risk scores, and assessment of cardiac microvasculature[6–11].

[1]Biomedical Sciences Research Institute, Ulster University, Cromore Road, Coleraine BT52 1SA, UK. [2]Clinical Studies Group, Randox Laboratories Ltd, 55 Diamond Road, Crumlin BT29 4QY, UK. [3]Department of Cardiology, Royal Victoria Hospital, Belfast Health and Social Care Trust, 274 Grosvenor Road, Belfast BT12 6BA, UK. [4]VAMPIRE Project, Computing (SSEN), University of Dundee, Dundee DD1 4HN, UK. [5]Nanotechnology and Integrated Bioengineering Centre (NIBEC), Ulster University, Jordanstown BT37 0QB, UK. ✉email: tara.moore@ulster.ac.uk

Current European Society of Cardiology (ESC) clinical guidelines recommend the systematic assessment of cardiovascular (CV) risk in men > 40 years and in women > 50 years or post-menopausal with no CV risk factors[10]. ESC assessment of risk for asymptomatic individuals utilises the Systematic Coronary Risk Estimation (SCORE) assessment tool, whilst National Institute for Clinical Excellence (NICE) advocates the use of QRISK3[12,13]. Both tools take into consideration conventional vascular risk factors to estimate long-term CV risk. The results of these estimates of risk are then used to inform GPs' decisions with regards to primary preventative therapies and overall long-term risk. The risk score obtained may be modified by the presence of pre-existing medical conditions that were not taken into consideration during the initial risk calculation (e.g. chronic kidney disease or diabetes mellitus); or with the detection of preclinical asymptomatic vascular damage using imaging modalities (e.g. computed tomography (CT) coronary calcium score, carotid ultrasound or ankle brachial pressure index[13]). All pre-existing screening methods are limited either by the exposure of the patient to ionizing radiation (CT); or by the need for expensive imaging modalities requiring operator expertise to perform and interpret (carotid ultrasound)[13,14]. Due to the global and regional health and socioeconomic implications of CAD, there is a need to identify novel factors for screening asymptomatic individuals for early detection of CAD.

Previously heart-type fatty acid-binding protein (H-FABP), for example, has been shown to be an early blood diagnostic biomarker of MI[15]. H-FABP is detected in blood within 30 min of an ischaemic event. Measurement of H-FABP with troponin proved to be a reliable diagnostic tool for the early diagnosis of MI and a valuable rule out test at presentation to the emergency department[15,16]. Cholesterol is usually measured in screening > 40-year-old males and > 50-year-old females. Measurement of biomarkers in addition to cholesterol may provide further information to identify individuals at risk of CAD in asymptomatic individuals as a screening tool.

Microcirculatory studies have demonstrated the association of inflammation with atherosclerosis[17–20]. In addition, it has been shown that endothelial dysfunction in the microcirculation is an early manifestation and marker of vascular disease[21]. Microcirculatory changes have been observed in patients with hypertension, diabetes, sickle cell disease and sepsis[17,21–23]. A change in microcirculation is a potential marker for determining risk of potential major adverse cardiovascular events (MACE). These changes may manifest in changes in blood biomarker levels associated with these processes [e.g. NT-proBNP, interleukin-6 (IL-6), C-reactive protein (CRP), H-FABP, high density lipoprotein (HDL), fibrinogen, apolipoproteins, adiponectin, HDL-3 and monocyte chemoattractant protein-1 (MCP-1)].

In addition, the networks of the human eye allow examination of the microcirculation at the anterior (ocular adnexum) and posterior (retina) aspect that can easily be visualised and accessed non-invasively[24]. Changes to the retinal vessel diameters show evidence of diseases that are conventional risk factors for CAD (e.g. diabetes and hypertension)[25–27] and hence could play a pathophysiological role in CVD risk stratification and prediction[28]. Blood flow within the conjunctival vasculature can be directly visualised and hence assessment of microcirculatory parameters (e.g. velocity (V), flow (Q), wall shear rate (WSR)) can also be measured non-invasively[29–31]. The study by Brennan et al.[31] assessed groups of subjects with and without hypertension, diabetes mellitus, dyslipidaemia, reduced left ventricular ejection fraction (< 50%), as well as smokers vs. non-smokers. The results show only the blood flow rate (pl/s) increased significantly in diabetics vs. non-diabetics respectively (181 ± 61 vs. 151 ± 39 pl/s, $p = 0.04$). Previous studies have identified conjunctival microvascular changes in diseases such as sickle cell, hypertension and diabetes mellitus[32,33].

The aim of this study was to develop a screening tool that could be used to identify patients at risk of CAD. Our previous study detected changes in conjunctival microvascular measurements between control and post-MI patients[31]. As part of the study, blood samples were collected to determine if blood biomarkers could be used in conjunction with microvascular measurements to improve the diagnostic potential of the test.

Methods

Study population. In this case–control MACE study, we compared a cohort of inpatients with severe cardiovascular phenotype after an acute MI with a healthy gender-matched patient cohort. Participants < 18 years were excluded from the study. All study participants were recruited between January 2018 and November 2019. Participants were eligible for inclusion in the 'healthy' cohort if they had no previous history of CAD.

Patients were eligible for inclusion in the post-MI cohort if they had been admitted to hospital with a diagnosis of MI that fulfilled the European Society of Cardiology (ESC) 4th Universal definition of type 1 MI. This is defined as acute myocardial injury with clinical evidence of acute myocardial ischaemia. A fall and/or rise of cardiac troponin (cTn) with 1 or more values beyond the 99th percentile of the Upper Reference Limit (URL), in addition to one or more of the following: evidence of new ischaemic ECG changes; pathological Q waves; current loss of myocardium or regional wall motion abnormality in line with an ischaemic aetiology; and coronary thrombus[34].

The study complied with ethical principles on human experimentation (Declaration of Helsinki) and was approved by the office for Research Ethics Committee Northern Ireland (ORECNI) (IRAS Reference-166742), and Research Governance Committee of Belfast Trust (Trust Reference-15144TM-AS). Written informed consent was obtained from each participant prior to recruitment. The study was conducted in accordance with Standard for Reporting Diagnostic Accuracy (STARD) guidelines[35].

Clinical data collection. All participants were asked to complete a clinical questionnaire detailing baseline demographics, past medical history, current medications, family history of medical conditions and lifestyle information. Electronic healthcare records were reviewed following ethical approval and participants' consent for medical history to ensure accuracy. Baseline measurement of blood pressure, heart rate, oxygen saturations, height, and weight were also performed.

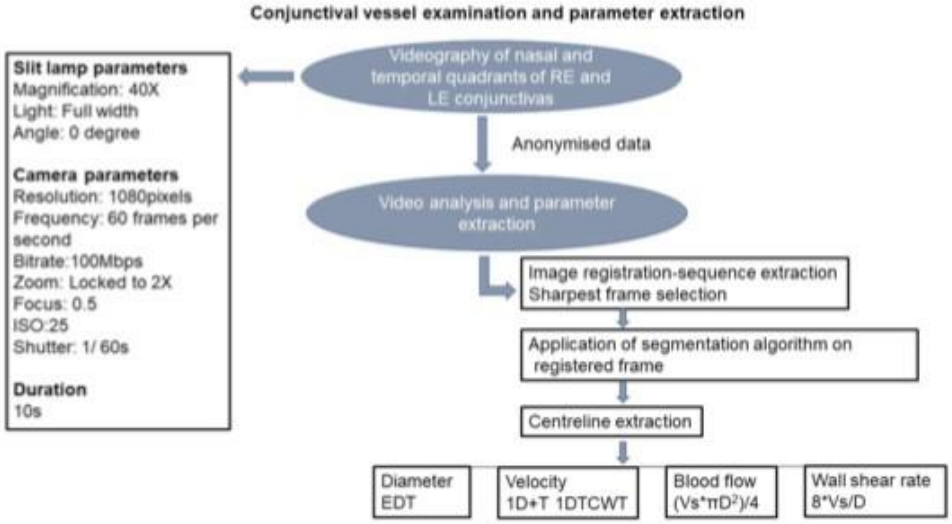

Figure 1. Vessel parameter data collection. *RE* Right Eye, *LE* Left Eye, *EDT* Euclidean Distance Transform, *1D + T* 1 Dimension + Time, *CWT* Continuous Wavelet Transform, *Vs* Cross Sectional Velocity, *D* Diameter.

Blood sampling and laboratory methods. For biomarker assessment, 24mls of venous blood was sampled. Serum and plasma samples were analysed by Randox Clinical Laboratory Services (RCLS), (Antrim, UK) on cytokine arrays (Randox Laboratories Ltd, Crumlin, UK); using an Evidence Investigator analyser (Randox Laboratories Ltd, Crumlin, UK) for the following proteins: Cytokine array 1: Interleukin (IL)-1α, -1β, -2, -4, -6, -8, -10, vascular endothelial growth factor (VEGF), epidermal growth factor (EGF), tumour necrosis factor alpha (TNF-α), interferon gamma (IFNγ) and MCP-1. H-FABP, adiponectin, homocysteine and HDL-3 were measured on the RX Imola analyser (Randox, Crumlin, UK). Folate and vitamin B_{12} were measured on a Cobas8000 (Roche, Basel, Switzerland).

Asymmetric dimethylarginine (ADMA) and leucine-rich alpha-2-glycoprotein-1 (LRG-1) were assessed by ELISA, according to manufacturer's instructions (ELISAgenie, Ireland). The limits of detection (LOD) for the biomarkers were as follows: IL-1α 0.19 pg/ml; IL-1β 0.26 pg/ml; IL-2 2.97 pg/ml; IL-4 2.12 pg/ml; IL-6 0.12 pg/ml; IL-8 0.36 pg/ml; IL-10 0.37 pg/ml, VEGF 3.24 pg/ml; EGF 1.04 pg/ml; TNF-α 0.59 pg/ml; IFNγ 0.44 pg/ml; MCP-1 3.53 pg/ml; H-FABP < 2.94 ng/ml; adiponectin 0.18 µg/ml; folate 2.72 nmol/l; homocysteine 1.74 µmol/l; vitamin B_{12} 73.8 pmol/l; HDL-3 4 mg/dl; plasma ADMA < 0.938 µmol/L; plasma LRG-1 < 0.0047 µg/ml. Results below the LOD were inputted as 90% of the LOD[36].

Troponin, lipids, NT-proBNP, urate, urea and electrolytes and all other biochemical measurements, were analysed by clinical staff at the Kelvin Building Laboratories, Royal Victoria Hospital, Belfast. Apo-lipoprotein A and B were analysed by the Biochemistry Department, Cardiff and Vale University Hospital, UK as reported previously[31].

Conjunctival vessel imaging. Conjunctival microvascular imaging was performed using our previously described non-invasive imaging tool (iPhone 6s with slit lamp biomicroscope) and semi-automated software; developed by the VAMPIRE centre (Dundee) and NIBEC (Ulster University) for quantifying vessel haemodynamic properties (vessel diameter (D), axial velocity (Va), cross-sectional velocity (Vs), Q, and WSR)[30,37,38]. The process is summarised as a flow diagram in Fig. 1.

Briefly, the imaging tool consisted of a 2X magnification device (Apple iPhone 6s) adapted as an eye piece of a slit-lamp biomicroscope (Topcon SL-D4) with a 40 × magnification lens. A third-party camera application (ProMovie Recorder) was used for controlling camera settings (focus, shutter speed and ISO). Conjunctival imaging may take around 5 to 10 min per patient. Videos were obtained from conjunctival vessels in the nasal and temporal bulbar conjunctivas while the participants focused on a fixation target attached to the slit lamp. A total of 4 videos per participant were obtained in 40 s; each video was captured at 60 frames per second for 10 s. While all videos were captured under the same, or similar, lighting conditions in a hospital setting, the brightness of the light from the slit-lamp source rendered any small fluctuations in ambient lighting insignificant. Anonymised videos taken during the eye examinations were processed and analysed by researchers blinded to the participant baseline demographics and cohort allocation at Dundee University and Ulster University. They were analysed with set-up specific semi-automated software[38]. Measurements from vessels of both eyes were combined for the estimation of overall mean of each parameter per patient (patient's mean).

Variables	Control n = 66	Post-MI n = 66	p value
Age (years)	52.50 ± 9.73	56.73 ± 11.41	0.039
Gender (males)	45/66 (68.2%)	52/66 (78.8%)	0.168
Height (cm)	168.21 ± 10.68	170.77 ± 9.34	0.262
Weight (kg)	81.40 ± 22.72	83.59 ± 14.93	0.186
Body mass index (kg/m^2)	28.71 ± 7.66	28.62 ± 4.68	0.306
Systolic BP (mmHg)	128 ± 16	120 ± 16	0.006
Diastolic BP (mmHg)	76 ± 10	73 ± 11	0.066
Heart rate (beats/min)	71 ± 10	73 ± 12	0.299
Hypertension	8/66 (12.1%)	31/66 (47.0%)	0.001
Diabetes	2/66 (3.0%)	15/66 (22.7%)	0.001
COPD	6/66 (9.1%)	8/66 (12.1%)	0.572
Hypercholesterolemia	17/64 (26.6%)	36/66 (54.5%)	0.001
Previous MI	0/66 (0%)	9/66 (13.6%)	0.002
Heart failure	0/66 (0%)	6/65 (9.2%)	0.012
Stroke	0/66 (0%)	1/66 (1.5%)	0.315
Smoking (yes)	29/66 (43.9%)	43/66 (65.2%)	0.014
Family history of IHD	21/66 (31.8%)	38/66 (57.6%)	0.003

Table 1. Demographic and clinical characteristics (mean ± SD). *COPD* chronic obstructive pulmonary disease, *IHD* ischaemic heart disease, *BP* blood pressure.

Estimation of conjunctival microcirculatory parameters. Estimation of blood vessel parameters has been previously described[30,37–39]. Video sequences with minimal motion artefact were selected. The sharpest frame in the sequence was selected as a reference frame and all other frames registered to it. A segmentation algorithm was applied to segment vessels before vessel centrelines were extracted for estimating the dynamic properties of the vessels. Euclidean Distance Transformation was used for estimation of vessel diameter. The axial velocity (Va) was estimated based on spatial–temporal image (STI) via applying one dimension of space plus time (1D + T) continuous wavelet transform (1DTCWT)[40]. Blood flow was calculated from the product of the cross-sectional velocity (Vs) and diameter (D), using the formula, $(Vs.\pi D^2)/4$. Wall shear rate was calculated by the formula $8Vs/D$[30,37,38].

Statistical analysis. Statistical analyses were performed using IBM SPSS v25 and R version 4.1.2[41]. The following statistics were analysed on the appropriate data: descriptive statistics (mean ± SD) and percentages for summarizing parametric and nominal data, respectively; Chi square and Pearson's tests for determining the association and correlation between variables; and independent t-test for differences between group means for parametric data. Where the assumptions of t-test were unmet, the Mann–Whitney *U* test or Wilcoxon rank-sum test was used. Variable medians were compared when distributions were similar but mean ranks were compared when distributions were dissimilar. Binary logistic regression and receiver operator characteristic (ROC) curves were used to test sensitivity and specificity. Normality was assessed by Shapiro Wilk test ($p > 0.05$). Data transformation was applied when the assumption of normality was unmet. Statistical significance was set at an α-level $p < 0.05$.

Results

Demographic characteristics. A total of n = 132 participants were recruited to the MACE study. There was an equal number of participants in each group; post-MI n = 66 and healthy controls n = 66. Post MI cases were recruited 2.53 ± 3.44 days (range 0–21 days) after hospital admission following type 1 MI. There was a significant difference between the mean ages of the control and MI groups ($p = 0.039$) but no significant difference between gender distribution ($\chi^2(1) = 1.91$, $p = 0.168$). Demographic and clinical characteristics are described in Table 1.

Clinical and lifestyle characteristics. None of the participants in the control group had previous MI (control: 0/66 (0.00%) vs. post-MI: 9/66 (13.6%), heart failure (control: 0/66 (0.00%) vs. post-MI: 6/66 (9.2%) or stroke (control 0/66 (0.00%) vs. post-MI:1/66 (1.5%), $p < 0.05$ for all variables). There were more smokers in the post-MI group; 43/66 (65.2%) vs. 29/66 (43.9%); $p = 0.014$, respectively. No significant differences in height were found between the cohorts. The mean and standard deviation values of height (cm) for both cohorts, controls vs. MI respectively were 168.21 ± 10.68 cm vs. 170.77 ± 9.34 cm, $p = 0.262$.

Comparison of microvascular parameters and biomarkers. Results of the comparison for microvascular parameters between groups are described in Table 2.

A summary of biomarker results between the control and post-MI group are described in Table 3.

Variables	Control n = 66	Post-MI n = 66	p value
Diameter (D, μm)	21.45 ± 3.03	22.79 ± 3.07	0.012
Axial velocity (Va, mm/s)	0.54 ± 0.05	0.50 ± 0.06	0.001
Cross-sectional velocity (Vs, mm/s)	0.38 ± 0.04	0.35 ± 0.04	0.001
Blood flow (Q, pl/s)	159.66 ± 47.27	161 ± 48.12	0.457
Wall shear rate (WSR, s^{-1})	167.78 ± 34.37	143.59 ± 28.56	0.001

Table 2. Ocular microvascular parameters (mean ± SD).

Ocular-biomarker algorithm derivation. Combining biomarker and ocular measurements may provide a novel method of identifying individuals at risk of CAD. Using forward and backward Wald logistic regression identified the combination of Vs, NT-proBNP and adiponectin as having the highest predictive ability to discriminate the post-MI group from control; with the fewest variables suitable for the patient cohort size for the study ($\chi^2(3) = 111.74$, $p < 0.05$). The model explained 80.4% (Nagelkerke R^2) of the variance in CAD and correctly classified 90.1% of cases. Hosmer and Lemeshow test for goodness of fit was $\chi^2(8) = 6.83$, $p = 0.55$; sensitivity 93.0%, specificity 91.5%, positive predictive value (PPV) 91.4%, negative predictive value (NPV) 93.1%; area under receiver operator characteristic curve (AUROC) 0.967 (Table 4 and Fig. 2). In comparison, the QRISK3 score had a reduced sensitivity (71.7%), specificity (64.9%), PPV = 68.3% and NPV = 68.5% as shown in Table 4 and Supplementary Fig. 1.

Discussion

The aim of this case–control study was to evaluate the feasibility for using conjunctival microvascular parameters assessed non-invasively, in combination with biomarkers as a potential screening modality for CAD. This was achieved by comparing conjunctival imaging parameters and blood-based biomarkers in patients with established CAD and severe CVD phenotype (post-MI) with a control group of healthy volunteers.

Of the five conjunctival microvascular parameters assessed, four (diameter, axial velocity, cross-sectional velocity and wall shear rate) were significantly different between the post-MI and controls. Conjunctival vessel diameter was significantly higher in the post-MI group, however axial and cross-sectional velocities were lower compared with the control group. In addition, wall shear rate was lower in the post-MI group. An algorithm which included both conjunctival and biomarker measurements (microvascular velocity, adiponectin and NT-proBNP) was identified that differentiated the post-MI from control (AUROC 0.967, sensitivity 93.0%, specificity 91.5%) (Table 4 and Fig. 2). Application of this novel algorithm could be used to screen asymptomatic individuals for atherosclerotic disease.

Reduced blood velocity, elevated NT-proBNP and lower adiponectin reflect pathological cardiovascular conditions. The main function of the microcirculation is regulation of vascular resistance and oxygen perfusion of tissues. Therefore, decreased velocity and increased vessel diameter in the post-MI group, opposes the normal Poiseuille's law of blood flow dynamics, suggesting underlying microvascular dysfunction[42].

Adiponectin and NT-proBNP are implicated in the pathogenesis and pathophysiology of CAD, for example, low levels of adiponectin (< 4.0 μg/mL) have been reported to be associated with an increased risk of CAD[43]. Low levels of adiponectin reflect underlying abnormal lipid metabolism, inflammation and is a contributor of atherosclerosis and subsequent vascular events[43–45].

This study evaluated biomarkers of inflammation and endothelial dysfunction associated with CAD. A reduced conjunctival wall shear rate was observed in post-MI compared with control. Potential screening algorithms for CAD incorporating biomarkers and conjunctival blood vessel parameters have been identified (Table 4). These data suggest that changes in ocular microvascular parameters e.g. cross-sectional velocity, combined with biomarkers, have potential benefits for detecting atherosclerotic heart disease.

Detecting inflammation and endothelial dysfunction may offer the earliest opportunity to institute primary preventative therapies, lowering the risk of major adverse cardiac events. Endothelial dysfunction occurs in the initial stages of the ischemic cascade by promoting the development of atherosclerosis[46]. Reduction in wall shear rate and stress are associated with atherosclerotic plaque development and progression in coronary microvascular dysfunction[42,47]. Endothelial cells are regulators of inflammation; chronic inflammation is also an etiology of endothelial dysfunction. Hence, an understanding of the relationship and underlying pathophysiological mechanisms of endothelial dysfunction and inflammation is vital.

The authors of this report acknowledge that MI triggers inflammation aimed at enhancing healing and tissue repair which resolves between 2 and 4 weeks post-infarction[48–50]. Considering the recruitment interval of the post-MI group, post-infarct inflammation potentially could contribute to the inflammatory mediators released to promote healing[51]. However, the mediators have the potential of aggravating the existing atherosclerotic plaques leading to recurrent MI. Assessment of the relationship between cross-sectional velocity and biomarkers of endothelial dysfunction has potential utility in the screening of both asymptomatic and symptomatic CVD for stratifying risk of future events. This report suggests that the proposed algorithm identified in this study is tested and validated in a follow up study.

Biomarkers/ocular parameters	AUROC	Sensitivity %	Specificity %	PPV%	NPV%
Log_{10} NT-proBNP, adiponectin, log_{10} H-FABP, Va	0.977	94.7	91.5	91.5	94.7
Log_{10} NT-proBNP, log_{10} adiponectin, log_{10} H-FABP, Vs	0.976	93.0	93.2	93.0	93.2
Log_{10} NT-proBNP, log_{10} adiponectin, Vs	**0.967**	**93.0**	**91.5**	**91.4**	**93.1**
Log_{10} NT-proBNP, log_{10} adiponectin, Va	0.966	94.7	93.2	93.1	94.8
Log_{10} H-FABP, log_{10} NT-proBNP, Va	0.953	88.1	91.9	91.2	89.1
Log_{10} H-FABP, log_{10} NT-proBNP, Vs	0.953	86.4	90.3	89.5	87.5
Log_{10} H-FABP, log_{10} NT-proBNP, log_{10} WSR	0.936	84.7	88.7	87.7	85.9
Log_{10} NT-proBNP, Vs	0.926	85.0	83.9	83.6	85.2
Log_{10} NT-proBNP, Va	0.925	83.3	85.5	84.7	84.1
IL-6, Vs	0.840	76.2	76.2	76.2	76.2
Log_{10} H-FABP, Vs	0.830	73.0	76.6	75.4	74.2
Log_{10} H-FABP, Va	0.815	73.0	71.9	71.9	73.0
CRP, D	0.810	79.4	67.2	71.4	75.9
Log_{10} adiponectin, log_{10} WSR	0.769	76.3	60.3	66.2	71.4
Log_{10} adiponectin, Va	0.721	76.2	53.1	61.5	69.4
Log_{10} adiponectin, D	0.702	72.1	54.2	62.0	65.3
Vs	0.706	63.1	73.4	70.7	66.2
Log_{10} adiponectin	0.674	65.6	62.5	63.6	64.5
Log_{10} NT-proBNP	0.897	78.7	90.6	88.9	81.7
QRISK3 score	0.732	71.7	64.9	68.3	68.5
Age (years)	0.604	59.1	57.6	58.2	58.5

Table 4. Multivariate logistic regression with biomarkers and ocular parameters for detecting CAD. Significant values are in bold. *CRP* C-reactive protein, *H-FABP* heart-type fatty acid-binding protein, *IL-6* interleukin-6, *NT-proBNP* N-terminal pro brain natriuretic peptide, *D* vessel diameter, *Va* axial velocity, *Vs* cross-sectional velocity, *WSR* wall shear rate, *AUROC* area under receiver operator characteristic curve, *PPV* positive predictive value, *NPV* negative predictive value.

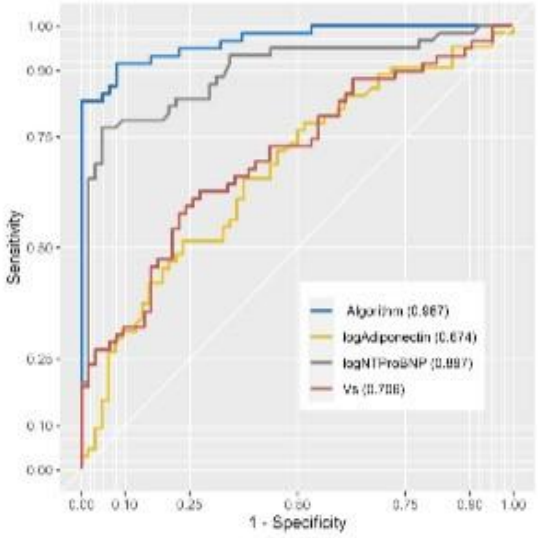

Figure 2. ROC curve of ocular-biochemical score.

Study limitations

The small sample size had a tendency of generating false-positive errors (type 1)[52]. Hemorheological parameters respond differently to the cardiac cycle[53]. Hence, lack of differentiation of vessels has the potential of concealing true parameter values leading to biases in results and conclusions. Another study limitation relates to known confounding factors of vascular alteration including, but not limited to, age, lifestyle and medical factors[3]. Underlying

medical factors with known effects on microvasculature include systemic blood pressure, hypercholesterolaemia, and diabetes. Heart failure and lifestyle factors such as smoking have known effects on the microvasculature. We acknowledge the sample size as the major study limitation on statistics on confounding factors, comorbidities, routine medication and hence recommend a larger study population for validation.

Conclusion

This study demonstrated the potential for a non-invasive ocular screening modality to detect conjunctival microvascular dysfunction in patients with overt atherosclerotic heart disease. The novel algorithm identified, combines ocular parameters with biomarkers that could distinguish between control and post-MI groups. The assessment of the conjunctival microcirculation is a rapid non-invasive test that can easily compliment blood investigations and existing lifestyle factors for CVD screening and risk stratification; however, this would need further validation as a screening tool in a larger sample of asymptomatic people.

Received: 7 October 2021; Accepted: 15 March 2022
Published online: 21 April 2022

References

1. Institute of Health Metrix and Evaluations [IHME]. Global burden of disease study 2017. *Lancet* (2017).
2. Braun, M. M. & Stevens, W. A. Stable coronary artery disease: Treatment. *Am. Fam. Physician* **97**, 376–384 (2018).
3. British Heart Foundation. *UK Factsheet*, 1–21 (British Heart Foundation, 2020).
4. World Economic Forum. *The Global Economic Burden of Non-communicable Diseases, Harvard School of Public Health*. (2011).
5. Wilkins, E. *et al. European Cardiovascular Disease Statistics 2017 edition* 192 (European Heart Network, 2017).
6. Vasan, R. S. Biomarkers of cardiovascular disease: Molecular basis and practical considerations. *Circulation* **113**, 2335–2362 (2006).
7. McQueen, M. J. *et al.* Lipids, lipoproteins, and apolipoproteins as risk markers of myocardial infarction in 52 countries (the INTERHEART study): A case–control study. *Lancet* **373**, 224–233 (2008).
8. Yusuf, S. *et al.* Effect of potentially modifiable risk factors associated with myocardial infarction in 52 countries (the INTERHEART study): Case-control study. *Lancet* **17**, 937–952 (2004).
9. Karmali, K. *et al.* Risk scoring for the primary prevention of cardiovascular disease (review) summary of findings for the main comparison. *Cochrane Database Syst. Rev.* **1**, 1–127. https://doi.org/10.1002/14651858.CD006887.pub4 (2017).
10. Piepoli, M. F. *et al.* 2016 European Guidelines on cardiovascular disease prevention in clinical practice the Sixth Joint Task Force of the European Society of Cardiology and Other Societies on Cardiovascular Disease Prevention in Clinical Practice (constituted by representative). *Eur. J. Prev. Cardiol.* **23**, 1–96 (2016).
11. Pries, A. R. *et al.* A review of methods for assessment of coronary microvascular disease in both clinical and experimental settings. *Cardiovasc. Res.* **80**, 165–174 (2008).
12. NICE. *Impact Cardiovascular Disease Prevention*.
13. Piepoli, M. F. *et al.* 2016 European Guidelines on cardiovascular disease prevention in clinical practice. *Eur. Heart J.* **37**, 2315–2381 (2016).
14. Driessen, R. S., Raijmakers, P. G., Stuijfzand, W. J. & Knaapen, P. Myocardial perfusion imaging with PET. *Int. J. Cardiovasc. Imaging* **33**, 1021–1031 (2017).
15. Mcmahon, C. G. *et al.* Diagnostic accuracy of heart-type fatty acid-binding protein for the early diagnosis of acute myocardial infarction. *Am. J. Emerg. Med.* **30**, 267–274 (2012).
16. Navarro-Paredes, C. *et al.* Diagnostic performance of a combination biomarker algorithm for rule-out of acute myocardial infarction at time of presentation to the emergency department, using heart-type fatty acid-binding protein and high-sensitivity troponin T tests. *J. Clin. Exp. Cardiol.* **9**, 1–9 (2018).
17. Lockhart, C. J., Hamilton, P. K., Quinn, C. E. & Mcveigh, G. E. End-organ dysfunction and cardiovascular outcomes: the role of the microcirculation. *Clin. Sci.* **116**, 175–190 (2009).
18. Stokes, K. Y. & Granger, D. N. The microcirculation: A motor for the systemic inflammatory response and large vessel disease induced by hypercholesterolaemia?. *J. Physiol.* **562**, 647–653 (2005).
19. Pober, J. S. & Sessa, W. C. Evolving functions of endothelial cells in inflammation. *Nat. Rev. Immunol.* **7**, 803–815 (2007).
20. Savoia, C. & Schiffrin, E. L. Vascular inflammation in hypertension and diabetes: Molecular mechanisms and therapeutic interventions. *Clin. Sci.* **112**, 375–384 (2007).
21. Abularrage, C. J. *et al.* Evaluation of the microcirculation in vascular disease. *J. Vasc. Surg.* **42**, 574–581 (2005).
22. Charlton, M., Sims, M., Coats, T. & Thompson, J. P. The microcirculation and its measurement in sepsis. *J. Intensive Care Soc.* **18**, 221–227 (2017).
23. Menaa, F., Khan, B. A., Uzair, B. & Menaa, A. Sickle cell retinopathy: Improving care with a multidisciplinary approach. *J. Multidiscip. Healthc.* **10**, 335–346 (2017).
24. Jiang, H. *et al.* Human conjunctival microvasculature assessed with a retinal function imager (RFI). *Microvasc. Res.* **85**, 134–137 (2013).
25. De Jong, F. *et al.* Retinal vascular caliber and risk of dementia. *Neurology* **76**, 816–821 (2011).
26. Ikram, M. K. *et al.* Are retinal arteriolar or venular diameters associated with markers for cardiovascular disorders? The Rotterdam study. *Investig. Ophthalmol. Vis. Sci.* **45**, 2129–2134 (2004).
27. Ikram, M. K. *et al.* Retinal vessel diameters and risk of hypertension. *Hypertension* **47**, 189–194 (2006).
28. Rim, T. H. *et al.* Deep-learning-based cardiovascular risk stratification using coronary artery calcium scores predicted from retinal photographs. *Lancet Digit. Heal.* **3**, e306–e316 (2021).
29. Khansari, M. M. *et al.* Automated fine structure image analysis method for discrimination of diabetic retinopathy stage using conjunctival microvasculature images. *Biomed. Opt. Express* **7**, 2597 (2016).
30. Brennan, P. F. *et al.* Assessment of the conjunctival microcirculation in adult patients with cyanotic congenital heart disease compared to healthy controls. *Microvasc. Res.* **136**, 104167 (2021).
31. Brennan, P. F. *et al.* Assessment of the conjunctival microcirculation for patients presenting with acute myocardial infarction compared to healthy controls. *Sci. Rep.* **11**, 1–9 (2021).
32. Cheung, A. T. W. *et al.* Microvascular abnormalities in sickle cell disease: A computer-assisted intravital microscopy study. *Sci. Rep.* **99**, 3999–4005 (2011).
33. Wong, T. Y. *et al.* Computer-assisted measurement of retinal vessel diameters in the Beaver Dam eye study: Methodology, correlation between eyes, and effect of refractive errors. *Ophthalmology* **111**, 1183–1190 (2004).
34. Thygesen, K. *et al.* Fourth universal definition of myocardial infarction (2018). *Eur. Heart J.* **40**, 237–269 (2019).

35. Cohen, J. F. *et al.* STARD 2015 guidelines for reporting diagnostic accuracy studies: Explanation and elaboration. *BMJ Open* **6**, 1–17 (2016).
36. Kurth, M. J. *et al.* Acute kidney injury risk in orthopaedic trauma patients pre and post surgery using a biomarker algorithm and clinical risk score. *Sci. Rep.* **10**, 20005–20005 (2020).
37. Brennan, P. F. *et al.* Cardiac-gated slit lamp videography as a novel approach to assessing a microcirculatory. *Netw. R. Vict. Hosp.* **44**, 1–4 (2017).
38. Brennan, P. F. *et al.* Quantitative assessment of the conjunctival microcirculation using a smartphone and slit-lamp biomicroscope. *Microvasc. Res.* **126**, 103907 (2019).
39. Jerman, T., Pernus, F., Likar, B. & Spiclin, Z. Enhancement of vascular structures in 3D and 2D angiographic images. *IEEE Trans. Med. Imaging* **35**, 2107–2118 (2016).
40. Duval-Destin, M. Spatio-temporal wavelet: Appication to the analysis of moving. *Prog. Wavelet Anal. Appl.* **1**, 1–10 (1993).
41. R Core Team. *R: A language and environment for statistical computing*. https://www.R-project.org/ (R Foundation for Statistical Computing, Vienna, Austria, 2021).
42. Koutsiaris, A. G., Tachmitzi, S. V. & Batis, N. Wall shear stress quantification in the human conjunctival pre-capillary arterioles in vivo. *Microvasc. Res.* **85**, 34–39 (2013).
43. Kumada, M. *et al.* Association of hypoadiponectinemia with coronary artery disease in men. *Arterioscler. Thromb. Vasc. Biol.* **23**, 85–89 (2003).
44. Coughlin, C. C. *et al.* Effect of marked weight loss on adiponectin gene expression and plasma concentrations. *Obesity* **15**, 640–645 (2007).
45. Madeira, I. R. *et al.* Impact of obesity on metabolic syndrome components and adipokines in prepubertal children. *J. Pediatr.* **85**, 261–268 (2009).
46. Corban, M. T. & Lerman, L. O. Endothelial dysfunction cardiovascular disease pathophysiology hidden in plain sight. *Arter. Thromb Vasc. Biol.* **7**, 1272–1274 (2019).
47. Samady, H. *et al.* Coronary artery wall shear stress is associated with progression and transformation of atherosclerotic plaque and arterial remodeling in patients with coronary artery disease. *Circulation* **124**, 779–788 (2011).
48. Kandat, T. & Takahashi, T. Interleukin-6 and cardiovascular diseases. *Jpn Hear. J* **45**, 183–193 (2004).
49. Szekely, Y. & Arbel, Y. A review of interleukin-1 in heart disease: Where do we stand today?. *Cardiol. Ther.* **7**, 25–44 (2018).
50. Vanhaverbeke, M. *et al.* C-reactive protein during and after myocardial infarction in relation to cardiac injury and left ventricular function at follow-up. *Clin. Cardiol.* **41**, 1201–1206 (2018).
51. Frangogiannis, N. G. The inflammatory response in myocardial injury, repair, and remodelling. *Nat. Rev. Cardiol.* **11**, 255–265 (2014).
52. Hackshaw, A. Small studies: Strengths and limitations. *Eur. Respir. J.* **32**, 1141–1143 (2008).
53. Chen, H. C., Patel, V., Chen, J., Rassam, S. M. & Kohner, E. M. Vessel diameter changes during the cardiac cycle. *Eye* **8**, 97–103 (1994).

Author contribution

Designing studies: T.C.B.M., M.A.N., M.W.R., M.S.S., E.T., J.A.D.M., D.D.F., A.A., P.B., M.J.K., J.L., P.F: Data Gathering: A.A., J.S.M., P.B., A.J.M, M.J., J.A.M: Research Database Preparation and Auditing: A.A., J.S.M., M.A.N., M.W.R., T.C.B.M. J.W.; Research Data Analysis: A.A., J.S.M., M.W.R., J.W; Manuscript Preparation: A.A., J.S.M., M.W.R., M.A.N., T.C.B.M., P.B., J.A.M., M.S.S., J.A.D.M, M.J.K., J.W., J.L., P.F: Editing of final version of manuscript: A.A., J.S.M., M.W.R., M.J.K., J. W, M.A.N., T.C.B.M, J.A.M., P.B.

Competing interests

Mark Ruddock, Mary Jo Kurth, Joanne Watt, and John Lamont are employees of Randox Laboratories Ltd but hold no shares in the Company. Peter Fitzgerald is the Managing Director and owner of Randox Laboratories Ltd. A patent has been filed to protect the biomarkers and biomarker combinations disclosed in this study.

Additional information

Supplementary Information The online version contains supplementary material available at https://doi.org/10.1038/s41598-022-10491-7.

Correspondence and requests for materials should be addressed to T.C.B.M.

Reprints and permissions information is available at www.nature.com/reprints.

Publisher's note Springer Nature remains neutral with regard to jurisdictional claims in published maps and institutional affiliations.

Appendix II

www.nature.com/scientificreports

scientific reports

Check for updates

OPEN

Assessment of the conjunctival microcirculation for patients presenting with acute myocardial infarction compared to healthy controls

Paul F. Brennan[1,2✉], Andrew J. McNeil[2], Min Jing[4], Agnes Awuah[2], Julie S. Moore[2], Jonathan Mailey[1], Dewar D. Finlay[4], Kevin Blighe[2], James A. D. McLaughlin[4], M. Andrew Nesbit[2], Emanuele Trucco[3], Tara C. B. Moore[2] & Mark S. Spence[1]

Microcirculatory dysfunction occurs early in cardiovascular disease (CVD) development. Acute myocardial infarction (MI) is a late consequence of CVD. The conjunctival microcirculation is readily-accessible for quantitative assessment and has not previously been studied in MI patients. We compared the conjunctival microcirculation of acute MI patients and age/sex-matched healthy controls to determine if there were differences in microcirculatory parameters. We acquired images using an iPhone 6s and slit-lamp biomicroscope. Parameters measured included diameter, axial velocity, wall shear rate and blood volume flow. Results are for all vessels as they were not sub-classified into arterioles or venules. The conjunctival microcirculation was assessed in 56 controls and 59 inpatients with a presenting diagnosis of MI. Mean vessel diameter for the controls was 21.41 ± 7.57 µm compared to 22.32 ± 7.66 µm for the MI patients ($p < 0.001$). Axial velocity for the controls was 0.53 ± 0.15 mm/s compared to 0.49 ± 0.17 mm/s for the MI patients ($p < 0.001$). Wall shear rate was higher for controls than MI patients (162 ± 93 s^{-1} vs 145 ± 88 s^{-1}, $p < 0.001$). Blood volume flow did not differ significantly for the controls and MI patients (153 ± 124 pl/s vs 154 ± 125 pl/s, $p = 0.84$). This pilot iPhone and slit-lamp assessment of the conjunctival microcirculation found lower axial velocity and wall shear rate in patients with acute MI. Further study is required to correlate these findings further and assess long-term outcomes in this patient group with a severe CVD phenotype.

Globally cardiovascular disease (CVD) is a leading cause of morbidity and mortality with an estimated 17.7 million people dying from CVD each year[1]. CVD also represents a substantial economic burden and in Northern Ireland alone, it is estimated that around £400 million per year is spent on CVD[2]. Cardiovascular screening and primary prevention are important elements of the healthcare system. CVD risk models such as the Q-Risk 3 score provide a 10-year estimate of the likelihood of a patient sustaining a major adverse cardiovascular event (MACE) occurring e.g. myocardial infarction (MI), cerebrovascular accident (CVA)[3,4].

Microcirculatory dysfunction represents the earliest stages of CVD[5]. Microvascular networks that are readily-accessible for evaluation include the retinal circulation, sublingual circulation and nail-fold circulation[6–8]. The conjunctival microcirculation gains its blood supply from the anterior ciliary branch of the ophthalmic artery[9]. Conjunctival microcirculatory parameters, namely diameter (D), axial velocity (Va), blood volume flow (Q) and wall shear rate/stress (WSR/WSS) have previously been assessed using a non-invasive combination of a slit-lamp biomicroscope and digital charge-coupled device (CCD) camera[10–16]. The study of the conjunctival microcirculation, using these methods, has been applied to patients at high CVD-risk e.g. post CVA, diabetic retinopathy[17,18]. Correlation between conjunctival microcirculatory abnormalities and CVD risk calculation,

[1]Department of Cardiology, Royal Victoria Hospital, Belfast Health and Social Care Trust, Belfast, UK. [2]Biomedical Sciences Research Institute, Ulster University, Coleraine, UK. [3]VAMPIRE project, Computing (SSEN), University of Dundee, Dundee, UK. [4]Nanotechnology and Integrated Bioengineering Centre (NIBEC), Ulster University, Jordanstown, UK. ✉email: paul.brennan@belfasttrust.hscni.net

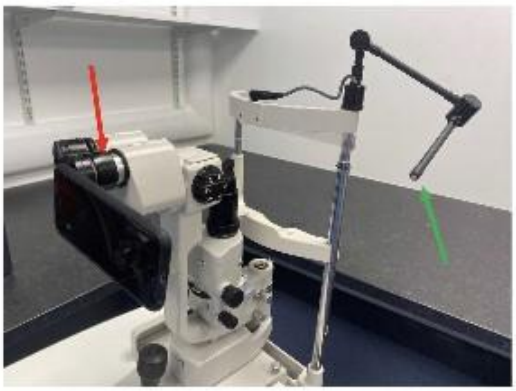

Figure 1. The iPhone 6s, TopCon SL-D4 imaging system with the Zarf bespoke adapter (red arrow) and TopCon external fixation target (green arrow).

using the Framingham Risk Score has also been reported[19,20]. Haemoglobin video imaging (HVI) has recently been described for assessing the branching patterns within the conjunctival circulation[21].

Assessment of the conjunctival microcirculation in patients with acute MI, has not been described. A prior rabbit model[22], however, demonstrated a relationship between conjunctival venous diameter velocity, blood volume flow and the administration of either the potent vasoconstrictor alpha-adrenergic agonist phenylephrine or the negatively inotropic beta-adrenergic blocker esmolol. Nail-fold capillary diameters have been shown to be more dilated in patients with chronic heart failure (CHF) compared to controls[23]. These responses of the microcirculation to alterations in vasoreactivity, cardiac inotropy and heart failure status could all potentially be encountered in patients with acute MI.

We recently reported the feasibility of assessing the conjunctival microcirculation using an iPhone 6s (Apple, USA) and slit-lamp biomicroscope in a group of low CVD-risk controls[24]. The purpose of this study was to quantifiably assess the conjunctival microcirculation of patients that had recently suffered an acute type 1 MI, based on the 4th universal definition of MI compared to a group of age- and sex-matched controls[25].

Methods

Study design. We conducted a prospective study (Integrated Research Application System study number 166742) of inpatients who had suffered a recent myocardial infarction compared to a group of low CVD risk controls at the Royal Victoria Hospital, Belfast, United Kingdom. All subjects were screened and provided with verbal and written information and consented prior to study enrolment. Informed consent was obtained from all participants. Participants were recruited to the study in accordance with the Declaration of Helsinki. The experimental protocol was approved by the Research Ethics committee in the Belfast Health and Social Care Trust (BHSCT) and Ulster University (UU).

Criteria for the MI patients included that they were currently an inpatient with acute type 1 MI, not pregnant and greater than 17 years age. Key inclusion criteria for the control patients was that they were of low CVD risk and did not have prior history of coronary artery disease, MI, stroke, diabetes or uncontrolled systemic hypertension. Exclusion criteria for both groups included inability to consent, a history of recent conjunctival inflammation, prior refractive surgery, use of ocular medications (excluding artificial tears) and current use of contact lenses. In addition to the exclusion screening questionnaire all patients were examined by a clinical optometrist at the time of conjunctival imaging to assess for active signs of inflammation or dry eyes.

Baseline characteristics and quantitative conjunctival microcirculatory parameters were compared between both patient groups. The Q-Risk 3 score was calculated to estimate the 10-year risk of MACE for the control group.

The definitions of ST elevation and Non-ST elevation MI (STEMI, NSTEMI) were as described in the respective European Society of Cardiology guidelines[26,27].

Baseline clinical data and characteristics were obtained using the recruitment questionnaire, the inpatient clinical notes (if an acute MI patient), the hospital cardiology database (Cardiovascular Information System Tomcat, Phillips, Eindhoven, Netherlands) and the patient's Northern Ireland Electronic Care Record (NIECR). Long-term clinical outcomes were determined using NIECR.

Conjunctival assessment. Conjunctival microcirculation image acquisition for both eyes was performed under the same settings for all patients. Using our previously reported methods[24] we acquired images using a Topcon SL-D4 (Topcon Medical Systems Inc., USA), an iPhone 6s smartphone (Apple, Inc, USA) and a bespoke adapter (Zarf Enterprises Inc., USA) as illustrated in Fig. 1. The optimal configuration was set at a resolution of 1920 × 1080 pixels, captured at 60 frames per second. Using the third-party application "ProMovie Recorder" (http://www.promovieapp.com) we locked the video zoom setting at magnification 2×, providing a 1:1- pixel mapping of the camera sensor at 1080 pixel resolution. We acquired 5–10 s videos of the conjunctival micro-

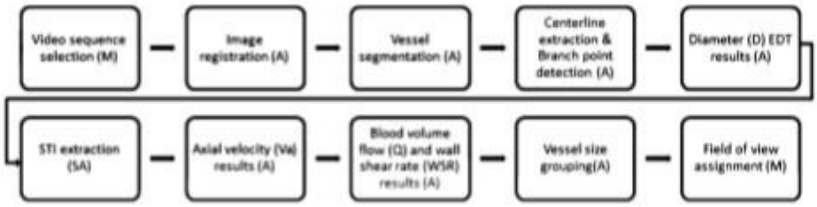

Figure 2. Flow-chart illustrating the individual processing stages from image registration to results output. Each step is labelled as automatic (A), manual (M) or semiautomatic (SA).

circulation medial and lateral to the iris, this generating four videos per subject. An external fixation target was used to minimise blinking and eye motion. A processed stabilised video of the left nasal conjunctival microcirculation is provided in Supplementary Video file 1.

We quantifiably assessed diameter (D), axial velocity (Va), blood volume flow (Q) and wall shear rate (WSR) in vessels with observable flow.

MALTAB R2019b (MathWork, USA) was used for programming. The sharpest frame in the sequence was automatically selected as a reference frame and all other frames registered to it. The Matlab function imregister.m was used for automatic registration. Automatic vessel filtering was implemented using Matlab code available in[28] Vessel centreline extraction and branch/end-point detection was automatically applied to the image using Matlab function bwmorph.m.

The Euclidean Distance Transform (EDT) principle was used to calculate vessel diameter (D). The value at each pixel of EDT map was automatically calculated based on the Euclidean distance between the pixel and its nearest nonzero pixel in the binary vessel image. The vessel centreline was used to obtain the central EDT values and radius along the vessel axis. The final vessel diameter estimation is provided by averaging the diameters found along the length of the vessel.

Axial velocity was estimated based on the spatial–temporal image (STI) obtained from the vessel segment and continuous wavelet transform (CWT) method, with the change in STI intensity reflecting erythrocyte movement through the vessel. The (CWT) has been applied as a spatio-temporal filter for motion capture for 1-dimension plus time (1D + T) signals[29–31]. The STI is a time sequence signal denoted as $\boldsymbol{I(x,t)}$, where each value in the image represents the intensity at the position x in the corresponding vessel centreline and time point t. The change in STI intensity reveals the blood flowing through the vessel within the given time (or video frames) and as described previously this was performed semi-automatically[24].

The blood volume flow rate (Q) was automatically calculated based on the principles defined in previous works[11,24] by the product of the cross-sectional velocity V_s and the cross-sectional area (assuming a circular cross-section (1)):

$$Q = V_s \frac{\pi D^2}{4} \tag{1}$$

The wall shear rate (WSR) was calculated by dividing the cross-sectional velocity by the diameter as evidenced in (2)

$$WSR = \frac{8V_s}{D} \tag{2}$$

For microvessel diameters less than approximately 20 µm, a velocity profile cannot be used in the ordinary sense in order to estimate V_s[32]. Therefore, V_s is obtained based on a profile factor function that has been previously described in other work[33], in which the relationship between the cross-sectional velocity V_s and axial velocity V_a is represented as:

$$V_s = \begin{cases} V_a & when\ D/D_c \le 0.6, \\ \frac{V_a}{1.58\left(1-e^{-\sqrt{2D/D_c}}\right)}, & when\ D/D_c > 0.6. \end{cases} \tag{3}$$

where D_c is the size of the average human erythrocyte diameter that is 7.65 µm as described in[33].

Figure 2 is a flow-chart illustrating the processing stages.

Methodology repeatability was assessed by one observer analysing the video sequences for 5 control subjects twice, blinded to the clinical and demographic details of each subject. The repeated measurements were obtained from 38 vessel segments (5–9 per subject) and sample size was similar to other well-established conjunctival analysis work[16]. Differences in the four main measured parameters (D, Va, Q, WSR) were compared. Coefficients of repeatability (CR) were calculated using conventional approaches[33]. The mean difference for D was − 0.01 ± 0.04 µm, CR 0.08 µm (95%CI − 0.09 µm to 0.07 µm) and for Va was 0.002 mm/s ± 0.01 mm/s, CR 0.02 mm/s (95%CI − 0.02 mm/s to 0.02 mm/s). The mean difference for Q was 0.03 ± 2.14 pl/s, CR 4.19 pl/s (95%CI − 4.1 pl/s to 4.2 pl/s) and for WSR was 0.78 ± 4.17 s^{-1}, CR 8.18 s^{-1} (95%CI − 7.4 to 9.0 s^{-1}). These results supported acceptable repeatability of vessel segment analysis using our current technical approach.

Baseline characteristic	Control (n = 56)	MI (n = 59)	p value
Age, years ± SD	53 ± 10	57 ± 12	0.07
Male sex n (%)	38 (68)	47 (80)	0.15
Q-Risk 3 score ± SD (%)	8.1 ± 7.6	Not applicable	
Clinical IHD n (%)	0	11 (18.6)	**< 0.001**
Prior MI n (%)	0	8 (13.6)	**0.006**
Prior stroke n (%)	0	1 (1.7)	1
Hypertension n (%)	7 (12.5)	21 (35.6)	**0.004**
Diabetes mellitus n (%)	0	12 (20.3)	**0.002**
Dyslipidaemia n (%)	11 (19.6)	25 (42.4)	**0.009**
Smoking history n (%)	21 (37.5)	36 (61)	**0.01**
COPD n (%)	4 (7.1)	2 (3.4)	0.43
Creatine clearance, ml/min ± SD	84 ± 29	91 ± 37	0.56
Haemoglobin, g/l ± SD	146 ± 11	142 ± 15	0.08
Haematocrit, l/l ± SD	0.43 ± .03	0.42 ± .04	0.29
Platelet count, 10^{99}/l ± SD	263 ± 43	259 ± 64	0.27

Table 1. Summary of baseline characteristics for the healthy control and acute MI populations. Bold values are statistically significant ($p < 0.05$). *IHD* ischaemic heart disease, *MI* myocardial infarction, *COPD* chronic obstructive pulmonary disease.

To overcome the heterogenous anatomical properties of the conjunctival microcirculation we applied a vessel grouping classification to our results based on vessel diameter i.e. group 1 (D < 11 µm), group 2 (D 11–16 µm), group 3 (D 16–22 µm) and group 4 (D > 22 µm)[10,24]. Vessels were not separated into venules or arterioles and results are provided for all vessels.

Statistical analysis. For statistical analysis SPSS for Apple iOS version 25 (property of IBM) was used. Continuous variables were described using the mean, standard deviation of the mean and 95% confidence intervals (CI). The median was applied if the continuous variable was not normally distributed. Kolmogorov–Smirnov testing was used to assess normality of the continuous variables. Categorical variables were expressed as a number and percentage of the total category number to which the variable belonged.

Normally distributed variables were compared between the two populations using the independent-samples t-test. Non-normally distributed continuous variables were compared using non-parametric tests e.g. Mann–Whitney U test. Categorical comparisons were made between the two groups using Pearson Chi-Square or Fisher's exact test.

A one-way analysis of variance (ANOVA) was used to compare differences between the two groups based on the vessel group classifications and the fields of view imaged, followed by post-hoc testing where indicated to assess the origin of the statistical significance. Bonferroni post-hoc testing was applied if normal variance was assumed and Games-Howell if normal variance could not be assumed.

An α-level of less than 0.05 was determined to be of statistical significance. As this was an exploratory pilot study a formal power calculation was not performed. Results are described based on the number of vessel segments. A total of 4163 vessel segments were analysed and reported in the results section (controls 1904 total, 34 per patient vs MI 2259 total, 38 per patient) providing a large number of vessels for comparison. The parameters for each study group from all vessel segments across the four videos were averaged for each patient prior to overall analysis. When vessel groups were compared (1–4), however, each parameter was averaged for all vessel segments falling within that vessel group.

Results

Baseline characteristics. Between the 31st January 2018 and 15th March 2019, 115 patients were recruited to this study. 48.7% (56/115) patients were healthy controls and 51.3% (59/115) were patients post-acute MI. The mean age for the control population was 53 ± 10 years compared to 57 ± 12 years for the acute MI patients ($p = 0.07$). 68% (38/56) the control population were male compared to 80% (47/59) of the acute MI patients ($p = 0.15$). The MI patients had a higher proportion of diabetes mellitus, systemic hypertension and smoking. The baseline Q-Risk 3 score for the controls was 8.1 ± 7.6%. Baseline characteristics are summarised in Table 1.

At the time of recruitment both groups were normotensive, with the control population having a significantly higher systolic (129 ± 16 mmHg vs. 121 ± 17 mmHg, $p = 0.01$) blood pressure and higher diastolic (77 ± 10 mmHg vs. 74 ± 11 mmHg, $p = 0.10$) blood pressure, but this did not reach statistical significance. This is explained by the appropriate administration of blood pressure (BP)-lowering medications, either newly started or long-term, for 95% of the MI population at the time of recruitment and patient medications are summarised in Table 2.

Within the MI group 21 (36%) had STEMI and 38 (64%) NSTEMI. There were no differences in mean age or sex of either MI group. The median time to recruitment post MI event was 1 day (interquartile range IQR 1–3, overall range day 0–22). 81% patients were recruited within 3 days of their MI, 91.5% within the first week and 98.3% within 2 weeks. 49 (83%) of the MI patients had percutaneous coronary intervention (PCI), 6 (10%) had

Medication	Control population (n = 56)	MI population (n = 59)	p value
Aspirin, n (%)	5 (8.9)	58 (98.3)	**< 0.001**
Ticagrelor, n (%)	0	52 (88.1)	**< 0.001**
Clopidogrel, n (%)	0	2 (3.4)	0.50
Prasugrel, n (%)	0	0	n/a
ACE inhibitors, n (%)	5 (8.9)	41 (69.5)	**< 0.001**
Angiotensin receptor blockers, n (%)	1 (1.8)	7 (11.9)	0.10
Mineralocorticoid antagonists, n (%)	0	11 (18.7)	**0.003**
Beta-blockers, n (%)	3 (5.4)	53 (89.8)	**< 0.001**
Any BP-lowering medication, n (%)	7 (12.5)	56 (95)	**< 0.001**
Statins, n (%)	8 (14.3)	55 (93.2)	**< 0.001**

Table 2. Pharmacological therapy at the time of recruitment. Bold values are statistically significant ($p < 0.05$).

Baseline characteristic	STEMI (n = 21)	NSTEMI (n = 38)	p value
Age, years ± SD	55 ± 13	59 ± 11	0.20
Male sex, n (%)	17 (81)	30 (79)	1
Creatine clearance, ml/min ± SD	99 ± 50	89 ± 24	0.41
Diabetes mellitus, n (%)	2 (9.5)	10 (26.3)	0.18
Hypertension, n (%)	5 (23.8)	16 (42)	0.25
LVEF < 50%, n (%)	12 (57)	15 (38.5)	0.42
TnThs, mmol/l ± SD	3645 ± 3438	527 ± 1077	0.001
NT-proBNP, ng/L ± SD	1288 ± 1377	825 ± 1190	0.22
LDL, mmol/l ± SD	3.2 ± 1.7	2.6 ± 1.3	0.16
Cholesterol/HDL ratio ± SD	4.2 ± 0.4	4.2 ± 1.6	0.83
HbA1c, mmol/l ± SD	41 ± 5	49 ± 17	0.09
Time in hospital, days (IQR)	4 (2–6.5)	9 (2–10.5)	0.17

Table 3. Baseline characteristics and biomarkers for the STEMI and NSTEMI populations. *SD* standard deviation, *STEMI* ST segment elevation myocardial infarction, *NSTEMI* non ST segment elevation myocardial infarction, *TnThs* high-sensitivity troponin T, *NT-proBNP* N terminal pro brain natriuretic peptide, *LDL* low density lipoprotein, *HDL* high density lipoprotein, *HbA1c* glycated haemoglobin, *LVEF* left ventricular ejection fraction, *IQR* interquartile range.

coronary artery bypass grafts (CABG) and 4 (7%) patients were medically managed without coronary revascularisation. 28 (47%) of MI patients were recruited prior to coronary revascularisation with the remaining 31 (53%) of MI patients recruited after revascularisation. The breakdown of STEMI, in order of most to least frequent and based on the presenting electrocardiogram's (ECG) suggested territory of infarction, was 47.7% (n = 10) inferior, 33.3% (n = 7) anterior, 9.5% (n = 2) lateral and 9.5% (n = 2) posterior/inferolateral.

Left ventricular systolic dysfunction, based on a left ventricular ejection fraction < 50%, was observed in 46% (n = 27) MI patients on their pre-discharge transthoracic echocardiogram (TTE). 8.5% (n = 5) patients had severe left ventricular systolic dysfunction (ejection fraction < 35%) on TTE. There was no in-hospital mortality, further MI or stroke. No patients had an implantable cardioverting defibrillator (ICD) or permanent pacemaker (PPM) implanted. The STEMI group had a statistically higher TnThs compared to the NSTEMI group (3645 ± 3438 mmol/l vs. 527 ± 1077 mmol/l, p = 0.001) but creatinine clearance, Nt-proBNP and baseline lipid profiles did not differ, significantly, between the two groups. Baseline comorbidities were similar between the STEMI and NSTEMI group and are summarised in Table 3.

STEMI patients had a shorter total admission duration than NSTEMI patients (4.2 ± 3 days vs. 9.2 ± 13 days, p = 0.17). STEMI patients were treated via our regional primary PCI pathway with immediate revascularisation whereas the mean time to NSTEMI patient revascularisation was 5.6 ± 7 days. The mean time for NSTEMI patients to revascularisation with PCI was 2 ± 2 days compared to 18 ± 8 days for CABG (p < 0.001) and the PCI patients also had significantly shorter stays post revascularisation (2.3 ± 3 days vs. 13 ± 12 days, p < 0.001).

Repeat revascularisation occurred in 17% (n = 10) patients during a median follow-up of 361 days. The majority of repeat revascularisation was planned (70%, n = 7). Unplanned revascularisation occurred in 30% (n = 3) of the MI repeat revascularisation group. Culprit vessel revascularisation occurred in 30% (n = 3) of this group. There were no cases of stent thrombosis during follow-up.

Only one patient was readmitted with HF presentation within 1 year. There was no cardiac mortality during follow-up. One MI patient died of lung adenocarcinoma (diagnosed after recruitment) during follow-up.

Haemodynamic parameter	Controls (n = 56)	MI patients (n = 59)	p value
D, μm ± SD	21.43 ± 7.57	22.32 ± 7.66	**< 0.001**
Va, mm/s ± SD	0.53 ± 0.15	0.49 ± 0.17	**< 0.001**
Q, pl/s ± SD	153 ± 124	154 ± 125	0.84
WSR, s^{-1} ± SD	162 ± 93	145 ± 88	**< 0.001**

Table 4. Summary of conjunctival microcirculatory parameters for all vessel sizes for both populations. Bold values are statistically significant ($p < 0.05$). *D* diameter, *SD* standard deviation, *Va* axial velocity, *Q* blood volume flow, *WSR* wall shear rate, *MI* myocardial infarction.

Conjunctival analysis. Conjunctival microvascular videos were captured for all 115 patients. There were no reported complications or adverse outcomes associated with image acquisition. Processing of images and subsequent microvascular quantitative assessment was performed in an independent laboratory, blinded to the patient baseline characteristics and history to avoid bias.

A total of 4163 (control 1904 total, 34 per patient vs. MI 2259 total, 38 per patient) vessel segments were analysed for the two populations, with no significant differences in the mean number of vessel segments analysed per patient group ($p > 0.05$).

The mean vessel diameter for the controls was 21.41 ± 7.57 μm (95% CI 21.08–21.76 μm) which was significantly lower than the 22.32 ± 7.66 μm (95% CI 22–22.64 μm) for the MI patients ($p < 0.001$). The mean axial velocity (Va) for the MI population was 0.49 ± 0.17 mm/s (95% CI 0.49–0.50 mm/s) which was significantly lower than the control populations mean Va of 0.53 ± 0.15 mm/s (95% CI 0.52–0.53 mm/s ($p < 0.001$)).

Overall mean blood volume flow (Q) did not differ significantly between the control and MI groups (153 ± 124 pl/s (95% CI 147–157 pl/s) vs. 154 ± 125 pl/s (95% CI 149–159 pl/s), $p = 0.84$). Wall shear rate (WSR) was significantly lower in the MI population, compared to the healthy controls (control 162 ± 93 s^{-1} (95% CI 118–166 s^{-1}) vs. MI 145 ± 88 s^{-1} (95% CI 141–149 s^{-1}), $p < 0.001$). Table 4 summarises the differences between the two study groups.

Microcirculatory parameters were sub-analysed between the two groups based on the four vessel size groupings described above. The largest diameter vessels (group 4, > 22 μm) were the most frequently observed vessels with vessel frequency decreasing from group 4 down to group 1.

Axial velocity (Va) was lower for the MI patients through all vessel size groups, meeting statistical significance for groups 2–4. Blood volume flow (Q) was also lower for MI patients in all vessel size groups and this met statistical significance for the most numerically abundant vessels i.e. groups 3 and 4. Wall shear rate (WSR) was consistently lower for the MI patients for all vessel groups and met statistical significance for groups 2–4. Table 5 is a summary of the microcirculatory comparisons for each of the four vessel size groups.

The conjunctival measurements were compared between the STEMI and NSTEMI patient groups. Despite the differences in presentation, myocardial biomarkers and prevalence of left ventricular systolic dysfunction there were no significant differences between the two groups with respect to any of the conjunctival measurements as summarised in Supplementary Table 1.

Within the MI population sub-group analysis of specific comorbidities the only significant difference in microcirculatory parameters was a higher Q (181 ± 61 pl/s vs 151 ± 39 pl/s, $p = 0.04$) in diabetic (DM) patients (n = 12) compared to non-diabetics (n = 47) as presented in Fig. 3.

No significant differences were noted for the remainder of the microcirculatory parameters on subgroup analysis of smoking st.atus, impaired LV systolic function (LVEF < 50%), systemic HTN and hypercholesterolaemia. Supplementary Figure 1a–c illustrate the microcirculatory parameters sub-group analysis.

Discussion

Our study demonstrated differences in conjunctival microcirculatory parameters for a group of high CVD risk patients post-MI compared to a group of healthy volunteers. The physiological changes and endothelial dysfunction, associated with atherosclerosis and CVD, typically manifest earliest in the microvasculature within the body[5]. The progressive process which leads to myocardial ischaemia is known as the ischaemic cascade[34]. This process begins with localised metabolic and endothelial function changes in the coronary circulation. Perfusion defects typically occur next in this cascade, followed by cardiac myocyte dysfunction and changes in the patient ECG which can result in angina or MI.

There was a significant reduction in Va for patients with history of recent acute MI compared to the healthy controls, suggestive of endothelial dysfunction and this is consistent with prior findings in patients with other forms of CVD[17,18,35]. Slower coronary flow has previously been associated with atherosclerosis and increased risk of obstructive coronary artery disease[36] and our findings would suggest a possible correlation between diminished epicardial blood flow and conjunctival Va. The most pronounced statistical differences for Va between the two study groups were observed for vessel size groups 2–4.

Overall blood volume flow (Q) did not differ significantly between the two study groups but was significantly lower in the MI group for vessel groups 3 and 4. These were the most numerically abundant vessel groups in the study. This may be explained by the distribution of venules and arterioles across the vessel size groupings. Differences in conjunctival Q was not reported in other studies of the conjunctival microcirculation in high CVD risk patients e.g. ischaemic stroke patients and diabetic patients[17,18].

Haemodynamic parameter	Control group (n = 56)	MI population (n = 59)	p value
Group 1 (< 11 µm)	**No. vessels 165**	**No. vessels 178**	
D, µm ± SD	9.12 ± 1.33	9.04 ± 1.36	0.64
Va, mm/s ± SD	0.49 ± 0.14	0.46 ± 0.15	0.08
Q, pl/s ± SD	26 ± 10	24 ± 10	0.15
WSR, s^{-1} ± SD	357 ± 132	339 ± 128	0.22
Group 2 (11–16 µm)	**No. vessels 325**	**No. vessels 324**	
D, µm ± SD	13.55 ± 1.47	13.70 ± 1.35	0.205
Va, mm/s ± SD	0.49 ± 0.14	0.46 ± 0.16	**0.02**
Q, pl/s ± SD	54 ± 19	52 ± 21	0.13
WSR, s^{-1} ± SD	221 ± 70	205 ± 75	**0.005**
Group 3 (16–22 µm)	**No. vessels 512**	**No. vessels 571**	
D, µm ± SD	19.16 ± 1.78	19.26 ± 1.72	0.382
Va, mm/s ± SD	0.51 ± 0.14	0.47 ± 0.16	**< 0.001**
Q, pl/s ± SD	105 ± 35	99 ± 39	**0.001**
WSR, s^{-1} ± SD	152 ± 45	140 ± 49	**< 0.001**
Group 4 (> 22 µm)	**No. vessels 902**	**No. vessels 1186**	
D, µm ± SD	27.81 ± 4.91	28.14 ± 4.93	0.06
Va, mm/s ± SD	0.55 ± 0.16	0.52 ± 0.17	**< 0.001**
Q, pl/s ± SD	239 ± 129	228 ± 128	**0.01**
WSR, s^{-1} ± SD	111 ± 35	102 ± 37	**< 0.001**

Table 5. Comparison of conjunctival microcirculatory parameters based on vessel group. Bold values are statistically significant ($p < 0.05$). *D* diameter, *SD* standard deviation, *Va* axial velocity, *Q* blood volume flow, *WSR* wall shear rate, *MI* myocardial infarction.

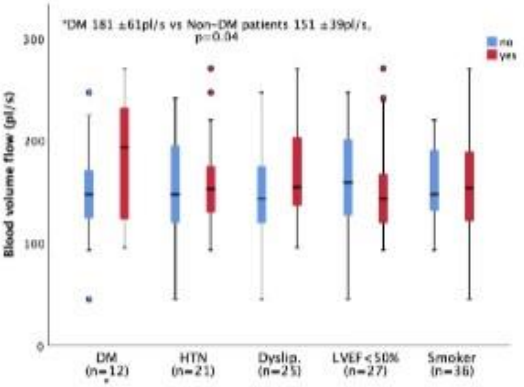

Figure 3. Sub-group analysis of MI patients with respect to microvessel blood volume flow (Q). n denotes the number of "yes" for each sub-group. *DM* diabetes mellitus, *HTN* hypertension, *Dyslip.* dyslipidaemia, *LVEF < 50%* left ventricular ejection fraction less than 50%, *Smoker* active smoker or ex-smoker vs no history smoking.

WSR was significantly reduced for the MI patients compared to the healthy controls, and this was consistent throughout all the vessel groups. Reduced WSR has previously been reported in patients at risk of CVD[15,18]. WSR has an important role in endothelial function[37,38] and reduced WSR can lead to abnormal vascular wall remodelling[39]. Wall shear stress (WSS) is a direct product of WSR and plasma viscosity. Patients suffering type 1 acute MI have epicardial macrocirculatory disease[24]. Microcirculatory dysfunction, in the form of reduced WSS, has been reported in the coronary arteries of acute coronary syndrome patients with high-risk plaques[40]. Our findings would suggest that reduced WSR has a potential role in identifying those patients at high risk of MACE.

To our knowledge, at the time of writing, we are the only group to report findings and differences in conjunctival microcirculatory parameters for MI patients compared to healthy volunteers.

A potential limitation is that we studied the microcirculatory parameters without separating vessels into arterioles and venules. Differentiation between venules and arterioles has been reported previously based on the manually observed direction of flow within each vessel[10,11]. A major limitation of this method though is human

error and the inability to reliably identify branching patterns. Automated differentiation of vessels into venules and arterioles would take require extensive technical development and was not possible within the confines of this pilot study. Haemoglobin video imaging (HVI) may also have the potential to help assess the conjunctival vessel hierarchy and vessel distribution[21] but our methods would require further technical development to allow for integration into our model. Vessel differentiation may explain the statistical differences in blood volume flow that were only appreciated for group size 3–4 vessels. Another limitation is the inter-visit variability in conjunctival measurements. All MI patients and controls were recruited at one time-point. Previous studies have described the inter-visit variability of conjunctival measurements in both healthy controls[41] and diabetic retinopathy patients[42]. The majority of the MI patients had received at least one dose of routinely prescribed medications (ACE inhibitor, beta-blocker) and all MI patients received dual antiplatelet therapy. These medications could contribute to the results observed between the two groups but the median time to recruitment post MI was 1 day and the vast majority would have only had a one-two doses of these drugs. As anticipated, there was a higher prevalence of diabetes mellitus, smoking history, systemic hypertension and dyslipidaemia in the MI group highlighting the severe CVD phenotype of MI patients. The subsequent sub-group analysis only demonstrated a significant difference in microcirculatory parameters for blood volume flow (Q) in patients with or without diabetes mellitus. This is a pilot investigation of MI patients conjunctival assessment and conventional sample size estimation was not feasible thus our findings are largely exploratory. Finally, vessels of smaller size were less abundant than the larger vessels but using our methods we still provided good results representation from the smaller vessel groups.

In conclusion this study using a slit-lamp biomicroscope and iPhone combination found lower axial velocity and wall shear rate in acute MI patients compared to healthy controls. In addition for MI patients, blood volume flow was lower in larger vessels compared to healthy controls. These results and the application of these methods have potential as an adjunct in cardiovascular risk assessment and screening which merit further development and study.

Data availability

The datasets generated during and/or analysed during the current study are available from the corresponding author on reasonable request.

Received: 22 July 2020; Accepted: 23 March 2021
Published online: 07 April 2021

References

1. http://www.who.int/cardiovascular_diseases.
2. Bhatnagar, P. *et al.* The epidemiology of cardiovascular disease in the UK 2014. *Heart* **101**, 1182–1189 (2015).
3. Hippisley-Cox, J., Coupland, C. & Brindle, P. Development and validation of QRISK3 risk prediction algorithms to estimate future risk of cardiovascular disease: Prospective cohort study. *BMJ* **357**, 2099 (2017).
4. Hippisley-Cox, J. *et al.* Predicting cardiovascular risk in England and Wales: Prospective derivation and validation of QRISK2. *BMJ* **336**, 1475–1482 (2008).
5. Stokes, K. Y. & Granger, D. N. The microcirculation: A motor for the systemic inflammatory response and large vessel disease induced by hypercholesterolaemia?. *J. Physiol.* **562**, 647–653 (2005).
6. Zhong, Z., Petrig, B. L., Qi, X. & Burns, A. In vivo measurement of erythrocyte velocity and retinal blood flow using adaptive optics scanning laser ophthalmoscopy. *Opt. Express.* **16**(17), 12746–12756 (2018).
7. Demir, S. U. *et al.* An automated method for analysis of microcirculation videos for accurate assessment of tissue perfusion. *BMC Med. Imaging.* **12**, 37 (2012).
8. Fagrell, B., Fronek, A. & Intaglietta, M. A microscope-television system for studying flow velocity in human skin capillaries. *Am. J. Physiol.* **233**(2), 318–321 (1997).
9. Van Buskirk, E. M. The anatomy of the limbus. *Eye* **3**(2), 101–108 (1989).
10. Khansari, M. M., Wanek, J., Felder, A. E., Camardo, N. & Shahidi, M. Automated assessment of hemodynamics in the conjunctival microvasculature network. *IEEE Trans. Med. Imaging* **35**, 605–611 (2016).
11. Koutsiaris, *et al.* Volume flow and wall shear stress quantification in the human conjunctival capillaries and post-capillary venules in vivo. *Biorheology* **44**(5), 375–386 (2007).
12. Shahidi, M., Wanek, J., Gaynes, B. & Wu, T. Quantitative assessment of conjunctival microvascular circulation of the human eye. *Microvasc. Res.* **79**(2), 109–113 (2010).
13. Koutsiaris, A. G. *et al.* Blood velocity pulse quantification in the human conjunctival pre-capillary arterioles. *Microvasc Res.* **80**(2), 202–208 (2010).
14. Kord Valeshabad, A. *et al.* Changes in conjunctival hemodynamics predict albuminuria in sickle cell nephropathy. *Am. J. Nephrol.* **41**(6), 487–493 (2015).
15. Jiang, Y., Kohara, K. & Hiwada, K. Low wall shear stress in carotid arteries in subjects with left ventricular hypertrophy. *Am. J. Hypertens.* **13**, 892–898 (2000).
16. Wang, L. *et al.* Vessel sampling and blood flow velocity distribution with vessel diameter for characterizing the human bulbar conjunctival microvasculature. *Eye Contact Lens.* **42**(2), 135–140 (2016).
17. Kord Valeshabad, A. *et al.* Feasibility of assessment of conjunctival microvascular hemodynamics in unilateral ischemic stroke. *Microvasc. Res.* **100**, 4–8 (2015).
18. Khansari, *et al.* Assessment of conjunctival microvascular hemodynamics in stages of diabetic microvasculopathy. *Sci. Rep.* **7**, 45916 (2017).
19. Berry, J. D., Donald, M. L. J., Garside, D. B. & Greenland, P. Framingham risk score and prediction of coronary heart disease health in young men. *Am. Heart J.* **154**(1), 80–86 (2007).
20. Karanam, V., Tamariz, L., Batawi, H., Wang, J. & Galor, A. Functional slit lamp biomicroscopy metrics correlate with cardiovascular risk. *Ocul. Surf.* **17**, 64–69 (2019).
21. Meyer, P. A. R. Re-orchestration of blood flow by micro-circulations. *Eye* **32**, 222–239 (2018).
22. Gaynes, B., Teng, P. Y., Wanek, J. & Shahidi, M. Feasibility of conjunctival hemodynamic measurements in rabbits: Reproducibility, validity, and response to acute hypotension. *Microcirculation* **19**(6), 521–529 (2012).
23. Houben, A., Beljaars, J., Hofstra, L., Kroon, A. & De Leeuw, P. Microvascular abnormalities in chronic heart failure: A cross-sectional analysis. *Microcirculation* **10**(6), 471–478 (2003).

24. Brennan, P. F. *et al.* Quantitative assessment of the conjunctival microcirculation using a smartphone and slit-lamp biomicroscope. *Microvasc. Res.* **126**, 103907 (2019).
25. Thygesen, K. *et al.* Fourth universal definition of myocardial infarction (2018). *Eur. Heart J.* **40**, 237–269 (2019).
26. Ibanez, B. *et al.* 2017 ESC Guidelines for the management of acute myocardial infarction in patients presenting with ST-segment elevation. *Eur. Heart J.* **39**, 119–177 (2018).
27. Roffi, M. *et al.* 2015 ESC Guidelines for the management of acute coronary syndromes in patients presenting without persistent ST-segment elevation. *Eur. Heart J.* **37**(3), 267–315 (2016).
28. Jerman T. Jerman Enhancement Filter (https://github.com/timjerman/JermanEnhancementFilter), GitHub. Accessed December 2020. (2020).
29. Duval-Destin, M. & Murenzi, R. Spatio-temporal wavelet: Application to the analysis of moving patterns. In *Progress in Wavelets Analysis and Applications. FrontiReres, Gif-sur-Yvette* 399–408 (1993)
30. Wang, R., Zhao, Y., Tang, Y. & Yuan, Y. A spatio-temporal filtering method for motion estimation. In *The 6th International Conference on Computer Science and Education (ICCSE), ThC* Vol. 6, no. 3, 830–834 (2011)
31. Hong, L., Ruan, Y., Li, W., Wicker, D. & Layne, J. Energy-based video tracking using joint target density processing with an application to unmanned aerial vehicle surveillance. *Comput. Vis. IET* **2**(1), 1–12 (2008).
32. Koutsiaris, A. G., Tachmitzi, S. & Batis, N. Wall shear stress quantification in the human conjunctival pre-capillary arterioles in vivo. *Microvasc. Res.* **85**, 34–39 (2013).
33. Koutsiaris, A. G. Volume flow estimation in the precapillary mesenteric microvasculature in vivo and the principle of constant pressure gradient. *Biorheology* **42**(6), 479–491 (2005).
34. Maznyczka, A., Sen, S., Cook, C. & Francis, D. P. The ischaemic constellation: an alternative to the ischaemic cascade-implications for the validation of new ischaemic tests. *Open Heart* **2**, e000178 (2014).
35. Cheung, A. T. W. *et al.* Microvascular abnormalities in the bulbar conjunctiva of patients with type 2 diabetes mellitus. *Endocr. Pract.* **7**, 358–363 (2001).
36. Sadr-Ameli, M. A. *et al.* Coronary slow flow: Benign or ominous?. *Anatol. J. Cardiol.* **15**(7), 531–535 (2014).
37. Koutsiaris, A. G. *et al.* Wall shear stress in the human eye microcirculation in vivo, segmental heterogeneity and performance in vitro. *Clin. Hemorheol. Microcirc.* **63**, 15–33 (2016).
38. Ando, J. *et al.* Shear stress inhibits adhesion of cultured mouse endothelial cells to lymphocytes by downregulating VCAM-1 expression. *Am. J. Physiol. Cell Physiol.* **267**, 679–687 (1994).
39. Gibbons, G. H. & Dzau, V. J. The emerging concept of vascular remodelling. *N. Engl. J. Med.* **330**, 1431–1438 (1994).
40. Chatzizisis, Y. S. *et al.* Association of global and local low endothelial shear stress with high-risk plaque using intracoronary 3D optical coherence tomography: Introduction of 'shear stress score'. *Eur. Heart J. Cardiovasc. Imaging.* **18**(8), 888–897 (2017).
41. Xu, Z. *et al.* Measurement variability of the bulbar conjunctival microvasculature in healthy subjects using functional slit lamp biomicroscopy (FSLB). *Microvasc. Res.* **101**, 15–19 (2015).
42. Khansari, M., Tan, M., Karamian, P. & Shahidi, M. Inter-visit variability of conjunctival microvascular hemodynamic measurements in healthy and diabetic retinopathy subjects. *Microvasc. Res.* **118**, 7–11 (2018).

Author contributions

The specific contributions made by authors were as following. Concept and design of the work: P.F.B., A.A., A.J.M., M.J., D.D.F., J.A.D.M., A.N., E.T., T.C.B.M., M.S.S.; data collection: P.F.B., A.A., J.M., S.M., K.B.; data analysis and interpretation: P.F.B., A.A., M.J., A.J.M.; drafting the article: P.F.B., M.S.S.; critical revision of the article: all authors; final approval for publication: all authors. P.F.B. is the guarantor of this study and takes responsibility for the contents of the manuscript.

Funding

This project was funded by the Heart Trust fund, Royal Victoria Hospital, Belfast; the Regional Medical Cardiology Centre (RMCC), Royal Victoria Hospital, Belfast; Northern Ireland Chest Heart and Stroke (NICHS) and the Ulster University all of which are located in Northern Ireland, United Kingdom. The work, in part, for image processing and microcirculatory parameters estimation was funded by Interreg SEUPB funding associated with Eastern Corridor for Medical Engineering (ECME).

Competing interests

The authors declare no competing interests.

Additional information

Supplementary Information The online version contains supplementary material available at https://doi.org/10.1038/s41598-021-87315-7.

Correspondence and requests for materials should be addressed to P.F.B.

Reprints and permissions information is available at www.nature.com/reprints.

Publisher's note Springer Nature remains neutral with regard to jurisdictional claims in published maps and institutional affiliations.

Appendix III

ABSTRACT

Tools Share

Jump to

Abstract

Footnotes

SESSION TITLE: NOVEL APPROACHES FOR DETECTING AND TREATING MICROVASCULAR DYSFUNCTION

Abstract 11054: A Novel Method of Conjunctival Vascular Screening to Detect Hemodynamic Alterations in Patients with Coronary Microvascular Disease

Jonathan A Mailey, Julie S Moore, Paul F Brennan, Min Jing, Agnes Awuah, James A McLaughlin, Andrew A Nesbit, Andrew T Nesbit and Mark S Spence

Originally published 8 Nov 2021 | https://doi.org/10.1161/circ.144.suppl_1.11054 | Circulation. 2021;144:A11054

Abstract

Introduction: A large proportion of patients with cardiovascular disease (CVD) remain asymptomatic until presentation with myocardial infarction. Conventional CV risk assessment can be augmented by investigations such as CT coronary artery calcium scoring; but are limited by cost, availability and exposure to ionizing radiation.

This study utilizes the conjunctiva as a network of blood vessels that can be assessed non-invasively in order to compare hemodynamic parameters in patients with and without established coronary microvascular disease (MVD).

Methods: We assessed the conjunctival microcirculation of patients diagnosed with angina undergoing invasive coronary angiography and physiological evaluation of epicardial stenoses and MVD. All patients had haemodynamically insignificant epicardial disease (FFR ≥0.80). Conjunctival imaging was performed using an adapted iPhone 11pro and slit-lamp biomicroscope. We compared a cohort of patients with MVD (IMR ≥25); to a group of controls without MVD (IMR <25).

Results: A total of 54 patients were included (19 MVD and 35 controls). **Table 1** demonstrates a comparison of baseline demographics and hemodynamics between the groups. A total of 866 conjunctival vessels were analysed (366 MVD and 500 controls) and the differences in microvascular parameters between groups determined (**Table 2**). Statistically significant differences were observed in axial velocity, cross sectional velocity and blood flow rate.

Conclusion: This study demonstrates the ability to non-invasively detect abnormal microvascular function. The conjunctival microcirculation therefore has potential merit to complement conventional CV risk screening.

Circulation

November 16, 2021
Vol 144, Issue
Suppl_1

Article Information

Article Metrics View all metrics

Downloads Citations

No data available.

Total 6 Months 12 Months

https://doi.org/10.1161/circ.144.suppl_1.11054

Originally published November 8, 2021

Check for updates

Keywords

Ischemic heart disease

Cardiovascular disease

Tools Share

Jump to

Abstract

Footnotes

Appendix IV

[1] These authors contributed equally to this study.

Accepted 4 January 2022
Available online 10 January 2022

https://doi.org/10.1016/j.jinf.2022.01.004

Cross reactivity of spike glycoprotein induced antibody against Delta and Omicron variants before and after third SARS-CoV-2 vaccine dose in healthy and immunocompromised individuals

Dear Editor,

SARS-CoV-2 variants of concern threaten evasion of natural and vaccine-induced immunity. There is an urgent need to know how effective different vaccine strategies will be in reducing the transmission of and disease severity arising from the Omicron variant of concern (VOC). In the UK, two main vaccines have formed the basis of the national immunisation strategy: the AstraZeneca ChAdOx1 nCoV-19 vaccine (AZ)[1] and the Pfizer-BioNtech 162b2 COVID-19 vaccine (PFZ).[2] Both elicit immune responses directed against the original wildtype SARS-CoV-2 (Wuhan) spike glycoprotein and both have been shown to reduce the incidence of severe disease in clinical trials.[1,2] In mid-2021, the Delta VOC became dominant worldwide and led to the widespread deployment of booster immunisations using mRNA vaccines. In late November 2021, the Omicron VOC rapidly emerged displaying even greater transmissibility and has become the dominant SARS-CoV-2 virus in the UK and across

the world.[3] These rapid shifts in the pre-dominance of VOC outpaces and impairs the development and testing in clinical trials of new VOC-tailored vaccines. We do not yet know how well the different vaccine strategies applied in the UK will reduce the transmission of and severity of disease arising from rapidly emerging VOC in the general population and immunological vulnerable subgroups.

We have used the core design of an anti-IgG/A/M SARS-CoV-2 ELISA[4,5] to measure IgG antibodies specific for spike protein from the original Wuhan strain,[6] B.1.617.2 (Delta - Abingdon Health) and B.1.1.529 (Omicron - SinoBiological China). In addition, we assayed serial dilutions (250 – 7.8 IU/mL) of the WHO standard NIBSC 20/136[7] and the therapeutic monoclonal antibody therapy Sotrovimab (Glaxo Smith Kline) the base concentration of which is 62.5 mg/ml and a 500 mg dose is given to patients. We have used these ELISAs to determine cross-reactivity of spike glycoprotein induced antibody against Delta and Omicron variants before and after third SARS-CoV-2 vaccine dose.

We have recruited three well-characterised cohorts: firstly, a health care worker cohort from University Hospitals Birmingham from the *Determining the immune response to SARS-CoV-2 infection in convalescent health care workers (COCO)* study, who had PFZ as their primary two-dose vaccine course followed by PFZ booster (PPP cohort). Secondly, individuals classed as clinically extremely vulnerable (CEV) attending general practice for vaccination in Ulster, who had the AZ vaccine as their primary two-dose vaccine course followed by a PFZ third dose (AAP). Lastly, individuals on haemodialysis under renal care at the University Hospitals Birmingham; 70.3% of which had AZ as their primary course (HD cohort) followed by a PFZ third dose. Serum samples were taken 6 months following their second vaccination of their primary course, prior to the third dose with PFZ, and also 28 days following vaccination.

There was evidence of suboptimal seropositivity 6 months post primary dose of vaccination in all groups but particularly amongst HD and CEV patients. Samples taken 6 months post-primary vaccine course showed that for the HD cohort, 58.9% of individuals were seropositive against the Wuhan strain, 34.4% against Delta and 62.2% against Omicron strains. For the PPP cohort, seropositivity was maintained at 92.2% against Wuhan, 90% against Delta and 91.1% against Omicron strains. For the AAP cohort, seropositivity was 62.5% against Wuhan, 45.8% against Delta and 91.7% against Omicron strains (Fig. 1a-c).

Post third vaccine dose, there was a significant increase in the percentage of individuals who were seropositive and a rise in the median serum antibody concentration (as measured by optical density or OD) of these seropositive individuals. For the HD cohort, seropositivity was 98.8% against the Wuhan, 97.6% against Delta and 100% against Omicron strains. For the PPP and AAP cohorts seropositivity was 100% against all 3 strains . The increase in median OD following vaccination in HD patients was 2.46 to 2.98 ($p<0.0001$) for the Wuhan, 1.94 to 2.49 (non-significant (ns)) for Delta, and 1.37 to 2.84 ($p<0.0001$) for Omicron strains. The increase in median OD for the PPP cohort against the Wuhan strain was 2.62 to 2.88 (ns), for Delta 2.33 to 3.08 ($p<0.0001$) and for Omicron 1.71 to 3.37 ($p<0.0001$). For the AAP cohort, for the Wuhan strain the increase was from 2.38 to 3.52 ($p<0.0001$), for Delta 2.98 to 3.45 ($p = 0.0044$) and for Omicron 1.17 to 3.46 ($p<0.0001$). We also compared antibody concentrations following booster immunisation between the PPP and AAP groups: in the AAP group there was a higher median OD for the Wuhan (2.88 v 3.52, $p<0.0001$) and Delta strains (3.08 v 3.45, $p = 0.0022$) but not for the Omicron strain (3.37 v 3.46, ns) compared to the PPP group suggesting heterologous vaccine strategies may demonstrate enhanced immunogenicity against these SARS-CoV-2 variants.

Lastly, the WHO NIBSC 20/136 standard was run as a standard curve in the Wuhan, Delta and Omicron ELISAs and no significant loss of antibody binding was observed against any VOC (Supplementary Figure 1a). Similarly, a dilution series from 6.5 mg/ml to 0.003 mg/ml of Sotrovimab (GSK) found no loss of antibody binding against Omicron (Supplementary Figure 1b). Strong correlations exist between antibody binding and neutralisation[8] and between the presence of neutralising antibodies and protection against severe COVID-19.[9]

Understanding the pre-existing seroprevalence of antibodies directed against novel SARS-CoV-2 VOC and their induction following third-primary or booster immunisation is of critical importance in guiding public health policy during the ongoing SARS-CoV-2 pandemic. This knowledge is of particular relevance to immunologically vulnerable groups who either do not make a robust serological response to vaccination or fail to retain a serological response over time. In this study, we provide evidence supporting the need of a third dose of vaccination due to a waning antibody response at 6 months and the broadly cross-reactive humoral immunogenicity of the third vaccine dose against rapidly evolving SARS-CoV-2 VOC in healthy, CEV, and HD patients. However, it is important to note that antibody binding doesn't necessarily equate with functionality of antibodies, particularly in immunosuppressed individuals. Therefore, this is the best-case scenario and this study will need to be repeated with neutralisation assays going forward.

Ethical approval

The COCO study was ethically approved for this work by the London - Camden and Kings Cross Research Ethics Committee on behalf of the United Kingdom Health Research Authority – reference 20/HRA/1817. The Haemodialysis study was ethically approved for this work by the North West Preston Research Committee on behalf of the United Kingdom Health Research Authority for the National Institute of Health Research Coronavirus Immunological Analysis study – reference 20/NW/ 0240. The Ulster study was ethically approved for this work by the Office of Research Ethics Committee for Northern Ireland on behalf of the United Kingdom Health Research Authority - reference 20/WM/0184. The pre-2019 health controls was ethically approved for this work by the University of Birmingham Research Ethics Committee, United Kingdom - reference ERNE_16–178 (2002/201, Amendment Number 4).

Acknowledgments

We thank the staff and patients that have kindly volunteered for this study. Thanks also to Abingdon Health for the Wuhan and Delta antigens. The authors would like to acknowledge the COVID-HD Birmingham Study Group and PITCH consortium that have enabled this work, the staff of the Clinical Immunology Service, managed by Tim Plant, who helped process the healthcare worker and haemodialysis samples and Dr. Margaret Goodall for her expertise in antibody production and assay development. The authors would also like to acknowledge the National Institute for Health Research (NIHR)/Wellcome Trust Birmingham Clinical Research Facility and University Hospitals Birmingham Research and Development team, in particular the research nurses that enabled the sample consent and sample collection including Mary Dutton, Lesley Fifer, Sinead White, Natalie Walmsley-Allen, Lucy Atchinson-Jones, Kulli Kuningas, Margaret Carmody, Rani Maria Joseph, Christopher McGhee, Shannon Page and Michelle Bates. Also, The Ulster Pandemic Study team. The COCO/PITCH healthcare worker cohort was funded by the United Kingdom Department of Health and Social Care and United Kingdom Research and Innovation COVID-19 Rapid Response Rolling Call as part of the PITCH Consortium. The HD cohort was funded by the United Kingdom Research and Innovation

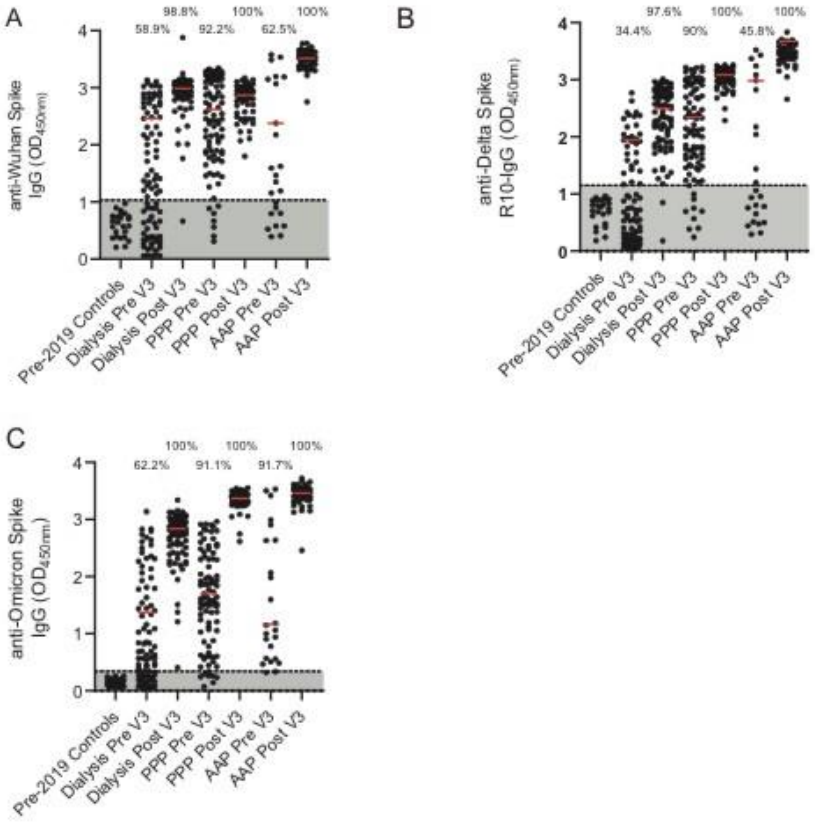

Fig. 1. Percentage of cohort with antibodies against Wuhan, Delta and Omicron strain.
A-Detection of anti- Wuhan spike IgG in pre-2019 controls, a dialysis population, a cohort of health care workers who have had three PFZ vaccines and a Clinically Extremely Vulnerable population in general practice who have had two AZ and one PFZ vaccine. Results are given for pre and post 3rd dose of vaccination. Percentage of cohort that are considered seropositive are included above the dot plots. The red line represents the median of the seropositive individuals in that cohort.
B-Detection of anti-Delta spike IgG for the same populations.
C-Detection of anti- Omicron spike IgG for the same populations
Pre- pre-3rd dose of vaccine and 6 months post 2nd dose. Post- 28 days post 3rd dose of vaccine. PPP- 3 Pfizer-BioNtech vaccines given in this cohort. AAP- two AstraZeneca ChAdOx1 nCoV-19 vaccines and the one Pfizer-BioNtech vaccine given in this cohort. (For interpretation of the references to colour in this figure legend, the reader is referred to the web version of this article.)

COVID-19 Rapid Response Rolling Call. The COVID-HD Birmingham Study Group include Claire Backhouse, Anna Casey, Lynsey Dunbar, Beena Emmanuel, Megan Fahy, Alexandra Godlee, Paul Moss, Peter Nightingale, Liz Ratcliffe, Stephanie Stringer, Matthew Tabinor, Sian Faustini, Adam Cunningham, Alex Richter, Lorraine Harper. The PITCH study Group include Susanna Dunachie, Paul Klenerman, Lance Turtle, Thushan de Silva, Christopher Duncan, Rebecca Payne, Alex Richter, Ellie Barnes, Miles Carroll, Alexandra Deeks, Christina Dold.

Supplementary materials

Supplementary material associated with this article can be found, in the online version, at doi:10.1016/j.jinf.2022.01.002.

References

1. Voysey M., Clemens S.A.C., Madhi S.A., Weckx L.Y., Folegatti P.M., Aley P.K.. Safety and efficacy of the ChAdOx1 nCoV-19 vaccine (AZD1222) against SARS–CoV-2: an interim analysis of four randomised controlled trials in Brazil, South Africa, and the UK. *Lancet* 2021;**397**(10269):99–111 Jan.
2. Polack F.P., Thomas S.J., Kitchin N., Absalon J., Gurtman A., Lockhart S.. Safety and Efficacy of the BNT162b2 mRNA Covid-19 Vaccine. *N Engl J Med* 2020;**383**(27):2603–15 Dec.
3. England P.H. SARS-CoV-2 variants of concern and variants under investigation in England. Sage. 2021;(April).
4. Cook A.M., Faustini S.E., Williams L.J., Cunningham A.F., Drayson M.T., Shields A.M.. Validation of a combined ELISA to detect IgG, IgA and IgM antibody responses to SARS-CoV-2 in mild or moderate non-hospitalised patients. *J Immunol Methods* 2021:494 Jul 1.
5. Faustini S.E., Jossi S.E., Perez-Toledo M., Shields A.M., Allen J.D., Watanabe Y.. Development of a high-sensitivity ELISA detecting IgG, IgA and IgM antibodies to the SARS-CoV-2 spike glycoprotein in serum and saliva. *Immunology* 2021;**164**(1):135–47 Sep 1.
6. Watanabe Y., Allen J.D., Wrapp D., McLellan J.S., Crispin M.. Site-specific glycan analysis of the SARS-CoV-2 spike. *Science* 2020;**369**(6501) Jul 17330-3. Available from: https://pubmed.ncbi.nlm.nih.gov/32366695/.
7. NIBSC NI for BS andControls. WHO International Standard First WHO International Standard for anti-SARS-CoV-2 Immunoglobulin (human) NIBSC Code: 20/136 Instructions for Use (Version 2.0, Dated 17/12/2020). Potters Bar, Hertfordshire, EN6 3QG.
8. Earle K.A., Ambrosino D.M., Fiore-Gartland A., Goldblatt D., Gilbert P.B., Siber G.R.. Evidence for antibody as a protective correlate for COVID-19 vaccines. *Vaccine* 2021 Jul 22;**39**(32):4423–8 Available from: https://pubmed.ncbi.nlm.nih.gov/34210573/.
9. Khoury D.S., Cromer D., Reynaldi A., Schlub T.E., Wheatley A.K., Juno J.A..

Neutralizing antibody levels are highly predictive of immune protection from symptomatic SARS-CoV-2 infection. *Nat Med* 2021;**27**(7):1205–11 Jul 1Available from: https://pubmed.ncbi.nlm.nih.gov/34002089/.

Sian Faustini
Institute of Immunology and Immunotherapy, College of Medical and Dental Sciences, University of Birmingham, Birmingham, United Kingdom

Adrian Shields
Institute of Immunology and Immunotherapy, College of Medical and Dental Sciences, University of Birmingham, Birmingham, United Kingdom
University Hospitals Birmingham National Health Service (NHS) Foundation Trust, Birmingham, United Kingdom

Gemma Banham, Nadezhda Wall
Institute of Clinical Sciences, College of Medical and Dental Sciences, University of Birmingham, Birmingham, United Kingdom
University Hospitals Birmingham National Health Service (NHS) Foundation Trust, Birmingham, United Kingdom

Saly Al-Taei, Chloe Tanner, Zahra Ahmed, Elena Efstathiou, Neal Townsend, Margaret Goodall, Tim Plant, Marisol Perez-Toledo, Aleksandra Jasiulewicz
Institute of Immunology and Immunotherapy, College of Medical and Dental Sciences, University of Birmingham, Birmingham, United Kingdom

Ruth Price
Biomedical Sciences Research Institute, Ulster University, Northern Ireland

James McLaughlin
Nanotechnology and Integrated Bioengineering Centre, Ulster University, Northern Ireland

John Farnan
The Group Surgery, 257 North Queen Street, Belfast, Northern, Ireland

Julie Moore, Louise Robertson, Andrew Nesbit, Grace Curry
Biomedical Sciences Research Institute, Ulster University, Northern Ireland

Amy Black
The Group Surgery, 257 North Queen Street, Belfast, Northern, Ireland

Adam Cunningham
Institute of Immunology and Immunotherapy, College of Medical and Dental Sciences, University of Birmingham, Birmingham, United Kingdom

Lorraine Harper
University Hospitals Birmingham National Health Service (NHS) Foundation Trust, Birmingham, United Kingdom
Institute of Applied Health, University of Birmingham, Birmingham, United Kingdom

Tara Moore
Biomedical Sciences Research Institute, Ulster University, Northern Ireland
Nanotechnology and Integrated Bioengineering Centre, Ulster University, Northern Ireland
Avellino labs USA 1505 Adams Drive Menlo Park, CA 94025 USA

Mark Drayson
Institute of Immunology and Immunotherapy, College of Medical and Dental Sciences, University of Birmingham, Birmingham, United Kingdom

Alex Richter*[1]
Institute of Immunology and Immunotherapy, College of Medical and Dental Sciences, University of Birmingham, Birmingham, United Kingdom
University Hospitals Birmingham National Health Service (NHS) Foundation Trust, Birmingham, United Kingdom

*Corresponding author at: Clinical Immunology Service, Institute of Immunology and Immunotherapy, Medical School, University of Birmingham, Edgbaston, B15 2TT.
E-mail addresses: s.e.faustini@bham.ac.uk (S. Faustini), a.m.shields@bham.ac.uk (A. Shields), emma.banham@nhs.net (G. Banham), nadya.wall@nhs.net (N. Wall), s.al-taei@bham.ac.uk (S. Al-Taei), c.l.tanner@bham.ac.uk (C. Tanner), a.zahra@bham.ac.uk (Z. Ahmed), e.efstathiou@bham.ac.uk (E. Efstathiou), n.j.townsend@bham.ac.uk (N. Townsend), dm.goodall@bham.ac.uk (M. Goodall), tplant.1@bham.ac.uk (T. Plant), m.perez-toledo@bham.ac.uk (M. Perez-Toledo), a.jasiulewicz@bham.ac.uk (A. Jasiulewicz), rk.price@ulster.ac.uk (R. Price), jad.mclaughlin@ulster.ac.uk (J. McLaughlin), john.farnan@doctors.org.uk (J. Farnan), Moore-J66@ulster.ac.uk (J. Moore), lrobertson@ulster.ac.uk (L. Robertson), a.nesbit@ulster.ac.uk (A. Nesbit), G.Curry@ulster.ac.uk (G. Curry), AmyBlack@doctors.org.uk (A. Black), a.f.cunningham@bham.ac.uk (A. Cunningham), lharper@bham.ac.uk (L. Harper), tara.moore@ulster.ac.uk (T. Moore), m.t.drayson@bham.ac.uk (M. Drayson), a.g.richter@bham.ac.uk (A. Richter)

[1] On behalf of the COVID-HD Birmingham study group and the PITCH consortium

Accepted 4 January 2022
Available online 10 January 2022

https://doi.org/10.1016/j.jinf.2022.01.002

Control of COVID-19 in China likely reduced the burden of multiple other infectious diseases

Dear Editor,

We read with great interest the analyses that suggested the control measures for COVID-19 likely reduced the infections of tuberculosis and influenza, but not the infections of human immunodeficiency virus and hepatitis C virus, possibly because these four diseases are transmitted through different routes.[1–3] In theory, the similar effects could be observed on multiple infectious diseases in China, because China also implemented strict and costly measures, such as lockdown of cities, mass restriction of travelling and gathering, mass isolation, mass mask wearing, and mass disinfection, for the control of COVID-19 caused by SARS-CoV-2 in 2020.[4] Here we provided data to test this theoretical inference that is important for calculating the benefits of the strict and costly measures for combating the COVID-19 pandemic.

Over 30 important infectious diseases were listed as Class A or B infectious diseases in China. The numbers of new cases of these diseases are reported monthly at the official website of National Health Commission of China (http://www.nhc.gov.cn/jkj/s3578/new_list.shtml). We collected these numbers of the years 2010–2020 from this official website. We excluded the numbers of the pandemic H1N1 subtype influenza, hepatitis D, human in-

Appendix V

www.nature.com/scientificreports

scientific reports

Check for updates

OPEN

User experience of home-based AbC-19 SARS-CoV-2 antibody rapid lateral flow immunoassay test

Min Jing[1], Raymond Bond[2], Louise J. Robertson[3], Julie Moore[3], Amanda Kowalczyk[3], Ruth Price[3], William Burns[1], M. Andrew Nesbit[3], James McLaughlin[1]✉ & Tara Moore[3,4]✉

The urgent need to scale up testing capacity during the COVID-19 pandemic has prompted the rapid development of point-of-care diagnostic tools such as lateral flow immunoassays (LFIA) for large-scale community-based rapid testing. However, studies of how the general public perform when using LFIA tests in different environmental settings are scarce. This user experience (UX) study of 264 participants in Northern Ireland aimed to gather a better understanding of how self-administered LFIA tests were performed by the general public at home. The UX performance was assessed via analysis of a post-test questionnaire including 30 polar questions and 11 7-point Likert scale questions, which covers the multidimensional aspects of UX in terms of ease of use, effectiveness, efficiency, accuracy and satisfaction. Results show that 96.6% of participants completed the test with an overall average UX score of 95.27% [95% confidence interval (CI) 92.71–97.83%], which suggests a good degree of user experience and effectiveness. Efficiency was assessed based on the use of physical resources and human support received, together with the mental effort of self-administering the test measured via NASA Task Load Index (TLX). The results for six TLX subscales show that the participants scored the test highest for mental demand and lowest for physical demand, but the average TLX score suggests that the general public have a relatively low level of mental workload when using LFIA self-testing at home. Five printed LFIA testing results (i.e. the 'simulated' results) were used as the ground truth to assess the participant's performance in interpreting the test results. The overall agreement (accuracy) was 80.63% [95% CI 75.21–86.05%] with a Kappa score 0.67 [95% CI 0.58–0.75] indicating substantial agreement. The users scored lower in confidence when interpreting test results that were weak positive cases (due to the relatively low signal intensity in the test-line) compared to strong positive cases. The end-users also found that the kit was easier to use than they expected ($p < 0.001$) and 231 of 264 (87.5%) reported that the test kit would meet their requirements if they needed an antibody testing kit. The overall findings provide an insight into the opportunities for improving the design of self-administered SARS-CoV-2 antibody testing kits for the general public and to inform protocols for future UX studies of LFIA rapid test kits.

Timely and accurate diagnostic testing plays an important role in preventing and controlling the spread of COVID-19. Several diagnostic techniques for SARS-CoV-2 have been recommended by the World Health Organisation (WHO)[1]: (1) detection of viral RNA via nucleic acid amplification tests (NAAT), such as real-time reverse transcription polymerase chain reaction (PCR); (2) detection of viral antigens through immunodiagnostic techniques, such as rapid diagnostic tests via lateral flow assays (LFIAs), and (3) detection of host antibodies through serological techniques, such enzyme linked immunosorbent assays (ELISAs). According to WHO[1], NAAT is recommended as the reference standard since it is the most sensitive and specific; alternatively, rapid tests by LFIAs offer an opportunity to scale up testing capacity.

Given the importance of monitoring the presymptomatic or paucisymptomatic transmission of COVID-19[2,3], large-scale community-based rapid testing[4,5] becomes very important, which, however, is difficult to achieve by PCR testing because it can take at least one day[6] or longer from requesting a test to receiving a result. Governments have invested enormous resources to scale up testing capacity and many countries have adopted the rapid diagnostic tests via LFIAs[5–9]. Although many studies have reported the performance of PCR[10–13] and LFIA as a

[1]Nanotechnology and Integrated Bioengineering Centre (NIBEC), School of Engineering, Ulster University, Jordanstown, UK. [2]School of Computing, Ulster University, Jordanstown, UK. [3]Biomedical Sciences Research Institute, Ulster University, Coleraine, UK. [4]Avellino USA, 1505 Adams Drive, Menlo Park, CA 94025, USA. ✉email: jad.mclaughlin@ulster.ac.uk; tara.moore@ulster.ac.uk

diagnostic tool for COVID-19[14–16], there is a lack of user experience (UX) studies that investigate how the LFIA test kits are used by the general public for mass testing in different environmental settings, which is the gap in the literature that this study aimed to fill.

As well-established, low-cost, rapid and highly efficacious PoC devices, LFIAs have been developed for home pregnancy tests[17,18], HIV[19,20], Influenza A (H1N1)[21], and more recently for COVID-19 antibody testing[22–26]. The UX studies for LFIA are commonly focused on evaluation for the accuracy in interpreting the test results and gathering the user response via questionnaire[17,19,23]. For example, a study[19] for HIV self-testing based on 150 lay users conducting unsupervised self-testing aimed to assess whether the participants can correctly conduct all steps of the test. Results show that errors were found in the sample collection and transfer, as well as difficulties in interpreting the results. Another study[17] investigated the usability and performance of seven visual home pregnancy tests that were available in Europe where each device claimed different sensitivity and accuracy scores. The study included 250 volunteers from the UK, who performed the test at home and at a study site. The usability study was evaluated by user scores based on 7-point Likert rating scales. Note these two UX studies were not for COVID-19 and they also did not cover the multidimensional aspects of UX analysis presented in this study.

There are limited studies involving user experience based on LFIAs for COVID-19[23,26]. A study for usability and acceptability[23] was conducted for self-administered COVID-19 antibody testing in a home environment, which recruited 10,600 and 3800 participants in England for using two types of LFIAs. The presented usability analysis was summarised by descriptive statistics based on data from questionnaires, which identified the difficulties in the use of the lancet, and a need for clearer instructions for using the kit and interpreting the results. Agreement between the participant and a clinician's interpretation of the results of the testing kits was assessed using Kappa scores and resulted in 0.72 and 0.89 scores for the two LFIA tests respectively. Another UX study for self-administrated SARS CoV-2 antibody testing kit was conducted in an in-car setting[26] based on 1544 participants in Northern Ireland. The UX analysis based on 28 5-point Likert ratings from a post-test questionnaire suggested a good degree of UX and substantial agreement (Kappa score 0.75) in the interpretation of the test results by the participant and researcher. Analysis of the free-text responses in the survey suggests that the UX could be improved for blood-sample collection by modifying the method of sample transfer to the test device, and for interpretation of the results by giving clearer instructions.

The purpose of this UX study was to investigate the general public's interaction with the LFIA testing kit at home, to identify the areas of difficulty encountered during testing, and to reveal valuable information and design opportunities for future improvement. The contribution of this study to literature includes three aspects: (1) Unlike other LFIA usability studies for COVID-19[23,26] that were focused on the usability/acceptability and assessment of accuracy in interpreting test results, this current study carried out a more in-depth analysis, which covered the multidimensional aspects of UX including the ease of use, effectiveness, efficiency, accuracy (in interpreting the test results) and satisfaction. (2) To investigate how the participants perform in reading different test results, five types of LFIA test results were simulated and printed in the cards for participants to read. Using the simulated test results provides the controlled variation of test results, therefore, enabled us to gain a better understanding of how participants performed when reading different test results. (3) To assess various aspects of mental workload involved for home-based LFIA testing, National Aeronautics and Space Administration (NASA) task load index (TLX)[27] was applied to estimate the user's perceived cognitive demand of the task undertaken by the user. Workload assessment is valuable for the overall design of the test system as it may help to make the equipment and test procedure more user-friendly and potentially reduce error and improve effectiveness and customer acceptance.

The overall findings of this UX study will help the design of LFIA rapid testing for SARS-CoV-2 antibody and inform protocols for future studies, which may not only improve the LFIA testing performance by the general public but also have implications for coronavirus related public health planning.

Materials and methods

Test kit. The test kit used in this study was the AbC-19 Rapid Test developed by Abingdon Health, which has been approved for professional use in the UK and EU[28] and has been used in another UX study for self-administrated LFIA for COVID-19 antibody testing in cars[26]. The AbC-19 Rapid Test is a single-use test for the detection of SARS-CoV-2 IgG antibodies in human capillary whole blood. Using a blood sample from a finger-stick puncture the test will identify the presence of IgG antibodies against the trimeric spike protein of SARS-CoV-2 virus (the virus responsible for the COVID-19 disease), signifying a recent or previous infection by the virus.

The test kit materials include: one test, two single-use lancets, one blood collector, one test solution vial, a waste bag and instructions. The steps for performing the testing are outlined in the instructions (provided in Supplementary file): (a) hands were cleaned using warm water only; (b) the blood sample was taken from the ring or middle finger of the non-dominant hand by using the lancet; (c) the blood was collected using the blood collector; (d) blood was added to the test sample hole, and the test solution was then applied to the sample hole and the test allowed to develop; (e) after 20 min, if the C-line appears (indicating the test was performed successfully), the test results were interpreted by looking at the viewing window. Figure 1 illustrates the LFIA testing device and examples of results: (a) structure of the device showing the sample hole, viewing window with the control line (C-line) and test line (T-Line) as an example of positive result; (b) example of negative result; (c) example of invalid (without C-line).

Participants. The home-based study was conducted from October to December 2020 in Northern Ireland (NI). The recruitment strategy was targeted email recruitment from our existing Pandemic Database. We targeted those with families and then a range of age, gender and education groups, which resulted in an over-recruitment of 55. From this 10 were excluded due to incomplete registrations. From the remaining groups,

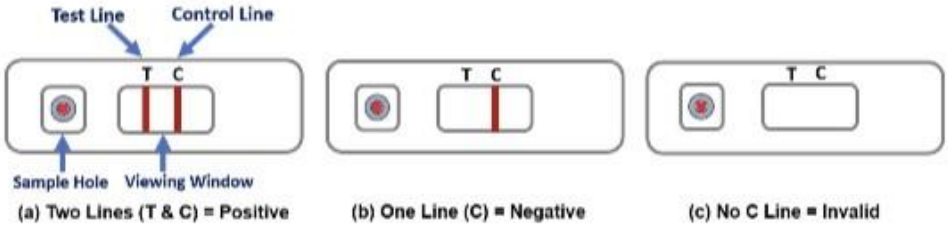

Figure 1. Illustration of the LFIA testing device: (**a**) structure of the testing device showing the sample hole, viewing window with the control line and test line as an example of positive result; (**b**) an example of negative result, and (**c**) example of invalid (without C-line).

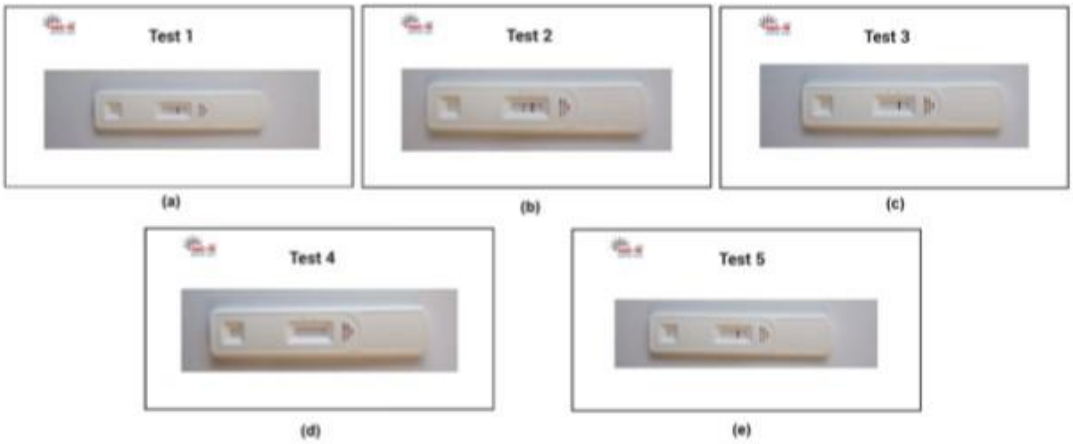

Figure 2. Examples of five printed test results that were designed for the study: (**a**) T1: positive; (**b**) T2: strong positive; (**c**) T3: negative; (**d**) T4: invalid, and (**e**) T5: weak positive.

participants were selected based on age, gender, and education using the NI census data[29] to achieve as balanced an overall cohort as representative of the NI population as possible. We had over-recruited middle-aged (31–50 years) females with a degree or higher and selected every 2nd entry—removing 45 participants.

Participants were invited to complete an online consent form and questionnaire via REDCap (www.project-redcap.org), which collected data such as gender, age, education, COVID-like symptoms, etc. The participants received Amazon vouchers after they completed the study. All participants were members of the public in NI and included children above the age of 7 years old and adults. Informed consent was obtained prior to commencing the study. Consent could only be given by individuals who were capable of independently understanding the information provided. Consent for children (< 18 years) was provided by their parent/guardian alongside child assent. Older participants and participants under 18 years old could be assisted by a family member or parent/guardian to complete the test and questionnaire.

Study design. Difficulties in interpreting results appear to be one of the most common issues reported in UX studies for LFIA testing[19,20,22,23,26]. Our recent study for LFIA self-testing of SARS-CoV-2 IgG antibodies in cars[26] suggested that the users found it difficult to interpret the results with the faint T-lines and hence resulted in false negative readings. One possible reason for the faint T-lines might be due to the dynamic changes in IgG levels among COVID-19 patients as some studies have suggested the rapid decay of anti-SARS-CoV-2 IgG in early infection[30–32] and in the recovery stage[33]. Although most LFIA testing are qualitative and there is still a lack of quantitative studies for COVID-19 antibodies, a recent study[34] has explored the quantitative analysis of LFIAs for early risk assessment of cardiovascular disease, in which the data show that the intensity of T-line changes according to eight different c-reactive protein (CRP) concentration levels.

To investigate how the participants performed in reading the test results with different T-line intensities, five simulated LFIA test results were printed in the cards, as shown in Fig. 2: (a) Test-1 (T1): positive; (b) Test-2 (T2): strong positive; (c) Test-3 (T3): negative; (d) Test-4 (T4): invalid and (e) Test-5 (T5): weak positive. The design of these five LFIA was based on the findings from our recent study for LFIA self-testing conducted in cars[26], in which the false negative results comprised mostly of faint test lines (like T5). The faint T-line may be reflective of the level of antibodies present in the blood of subjects who may have been infected in March 2020 during the

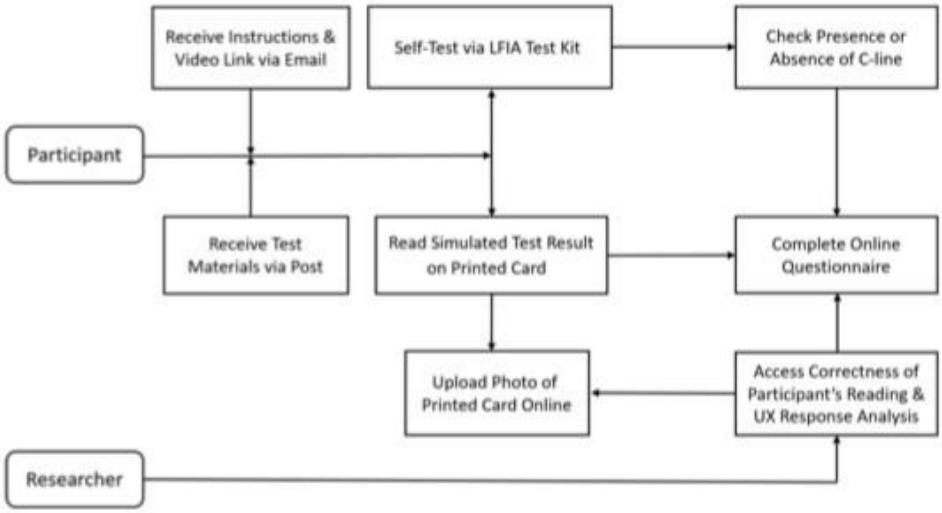

Figure 3. The diagram for the study design.

first wave of COVID-19 within Northern Ireland whilst that study was conducted almost 6 months later. Using the simulated test results helps to provide the controlled variation of T-line intensity, which enabled us to gain a better understanding of how participants performed when reading different test results.

The diagram for the study design is presented in Fig. 3. Participants received the test kits via post and were given prior access to written instructions and a video on YouTube[35] before using the test. Participants were asked to follow the instructions provided and to complete three tasks: (1) apply blood sample to the testing kit, wait for the C-line to develop and answer whether they have observed the C-line in the test, and upload a photo of their finished test. Note the purpose of this task was not to test for the actual existence of the COVID-19 antibodies but to assess the participants' ability to complete the test successfully via observing the presence of C-line and identifying the reasons for failure and areas of difficulties. Therefore, the participants needed to follow all steps in instruction to apply the test to themselves to develop the C-line. (2) interpret the test result printed on a card, which was randomly selected for them from five simulated test results (as in Fig. 2) and choose the reading that most closely matched their interpretation from the four options provided: positive, negative, failed/invalid and unsure. They were also asked to upload the photo of their printed card, which was used by the researchers to assess the correctness of the participants' readings via comparing to the ground truth; (3) complete the post-test questionnaire online. Note, assessment of participants' reading for actual LFIA testing results against the clinicians' or researchers' results have been done in two related studies at home[23] and in cars[26], which was not the purpose of this study. Therefore, the participants' reading against ground truth (in printed cards) was used in this study.

UX analysis. The data regarding the UX of the testing kit were collected from the post-test questionnaire (provided in Supplementary Information). The questionnaire was based on modification and extension of the recent UX study for LFIA self-testing in cars[26]. To simplify the task for the end-users, the 5-point Likert rating questions used in the previous study[26] were replaced by polar questions. Furthermore, two new question sections were added for assessment of TLX[27] and satisfaction.

The questionnaire comprised of 13 sections and each section entailed 3 to 6 questions, which included 30 polar questions and 11 Likert rating questions in total. There were 27 of 30 polar questions measured the UX of a particular aspect of the testing kit, which include: (Q1) outer packaging; (Q2) collection of finger prick blood sample; (Q3) application of sample to test; (Q4) application of test solution to LFIA device; (Q5) development of a control line and interpretation of results; (Q6) instructions for use; (Q7) risks and warnings. The remaining 3 polar questions were focused on the completion of test (Q8a), whether participants received help (Q9c) and interpretation of the results (Q10c). There were 11 7-point Likert rating scales in the two sections (Q11 and Q12). Q11 was designed for obtaining the task load index (TLX)[27] and Q12 was for assessing the comfort and acceptability of the end-users for the test kit. The presentation of the UX analysis was organised in five areas: (1) ease of use; (2) effectiveness; (3) efficiency; (4) accuracy and (5) satisfaction, which are explained in detail next.

(1) *Ease of use* Ease of use was evaluated based on the UX and usability scores, a percentage of ratings from the polar questions in Q1–Q7, by counting "Yes" from all answers then normalised to 100. The summative scores (sum of scores normalised as a percentage) for all participants in each section were calculated and analysed. Although there are diverse definitions of UX, most agree that UX is more than just a sum of a product's usefulness and usability[36–38]. Both UX and usability were analysed using the same approaches in our early study[26], in which UX was considered a higher level construct (where usability is a sub-component). All polar questions

in Q1–Q7 (except Q2e and Q6b for efficiency) were used for calculating UX scores. Questions not describing the usability constructs, Q1a, Q2d, Q4d, Q7a, Q7b, Q7c, Q7d and Q7e were removed for the usability analysis.

(2) *Effectiveness* ISO9241 defines effectiveness as "the accuracy and completeness with which specified users can achieve specified goals in particular environments", hence effectiveness was assessed by the test completion rate. A presence of C-line within the test window indicates a successful completion of test. The number of users who completed the test (via achieving a C-line) was examined and the reasons for failure and areas of difficulty to complete the test were analysed.

(3) *Efficiency* ISO9241 defines efficiency as "the resources expended in relation to the accuracy and completeness of goals achieved". Here efficiency was assessed in the following aspects: physical resource, human support and mental workload. For physical resource, feedback was gathered on the users' responses to whether the second lancet was used (Q2e), how usable the instructions were (Q6b) and the frequency of consulting instructions (Q6f). For human support, the percentage of those who requested help from others was obtained and analysed (Q9c). NASA's TLX was applied to assess the mental workload. Independent studies have found TLX to be a valid measure of subjective workload[27,39,40] and has become the gold standard for measuring subjective workload across a wide range of applications from healthcare[41–43] to technology domains[44]. TLX is a six-item scale and each item represents a different aspect of workload: Mental Demand (MD), Physical Demand (PD), Temporal Demand (TD), Effort (EF), Performance (PE) and Frustration (FR). Research has shown that the raw TLX (without weighting the contribution of each factor in a predefined manner) has a high correlation with the weighted one[45], but is more time efficient and simpler to apply[46,47], therefore no weighting was applied for TLX in this study. To aid in interpretation and simplify use, the items are combined into a single summed unweighted score representing the latent construct of overall workload experienced by the individual during a specific time, event or situation[44,46]. Like previous studies[46,48], we simplified the original 21-point TLX Likert scale questions to 7-point. Like many studies based on raw TLX[49], all ratings for six subscales were normalised to 100 and the final TLX score was the mean of six subscale ratings. We further investigated whether there are differences in mental workload for people of different ages and education levels. Like another study[26], we categorised the participants into four age groups (as shown in Table 1, 7–17, 18–30, 31–60 and age above 60) and four educational attainments (Master/PhD, Honours Degree, A-level/NVQ (National Vocational Qualifications) and Primary/Secondary/Other education). For every group, the TLX scores were calculated and the pair-wise Wilcoxon tests were performed between the groups.

(4) *Accuracy* For clarity, the focus of this study was not to address or report on the diagnostic accuracy of the LFIA test to detect antibodies against SARS-CoV-2 virus[50], instead, the focus was to assess the user experience of the test kit. The simulated LFIA test results were used, which provided the controlled variation of T-line intensity and enabled us to gain a better understanding of how participants performed when reading the test results. The correctness of participants' reading for the printed test results were assessed by researchers by comparing to the ground truth. The accuracy was measured based on the agreement rate and Kappa score. Further investigation was carried out on which types of test results the members of the public most often misinterpreted.

(5) *Satisfaction* ISO 9241 defines satisfaction as "the comfort and acceptability of the work system to its users and other people affected by its use". The feedback on satisfaction was gathered in Section Q12. Similar to a recent UX study[23] based on self-testing for COVID-19 at home, in which the acceptability was assessed by the end users' willingness to perform finger-prick antibody tests, the question used in this study was to assess whether the users think the test kit meets their requirements (Q12a). Furthermore, to assess the comfort, questions asked the end users' perceived ease of using the test kit before and after testing (Q12b and Q12c) and the confidence in both completing the LFIA test and reading the test results (Q12d and Q12e).

Statistical analysis. The Chi-square test was applied to assess the differences between two proportions. Wilcoxon rank-sum tests were applied for data that were not normally distributed as indicated by the Kolmogorov–Smirnov-test. Bonferroni correction[51] was applied to adjust the significance level α during multiple hypothesis testing. The effect size for Chi-square test was measured by ϕ coefficient proposed by K. Pearson[52]. The effect size η^2 for Wilcoxon rank-sum tests was calculated using the z-scores of rank-sum tests as proposed by Cohen[53]. The effect size for t-test was calculated based on Cohen's d[54].

The agreement rate was assessed by the percentage of cases where the results interpreted by the participants' agreed with the printed test results (the ground truth). Kappa statistics[55–57] was also applied to evaluate the agreement, which was the metric of choice in COVID-19 antibody self-testing study[23,26] and HIV rapid diagnostic tests[58–60]. The range of Kappa scores can be interpreted as follows[61]: < 0 = poor agreement, 0.00–0.20 = slight agreement, 0.21–0.40 = fair agreement, 0.41–0.60 = moderate agreement, 0.61–0.80 = substantial agreement, and > 0.8 = almost perfect agreement.

All data analyses were performed using MATLAB2019b (MathWorks, USA) and Microsoft Excel for Microsoft 365 (MSO 32-bit).

Ethical approval. This study was approved by Ulster University Research Ethics committee (Ref: REC/20/0043) in full adherence to the Declaration of Helsinki. All participants provided fully informed consent. Informed consent for children (<18 years) was obtained from parents/guardians alongside assent from the child.

Results

Characteristics of study participants. There were 264 individuals participated in the study and the characteristics of the participants are provided in Table 1, which presents the proportion of participants in gender, age, education and ethnicity. The histograms of age distribution (for male and female) are presented as in Fig. 4a.

Characteristics	Groups	Proportions n (%)
No. of participants	All	264 (100)
Gender	Male	85 (32.2)
	Female	178 (67.4)
	Prefer not to say	1 (0.4)
Age [7–79, 45.0 ± 17.4]	7–17 (12.9 ± 2.5)	30 (11.3)
	18–30 (24.7 ± 3.8)	26 (9.9)
	31–60 (47.4 ± 7.7)	160 (60.6)
	60 + (68.3 ± 5.3)	48 (18.2)
Education	Ph.D	13 (4.9)
	Master	48 (18.2)
	Honours degree	73 (27.7)
	A-Level /level3 NVQ/diploma	59 (22.3)
	Secondary School Education	32 (12.1)
	Some Secondary Education	1 (0.4)
	Other Education	9 (3.4)
	Missing	29 (11.0)
Ethnicity	White	262 (99.2)
	Other	2 (0.8)

Table 1. Characteristics of study participants. The values for age are presented in the range, mean ± standard deviation (SD).

It is noticed that female participants were slightly over-represented (as also shown in Table 1 that 178 of 264 (67%) participants are females). The percentages of participants in four educational groups are shown in Fig. 4b, which shows less participants in Primary/Secondary/Other education (shown as 'Other') when compared to the other groups. However, every effort has been made to achieve as balanced an overall cohort as possible.

Ease of use. There were 30 polar questions in ten sections in the questionnaire, the participants' answers for each polar question were counted. The percentage of the counts are provided in Fig. 5. The p-values from Chi-square tests suggest statistical significance ($p < 0.001$) and the effect sizes suggest medium or large effect except for Q6b ($\phi = 0.20$ indicating small effect).

The sections Q1 to Q7 were devoted to specific aspects of the testing kit and used to assess the ease of use. The summative UX scores (sum of scores normalised as a percentage) for 264 participants from Q1 to Q7 were calculated (in which Q2e and Q6b were excluded and analysed for efficiency), and the mean and standard errors are presented in Fig. 6a. With the mean of each section higher than 93.11% and an overall average 95.27% (95% CI 92.71–97.83%), the public found the test kit relatively easy to use. Figure 6a also suggests the areas that could be improved, i.e., the application of test solution to LFIA device (Q4). A relatively low score was found in Q7e with 78.8% confirming that the unused second lancet was clicked prior to disposal, which suggests more effort will be needed to increase the users' awareness of the risks of unused lancet.

Similar to the approach used in another study[26], to assess the usability, we removed the questions Q1a, Q2d, Q4d, Q7a, Q7b, Q7c, Q7d and Q7e because they were not related to the usability construct. The summative usability scores were then calculated for the remaining 17 questions. The results of usability scores with mean and standard errors are given in Fig. 6b. The means for each section are higher than 93.7% with an overall average of 96.2% (95% CI 93.8–98.5%).

It can be seen in Fig. 6a that the scores for section Q2 (relating to collection of the blood sample) and section Q4 (relating to application of test solution to LFIA device) are lower than those in Fig. 6b. The reason for this was due to Q2d and Q4d being excluded from calculating usability scores. From Fig. 5, we can see that participants scored relatively low (91.3%) for Q2d ("The correct amount of blood was collected from the finger prick puncture') and 81.1% for Q3d ("The blood was easily expelled from the blood collector to the test'), which suggests that these were the barriers to optimal user experience. Q4d asked if there was any test solution remaining in the container, which has a relatively low score of 88.3%, which suggests that some users might not realise that they should have used all of the test solution.

Effectiveness. Effectiveness was assessed by test completion rate (Q5), in which 255 of 264 (96.6%) participants successfully completed the test after obtaining the control line, suggesting a good degree of effectiveness of the test kit. There were 9 participants for whom the test failed, in which 1 of 9 (11.1%) came from the age 18-30 group, 6 of 9 (66.7%) from age 30–60 group and 2 of 9 (22.2%) were aged over 60. The reasons for failure (Q8b) with multiple choices are summarised in Fig. 7a. The most common reason for failure was failure to add the blood sample to the test followed by failure to get a sufficiently sized drop of blood to form.

All participants also identified other areas of difficulty in their experience that did not lead to a test failure. There was a total of 318 choices received from 264 participants and the proportion in total choices is shown in

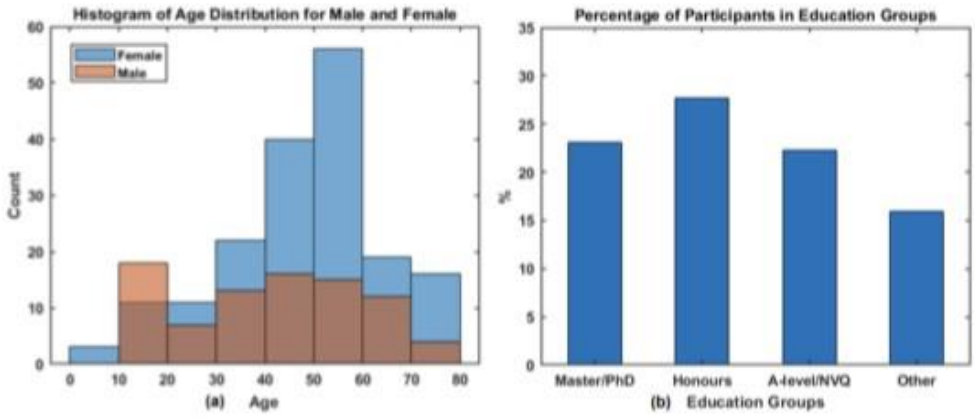

Figure 4. (**a**) The histogram of age distribution for female and male participants; (**b**) percentage of participants in four education groups.

Fig. 7b. It can be seen that 142 of 318 (45%) responders had no difficulty in completing the test, however the most difficult part of the test, as reported by 54 of 318 (17%) was collecting the blood using the blood collector. This was followed by 38 of 318 (12%) who said that their difficulty was adding the blood sample to the test, which was also reported as the main reason for failure.

Questions	Yes (%)	No (%)	P-values	Effect Size
Q1a: Did the packaging provide sufficient protection to the kit materials?	97.0	3.0		1.33
Q1b: Were the kit materials easily accessed?	98.5	1.5		1.37
Q1c: Did the packaging provide clear information to the type of test and materials inside?	98.1	1.9		1.36
Q2a: The lancet was easily identified.	97.7	2.3		1.35
Q2b: The lancet cap was easy to remove.	98.5	1.5		1.37
Q2c: The fingerpick puncture was easy to perform.	94.3	5.7		1.25
Q2d: The correct amount of blood was collected from the fingerpick puncture.	91.3	8.7		1.17
Q2e: The second lancet was required to be used.	25.8	74.2		0.69
Q3a: The test device was easily identified.	98.9	1.1		1.38
Q3b: The test was easy to remove from the foil packaging.	95.1	4.9		1.27
Q3c: The correct place to apply the sample ('sample hole') was easily identified.	100.0	0.0		1.41
Q3d: The blood was easily expelled from the blood collector to the test.	81.1	18.9		0.88
Q4a: The test solution was easily identified.	99.2	0.8		1.39
Q4b: The twist cap was easy to remove.	90.2	9.8		1.14
Q4c: The test solution was easily applied to the sample hole on the device.	96.2	3.8		1.31
Q4d: There was no test solution left in the container.	88.3	11.7	< 0.001	1.08
Q5: A control line (C-line) was present within the test window.	96.6	3.4		1.33
Q6a: The instructions provided were easy to follow.	98.1	1.9		1.36
Q6b: The instruction video was watched prior to performing the test.	57.2	42.8		0.20
Q6c: The user steps were simple and easy to perform.	96.2	3.8		1.31
Q6d: The items in the kit were appropriately labelled.	95.1	4.9		1.27
Q6e: The test is in an easy to use format.	95.8	4.2		1.30
Q7a: The lancet was understood to contain a needle.	95.5	4.5		1.29
Q7b: The risks associated with the lancet was clearly understood.	97.7	2.3		1.35
Q7c: The potential for small components to be a choking hazard was clearly understood.	94.7	5.3		1.26
Q7d: The correct way to dispose of the kit following use was understood.	99.2	0.8		1.39
Q7e: If unused the second lancet was clicked prior to disposal.	78.8	21.2		0.81
Q8a: Was the test completed and the control line obtained?	96.6	3.4		1.32
Q9c: Did you receive help from another person throughout the study?	17.4	82.6		0.92
Q10c: The results of the printed test provided on the card was easily interpreted based on the information provided in the instructions.	94.7	5.3		1.26

Figure 5. Summary of participants' responses to polar questions survey together with p-values and effect size ϕ.

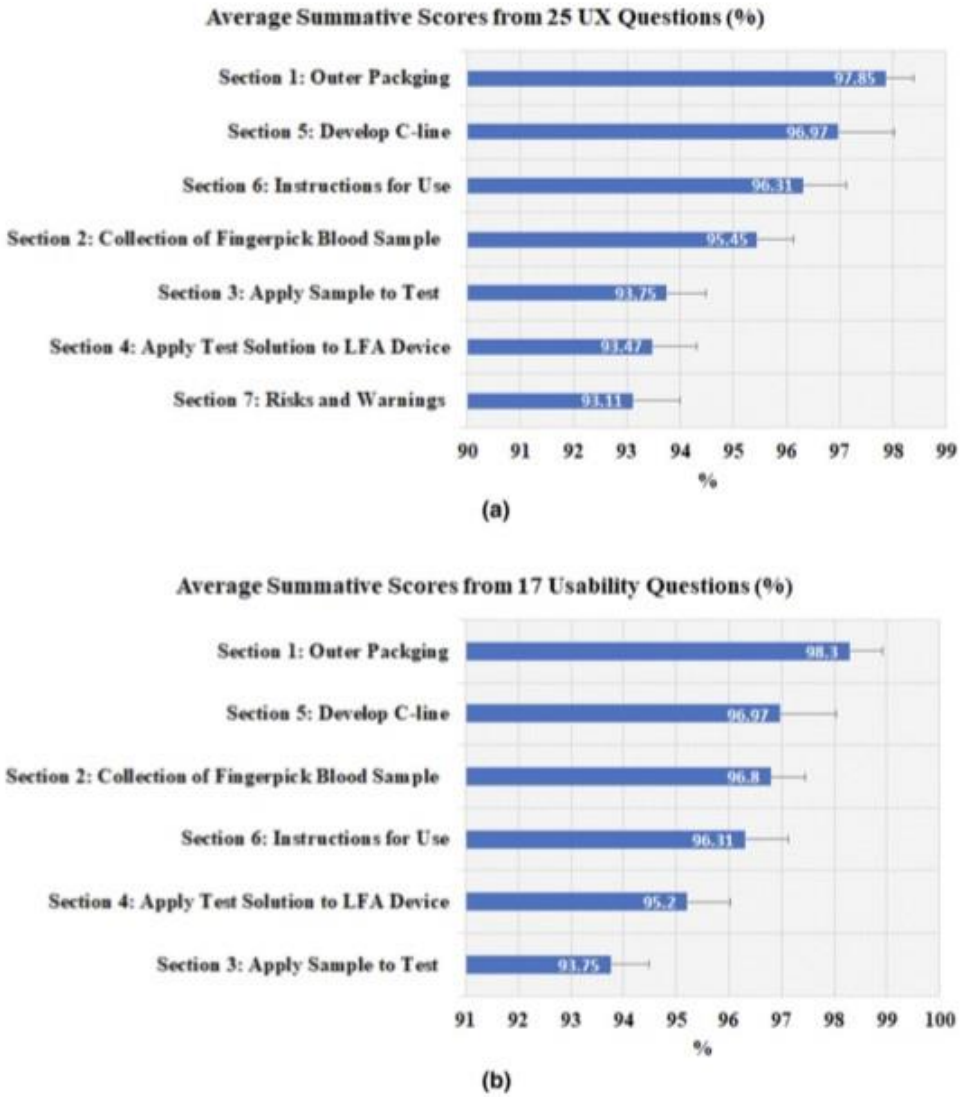

Figure 6. Average summative scores based on: (**a**) 25 UX questions; (**b**) 17 questions related to usability construct only. The error bars represent the standard errors (n = 264).

Efficiency.

(1) *Physical resource* The response to Q2e shows that 74.2% participants completed test using only one lancet suggesting user efficiency without the need for the spare lancet (each test kit included two lancets). Regarding the instruction video, answers to Q6b indicate that 57.2% of users watched the instruction video prior to performing the test, yet according to answers for Q5, 96.6% of users completed the test successfully, which suggests that the procedure was relatively easy to understand and implement even if not all users watched the video. For 9 users who failed the test, 6 of them watched the video before test, which may suggest that watching the video or not may have no direct impact on the failure of the test.

Question Q6f asked how many times the participant consulted the instructions during the test. As seen in Table 2, the majority of participants, 214 of 264 (81.1%) consulted the instructions 1–3 times, 42 of 264 (15.9%) consulted instructions 4–6 times, 5 participants consulted the instructions 7–9 times and only 3 consulted instructions more than 10 times. Among the 3 people who consulted the instructions at least 10 times and 5

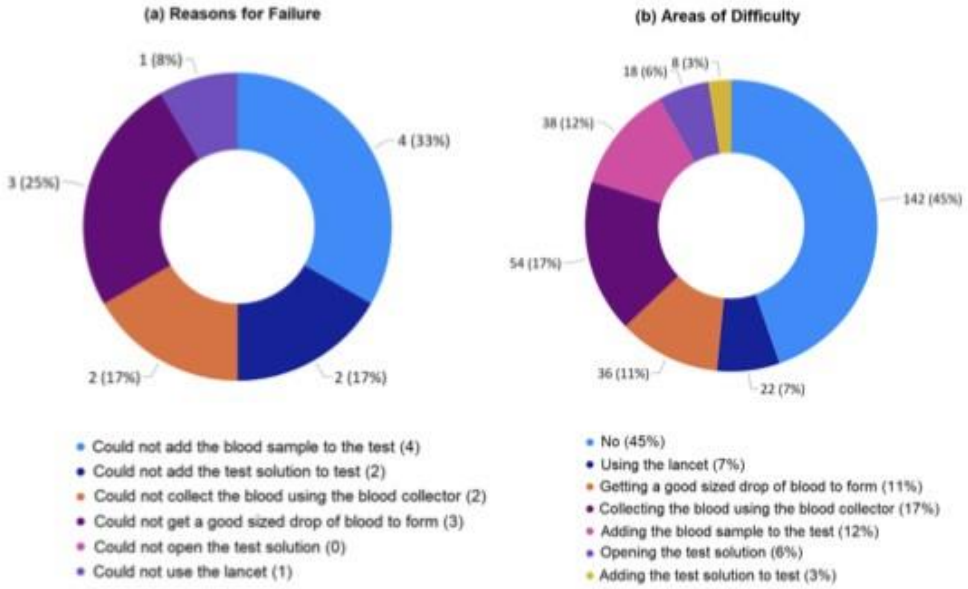

Figure 7. Summary for: (**a**) reasons for failure to complete the test based on 12 multiple choices; (**b**) areas of difficulty during the test based on 318 multiple choices.

Number of times users consulted the instructions	Age 7–17	Age 18–30	Age 31–60	Age 60+	Total
1–3	23	22	131	38	214 (81.1%)
4–6	5	2	25	10	42 (15.9%)
7–9	1	1	3	0	5 (1.9%)
10 +	1	1	1	0	3 (1.1%)
Total	30	26	160	48	264 (100%)

Table 2. Number of times the participants consulted the instructions in four age groups.

Number of times users consulted the instructions	Watched video	Didn't watch video	Total
1–3	127	87	214
4–6	23	19	42
7–9	0	5	5
10 +	1	2	3

Table 3. Number of times the participants consulted the instructions for those watched the instruction video and those did not.

people who consulted instructions 7–9 times, none of them were over 60 years old. Among 214 who consulted instruction 1–3 times, no significant difference was found between four age groups (as shown in Supplementary Table S1).

We cross examined the answers from the participants who watched the instruction video vs those who did not. From Table 3, it shows that among the 214 who consulted the instruction 1–3 times, 87 of 214 (40.7%) did not watch the video, which is the lowest proportion in the four categories; 5 of 5 (100%) and 2 of 3 (66.7%) that didn't watch the video consulted the instructions 7–9 times and more than 10 times, respectively. It appears that the higher the proportion of users who didn't watch the video, the more times they consulted the instructions, which indicates the effectiveness of the video in informing participants.

(2) *Human support (help received)* The question Q9c asked whether the participants received help from another person during the study. The answers suggest that 218 of 264 (82.6%) completed the test independently

Received help	Age 7–17	Age 18–30	Age 31–60	Age 60 +	Total
Yes	21 (70%)	2 (8%)	12 (8%)	11 (23%)	46 (17%)
No	9 (30%)	24 (92%)	148 (92%)	37 (77%)	218 (83%)
Total	30	26	160	48	264

Table 4. Number of participants in four age groups that received help from others during the test.

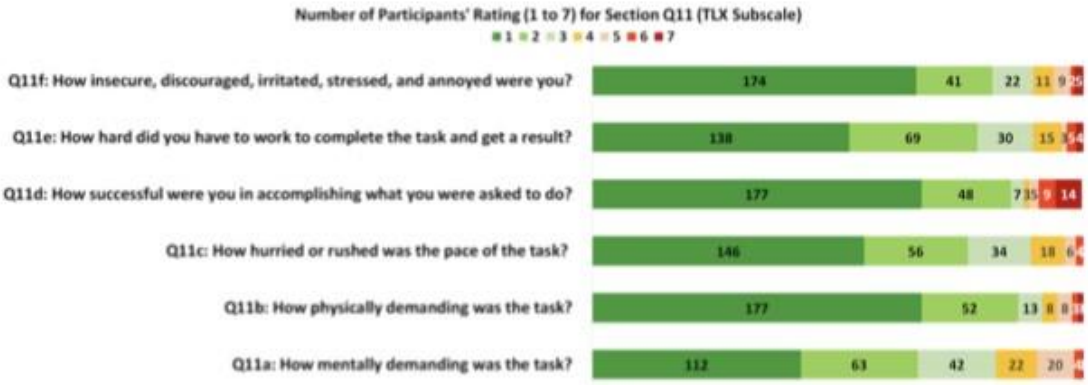

Figure 8. Summary of number of participants' rating in six TLX subscales.

without another person's help and of 46 of 264 (17.4%) requested help from others. We examined the participants who requested help in each age group and results are given in Table 4. The table shows that 21 of 30 (70%) in the age group 7–17 requested help from others, which is significantly higher than the rest three age groups (p-values < 0.001 and effect size $\phi > 0.46$ as presented in Supplementary Table S2). There are 11 of 48 (23%) from the age group 60+ also requested help, which is significantly higher than those in age group 31–60 ($p = 0.003$, effect size $\phi = 0.21$). The results suggest that additional support is needed for these two age groups (< 18 and 60+) during the self-administrated test.

(3) *Mental workload* The counts for six TLX subscales are presented in the Fig. 8, in which each item has a scale rating from 1 to 7. The results of mean and SD of TXL scores and six workload subscales (n = 264, normalised to 100) are provided in Fig. 9a, in which the mental demand (MD) has the highest score (31.5 ± 19.7), followed by Effort (EF) (27.0 ± 18.3), temporal demand (TD) (26.3 ± 16.8), own performance (OP) (26.2 ± 23.8), frustration (FR) (24.8 ± 18.9), and physical demand (PD) has the lowest score (23.3 ± 17.2). The overall workload TLX score is 26.5 ± 19.1.

A further investigation was carried out to study the mental workload for four age groups (AGs) and four education groups (EGs). Fig. 9b presents a bar chart for the average of six TLX subscales from the participants in four age groups. The results show that among all factors, mental demand (MD) appears to score the highest in three of four groups, which suggests that the participants considered the task more mentally demanding when compared to other factors. The age group AG4 (60+) gave the highest score for mental demand and AG3 (31–60) has the lowest MD score. The three groups (AG1, AG2 and AG4) scored high for physical demand (PD) and frustration (FR). But AG4 (60+) and AG1 (< 18) did not score the highest for temporal demand (TD), perhaps due to both groups received helps from others (as shown in the results in Table 4). For the overall workload TLX, the AG3 (31–60) has the lowest score, which suggests that the AG3 considered the test having less mental workload when compared to the other AGs. Fig. 9c presents the bar chart for mean of six TLX subscales for the participants in each of the four EGs. Similar to that in the age groups, mental demand (MD) appears to score the highest among all four groups. For the overall TLX scores, the EG2 (Honours) appears to score higher than the rest and EG3 (A-level) has the lowest TLX score.

One-sample Kolmogorov–Smirnov tests were performed for each group and the results suggest the scores do not have a standard normal distribution. The paired Wilcoxon rank sum tests were applied to access the medium differences between the groups. The significance level α was set as 0.008 via Bonferroni corrections. The results of p-values and effect size η^2 based on the age groups are presented in Table 5 and no significant differences were found in the paired comparison. The results for education groups are given in Table 6, EG1 (Master/PhD) and EG2 (Honours) appear to score significantly higher than EG3 (A-levels) but both have small effect sizes. No statistical significance was found for other paired tests. Overall, the average TLX for each group is lower than 30

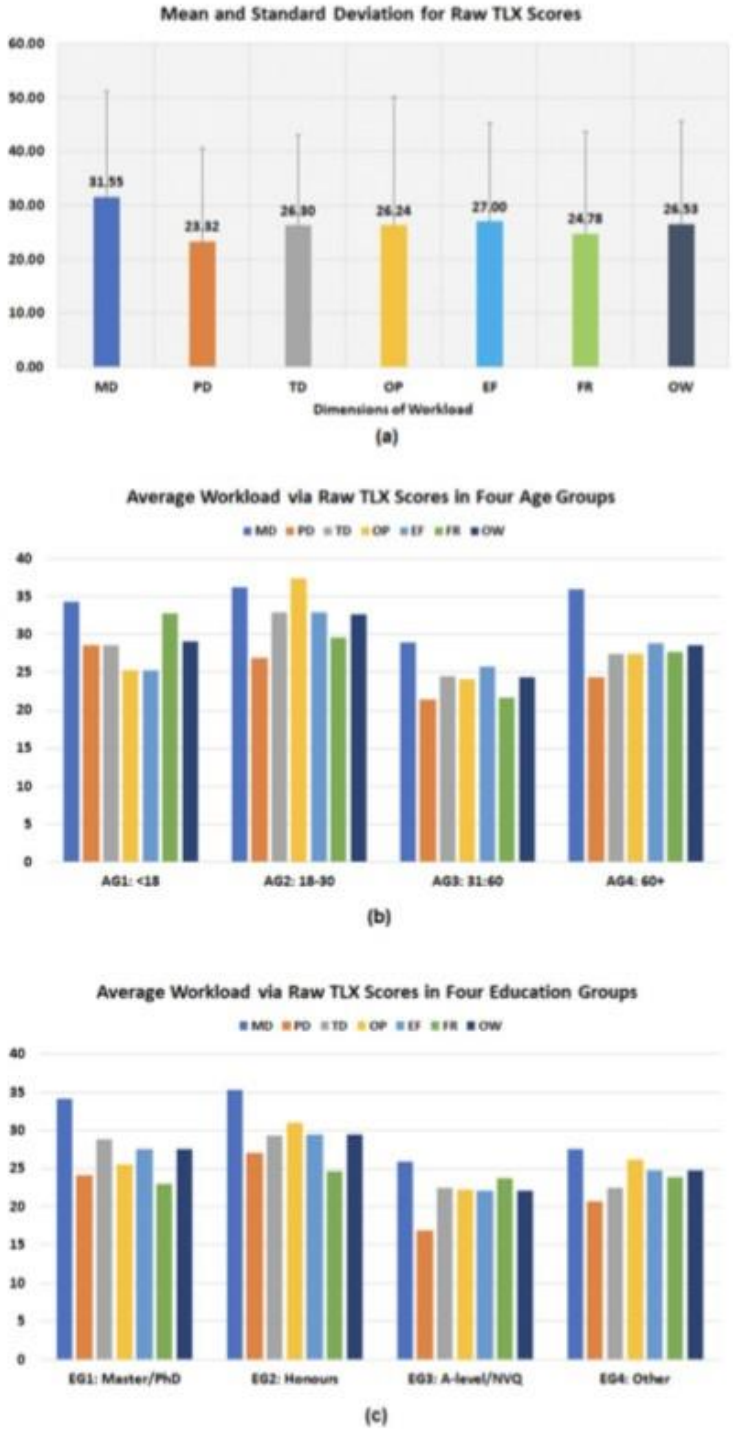

Figure 9. Results of TLX and six subscales: (**a**) mean and standard deviation based on all participants (n = 264); (**b**) mean based on participants from four age groups (AGs); (**c**) mean based on participants from four education groups (EGs).

Age groups	AG1 7–17	AG2 18–30	AG3 31–60	AG4 60+
AG1 7–17	1 (0)	–	–	–
AG2 18–30	0.372 (0.119)	1 (0)	–	–
AG3 31–60	0.320 (− 0.072)	0.026 (− 0.164)	1 (0)	–
AG4 60 +	0.824 (0.025)	0.382 (− 0.102)	0.092 (0.117)	1 (0)

Table 5. p-values and effect size η^2 (in bracket) based on paired Wilcoxon tests for TLX scores in four age groups.

Education groups	EG1: Master/PhD	EG2: Honours	EG3: A-Levels	EG4: Other
EG1: Master/PhD	1 (0)	–	–	–
EG2: Honours	0.773 (0.025)	1 (0)	–	–
EG3: A-Levels	0.002 (− 0.281)	0.002 (− 0.265)	1 (0)	–
EG4: Other	0.088 (− 0.168)	0.069 (− 0.170)	0.470 (0.072)	1 (0)

Table 6. p-values and effect size η^2 (in bracket) based on paired Wilcoxon tests for TLX scores four education groups.

		Printed cards' results n (%)						
		Positive (T1)	Strong positive (T2)	Weak positive (T5)	Total positive	Negative (T3)	Invalid (T4)	Total
Participant results: n (%)	Positive	43 (16.3)	29 (11.0)	48 (18.2)	120 (45.5)	2 (0.8)	1 (0.4)	123 (46.6)
	Negative	14 (5.3)	8 (3.0)	13 (4.9)	35 (13.3)	59 (22.3)	7 (2.7)	101 (38.3)
	Invalid	0 (0.0)	0 (0.0)	2 (0.8)	2 (0.8)	2 (0.8)	25 (9.5)	29 (11.0)
	Unsure	1 (0.4)	0 (0.0)	1 (0.4)	2 (0.8)	1 (0.4)	8 (3.0)	11 (4.2)
	Total	58 (22.0)	37 (14.0)	64 (24.2)	159 (60.2)	64 (24.2)	41 (15.5)	264 (100)

Table 7. Results read by the participants and the ground truth provided in the printed cards. The values in the brackets show the percentage of the results related to total number of results (n = 264).

indicating a relatively low level of mental workload compared to the reported reference values for TLX[49] in the domain of manual labour and when using handheld devices .

Accuracy: agreement between participant-interpreted and printed results. The results interpreted by the participants were compared to the ground truth from the printed cards. The summary of the results is presented in Table 7. The rows of the table are the participants' results (via answers to Q10b) in four categories: positive, negative, invalid and unsure. The columns show their printed cards that can be one of the five categories: positive (T1), strong positive (T2), weak positive (T5), negative (T3) and invalid (T4). The column of 'Total Positive' is the sum of all positives (T1, T2 and T5). The agreement rate between participants' results and the ground truth (based on the counts for total positive, negative and invalid) is 80.63% [95% CI 75.21–86.05%], and the Kappa score is 0.67 [95% CI 0.58–0.75] which suggests a substantial agreement between the results interpreted by the participant and the ground truth.

As seen in Table 7, there were 35 False Negative (FN) cases which the participants interpreted the results as negative, but the printed cards were positive. There are 13 of 35 (37.14%) FN cases were 'weak positives' (T5) and 14 of 35 (40%) FN cases were positive (T1), but only 8 of 35 (22.85%) cases were 'strong positive' (T2) cases and 7 of 35 (20%) were invalid (T4) cases. This suggests that results from the categories of positive (T1) and weak positive (T5) were more difficult to interpret due to the relatively low signal intensity in the test-line when compared to the strong positive (T2) cases.

Satisfaction. The answers to Q12 helped to assess the comfort and acceptability (the satisfaction) the users perceived for the test kit and the results for the rating counts are summarised in Fig. 10. The answers for Q12a show that 231 of 264 (87.5%) scored over 5, which suggest that majority of users considered the capability of the test kit meet their requirements.

The scores from Q12b and Q12c were the responses on the user-perceived ease of using the kit after and before the test, respectively. A boxplot based on the scores from Q12b and Q12c are given in Fig. 11a. The higher median of Q12b than Q12c suggest that the participants found the kit was easier to use than they expected ($p < 0.001$, effect size $d = 1.41$).

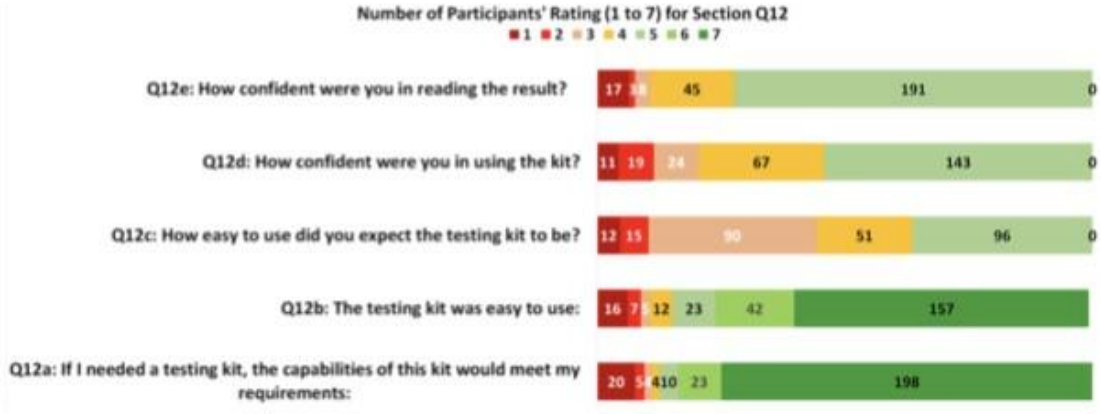

Figure 10. The counts for the 7-point Likert rating scores for question section Q12 (which helps to assess the comfort and acceptability).

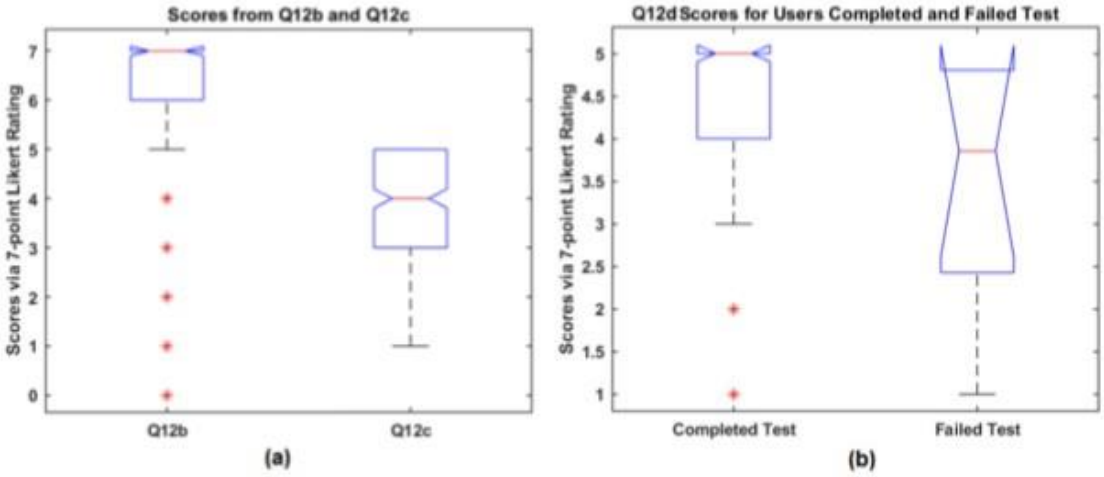

Figure 11. The boxplot for: (**a**) scores from Q12b and Q12c to assess the user-perceived ease of using the kit after and before the test; (**b**) scores for Q12d (to assess the confidence in using the kit) from the users who completed and failed the test.

In terms of the confidence in using the kit (Q12d), as seen in Fig. 10, the highest score was 5 received from 143 of 264 (54.2%), 67 of 264 (25.4%) scored 4, which suggest the relatively low confidence the users felt in using the kit. However, the answers to Q5 show that 255 of 264 (96.6%) users successfully completed the test, which suggests that even the participants who felt a lack of confidence still managed to complete the test. A boxplot for Q12d scores from those who completed and failed the test is given in Fig. 11b, which shows a higher score in confidence for those who completed the test than those who failed to do so although no significance was found (rank sum test $p = 0.09$, effect size $\eta^2 = 0.102$).

In terms of the confidence in reading the result (Q12e), as in Fig. 10, 191 of 264 (72.3%) gave the highest score 5, 45 of 264 (17.1%) scored 4, and 17 of 264 (6.4%) scored only 1. We further examined what type of tests the users were less confident to read for those 73 users who scored under 5, and the results are given in Table 8. It is noted that the highest number 18 of 73 (24.7%) was from 'Invalid', but there are 32 of 73 (43.8%) from the combination of T1 and T5 in those scored less than 5. The results suggest that for the tests T1 and T5, the participants felt less confident in reading compared to the rest, which concord with the findings pertaining to the accuracy of reading test results (in Table 7).

Feedback. The areas for future improvement have been identified from the user feedback. There were 123 free text comments received from the participants, which can be summarised in several aspects related to difficulty in using the test kit, instructions, risks/safety warnings, and UX study design. A total of 36 out of 123 (28%) users found the blood collector was difficult to use, such as the issues related to blood sample collecting included the blood bubbled into the test, difficult to expel blood, or unsure of the size of drop of blood required.

Q12e	Printed cards' results					
	Positive (T1)	Strong positive (T2)	Weak positive (T5)	Negative (T3)	Invalid (T4)	Total
Scores < 5	15	8	17	15	18	73

Table 8. The counts for participants' confidence levels scored under 5 when reading the result (Q12e) and the ground truth provided in their printed cards.

Similar issues have been reported in the previous car-based study[26]. Regarding the instructions, 9 of 123 (7.3%) found it helpful to watch the video before the test, three users pointed out the layout of the instruction booklet was not easy to read, and two users raised the issue of hygiene and suggested the instruction should advise washing hands after the test.

Some users were concerned by the dexterity required to complete the test as they found it was difficult due to either shaky hands (two users), poor eyesight (one user), or disability (one user). One younger user was concerned that the task could be difficult for the elderly in terms of comprehending a large amount of information and uploading photos via mobile device. Therefore, extra help and consideration will be needed for those vulnerable people.

In terms of UX study design, six users found the amount of information required to read and the paperwork to process was overwhelming and off-putting. Three users mentioned that they were unclear about the purpose of using the printed test cards. Four users reported that they had a technical issue when uploading images using their mobile devices and had to use a laptop or send photos via their email. Six users suggested that plaster and tissue should be provided in the kit for the users. Four users mentioned the package received via postal were damaged, which suggests that a better package may be needed if using the postal service to deliver the test kits in the future.

Discussion

This paper presents a home-based UX study for SARS-CoV-2 antibody rapid test kit via simulated LFIA testing. A summary of UX analysis methods used in this study and two related studies[23,26] is provided in Table 9, which highlights the contribution of this study to the literature. Although containing a relatively smaller sample size than the other two studies, this study carried out a more in-depth analysis that covered the multidimensional aspects of UX analysis in terms of ease of use, effectiveness, efficiency, accuracy and satisfaction.

(1) For ease of use, study-1[23] used 4 10-point Likert ratings to check the user's understanding of the instruction and ability to perform the test, this study contained 25 of 30 polar questions that measured the UX of a particular aspect of the testing kit (as seen in Fig. 6). The design of questions simplified the users' tasks by replacing the 5-point Likert ratings used the study-2[26] by the polar questions. A similar average UX score (95.27%) was obtained as in study-2[26] (96.03%), which suggests the good user experience of the test kit for both using the AbC-19 LFIA test kit in cars and at home.

(2) In terms of effectiveness, similar as highlighted in study-1[23], the common difficult areas for completing the test were applying the blood drop to the test and collecting the blood using the blood collector (as in Fig. 7), which suggests these areas should be the focus for design improvement in the future.

(3) In terms of efficiency, this study assessed the use of the physical resource, number of times to consult the instruction, use of instruction videos, human support, and mental workload, together with cross-examination for age and education groups. The results suggest the usefulness of the instruction video and recommend that additional support is needed for two age groups (< 18 and 60+) during the self-administrated test. NASA's TLX was applied to assess the users' perceived cognitive demand of the tasks, which may potentially help to reduce error and improve customer acceptance. As seen in Fig. 9, the participants scored the test highest for mental demand (31.5 ± 19.7) and lowest for physical demand (23.3 ± 17.2), the overall workload TLX score is 26.5 ± 19.1. A paper conducted a meta-analytic review[49] about reference values and subscale patterns for TLX based on 556 studies across 18 domains, 4 technology areas and 6 global regions. All papers selected in this review were based on raw TLX including six subscales, the values for six subscales were rescaled to the 0–100 range and TLX was calculated as the mean of the subscales, which was the same approach used in our study. According to this review paper[49], the average TLX score when used for the domain of manual labour (physical work) is 56 ± 12, and the average TLX when using handheld devices is 35 ± 16. In comparison, the TLX score (26.5 ± 19.1) achieved for the LFIA rapid test kit in this study is lower than these two aforementioned TLX scores for the domain of manual labour and when using handheld devices, which suggests that the general public have a relatively low level of mental workload when using LFIA self-testing at home.

(4) For assessment of accuracy, substantial agreement was found via Kappa scores in all studies. In two related studies, the participants' reading for actual LFIA testing results were compared to the clinicians' or researchers' results. Simulated test results were applied in this study, in which a controlled variation of T-line and C-line helped us to assess how participants performed when reading different types of test results. The results suggest that the categories of positive (T1) and weak positive (T5) were more difficult to interpret due to the relatively low T-line intensity when compared to the strong positive (T2) cases.

(5) The assessment of satisfaction suggests that the end-users felt less confident in reading tests of T1 (positive), T5 (weak positive), and T4 (invalid) compared to the rest. However, overall the users felt the test kit

	Study-1[23]	Study-2[26]	This study
Environment	At home	In car	At home
Sample size	N1: 10600; N2: 3800	1544	264
Number of questions	17	28	41
Ease of use	4 10-point Likert ratings	28 5-point Likert ratings (analysis for age & education groups)	25 polar questions
Effectiveness			
Completion rate (with valid C-line)	N1: 91.5%; N2: 94.4%	Not recorded	96.7%
Identify reasons for failure	Yes	Not recorded	Yes
Identify areas of difficulty	Yes	Yes	Yes
Efficiency			
Use of physical resource	Not recorded	Yes	Yes
Frequency to consult the instructions	Not recorded	Yes (analysis for age groups)	Yes (analysis for age groups)
Use of instruction video	Not recorded	Yes	Yes
Human support	Yes	Not recorded	Yes (analysis for age groups)
Mental workload	Not recorded	Not recorded	Yes (analysis for age & education groups)
Accuracy (Kappa score)	N1: 0.72, N2: 0.89 (real test results)	0.75 (real test results)	0.67 (simulated test results)
Satisfaction (acceptability)	2 polar questions	Not recorded	5 7-point Likert ratings

Table 9. Comparison of UX analysis methods used in this study and two related studies for LFIA self-testing for COVID-19.

was easier to use than they expected and a majority (87%) of users scored 5 over 7 and considered that the capability of the test kit met their requirements.

The findings from using simulated test results may also suggest the potential need for further investigation of the quantitative analysis of different COVID-19 antibody levels. Although there are studies that have reported the dynamic changes of SARS-CoV-2 antibody response[30,31,62], there is a lack of investigation of the relationship between the T-line intensity and SARS-CoV-2 antibody levels in the literature. Some researchers[30] are concerned that the reduction in SARS-CoV-2 IgG and neutralising antibody levels in the early recovery phase might have implications for immunity strategy. Another study[31] also suggests further studies will be needed to define a quantitative protection threshold and rate of decline of antiviral antibodies beyond 90 days. Future work to investigate the relationship between the T-line intensity and SARS-CoV-2 antibody levels may provide new insight to fill these gaps in the literature.

Furthermore, the methodology and findings in this study may also provide values to other types of LFIA applications, not just COVID-19. For example, a better understanding of the area of difficulties in self-testing may help to improve the LFIA testing performance at home in general, also the approach for cross-examination of groups (age/education) helps to uncover the potential issues in different groups of the end-users so the additional support can be provided for those in need, such as the users who are younger than 18 and over 60.

Limitations of this study include the following aspects: (1) The questionnaire used in this study was based on modification and extension of our previous study for UX study of LFIA testing COVID-19 in cars[26], which was not a validated questionnaire but was specifically designed for our study. Since we found there was a lack of well-defined measurement metrics for UX related to LFIA self-testing. Those related studies[17,19,22,23] mainly focused on the assessment of accuracy in interpreting test results and tried to identify specific issues for their study based on the feedback received from their questionnaires. The questions in the industry standard benchmark for usability measures like SUS[63] or USE[64] were unsuitable for our study, such as the SUS question "I think that I would like to use this system frequently", and the USE questions "It helps me be more effective", "It helps me be more productive", which are not applicable to the LFIA testing for COVID-19. Therefore, we applied self-defined measurements for UX analysis together with NASA-TLX for assessment of mental workload to explore the multiple aspects of user experiences. Modification of SUS questions as suggested in other study[65] can be considered in the future study. (2) The assessment of mental workload based on the measure of TLX may be limited via only comparing to the reference value recommended in the literature[49], rather than proposing criteria for target NASA-TLX for the home-based LFIA testing, which is beyond the scope of this study but will be considered in the future work. (3) Compared to related studies[23,26], this study has relatively small samples. Also due to the restraints of responses to recruitment, some groups were over-represented (females) while other groups were under-represented (males). In terms of age distribution, according to NI 2011 Census[29], 13.18% of the NI population (1.8 million) are aged 8-17 and 18.73% are aged over 60. For this study, we have 30 of 264 (11.3%) from under 18 and 48 of 264 (18.2%) from the group of age over 60, which was broadly similar to the NI population profile, but more volunteers with primary or secondary education will need to be included to improve the analysis related to the education groups.

33. Zhou, W. *et al.* The dynamic changes of serum IgM and IgG against SARS-CoV-2 in patients with COVID-19. *J. Med. Virol.* **93**, 924–933 (2021).
34. Jing, M. *et al.* Enhance categorisation of multilevel high-sensitivity cardiovascular biomarkers from lateral flow immunoassay images via neural networks and dynamic time warping. In *2020 IEEE International Conference on Image Processing (ICIP)*, 365–369 (IEEE, 2020).
35. Abingdon Health instruction video. *Youtube* https://youtu.be/WqT2z8jCEHs (2020).
36. Alben, L. Quality of experience: Defining the criteria for effective interaction design. *Interactions* **3**, 11–15 (1996).
37. Hassenzahl, M. & Wessler, R. Capturing design space from a user perspective: The repertory grid technique revisited. *Int. J. Hum. Comput. Interact.* **12**, 441–459 (2000).
38. Hassenzahl, M. & Tractinsky, N. User experience-a research agenda. *Behav. Inf. Technol.* **25**, 91–97 (2006).
39. Rubio, S., Díaz, E., Martín, J. & Puente, J. M. Evaluation of subjective mental workload: A comparison of SWAT, NASA-TLX, and workload profile methods. *Appl. Psychol.* **53**, 61–86 (2004).
40. Xiao, Y., Wang, Z., Wang, M. & Lan, Y. The appraisal of reliability and validity of subjective workload assessment technique and NASA-task load index. *Chin. J. Ind. Hyg. Occup. Dis.* **23**, 178–181 (2005).
41. Weinger, M. B. *et al.* Quantitative description of the workload associated with airway management procedures. *J. Clin. Anesth.* **12**, 273–282 (2000).
42. Lopez, K. D., Gerling, G. J., Cary, M. P. & Kanak, M. F. Cognitive work analysis to evaluate the problem of patient falls in an inpatient setting. *J. Am. Med. Inform. Assoc.* **17**, 313–321 (2010).
43. Yurko, Y. Y., Scerbo, M. W., Prabhu, A. S., Acker, C. E. & Stefanidis, D. Higher mental workload is associated with poorer laparoscopic performance as measured by the NASA-TLX tool. *Simul. Healthc.* **5**, 267–271 (2010).
44. Hart, S. G. Nasa-task load index (NASA-TLX); 20 years later. In *Proceedings of the human factors and ergonomics society annual meeting*, vol. 50, 904–908 (Sage publications Sage CA, 2006).
45. Grier, R. A. How high is high? A meta-analysis of NASA-TLX global workload scores. In *Proceedings of the Human Factors and Ergonomics Society Annual Meeting*, vol. 59, 1727–1731 (SAGE Publications Sage CA, 2015).
46. Hendy, K. C., Hamilton, K. M. & Landry, L. N. Measuring subjective workload: When is one scale better than many?. *Hum. Factors* **35**, 579–601 (1993).
47. Nygren, T. E. Psychometric properties of subjective workload measurement techniques: Implications for their use in the assessment of perceived mental workload. *Hum. Factors* **33**, 17–33 (1991).
48. Svensson, E., Angelborg-Thanderez, M., Sjöberg, L. & Olsson, S. Information complexity-mental workload and performance in combat aircraft. *Ergonomics* **40**, 362–380 (1997).
49. Hertzum, M. Reference values and subscale patterns for the task load index (TLX): A meta-analytic review. *Ergonomics* **64**(7), 869–878 (2021).
50. Robertson, L. J. *et al.* Evaluation of the IgG antibody response to SARS-CoV-2 infection and performance of a lateral flow immunoassay: Cross-sectional and longitudinal analysis over 11 months. *BMJ Open* **11**, e048142 (2021).
51. Weisstein, E. W. Bonferroni correction. *https://mathworld.wolfram.com/* (2004).
52. Cramér, H. *Mathematical Methods of Statistics (PMS-9)*, Vol. 9 (Princeton university press, 2016).
53. Cohen, J. *Statistical Power Analysis for the Behavioral Sciences* (Academic Press, 2013).
54. Fritz, C. O., Morris, P. E. & Richler, J. J. Effect size estimates: Current use, calculations, and interpretation. *J. Exp. Psychol. General* **141**, 2 (2012).
55. Cohen, J. A coefficient of agreement for nominal scales. *Educ. Psychol. Meas.* **20**, 37–46 (1960).
56. Fleiss, J. L., Levin, B. & Paik, M. C. *Statistical Methods for Rates and Proportions* (Wiley, 2013).
57. Viera, A. J. *et al.* Understanding interobserver agreement: The kappa statistic. *Fam. Med.* **37**, 360–363 (2005).
58. Lee, V. J. *et al.* User acceptability and feasibility of self-testing with HIV rapid tests. *JAIDS J. Acquir. Immune Defic. Syndr.* **45**, 449–453 (2007).
59. Figueroa, C. *et al.* Reliability of HIV rapid diagnostic tests for self-testing compared with testing by health-care workers: A systematic review and meta-analysis. *Lancet HIV* **5**, e277–e290 (2018).
60. Kurth, A. E. *et al.* Accuracy and acceptability of oral fluid HIV self-testing in a general adult population in Kenya. *AIDS Behav.* **20**, 870–879 (2016).
61. McHugh, M. L. Interrater reliability: The kappa statistic. *Biochem. Med. Biochemia medica* **22**, 276–282 (2012).
62. Feng, X. *et al.* Longitudinal profiling of antibody response in patients with COVID-19 in a tertiary care hospital in Beijing, China. *Front. Immunol.* **12**, 700 (2021).
63. Brooke, J. SUS: a 'quick and dirty'usability. In Jordan, P. W., Thomas, B., McClelland, I. L. & Weerdmeester, B. (eds.) *Usability Evaluation in Industry*, 189–194 (CRC Press, 1996).
64. Lund, A. M. Measuring usability with the use questionnaire12. *Usability Interface* **8**, 3–6 (2001).
65. Lewis, J. R. & Sauro, J. Can I leave this one out? The effect of dropping an item from the SUS. *J. Usability Stud.* **13**, 38–46 (2017).

Acknowledgements

We are extremely grateful to all the people of Northern Ireland who took part in this study during the pandemic. We also acknowledge the European Union's INTERREG VA Programme [Grant ID:IVA5034, managed by the Special EU Programmes Body (SEUPB)] funding associated with Eastern Corridor for Medical Engineering (ECME) in relation to data analysis and UK-RTC provided the test kits and funding of expenses.

Author contributions

T.M. and J.M.L. designed, coordinated and supervised the project, participated in interpretation of results and provided the critical comments for the manuscript; R.B. designed the research questions, supervised the data analysis, participated in interpretation of results and provided the comments for the manuscript; M.J. conducted the data analysis including technical implementation and interpretation of results, drafted the manuscript with inputs from all authors; A.N. participated in interpretation of results and provided the comments for the manuscript; A.N., R.P. participated in participants recruiting, collected the original post-study data; T.M., A.N., L.R., J.M., A.K. and R.P. obtained ethical approval, coordinated data collection and ensured adherence to all research governance issues; W.B. designed and controlled the data base and digitalised all original post-study data for analysis; All authors reviewed the manuscript and approved the final version of the manuscript.

Competing interests

The authors declare no competing interests.

Appendix VI

www.nature.com/scientificreports

scientific reports

Check for updates

OPEN

User experience analysis of AbC-19 Rapid Test via lateral flow immunoassays for self-administrated SARS-CoV-2 antibody testing

Min Jing[1], Raymond Bond[1], Louise J. Robertson[2], Julie Moore[2], Amanda Kowalczyk[2], Ruth Price[2], William Burns[1], M. Andrew Nesbit[2], James McLaughlin[1]✉ & Tara Moore[2,3]✉

Lateral flow immunoassays are low cost, rapid and highly efficacious point-of-care devices, which have been used for SARS-CoV-2 antibody testing by professionals. However, there is a lack of understanding about how self-administered tests are used by the general public for mass testing in different environmental settings. The purpose of this study was to assess the user experience (UX) (including usability) of a self-testing kit to identify COVID-19 antibodies used by a representative sample of the public in their cars, which included 1544 participants in Northern Ireland. The results based on 5-point Likert ratings from a post-test questionnaire achieved an average UX score of 96.03% [95% confidence interval (CI) 95.05–97.01%], suggesting a good degree of user experience. The results of the Wilcoxon rank sum tests suggest that UX scores were independent of the user's age and education level although the confidence in this conclusion could be strengthened by including more participants aged younger than 18 and those with only primary or secondary education. The agreement between the test result as interpreted by the participant and the researcher was 95.85% [95% CI 94.85–96.85%], Kappa score 0.75 [95% CI 0.69–0.81] (indicating substantial agreement). Text analysis via the latent Dirichlet allocation model for the free text responses in the survey suggest that the user experience could be improved for blood-sample collection, by modifying the method of sample transfer to the test device and giving clearer instructions on how to interpret the test results. The overall findings provide an insight into the opportunities for improving the design of SARS-CoV-2 antibody testing kits to be used by the general public and therefore inform protocols for future user experience studies of point-of-care tests.

The SARS-CoV-2 pandemic has provided an impetus for the rapid development of laboratory and point-of-care (PoC) diagnostic serological assays, which would meet a clinical need and fulfil epidemiological requirements including vaccine response monitoring and research needs. Commercial professional tests including lab-based immunoassays and lateral flow immunoassays (LFIA)[1] were released into the market over very short time frames. Well established, low-cost, rapid and highly efficacious PoC devices in the form of LFIA have been developed for home pregnancy tests[2,3], HIV[4,5], Influenza A (H1N1)[6], and more recently for COVID-19 antibody testing[7–10]. Given the research community is currently trying to establish how long COVID-19 antibodies persist[11,12], the capability to rapidly test for the presence of these antibodies is a vital tool for understanding coronavirus related public health planning.

According to Ara Darzi, Director of the Institute of Global Health Innovation, "The testing landscape is like the wild west with no rules, no standards, and widely varying reliability. Even the most accurate test is useless unless it is usable"[13]. Given the novelty of COVID-19, there is a paucity of research related to the user experience of COVID-19 related products, services, and testing kits by the general public. One study[7] which evaluated a SARS-CoV-2 antibody test by LFIA stated that their patient and public involvement activities found that

[1]Faculty of Computing, Engineering and the Built Environment, Ulster University, Jordanstown, UK. [2]Biomedical Sciences Research Institute, Ulster University, Coleraine, UK. [3]Avellino USA, 1505 Adams Dr, Menlo Park, CA 94025, USA. ✉email: jad.mclaughlin@ulster.ac.uk; tara.moore@ulster.ac.uk

"user-expressed difficulties interpreting results motivated us to investigate agreement between self-reported and clinician-reported results". Hence, a follow-up usability and acceptability study[8] recruited members of the public who self-administered an antibody test in a home environment. Feedback from pilot testing with 315 volunteers helped the design of a nationally representative study using two types of LFIAs (by Guangzhou Wondfo Biotech Co Ltd and Fortress Orient Gene Biotech Co Ltd) with 10,600 and 3,800 participants in England, completed by 97.5% and 97.8% of respondents[8], respectively. Agreement between the participant and clinician interpretation of the results of the testing kits achieved Kappa scores of 0.72 and 0.89 for two LFIA tests respectively. The presented usability analysis was only summarised by descriptive statistics based on data from questionnaires, which identified the difficulties in use of the lancet, a need for clearer instructions for using the kit and interpretation of results.

The purpose of our study was to evaluate whether the LFIA test can be easily understood and effectively self-administered by a sample of citizens, without incidents of difficulty, confusion, or failure due to the test design. Testing kits need to be user-friendly and intuitive for the majority of the citizens to perform the test correctly. The UX analysis will help to improve the design of testing kits and inform protocols for future studies. This study was led by Ulster University researchers, using the AbC-19 Rapid Test developed by Abingdon Health. When this study was conducted, this device was approved for professional use in the UK and EU[14]. Unlike the previously published study[8] that was conducted in a home setting, in the study presented here, the tests were carried out in an in-car setting at a university car park (due to the social distancing rules during the pandemic, the car park was an environment in which this study could be safely conducted). The participants self-administered the test in their own cars (overseen by the researchers), which had different environmental conditions and spatial constraints compared to a home or laboratory setting.

To evaluate the participants' ability to interpret their test result, we analysed the agreement between a participant's self-reported result and the researcher's interpretation of the same test, coupled with a post-test questionnaire to collect data regarding the user experiences of the testing kit. Several studies related to user experience of LFIA self-testing conducted the analysis have used the similar approach (via evaluation of agreement and questionnaire)[2,4,8]. Apart from studying the post-test survey data, we carried out the UX analysis based on user's age and education attainment. Testing the user experience of a product across educational levels and age is important to show if a product is user friendly and independent of age and education, thereby the product can be reliably released into communities with the reasonable expectation that it can be safely and intuitively used by users of various demographics. Research from the usability literature[15] suggests the importance of considering age in testing which helps further justify this research question. Furthermore, we also carried out text analysis based on the users' free text responses to open questions in the survey, which helped identify opportunities to improve the design of these testing kits. In this paper, we answer the following research questions:

- Do members of the public find the testing kit easy to use?
- Is ability to use the testing kit independent of age and education level?
- Which testing kit user experience issues are identified?
- What is the agreement rate between the results as interpreted by participants and researchers?

For clarity, this paper does not attempt to address or report on the diagnostic accuracy of the LFIA to detect antibodies against SARS-CoV-2 virus, but instead is a study that was focused on the user experience and the agreement rate between participants and trained researchers when interpreting the test results.

Materials and methods

Materials. The AbC-19 Rapid Test is a single-use test for the detection of SARS-CoV-2 IgG antibodies in human capillary whole blood. Using a blood sample from a finger-stick puncture the Rapid Test will identify the presence of IgG antibodies against the trimeric spike protein of SARS-CoV-2 virus (the virus responsible for the COVID-19 disease), signifying a recent or previous infection by the virus. The test kit materials include: one test, two single-use lancets, blood collector, test solution, waste bag and instructions. Fig. 1 presents: (a) structure of the testing device showing the sample hole, viewing window with the control line (C-line) and test line (T-Line) as an example of positive result; (b) example of negative result.

To perform testing, the participants followed the steps provided in the instruction (in Supplementary file): (a) hands were cleaned using warm water only; (b) the blood sample was taken from the ring or middle finger of the non-dominant hand by using the lancet; (c) the blood was collected using the blood collector; (d) blood was added to the test sample hole, and the test solution was then applied to the sample hole; (e) after 20 minutes, if C-line appears (indicating the test was performed successfully), the test results were interpreted by looking at the viewing window.

Participants and study setup. Potential participants who had expressed an interest in taking part in the study following either university or media publicity were invited to complete an online consent form and questionnaire which collected data such as gender, age, education, COVID-like symptoms etc. Individuals from each age/gender group were randomly selected to achieve as balanced an overall cohort as representative of the NI population as possible. No financial or other types of incentives were received by the participants.

All participants were members of the public in Northern Ireland and included children above the age of 8 years old and adults. Data collection was completed over 2 days, on 4th and 5th September 2020 in a car park at Ulster University (address: Newtownabbey, Co. Antrim, Northern Ireland, UK). Informed consent was obtained prior to commencing the study. Consent for children was provided by their parent/guardian. Consent could only

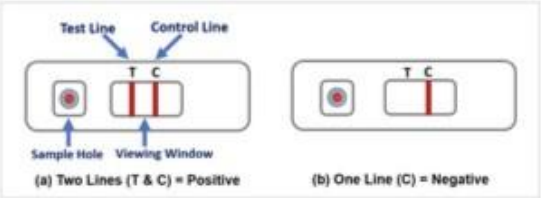

Figure 1. (**a**) structure of the testing device showing the sample hole, viewing window with the control line and test line as an example of positive result; (**b**) an example of negative result.

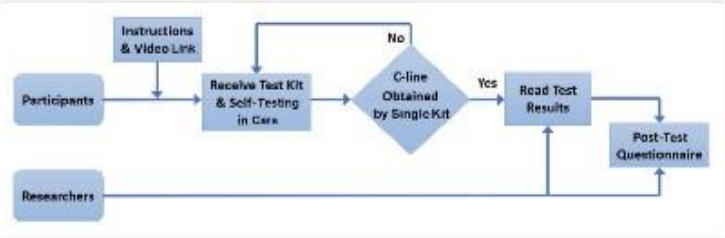

Figure 2. The diagram for the study flow.

be given by individuals who were capable of independently understanding the information provided. Participants aged between 8 and 17 years old could be assisted by their parent/guardian.

A diagram to illustrate the study flow is presented in Fig. 2. Participants were given prior access to written instructions and a video on YouTube[16] before the test. On arrival they were directed to a parking space, given a test kit and performed the self-test within their cars. If no C-line was visible by using a single test kit, the participant was asked to repeat the testing procedure. After participants obtained their results, a researcher (one of 20 trained volunteers from university staffs and post-graduate students) would interpret the same tests performed by participants. Interpretation of any queried results, e.g. a very weak T-line, lack of a C-line in LFIA, was undertaken by three highly experienced LFIA users. The researchers also gathered participant responses to a post-test questionnaire.

UX and usability analysis. According to ISO definition (ISO 9241-11)[17], usability is related to "effectiveness, efficiency and satisfaction with which specified users achieve specified goals in particular environments", whilst user experience is "A person's perceptions and responses that result from the use and/or anticipated use of a product, system or service. (ISO 9241-210)[18]. Although there are diverse definitions of UX, most agreed that UX is more than just a product's usefulness and usability[19–21]. The aim of UX analysis in this study was to examine the user's interaction with the testing kit and to identify the areas of difficulty encountered during testing; the aim of usability analysis was to assess whether the testing kit was easy for users to complete the test successfully. Both UX and usability were analysed, in which UX was considered a higher level construct (where usability is a sub-component).

The data for the UX and usability analysis were collected from the post-test questionnaire (provided in Supplementary file). The questionnaire was comprised of seven sections each of which included 3 to 6 questions based on 5-point Likert rating scales, which measure the UX or usability of a particular aspect of the testing kit. There were 28 Likert ratings in the seven sections which include: (Q1) outer packaging; (Q2) collection of finger-prick blood sample; (Q3) application of sample to test; (Q4) application of test solution to the lateral flow device; (Q5) development of a control line and interpretation of results; (Q6) instructions for use; (Q7) risks and warnings. We considered that all questions in the survey that were related to UX. Questions not describing the usability constructs, Q1a, Q2d, Q2e, Q2f, Q4d, Q7a, Q7b, Q7c and Q7d, were removed for the usability analysis. The ratings for the questions in a section were counted and normalised as a percentage to provide a UX or usability score.

Age and education. A key concern for the LFIA self-testing is to ensure that the testing kit is inclusive and usable to as many members of the public as possible, including the older population and those with lower educational attainment. To study whether the scores were affected by age or education levels, we categorised the participants into four age groups (8-17, 18-30, 31-60 and age above 60) and four educational attainments (Master/PhD, Honours Degree, A-level/NVQ (National Vocational Qualifications) and Primary/Secondary/Other education). The range and the size of each age group are given in Table 1. Since older people generally suffer more by

the SARS-CoV-2 virus due to their relative weak immune system, and that younger children may need assistance from a parent/guardian, we had additional discussion for these cohorts (those aged 8-17 and those aged over 60).

Statistical analysis. Statistical analysis was carried out to assess whether the UX and usability scores were independent of the education and the age of the participant based on the Wilcoxon rank-sum tests (for data that were not normally distributed). The Bonferroni correction[22] was applied to adjust the significance level during multiple hypothesis testing.

Kappa statistic[23–25] was used to evaluate the agreement between the participant and researcher interpreted results, which has been the metric of choice in a home-based COVID-19 antibody self-testing study[8] and HIV rapid diagnostic tests[26–28]. (Kappa score was calculated using MATLAB source code[29]). The range of Kappa scores can be interpreted as follows[30] :< 0 = poor agreement, 0.00–0.20 = slight agreement, 0.21–0.40 = fair agreement, 0.41–0.60 = moderate agreement, 0.61–0.80 = substantial agreement, and> 0.8 = almost perfect agreement. The agreement rate was also measured by the percentage of cases where the participant and the researcher agreed when interpreting the test result.

Text analysis. Text analysis was performed on the participants' comments using natural language processing (NLP) techniques, in which each comment was considered as a single document and all comments are considered as the corpus. The processing steps included: (1) the actual number of comments was determined by removal of empty documents; (2) texts were tokenized to break up the comments and represent them as a collection of words; (3) the words were lemmatised, a process of normalisation to reduce words to their root form, e.g. "disposal" and "dispose" become "dispos"; (4) punctuation was erased; (5) stop words (such as "and", "of", and "the") were removed; (6) words with two or fewer characters and words with 15 or more characters were removed. After processing, a bag-of-words (BoW) was created to present the word frequency in each comment. The importance of a word in the document can be ranked by the word frequency. The concept of BoW was initially used in a linguistic context[31] but has been widely used for text classification[32] and computer vision[33]. The latent Dirichlet allocation (LDA) model[34] was applied to the BoW to discover the topics based on the word probabilities. The number of topics for all comments was estimated based on comparing the goodness-of-fit of LDA models. The word clouds were used to visualise the key topics learned from users feedback by LDA.

All data analyses were performed using MATLAB (MathWorks, USA) and Microsoft Excel for Microsoft365 (MSO 32-bit).

Ethical approval. This study was approved by Ulster University Institutional Ethics committee (Ref: REC/20/0043) in full adherence to the Declaration of Helsinki. All participants provided fully informed consent. Informed consent for children in this study was obtained from their parents/guardian.

Results

Characteristics of study participants. Initially 2100 individuals were invited to take part, which included participants from a database of individuals who expressed an interest in taking part in the research alongside individuals who had previously volunteered and had been shown to have antibodies to SARS-Cov-2 virus. Not everyone who made a booking participated, some attended but were excluded if a consent form was missing. The final dataset for this study included 1544 participants and the characteristics are provided in Table 1, which presents the proportion of participants in gender, age, education and ethnicity.

The histograms of age distribution (for male and female) are presented as in Fig. 3a. It is noticed that female participants were over-represented in middle-age groups, which was due to the fact that we had more female volunteers than male (as shown in Table 1 that 60% of 1544 participants are females). The percentages of participants in four educational groups are shown in Fig. 3b, which shows fewer participants in Primary/Secondary/Other education (shown as 'Other') than other groups. However, every effort has been made to achieve as balanced an overall cohort as possible.

Ease of use. The participants were asked to give scores from 1 to 5 for 28 Likert style questions in seven sections of the questionnaire (provided in Supplementary Information) and 1539 provided the scores. The seven sections were devoted to specific aspects of the testing kit. The participants' scores for each question were counted and the percentage of the counts are provided in Table 2.

To assess the overall UX scores for each section of the questionnaire, the summative scores (sum of ratings for all questions normalised as a percentage) for 1539 participants in each section were calculated and the mean and standard errors are presented in Fig. 4a. The means for each section are higher than 92.5% with an overall average of 96.03% (SD = 0.05, 95% CI 95.05-97.01%). The results suggest an overall good user experiences by the public although the testing experience for the collection of the blood sample (Q2) and the application sample to the test (Q3) will need further improvement in the future.

To assess the usability, we removed the questions Q1a, Q2d, Q2e, Q2f, Q4d, Q7a, Q7b, Q7c and Q7d which were not related to the usability construct, and then calculated the summative scores for the remaining 20 questions. The results of usability scores with mean and standard errors are given in Fig. 4b. The means for each section are higher than 94.2% with an overall average of 96.66% (SD = 0.2, 95% CI 93.03-95.37%). It is noticed that section Q2 (relates to collection of the blood sample) has the second highest usability score but the lowest UX score, for the rest, the order of scores (from high to low) remains unchanged. The reason for this was due to usability analysis excluded Q2d and Q2e. From Table 2, we can see that participants scored relatively low for Q2d ("The correct amount of blood was collected from the finger prick puncture") and Q2e ("The bleeding stopped without the need to apply pressure"), which suggest they were the difficult areas in user experience.

Characteristics	Groups	Proportions n (%)
Number of Participants	All	1544 (100)
Gender	Male	613 (39.7)
	Female	927 (60.0)
	Other	4 (0.3)
Age [8-85, 47 ± 14.1]	8–17 (11.8 ± 3.7)	20 (1.3)
	18–30 (25.9 ± 3.5)	191 (12.4)
	31–60 (45.4 ± 8.3)	1046 (67.7)
	60+ (66.9 ± 4.9)	287 (18.6)
Education	PhD	76 (4.9)
	Master's	362 (23.4)
	Honours Degree	539 (34.9)
	A-Level / NVQ	307 (19.9)
	Secondary School Education	186 (12.1)
	Some Secondary Education	36 (2.3)
	Primary Education	7 (0.5)
	Other Education	31 (2.0)
Ethnicity	White	1530 (99.1)
	Mixed	5 (0.32)
	Asian / Chinese / British Asian	4 (0.26)
	White African	1 (0.064)
	A-level / NVQ	1 (0.064)
	Middle East	1 (0.064)
	Irish Traveler	1 (0.064)
	Other	2 (0.128)

Table 1. Characteristics of study participants. The values for age are presented in the range (mean ± standard deviation (SD)).

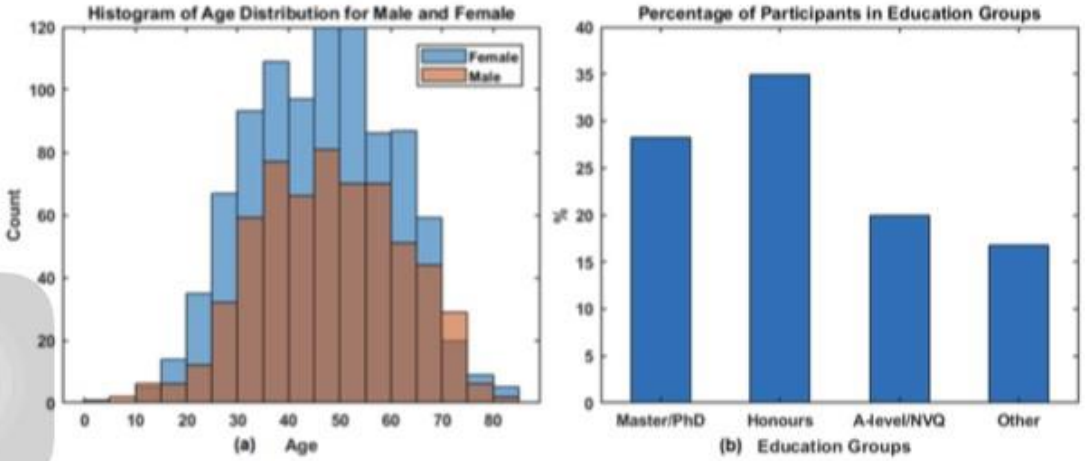

Figure 3. (**a**) The histogram of age distribution for female and male participants; (**b**) percentage of participants in four education groups.

Use of resource. Question Q2f and Q6f assessed the efficiency in use of resource. Q2f asked whether the second lancet was required for the test, in which 19.95% (307 of 1539) answered 'yes'. We cross-examined how many of those required the second lancet in each age group and the results are summarised in Table 3. It appears that the highest proportion 32% (46 of 190) comes from the young adult age group 18-30. Moreover, age groups 8-17 and those over 60 years old appeared to have the least need for a second lancet when compared to the other groups. No statistical significance was found (Chi-square tests p-values provided in Supplementary Table.S6).

Question Q6f asked how many times the participant consulted the instructions during the test. We cross examined the answers from the participants in the four age groups and the results are given in Table 4. The

	Questions	Score count (%)				
		1	2	3	4	5
Q1a	Did the packaging provide sufficient protection to the kit materials?	0.06	0.06	0.13	1.75	97.99
Q1b	Were the kit materials easily accessed?	0.13	0.39	1.10	3.70	94.67
Q1c	Did the packaging provide clear information to the type of test and materials inside?	0.13	0.45	1.04	3.25	95.13
Q2a	The lancet was easily identified.	0.32	0.39	0.97	2.86	95.45
Q2b	The lancet cap was easy to remove.	0.32	0.26	1.88	6.43	91.10
Q2c	The fingerpick puncture was easy to perform.	1.10	0.97	4.55	6.50	86.87
Q2d	The correct amount of blood was collected from the fingerpick puncture.	3.05	4.48	8.32	8.38	75.76
Q2e	The bleeding stopped without the need to apply pressure.	10.33	5.13	10.27	6.04	68.23
Q2f	The second lancet was required to be used.	Yes	19.95		No	80.05
Q3a	The test device was easily identified.	0.32	0.39	0.45	2.08	96.75
Q3b	The test was easy to remove from the foil packaging.	0.84	0.97	2.86	4.48	90.84
Q3c	The correct place to apply the sample ('sample hole') was easily identified.	0.26	0.26	1.36	3.38	94.74
Q3d	The blood was easily expelled from the blood collector to the test.	8.38	7.47	10.33	8.71	65.11
Q4a	The test solution was easily identified.	0.71	0.39	0.71	2.40	95.78
Q4b	The twist cap was easy to remove.	1.56	1.36	4.55	7.34	85.19
Q4c	The test solution was easily applied to the sample hole on the device.	0.58	1.36	4.55	7.47	86.03
Q4d	There was no test solution left in the container.	0.32	0.32	0.52	1.95	96.88
Q5a	Clearly understood that the C line is a control line.	3.38	0.78	1.82	1.82	92.20
Q5b	Clearly understood that the T line is a test line.	2.99	0.65	1.69	1.69	92.98
Q5c	A control line was easily identified within the test window.	0.65	0.20	0.52	1.24	97.40
Q5d	Results were easily interpreted based on the information provided in the instructions.	1.43	1.04	1.30	1.82	94.41
Q6a	The instructions provided were easy to follow.	0.32	0.45	1.62	4.29	93.31
Q6b	The user steps were simple and easy to perform.	0.26	0.39	1.56	5.26	92.53
Q6c	The items in the kit were appropriately labelled.	2.79	1.95	4.09	6.43	84.73
Q6d	The test is in an easy to use format.	0.06	0.45	1.43	5.72	94.41
Q7a	The lancet was understood to contain a needle.	1.36	0.78	2.21	2.47	93.18
Q7b	The risks associated with the lancet was clearly understood.	2.60	1.30	2.21	2.34	91.55
Q7c	The potential for small components to be a choking hazard was clearly understood.	4.16	1.88	3.12	2.86	87.98
Q7d	The importance of disposing the kit materials in general waste and not within the recycling was understood.	2.92	1.43	2.53	2.73	90.38

Table 2. The questions and participants' score counts in % (n=1539).

majority 74.2% (1142 of 1539) participants consulted the instructions 1-3 times, 299 of 1539 needed to refer to the instructions 4-6 times, 64 participants read the instructions 6-9 times and 34 did more than 10 times. Among the 34 people who consulted the instructions at least 10 times, only 2.9 % (1 of 34) were aged under 18, 23.5% (8 of 34) were over 60 years old, and age group 31–60 refer to instructions more frequently than other groups (significance was found in Chi-square tests results given Supplementary Table S7).

Age groups and education levels. The boxplot of average summative scores for the different groups are presented in Fig. 5: (a) UX scores by education group; (b) usability scores by education groups; (c) UX scores by age groups and (d) usability scores by age groups, respectively. In the boxplot, the central line indicates the median, whilst the bottom and top lines represent the 25*th* and 75*th* percentiles, respectively, (with outliers plotted as an asterisk).

To assess whether the scores have a normal distribution, one-sample Kolmogorov-Smirnov tests were performed for each group and all results show a $p < 0.001$, which suggest that the scores do not have a standard normal distribution. (The histogram for UX scores and usability scores for education and age groups are provided from Supplementary Figure S.1 to Figure S.4. Therefore the paired Wilcoxon rank sum tests were applied to access the medium differences between the groups. Bonferroni corrections were used for multiple hypothesis testing, hence the significance level α was as $0.05/6 = 0.0083$.

The p-values of differences in results for education groups are given in Tables 5 and 6, and those for the age groups are presented in Tables 7 and 8. No significant differences were found between age groups and education groups. The results based on the data collected for this study show that the UX scores and usability scores are independent of users' age and educational attainment. However, this is based on the dataset that lacks representation from some groups, such as age 8-17 and those with primary or secondary education, the current finding could be improved by recruiting more participants in these groups in a future study.

Free text analysis: factors to consider for enhancing usability. The topics in free text learned by the LDA model[34] are presented by word clouds in Supplementary Figure S.5, which suggest the key topics including

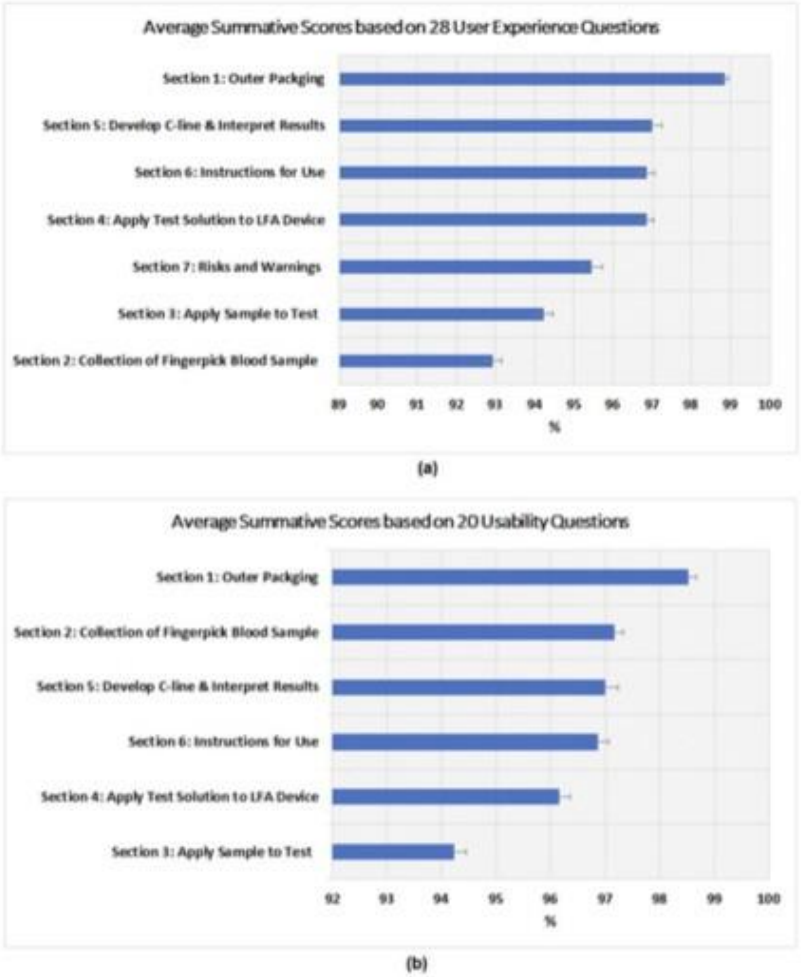

Figure 4. Average summative scores for 1539 responses based on: (**a**) all 28 UX questions; (**b**) 20 questions related to usability construct only. The error bars represent the standard errors.

Second lancet needed	Age: 8–17	Age: 18–30	Age: 31–60	Age: 60+	Total
Yes	3	46	206	52	307
No	17	144	837	234	1232
Ratio (Yes/No)	0.18	0.32	0.25	0.22	0.25

Table 3. Number of participants in four age groups that required the second lancet to complete the test.

Times consulted instruction	Age: 8–17	Age: 18–30	Age: 31–60	Age: 60+	Total
1–3	15	137	769	221	1142
4–6	4	44	200	51	299
7–9	0	8	50	6	64
10+	1	1	24	8	34

Table 4. Number of times the participants consulted the instructions in four age groups.

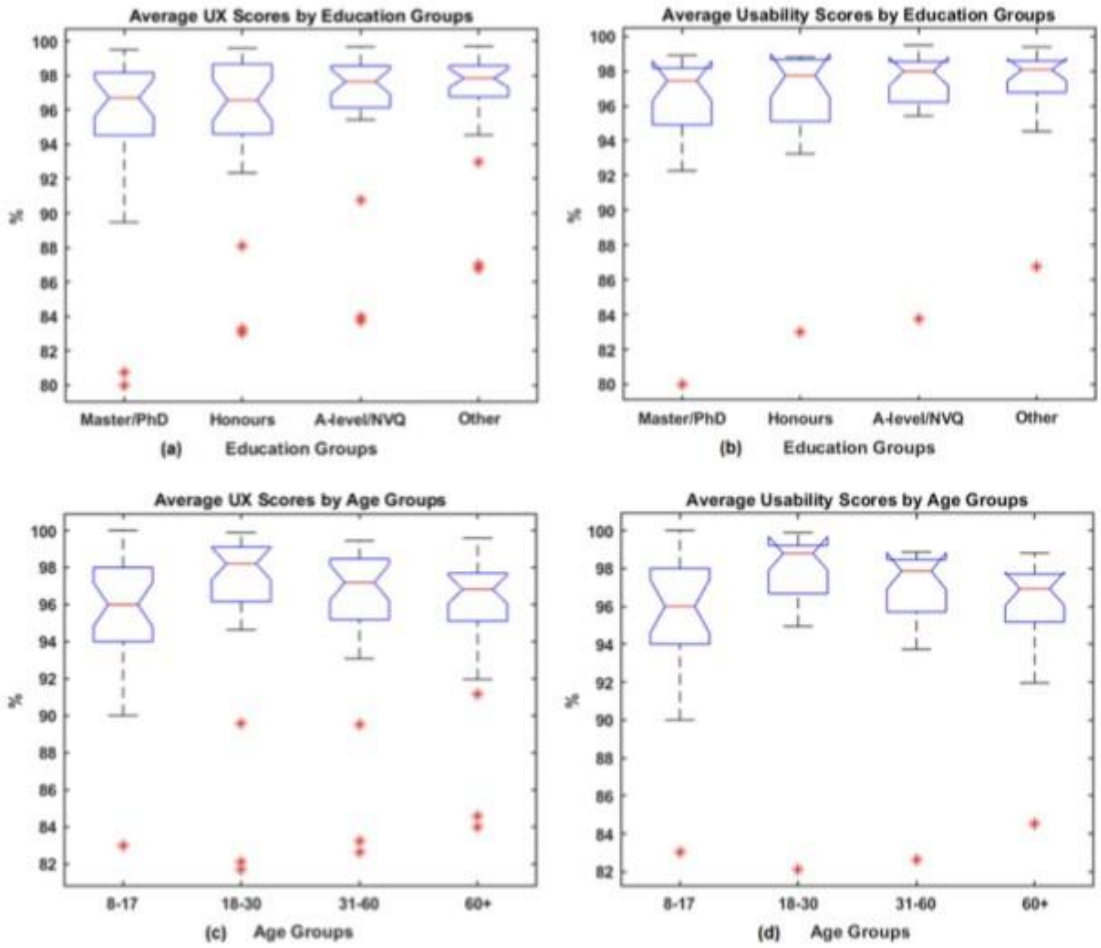

Figure 5. Boxplot for average of: (a) UX scores by education groups; (b) Usability scores by education groups; (c) UX scores by age groups and (d) Usability scores by age groups.

Education groups	Master/PhD	Honours	A-levels	Other
Master/PhD	1	–	–	–
Honours	0.6288	1	–	–
A-Levels	0.1030	0.2547	1	–
Other	0.0701	0.2315	0.7369	1

Table 5. *P* values based on paired Wilcoxon tests for UX scores in four education groups.

Education groups	Master/PhD	Honours	A-levels	Other
Master/PhD	1	–	–	–
Honours	0.5427	1	–	–
A-levels	0.1895	0.4734	1	–
Other	0.1197	0.4651	0.7557	1

Table 6. P-values based on paired Wilcoxon tests for usability scores in four education groups.

Age groups	8–17	18–30	31–60	60+
8–17	1	–	–	–
18–30	0.1061	1	–	–
31–60	0.5384	0.0868	1	–
60+	0.5602	0.0338	0.4173	1

Table 7. P-values based on paired Wilcoxon tests for UX scores from four age groups.

Age groups	8–17	18–30	31–60	60+
8–17	1	–	–	–
18–30	0.0598	1	–	–
31–60	0.2848	0.0601	1	–
60+	0.5070	0.0114	0.1332	1

Table 8. P-values based on paired Wilcoxon tests for usability scores from four age groups.

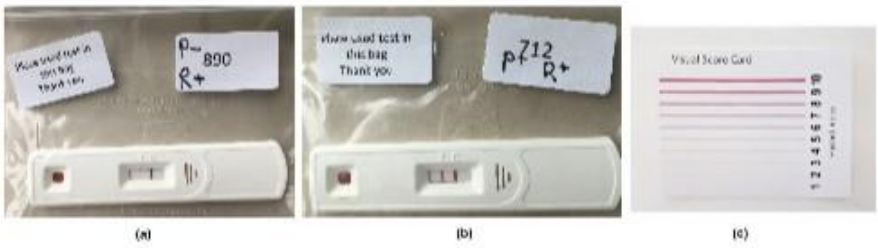

(a) (b) (c)

Figure 6. Examples of two test kits placed in the polyester bag (to prevent cross-contamination): (**a**) participant's result read as negative (P-) and researcher's was positive (R+); (b) both participant and researcher's results were positive (P+ and R+); (**c**) a visual score card for T-lines.

'blood', 'video', 'lancet', 'line', 'bubble', 'instruction', 'test' and 'sample'. The examples of user comments in each of five comment sections are provided in Supplementary Tables S1 to S5, which include: (1) key words based on word frequency; (2) the popularity of the key word, in which the proportion shows the percentage of the comments mentioned this word related to total users; and (3) representative samples of user comments related to the key word.

The analysis of user comments on applying sample to test (Q3; Supplementary Table S1) suggest a total of 26.58% (421 of 1544) subjects provided a free text response, in which 44.90% (189 of 421) were related to the 'blood', and specifically 25% of 421 related to the blood collector. The analysis of the text responses based on the application of test solution to the lateral flow device (Q4) are summarised in Supplementary Table S2. A total of 16.90% (261 of 1544) subjects provided a response, and 29.50% of 261 related to (blood) bubbling leaving the transfer device which made transfer difficult, and 23.75% of 261 were related to the issues with the test solution. The analysis of the user comments related to the control line and the interpretation of the test result (Q5: Supplementary Table S3) show that a total of 15.22% (235 of 1544) commented on this aspect and 22.55% of 235 were related to the lines in the test. The responses related to instructions (Q6: Supplementary Table S4) suggest that a total of 22.60% (349 of 1544) provided a response to this question, in which 109 of 349 pointed out the importance of the video to demonstrate the test. Finally, the analysis of free text related to the potential misuse of the testing kit (Q8: Supplementary Table S5). A total of 31.99% (494 of 1544) subjects provided comments, where 84.82% of 494 reported no issues found, 9.31% of 494 were related to the potential misuse of the spare lancet and 2.02% of 494 were related to the supervision of children when self-administering the test .

Agreement between participant-interpreted and researcher-interpreted results. Two examples of the test kit is given in Fig. 6, in which the test kit was placed in a polyester bag to prevent cross-contamination. Fig. 6a shows an example that the result from participant was negative (indicated as 'P-' on the bag) and researcher read it as positive ('R+'). It can be seen that the T-line was difficult to read even when the picture was taken under good light condition. Fig. 6b shows an example with both participant and researcher's results were positive (P+ and R+). Fig. 6c presents a visual score card for T-lines according to the level of antibodies present in the blood. It can be seen that a T-line that is attributed a score of 1/10 is a relatively faint line.

	Researcher results n(%)			
	Positive	Negative	Invalid	Total
Participant results				
Positive	109 (7.1)	2 (0.1)	0 (0.0)	1431 (92.7)
Negative	62 (4.0)	1369 (88.7)	0 (0.0)	111 (7.2)
Invalid	0 (0.0)	0 (0.0)	1 (0.1)	1 (0.1)
Total	171 (11.0)	1371 (88.9)	1 (0.1)	1543 (100)

Table 9. Results based on self-test in cars interpreted by the participants and the researchers. The values in the brackets show the percentage of the results related to total number of results (n=1543).

It was difficult to read the test results due to the difficult weather conditions and the need to put samples within a translucent plastic bag, especially for those faint T-lines due to low signal intensity. Interpretation of any queried results, e.g. a very weak T-line, was undertaken by three highly experienced LFIA users. These consisted in the most part of faint test lines (scored 1/10 in visual score card in Fig. 6c) that are difficult to read and perhaps reflective of the level of antibodies present in the blood of subjects who may have been infected in March 2020 during the first wave of COVID-19 within Northern Ireland whilst this study was conducted in September 2020 almost 6 months later.

The participants' self-testing results were compared to those obtained from the researchers. The results of agreement are presented in Table 9. Among 1544 participants, one test failed and one result from the researcher was lost. A total of 1478 of 1542 participants interpreted the result in the same way as the corresponding researchers. The observed agreement rate is 95.85% [95% CI 94.85 – 96.85%] with the Kappa score of 0.75 [95% CI 0.69–0.81], which suggests substantial agreement in the results interpreted by participants and researchers.

Discussion

This paper presented the findings of UX analysis for a LFIA self-testing kit to identify COVID-19 antibodies used by 1544 participants from Northern Ireland. The UX analysis assessed the scores obtained from different age and education groups, the agreement between the results interpreted by participants and researchers, and identified the potential issues of the testing kit. The results suggest a substantial agreement (Kappa score 0.75) between members of the public and the researchers in the interpretation of the antibody testing kit results. The agreement rate is consistent with another recent study[8] based on LFIA self-testing at home.

The difficulties in interpreting results appear to be one of the common issues reported in the usability studies for LFIA testing[4,5,7,8]. In this study, there were 62 of 1543 (4.02%) participants who interpreted the results as negative but the researcher queried the results as positive. The misinterpretation of the tests could be due to many reasons including environmental issues (test results being viewed through a weather protecting polyester bag under poor light), or ambiguous T-lines with low signal intensity which may occur with very low levels of antibodies being present in the test result. The comments received by participants also suggest that the T-line with low intensity may confuse the users to determine whether the result corresponded to a positive result.

In a related study[8] for the home based COVID-19 antibody self-testing, the clinician interpretations of the results were based on inspecting a photograph of the test received from the participants as opposed to having the physical test available. This was different to our study where the researchers interpreted the result based on having the physical test available, which is arguably higher fidelity given that photographs are resolution dependent, and that the lighting environments and exposure may affect the photo capture of faint lines in the test result. For example, we noted that faint lines (typically scored a 1/10 using an approved score card from the manufacturer) were visible to the naked eye but not visible on a photograph. Nevertheless, our study achieved a similar agreement rate to the rate reported in the related study[8].

This study provided scope for future work to improve self-administered tests. One area for improvement highlighted by this user experience study would be to avoid members of the public misinterpreting some positive results as a negative result. Improvements in the LFIA conjugation protocols or media type can enhance the brightness of the lines at low antibody levels but this can be at the expense of false positives. Improving the instructions can help, which can include more information regarding the variation of line intensities to help the users make the correct decision or including simple improvements to the visual format of the instructions. Alternatively, some studies have proposed the use of a machine learning based approach to automatically read the result for LFIA testing via smartphone technology[35,36]. The smartphone 'app' can assist users and indeed help reduce the uncertainty in their interpretation by comparing pixel intensities after detecting the T-line as the region of interest, although the performance of the algorithm might be affected by poor lighting. More advanced systems could incorporate deep learning approaches[37–39] and the complementary metal-oxide semiconductor (CMOS) reader to reading the results[39].

One noticeable limitation of this study was that we did not use the industry standard usability measures, such as two widely used and psychometrically validated measures of usability, System Usability Scale (SUS)[40] and the Usability, Satisfaction, Effectiveness scale (USE)[41]. This was due to the fact that we found some of SUS or USE questions inappropriate for this study. For example, one SUS question states: "I think that I would like to use this system frequently", which is not applicable to the LFA testing for Covid antibody. Some USE questions for

'Usefulness' are not suitable for this study, such as 'It helps me be more effective', 'It helps me be more productive', 'It gives me more control over the activities in my life', and 'It makes the things I want to accomplish easier to get done'.

We notice that there is a lack of well-defined measurement metrics for UX and usability related to LFIA self-testing. Most related studies[2,4,7,8] focused on assessment of accuracy in interpreting test results and tried to identify the issues based on the feedback received from the questionnaire. Therefore, we applied self-defined measurements for UX and usability because the purpose of this study was not only to assess the ease of use the testing kit (usability), but also to identify the difficult areas or warnings from the user experiences. We believe that the outcomes from the UX analysis provided the valuable information for the future studies. Furthermore, there are other scales that are arguably related to UX that could be used, for example the NASA TLX scale[42] can be used to assess the mental workload, which will be considered in the future study.

In addition, although we were able to randomly select individuals from each age/gender group to best represent the NI population, due to the restraints of responses to recruitment, some groups were over-represented (females) while other groups were under-represented (males). In terms of age distribution, as shown in Figure S.6, 13.18% of NI population (1.8 millions) are age 8-17 and 18.73% are age over 60 (according to NI 2011 Census[43]). For this study, we have 18.6% (of 1544) from group of age over 60 which is similar to the figure from NI population, however, we only have 1.3% participants in group 8-17 due to the difficulties in recruitment. Also more volunteers with primary or secondary education will need to be included in order to strengthen the finding that the test kit is user-friendly, independent of age and education.

One of other limitations includes the fact that the test was carried out in a university car park within a car. Cars are not the ideal environment to self-administer tests, especially if the lighting is poor, however this was difficult to control during the pandemic due to safety concerns and logistics of conducting such research during strict lockdown controls. Another limitation is that the survey was comprised of a large set of questions where subjects could have questionnaire fatigue, which can affect the veracity of some of the answers that are provided towards the end of the survey. Moreover, the survey consisted of Likert rating style questions where each question had a positive connotation. Hence, the highest rating of 5 is always denoted as a positive score, and the questions could suffer from this type of bias towards positive ratings.

Nevertheless, members of the public provided very high ratings regarding the usability of the kit and the ratings are independent of user age and education attainment. This suggests that the kit can be used as a user-friendly device for widespread use in the population. The user comments also suggest that the utility of the video was helpful for displaying the instructions and for providing an intuitive way to demonstrate how to use the kit, also the importance of providing the tray for using this kit in a car environment. Future work is also needed to improve the collection of the blood sample and the application sample to the test. Testing the UX of the kit may be conducted from an accessibility point of view, such as amongst people with hearing or visual impairments or indeed with intellectual disabilities.

Conclusion

We conducted a user experience study of a self-administered SARS-CoV-2 antibody test in cars based on a total of 1544 members of the public in Northern Ireland. The statistical analysis found substantial agreement between the results interpreted by participants and researchers. The participants also perceived the kit to be user-friendly by providing high ratings in the post-test questionnaire. The user feedback identified that some areas need improvement, such as collecting blood samples and applying the sample to the test which are two areas that the participants found more difficult, as well as faint test lines which may cause misinterpretations of the result. In conclusion, the results from the user experience analysis are encouraging, and the findings will help to improve the design of SARS-CoV-2 antibody testing kits and inform protocols for future UX studies.

Received: 19 February 2021; Accepted: 7 June 2021
Published online: 07 July 2021

References

1. Sheridan, C. Coronavirus testing finally gathers speed. *Nature Biotechnology News* (2020-11-05).
2. Boxer, J., Weddell, S., Broomhead, D., Hogg, C. & Johnson, S. Home pregnancy tests in the hands of the intended user. *J. Immunoass. Immunochemistry* **40**, 642–652 (2019).
3. Valanis, B. G. & Perlman, C. S. Home pregnancy testing kits: prevalence of use, false-negative rates, and compliance with instructions. *Am. J. Public Health* **72**, 1034–1036 (1982).
4. Peck, R. B. *et al.* What should the ideal HIV self-test look like? a usability study of test prototypes in unsupervised HIV self-testing in kenya, malawi, and south africa. *AIDS Behav.* **18**, 422–432 (2014).
5. Ndlovu, Z. *et al.* Diagnostic performance and usability of the visitect cd4 semi-quantitative test for advanced HIV disease screening. *PLoS ONE* **15**, e0230453 (2020).
6. Rodriguez, N. M. *et al.* based rna extraction, in situ isothermal amplification, and lateral flow detection for low-cost, rapid diagnosis of influenza a (H1N1) from clinical specimens. *Anal. Chem.* **87**, 7872–7879 (2015).
7. Flower, B. *et al.* Clinical and laboratory evaluation of SARS-CoV-2 lateral flow assays for use in a national COVID-19 seroprevalence survey. *Thorax* (2020).
8. Atchison, C. *et al.* Usability and acceptability of home-based self-testing for Severe Acute Respiratory Syndrome (SARS-CoV-2) antibodies for population surveillance. *Clin. Infect. Dis.* **72**, e384–e393 (2020).
9. Deeks, J. J. *et al.* Antibody tests for identification of current and past infection with SARS-CoV-2. *Cochrane Database Syst. Rev.* **6**, 1-306 (2020).
10. Pollán, M. *et al.* Prevalence of SARS-CoV-2 in spain (ene-covid): a nationwide, population-based seroepidemiological study. *The Lancet* **396**, 535–544 (2020).

11. Iyer, A. S. *et al.* Persistence and decay of human antibody responses to the receptor binding domain of SARS-CoV-2 spike protein in COVID-19 patients. *Sci. Immunol.* **5**, eabe0367, 1-13 (2020).
12. Isho, B. *et al.* Persistence of serum and saliva antibody responses to SARS-CoV-2 spike antigens in COVID-19 patients. *Sci. Immunol.* **5**, (2020).
13. Torjesen I. Covid-19: Home testing programme across England aims to help define way out of lockdown. *BMJ.* **369**: m1799, (2020).
14. Abingdon Health. UK COVID-19 rapid antibody tests approved for professional use. *Company News* (2020-07-30).
15. Sonderegger, A., Schmutz, S. & Sauer, J. The influence of age in usability testing. *Appl. Ergon.* **52**, 291–300 (2016).
16. Abingdon Health instruction video. *Youtube* https://youtu.be/WqT2z8jCEHs *(2020).*
17. Bevan, N. Iso 9241: Ergonomic requirements for office work with visual display terminals (vdts)-part 11: Guidance on usability. *Ti* **159**, 61 (1998).
18. Bevan, N. What is the difference between the purpose of usability and user experience evaluation methods. In *Proceedings of the Workshop UXEM*, vol. 9, 1–4 (Citeseer, 2009).
19. Alben, L. Quality of experience: defining the criteria for effective interaction design. *Interactions* **3**, 11–15 (1996).
20. Hassenzahl, M. & Wessler, R. Capturing design space from a user perspective: the repertory grid technique revisited. *Int. J. Hum–Comput. Interact.* **12**, 441–459 (2000).
21. Hassenzahl, M. & Tractinsky, N. User experience-a research agenda. *Behav. Inf. Technol.* **25**, 91–97 (2006).
22. Weisstein, E. W. Bonferroni correction. *MathWorld-A Wolfram Web Resource*. https://mathworld.wolfram.com/ (2004)
23. Cohen, J. A coefficient of agreement for nominal scales. *Educ. Psychol. Meas.* **20**, 37–46 (1960).
24. Fleiss, J. L., Levin, B. & Paik, M. C. *Statistical Methods for Rates and Proportions* (Wiley, 2013).
25. Viera, A. J. *et al.* Understanding interobserver agreement: the kappa statistic. *Fam. Med.* **37**, 360–363 (2005).
26. Lee, V. J. *et al.* User acceptability and feasibility of self-testing with HIV rapid tests. *JAIDS J. Acquir. immune Defic. Syndromes* **45**, 449–453 (2007).
27. Figueroa, C. *et al.* Reliability of HIV rapid diagnostic tests for self-testing compared with testing by health-care workers: a systematic review and meta-analysis. *The lancet HIV* **5**, e277–e290 (2018).
28. Kurth, A. E. *et al.* Accuracy and acceptability of oral fluid HIV self-testing in a general adult population in Kenya. *AIDS Behav.* **20**, 870–879 (2016).
29. Cardillo, G. Cohen's Kappa: compute the Cohen's kappa ratio on a square matrix. *GitHub* https://github.com/dnafinder/Cohen *(2007).*
30. McHugh, M. L. Interrater reliability: the kappa statistic. *Biochem. Med. Biochem. Med.* **22**, 276–282 (2012).
31. Harris, Z. S. Distributional structure. *Word* **10**, 146–162 (1954).
32. Sriram, B., Fuhry, D., Demir, E., Ferhatosmanoglu, H. & Demirbas, M. Short text classification in twitter to improve information filtering. In *Proceedings of the 33rd International ACM SIGIR Conference on Research and Development in Information Retrieval*, 841–842 (2010).
33. Sivic, J. & Zisserman, A. Efficient visual search of videos cast as text retrieval. *IEEE Trans. Pattern Anal. Mach. Intell.* **31**, 591–606 (2008).
34. Blei, D. M., Ng, A. Y. & Jordan, M. I. Latent dirichlet allocation. *J. Mach. Learn. Res.* **3**, 993–1022 (2003).
35. Eltzov, E. *et al.* Lateral flow immunoassays-from paper strip to smartphone technology. *Electroanalysis* **27**, 2116–2130 (2015).
36. Quesada-González, D. & Merkoçi, A. Mobile phone-based biosensing: an emerging "diagnostic and communication" technology. *Biosens. Bioelectron.* **92**, 549–562 (2017).
37. Zeng, N., Wang, Z., Zhang, H., Liu, W. & Alsaadi, F. E. Deep belief networks for quantitative analysis of a gold immunochromatographic strip. *Cognit. Comput.* **8**, 684–692 (2016).
38. Carrio, A., Sampedro, C., Sanchez-Lopez, J. L., Pimienta, M. & Campoy, P. Automated low-cost smartphone-based lateral flow saliva test reader for drugs-of-abuse detection. *Sensors* **15**, 29569–29593 (2015).
39. Jing, M. *et al.* Enhance categorisation of multilevel high-sensitivity cardiovascular biomarkers from lateral flow immunoassay images via neural networks and dynamic time warping. In *2020 IEEE International Conference on Image Processing (ICIP)*, 365–369 (IEEE, 2020).
40. Brooke, J. SUS: a "quick and dirty'usability. In Jordan, P. W., Thomas, B., McClelland, I. L. & Weerdmeester, B. (eds.) *Usability evaluation in industry*, 189–194 (CRC press, 1996).
41. Lund, A. M. Measuring usability with the use questionnaire12. *Usability Interface* **8**, 3–6 (2001).
42. Hart, S. G. & Staveland, L. E. Development of NASA-TLX (Task Load Index): results of empirical and theoretical research. In *Advances in Psychology*, vol. 52, 139–183 (Elsevier, 1988).
43. NISRA. 2011 Census Population Tables. *Northern Ireland Statistics and Research Agency (NISRA)* https://www.nisra.gov.uk/publications/2011-census-population-tables *(2014).*

Acknowledgements

We are extremely grateful to all the people of Northern Ireland who took part in this study during the pandemic. We acknowledge Dr. Tony Byrne for use of the Safe Water laboratory and Professor Gareth Davison for laboratory space and equipment during the pandemic within a locked down University. We also acknowledge the European Union's INTERREG VA Programme (Grant ID:IVA5034, managed by the Special EU Programmes Body (SEUPB)) funding associated with Eastern Corridor for Medical Engineering (ECME) in relation to data analysis and UK-RTC provided the test kits and funding of expenses. Finally, we appreciate all the comments from the reviewers which enabled us to improve the presentation and scientific contribution of this work.

Author contributions

T.M. and J.ML. designed, coordinated and supervised the project, participated in interpretation of results and provided the critical comments for the manuscript; R.B. designed the research questions, supervised the data analysis and participated in interpretation of results and drafting the manuscript; M.J. conducted the data analysis including technical implementation and interpretation of results, drafted the manuscript with inputs from all authors; A.N., R.P. participated in participants recruiting, collected the original post-study data; T.M., A.N., L.R., J.M., A.K. and R.P. obtained ethical approval, coordinated car park data collection and ensured adherence to all research governance issues; W.B. designed and controlled the data base and digitalised all original post-study data for analysis; All authors reviewed and provided comments for the manuscript, read and approved the final version of the manuscript.

Appendix VII

Clinical Immunology Communications 2 (2022) 130–135

Contents lists available at ScienceDirect

Clinical Immunology Communications

journal homepage: www.elsevier.com/locate/clicom

Full Length Article

Evaluation of the performance of a lateral flow device for quantitative detection of anti-SARS-CoV-2 IgG

J.S. Moore [a,b], L.J. Robertson [a,b], R. Price [a], G. Curry [a,b], J. Farnan [c], A. Black [c], M.A. Nesbit [a,b], J.A. McLaughlin [b,d], T. Moore [a,b,*]

[a] Biomedical Sciences Research Institute, Ulster University, Northern Ireland, United Kingdom
[b] Integrated Diagnostics Laboratory, Ulster University, 3-5a Frederick St, Belfast, Northern Ireland, United Kingdom
[c] The Group Surgery, 257 North Queen Street, Belfast, Northern Ireland, United Kingdom
[d] Nanotechnology and Integrated Bioengineering Centre, Ulster University, Northern Ireland, United Kingdom

ARTICLE INFO

Keywords:
SARS-CoV-2
Lateral flow immunoassay
Antibody
Vaccine
Variant

ABSTRACT

Introduction: The AbC-19™ lateral flow immunoassay (LFIA) performance was evaluated on plasma samples from a SARS-CoV-2 vaccination cohort, WHO international standards for anti-SARS-CoV-2 IgG (human), individuals ≥2 weeks from infection of RT-PCR confirmed SARS-CoV-2 genetic variants, as well as microorganism serology.

Methods: Pre-vaccination to three weeks post-booster samples were collected from a cohort of 111 patients (including clinically extremely vulnerable patients) from Northern Ireland. All patients received Oxford-AstraZeneca COVID-19 vaccination for the first and second dose, and Pfizer-BioNTech for the third (first booster). WHO international standards, 15 samples from 2 variants of concern (Delta and Omicron) and cross-reactivity with plasma samples from other microorganism infections were also assessed on AbC-19™.

Results: All 80 (100%) participants sampled post-booster had high positive IgG responses, compared to 38/95 (40%) participants at 6 months post-first vaccination. WHO standard results correlated with information from corresponding biological data sheets, and antibodies to all genetic variants were detected by LFIA. No cross-reactivity was found with exception of one (of five) Dengue virus samples.

Conclusion: These findings suggest BNT162b2 booster vaccination enhanced humoral immunity to SARS-CoV-2 from pre-booster levels, and that this antibody response was detectable by the LFIA. In combination with cross-reactivity, standards and genetic variant results would suggest LFIA may be a cost-effective measure to assess SARS-CoV-2 antibody status.

Introduction

The SARS-CoV-2 pandemic has been ongoing since 2019. The vaccination programme for the population of the United Kingdom commenced in December 2020. Since the start of July 2022, over 1400,000 first vaccinations, 1300,000 second vaccinations (approximately ≥8–12 weeks following the first dose) and 1100,000 third "booster" vaccinations (approximately 3 months following the second dose) have been administered in Northern Ireland [1]. However, the emergence of new variants, alongside the waning of antibody levels over time, warrants further investigation and monitoring of both the vaccine-induced immune response and the immune response from SARS-CoV-2 infection. SARS-CoV-2 IgG may be detected in saliva, sputum, bronchoalveolar lavage fluid or blood samples [2]. Our previous study [3] assessed plasma samples from participants for anti-SARS-CoV-2 spike protein IgG from pre-vaccination to six months after their first vaccination, as well as documented reports of SARS-CoV-2 infection from participants (i.e., the differences in antibody levels in participants that had been infected at some point within the vaccination process). The objective of this study is to semi-quantitatively assess the performance of the AbC-19™ lateral flow immunoassay on a selection of plasma samples which includes post booster vaccination, WHO international standards genetic variants and microorganism serology.

Methods

Study design

The eligibility criteria for the study required that participants be >18 years old with no contraindications to providing a blood sample, and that they were scheduled to receive the COVID-19 vaccine. All participants provided fully informed written consent prior to enrolment in

* Corresponding author at: Biomedical Sciences Research Institute, Ulster University, Northern Ireland, United Kingdom.
E-mail address: tara.moore@ulster.ac.uk (T. Moore).

https://doi.org/10.1016/j.clicom.2022.09.001
Received 2 September 2022; Received in revised form 13 September 2022; Accepted 13 September 2022

Table 1
Timepoint description.

Timepoint (TP)	Description
1	Pre first vaccination
2	3 weeks post first vaccination
3	Pre second vaccination
4	3 weeks post second vaccination
5	6 months post first vaccination
6	9 months post first vaccination
7	Post booster vaccination

the study. The study was approved by the South Birmingham Research Ethics Service (REC 20/WM/0184, IRAS 286,041), and adhered to the Declaration of Helsinki.

Venous blood samples were collected from study participants in approximately 10 ml EDTA vacutainers and centrifuged at 3000 rpm for 15 min at 4 °C. The plasma was aliquoted and stored at −80 °C with a maximum freeze-thaw cycle of 1 upon testing on AbC-19™. The patients within the vaccine cohort received the Oxford-AstraZeneca COVID-19 vaccination for the first and second dose, and the Pfizer-BioNTech (BNT162b2) for the third dose (first booster). The sampling time points are described in Table 1. At each sampling time point participants received a questionnaire, and positive COVID-19 rapid antigen or PCR test results were recorded, as well as details of infection that include symptom severity (defined as mild, moderate or severe).

In this study we also assess the comorbidities and the medications of the clinically extremely vulnerable (CEV) participants. CEV patients would now be defined as high risk for death or serious illness from COVID, however, at the point of recruitment patients were categorized as CEV or non-CEV. The 10 genetic variant samples (5 samples per variant of concern to include Delta (mutations; G142D, E156-F157, R158G, L452R, T4278K) and Omicron (B.1.1.529) were sourced and tested on the AbC-19™ device by Abingdon Health (York, UK). The WHO international standards were obtained from NIBSC (National Institute for Biological Standards, Herts, UK). The 101 microorganism serology samples, as listed in Table S2., were obtained from AbBaltis (Kent, UK), Trina (Trina Bioreactives AG, Switzerland) and NIBSC.

The AbC-19™ Rapid Test lateral flow immunoassay was used in accordance with manufacturer's instructions to test the plasma samples for anti-SARS-CoV-2 IgG (including neutralising antibodies to the trimeric spike protein). To allow for comparison of the immune response post-booster vaccination, the semi-quantitative approach, as documented within our earlier study [3] was implemented as follows;

Negative= AbC-19™ score of 0
Low positive= AbC-19™ score of 1–2
High positive= AbC-19™ score of 4–10

Statistical analysis

All data analysis was carried out using SPSS for Windows version 27 (property of IBM). Continuous data was described using the mean ± standard error of the mean and 95% confidence intervals. Differences were tested using the Mann Whitney U test. Categorical data was described by number and percentages. One-way analysis of variance (ANOVA) was used to compare the differences between groups and the Games-Howell post hoc test was applied.

Results

Vaccinated sample demographics

From our initial cohort of 111 participants, as documented by Robertson et al. [3], we were able to follow-up on 24 participants at TP6 (all except for 1 participant were followed up at TP7) and 80 participants for TP7. CEV participants accounted for 53.2% of the total cohort (59/111). Of the 59 CEV participants, 19 (32.2%) were hypertensive, 10 had cardiovascular disease (16.9%), 8 were diabetic (13.6%), 15 were asthmatic (25.4%) and 10 had cancer (17.0%). Additionally, 20 of the CEV participants had more than one medical condition. The majority of CEV participants were on medications (84.7%), with the most common medication within this cohort being statins (37.3%).

Immune response post-booster vaccination (TP7)

The results of the anti-SARS-CoV-2 IgG AbC-19™ test shown in Fig. 1 demonstrate high positive IgG antibody levels for all 80 participants sampled at TP7. There was a significant mean increase in AbC-19™ score of 5.73 between TP5 and TP7 as shown in Fig. S2 ($p<0.0001$). TP5 AbC-19™ scores ranged from 0 to 10, whilst TP7 AbC-19™ scores ranged from 5 to 10.

Furthermore, the one participant previously reported to be SARS-CoV-2 IgG negative within the cohort following second vaccination (TP4), returned a high positive (5) AbC-19™ score following booster vaccination (TP7) for. The participant was CEV and reported having no medical history of SARS-CoV-2 infection. A further 6 participants who tested IgG negative at TP5, and an additional 3 participants who tested negative at TP6 all elicited an immune response following their booster vaccination. The AbC-19™ scores of the 6 negative individuals at TP5 increased by 6, 8, 9, 6, 7 and 5. The AbC-19™ scores of the 3 negative individuals at TP6 increased by 10, 8 and 9. These individuals were all low positives at TP4.

Effect of previous SARS-CoV-2 infection on response to booster vaccination

SARS-CoV-2 infection confirmed by rapid antigen or PCR test was recorded. The AbC-19™ score of the 17 participants who had previously been infected with SARS-CoV-2 was compared with the scores of those who reported no infection (Fig. 2). The scores of those who reported previous infection were significantly higher, increased by a mean AbC-19™ score of 0.8 ($p = 0.049$). Multiple comparisons analysis is presented in Table S1 for infection status and grade. However, there is no difference in the scores when stratified for symptomatic or non-symptomatic infection, as shown in Fig. 3. Furthermore, the mean increase in AbC-19™ score was significantly less for the infected individuals at 5.80 compared to those not previously infected at 2.43, as shown in Figure S3 ($p = 0.001$). Therefore, this difference is likely to be due to infected individuals having already increased antibody levels.

The immune response elicited by the booster vaccination in the CEV was compared to those not CEV. Although the mean response to the booster vaccine was stronger in non-CEV participants, the 0.23 increase in the mean AbC-19™ score for the 32 non-CEV participants compared to the 48 CEV participants was not statistically significant ($p = 0.49$) (Fig. 4). Similarly, the 0.41 increase in the mean AbC-19™ score found at TP5 for 35 non-CEV compared to 54 CEV participants was not statistically significant ($p = 0.522$).

WHO international standards and genetic variants

The MDCG (2021) guidelines advocate the testing of the WHO International SARS-CoV-2 IgG NIBSC standards, genetic variants, and potentially interfering/cross-reacting serology [4]. The WHO international SARS-CoV-2 IgG NIBSC standards were developed for the purposes of standardization and calibration of SARS-CoV-2 IgG antibody tests [5]. This analysis was performed to assess if the AbC-19™ could correctly rank the standards in accordance with the NIBSC ranking, as well as to investigate if the AbC-19™ was able to detect antibodies to a selection of genetic variants. The WHO international standards performed as expected in accordance with the ranking of the NIBSC standards (*S*=spike protein, *N*=nucleocapsid); NIBSC 20/150 (high) scored 6, 20/148 (mid) scored 3–4, 20/144 (low S, high N) scored 1–2, 20/140 (low) scored 1,

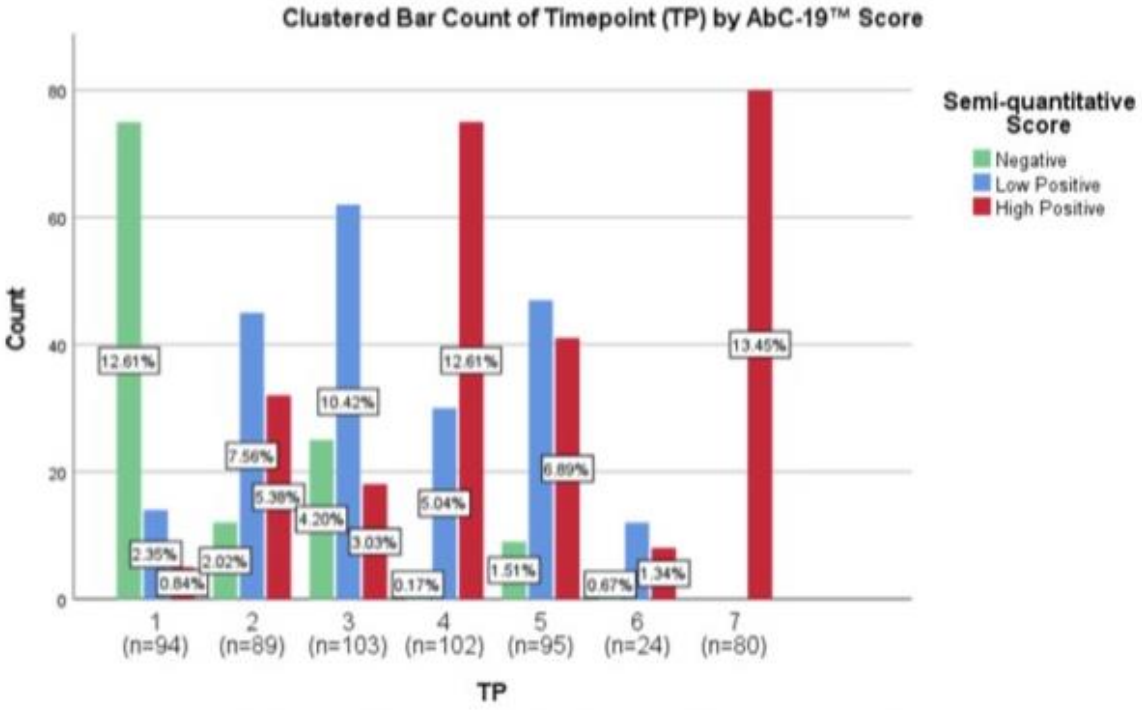

Fig. 1. Semi-quantitative scoring of AbC-19™ result for participants at seven time points.

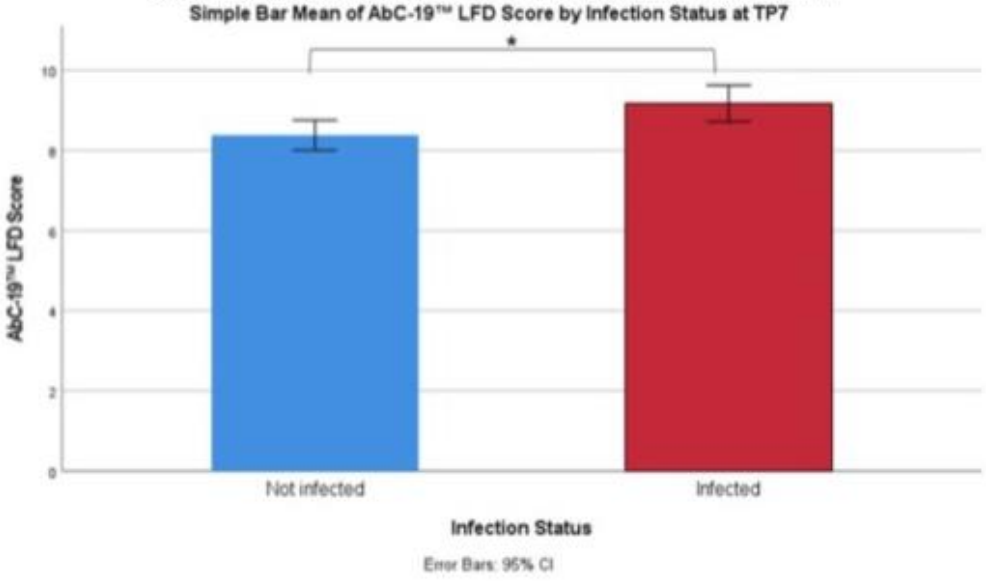

Fig. 2. AbC-19™ score by infection status for TP7.
Not infected n = 63 vs Infected n = 17 (Pre-Vaccination n = 7, TP1-TP7 n = 10). LFD= Lateral Flow Device.

20/142 (negative) scored 0 and 21/234 (high) scored 6. The results of the genetic variant samples are presented in Table 2.

Cross-reactivity

This cross-reactivity analysis was carried out to evaluate the cross-reactivity to antibodies elicited by other microbial infections. There were 101 microorganism serology samples tested on AbC-19™ as documented in Table S2. No cross-reactivity was detected in any sample with the exception of a marginal cross-reactivity that was observed in one of five pre-pandemic dengue serology samples with a score of 1 on AbC-19™, and as confirmed by repeat testing and multiple observers.

Discussion

Vaccination and infection

In this study we assessed both samples from infected individuals and samples from vaccinated individuals. Assessment of SARS-CoV-2 antibodies provides a better understanding of the immune response to both

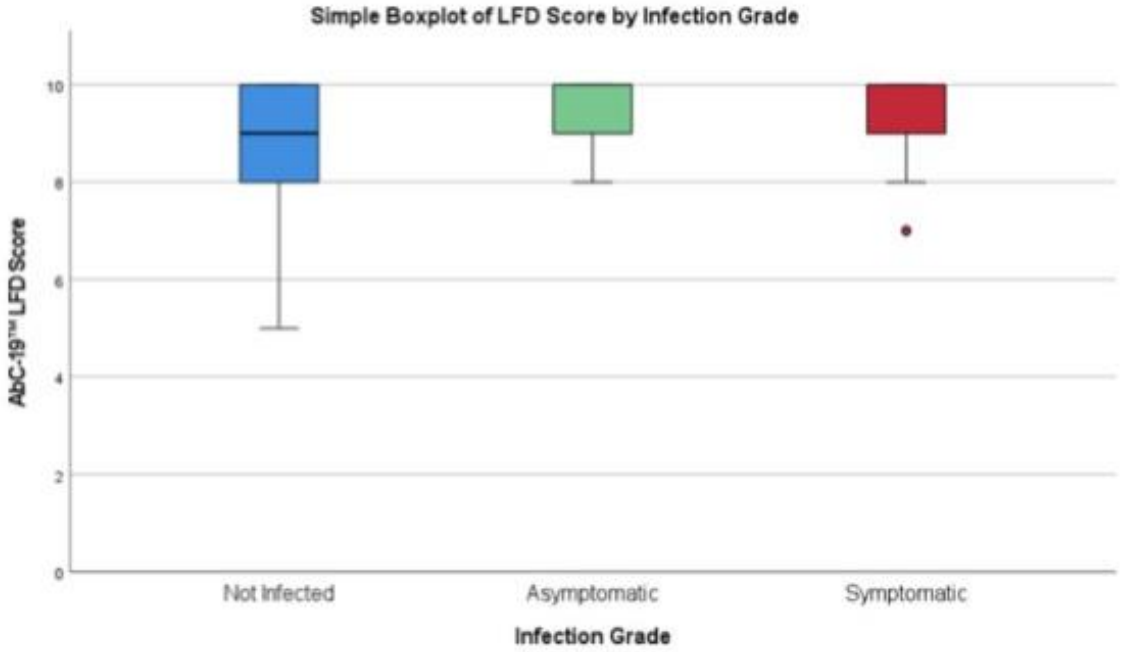

Fig. 3. AbC-19™ score by infection grade for TP7.
Not infected $n = 63$, Asymptomatic $n = 7$ (Non-CEV $n = 3$, CEV $n = 4$), Symptomatic $n = 10$ (Mild $n = 4$ (Non-CEV $n = 2$, CEV $n = 2$), Moderate $n = 3$ (Non-CEV $n = 2$, CEV $n = 1$), Severe $n = 3$ (Non-CEV $n = 0$, CEV $n = 3$)).

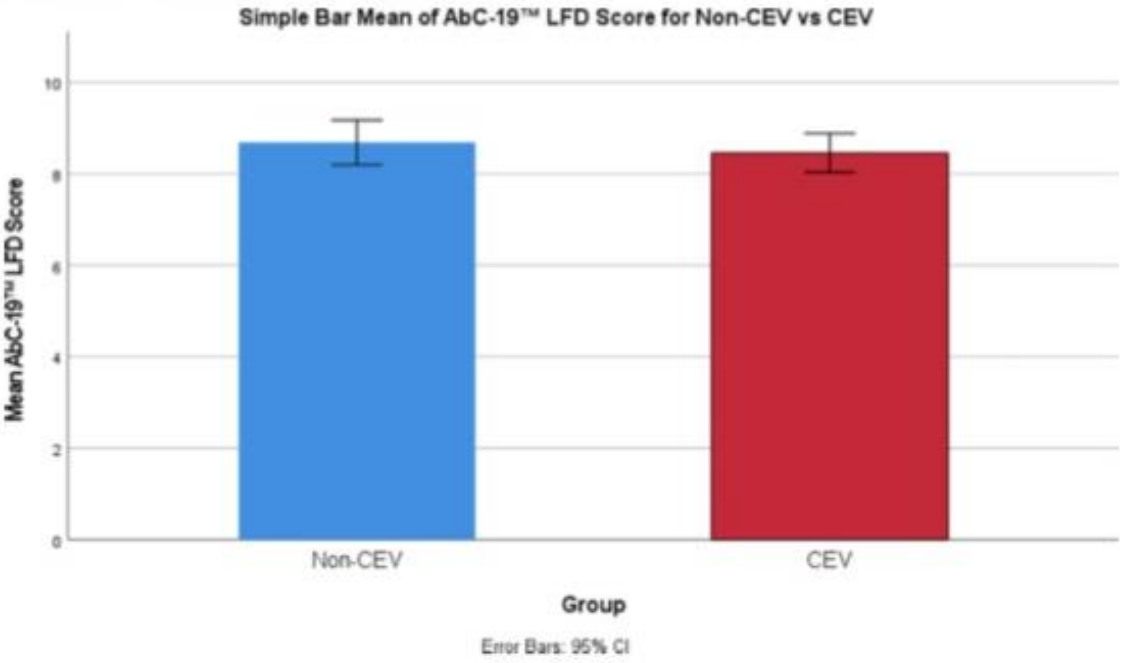

Fig. 4. AbC-19™ score for Non-CEV vs CEV at TP7.
Non-CEV ($n = 32$) vs CEV ($n = 48$).

vaccination, as well as infection. For example, in a recent study the odds of infection by Omicron were shown to be higher than that of Delta [6]. Additionally, Beaney et al. [7] also found significant variation over time for hospitalization and mortality risk from SARS-CoV-2 infection. These findings may suggest continual monitoring of infection and immune response is crucial with the emergence of new variants. In the same study by Chaguza et al., there was shown to be a lower PCR test positivity rate after three mRNA vaccine doses, highlighting the importance of booster vaccinations.

There are few studies assessing the SARS-CoV-2 immune response of samples from vaccinated individuals compared to those of infected individuals [8], The conclusions of the studies by Salvagno et al. [9] and Chuguza et al., recognized the need for booster vaccinations following a decline in antibody levels after 6 months. This is particularly important given the indication of protection from COVID-19 associated with [10], as well as reports of reduction in risk of symptomatic infection in correlation with higher levels of immune markers to include anti-spike, anti-receptor binding domain and neutralising antibodies [11].

Table 2
Genetic variants.

Sample	Operator 1						Operator 2						Average T-Line	Mode T-Line	Max	Min
	Rep 1		Rep 2		Rep 3		Rep 1		Rep 2		Rep 3					
	C1	T1	C2	T2	C3	T3	C1	T1	C2	T2	C3	T3				
1. Delta	10	1	10	1	10	1	9	1	9	1	9	1	1.00	1	1	1
2. Delta	10	3	10	3	10	2	9	3	9	3	9	2	2.67	3	3	2
3. Delta	10	2	10	2	10	2	9	2	9	3	9	2	2.17	2	3	2
4. Delta	10	2	10	2	10	2	9	2	9	1	9	1	1.67	2	2	1
5. Delta	10	4	10	3	10	3	9	4	9	3	9	3	3.33	3	4	3
6. Omicron	10	7	10	7	10	6	9	7	9	7	9	7	6.83	7	7	6
7. Omicron	10	6	10	6	10	6	9	6	9	6	9	6	6.00	6	6	6
8. Omicron	10	4	10	5	10	5	9	4	9	4	9	4	4.33	4	5	4
9. Omicron	10	7	10	5	10	6	9	6	9	6	9	6	6.00	6	7	5
10. Omicron	10	7	10	7	10	6	9	7	9	7	9	7	6.83	7	7	6
Buffer alone	0	0	0	0	0	0	0	0	0	0	0	0	0	0	0	0

Rep= Repeat, C= Control-Line and *T* = T-Line.

The study presented here obtained from the vaccinated cohort aimed to address this matter further.

The high positive anti-SARS-CoV-2 IgG response to the booster vaccine was found to be significantly increased for those who were previously infected, reflecting the findings from our previous study [3]. Although all participants scored high positive AbC-19™ results at TP7. Contrastingly, results from the study by Reynolds et al. [12] suggest that after the third vaccine dose the anti-spike protein S1 receptor binding domain antibody response increased to similar levels in all 3 groups assessed (Wuhan variant infected, Alpha variant infected and uninfected). However, this study used lab-based immunoassays such as ROCHE Elecsys electrochemiluminescence immunoassay (ECLIA).

Genetic variants and who international standards

The MDCG (2021) guidelines propose acceptable performance metrics of a SARS-CoV-2 IgG immunoassay to be ≥90% diagnostic sensitivity for samples taken >21 days post symptom onset (for ≥400 samples), and a high specificity value of >99% (for ≥400 samples from non-vaccinated and non-infected individuals) should also be met. However, MHRA (2022) guidelines suggest a minimum clinical sensitivity and specificity of >98% [13]. In the evaluation of analytical sensitivity, the AbC-19™ LFIA successfully profiled the WHO International standard results by correctly identifying those samples with negative, low, mid and high antibody levels. The results of this study also show successful detection of a neutralising humoral antibody response for the 2 variants (Delta and Omicron). In our earlier collaborative study, we reported cross-reactivity of spike glycoprotein induced antibody against the Delta and Omicron variants pre and post booster vaccination in a range of non-CEV and CEV individuals [14]. Therefore, SARS-CoV-2 immunoassays may prove to be a valuable tool in the monitoring and response to new variants with the possibility of immune escape [15]. However, the performance of the existing LFD test should be measured for each new variant to ensure that the test performs to the required standard.

Cross-reactivity

Cross-reactivity of samples from dengue serology as well as malaria serology samples have previously been reported to present false positive results on SARS-CoV-2 assays [16]. Therefore, whilst only 1 out of the 5 Dengue samples tested demonstrated this weak cross-reactivity on AbC-19™, this should still be taken into consideration to prevent overestimating SARS-CoV-2 seroprevalence in regions where these infections are widespread. However, it is likely that this positive result was due to non-specific binding of the anti-dengue IgG in this one sample [17]. Furthermore, the MHRA (2022) guidelines desired criteria are met as no cross-reactivity with any other coronaviruses or respiratory pathogen antibody positive serology was detected, and Dengue is not presented in the list for analytical specificity analysis.

Limitations

This study examines only the humoral antibody response and not the cellular antibody response. Additionally, given the longitudinal nature of the study it was anticipated that vaccinated participants may not attend all sampling timepoints. Lastly, we acknowledge this study is limited as it only reports on the results from one immunoassay and Salvagno et al. [18] suggest that assessment of pre and post booster humoral response is dependant on the immunoassay used.

In conclusion, the AbC-19™ immunoassay detected high positive IgG responses post-booster for all 80 participants sampled. Furthermore, the AbC-19™ test also successfully classified all WHO international standards and detected IgG responses with all genetic variants tested. Cross-reactivity was only observed with one dengue serology sample. Therefore, the AbC-19™ immunoassay would be a cost-effective tool to indicate antibody status.

Authorship statement

all authors meet the ICMJE authorship criteria.

ICMJE statement

TM and JADM conceived the study. LJR, GC, JSM and TM performed all laboratory analyses. JSM, LJR and GC analysed data. JSM performed all statistical analyses/interpretations and produced figures. TM, RKP, MAN, JF and AB coordinated participant recruitment, consent and sampling. LJR, JSM and GC performed sample collection and processing. JSM, LJR, MAN and TM wrote the manuscript. All authors reviewed and approved the final manuscript.

Funding

The study was funded by Abingdon Health, United Kingdom who also provided the AbC-19™ testing devices. Abingdon Health had no other involvement in the study.

Declaration of Competing Interest

The authors declare the following financial interests/personal relationships which may be considered as potential competing interests: Professor Tara Moore acted as a consultant for Abingdon Health during the final period of sampling. At time of conception and commencement of this study, none of the authors received payment from Abingdon Health.

Supplementary materials

Supplementary material associated with this article can be found, in the online version, at doi:10.1016/j.clicom.2022.09.001.

References

[1] Department of Health. (2022) Available at: https://covid-19.hscni.net/ni-covid-19-vaccinations-dashboard/ [Accessed 4 July 2022]

[2] W. Zhang, B.Y. Chua, K.J. Selva, L. Kedzierski, T.M. Ashhurst, E.R. Haycroft, S.K. Shoffner-Beck, L. Hensen, D.F. Boyd, F. James, E. Mouhtouris, Nat. Commun. 13 (1) (2022 May 19) 1–8.

[3] L.J. Robertson, R. Price, J.S. Moore, G. Curry, J. Farnan, A. Black, K. Blighe, M.A. Nesbit, J.A. McLaughlin, T. Moore, Vaccine 40 (18) (2022 Apr 20) 2535–2539.

[4] Medical Devices Coordination Group (MDCG). (2021) Available at: https://ec.europa.eu/health/system/files/2022-02/mdcg_2021-21_en.pdf [Accessed 4 July 2022].

[5] European Centre for Disease Prevention and Control. Available at: https://www.ecdc.europa.eu/sites/default/files/documents/Considerations-for-the-use-of-antibody-tests-for-SARS-CoV2-first-update.pdf [Accessed 4 July 2022].

[6] C. Chaguza, A. Coppi, R. Earnest, D. Ferguson, N. Kerantzas, F. Warner, H.P. Young, M.I. Brehan, K. Billig, R.T. Koch, K. Pham, Medicine (2022 Apr 6).

[7] T. Beaney, A.L. Neves, A. Alboksmaty, H. Ashrafian, K. Flott, A. Fowler, J.R. Benger, P. Aylin, S. Elkin, A. Darzi, J. Clarke, Nat. Commun. 13 (1) (2022 Apr 29) 1–0.

[8] L. Mulder, B. Carrères, F. Muggli, A. Zollinger, J. Corthésy, A. Klijn, G. Togni, J. Clin. Med. 11 (8) (2022 Jan) 2100.

[9] G.L. Salvagno, B.M. Henry, L. Pighi, S. De Nitto, G. Gianfilippi, G. Lippi, Clin. Chem. Lab. Med. (CCLM) 60 (2) (2022 Jan 1) e29–e31.

[10] C.M. Worsley, M.A. van der Mescht, D. Hoffmann, P.W. Meyer, V. Ueckermann, T.M. Rossouw, J. Infect. 85 (3) (2022 Sep) 334.

[11] S. Feng, D.J. Phillips, T. White, H. Sayal, P.K. Aley, S. Bibi, C. Dold, M. Fuskova, S.C. Gilbert, I. Hirsch, H.E. Humphries, Nat. Med. 27 (11) (2021 Nov) 2032–2040.

[12] C.J. Reynolds, J.M. Gibbons, C. Pade, K.M. Lin, D.M. Sandoval, F. Pieper, D.K. Butler, S. Liu, A.D. Otter, G. Joy, K. Menacho, Science 375 (6577) (2022 Jan 14) 183–192.

[13] Medicines and Healthcare products Regulatory Agency (MHRA). (2022) Available at: https://www.gov.uk/government/publications/how-tests-and-testing-kits-for-coronavirus-covid-19-work/target-product-profile-antibody-tests-to-help-determine-if-people-have-recent-infection-to-sars-cov-2-version-2 [Accessed 4 July 2022].

[14] S. Faustini, A. Shields, G. Banham, N. Wall, S. Al-Taei, C. Tanner, Z. Ahmed, E. Efstathiou, N. Townsend, M. Goodall, T. Plant, J. Infect. 84 (4) (2022 Apr 1) 579–613.

[15] D. Tian, Y. Sun, J. Zhou, Q. Ye, J. Med. Virol. 94 (3) (2022 Mar) 847–857.

[16] C. Yek, V.S. Nam, R. Leang, D.M. Parker, S. Heng, K. Souv, S. Sovannaroth, M. Mayxay, S. Abubakar, R.T. Sasmono, N.D. Tran, Front. Trop. Dis. 2 (2021) 788590.

[17] J. Henrina, I.C. Putra, S. Lawrensia, Q.F. Handoyono, A. Cahyadi, SN Comprehens. Clin. Med. 2 (8) (2020 Aug) 1109–1119.

[18] G.L. Salvagno, B.M. Henry, G. Lippi, Int. J. Infect. Dis. 111 (2021 Oct 1) 65–67.

Appendix VIII

Vaccine 40 (2022) 2535–2539

Contents lists available at ScienceDirect

Vaccine

journal homepage: www.elsevier.com/locate/vaccine

Short communication

IgG antibody production and persistence to 6 months following SARS-CoV-2 vaccination: A Northern Ireland observational study

Louise J. Robertson [a], Ruth Price [a], Julie S. Moore [a], Grace Curry [a], John Farnan [b], Amy Black [b], Kevin Blighe [a], M. Andrew Nesbit [a], James A.D. McLaughlin [c,d], Tara Moore [a,d,e,*]

[a] Biomedical Sciences Research Institute, Ulster University, Northern Ireland, United Kingdom
[b] The Group Surgery, 257 North Queen Street, Belfast, Northern Ireland, United Kingdom
[c] Nanotechnology and Integrated Bioengineering Centre, Ulster University, Northern Ireland, United Kingdom
[d] Integrated Diagnostics Laboratory, Ulster University, 3-5a Frederick St, Belfast, Northern Ireland, United Kingdom
[e] Avellino, 1505 Adams Dr, Menlo Park, CA 94025, United States

ARTICLE INFO

Article history:
Received 28 October 2021
Received in revised form 19 January 2022
Accepted 28 February 2022
Available online 3 March 2022

Keywords:
COVID-19
SARS-CoV-2
Oxford-AstraZeneca ChAdOx1
COVID-19 vaccination
Antibody response
Adenovirus vector-based vaccine

ABSTRACT

Background: This study evaluates spike protein IgG antibody response following Oxford-AstraZeneca COVID-19 vaccination using the AbC-19™ lateral flow device.
Methods: Plasma samples were collected from n = 111 individuals from Northern Ireland. The majority were >50 years old and/or clinically vulnerable. Samples were taken at five timepoints from pre-vaccination until 6-months post-first dose.
Results: 20.3% of participants had detectable IgG responses pre-vaccination, indicating prior COVID-19. Antibodies were detected in 86.9% of participants three weeks after the first vaccine dose, falling to 74.7% immediately prior to the second dose, and rising to 99% three weeks post-second vaccine. At 6-months post-first dose, this decreased to 90.5%. At all timepoints, previously infected participants had significantly higher antibody levels than those not previously infected.
Conclusion: This study demonstrates that strong anti-spike protein antibody responses are evoked in almost all individuals that receive two doses of Oxford-AstraZeneca vaccine, and which largely persist beyond six months after first vaccination.

1. Introduction

The global impact of the COVID-19 pandemic resulted in a race to find a safe and effective vaccine. In December 2020, the Pfizer BioNTech (PFZ) vaccine was approved for use in the UK, shortly followed by the ChAdOx1 Oxford-AstraZeneca (OAZ)[1] vaccine. The OAZ vaccine, an adenovirus vector vaccine is a modified, non-replicating, chimpanzee adenovirus which contains DNA coding for SARS-CoV-2 spike protein [1]. The first data on efficacy showed it was 64% effective after first dose and 70% after second [1]. SARS-CoV-2 neutralising antibodies were reported in 91% of participants following the first dose, and 99–100% following a second dose [2,3].

The UK Rapid Test Consortium (UK-RTC) was founded in response to a UK Government call for development of a rapid antibody test for use nationally. The consortium developed the AbC-19™ lateral flow device (LFD) antibody test now approved in Europe and UK for professional use and is available for sale. AbC-19™ is an easy-to-use, accurate and reliable neutralising antibody rapid test indicating positive antibody response post-infection or presence of neutralising antibodies post-vaccine [4]. Testing can take place in a wide range of environments and by a range of individuals from varying educational backgrounds as shown in our previously published data [5].

Antibody testing is vital to inform understanding of the prevalence of SARS-CoV-2 virus in the population. It is important for understanding response to emerging variants, detecting differences in levels of immunity (vaccinated immunity versus infection-acquired immunity) and their durability. Strategic antibody screening will inform the need for boosters and vaccination strategies globally [6].

This study assesses SARS-CoV-2 IgG antibody status at five timepoints during vaccination against COVID-19 disease with the OAZ vaccine using the AbC-19™. We also assess natural COVID-19 infection before and during these six months and report the impact of infection pre- and post-vaccination on antibody levels.

* Corresponding author at: Integrated Diagnostics Laboratory, Ulster University, 3-5a Frederick St, Belfast, BT12NR, United Kingdom
E-mail address: tara.moore@ulster.ac.uk (T. Moore).
[1] OAZ – Oxford-AstraZeneca ChAdOx1 COVID-19 Vaccine.

https://doi.org/10.1016/j.vaccine.2022.02.087
0264-410X/

2. Methods

The study was an observational study conducted over 5 time-points (up to 6 months post-first dose) on patients scheduled to receive the OAZ COVID-19 vaccine. The study was approved by the South Birmingham Research Ethics Service (REC 20/WM/0184, IRAS 286041) and all participants provided fully informed written consent prior to taking part. All work was carried out in accordance with the Declaration of Helsinki.

Participants were recruited by word-of-mouth or recruitment poster on the day of their first or second vaccination at a GP clinic in Belfast, Northern Ireland. A small number of participants (n = 12) were enrolled at the time of their second vaccination, so were only sampled at two timepoints. All participants provided informed consent, basic demographic information and details of any previous positive SARS-CoV-2 test result using REDCap electronic data capture tools hosted at Ulster University (https://www.project-redcap.org/). PANDEMIC study participants that had previously tested positive for COVID-19 were also invited to join the study via email. Participants were eligible for the study if they were over 18 years of age and could attend a blood sample clinic at the time of their first or second vaccination. Exclusion criteria included anyone with a blood disorder or contraindication to giving a blood sample, or anyone currently exhibiting symptoms of COVID-19. Samples were taken at five time-points: just before first vaccination (TP1), 3 weeks after first vaccination (TP2), just before second vaccination (TP3), 3 weeks after the second vaccination (TP4) and 6 months following first vaccination (TP5), as shown in Supplementary Table 1.

An EDTA-plasma (10 ml) sample was collected at each time point from each participant. All blood samples were processed within 2 h of collection in refrigerated centrifuges (15 min, 3000 rpm, 4 °C). Samples were stored at −80 °C until analysis. Analyses were performed on AbC-19™ at Ulster University according to manufacturer's instructions. Assays were performed with samples in batches of 10, with one researcher adding 2.5 μL of EDTA-plasma to the assay and a second adding 100 μL of buffer immediately following sample addition. After 20 min, the strength of resulting test line was scored, independently by three experienced blinded observers, from 0–10 according to a visual score card (Figure S1). In qualitative mode, a score ≥1 is positive. Using the semi-quantitative approach, scores of 1, 2 and 3 are low positive whilst scores of 4, 5, 6, 7, 8, 9 and 10 are high positive.

All data was analysed using Microsoft Excel and GraphPad Prism 9 with figures generated in Prism. Differences between RT-PCR positive and no RT-PCR results were analysed using two tailed unpaired Welchs *t*-test and 6 months post vaccine group compared by Brown-Forsythe and Welch one-way ANOVA.

3. Results

We assessed SARS-CoV-2 IgG antibody status in a total of 111 participants using the AbC-19™ at five timepoints to determine antibody response to OAZ vaccination. AbC-19™ results were graded quantitatively, then classified semi-quantitatively as directed by the manufacturer: test lines were graded as negative, low positive or high positive as described above (Figure S1).

The initial samples were collected at a Belfast GP clinic during March 2021, when access to vaccination was limited to those aged 50 years and above, or those classified as vulnerable or clinically extremely vulnerable. A small number of participants were recruited from previous PANDEMIC study phases who were eligible for vaccination and previously tested positive for COVID-19 [4]. The cohort consisted of 55% female (n = 61, aged 28–89 years, median 51 years) and 45% male (n = 50, aged 24–82 years, median 51 years) subjects, with an overall age range of 24–89 years (median 51 years old). A total of n = 14 participants had tested positive by RT-PCR for SARS-CoV-2 infection before being vaccinated, with a range of 47–219 days (median 104 days) between the positive result and first vaccination.

Samples were collected from n = 94 participants at the time of first vaccination (TP1) with n = 75 (79.7%) scoring negative by AbC-19™ (n = 4 previously infected, Fig. 1). 14 samples scored low positive (14.9%) and 5 scored high positive (5.3%). Of the 19 participants with a positive result (n = 14 low positive, n = 5 high positive) at 1st dose, 8 had previously reported that they had been infected with COVID-19 (n = 5 low, n = 3 high; Fig. 1).

Participants (n = 89) were sampled again at 3-weeks post-first vaccination (TP2). By this time, 86.5% (77/89) of participants had antibodies detectable by AbC-19™: 45/77 were scored as low positive and 32/77 as high positive. All previously infected participants had detectable antibodies (Fig. 1). Two of the three participants, not reported as previously RT-PCR positive but AbC-19™ positive, and presumably seropositive at 1st dose, had a robust IgG response, comparable to RT-PCR positive participants, with low positive AbC-19™ scores at TP1 and high positive scores at TP2 (Figure S2).

At time of second vaccination (TP3), antibody levels had fallen. The number scoring as high positive reduced to 16 (from 32 at TP2) and the number scoring negative for SARS-CoV-2 IgG increased to 25 (from 12 at TP2). Overall, 75.7% (78/103) of participants showed detectable antibodies as either low or high positive.

Three weeks after the second dose (TP4), all but one participant showed antibodies detectable by AbC-19™ (99%, 101/102). 30 participants had low positive scores (29.4%) while 71 had high positive scores (69.6%). These data indicate a robust IgG response to OAZ vaccination (Fig. 1).

Participants were sampled again 6 months after receiving their first vaccination (TP5), and antibody levels remained detectable in 86/95 (90.5%) of participants, including all who were infected prior to first vaccination (n = 10 sampled). The proportion of high positive AbC-19™ scores reduced somewhat to 38/95 (40%) while 47/95 (49.5%) had low positive antibody levels.

Overall, antibody levels increased at 3 weeks after each dose of vaccine, while there was a slight drop in AbC-19™ score before the second dose and a larger drop over the 6 months following second dose (Figure S2). Individuals with a reported previous COVID-19 infection had a significantly higher quantitative AbC-19™ score than those without at all timepoints ($p < 0.05$ to $p < 0.0001$), with the largest difference seen between these groups at TP2 (Fig. 2a-e). After providing a sample at TP4, five participants became infected with SARS-CoV-2 (and tested positive by RT-PCR) all of whom scored high positive by AbC-19™ at TP5, with scores significantly higher than doubly vaccinated, uninfected participants ($p < 0.0001$, Fig. 2e). Infection prior to vaccination had no signifi-

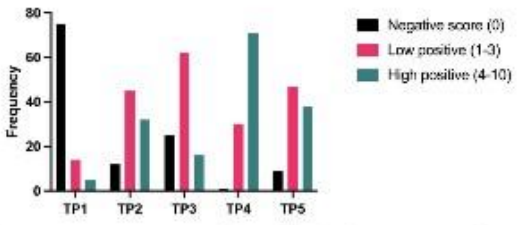

Fig. 1. Semi-quantitative scoring of AbC-19™ result for participants at five time points. TP1 = before 1st vaccination, TP2 = 3 weeks after 1st vaccination, TP3 = before 2nd vaccination, TP4 = 3 weeks after 2nd vaccination and TP5 = 6 months after 1st vaccination.

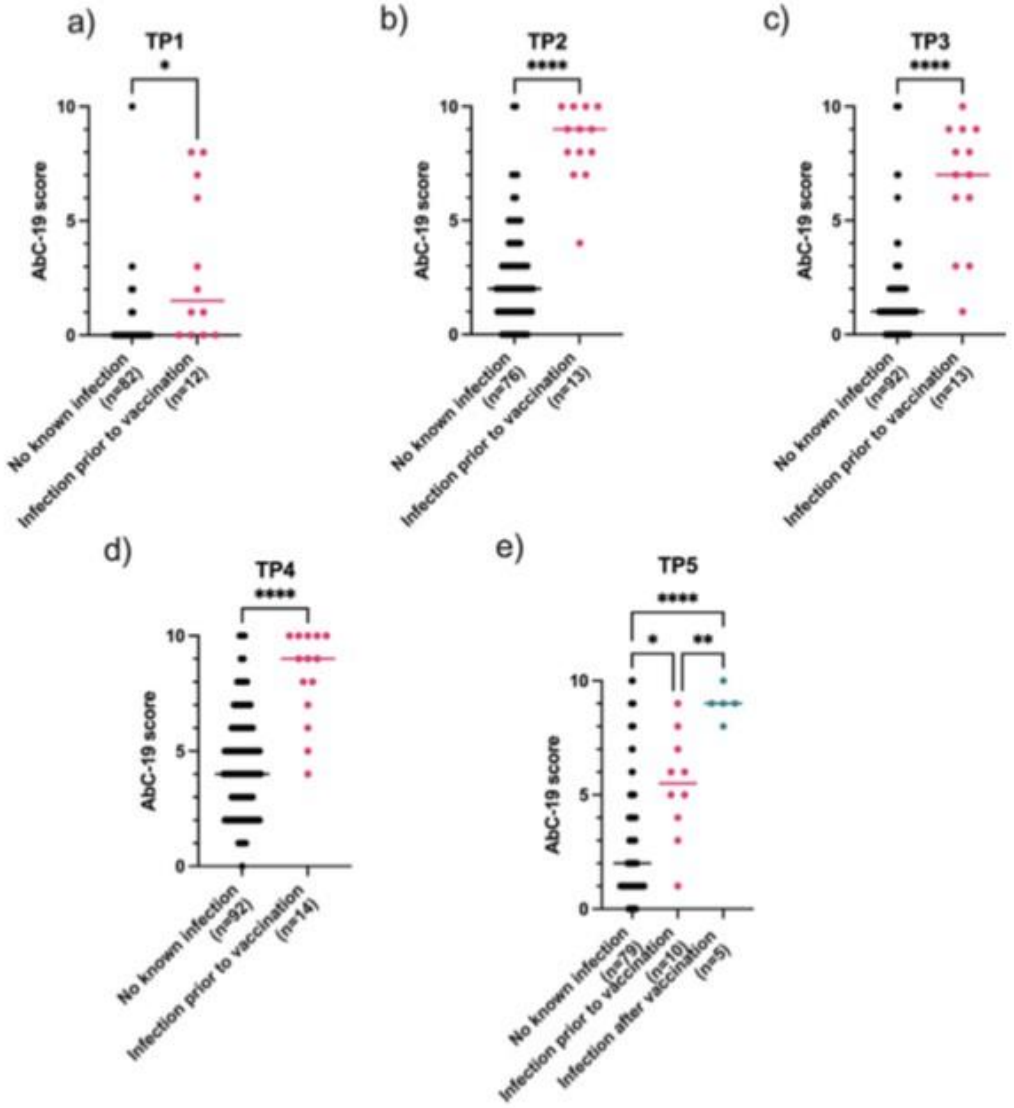

Fig. 2. AbC-19™ quantitative score between previously RT-PCR positive, no known infection groups and infection after vaccination at all time points (where relevant). TP1 = before 1st vaccination, TP2 = 3 weeks after 1st vaccination, TP3 = before 2nd vaccination, TP4 = 3 weeks after 2nd vaccination and TP5 = 6 months after 1st vaccination. Differences in means analysed using Welchs two-tailed unpaired *t*-test or Brown-Forsythe and Welch ANOVA (median *=p < 0.05, **P < 0.01, ****=p < 0.0001).

cant effect on the reduction in AbC-19™ scores observed between the two final timepoints (no infection- mean change −1.772, infection prior to vaccination mean change −3.1, p = 0.128, Fig. 3).

4. Discussion

We have previously shown good laboratory validation performance metrics for AbC-19™ detection of SARS-CoV-2 spike protein IgG antibody in a laboratory-based setting with a sensitivity of 97.58% (95% CI, 95.28%-98.95%) on a cohort of known positives, and specificity of 99.59% (95% CI, 98.53 %- 99.95%) on known negatives, including 223 pre-pandemic samples [4]. We demonstrated excellent overall agreement between antibody levels when measured by three other immunoassays (Roche Elecsys Anti-SARS-CoV-2 IgG/IgA/IgM against the SARS-CoV-2 Nucleocapsid antigenic region (Roche Diagnostics, Basel, Switzerland), the Abbott SARS-CoV-2 IgG assay against the same antigenic region (Abbott Diagnostics, Abbott Park, Illinois, USA) and EuroImmun Anti-SARS-CoV-2 ELISA-IgG against the S1 domain of the spike (antigenic) protein of SARS-CoV-2 (EuroImmun UK, London, UK). We also demonstrated that detectable spike protein IgG antibody may persist for more than 10 months after RT-qPCR-confirmed infection especially in cases where initial antibody reading was high on a scale of 1 to 10. The kinetics of antibody response following vaccination have been examined but have largely concentrated on mRNA vaccines (PFZ and Moderna). In a study using AbC-19™

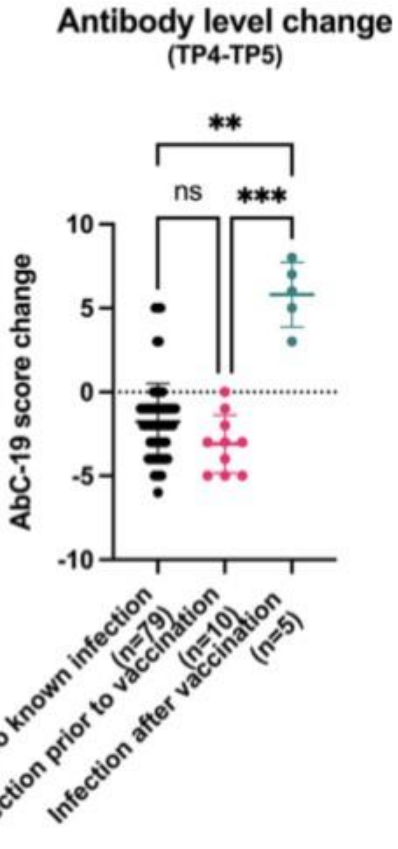

Fig. 3. Change in AbC-19™ quantitative score between TP4 (3 weeks after 2nd vaccination) and TP5 (6 months after first vaccination). Differences in means analysed using Brown-Forsythe and Welch ANOVA. ns = not significant, **=P < 0.01, ***=p < 0.001.

to compare IgG antibodies in participants double-vaccinated with either PFZ or OAZ vaccination, Ebanks et al (2021) showed a greater antibody response following PFZ, though a higher OAZ cohort median age may account for the reduced IgG response observed [7].

Here, we used the AbC-19™ to determine the kinetics of the response to the OAZ vaccination at various timepoints through the vaccination program. 86.5% of participants mounted a detectable IgG antibody response to the first vaccine dose, falling to 74.7% immediately prior to the second dose, and rising to 99% after it, with previously infected participants having a significantly higher quantitative AbC-19™ score than those without at all timepoints. These results are in close agreement with similar studies of antibody response to the OAZ, PFZ and Moderna vaccines measured using a variety of assays – LFD, chemiluminescent immunoassays (CLIA), and chemiluminescent microparticle assays (CMIA) [8–13]. In all studies, almost all participants mount a detectable antibody response to two doses of vaccine that is greater in previously infected individuals (either known RT-PCR positive or seropositive at baseline).

Antibody levels have been shown to decline over time following vaccination, but remain detectable for more than 6 months after second vaccination [9,14,15]. Titres of neutralizing antibodies have been shown to decay faster in never infected vaccinated individuals than in those infected prior to vaccination [16]. No significant difference in the reduction of AbC-19™ scores between previously infected and never infected individuals was observed in this study (Fig. 3).

Infection following the second dose of vaccine in previously uninfected individuals results in a high IgG antibody titre with a mean increase in AbC-19™ score of 5.8, significantly higher ($p<0.0001$) than the mean decrease in AbC-19™ score of 1.7 observed in doubly vaccinated, uninfected individuals (Fig. 3). Similar immune responses to post-vaccination infection were observed in nursing home residents infected following a second dose of PFZ vaccine [17].

The present study has limitations. Firstly, the largest portion of participants came from the 50+ year old age group being called for vaccination at the time of the study and were representative of the ethnic diversity of the area of Belfast, in which they were recruited (2.2% belonging to minority ethnic groups) [18]. The data that was obtained from younger participants was limited to those individuals called for vaccination due to underlying health problems. Secondly, we assessed antibody levels semi-quantitatively with the AbC-19™, a device which we already demonstrated to have a good correlation between other commercially available assays (Roche, Abbott, Eurolmmun) [4]. Additionally, a drop in antibody levels in undiluted serum of individuals with high positive (10) scores may not be detected. Dilution of serum samples by 10- or 100-fold may be necessary [11]. Thirdly, only the humoral (antibody) immune response was measured in this study; cellular (T cell) responses to vaccination were not investigated. Two vaccine doses have been shown to be required for maximal T cell response, which importantly appear to be directed against SARS-CoV-2 epitopes conserved between the SARS-CoV-2 variant used in the OAZ vaccine and the variants of concern that have subsequently emerged [19].

In summary, this study demonstrates via AbC-19™ that two doses of the OAZ ChAdOx1 vaccine elicits strong anti-spike protein antibody responses in almost all vaccinated individuals which persist for most individuals beyond six months after first vaccination. The utility of the 20-minute response time AbC-19™ rapid test in confirming this antibody response is also demonstrated. Further follow-up of this cohort at later time points will monitor further decline in antibody levels and help inform the likely need for additional vaccine or booster doses, particularly tailored to emerging strains or for people in whom the greatest decline in antibody levels is seen with time.

Funding

The study was funded by Abingdon Health, United Kingdom who also provided the AbC-19™ testing devices. Abingdon Health had no other involvement in the study.

Declaration of Competing Interest

The authors declare the following financial interests/personal relationships which may be considered as potential competing interests: Professor Tara Moore acted as a consultant for Abingdon Health during the final period of sampling. At time of conception and commencement of this study, none of the authors received payment from Abingdon Health.

Acknowledgements

The study is sponsored by Abingdon Health, United Kingdom. We thank the phlebotomists and staff at the Group Surgery who

made this study possible. Most importantly we are indebted to the participants who donated blood samples during this study.

Appendix A. Supplementary data

Supplementary data to this article can be found online at https://doi.org/10.1016/j.vaccine.2022.02.087.

References

[1] Voysey M, Clemens SAC, Madhi SA, Weckx LY, Folegatti PM, Aley PK, et al. Safety and efficacy of the ChAdOx1 nCoV-19 vaccine (AZD1222) against SARS-CoV-2: an interim analysis of four randomised controlled trials in Brazil, South Africa, and the UK. Lancet 2021;397:99–111. https://doi.org/10.1016/S0140-6736(20)32661-1.

[2] Folegatti PM, Ewer KJ, Aley PK, Angus B, Becker S, Belij-Rammerstorfer S, et al. Safety and immunogenicity of the ChAdOx1 nCoV-19 vaccine against SARS-CoV-2: a preliminary report of a phase 1/2, single-blind, randomised controlled trial. Lancet 2020;396:467–78. https://doi.org/10.1016/S0140-6736(20)31604-4.

[3] Ramasamy MN, Minassian AM, Ewer KJ, Flaxman AL, Folegatti PM, Owens DR, et al. Safety and immunogenicity of ChAdOx1 nCoV-19 vaccine administered in a prime-boost regimen in young and old adults (COV002): a single-blind, randomised, controlled, phase 2/3 trial. Lancet 2020;396:1979–93. https://doi.org/10.1016/S0140-6736(20)32466-1.

[4] Robertson LJ, Moore JS, Blighe K, Ng KY, Quinn N, Jennings F, et al. Evaluation of the IgG antibody response to SARS CoV-2 infection and performance of a lateral flow immunoassay: cross-sectional and longitudinal analysis over 11 months. BMJ Open 2021;11:e048142. https://doi.org/10.1136/bmjopen-2020-048142.

[5] Jing M, Bond R, Robertson LJ, Moore J, Kowalczyk A, Price R, et al. User experience analysis of AbC-19 Rapid Test via lateral flow immunoassays for self-administrated SARS-CoV-2 antibody testing. Sci Rep 2021;11:14026. https://doi.org/10.1038/s41598-021-93262-0.

[6] Bonanni P, Cantón R, Gill D, Halfon P, Liebert UG, Crespo KAN, et al. The Role of Serology Testing to Strengthen Vaccination Initiatives and Policies for COVID-19 in Europe. COVID 2021;1:20–38. https://doi.org/10.3390/covid1010004.

[7] Ebanks D, Faustini S, Shields A, Parry H, Moss P, Plant T, et al. Cross reactivity of serological response to SARS-CoV-2 vaccination with viral variants of concern detected by lateral flow immunoassays. J Infect 2021;83:e18–20. https://doi.org/10.1016/j.jinf.2021.07.020.

[8] Demonbreun AR, Sancilio A, Velez MP, Ryan DT, Saber R, Vaught LA, et al. Comparison of IgG and neutralizing antibody responses after one or two doses of COVID-19 mRNA vaccine in previously infected and uninfected individuals. EClinicalMedicine 2021;38:101018. https://doi.org/10.1016/j.eclinm.2021.101018.

[9] Doria-Rose N, Suthar MS, Makowski M, O'Connell S, McDermott AB, Flach B, et al. Antibody Persistence through 6 Months after the Second Dose of mRNA-1273 Vaccine for Covid-19. N Engl J Med 2021;384:2259–61. https://doi.org/10.1056/NEJMc2103916.

[10] Eyre DW, Lumley SF, Wei J, Cox S, James T, Justice A, et al. Quantitative SARS-CoV-2 anti-spike responses to Pfizer-BioNTech and Oxford-AstraZeneca vaccines by previous infection status. Clin Microbiol Infect Off Publ Eur Soc Clin Microbiol Infect Dis 2021. https://doi.org/10.1016/j.cmi.2021.05.041.

[11] Parry H, Bruton R, Stephens C, Brown K, Amirthalingam G, Otter A, et al. Differential immunogenicity of BNT162b2 or ChAdOx1 vaccines after extended-interval homologous dual vaccination in older people. Immun Ageing 2021;18:34. https://doi.org/10.1186/s12979-021-00246-9.

[12] Pezzati L, Giacomelli A, Mileto D, Conti F, Gagliardi G, Rizzo A, et al. Rapid lateral-flow immunochromatographic tests to assess anti N/S IgG seropositivity after BNT162b2 vaccine: A cross-sectional study: Rapid lateral-flow immunochromatographic tests after BNT162b2 vaccine. J Infect 2021;83:381–412. https://doi.org/10.1016/j.jinf.2021.05.029.

[13] Salvagno GL, Henry BM, Pighi L, De Nitto S, Gianfilippi GL, Lippi G. Three-month analysis of total humoral response to Pfizer BNT162b2 mRNA COVID-19 vaccination in healthcare workers. J Infect 2021;83:e4–5. https://doi.org/10.1016/j.jinf.2021.06.024.

[14] Glück V, Grobecker S, Köstler J, Tydykov L, Bertok M, Weidlich T, et al. Immunity after COVID-19 and vaccination: follow-up study over 1 year among medical personnel. Infection 2021:1–8. https://doi.org/10.1007/s15010-021-01703-9.

[15] Levin EG, Lustig Y, Cohen C, Fluss R, Indenbaum V, Amit S, et al. Waning Immune Humoral Response to BNT162b2 Covid-19 Vaccine over 6 Months. N Engl J Med 2021. https://doi.org/10.1056/NEJMoa2114583.

[16] Vicenti I, Basso M, Gatti F, Scaggiante R, Boccuto A, Zago D, et al. Faster decay of neutralizing antibodies in never infected than previously infected healthcare workers three months after the second BNT162b2 mRNA COVID-19 vaccine dose. Int J Infect Dis IJID Off Publ Int Soc Infect Dis 2021;112:40–4. https://doi.org/10.1016/j.ijid.2021.08.052.

[17] Urlaub D, Wolfsdorff N, Durak D, Renken F, Watzl C. SARS-CoV-2 infection shortly after BNT162b2 vaccination results in high anti-spike antibody levels in nursing home residents and staff. Immunity, Inflamm Dis 2021;n/a. https://doi.org/https://doi.org/10.1002/iid3.525.

[18] Northern Ireland Statistics and Research Agency. Census 2011: Key Statistics for Northern Ireland. n.d.

[19] Skelly DT, Harding AC, Gilbert-Jaramillo J, Knight ML, Longet S, Brown A, et al. Two doses of SARS-CoV-2 vaccination induce robust immune responses to emerging SARS-CoV-2 variants of concern. Nat Commun 2021;12. https://doi.org/10.1038/s41467-021-25167-5.

Appendix IX

Open access Original research

BMJ Open

Evaluation of the IgG antibody response to SARS CoV-2 infection and performance of a lateral flow immunoassay: cross-sectional and longitudinal analysis over 11 months

Louise J Robertson ,[1] Julie S Moore,[1] Kevin Blighe ,[1] Kok Yew Ng ,[2] Nigel Quinn,[3] Fergal Jennings,[3] Gary Warnock,[4] Peter Sharpe,[3] Mark Clarke,[5] Kathryn Maguire,[5] Sharon Rainey,[5] Ruth K Price ,[1] William P Burns ,[2] Amanda M Kowalczyk,[1] Agnes Awuah ,[1] Sara E McNamee ,[2] Gayle E Wallace,[6] David Hunter,[6] Steve Sager,[1] Connie Chao Shern ,[7] M Andrew Nesbit ,[1] James A D McLaughlin ,[2] Tara Moore [1,7]

To cite: Robertson LJ, Moore JS, Blighe K, *et al*. Evaluation of the IgG antibody response to SARS CoV-2 infection and performance of a lateral flow immunoassay: cross-sectional and longitudinal analysis over 11 months. *BMJ Open* 2021;**11**:e048142. doi:10.1136/bmjopen-2020-048142

► Prepublication history and additional supplemental material for this paper are available online. To view these files, please visit the journal online. To view these files, please visit the journal online (http://dx.doi.org/10.1136/bmjopen-2020-048142).

Received 21 December 2020
Accepted 27 May 2021

For numbered affiliations see end of article.

Correspondence to
Prof Tara Moore;
tara.moore@ulster.ac.uk

ABSTRACT

Objective To evaluate the dynamics and longevity of the humoral immune response to SARS-CoV-2 infection and assess the performance of professional use of the UK-RTC AbC-19 Rapid Test lateral flow immunoassay (LFIA) for the target condition of SARS-CoV-2 spike protein IgG antibodies.

Design Nationwide serological study.

Setting Northern Ireland, UK, May 2020–February 2021.

Participants Plasma samples were collected from a diverse cohort of individuals from the general public (n=279), Northern Ireland healthcare workers (n=195), pre-pandemic blood donations and research studies (n=223) and through a convalescent plasma programme (n=183). Plasma donors (n=101) were followed with sequential samples over 11 months post-symptom onset.

Main outcome measures SARS-CoV-2 antibody levels in plasma samples using Roche Elecsys Anti-SARS-CoV-2 IgG/IgA/IgM, Abbott SARS-CoV-2 IgG and EuroImmun IgG SARS-CoV-2 ELISA immunoassays over time. UK-RTC AbC-19 LFIA sensitivity and specificity, estimated using a three-reference standard system to establish a characterised panel of 330 positive and 488 negative SARS-CoV-2 IgG samples.

Results We detected persistence of SARS-CoV-2 IgG antibodies for up to 10 months post-infection, across a minimum of two laboratory immunoassays. On the known positive cohort, the UK-RTC AbC-19 LFIA showed a sensitivity of 97.58% (95.28% to 98.95%) and on known negatives, showed specificity of 99.59% (98.53 % to 99.95%).

Conclusions Through comprehensive analysis of a cohort of pre-pandemic and pandemic individuals, we show detectable levels of IgG antibodies, lasting over 46 weeks when assessed by EuroImmun ELISA, providing insight to antibody levels at later time points post-infection. We show good laboratory validation performance metrics for the AbC-19 rapid test for SARS-CoV-2 spike protein IgG antibody detection in a laboratory-based setting.

Strengths and limitations of this study

- This paper describes a non-clinical laboratory evaluation and comparison of the ability of three different immunoassays to detect SARS-CoV-2 antibodies in the same samples, detecting different subtypes of antibodies against different targets of the viral antigenic repertoire that does not rely on PCR positivity as definition of expected test outcome, to provide a panel of known antibody positive and antibody negative serology for evaluation of newly developed immunoassays.
- This study demonstrates AbC-19 lateral flow point-of-care detection of IgG antibodies to the full trimeric spike protein of SARS-CoV-2 virus, the antibodies made in response to the vaccines used globally, in a large cohort of subjects, more than 10 months post-infection, across a broad age range (18–78 years).
- This study assesses correlation between approved laboratory-based assays and the AbC-19 lateral flow point-of-care lateral flow test for the detection of SARS-CoV-2 antibodies in characterised cohorts of known positive and negative plasma samples in an evaluation conducted according to Medicines and Healthcare products Regulatory Agency guidelines during a pandemic.
- Longitudinal data detecting IgG antibodies more than 10 months from infection were collected as sequential samples over time through a convalescent plasma donation programme.

INTRODUCTION

The WHO declared a pandemic in March 2020 due to SARS-CoV-2, identified in late 2019 in Wuhan, China, causing COVID-19 disease.[1 2]

Strengths and limitations of this study

- This study was conducted in a standardised setting with very experienced users on plasma characterised as positive or negative for the presence of antibodies using a reference standard, alongside one other assay which may introduce a possible spectrum bias and may not reflect the true performance metrics of the assay evaluated when translated to real-life settings, using finger prick blood samples and in which pretest probability would impact greatly on positive and negative predictive values.

A global race ensued to develop diagnostic assays, with the most common being viral RNA detection (reverse transcription-quantitative PCR (RT-qPCR) assays), to detect acute infection.[3] RT-qPCR assays are labour and reagent intensive, limited by a short temporal window for positive diagnosis, and exhibit potential for false negative results.[4] Evidence suggests sensitivity of RT-qPCR can be as low as 70%.[5] False positive rates between 0.8% and 4.0% have been reported in the UK and are dependent on the cycle threshold values accepted as indicating infection, the number of SARS-CoV-2 genes analysed and the proportion of asymptomatic individuals tested.[6 7] Lockdown measures and 'flattening the curve' strategies in the UK meant many infected individuals were instructed to self-isolate and were not offered a diagnostic RT-qPCR, with much of the testing limited to patients admitted to hospital, who perhaps reflect a more severely infected cohort. Consequently, a potentially large number of cases were unconfirmed or undetected.[8]

The ability to accurately detect SARS-CoV-2 specific antibodies, which develop after an immune response is evoked, is vital for building biobanks of convalescent sera for treatment, monitoring immune response to infection alongside surveillance studies and assessing responses to vaccination programmes.

Commercial serology immunoassays are mostly laboratory based and measure IgG antibody levels in plasma or serum. Alternatively, lateral flow immunoassays (LFIAs) require a finger prick blood sample and can be used at point-of-care (POC) or in the home; particularly important in the context of lockdown enforcement during the pandemic. A limited number of laboratory-based chemiluminescence immunoassays are approved for use in the UK including the Roche Elecsys Anti-SARS-CoV-2 IgG/IgA/IgM against the SARS-CoV-2 Nucleocapsid antigenic region (Roche Diagnostics, Basel, Switzerland) and the Abbott SARS-CoV-2 IgG assay against the same antigenic region (Abbott Diagnostics, Abbott Park, Illinois, USA).

The complexities of the humoral immune response to SARS-CoV-2 are a much-debated topic. In a US study, approximately 1 in 16 individuals lacked detectable IgG antibodies up to 90 days post-symptom onset, despite previous RT-qPCR-confirmed infection.[9] Patients who remain asymptomatic may mount a humoral immune response which is short lived, with detectable levels of antibody falling rapidly.[10] This, alongside the lack of RT-qPCR test availability across the UK, has hindered the development of a well-characterised gold standard serology test for IgG antibodies to SARS-CoV-2.

Herein, we describe the use of Roche and Abbott commercial immunoassays, as well as the EuroImmun Anti-SARS-CoV-2 ELISA-IgG against the S1 domain of the spike (antigenic) protein of SARS-CoV-2 (EuroImmun UK, London, UK) to characterise pre-pandemic and pandemic COVID-19 blood samples (n=880) from within Northern Ireland and report on longevity of IgG antibodies detected. Furthermore, we follow IgG antibody levels in convalescent plasma donors (n=101 individuals) for up to 11 months. Currently, there is no gold standard assay for comparison, therefore we aimed to establish a reference based on a positive COVID-19 antibody status. We present results of a laboratory evaluation of the UK-RTC AbC-19 with a target condition of antibodies against a cohort of 330 known IgG antibody positive samples according to this 'positive by two' system and 488 negative samples (223 pre-pandemic assumed negative and 265 known negative) for IgG to SARS-CoV-2.

METHODS

Participant samples

The flow of participant samples is summarised in online supplemental figure 1. A small cohort (n=19) of anonymised plasma samples were obtained from a partner USA laboratory for initial protocol development only. All participants provided informed consent. An online recruitment strategy was employed, with the study advertised through internal Ulster University email, website and social media. A BBC Newsline feature providing the pandemic study email address also prompted interest from the general population. The first 800 respondents who expressed interest were provided with an online patient information sheet, consent form and health questionnaire and invited to register to attend a clinic. Participants were eligible for the study if they were over 18 years of age. Exclusion criteria included anyone with a blood disorder or contraindication to giving a blood sample, or anyone currently exhibiting symptoms of COVID-19. To enrich the cohort for samples potentially positive for SARS-CoV-2 IgG antibody, further participants were invited if they had previously tested PCR positive or had the distinctive symptom of loss of taste and smell. Blood sampling clinics were held at locations around Northern Ireland between May and July 2020 resulting in collection of 263 10 mL EDTA plasma samples from 263 separate study participants. Additional anonymised plasma samples were obtained from Southern Health and Social Care Trust (SHSCT) healthcare workers (n=195) and Northern Ireland Blood Transfusion Service (NIBTS, n=184) through convalescent plasma programmes. NIBTS convalescent plasma samples continued to be collected throughout 2020–early 2021, with a total of n=897 from n=676 individuals, including n=183 samples from the cross-sectional cohort. Individuals from this programme with a positive RT-qPCR

result and EuroImmun starting value >6 were sequentially sampled over a period of up to 46 weeks resulting in a cohort of n=101 individuals, n=296 samples (including n=47 individuals from the cross-sectional cohort).

Pre-pandemic samples (prior to June 2019, n=136) were obtained from Ulster University Ethics Committee-approved studies with ongoing consent and from NIBTS (n=200, more than 3 years old). Plasma samples were used at no more than three freeze–thaw cycles for all analyses reported within this manuscript.

Clinical information

Basic demographic information and data with regard to probable or definite prior infection with SARS-CoV-2 were obtained from PANDEMIC Study participants through the secure online questionnaire requiring responses about positive RT-qPCR result and/or time from symptom onset. Anonymised participant samples from the USA, SHSCT and NIBTS were provided with age, gender and time since PCR positive, where a previous test had been carried out.

Laboratory-based immunoassays

Details of laboratory immunoassays are summarised in online supplemental methods and online supplemental table 1.

UK-RTC AbC-19 LFIA

All analyses were performed on UK-RTC AbC-19 Technical Transfer 3 devices at Ulster University according to manufacturer's instructions (details in online supplemental table 1). Assays were performed as cohorts, with samples in batches of 10, with one researcher adding 2.5 µL of plasma to the assay and a second adding 100 µL of buffer immediately following sample addition. After 20 min, the strength of each resulting test line was scored from 0 to 10 according to a visual score card (scored by three researchers; online supplemental figure 2). A score ≥1 was positive. Details of samples used for analysis for detection of antibodies are available in online supplemental methods.

Statistical analysis

As per Daniel,[11] a minimum sample size based on prevalence can be calculated using the following formula: $n = \frac{Z^2 P(1-P)}{d^2}$, where n=sample size, Z=Z statistic for a chosen level of confidence, P=estimated prevalence and d=precision. Assuming a prevalence of SARS-CoV-2 of 10% and a precision of 5%, we estimate that the required sample size at 99% confidence (Z=2.58) to be 240 individuals. If the true prevalence is lower, 5%, the estimated required sample size given a precision of 2.5% is 506 individuals. A minimum sample size of 200 known positives and 200 known negatives is given within Medicines and Healthcare products Regulatory Agency guidelines for SARS-CoV-2 LFIA antibody immunoassays.[12]

Statistical analysis was conducted in in R V.4.0.2.[13] To assess discordance between test results, data were first filtered to include individuals with an Abbott test result in the range ≥0.25–≤1.4, with a 2×2 contingency table produced that comprised all possible combinations of (concordant|discordant) test results (within|outside) of this range. A p value was derived via a Pearson χ^2 test after 2000 p value simulations via the stats package.

AbC-19 LFIA performance analyses were performed using MedCalc online (MedCalc Software, Ostend, Belgium). Receiver operating characteristic curve analysis was performed via the pROC package. To compare test result (positive|negative) with age, a binary logistic regression model was produced with test result as outcome—a p value was then derived via χ^2 analysis of variance. To compare time against test result (encoded continuously), a linear regression was performed. We calculated median per time period and then converted these to log (base 2) ratios against the positivity cut-off for each assay. All plots were generated via ggplot2 or custom functions using base R.[14]

RESULTS

We analysed samples from a mixed cohort of individuals from the general public (n=279), Northern Ireland healthcare workers (n=195), pre-pandemic blood donations and research studies (n=223), and through a convalescent plasma programme (n=183). Antibody levels in plasma from these 880 individuals were assessed using the three SARS-CoV-2 immunoassays: EuroImmun IgG, Roche Elecsys IgG/IgM/IgA and Abbott Architect IgG (online supplemental table 1 and online supplemental figure 3). This included a cohort of 223 pre-pandemic plasma samples collected and stored during 2017 to end of May 2019 to determine assay specificity. Of the 657 participants whose samples were collected during the pandemic, 267 (40.64%) previously tested RT-qPCR positive with a range of 7–173 days since diagnosis. A total of 225 participants gave time since self-reported COVID-19 symptoms, with a range of 5–233 days from symptom onset, while 195 had no symptom or PCR data available. Samples collected in 2020 (n=657) ranged from 19 to 78 years of age with a median (IQR) of 43 years (±22), and n=454 were women and n=200 men (n=3, not disclosed). Pre-pandemic samples (n=223) ranged from 20 to 87 years of age with median (IQR) of 50 years (±20) and consisted of n=88 women and n=135 men.

Laboratory-based antibody immunoassays

A positive result for antibody on one or more of the three laboratory immunoassays was recorded for 385 of 657 (58.6%) participants who provided a sample during the pandemic. By EuroImmun ELISA, 346 were positive, 20 borderline and 291 were negative. The Roche assay detected 380 positive and 277 negative, while Abbott determined 310 positive and 347 negative (online supplemental table 2 and online supplemental figure 3). The median age across all age groups combined was lower for participants testing positive across each of

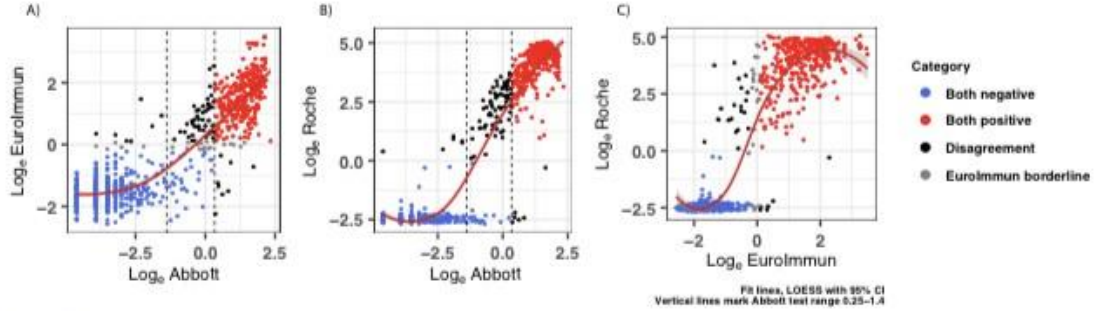

Figure 1 Two-way correlation scatter plots comparing (A) EuroImmun, (B) Abbott and (C) Roche immunoassays. Pearson χ^2 test was used to assess correlations. The results for each test were log transformed to ensure results follow a normal distribution. Negative agreement shown as blue dots, red dots show positive agreement for the two immunoassays, while black dots show disagreement and grey dots as the EuroImmun borderline results. Vertical lines mark the Abbott test range 0.25–1.4. n=880. The graphs show positive correlations between all immunoassays evaluated, with the fewest disagreement of results between the log of Roche and the log of EuroImmun. Fit lines locally estimated scatterplot smoothing (LOESS), with 95% CI shaded.

the immunoassays (median (SD) for positive vs negative, respectively: EuroImmun, 41 (13.16) vs 48 (12.95); Roche, 42 (13.08) vs 48 (13.00); Abbott, 41 (13.18) vs 47 (13.09)) (online supplemental figure 4, p<0.0001). When segregated by age group, however, differences were less apparent in certain groups (online supplemental figure 5). Excluding the pre-pandemic cohort, this gap reduced but remained statistically significant: EuroImmun, 41 (13.18) vs 45 (12.49); Roche, 42 (13.15) vs 45 (12.49); Abbott, 41 (13.26) vs 44 (12.63) (p<0.01) (median (SD) for positive vs negative). Of note, out of 267 individuals with a previous positive RT-qPCR result for SARS-CoV-2 viral RNA, 14 (5.2%, online supplemental figure 3A) did not show detectable antibodies by any of the three immunoassays, with no association found with age, gender or time between test and blood draw (data not shown).

The three commercial laboratory immunoassays provide a ratio value that increases with IgG antibody titre. When correlation between these values is assessed, good overall agreement is observed between the three immunoassays (figure 1A–C and online supplemental figure 9). As highlighted by Rosadas *et al*,[15] we also see significant disagreement in the Abbott 0.25–1.4 range when compared with EuroImmun and Roche (figure 1; X^2 p values: EuroImmun vs Abbott, p<0.001; Roche vs Abbott, p<0.001).

Duration of humoral response to SARS-CoV-2

In a cross-sectional analysis of antibodies over time, we found IgG antibodies could still be detected in individuals (excluding pre-pandemic) across all three immunoassays used up to week 20 (day 140) (figure 2). We note a statistically significant decrease in signal with respect to time across each assay (p value (estimate slope)): EuroImmun, p=0.028 (−0.823); Roche, p=0.002 (−0.125); Abbott, p<0.0001 (−3.673). These remained statistically significant after adjustment for age. Antibody levels (expressed as a ratio of median result per time point divided by positivity cut-off; table 1) peaked at week 1–2 for EuroImmun (1.33) and Abbott (1.64), though reached highest levels at week 9–12 when measured by Roche (5.45). By week 21–24, median score for all tests had dropped below the positivity cut-off, though a small number of samples remained above the positive cut-off at these later time points (figure 2).

Samples from the NIBTS convalescent plasma programme continued to be collected throughout 2020–early 2021. A total of n=897 samples from n=676 individuals were collected, 744 of 883 tested by EuroImmun were positive (>1.1, with values range of 0.051–34.361), 556 of 749 tested by Abbott were positive (>1.4, with values ranging from 0.01 to 8.85). Individuals with a positive RT-qPCR result and a EuroImmun result >6 were sequentially sampled (with median 3, range 2–9 samples per individual), and analysed by both EuroImmun (n=101 individuals) and Abbott immunoassays (n=75 individuals). Median age (IQR) for this cohort is 51 years (±21) with a range from 18 to 70 years and n=27 women, n=74 men. Longitudinal analysis shows persistence of detectable IgG antibodies until up to 302 days (43 weeks) by Abbott immunoassay (at which point this assay was discontinued at NIBTS) and 323 days (46 weeks) by EuroImmun ELISA, with a gradual decline over time (online supplemental figure 6). None of the individuals who were initially positive by EuroImmun SARS-CoV-2 S1 IgG assay dropped to below the EuroImmun positivity threshold (>1.1) over the course of the follow-up, while 26 who were initially positive by Abbott SARS-CoV-2 NP IgG fell below the Abbott threshold (>1.4).

UK-RTC AbC-19

Using the commercial immunoassays described, we established a well-characterised serology sample set of 'known positive' and 'known negative' for IgG antibodies

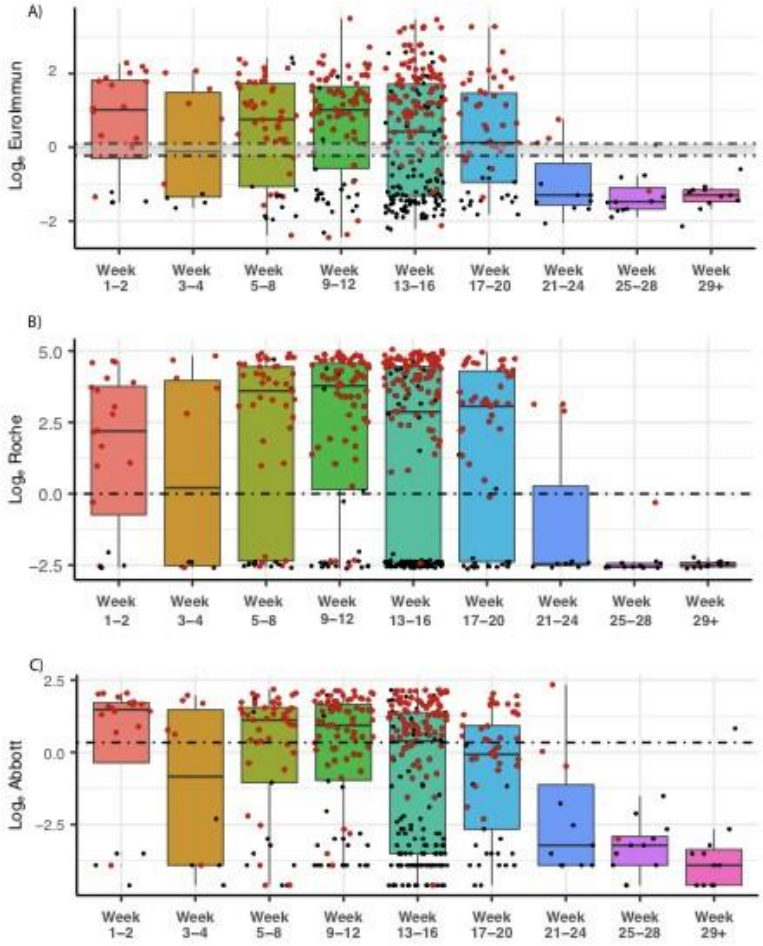

Figure 2 SARS-CoV-2 antibody levels by (A) EuroImmun, (B) Roche and (C) Abbott, relative to weeks since first reported symptoms or positive PCR result (where data available, n=685). RT-PCR-positive individuals are denoted by red dots, while individuals with time since symptom data are denoted in black. Dashed lines delineate log$_e$ equivalent of positivity threshold (EuroImmun 1.1, Roche 1.0, Abbott 1.4) for each test, and the negativity threshold for EuroImmun (0.8; borderline result between the two lines). Black bars indicate median, within IQR boxes for EuroImmun/Roche/Abbott value. Red triangles indicate outliers, based on 1.5×IQR. RT-PCR, reverse transcription-PCR.

to SARS-CoV-2 to evaluate performance metrics for the UK-RTC AbC-19 Rapid LFIA.

AbC-19 detects IgG antibodies against the spike protein antigen, so we therefore required all samples to be positive by the EuroImmun SARS-CoV-2 IgG ELISA, which likewise detects antibodies against the S1 domain.[16] To develop this characterised cohort, samples were also required to be positive by a second immunoassay (Roche or Abbott). To analyse specificity of the AbC-19 LFIA for detection of SARS-CoV-2 IgG antibody, we assessed 350 plasma samples from participants classed as 'known negative for SARS-CoV-2 IgG antibody' on the AbC-19 LFIA. All samples were from individuals confirmed to be negative across all three laboratory assays (Roche, EuroImmun, Abbott). Using these positive n=304 and negative n=350 antibody cohorts, we determined a sensitivity for detecting SARS-CoV-2 IgG antibody of 97.70% (95% CI: 95.31% to 99.07%) and specificity of 100% (98.95% to 100.00%) for the AbC-19 LFIA (table 2).

Given a recent report of lower specificity in the AbC-19 LFIA[17] and the possibility of introducing sample bias, we revised our inclusion criteria for the negative cohort. For the pre-pandemic cohort, we included samples from all 223 individuals, regardless of results on other laboratory

Table 1 Antibody level ratios for assays over time

	Ratio median antibody level: assay positivity cut-off									
	Week									
	Pre-2020	1–2	3–4	5–8	9–12	13–16	17–20	21–24	25–28	29+
EuroImmun	−2.65	1.33	0.2	0.95	1.32	0.47	0.04	−2.01	−2.26	−2.01
Roche	−3.64	3.16	3.05	5.20	5.45	4.14	4.42	−3.54	−3.69	−3.61
Abbott	−5.54	1.64	−0.51	1.12	0.86	0.08	−0.59	−5.13	−5.13	−6.13
Sample number (n=)	223	20	10	52	90	202	53	11	12	11

Antibody level ratios for assays over time show varying peak levels depending on test. Calculated by first establishing the median per time period, then calculating log2 ratio for each period versus each respective assay positivity cut-off.

immunoassays. When this assumed negative pre-pandemic cohort was used for laboratory evaluation for target condition of antibodies, we observed a specificity of 99.55% (97.53% to 99.99%, table 2). We expanded the negative cohort to include all samples that matched our criteria (samples collected during the pandemic to be negative by all three laboratory assays and all pre-pandemic samples regardless of other immunoassay results). The specificity observed on this extended negative cohort of 488 samples was 99.59% (98.53% to 99.95%, table 2). For sensitivity analysis on a positive cohort (samples positive by EuroImmun and one other test), we were able to analyse all samples previously untested due to limited testing capacity and tested a positive cohort of 330 samples giving a sensitivity of 97.58% (95.28% to 98.95%, table 2). When we sorted samples analysed in both negative (n=488) and positive cohorts (n=330) by RT-qPCR status and assessed AbC-19 LFIA sensitivity by including only those that were RT-qPCR positive (n=227), the test showed a sensitivity of 92.07% (87.76% to 95.23%; online supplemental table 3 and online supplemental figure 3B). However, of the n=18 RT-qPCR-positive individuals negative for IgG antibodies by AbC-19, n=12 showed no detectable antibodies by all three laboratory assays (EuroImmun, Roche or Abbott), suggesting that antibodies are not present in those samples (online supplemental figure 3C).

When used as intended by the public, the AbC-19 LFIA provides binary positive/negative results. However, when assessing LFIA in the laboratory, each test line was scored against a scorecard by three independent researchers (0 negative, 1–10 positive; online supplemental figure 2). When compared with quantitative outputs from the Abbott, EuroImmun and Roche assays, the AbC-19 LFIA shows good correlation (Abbott r=0.84 (p<0.001); EuroImmun r=0.86 (p<0.001); Roche r=0.82 (p<0.001); online supplemental figures 3 and 7–9).

Analytical specificity and sensitivity of AbC-19 LFIA

We observed no cross-reactivity across samples with known H5N1 influenza, respiratory syncytial virus, influenza A, influenza B, *Bordetella pertussis*, *Haemophilus influenzae*, seasonal coronavirus NL63 and 229E on the AbC-19 LFIA (n=34 samples, n=8 distinct respiratory viruses; online supplemental table 4). Against a panel of external reference SARS-CoV-2 serology samples, the AbC-19 LFIA detected antibodies with scores commensurate to the EuroImmun ELISA scores (online supplemental figure 10 and online supplemental table 5).

DISCUSSION

Serological antibody immunoassays are an important tool in helping combat the SARS-CoV-2 pandemic. The duration of the humoral immune response is of particular importance, to inform an individual's protection following both natural infection and vaccination. Using a

Table 2 UK-RTC AbC-19 LFIA performance metrics against known antibody positive and known antibody negative cohorts

Total negative	True negative	False positive	Total positive	True positive	False negative	Sensitivity % (95 CI)	Specificity % (95 CI)
Pre-pandemic (n=223)							
223	222	1	n/a	n/a	n/a	n/a	99.55 (97.53 to 99.99)
Initially reported cohorts (n=654)							
350	350	0	304	297	7	97.70 (95.31 to 99.07)	100.00 (98.95 to 100.00)
Extended cohorts (n=818)							
488	486	2	330	322	8	97.58 (95.28 to 98.95)	99.59 (98.53 to 99.95)

LFIA, lateral flow immunoassay; n/a, not available.

large cohort of individuals across a wide age range (18–78 years), we assessed antibody levels across up to three laboratory immunoassays and perform a cross-sectional and longitudinal analysis over time. Our results show strong correlation between all three immunoassays, with shortcomings in the Abbott system output 0.25–1.4 range, as described previously, suggesting an overestimated positive cut-off (figure 1).[15]

Longitudinal studies on SARS-CoV-1 convalescent patients suggest that detectable IgG can still be present as long as 2 years after infection.[18] There are conflicting reports of the longevity of the humoral response to SARS-CoV-2 infection which differ in the make-up of the cohort studied, the assays used and the length of time since symptom onset. The longevity of IgG antibodies to both spike and nucleocapsid protein more than 10 months after RT-qPCR-positive status (and beyond in a small number of samples (figure 2 and online supplemental figure 6) is consistent with that observed in other recent studies.[19–21] In this study, samples were collected through a convalescent plasma programme (online supplemental figure 6), with individuals selected for sequential plasma donation based on an initial high EuroImmun assay score. In contrast to the time series analysis of healthcare workers recruited prospectively by Manisty *et al*,[22] we observed no cases where EuroImmun ELISA-measured anti-spike antibody levels fell below threshold, while a large number of Abbott measured anti-nucleocapsid antibody levels dropped below the positivity threshold (34.7%, 26 of 75). However, this may be an overestimate given the shortcomings of the Abbott assay described above (figure 1). In a similar longitudinal study of 51 symptomatic participants, Dan *et al* estimated that half-life ($t_{1/2}$) for IgG-spike (103 days) was longer than that for IgG-nucleocapsid (68 days), although with a considerable overlap of 95% CIs.[23]

In our more diverse cross-sectional cohort, we also note a statistically significant decline over time but levels remain detectable at 140 days (figure 2). We note that IgG levels reach their peak (Roche ratio 5.45 times threshold cut-off) as late as week 9–12 from first symptoms or a viral RNA RT-qPCR positive result, though this may be an artefact of lower number of participants at earlier time points (table 1). Robust antibody responses are produced in our cohorts across a wide age range (18–78 years old, figure 2 and online supplemental figure 6). We detect a slightly but significantly lower median age of participants testing positive (online supplemental figure 4); however, this is likely be due to cohort characteristics and not a true reflection of the population or indication of test performance.

A difficulty faced in validation of antibody diagnostic assays has been access to samples with known SARS-CoV-2 antibody status. As previously described, there is no clear gold standard reference against which to assess SARS-CoV-2 immunoassays. A positive RT-qPCR test has been used previously to indicate previous (COVID-19) SARS-CoV-2 infection, though this approach is limited by a high rate of false negatives and positives in RT-qPCR testing, failure in some cases to develop IgG antibodies (sero-silence or lack of antibody against the same antigenic component of the virus as the immunoassay used as a capture antigen) and the lack of RT-qPCR testing availability early in the pandemic.[3 5 24] SARS-CoV-2 IgG antibodies were undetectable in 14 of 267 (5.2%) of previously RT-qPCR SARS-CoV-2 viral RNA-positive participants in this study. It is unclear if this is due to insufficient/absent antibody production in these individuals at the time the sample was taken, or due to a false positive PCR result which may occur in the UK at a rate between 0.8% and 4.0%.[6] Self-assessment of symptoms for COVID-19 (disease) is a poor indicator of previous infection, even among healthcare workers.[25] Additionally, the kinetics of a SARS-CoV-2 virus infection contributes to the loss of sensitivity of RT-qPCR to detect virus with time, contributing to false negative RT-qPCR test results for individuals who may be late to present for virus detection tests.[5 26]

To assess sensitivity and specificity of the AbC-19 LFIA for its ability to detect SARS-CoV-2 antibody in a laboratory evaluation, we developed a reference standard for SARS-CoV-2 antibodies, which does not rely on a single test as reference. A similar approach was used in a recent seroprevalence study in Iceland, whereby two positive antibody results were required to determine a participant sample as positive for SARS-CoV-2 antibody.[24] Our evaluation of performance metrics for the UK-RTC AbC-19 LFIA to detect antibodies for SARS-CoV-2 gave 97.58% sensitivity and 99.59% specificity. In an evaluation of the AbC-19 tests, Mulchandani *et al* observed a specificity of 97.9% (97.2% to 98.4%) in a cohort of pre-pandemic samples and report a sensitivity of 92.5% (88.8% to 95.1%) for detecting previous infections (based on a previous RT-qPCR result) or 84.7% (80.6% to 88.1%) against the Roche Elecsys antibody test, which detects IgM/IgG/IgA SARS-CoV-2 antibodies to the nucleocapsid portion of SARS-CoV-2.[25] In RT-qPCR-positive individuals from our cohorts, the AbC-19 test showed a similar sensitivity of 92.07% (87.76% to 95.23%, online supplemental figure 3, online supplemental table 3). However, we demonstrate the drawbacks of this approach given that in 12 of 18 AbC-19 false negatives, none of the four immunoassays used (EuroImmun, Roche, Abbott or AbC-19) detected antibodies, suggesting either a false RT-qPCR result, a failure to produce IgG antibodies or sero-reversion before sample collection in these individuals. Another recent evaluation of the AbC-19 LFIA by Moshe *et al*[27] determined a sensitivity of 100% (98.1% to 100%) on laboratory sera, using a composite reference standard of antibody positive by either spike protein ELISA or hybrid double antigen binding assay (DABA) and specificity of 99.8% (98.9% to 100%) against pre-pandemic samples. However, when AbC-19 performance was analysed on matched finger prick and serum samples against the same antibody standard, a lower sensitivity was observed (finger prick 69% (53.8% to 81.3%), serum 92% (80% to 97.7%)).

In our study, strong correlation was observed in quantitative score between results on all immunoassays with

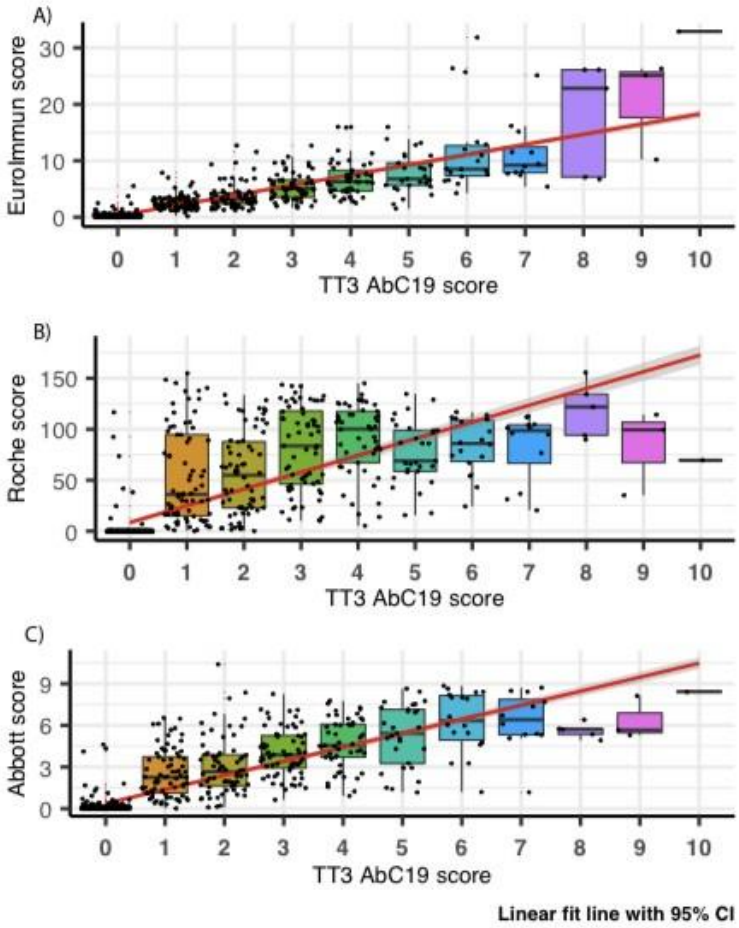

Figure 3 AbC-19 extended cohort (n=818) correlation to (A) EuroImmun, (B) Roche and (C) Abbott scores. Box plots overlaid on scatter plot, comparing AbC-19 TT3 test scores with EuroImmun, Roche and Abbott quantitative antibody values. Red linear line of best fit with 95% CI shaded in grey. Black bars indicate median, within IQR boxes for EuroImmun/Roche/Abbott value. Red triangles indicate outliers, based on 1.5×IQR. TT3, Technical Transfer 3.

the highest observed between EuroImmun and AbC-19 LFIA (online supplemental figures 8 and 9). This is to be expected, given both the AbC-19 LFIA and EuroImmun ELISA detect IgG antibodies against spike protein. Importantly, for the assessment of immunity to prior natural infection as well as to immunisation, IgG antibodies against SARS-CoV-2 spike protein detected by laboratory-based EuroImmun ELISA and AbC-19 LFIA are known to correlate with neutralising antibodies, which may confer future immunity.[23 28 29] Previous evaluations of sensitivity and specificity reported by Public Health England (PHE) showed a EuroImmun sensitivity of 72% and specificity of 99%, Abbott with sensitivity of 92.7% and specificity of 100%, and Roche with sensitivity of 83.9% and specificity of 100%.[30–32] The PHE analyses for each of these tests used previous infection (RT-qPCR-positive status) as a reference standard, the limitations of which are discussed above.

In the use of characterised 'known positive' and 'known negative' cohorts, one limitation of this study is its potential for spectrum bias, whereby our positive by two reference system may artificially raise the threshold for positive sample inclusion, possibly resulting in the overestimation of the sensitivity of any test evaluated.[33] However, similar issues have been raised when using previous RT-qPCR result or definitive COVID-19 symptoms as inclusion criteria given these will likely skew a cohort towards more severe disease, especially given issues of RT-qPCR availability outside of hospital settings during the first wave.[5] Importantly, our mixed origin of samples forming

the cohort provides a positive cohort for assessing assay sensitivity that includes individuals from the general public, healthcare workers and from convalescent plasma programmes. In the absence of a clear gold standard test, our system relies on no single test (each with their individual shortcomings) and instead takes an average of three. Our analysis of specificity on only pre-pandemic individuals (n=223) shows similar specificity (99.55%) to the larger mixed 'known negative cohort' (n=488, sensitivity 99.59%). We also demonstrate a high level of analytical specificity of the AbC-19 test with no cross-reactivity against a panel of other respiratory viruses, including SARS-CoV-1 NL63 and 229E (online supplemental table 4).

Our assessment of the AbC-19 LFIA in a laboratory setting, using characterised cohorts of known SARS-CoV-2 antibody positive and antibody negative plasma, shows good performance metrics for its ability to detect SARS-CoV-2 IgG antibodies following natural infection. We note our use of plasma from venous blood samples, as opposed to a finger prick blood sample as would be used in rapid testing scenarios.[27] Additionally, when the AbC-19 LFIA was used on our cohort, a number of the positive results scored low (1 of 10 using the scorecard under laboratory conditions, figure 3), with a faint test band visible to a trained laboratory scientist but perhaps difficult to identify as positive by individuals performing a single test (online supplemental figure 10). This faint line may be reflective of the longer time from infection for the Northern Ireland cohort used. If the AbC-19 LFIA is to be used in clinical settings, it is important to determine if all users observe the same results as observed in this laboratory evaluation.

This assessment of the AbC-19 LFIA does not provide data on how this test will perform in a seroprevalence screening scenario, but instead provides metrics for the performance of the test, where presence of SARS-CoV-2 antibodies is of interest, as opposed to previous COVID-19 infection. An important potential use of the AbC-19 LFIA would be in monitoring the immune response to vaccination, with most vaccines using SARS-CoV-2 spike protein antigens.[34]

CONCLUSION

We present a comprehensive analysis of pre-pandemic and two large pandemic cohorts (more than 700 individuals) and in a longitudinal analysis, show that IgG antibodies to SARS-CoV-2 antigens are detectable more than 10 months from positive RT-qPCR test. We use antibody positive status as an alternative to RT-PCR-positive status as a standard for assessing SARS-CoV-2 antibody assays and show strong performance for the UK-RTC AbC-19 LFIA rapid POC test in detecting SARS-CoV-2 antibodies. User experience in future studies in the real world is important and may alter the performance characteristics. Also, the effect of operator training will have direct effects on test performance. We welcome further clinical evaluation of the AbC-19 LFIA in large cohorts of symptomatic and asymptomatic individuals alongside large studies assessing vaccination outcomes in individuals to fully validate its implementation across all intended use cases.

Author affiliations
[1]Biomedical Sciences Research Institute, Ulster University, Coleraine, UK
[2]Nanotechnology and Integrated Bioengineering Centre, Ulster University—Jordanstown Campus, Newtownabbey, UK
[3]Clinical Biochemistry Laboratory, Southern Health and Social Care Trust, Portadown, UK
[4]Microbiology Laboratory, Southern Health and Social Care Trust, Portadown, UK
[5]Northern Ireland Blood Transfusion Service, Belfast City Hospital, Belfast, UK
[6]Royal Victoria Hospital, Belfast Health and Social Care Trust, Belfast, UK
[7]R&D, Avellino Labs USA, Menlo Park, California, USA

Acknowledgements We are extremely grateful to all the people of Northern Ireland who took part in this study and gave blood during the pandemic. We are indebted to the phlebotomists: Geraldine Horrigan and Pamela Taylor who conducted the blood draws while ensuring the highest possible level of safety to the participants. We are also grateful to Kingsbridge Private Hospital Group for sponsorship and providing everything needed for blood collection including the clinical rooms. We acknowledge Dr Tony Byrne for use of his laboratory and Professor Gareth Davison for laboratory space and equipment during the pandemic within a locked down university.

Contributors TM and JADM conceived the study. LJR, JSM and TM performed all laboratory analyses. LJR, SEM and KYN analysed data. KB performed all statistical analyses/interpretations and produced figures. NQ, FJ, GW and PS performed all Roche analyses and provided SHSCT cohort samples. MC, KM and SR performed all Abbott analyses and provided blood transfusion cohort samples. TM, RKP and MAN coordinated participant recruitment, consent and sampling. WPB and JADM developed online consent forms, questionnaires and databases. LJR, JSM, AMK, AA, GEW, DH, SS and CCS performed sample collection and processing. LJR and TM wrote the manuscript, with significant contributions from JSM, JADM, MAN and KB. All authors reviewed and approved the final manuscript.

Funding Costs for assays and laboratory expenses only will be paid by UK-RTC as is normal practice (UU-UK-RTC-2020-001). The authors have not been paid or financially benefited from this study. The advisory roles within CIGA Healthcare were unpaid temporary roles. This manuscript and associated data within this paper have only been used to build confidence into the overall device design and performance assessment of the UK RTC AbC-19 devices and such work was never commissioned for any government contractual consideration.

Competing interests None declared.

Patient consent for publication Not required.

Ethics approval All study participants provided informed consent. This study was approved by Ulster University Institutional Ethics Committee (REC/20/0043), South Birmingham REC (The PANDEMIC Study IRAS Project ID: 286041Ref 20/WM/0184) and adhered to the Declaration of Helsinki and Good Clinical Practice.

Provenance and peer review Not commissioned; externally peer reviewed.

Data availability statement Data are available on reasonable request to the corresponding author.

ORCID iDs
Louise J Robertson http://orcid.org/0000-0003-2926-1231
Kevin Blighe http://orcid.org/0000-0002-6322-6571
Kok Yew Ng http://orcid.org/0000-0003-1465-0592
Ruth K Price http://orcid.org/0000-0001-8765-2842
William P Burns http://orcid.org/0000-0002-6146-3434
Agnes Awuah http://orcid.org/0000-0002-4068-2216
Sara E McNamee http://orcid.org/0000-0003-1711-2714
Connie Chao Shern http://orcid.org/0000-0002-2772-9235
M Andrew Nesbit http://orcid.org/0000-0001-7222-4124
James A D McLaughlin http://orcid.org/0000-0001-6026-8971
Tara Moore http://orcid.org/0000-0002-7659-9326

REFERENCES

1 World Health Organisation. Rolling updates on coronavirus disease (COVID-19), 2020. Available: https://www.who.int/emergencies/diseases/novel-coronavirus-2019/events-as-they-happen
2 Lu R, Zhao X, Li J, *et al*. Genomic characterisation and epidemiology of 2019 novel coronavirus: implications for virus origins and receptor binding. *Lancet* 2020;395:565–74.
3 Petherick A. Developing antibody tests for SARS-CoV-2. *Lancet* 2020;395:1101–2.
4 Winichakoon P, Chaiwarith R, Liwsrisakun C, *et al*. Negative nasopharyngeal and oropharyngeal swabs do not rule out COVID-19. *J Clin Microbiol* 2020;58. doi:10.1128/JCM.00297-20. [Epub ahead of print: 23 04 2020].
5 Watson J, Richter A, Deeks J. Testing for SARS-CoV-2 antibodies. *BMJ* 2020;370:m3325.
6 Surkova E, Nikolayevskyy V, Drobniewski F. False-positive COVID-19 results: hidden problems and costs. *Lancet Respir Med* 2020;8:1167–8.
7 Omata M, Hirotsu Y, Sugiura H, *et al*. The dynamic change of antibody index against Covid-19 is a powerful diagnostic tool for the early phase of the infection and salvage PCR assay errors. *J Microbiol Immunol Infect* 2021. doi:10.1016/j.jmii.2020.12.009. [Epub ahead of print: 05 Jan 2021].
8 Black JRM, Bailey C, Przewrocka J, *et al*. COVID-19: the case for health-care worker screening to prevent Hospital transmission. *Lancet* 2020;395:1418–20.
9 Petersen LR, Sami S, Vuong N, *et al*. Lack of antibodies to SARS-CoV-2 in a large cohort of previously infected persons. *Clin Infect Dis* 2020:ciaa1685.
10 Long Q-X, Tang X-J, Shi Q-L, *et al*. Clinical and immunological assessment of asymptomatic SARS-CoV-2 infections. *Nat Med* 2020;26:1200–4.
11 Daniel WW. *Biostatistics : a foundation for analysis in the health sciences. 7th Edition*. New York: John Wiley & Sons, Ltd, 1999: 720.
12 Medicines and Healthcare product Regulatory Agency. Target product profile: antibody tests to help determine if people have immunity to SARS-CoV-2, 2020. Available: https://assets.publishing.service.gov.uk/government/uploads/system/uploads/attachment_data/file/881162/Target_Product_Profile_antibody_tests_to_help_determine_if_people_have_immunity_to_SARS-CoV-2_Version_2.pdf
13 The R Development Core Team. R: a language and environment for statistical computing. ISBN 3-900051-07-0 2017.
14 Wickham H. *ggplot2 elegant graphics for data analysis*. Berlin: Springer, 2016.
15 Rosadas C, Randell P, Khan M, *et al*. Testing for responses to the wrong SARS-CoV-2 antigen? *Lancet* 2020;396:e23.
16 UK-RTC and Abingdon Health. Charting the course to a post-COVID world. York, United Kingdom Abingdon Health; 2020. https://www.abingdonhealth.com/guides/abc-19tm-rapid-test-white-paper/ [Accessed Nov 2020].
17 Mulchandani R, Jones HE, Taylor-Phillips S, *et al*. Accuracy of UK Rapid Test Consortium (UK-RTC) "AbC-19 Rapid Test" for detection of previous SARS-CoV-2 infection in key workers: test accuracy study. *BMJ* 2020;371:m4262.
18 Wu L-P, Wang N-C, Chang Y-H, *et al*. Duration of antibody responses after severe acute respiratory syndrome. *Emerg Infect Dis* 2007;13:1562–4.
19 Vanshylla K, Di Cristanziano V, Kleipass F, *et al*. Kinetics and correlates of the neutralizing antibody response to SARS-CoV-2 infection in humans. *Cell Host Microbe* 2021. doi:10.1016/j.chom.2021.04.015. [Epub ahead of print: 03 May 2021].
20 Petersen MS, Hansen CB, Kristiansen MF. SARS-CoV-2 natural antibody response persists up to 12 months in a nationwide study from the Faroe Islands. *medRxiv* 2021.
21 Li C, Yu D, Wu X. Twelve-month specific IgG response to SARS-CoV-2 receptor-binding domain among COVID-19 convalescent plasma donors in Wuhan. *bioRxiv* 2021.
22 Manisty C, Treibel TA, Jensen M. Characterising heterogeneity and sero-reversion in antibody responses to mild SARS[?]CoV-2 infection: a cohort study using time series analysis and mechanistic modelling. *medRxiv* 2020.
23 Dan JM, Mateus J, Kato Y, *et al*. Immunological memory to SARS-CoV-2 assessed for up to 8 months after infection. *Science* 2021;371:eabf4063.
24 Gudbjartsson DF, Norddahl GL, Melsted P, *et al*. Humoral immune response to SARS-CoV-2 in Iceland. *N Engl J Med* 2020;383:1724–34.
25 Mulchandani R, Taylor-Phillips S, Jones H. Self assessment overestimates historical COVID-19 disease relative to sensitive serological assays: cross sectional study in UK key workers. *medRxiv* 2020.
26 Iyer AS, Jones FK, Nodoushani A, *et al*. Persistence and decay of human antibody responses to the receptor binding domain of SARS-CoV-2 spike protein in COVID-19 patients. *Sci Immunol* 2020;5:eabe0367.
27 Moshe M, Daunt A, Flower B, *et al*. SARS-CoV-2 lateral flow assays for possible use in national covid-19 seroprevalence surveys (react 2): diagnostic accuracy study. *BMJ* 2021;372:n423.
28 Iyer AS, Jones FK, Nodoushani A, *et al*. Dynamics and significance of the antibody response to SARS-CoV-2 infection. *medRxiv* 2020. doi: 10.1101/2020.07.18.20155374. [Epub ahead of print: 20 Jul 2020].
29 Addetia A, Crawford KHD, Dingens A, *et al*. Neutralizing antibodies correlate with protection from SARS-CoV-2 in humans during a fishery vessel outbreak with a high attack rate. *J Clin Microbiol* 2020;58.
30 Public Health England. Evaluation of the Abbott SARS-CoV-2 IgG for the detection of anti-SARSCoV-2 antibodies, 2020. Available: https://assets.publishing.service.gov.uk/government/uploads/system/uploads/attachment_data/file/890566/Evaluation_of_Abbott_SARS_CoV_2_IgG_PHE.pdf
31 Public Health England. Evaluation of the Euroimmun Anti-SARS-CoV-2 ELISA (IgG) serology assay for the detection of anti-SARS-CoV-2 antibodies, 2020. Available: https://assets.publishing.service.gov.uk/government/uploads/system/uploads/attachment_data/file/893433/Evaluation_of_Euroimmun_SARS_CoV_2_ELISA_IgG__1_.pdf
32 Public Health England. Evaluation of Roche Elecsys AntiSARS-CoV-2 serology assay for the detection of anti-SARS-CoV-2 antibodies. London, United Kingdom Public Health England; 2020. https://assets.publishing.service.gov.uk/government/uploads/system/uploads/attachment_data/file/891598/Evaluation_of_Roche_Elecsys_anti_SARS_CoV_2_PHE_200610_v8.1_FINAL.pdf [Accessed Nov 2020].
33 Hall MK, Kea B, Wang R. Recognising bias in studies of diagnostic tests part 1: patient selection. *Emerg Med J* 2019;36:431–4.
34 Jeyanathan M, Afkhami S, Smaill F, *et al*. Immunological considerations for COVID-19 vaccine strategies. *Nat Rev Immunol* 2020;20:615–32.